Technische Universität München

TUM School of Natural Sciences

Regulation of human tRNA expression during differentiation

Lexi Gao

Vollständiger Abdruck der von der TUM School of Natural Sciences der Technischen Universität München zur Erlangung des akademischen Grades einer

Doktorin der Naturwissenschaften (Dr. rer. nat.)

genehmigten Dissertation.

Vorsitz: Prof. Dr. Karl Duderstadt

Prüfer*innen der Dissertation: 1. Prof. Dr. Danny Nedialkova

2. Prof. Dr. Maria Colomé-Tatché

3. Prof. Dr. Nina Henriette Uhlenhaut

Die Dissertation wurde am 17.10.2023 bei der Technischen Universität München eingereicht und durch die TUM School of Natural Sciences am 13.12.2023 angenommen.

Publication list

Part of the results described in this thesis have been accepted for publication:

L. Gao[*]**,** A. Behrens[*], G. Rodschinka, S. Forcelloni, S. Wani, K. Strasser, D. D. Nedialkova. Selective gene expression maintains human tRNA anticodon pools during differentiation. *Nature Cell Biology*, *accepted in principle.*

[*]Authors contributed equally

Parts of the work described in this thesis were presented as talks at the following international scientific conferences:

L. Gao, G. Rodschinka, A. Behrens, S. Forcelloni, S. Wani, K. Strasser, D. D. Nedialkova. "Dynamics of human tRNA repertoires as a function of cell identity". EMBL Symposium "The Complex Life of RNA" (2022), Heidelberg, Germany.

L. Gao, A. Behrens, G. Rodschinka, S. Forcelloni, S. Wani, K. Strasser, D. D. Nedialkova. "Transfer RNA pools in human cells are controlled by selective gene expression". Paris-Munich Epigenetics Symposium (2023), Munich, Germany.

Table of contents

Abstract 1
Zusammenfassung 2
Chapter 1 - Introduction 4
1.1 tRNA biology 5
1.1.1 Eukaryotic tRNA biogenesis 5
1.1.2 tRNA structure 7
1.1.3 tRNA modifications 8
1.1.4 Codon-anticodon pairing 10
1.1.5 tRNA in translation 11
1.1.6 tRNA sequence diversity 14
1.1.7 Cell type-specific regulation of tRNA abundance 16
1.1.8 Codon demand and tRNA supply 17
1.1.9 High-resolution tRNA quantification by mim-tRNAseq 20
1.2 tRNA transcription by RNA polymerase III 22
1.2.1 RNA polymerase III 22
1.2.2 Type 1, 2 and 3 Pol III promoters 24
1.2.3 Pol III transcription factors 25
1.2.4 Pol III transcription complex assembly on a tRNA gene 26
1.3 Regulation of tRNA abundance by RNA polymerase III transcription 27
1.3.1 Regulation of Pol III transcription by cis-elements 27
1.3.2 Trans-regulating factors of tRNA transcription 29
1.3.3 Regulation of Pol III transcription by the epigenetic environment 30
1.3.4 Regulation of Pol III transcription by genomic context 31
1.3.5 Regulation of Pol III transcription by changes in protein composition 32
1.4 Regulation of Pol III transcription by MAF1 33
1.4.1 MAF1 33
1.4.2 mTORC1 35
1.5 tRNA and Pol III dysregulation and human diseases 36
1.6 Studying cell type-specific tRNA regulation in hiPSC-based models 37
1.7 Scope of this thesis 38
Chapter 2 - Results 39
2.1 Human tRNA pools are extensively remodeled at transcript level but remain largely stable at anticodon level during differentiation 41
2.1.1 Derivation of homogeneous cultures of cardiomyocytes, neuronal progenitor cells, and neurons by directed hiPSC differentiation 41
2.1.2 Analysis of mature tRNA abundance in hiPSC-derived models with mim-tRNAseq 45
2.1.3 tRNA transcript levels vary greatly across differentiation 47
2.1.4 tRNA anticodon and isotype pools vary to a much lesser extent 49

2.2 tRNA anticodon availability correlates with a stable codon usage and decoding rate across cell types. 51
2.3 tRNA anticodon levels are buffered through the stable expression of major isodecoders 57
2.4 Pol III transcription is restricted to housekeeping tRNA genes during differentiation 59
2.4.1 Optimization of Pol III ChIP-Seq 59
2.4.2 Pol III occupancy at tRNA genes predicts mature tRNA levels in human cells 66
2.4.3 Pol III binding is restricted to housekeeping tRNA genes during differentiation 68
2.4.4 Optimization of ATAC-Seq experimental workflow 72
2.4.5 Remodeling of chromatin at tRNA genes during differentiation 74
2.5 tRNA gene body and upstream sequences regulate differential Pol III recruitment 77
2.5.1 tRNAScan-SE scores alone are not sufficient to predict tRNA gene transcription 77
2.5.2 A- and B-box sequences within tRNA gene body are linked to Pol III occupancy 78
2.5.3 5' flanking regions contribute to differential Pol III occupancy at tRNA genes 82
2.5.4 The expression of tRNA-Arg-TCT-4-1 mirrors that of CADM3 in neurons 85
2.6 Reduced mTORC1 signaling triggers MAF1-dependent repression of a tRNA gene subset upon differentiation 88
2.6.1 The repression of specific tRNA genes upon hiPSC differentiation is not caused by the loss of RPC7α 88
2.6.2 Decreased mTORC1 signaling activates MAF1 in differentiated cells 95
2.6.3 MAF1 depletion relieves selective tRNA gene repression in differentiated cells 95
Chapter 3 - Discussion 98
Chapter 4 - Materials and Methods 105
4.1 Materials 106
4.2 Methods 111
Chapter 5 - Supplemental Data 139
5.1 Abbreviations 140
5.2 Supplementary tables 143
References 199
Acknowledgements 217

Abstract

A comprehensive understanding of tRNA regulation is crucial in identifying the molecular factors responsible for human diseases associated with tRNA dysregulation, and for devising effective therapeutics based on mRNA and tRNA. Despite its vital role in accurate and efficient mRNA decoding, tRNA pool composition and regulation in human cells is poorly characterized due to technical limitations of conventional tRNA quantification methods in capturing these highly similar, structured, and extensively modified molecules. Using the mim-tRNAseq workflow we recently developed for accurate tRNA quantitation, we measured tRNA expression in a human induced pluripotent stem cell (hiPSC) model cell line and the differentiated neuronal and cardiac cells. Combined with high resolution ribosome profiling, we demonstrated that despite significant alterations in tRNA repertoires, the abundance of mature tRNAs with specific anticodons that drives decoding rates remains largely constant across different cell types. Using ChIP-Seq for RNA Pol III and TFIIIB, we found that predicted human tRNA genes can be divided into three classes: housekeeping, inactive, and repressed during differentiation. Housekeeping genes, which account for one-third of predicted tRNA genes, are robustly transcribed throughout differentiation, and encode tRNA transcripts that constitute the majority of mature tRNAs within each anticodon family. Using ATAC-Seq and ChIP-Seq for histone marks, we discovered that housekeeping tRNA genes are in nucleosome-free regions marked by H3K4me3. By motif searching and experimental validation with CRISPR editing, we found that housekeeping tRNA genes have conserved intragenic promoter A- and B-box sequences and 5' flanking sequences enriched with GC- and polyA stretches. Mechanistically, we ruled out a role of the stem cell-specific Pol III subunit RPC7α in expanding tRNA repertoires in hiPSC. Instead, housekeeping tRNA genes were largely resistant to the MAF1-directed Pol III transcription repression that mediates the silencing of tRNA loci with low Pol III occupancy upon mTORC1 signaling decrease during hiPSC differentiation. Our findings uncover the mechanisms by which tRNA anticodon pools are maintained to ensure consistent decoding speed independently of cell identity, and reveal the role of mTORC1 in driving the selective expression of specific tRNAs during differentiation. By analyzing tRNA pool dynamics in a range of isogenic cell types and dissecting the upstream regulatory mechanisms and downstream effect on translation, the results presented in this thesis significantly advance our understanding of the tRNA expression in human cells and provide a framework for future studies of this type.

Zusammenfassung

Ein umfassendes Verständnis der tRNA-Regulierung ist von entscheidender Bedeutung für die Identifizierung von molekularen Faktoren, die für menschliche Krankheiten im Zusammenhang mit tRNA-Dysregulationen verantwortlich sind, und für die Entwicklung wirksamer Therapeutika auf der Grundlage von mRNA und tRNA. Trotz ihrer entscheidenden Rolle bei der genauen und effizienten mRNA-Dekodierung ist die Zusammensetzung und Regulierung des tRNA-Pools in menschlichen Zellen unzureichend charakterisiert, da herkömmliche tRNA-Quantifizierungsmethoden bei der Erfassung dieser hochgradig ähnlichen, strukturierten und stark modifizierten Moleküle technische Grenzen aufweisen. Mit Hilfe des mim-tRNAseq-Workflows, den wir kürzlich für eine genaue tRNA-Quantifizierung entwickelt haben, haben wir die tRNA-Expression in menschlichen induzierten pluripotenten Stammzellen (hiPSC) sowie in differenzierten neuronalen und kardialen Zellen gemessen. In Kombination mit hochauflösendem Ribosome profiling konnten wir zeigen, dass trotz signifikanter Veränderungen des tRNA-Repertoires die Häufigkeit reifer tRNAs mit spezifischen Anticodons, die die Dekodierungsraten vorantreiben, zwischen den verschiedenen Zelltypen weitgehend konstant bleibt. Mithilfe von ChIP-Seq für RNA Pol III und TFIIIB fanden wir heraus, dass die vorhergesagten menschlichen tRNA-Gene in drei Klassen eingeteilt werden können: Housekeeping, unterdrückte und inaktive Gene. Housekeeping-Gene, die ein Drittel der vorhergesagten tRNA-Gene ausmachen, werden während der gesamten Differenzierung robust transkribiert und kodieren tRNA-Transkripte, die die Mehrheit der reifen tRNAs innerhalb jeder Anticodon-Familie bilden. Mithilfe von ATAC-Seq und ChIP-Seq für Histonmarker entdeckten wir, dass Housekeeping-tRNA-Gene in nukleosomfreien Regionen liegen und durch H3K4me3 markiert sind. Durch Motivsuche und experimentelle Validierung mit CRISPR-Editing fanden wir heraus, dass Housekeeping-tRNA-Gene konservierte intragenische A- und B-Box-Sequenzen des Promotors und 5'-flankierende Sequenzen besitzen, die mit GC- und PolyA-Abschnitten angereichert sind. Wir konnten mechanistisch eine Rolle der stammzellspezifischen Pol III-Untereinheit RPC7α bei der Erweiterung des tRNA-Repertoires in hiPSC ausschließen. Stattdessen waren Housekeeping-tRNA-Gene weitgehend resistent gegen die MAF1-gesteuerte Pol-III-Transkriptionsunterdrückung, die das Silencing von tRNA-Loci mit geringer Pol-III-Besetzung bei Abnahme der mTORC1-Signalisierung während der hiPSC-Differenzierung vermittelt. Unsere Ergebnisse decken die Mechanismen auf, durch die tRNA-Anticodon-Pools

aufrechterhalten werden, um eine konsistente Dekodierungsgeschwindigkeit unabhängig von der Zellidentität zu gewährleisten, und zeigen die Rolle von mTORC1 bei der selektiven Expression spezifischer tRNAs während der Differenzierung auf. Durch die Analyse der tRNA-Pool-Dynamik in einer Reihe von isogenen Zelltypen und die Analyse der vorgelagerten Regulierungsmechanismen und der nachgelagerten Auswirkungen auf die Translation tragen die in dieser Arbeit vorgestellten Ergebnisse wesentlich zu unserem Verständnis der tRNA-Expression in menschlichen Zellen bei und bieten einen Rahmen für zukünftige Studien dieser Art.

Chapter 1 - Introduction

1.1 tRNA biology

1.1.1 Eukaryotic tRNA biogenesis

During translation, tRNAs help decode the genetic information into proteins by pairing their anticodons with matching codons in mRNA, thereby delivering amino acids to ribosomes, which incorporate them into the growing polypeptide chain. Given their central role in protein biosynthesis, tRNAs are highly conserved across organisms, and their biogenesis involves various processing steps and enzymes depending on the organisms. The order of processing events differs among the three kingdoms of life and for specific tRNA species, while the major steps are similar among eukaryotes and are outlined as follows (**Figure 1.1,** reviewed in (Hopper and Nostramo 2019):

1) Nuclear-encoded tRNA genes are transcribed by RNA polymerase III (Pol III) into pre-tRNAs. Pol III is recruited to tRNA genes through the interaction of transcription factor IIIC (TFIIIC) that recognizes two highly conserved promoter sequences named the A-box and B-box, which reside inside tRNA genes and overlap with highly conserved structural elements (D-loop and T-loop) in the mature tRNA transcripts (Kessler and Maraia 2021).

2) The 5’ leader sequence is removed by ribonuclease P (RNase P) (Lai et al. 2010). Complete processing of 3′ trailer sequences involves ribonuclease II, polynucleotide phosphorylase, and ribonucleases T and/or PH (Spickler and Mackie 2000; Cudny and Deutscher 1980; Deutscher, Marlor, and Zaniewski 1984).

3) The non-templated 3′ CCA tail is then added by a nucleotidyltransferase. The CCA tail protrudes from the tRNA as a single-stranded motif and is later recognized by the aminoacylation enzymes (Betat and Mörl 2015).

4) Mature tRNA transcripts are then recognized and exported from the nucleus into the cytoplasm by Los1/Xpo-t proteins as the so-called primary nuclear export. This recognition process is part of a quality control mechanism that ensures that incompletely processed and mutant RNAs are retained in the nucleus and degraded (Hellmuth et al. 1998).

5) The introns located one base 3’ to the anticodon in some tRNA species are excised by tRNA-splicing endonucleases docked on the outer surface of the mitochondria. These

endonucleases are composed of the proteins Sen2, Sen34, Sen15, and Sen54 (Song and Markley 2007). The subsequent 5' and 3' exon ligation and removal of the residual phosphate at the splice junction is catalyzed by tRNA ligase Trl1 and phosphotransferase, respectively (Trotta et al. 2006).

6) After the enzymatic addition of various chemical modifications to distinct nucleotides, spliced tRNA can undergo another round of transport between the nucleus and cytoplasm. The modified tRNA is trafficked back into the nucleus in a process called tRNA retrograde nuclear import and becomes the substrate for other modification enzymes. For the final step in tRNA maturation, the tRNA is transported back again to the cytoplasm, known as tRNA nuclear re-export, for further modification (Kramer and Hopper 2013).

7) Once modifications are completed, a functional tRNA needs to be charged with an amino acid to participate in protein synthesis. This involves the recognition and attachment of the correct amino acids by aminoacyl-tRNA synthetases (aaRS). Unique synthetase enzymes are usually available for each amino acid, so there are 20 synthetases in total. The synthetase-catalyzed reaction is coupled to the energy-releasing hydrolysis of ATP, producing high energy bonds between tRNAs and amino acids. The energy of these bonds is then used at a later stage in protein synthesis to link amino acids covalently to the growing polypeptide chains (Kaiser et al. 2020).

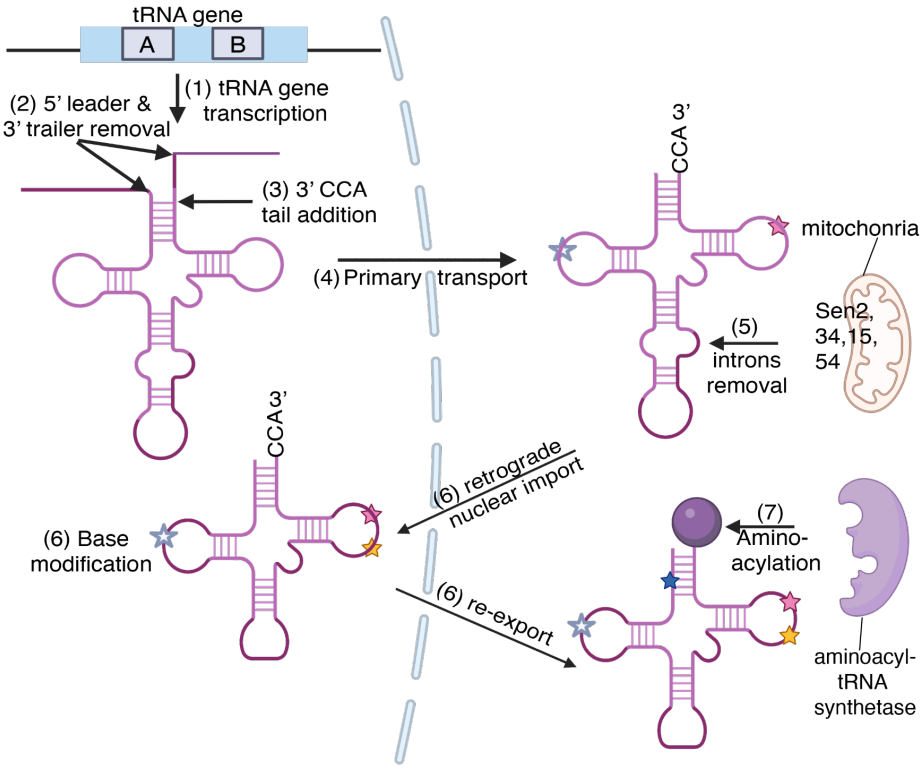

Figure 1.1. Schematic representation of eukaryotic tRNA biogenesis. Major steps of tRNA biogenesis and maturation are illustrated, as described in the text. The order of processing is labeled in the brackets.

1.1.2 tRNA structure

Mature tRNA transcripts are only 70 to 100 nucleotides long but fold into a complex three-dimensional structure. Base-pairing interactions lead to the formation of a cloverleaf-shaped molecule with four arms: the acceptor stem, to which amino acids are attached; the dihydrouridine (D) stem-loop that is involved in the recognition of the tRNA molecule by aminoacyl-tRNA synthetases; the anticodon stem-loop, which is responsible for recognizing mRNA codons, and the TψC (T) stem-loop that interacts with elongation factor and the ribosome during translation (ψ refers to pseudouridine) (**Figure 1.2**). tRNAs with a length of more than 76 nt often have an additional variable loop between the anticodon stem-loop and the T-loop. The cloverleaf undergoes further folding to form a compact L-shaped tertiary structure held together by additional hydrogen bonds between different regions. At one end of the L-shaped tRNA molecule is the anticodon domain, where a set of three consecutive nucleotides at positions 34, 35 and 36 pair with the complementary codon in an mRNA. At the other end of the tRNA sits a short single-stranded 3'-CCA region, where the amino acid that matches the mRNA codon is attached to the tRNA. The extensive chemical modifications and

secondary as well as tertiary structural contacts make tRNA molecules extremely stable, with a half-life of ~100 h for mature tRNAs in mammalian cells (Choe and Taylor 1972).

In addition to nuclear-encoded tRNA genes that give rise to cytoplasmic tRNAs, eukaryotes also have 22 mitochondrially encoded (mt) tRNAs. These molecules are less conserved and exhibit a non-canonical structure due to their shortened D- and T-loops. They are also synthesized and processed by distinct mechanisms from cytoplasmic tRNAs and were therefore not the focus of the work described in this thesis.

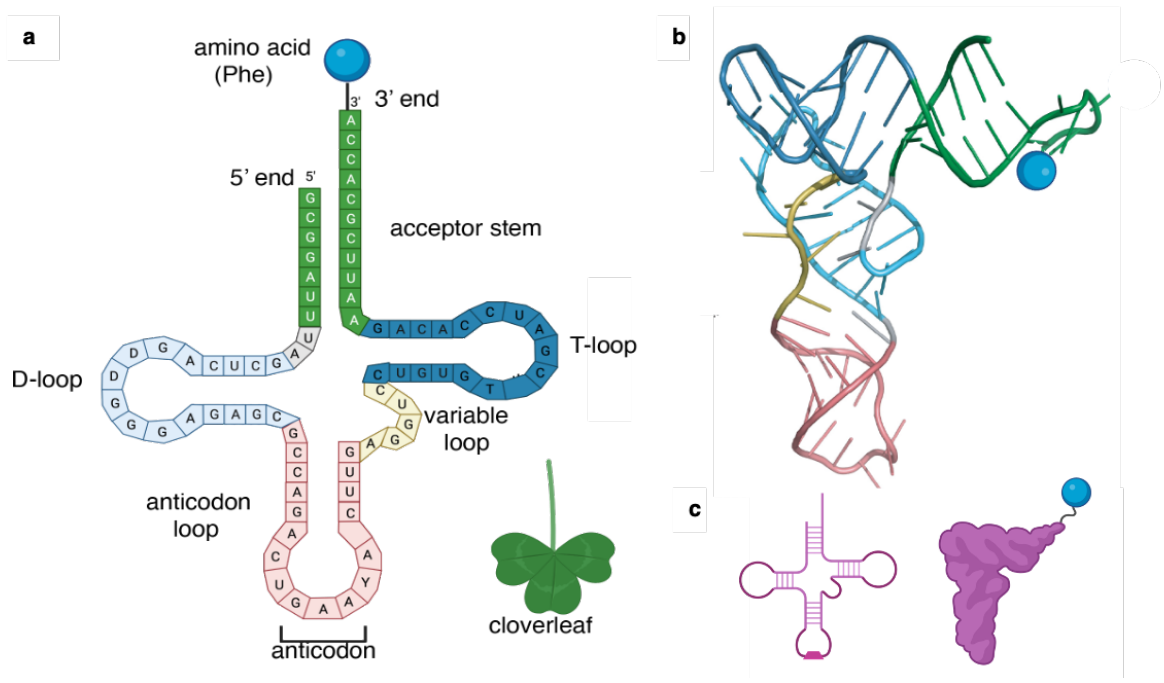

Figure 1.2. Various representations of a tRNA molecule specific for phenylalanine (Phe). a, Typical secondary structure and sequence of phenylalanine tRNA in the cloverleaf form. Highlighted from 5' to 3': acceptor stem, D-loop, anticodon-loop, anticodon, variable loop, T-loop acceptor stem and attached amino acid (Phe). Right bottom: A representative cloverleaf. **b**, View of a L-shaped tRNA molecule based on analysis using x-ray diffraction. Adapted from (Krahn, Fischer, and Söll 2020). **c**, Simplified tRNA icons used in this thesis (left: tRNA cloverleaf without amino acid; right: tertiary structure with amino acid).

1.1.3 tRNA modifications

During the processing of pre-tRNA transcripts (Section **1.1.1**), several rounds of modification occur both in the cytoplasm and nucleus. To date, over 120 different types of tRNA modifications are known, with up to 39 of these identified in human cytosolic tRNAs (Suzuki 2021; Boccaletto et al. 2021) (**Figure 1.3**).

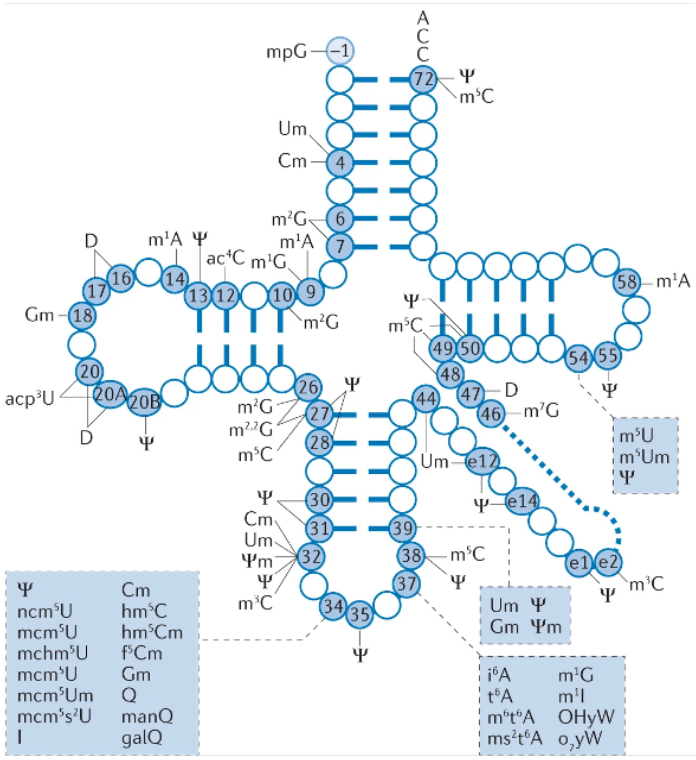

Figure 1.3. Modifications of human cytoplasmic tRNAs. Nucleotides subject to modification are assigned numbers, and the corresponding alterations are marked. The abbreviation for each RNA modification aligns with the MODOMICS RNA modification database. Adapted from (Suzuki 2021).

Nucleotides within the tRNA anticodon loop frequently undergo diverse modifications, which can regulate decoding by either facilitating or restricting wobble base pairing of tRNAs with non-cognate codons (Agris et al. 2018). For example, loss of modifications at the anticodon position 34, 5-methoxycarbonylmethyluridine (mcm^5U34) and its derivatives 5-methoxycarbonylmethyl-2-thiouridine (mcm^5s^2U34), has been demonstrated to slow down translation at cognate codons, triggering proteotoxic stress and protein misfolding (Nedialkova and Leidel 2015). I34 modifications, generated by hydrolytic deamination of adenosine at position 34 for recognizing U, C and A in codons, expands the decoding capacity. I34 is essential for *T. brucei* viability and its absence has been linked to various human diseases (Rubio et al. 2007; Torres et al. 2015; Torres et al. 2014). Decoding can also be modulated by modifications located beyond the tRNA anticodon region. For example, wybutosine (yW) modification and its derivatives hydroxywybutosine (OHyW) and peroxywybutosine (o_2yW) at position 37 of tRNA-Phe were shown to enhance the stability of interaction between position 36 and the first nucleotide in codon, maintaining the mRNA reading frames and enhancing the translation accuracy (Waas et al. 2007; Carlson et al. 1999), while lack of these modifications have been associated with cancer development (Rosselló-Tortella et al. 2020). N6-

Threonylcarbamoyladenosine (t^6A), another type of modification at the position 37 in cytoplasmic tRNAs, was found essential for imaginal discs cell survival in *Drosophila* and disruption of its biogenesis results in severe inherited human disorders (Rojas-Benítez, Eggers, and Glavic 2017; Thiaville, Iwata-Reuyl, and de Crécy-Lagard 2014). Failed introduction of the modification m^3C at position 32 in tRNA-Arg is linked to developmental delay (Lentini et al. 2020). Hypermodification of 5-methyluridine (m^5U) at tRNA position 54 of cytoplasmic tRNAs is linked to high recurrence of breast cancer (Hicks et al. 2010). The dependency of distinct symptoms on the loss of particular tRNA modifications suggest that various tissues and cell types exhibit different demands for modified tRNAs, which is of increasing interest to understand the cause, effects and mechanism of tRNA modification-related defects.

1.1.4 Codon-anticodon pairing

Successfully aminoacylated tRNAs can be used as "bridges" for linking the mRNAs and amino acids. In an mRNA, the instructions for building a polypeptide come in groups of three nucleotides called codons. Different combinations of the four nucleotides, adenine (A), uracil (U), cytosine (C), and guanine (G), give rise to 61 codons, including the AUG start codon which acts both as an initiation codon and also as the codon that specifies methionine, and three stop codons which mark the end of the coding sequence (**Figure 1.4**). The excess number of genetic codes (61) to amino acids (20) means that some amino acids are coded by more than one codon. The number of codons for each amino acid varies, while codons for the same amino acid mostly contain the same nucleotides at the first and second positions, and differ at the third position. The relationships between mRNA codons and amino acids are known as the genetic code (**Figure 1.4**).

A	R	D	N	C	E	Q	G	H	I	L	K	M	F	P	S	T	W	Y	V	
Ala	Arg	Asp	Asn	Cys	Glu	Gln	Gly	His	Ile	Leu	Lys	Met	Phe	Pro	Ser	Thr	Trp	Tyr	Val	stop
GCA GCC GCG GCU	AGA AGG CGA CGC CGG CGU	GAC GAU	AAC AAU	UGC UGU	GAA GAG	CAA CAG	GGA GGC GGG GGU	CAC CAU	AUA AUC AUU	UUA UUG CUA CUC CUG CUU	AAA AAG	AUG	UUC UUU	CCA CCC CCG CCU	AGC AGU UCA UCC UCG UCU	ACA ACC ACG ACU	UGG	UAC UAU	GUA GUC GUG GUU	UAA UAG UGA

Figure 1.4. The genetic code. The three-letter abbreviation for each amino acid is shown below the corresponding one-letter abbreviation, together with the codons displayed with the 5′-terminal nucleotide positioned on the left. Three codons serve as stop codons and do not encode any amino acid.

The anticodon bases in tRNA can be chemically modified after transcription, thereby facilitating the recognition of appropriate mRNA codons by the tRNA molecules and extending

their binding properties. For example, Inosine (I), produced by deamination of adenosine (A) with adenosine deaminase acting on tRNAs (ADATs) (**Figure 1.5**), allows base-pairing with U, C and A (Crick 1966; Gerber and Keller 1999).

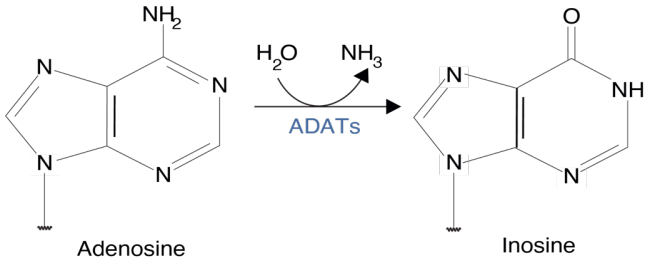

Figure 1.5. Adenosine deamination in tRNAs. ADAT enzymes facilitate the hydrolytic deamination from adenosine (A) to Inosine (I), wherein an adenosine undergoes the removal of an amine group, converted to inosine.

1.1.5 tRNA in translation

During translation, mRNA codons are read from the 5' end to the 3' end by tRNAs which has an anticodon, a set of three nucleotides that binds to a matching mRNA codon through base pairing, so that the first position of mRNA codon at the 5’ end is pairing with the third position of tRNA anticodon on its 3’end, and vice versa (**Figure 1.6a**). Codon-anticodon matching is key in the decoding and follows the basic principle of Waston Crick base pairing rules (A with U, C with G).

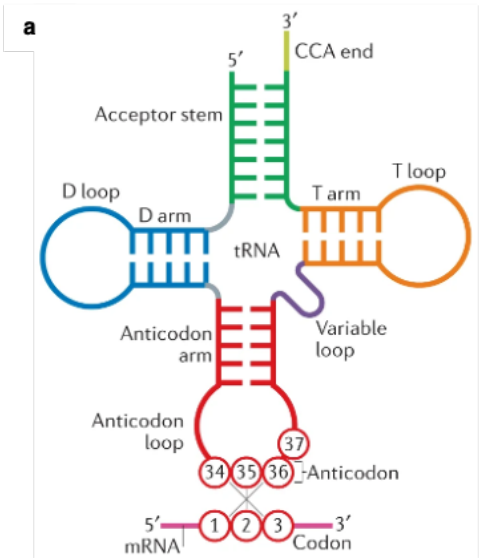

b

anticodon bases	wobble codon base
G	U,C
C	G
A	U,C,(A),G
U	U,(C),A,G
I	U,C,A

Figure 1.6. Base-pairing between mRNA codons and tRNA anticodons. a, Base-pairing between codon and anticodon exhibits higher stringency at codon positions 1 and 2, while unconventional pairing is permitted at the 3' base of mRNA codon. Adapted from (Suzuki 2021). **b**, Table showing wobble base-pairing. Adapted from

(Murphy and Ramakrishnan 2004). The nucleotides in the left column at the third (wobble) position of mRNA codon can form base pairs with the nucleotides in the second column at first position in tRNA anticodon.

However, bases do not always form pairs following the Watson-Crick base pairing rule and various non-Watson-Crick (or "wobble") base pairs are present. With accurate Watson-Crick base-pairing at the first two positions of the codons, ribosome allows more relaxed pairing and mismatch tolerance (or "wobble base pairing") at the third position of a codon (**Figure 1.6a,b**). For example, U at the first position of the tRNA anticodon pairs with G at the third position (wobble position) of the mRNA codon, in addition to the usual pairing with A. As a result, a single tRNA anticodon tRNA-Glu-UUC can decode multiple mRNA codons: 5'-GAA-3' (by Watson-Crick base pairing rules) and 5'-GAG-3' (by wobble pairing). While the basic concept of wobble pairing is consistent across most organisms, there can be some variations in the specific codon-anticodon interactions in certain species or organelles, such as mitochondria, some bacteria and archaea, which results in variations in the number of tRNA anticodons among different organisms, with more complex organisms generally having a larger set of tRNA anticodons to potentially fit their greater genetic and protein synthesis diversity (Santos and Del-Bem 2023). For example, while 57 anticodons are available in humans (Chan and Lowe 2009), bacteria makes it possible to accommodate the 20 amino acids to the 61 codons by utilizing as few as 31 distinct types of tRNA anticodons (Alamos et al. 2018).

The absence of specific tRNA anticodons throughout evolution also obliges some tRNAs to recognize more than one codon via "wobble" base-pairing. For example, the mRNA codon 5'-GCC-3' is theoretically decoded by tRNA anticodon tRNA-Glu-GGC, which is not expressed. As a result, codon 5'-GCC-3' can only be decoded by an tRNA-Ala-AGC with the adenine (A) post transcriptionally modified to inosine (I) at position 34, which can recognize U and C. The absence of tRNA anticodon tRNA-His-GUG requires codon 5'-CAU-3' to be decoded by tRNA-His-GUG, in which G at the anticodon wobble position pairs with U in the 3' end of the mRNA codon. Wobble base-pairing explains why so many of the alternative codons for an amino acid differ only in their third nucleotide.

With complementary base pairing between the mRNA codons and tRNA anticodons, each amino acid carried by the tRNA is added to the growing end of a polypeptide chain and the next codon on the mRNA chain is read again. The decoding and polypeptide chain building follows the following basic cycle (**Figure 1.7**):

- Aminoacyl-tRNA binding: An aminoacyl-tRNA carrying the correct amino acid and GTP-bound elongation factor EF1A approaches the vacant A site (A for "aminoacyl" site) on the ribosome. The binding of aminoacyl-tRNA to the A site involves base pairing between the tRNA's anticodon and the mRNA's codon. Initially, the ribosome allows multiple tRNA molecules to transiently bind to the A site and sample the mRNA, which can include both correct and incorrect tRNAs. This step involves dynamic sampling of available tRNAs before commitment to peptide bond formation (Lake 1977).
- Aminoacyl-tRNA accommodation: During this step, the ribosome undergoes a conformational change to firmly accommodate the correct aminoacyl-tRNA in the A site. If the correct codon-anticodon interaction is established and stable, GTP is hydrolyzed into GDP, which locks the tRNA into place in the A site and triggers the release of EF1A-GDP, allowing the aminoacyl-tRNA to be used in protein synthesis. Incorrect codon–anticodon pairing does not cause this conformational change, resulting in the dissociation of these tRNAs. In this way, the ribosome ensures that the codon-anticodon pairing is accurate and stable before proceeding to the next step (Valle et al. 2003).
- Peptide bond formation: A new peptide bond is formed between the existing peptide chain and the new amino acid at A site (Hiller et al. 2011).
- Translocation: The large ribosomal subunit translocates relative to the small subunit towards the 3’ of mRNA. The newly bound tRNA is now at peptidyl site (P site) of the large subunit and A site of the small subunit, while the preceding tRNA reside at exit site (E site) of the large subunit and P site on the small subunit. The binding of GTP-bound EF2 to the ribosome, followed by the hydrolysis of GTP facilitates the movement of tRNAs into their standard positions in the P and E sites, and was thought to be released from the post-translocation ribosome by the reverse rotation of the small ribosomal subunit (Frank et al. 2007).
- Deacyl-tRNA ejection: The small subunit then translocates three nucleotides through the ribosome, which leaves the ribosome with a fully empty A site, ready for the next aminoacyl-tRNA molecule to bind. The preceding tRNA without amino acid binding is ejected from the E site (Valle et al. 2003).

This cycle is repeated during the synthesis of a protein until stop codons are encountered, with each cycle adding one amino acid to the C-terminus of the polypeptide chain.

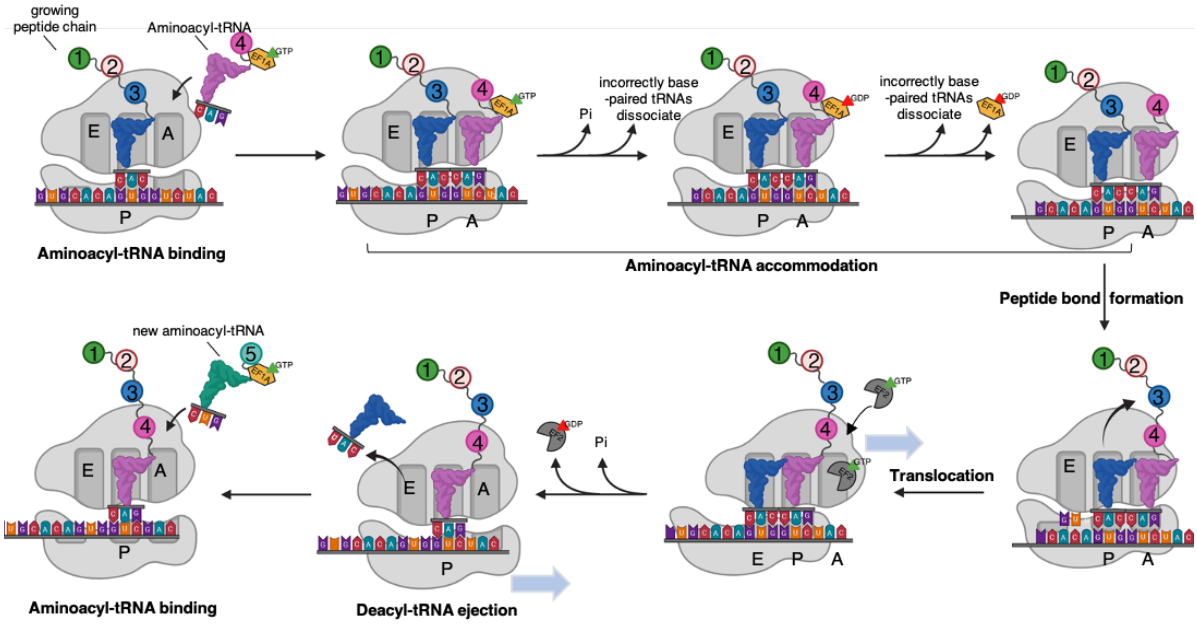

Figure 1.7. Schematic of translation elongation. The elongation process is as described in text. The E, P and A sites in the ribosome are labeled. The order of amino acids incorporated in the polypeptide chain is represented as numbers. GTP and GDP are labeled in green and red triangles, respectively. EF1A and EF2 are represented as orange and gray blocks, respectively. The blue-shaded arrow indicates the shifting direction of ribosome subunits.

1.1.6 tRNA sequence diversity

Because of the degeneracy of the genetic code, there can be multiple tRNA anticodon families that decode the same amino acid. Such tRNAs are referred to as "isoacceptors". (**Figure 1.8**). The number of tRNA isoacceptors encoded by predicted tRNA genes in eukaryotes can vary from 42 in *Saccharomyces cerevisiae* to 57 in *Homo sapiens*. Apart from the anticodon, there can be sequence variation in the tRNA body region.

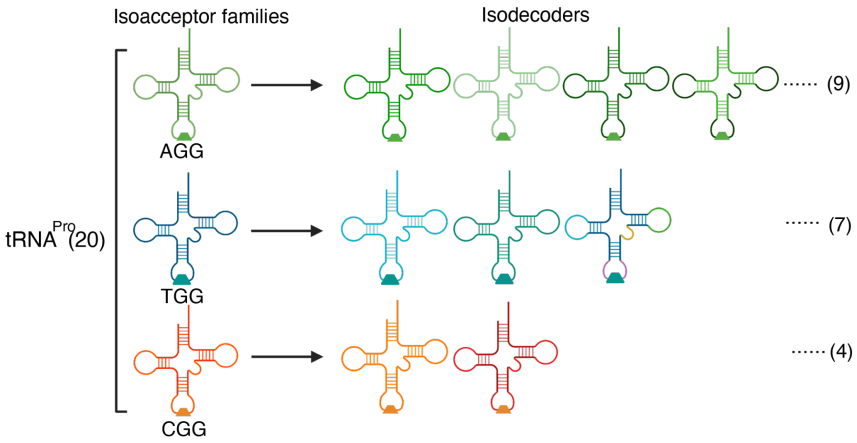

Figure 1.8. Representation of the sequence diversity in proline-decoding tRNAs in *Homo sapiens*. 20 transcripts of tRNA-Pro are grouped into three isoacceptor families, each of which contains the same anticodon

labeled as trapezoids with the same color. Different tRNA bodies are illustrated with different colors showing sequence variations within each anticodon family.

tRNA anticodon families can further consist of different isodecoders, which are tRNAs with the same anticodon but sequence differences elsewhere (**Figure 1.8**) (Goodenbour and Pan 2006). In contrast to the relatively similar number of isoacceptors, dramatic variations are displayed for the number of tRNA isodecoders among eukaryotes, ranging from 51 in *Saccharomyces cerevisiae*, 432 in humans and more than 3100 in zebrafish (Chan et al. 2021). With the same anticodon sequence, all isodecoders within each anticodon family read the same codon in translation, but different anticodons can have varied numbers of isodecoders in predicted tRNA genes. For example, in the human genome, there are 9 isodecoders encoded for the tRNA-Pro-AGG anticodon family, while only 4 for the tRNA-Pro-CGG family (**Figure 1.8**). Whether sequence diversity among tRNA isodecoders reflects functional variability is an open question. The presence of various tRNA isodecoders in eukaryotes was first simply viewed as an evolutionary consequence of neutral drift coinciding with genome expansion (Goodenbour and Pan 2006), and the spatial separation of genomic domains by tRNA genes may lead to fragile sites that facilitate genome evolution (McFarlane and Whitehall 2009). Later, some study supports functional substitution among isodecoders by showing that overexpressing different isodecoders, either *n-Tr21* (*tRNA-Arg-TCT-3-1*) or *n-Tr22* (*tRNA-Arg-TCT-1-1*), enhanced the overall tRNA-Arg-UCU abundance and successfully rescued the neurodegeneration caused by the mutations in *n-Tr20* (*tRNA-Arg-TCT-4-1*) and the ribosome rescue factor *Gtpbp2* (Kapur et al. 2020). While others proposed that differences in tRNA isodecoder expression can change the abundance of alternative products, such as tRNA fragments, pointing to non-canonical functions other than protein synthesis (Torres et al. 2019).

Why vertebrate genomes contain so many tRNA genes remains largely unclear. Some studies have suggested that it is because different tRNA isodecoders exhibit varying rates of translational efficiency. For example, in *Escherichia coli*, mutation of A32-U38 nucleotide pair in the tRNA body to a more common U32-A38 allows tRNA-Ala-GGC to read normally on cognate codons, but exceptionally more efficient on the near-cognate codons containing a single-nucleotide mismatch (Ledoux, Olejniczak, and Uhlenbeck 2009). Work in yeast has revealed that position 37 is important for tRNA-Arg-CCG binding with ribosomes by deleting the chromosomal genes of tRNA-Arg-CCG isoacceptor family and individually expressing single isodecoder species with mutations (Geslain et al. 2003). These data suggest that subtle

differences in the sequences of the tRNA isodecoders may modulate their aminoacylation efficiency and their interactions with the ribosome.

1.1.7 Cell type-specific regulation of tRNA abundance

Our incomplete understanding of tRNA regulation largely arises from the multicopy nature and simple promoter structure of tRNA genes, which makes it difficult to determine how individual tRNA genes could be differentially regulated in specific cellular contexts. Several studies have attempted to determine whether tRNA abundance differs in a cell type- and tissue- specific manner. Quantification by cDNA-free microarray-based methods found that tRNA levels varied among eight different human tissues and suggested that tRNA pool exhibits two distinct patterns during proliferation and differentiation, based on tRNA anticodons that match codons over-represented in genes related to cell cycle (Gingold et al. 2014). Using reverse transcription quantitative polymerase chain reaction (RT-qPCR) to quantify tRNAs, another study suggested that their levels change during stress in yeast (Torrent et al. 2018). However, these methods can only detect a subset of tRNAs but cannot distinguish among the highly similar ones (Dittmar et al. 2004), so the regulatory mechanisms of tRNA alterations among different cellular environments and states remain unclear.

While Pol III occupancy is commonly used as a proxy to measure tRNA gene activity (Barski et al. 2010b; Oler et al. 2010b; Canella et al. 2012; Rudolph et al. 2016), it is an indirect assessment of tRNA gene expression due to the multiple steps involved in tRNA biogenesis, and downstream post-transcriptional processing could lead to changes in mature tRNA abundance (Wolin and Matera 1999). However, due to the lack of high-resolution tRNA quantification method, how much Pol III transcription contributes to mature tRNA abundance in different cellular contexts remains to be elucidated.

The difference in abundance among tRNA isoacceptors can have functionally varying degrees of contribution in translation and some may have larger roles in gene expression regulation (Elf et al. 2003; Sørensen et al. 2005). Despite the lack of systematic comparison for involvement of isodecoders in specific cell type models, some hypotheses have been proposed In *Saccharomyces cerevisiae*, only about 3% of tRNA genes encode isodecoders, whereas in multicellular metazones such as human, nearly half of tRNA genes encode isodecoders (Orellana, Siegal, and Gregory 2022), suggesting that tRNA genes as well as isodecoders could be expressed in a tissue and cell type-specific manner. Indeed, studies have shown that a single

tRNA isodecoder can be specifically expressed in a particular tissue. This is the case for one of the five nuclear-encoded *tRNA-Arg-TCT* genes, *n-Tr20*, the mouse ortholog of human *tRNA-Arg-TCT-4-1*. *n-Tr20* is exclusively expressed in the mouse central nervous system (Ishimura et al. 2014). A single-nucleotide mutation of C-to-T at the nucleotide 50 located within the T stem loop of *n-Tr20*, together with loss of the ribosome rescue factor GTPBP2, causes ribosome stalling at the corresponding AGA codon and leads to neurodegeneration in mice (Ishimura et al. 2014). Human *tRNA-Arg-TCT-4-1* is also specifically expressed in brain tissue (Torres et al. 2019a). However, due to the heterogeneity of tissues and technical obstacles differentiating highly similar isodecoder sequences, the extent of variations among mature tRNA isodecoders among cell types and its functional impact is not understood.

1.1.8 Codon demand and tRNA supply

The redundancy of the genetic code gives rise to synonymous codons, which refer to different combinations of three nucleotides that can encode the same amino acid. This allows multiple distinct mRNA sequences to encode the same amino acid sequence. The unequal usage of synonymous codons in a particular organism or a specific gene is referred to as codon bias, which was suggested to coevolve with tRNA anticodon abundances to ensure accurate and efficient translation (Bulmer 1987; Rak, Dahan, and Pilpel 2018; Drummond and Wilke 2008). The elongation speed at which synonymous codons are decoded varies significantly, primarily based on two factors, codon usage and abundance of the matching tRNAs (**Figure 1.9a,b**). For example, the codon usage of Cys-TGC is less than its synonymous Cys-TGT (0.6 time), and the corresponding ribosome retention time at codon Cys-TGC is 1.5 times longer than codon Cys-TGT (Gardin et al. 2014). More commonly used codons are recognized by abundant tRNAs, which facilitates decoding and leads to more efficient translation than rarely used codons that have low transcriptome occurrence (Guimaraes et al. 2020). The balance between the codon demand and supply of tRNAs has been suggested to be crucial in determining optimal translation elongation rates, protein output, and protein folding (Rodnina et al. 2017) (**Figure 1.9c**). An imbalance between mRNA codon usage and tRNAs abundance supply can affect the translation elongation rate that may have wide implications for protein homeostasis and diseases (Orellana, Siegal, and Gregory 2022). For example, ribosomes were shown to pause at specific synonymous codons with loss of charging for tRNA-Arg-CGC and tRNA-Arg-CGU during arginine limitation, which reduced protein output and induced premature translation termination (Darnell, Subramaniam, and O'Shea 2018). Other work has shown that

overexpression of tRNA-Glu-UUC enhances the translation of mRNAs enriched with the cognate codons GAA and GAG leads to cancer metastasis, highlighting the importance of tRNA abundance in translation regulation (Goodarzi et al. 2016). tRNA levels quantified by hybridization-based method shows that overexpression of specific tRNA isoacceptors correlated with increased levels of oncoproteins from genes enriched with cognate codons of the tRNAs (Goodarzi et al. 2016). The codon-specific reprogramming of mRNA translation suggests that changes in the abundance or function of some specific tRNAs can particularly affect certain sets of mRNAs which contain a specific codon in high frequency, thereby contributing to the development of certain human diseases (Gillen, Waldron, and Bushell 2021). However, the extent to which each individual human tRNA contributes to protein synthesis is not yet known or determined. Moreover, due to different types of regulatory information overlapping in mRNA sequences, codon bias could be a result of selection for mutational biases, GC content of genes or genome, efficient translation, as well as differential transcription factor binding, mRNA stability and splicing (Rudolph et al. 2016; Frumkin et al. 2018; Parmley et al. 2007; Stergachis et al. 2013; Gu, Zhou, and Wilke 2010).

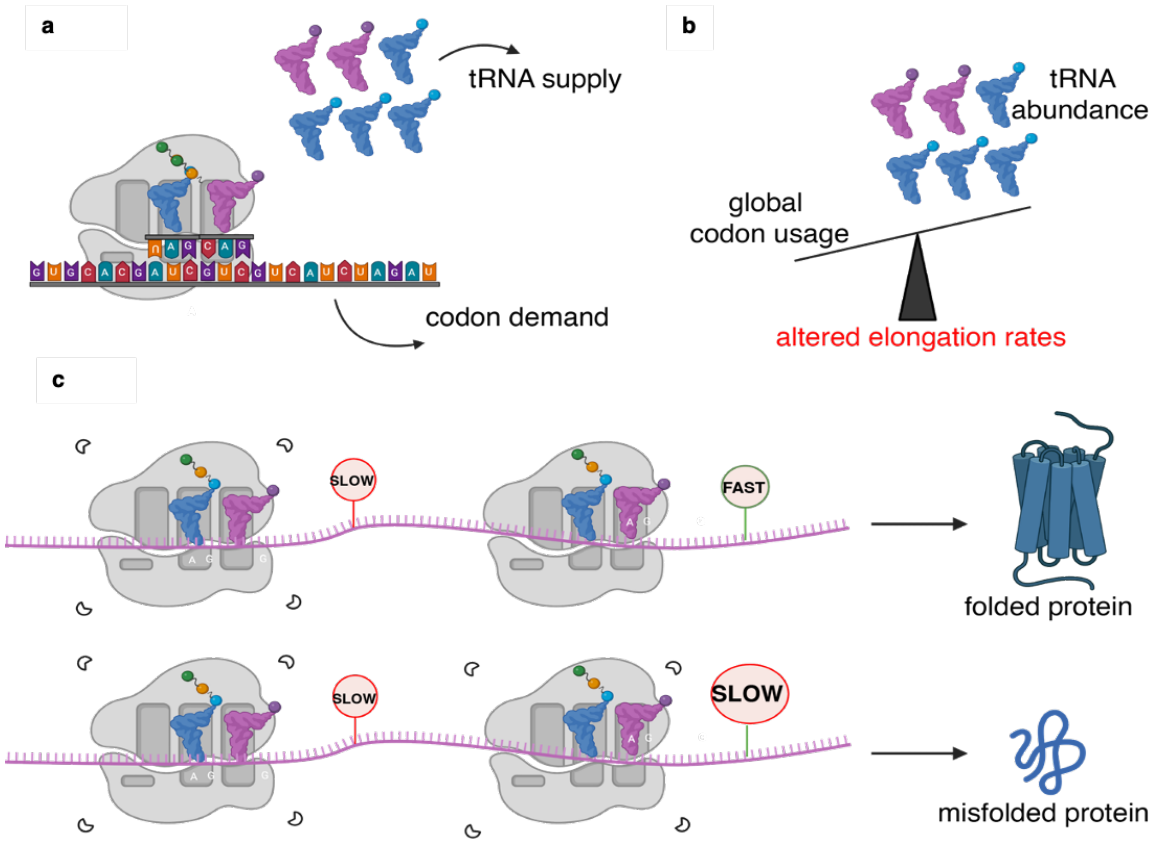

Fig 1.9. Codon demand and tRNA supply determine elongation rates and protein folding. a, Representative illustration showing the relationship between mRNA codon demand and tRNA abundance. **b**, Schematic

demonstration showing imbalance between global codon usage and tRNA abundance leading to altered elongation rates. **c**, Depiction for the impact of altered elongation rates on protein folding. Elongation rates are labeled as "SLOW" and "FAST" at specific codons.

The tRNA supply to codon demand balance can be influenced by multiple conditions, including tissue type, cellular state and environmental stress (Goodenbour and Pan 2006; Canella et al. 2010; Gogakos et al. 2017). For example, study in *Saccharomyces cerevisiae* showed that tRNA abundance was selectively altered in response to stress, which affects the translation rates of specific transcripts to increase the amounts of required proteins (Torrent et al. 2018). However, several studies have failed to identify a positive correlation between codon usage and tRNA abundance in multicellular organisms (Kudla et al. 2009; Pop et al. 2014), making the role of tRNA in setting elongation rates at specific codons controversial (Gobet et al. 2020b; Quax et al. 2015). This can be explained by the fact that organisms with larger genomes, such as humans, have higher tRNA gene redundancy with multicopy gene families (except for the unique gene coding for tRNA-Sec-UCA) (Percudani, Pavesi, and Ottonello 1997), which would decrease selection for specific codons (Quax et al. 2015). Moreover, larger genomes such as metazones often encode tRNA sequences with extensive similarity, and most of the studies quantify tRNA pools with cDNA-free microarrays (Dittmar, Goodenbour, and Pan 2006; Gingold et al. 2014), which only detect a limited number of tRNAs and cannot distinguish those with less than 8 nt difference (Dittmar et al. 2004), leading to challenges in accurately measuring tRNA abundance and understanding its impact on codon usage. Due to the lack of methods for accurate tRNA quantification, the exact tRNA repertoires in human cells are largely unknown, and whether changes in tRNA pools adjust the translation of specific genes in cell type-dependent manner also remains under debate (Gingold et al. 2014; Gao, Gallardo-Dodd, and Kutter 2022; Rudolph et al. 2016).

1.1.9 High-resolution tRNA quantification by mim-tRNAseq

The difficulties of quantifying tRNAs lies in the highly stable structure and abundant modifications of tRNAs, which often impede reverse transcription (RT) and yield truncated cDNA molecules with coverage bias towards the 3' end of the tRNA where RT is initiated. Moreover, the multicopy gene families and extensive sequence similarity among tRNAs, which can differ by as little as one nucleotide, can lead to considerable ambiguity during read alignment. Unlike hybridization-based microarray approaches, which suffer from limited accuracy and resolution, next-generation sequencing (NGS) has the potential to increase the

accuracy of tRNA quantification. Several tRNA sequencing methods have been applied in various species, but all of them have potential drawbacks. For example, Hydro-tRNAseq hydrolyzes tRNA transcripts into smaller RNA fragments before cDNA synthesis to counteract the influence of tRNA secondary structure on RT efficiency, while not considering the modification-induced RT stops (Gogakos et al. 2017). This workflow can therefore result either in short read libraries due to prematurely aborted cDNA synthesis at modified nucleosides, or an overrepresentation of transcripts with lower frequency of modifications that lead to premature RT stops. ARM-Seq removes common tRNA base methylations by enzymatic treatment with AlkB, but the differences in demethylase efficiency among various types of modifications result in biases during RT (Cozen et al. 2015). The most promising advance in RT optimization on tRNA template was made with the discovery of thermostable group II intron RT TGIRT (Qin et al. 2016; Mohr et al. 2013). This enzyme can synthesize cDNA from highly structured intron elements. Despite the improved RT reaction with TIGRT in approaches such as TGIRT-Seq and DM-tRNAseq, TGIRT has demonstrated relatively low efficiency and yield when applied to highly modified endogenous tRNAs (Zhao, Liu, and Pyle 2018; Zheng et al. 2015).

By optimizing the reaction conditions for TIGRT, our lab recently developed modification-induced misincorporation tRNA sequencing (mim-tRNAseq) (Behrens, Rodschinka, and Nedialkova 2021). Its library construction workflow enables near-complete tRNA modification readthrough, dramatically improving cDNA yield and the fraction of full-length products from tRNA templates (**Figure 1.10**, step 2). After stepwise total RNA and tRNA isolation, adapters were ligated to tRNA 3' ends and further served as the priming sites for cDNA synthesis with TGIRT. The reverse transcription efficiency of TIGRT was dramatically enhanced under lower reaction temperature, salt concentration and extended reaction time (Behrens and Nedialkova 2022). The following cDNA circularization step provides a template for the final library construction by PCR amplification.

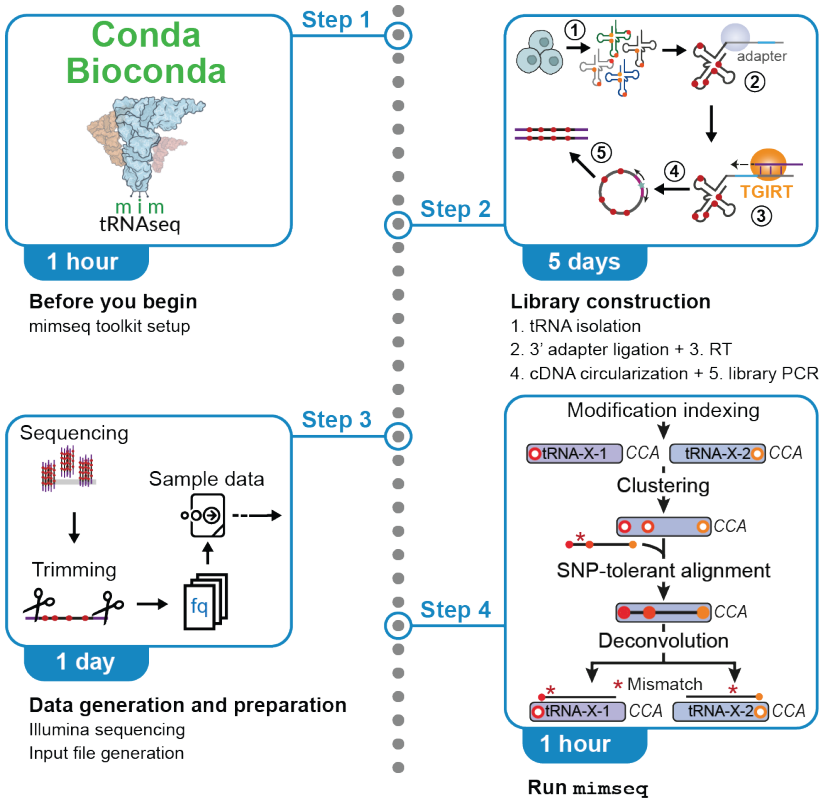

Figure1.10.Schematic of the experimental and computational workflows of mim-tRNAseq. Outline of four major steps in mim-tRNAseq, including toolkit environment setup with Bioconda, library construction, data generation and mim-tRNAseq running. Adapted from (Behrens and Nedialkova 2022).

Downstream tRNA read analysis has been another major obstacle to accurate tRNA quantitation due to the alignment bias against reads with misincorporations induced by modification readthrough during RT and the multimapping of tRNA reads from nearly identical transcripts. To minimize alignment alignment bias, mim-tRNAseq leverages the extensive annotation of tRNA modifications available in MODOMICS and uses this information to incorporate position-specific mismatch tolerance in the alignment process (**Figure 1.10**, step 4). This is combined with clustering of nearly identical tRNA genes that share an anticodon based on a sequence identity threshold (typically 95-97%), which nearly abolished multimapping (Behrens, Rodschinka, and Nedialkova 2021). The mim-tRNAseq computational pipeline also includes a deconvolution algorithm for restoring single-transcript resolution by assigning cluster-aligned tRNA reads to individual transcripts based on their unique mismatches to the cluster parent.

Thanks to the optimized experimental conditions and multiple advances in the sequencing data analysis workflow, sequencing bias was substantially alleviated and the number of full-length c DNA reads increased from 11% in DM-tRNAseq to 65%–83% in mim-tRNAseq (Behrens, Rodschinka, and Nedialkova 2021). Thus, mim-tRNAseq enables efficient and unbiased quantification of tRNA pools at single-transcript resolution, presenting an important solution to the long-lasting challenges in tRNA quantification and a major advance towards profiling mature tRNA abundance in different organisms and cell types.

1.2 tRNA transcription by RNA polymerase III

1.2.1 RNA polymerase III

tRNA genes are transcribed by RNA Polymerase III (Pol III), which is specialized in high level transcription of very short genes (<200nt) and also synthesizes other non-coding RNAs, including 5S ribosomal RNA (5S rRNA), the U6 spliceosomal RNA, and the 7SL signal recognition particle RNA (Schramm and Hernandez 2002).

Pol III is a 17-subunits complex containing a 9-subunit core that is decorated by three peripheral subcomplexes: the C8-C9 stalk, the C4-C5 heterodimer, and the C3-C6-C7 heterotrimer (**Figure 1.11**). The conserved core contains the two biggest catalytical DNA-interacting subunits RPC1 and RPC2 that are unique for Pol III, surrounded by five subunits (RPABC1, RPABC2, RPABC3, RPABC4, RPABC5) shared between Pol I, Pol II and Pol III (**Table 1.1**). Two additional subunits (RPAC1 and RPAC2) are shared between Pol I and Pol III (Wang et al. 2021).

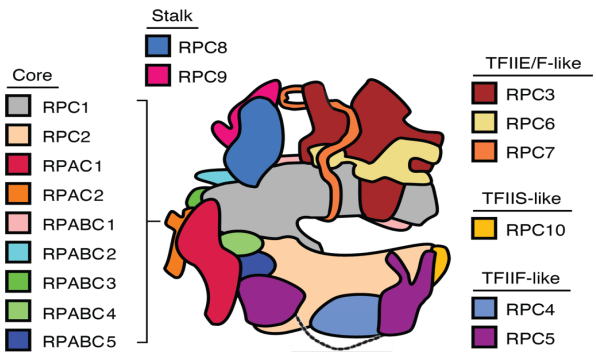

Figure 1.11. Schematic representation of human Pol III. The subunits of human Pol III complex are categorized based on their homology to Pol II counterparts and grouped into subcomplexes, represented in color code. Adapted from (Girbig et al. 2021a).

	PolI	PolII	PolIII
Polymerase Core	RPA1 RPA2 RPAC1 RPAC2 RPABC1 RPABC2 RPABC3 RPABC4 RPABC5	RPB1 RPB2 RPB3 RPB11 RPABC1 RPABC2 RPABC3 RPABC4 RPABC5	RPC1 RPC2 RPAC1 RPAC2 RPABC1 RPABC2 RPABC3 RPABC4 RPABC5
TFIIS-like	RPA12	RPB9	RPC10
Polymerase Stalk	RPA43	RPB4 RPB7	RPC9 RPC8
TFIIF-like	RPA49 RPA34	TFIIFα TFIIFβ	RPC4 RPC5
TFIIE-like		TFIIEα TFIIEβ	RPC3 RRC6 RRC7

Table 1.1. Conservation between the human RNA Polymerase I, II, and III subunits. Human polymerase I, II and III subunits are listed. Subunits are grouped into subcomplexes based on their functional and structural similarity to Pol II subunits.

The surrounding stalk subcomplex C8-C9 is anchored to the Pol III core via extensions of the largest Pol III subunit RPC1 (Hoffmann et al. 2015). The C9 subunit also interacts with the TFIIIB subunit BRF1 and interacts with initiation factors (Khoo et al. 2014). C4 and C5 are tethered to the lobe of Pol III with dimerization, similar to the Pol II general transcription factor TFIIF (Vannini and Cramer 2012; Fernández-Tornero et al. 2013). The peripheral TFIIE-like C3-C6-C7 heterotrimer is specific to Pol III and is important for interaction with TFIIIB as well as for promoter melting (Khoo et al. 2014; Wei and Chen 2018). Notably, as the only mammalian Pol III subunit variants identified, RPC7 was found in two isoforms based on database searches, RPC7α and RPC7β, encoded by two paralogous genes, *POLR3G* and *POLR3GL*, which are spatiotemporally regulated during development (Haurie et al. 2010; Wong et al. 2011). The subunit C10 mediates RNA cleavage in the catalytic center in Pol III pausing. It is homologous to the Pol II elongation and RNA cleavage factor TFIIS (Chédin et al. 1998).

1.2.2 Type 1, 2 and 3 Pol III promoters

There are three different types of promoters for Pol III transcription initiation (**Figure 1.12**). Type 1 promoters enable transcribing the 5S rRNA, a structural and functional component of the ribosome large subunit. tRNA transcription is initiated by type 2 promoters, and type 3 promoters are used to generate the U6 spliceosomal RNA, which catalyzes the excision of introns from pre-mRNA, and the 7SL signal recognition particle (SRP) RNA. Both type 1 and 2 promoters reside within the gene body without a TATA-box, with A-box and C-box in type

1 promoters, or A-box and B-box in type 2 promoters. The A-box in type 2 promoters is homologous to the type 1 promoter A-box, and in some species can be exchanged (Ciliberto et al. 1983). Transcription from type 1 promoter starts with the zinc finger protein TFIIIA binding to the A- and C-boxes (Engelke et al. 1980; Sakonju et al. 1981), which then directs TFIIIC recruitment and subsequently binding of TFIIIB and Pol III (Lassar, Martin, and Roeder 1983; Schramm and Hernandez 2002). A- and B-boxes containing type 2 promoters are recognized by TFIIIC, which then serves to recruit TFIIIB to the upstream region of the transcription start site (TSS) (Marzouki et al. 1986; Kassavetis et al. 1990). This is followed by Pol III recruitment and transcription initiation. The A- and B-boxes in tRNA genes overlap the highly conserved structural elements D and T stem loops in mature tRNA transcripts (Allison, Goh, and Hall 1983). Type 3 promoters are external and contains a TATA-box for recognition by TFIIIB component TBP (Schramm and Hernandez 2002), as well as a proximal sequence element (PSE) that is bound by snRNA activator protein complex (SNAPC), after which Pol III can be recruited.

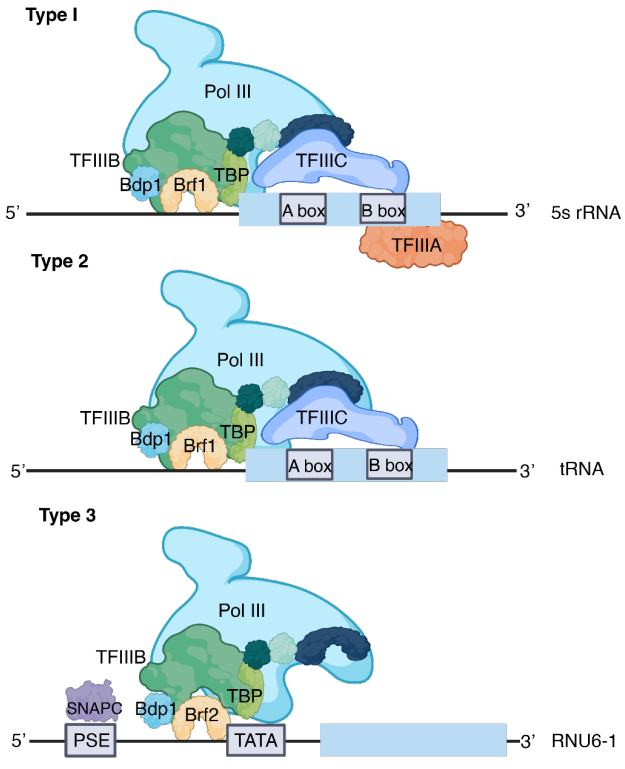

Figure 1.12. Three types of RNA polymerase III promoters and associated transcription factors. Cartoons illustrating Pol III promoter type 1, 2 and 3 (from top to bottom). Major elements depicted are intragenic promoters (A- and C-boxes for type 1, A- and B-boxes for type 2); PSE (Proximal Sequence Element) and TATA-box (for type 3); TFIIIA (for type 1); TFIIIC (for type 1 and 2); TFIIIB consisting of BDP1, TBP and BRF1 (for type 1 and 2) or BRF2 (for type 3) and SNAPC (SNRNA Activating Protein Complex) (for type 3).

1.2.3 Pol III transcription factors

TFIIIC is the largest Pol III transcription factor with a total mass of 520 kDa. It is composed of six subunits: TFIIIC220, TFIIIC110, TFIIIC102, TFIIIC90, TFIIIC63 and TFIIIC35. These subunits form two subcomplexes, τA and τB, which recognize the short intragenic A- box and B-box, respectively (Marzouki et al. 1986). While the position of the A-box and B-box elements is fixed relative to the 5' and 3' ends of the tRNA gene, the distance between them can vary due to the presence of introns and flexible tRNA arms (Marck et al. 1993). TFIIIC can assume different conformations according to the distance between the A-box and B-box, either in a compact globular shape when they are closely spaced, or extended as "dumb-bell shaped" with the two domains connected by a flexible linker when they are separated (Schultz et al. 1989). Given that τB binds to the B-box with higher affinity, it contributes the largest part of the affinity of TFIIIC interaction with DNA, and serves as an anchoring platform that facilitates the binding of τA to the A-box and subsequent recruitment of Pol III (Stillman and Geiduschek 1984).

Human TFIIIB comprises 3 proteins: TATA-box binding protein (TBP), TFIIB-related factor 1 or 2 (BRF1 or BRF2) and B double prime 1 (BDP1), which are only stably associated with each other when bound to DNA. TBP is shared by Pol I, II and III (Cormack and Struhl 1992; White, Jackson, and Rigby 1992) and was found to bend DNA itself or together with BRF1 in type 1 and 2 promoters (Kassavetis et al. 1990). It binds to a TATA-box in type 3 promoters (Hernandez 2001), which recruits a different TFIIB-related factor, BRF2. BRF1 contains a zinc ribbon domain and two cyclin repeats in its N terminal domain, characteristic of the TFIIB-related transcription factor family (Schramm and Hernandez 2002). BRF1 directly interacts with multiple TFIIIC subunits and Pol III subunits (Moir, Puglia, and Willis 2002; Khoo et al. 2014), and is essential for TFIIIB and Pol III function. Facilitated by binding of TFIIIC subunits and BRF1, BDP1 binds upstream of the TFIIIB-DNA complex ~8 bp from the TSS (Shah et al. 1999) opposite to BRF1, which is located downstream of the TBP-DNA core. BDP1 is involved in unpairing the upstream sequences (Kassavetis, Letts, and Geiduschek 2001).

1.2.4 Pol III transcription complex assembly on a tRNA gene

Bound TFIIIC directs the recruitment of TFIIIB by recruiting BRF1 through TFC102, followed by TBP binding (Hsieh et al. 1999). This complex facilitates the assembly of BDP1, which activates the initial melting of DNA sequences upstream of the TSS. The complete assembly

of TFIIIC and TFIIIB on type 2 promoters initiates the recruitment of Pol III. Pol III is bound to BRF1 through RPC9, which binds the non-transcribed strand upstream of the TSS, and RPC6, which interacts with both BRF1 and TBP. Once recruited, the Pol III-specific heterotrimer C3-C6-C7 activates the DNA double strands melting and transcription bubble formation, which extend downstream facilitated by BRF1 (Kassavetis et al. 1992). Transcription terminates when Pol III encounters a stretch of 7-8 Ts in the non-template strand (Turowski and Tollervey 2016). The binding of subunits C4, C5 and C10 transforms the elongation complex into a pre-termination complex, enabling termination signal recognition (Braglia, Percudani, and Dieci 2005; Landrieux et al. 2006).

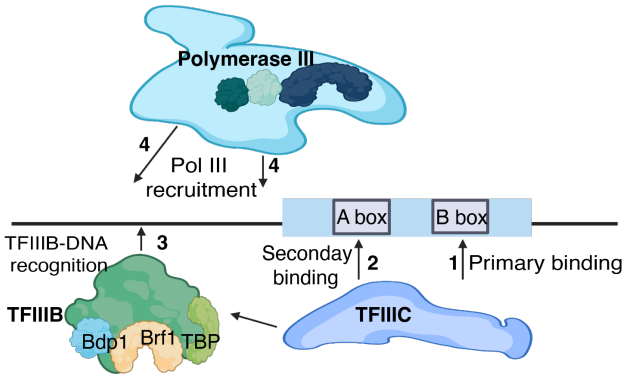

Figure 1.13. Pol III transcription complex assembly on a tRNA gene. The schematic illustration depicting the stepwise recruitment of TFIIIC, TFIIIB and Pol III to a tRNA gene. The major steps include primary and secondary binding by TFIIIC at A- and B-boxes, TFIIIC-directed recognition of TFIIIB, and Pol III recruitment of RNA. Order of the steps are marked as numbered arrows.

Interestingly, in the absence of TFIIIC at type 3 promoters, TFIIIB alone can also allow Pol III binding in *S. cerevisiae*, indicating that TFIIIB is the minimal transcription factor for Pol III transcription (Kassavetis et al. 1990). Indeed, for type 1 and 2 promoters, although TFIIIC is necessary for the initial round of transcription, it is dispensable once TFIIIB is bound and TFIIIC is thought to be removed from the promoter to make space for Pol III transcription (Kassavetis et al. 1990). *In vitro* studies support this hypothesis by demonstrating the high affinity between Pol III and TFIIIB even under stringent salt conditions, which disrupt TFIIIC-Pol III interaction (Cloutier et al. 2001; Stillman and Geiduschek 1984). Moreover, after the first cycle of synthesis, TFIIIB can retain Pol III for multiple rounds of transcription from the same locus through facilitated recycling (Ferrari and Dieci 2008; Ferrari et al. 2004; Jahn, Wingender, and Seifart 1987), a process in which the terminating Pol III quickly reattach to the same transcription unit with the TFIIIB pre-assembled on the DNA. The Pol III re-initiation

rate was shown to be faster than the initial transcription cycle due to the bending of DNA by TFIIIB (Dieci and Sentenac 1996; Ferrari et al. 2004).

1.3 Regulation of tRNA abundance by RNA polymerase III transcription

Given the functional and structural overlap between the internal tRNA promoters (A-box and B-box) with the conserved structural regions in mature tRNA (D-loop and T-loop) (Galli, Hofstetter, and Birnstiel 1981), it had been widely assumed that tRNA expression is exclusively regulated by these intrinsic promoter elements, and that no mechanisms for spatial and temporal control of tRNA gene expression exist. Accordingly, tRNA gene copy number is widely used as a measure of tRNA expression levels (dos Reis, Savva, and Wernisch 2004; Tuller et al. 2010; Mario dos Reis, Nucleic Acids Res. 2004; Tamir Tuller, Cell, 2010). However, recent studies have challenged this model, since tRNA genes with identical A- and B-boxes were found to be differentially expressed in diverse cell types, developmental stages and cellular conditions (Kutter et al. 2011b; Ishimura et al. 2014; Sagi et al. 2016). Notably, while nearly all predicted tRNA loci are occupied by Pol III in yeast, nearly half of the tRNA genes are inactive in murine and human cells (Torres 2019). All this evidence collectively points to the existence of various cis- and/or trans- factors modulating tRNA gene expression in multicellular organisms.

1.3.1 Regulation of Pol III transcription by *cis*-elements

A-box and B-box

In tRNA genes, the 11-bp A-box is located 12-20 nt downstream of the TSS, and the 11-base B-box is usually located 30-60 bp downstream (Galli, Hofstetter, and Birnstiel 1981). By comparing all bases with a frequency above 60% at A- and B-box in more than 80 different eukaryotic tRNAs, the consensus sequences for A- and B-boxes were initially extracted as 5'-TGGCNNAGTGG-3' and 5'-GGTTCGANNCC-3', respectively (Galli, Hofstetter, and Birnstiel 1981), which were later generalized to 5'-TRGYnnAnnnG3', and 5'-GWTCRAnnC-3' (n = any base, R = purine, Y = pyrimidine, W = A or T) (Marck et al. 2006). In yeast, the B-box was suggested to determine the binding strength to TFIIIC and initiation levels because of its high affinity to TFIIIC, while the A-box selects the correct TSS, supported by the finding that A-box sequences are more degenerate than B-box (Geiduschek and Tocchini-Valentini

1988). The A- and B- boxes were thought to be highly conserved, partly attributed to their encoding of the D and T loops in mature tRNA (Galli, Hofstetter, and Birnstiel 1981; Hofstetter, Kressman, and Birnstiel 1981). In line with the conservation, variation of the intragenic promoters was reported to be unrelated to tRNA gene expression in human HeLa and IMR90 cell lines (Canella et al. 2010; Oler et al. 2010b). However, in the mouse liver, minor differences at the variable positions in the A- and B-box were observed between tRNA genes with high or no Pol III occupancy (Canella et al. 2012). Another study also demonstrated that the sequence motif of the B-box differed between two subsets tRNAs that were enriched either during differentiation or proliferation, suggesting that internal promoter elements may contribute to tRNA expression regulation (Gingold et al. 2014).

5' and 3' flanking sequences

TFIIIC binding to internal tRNA promoters is followed by TFIIIB recruitment upstream of the TSS. Despite the central importance of TFIIIB binding to DNA for tRNA transcription mechanism, the 5' flanking sequences of tRNA genes vary dramatically (Arnold et al. 1986; Dingermann et al. 1982; Schramm and Hernandez 2002; Thornlow et al. 2018). Therefore, the contact between TFIIIB and the upstream DNA binding sequence was initially thought to be non-specific (Geiduschek and Kassavetis 2001). However, several have studies suggested that the upstream regions of certain tRNA genes contain conserved sequence elements with a regulatory role that influence promoter function in eukaryotes (Raymond, Raymond, and Johnson 1985). For example, a conserved sequence pattern with composite nature consisting of multiple motifs has been proposed to exist upstream of tRNA genes in *Saccharomyces cerevisiae*, and upstream sequences of tRNA genes with this pattern boost tRNA gene transcription by enhancing TFIIIB binding (Giuliodori et al. 2003). A TCAACA sequence motif was found spanning the TSS and was correlated with Pol III transcription initiation in both *Arabidopsis thaliana* and *Saccharomyces cerevisiae* (Yukawa et al. 2011). It is widely accepted that Pol III transcription terminates at well-conserved polyT stretches containing 4 or more consecutive thymidine residues that are locate around 20 bp downstream of the 3′ end of the mature tRNA coding sequence, and is bound by the La-protein (Orioli et al. 2012). The quality and strength of this terminator sequence can contribute to Pol III transcription efficiency and has been proposed to be part of Pol III promoters (Canella et al. 2012). Together, these findings indicate the presence of sequence patterns upstream and downstream of tRNA genes that may modulate their expression levels.

1.3.2 *Trans*-regulating factors of tRNA transcription

Apart from the core basal transcription factors, several *trans*-acting regulators have been implicated in the global regulation of Pol III in mammals, such as extracellular signal-regulated kinase (ERK). ERK functions through the Ras-Raf-MEK pathway and plays an important role in integrating external signals, such as epidermal growth factor (EGF), promoting cell growth and proliferation in various mammalian cell types (Downward 2003). ERK was shown to enhance tRNA synthesis by directly binding and phosphorylating the BRF1 subunit of TFIIIB (Felton-Edkins et al. 2003). In *Drosophila*, Erk signaling regulates Pol III output by inhibiting the nuclear localization and function of the Pol III repressor Maf1, thereby enhancing protein synthesis to promote cell growth (Sriskanthadevan-Pirahas et al. 2018).

The proto-oncogene protein c-Myc was also shown to be involved in the activation of Pol III transcription. c-Myc enhances cell growth and cell division by increasing ribosome biogenesis and translation (Campbell and White 2014). Chromatin immunoprecipitation (ChIP) has suggested that endogenous c-Myc may be present at tRNA and 5S rRNA loci in cultured mammalian cells and be recruited through binding to TFIIIB with its N-terminal transactivation domain (Gomez-Roman et al. 2003).

Casein kinase II (CK2), a Ser/Thr protein kinase, was also shown to regulate Pol III transcription through Maf1 (Graczyk et al. 2011) or TFIIIB (Ghavidel and Schultz 2001; Johnston et al. 2002) in both human and yeast cells. CK2 is involved in cell cycle control and DNA repair and has been associated with cell proliferation and transformation (Meggio and Pinna 2003; Homma and Homma 2008). CK2 can phosphorylate BRF1, leading to enhanced recruitment of TFIIIB (Landesman-Bollag et al. 2001; Faust et al. 1996; Yenice et al. 1994).

General negative regulators of Pol III transcription include the retinoblastoma tumor-suppressor protein (RB) and down-regulator of transcription 1 (DR1). Under limited nutrient availability, RB blocks the transition from G1 into S phase through binding to Pol II factor E2F. Unlike its role as histone deacetylases in Pol II transcription regulation, RB was shown to repress Pol III by binding and deactivating TFIIIB through disrupting its interaction with TFIIIC and Pol III (Sutcliffe et al. 2000). DR1 was also found to be associated with BRF1, which facilitates its recruitment to Pol III templates in mammalian cells, together with its dimerization partner DRAP1 (Kantidakis and White 2010). However, none of these proteins have been shown to have tRNA gene-specific effects on Pol III activity.

1.3.3 Regulation of Pol III transcription by the epigenetic environment

DNA methylation is an epigenetic process involving the addition of a methyl group to the fifth carbon atom of a cytosine ring in DNA by DNA methyltransferases (DNMTs), converting the cytosine bases to 5-methylcytosine (**Figure 1.14**). In humans, DNA methylation is found mainly on CpG dinucleotides, where it blocks the recruitment of transcription factors and results in gene silencing (Antequera and Bird 1999; Loyfer et al. 2023). During development, the patterns of DNA methylation change dynamically, which serves to regulate cell- and tissue-specific gene expression (Ghosh et al. 2010). Although DNA methylation has been profiled genome-wide with the advent of various high-throughput techniques (Yong, Hsu, and Chen 2016), its presence at tRNA genes and functional impact are not well understood. It is therefore not clear so far whether and to what extent DNA methylation regulates Pol III transcription and tRNA expression.

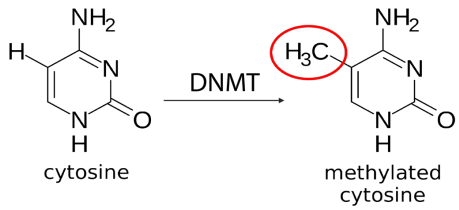

Figure 1.14. DNA methylation reaction catalyzed by DNMT. Schematic representation of the covalent transfer of a methyl group by DNA Methyltransferase (DNMT) to the fifth carbon of cytosines, which becomes 5-methylated cytosine. The added methylation group is highlighted in red.

Apart from DNA, histone proteins can also be methylated or acetylated on diverse lysine positions. Depending on the specific lysine residues being modified and the number of methyl groups added, histone methylation is linked to either repressed or active chromatin. H3K4me1/2/3 and H3K36me3 mark open chromatin (Pekowska et al. 2011; Wagner and Carpenter 2012), while H3K9me3 and H3K27me3 are associated with repressive chromatin and facultative heterochromatin, respectively (Kim and Kim 2012). H3K4me3 forms two peaks bracketing the TSS in Pol II genes, while it accumulates upstream of the TSS in human Pol III genes (Canella et al. 2012). The simultaneous deposition of H3K4me3 and H3K27me3 chromatin marks is a hallmark of bivalent Pol II genes preserved in a poised state, preventing them from being silenced while maintaining their potential for prompt activation in differentiation (Bernstein et al. 2006). H3K27me3 was reported to be positively correlated with Pol II pausing (Liu et al. 2017), the accumulation of transcriptionally engaged but paused Pol II proximal to promoters, generating a short transcript of 20–60 nucleotides (Rasmussen and

Lis 1993). However, whether these regulatory functions extend to Pol III genes is still not fully understood despite some correlation has been suggested between histone modifications and Pol III gene activity. For example, histone acetylation that marks open chromatin and active Pol II transcription, such as H3K9ac and H3K27ac, were also found on Pol III-transcribed non-coding RNA genes in Jurkat cells (Barski et al. 2010b). Similarly, Pol III–occupied tRNA loci were correlated with active Pol II histone marks (e.g., H3K36ac) and anticorrelated with repressive histone modifications (e.g., H3K36me3) in HeLa cells (Oler et al. 2010a). Actively-transcribed Pol III genes were found in close proximity to Pol II–dependent histone marks, such as H3K4me3, H3K4me2, H3K27ac and H3K9ac, in K562 cells (Moqtaderi et al. 2010b). Human embryonic stem cells H1 (H1 ES) also show a peak of H3K4me3 between the H3K27me3 and Pol III binding peaks, suggesting the role of H3K4me3 in "insulating" Pol III gene activity from the neighboring repressive H3K27me3 (Alla and Cairns 2014). Moreover, human TFIIIC has also been proposed to relieve chromatin-mediated repression of Pol III transcription via its intrinsic histone acetyltransferase (HAT) activity (Kundu, Wang, and Roeder 1999).

1.3.4 Regulation of Pol III transcription by genomic context

Similar to Pol II genes, many Pol III-transcribed genes are also found in nucleosome-free regions (NFR) (Bhargava 2013). tRNA genes have been proposed to prevent spreading of heterochromatin in both yeast and human cells (Raab et al. 2012). This was first supported by the finding that deletion of a tRNA gene located next to a transcriptionally silent chromatin region led to repression of a downstream gene (Donze and Kamakaka 2001). Just like insulators, which tend to cluster at specific sites in the genome, tRNA genes were also found to coalesce in the human nucleus (Raab et al. 2012). During macrophage development, tRNA gene transcription was found to be regulated in domains based on DNA loops, suggesting a role of maintaining chromosome structure and organization in tRNA gene regulation (Van Bortle, Phanstiel, and Snyder 2017).

Due to the general overlapping functions of histone modifications between Pol II and Pol III genes, as well as the association of tRNA genes with Pol II transcription factors such as c-myc, it has been proposed that Pol III transcription is positively influenced by the actively transcribed Pol II genes nearby (Oler et al. 2010b). Conversely, tRNA gene transcription by Pol III was found to suppresses transcriptional activity of nearby Pol II genes in *Saccharomyces cerevisiae*, due to clustering of tRNA genes in the proximity to the nucleolus (Pratt-Hyatt et al. 2006).

Some studies have proposed that rather than the linear distance of tRNA genes to active Pol II genes, long-range regulatory DNA interactions could actually alter the expression of specific tRNA genes in defined cellular contexts (Dekker and Misteli 2015). In *Drosophila*, 80% of Pol III-bound genes overlap with enhancer-like chromatin, marked by both H3K4me1 and H3K27Ac, while only 20% reside in Pol II promoters with H3K4me3, H3K4me2, H3K9ac (Alla and Cairns 2014). As the major gene-regulatory elements, enhancers control cell-type-specific gene expression through long distances looping to vicinity of their target gene promoters (Levine, Cattoglio, and Tjian 2014). However, whether human tRNA genes are associated with characterized Pol II enhancer elements has not been investigated to date.

Eukaryotes exhibit a significant variation in the distribution of tRNA genes. In mammalian genomes, they are often present in distinct clusters on specific chromosomes, such as chromosome 1 and 6 for humans, chromosome 13 for mice, and chromosome 5 for gorilla (Dixon et al. 2012; Raab et al. 2012; Hughes et al. 2023). This non-random arrangement raises the question as to whether tRNA gene expression is influenced by nearby tRNA gene activity, given that the spatial proximity of active genes to each other could raise the concentration of active polymerases in the distinct Pol III transcription “factories' observed in human cells, which could enable Pol III recycling (Pombo et al. 1999).

1.3.5 Regulation of Pol III transcription by changes in protein composition

In mammals, the Pol III subunit RPC7 is present in two forms, RPC7α and RPC7β, encoded by *POLR3G* on chromosome 5 and *POLR3GL* on chromosome 1 in humans. The two paralogous genes were predicted to derive from gene duplication in a common ancestor of vertebrates and encode proteins that have 46% amino acid identity (Renaud et al. 2014). RPC7α is highly abundant in stem cells, immortalized cancer cell lines, and at early developmental stages. Accordingly, the pluripotency transcription factors OCT4 and NANOG have been reported to bind the *POLR3G* TSS in humans (Wong et al. 2011). RPC7α was also suggested to maintain stem cell renewal, since decreased *POLR3G* expression results in loss of pluripotency and drives stem cell differentiation (Wong et al. 2011). During development, RPC7α levels drop substantially, and RPC7β becomes the predominant isoform in differentiated cells (Haurie et al. 2010; Wong et al. 2011; Lund et al. 2017). It has been hypothesized that dynamic variation of RPC7α abundance responds to growth cues, while RPC7β, which is maintained at a relatively low but stable level, provides a constitutive baseline for Pol III availability (Renaud et al. 2014).

RPC7α/RPC7β is incorporated into the ternary RPC3-RPC6-RPC7 subcomplex, which functions in Pol III transcription initiation by binding the Pol III clamp domain through RPC7 and interacting directly with TFIIIB through RPC6 (Kenneth, Marshall, and White 2008). ChIP-seq with IMR90 cells demonstrates that substitution of these two subunits in Pol III complex was not involved in gene target specificity, since Pol III with either RPC7α or RPC7β was detected with highly similar localization genome-wide (Renaud et al. 2014). In line with this, *POLR3GL* (RPC7β) was shown to functionally replace *POLR3G* (RPC7α) in mouse ESCs, based on that overexpression of *POLR3GL* rescues the differentiation deficiency in mouse ESCs with *POLR3G* knockout (Wang et al. 2020).

Given the seemingly functional equivalence between RPC7α and RPC7β, what could lead to the disparity in expression between these two forms during differentiation? Cryo-EM structures suggested that the human RPC1 clamp domain bound by RPC7 overlaps with the recently resolved structure of Pol III repressor Maf1 in *Saccharomyces cerevisiae*, and this interaction is only tightly formed with two residues exclusive to RPC7α, but not RPC7β, suggesting the inability of RPC7α-containing Pol III to be repressed by Maf1 (Vorländer et al. 2020; Girbig et al. 2021b). This evidence may provide bases for the enrichment of RPC7α in embryonic stem cells and cancer (Durrieu-Gaillard et al. 2018; Enver et al. 2005), as well as the increased tumor transformation with RPC7α overexpression (Haurie et al. 2010). However, this hypothesis has not been experimentally tested, so whether and how the loss of RPC7α-containing Pol III is related to MAF1 in differentiation remains elusive.

1.4 Regulation of Pol III transcription by MAF1

1.4.1 MAF1

Among the trans-factors with a negative influence on tRNA gene transcription, MAF1 is the most well-characterized and conserved Pol III repressor. Its regulation and mode of action have been documented in yeast (Graczyk, Cieśla, and Boguta 2018), fruit fly (Rideout, Marshall, and Grewal 2012), plants (Oliveira Andrade et al. 2020), mouse (Bonhoure et al. 2020), and human cells (Orioli et al. 2016). Human MAF1 is 28 kDa, while yeast Maf1 is 45 kDa. While yeast Maf1 undergoes phosphorylation on at least 6 sites (S90, S101, S177, S178, S209, S210) (Lee, Moir, and Willis 2009; Moir et al. 2006), human MAF1 is phosphorylated at three major residues (S60, S68, S75) by the mammalian target of rapamycin complex 1 (mTORC1) (Michels et al. 2010; Shor et al. 2010). In yeast, Pol III repression upon starvation, rapamycin

treatment and various stress conditions is mediated by Maf1 (Boisnard et al. 2009; Upadhya, Lee, and Willis 2002), which is dephosphorylated mainly by PKA and Sch9 (Moir et al. 2006; Huber et al. 2009). Under normal growth conditions with high mTORC1 activity in human cells, phosphorylated MAF1 is inactive, while in response to limited nutrient availability such as serum starvation, MAF1 is dephosphorylated and can repress Pol III transcription (Michels et al. 2010). In contrast to the well characterized nuclear translocation of yeast Maf1 upon dephosphorylation (Moir et al. 2006), there is no convincing evidence that supports the nuclear transport of human MAF1 (Michels et al. 2010), such as in HeLa cells which were found lack of MAF1 nuclear export upon changes in mTOR signaling (Kantidakis et al. 2010). This is supported by the fact that yeast Maf1 has two nuclear localization sequences (NLS) located at both the N-terminus and C-terminus, while no such NLS was identified in human MAF1 (Pluta et al. 2001).

This repression is most likely not via direct binding to DNA, as attempts to pull down Maf1 in ChIP have been unsuccessful in yeast (Desai et al. 2005) and in a mouse cell line expressing a tagged version of MAF1 protein (Bonhoure et al. 2015). Moreover, ChIP-Seq with an antibody directed against endogenous MAF1 in the liver from wild-type and *Maf1*$^{-/-}$ mice yielded similar DNA profiles, which did not correspond to any known Pol III loci (Bonhoure et al. 2015). Instead, cryo-EM structure of *Saccharomyces cerevisiae* Maf1 indicates that it binds to Pol III and allosterically repositions the C82/34/31 heterotrimer subcomplex, which would precludes Pol III to TFIIIB-bound promoters, thereby repressing transcription (Vannini et al. 2010). Yeast pull-down assays suggested that Maf1 binds to Brf1, which would block the recruitment of Brf1 to Pol III genes (Desai et al. 2005).

While MAF1 is not essential for cell viability, the phenotypes of its depletion can vary considerably in different organisms and experimental systems. For example, while MAF1 is associated with tumor suppression in PTEN-deficient cancer cells (Li et al. 2016), *Maf1*$^{-/-}$ mice are not tumor-prone, but instead have an extended lifespan, a lean phenotype and obesity resistance due to increased energy consumption (Bonhoure et al. 2015). Overexpression of MAF1 has also been reported to extend lifespan through mTORC1 in worms and flies (Cai and Wei 2016), which recapitulate the hypothesis that dietary restriction promotes health and leads to longer lifespan in animals (Mattison et al. 2017). Interestingly, recent data has also implicated MAF1 in cellular differentiation. For example, MAF1 promotes mesoderm induction of mouse embryonic stem cells (ESC) (Chen et al. 2018). Apart from lineage directed differentiation by MAF1 loss, at least one mechanism by which MAF1 functions to stimulate

adipogenesis is through its ability to repress Pol III-dependent transcription (Chen et al. 2018), although how this is achieved at a molecular level given MAF1's inability to bind DNA is unknown.

1.4.2 mTORC1

MAF1 is regulated by mTORC1, a key downstream effector of the phosphatidylinositol 3-kinase (PI3K)-AKT pathway, which promotes cell growth in response to nutrient availability and other environmental cues (**Figure 1.15)** (Bhaskar and Hay 2007; Laplante and Sabatini 2012). mTORC1 is inhibited under stress conditions, such as nutrient deprivation, resulting in MAF1 dephosphorylation (Michels et al. 2010). TSC1/TSC2 functions as the upstream inhibitors for mTORC1, and the major downstream targets of mTORC1 include the ribosomal protein S6 kinase 1 (S6K1) and 4EBP1, which binds to the eukaryotic translation initiation factor 4E (eIF4E) (Hay and Sonenberg 2004). Phosphorylation by mTORC1 activates S6K1, thereby promoting protein and lipid synthesis. mTORC1 phosphorylates 4EBP1 and releases it from eIF4E, which allows incorporation of eIF4E into translation initiation complexes and facilitates protein synthesis.

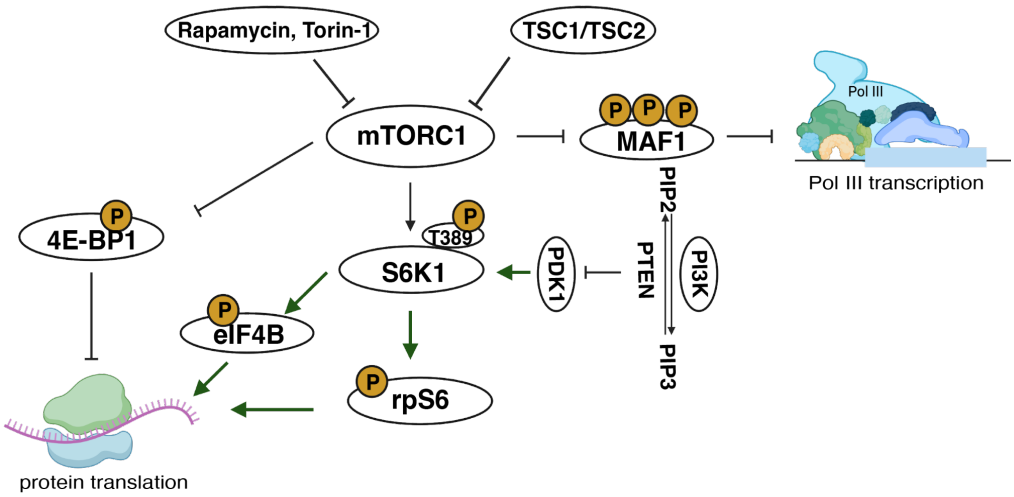

Figure 1.15. Schematic illustration of mTORC1 signaling pathways. mTORC1 stimulates phosphorylation of S6K1 at T389, which phosphorylates rpS6 (ribosomal protein S6) and eIF4B, and suppresses phosphorylation of 4EBP1, together promoting protein translation. mTORC1 phosphorylates and deactivates Pol III transcription repressor MAF1. mTORC1 activity can be repressed by rapamycin, Torin-1 and TSC1/TSC2. PTEN negatively regulates PI3K signaling by converting PIP3 to PIP2 and deactivates PDK1, subsequently inhibiting S6K1 phosphorylation. P indicates phosphorylation; PIP2 and PIP3 represent phosphatidylinositol-4,5-bisphosphate and phosphatidylinositol 3,4,5-trisphosphate, respectively.

High mTORC1 activity is necessary for the expression of key pluripotency genes, such as *POU5F1* and *NANOG*, and therefore for maintaining pluripotency in human ESC (Zhou, Su, et al. 2009). Reduced mTORC1 activity was shown during differentiation of neuronal cells and T cells from stem cells or specific progenitors (Zhang et al. 2022). How this reduction of mTORC1 activity impacts MAF1 and Pol III transcription upon differentiation is not understood.

1.5 tRNA and Pol III dysregulation and human diseases

Given their central role in protein synthesis, defects in tRNA function have been associated with numerous human diseases. The multiple steps in tRNA biogenesis can contribute to distinct human pathologies. Apart from the modification-related diseases that are briefly summarized in Section **1.1.3**, dysregulated tRNA abundance has been implicated in a wide range of diseases. For example, altered tRNA pools and charging levels in multiple myeloma (MM) have been proposed to accommodate for the varied demand in protein translation (Zhou, Goodenbour, et al. 2009). Overexpression of tRNA-Glu-UUC and tRNA-Arg-CCG was shown to promote breast cancer metastasis by enhancing ribosome occupancy at specific mRNAs with an overrepresentation of their cognate codons, which shift the cells towards pro-metastatic state (Goodarzi et al. 2016). Recently, changes in tRNA abundance was also identified as a marker for acute respiratory syndrome coronavirus 2 (SARS-CoV-2) infection and severity (Katanski et al. 2022). Mutations in Pol III subunits and Pol III transcription factors have also been linked to a wide range of diseases. For example, mutations of *POLR3A* and *POLR3B*, which encode the core Pol III subunits RPC1 and RPC2, decrease the levels of Pol III in the brain and are linked to leukodystrophies, which are characterized by demyelination and developmental defects of neurons (Bernard et al. 2011; Saitsu et al. 2011). Mutations in *POLR1C* and *POLR1D*, two subunits shared between Pol I and Pol III, are associated with Treacher Collins syndrome, which is characterized by bone and tissue underdevelopment (Noack Watt et al. 2016). *BRF1* mutations reduce BRF1 recruitment at tRNA target genes and alter Pol III transcription, thereby causing neurodevelopmental anomalies (Borck et al. 2015). Increased levels of Pol III subunits, TFIIIB and TFIIIC have also been found in different tumors (Fang et al. 2017; Winter et al. 2000), and in some cases were associated with poor prognosis (Zhong et al. 2016). Interestingly, Pol III has been detected in the cytoplasm, where it has been suggested to recognize and transcribe AT-rich DNA from foreign pathogens into intermediate RNAs, which activate innate immune responses (Ablasser et al. 2009; Chiu, Macmillan, and Chen 2009). As one of the

downstream targets of the growth regulator mTORC1, Pol III was found to restrict lifespan and survival in worms and flies (Filer et al. 2017). Collectively, these studies suggest that Pol III dysregulation is a hallmark of neurological diseases and cancer.

1.6 Studying cell type-specific tRNA regulation in hiPSC-based models

Much of what we currently know about eukaryotic tRNA biology is derived from studies with model organisms or tissues, or from work with primary or transformed cells, which have considerable disadvantages. Tissues are highly heterogeneous, and often contain multiple cell types, which can confound data analysis and interpretation. Primary cells are difficult to obtain and grow under laboratory conditions, whereas immortalized aneuploid cell lines are mostly tumor-derived and are characterized by dramatic genomic imbalances and gene expression abnormalities (Hanahan and Weinberg 2011). This makes their value questionable for understanding normal cell physiology, especially in the case of tRNA regulation, given that mature tRNA levels are in part controlled by gene copy number (dos Reis, Savva, and Wernisch 2004). Recently, human induced pluripotent stem cells (hiPSC) have become valuable research models for understanding human biology. hiPSC are reprogrammed from somatic cells by transducing four transcription factors: OCT4, KLF4, SOX2, and c-MYC (Takahashi and Yamanaka 2006). If somatic cells from healthy individuals are used, this enables the derivation of diploid hiPSC lines with a normal karyotype. The Human Induced Pluripotent Stem Cells Initiative (HipSci) has made several highly qualified reference hiPSC lines freely available for research use (Kilpinen et al. 2017). Genomic editing and gene expression manipulation in hiPSC have been largely facilitated by recent advances in the development of CRISPR/Cas9 system and inducible CRISPR interference (CRISPRi) (Mandegar et al. 2016). Moreover, highly efficient protocols have been established to differentiate hiPSC into a wide range of diverse cell types (Zakrzewski et al. 2019). These protocols recapitulate the natural process of somatic cell differentiation and have greatly facilitated the study of developmental processes. The differentiated cultures are isogenic and have purer cell composition than tissues, eliminating the genome instability and tissue heterogeneity as major confounding factors in gene expression studies with transformed cell lines. This makes hiPSC-derived cells a powerful model system for studying the regulation of gene expression during differentiation and in diverse cell types (Drubin and Hyman 2017).

1.7 Scope of this thesis

The work described in this thesis was aimed at gaining a quantitative and mechanistic understanding of how tRNA pools are regulated in distinct human cell types and during differentiation.

In chapter 2.1, we first set up a well-controlled model system, in which hiPSC are differentiated into cardiomyocytes (CM) or neuronal progenitor cells (NPC), which are further differentiated into neurons using small molecule-based approaches. We performed a quantitative characterization of tRNA pools across these cell types using mim-tRNAseq, and we analyzed the downstream effects of changed tRNA expression on translation elongation rates with ribosome profiling in chapters 2.2 and 2.3.

In chapter 2.4, we first optimized ATAC-Seq and ChIP-Seq workflows to enable the analysis of genome-wide occupancy of the Pol III subunit RPC1 and the TFIIIB subunit BRF1 in the hiPSC-based model system. We correlated Pol III occupancy with mature tRNA quantification from chapter 2.1 data to understand how Pol III transcription contributes to tRNA expression during differentiation. We also analyzed how chromatin status contributes to tRNA gene activity.

In chapter 2.5, we defined the sequence determinants governing Pol III occupancy at tRNA genes. The motifs we identified were validated experimentally by CRISPR/Cas9 genome editing. We also identified a potential mechanism for the dramatic upregulation of *tRNA-Arg-TCT-4-1* in neurons by identifying an overlapping enhancer of the nearby *CADM3* gene.

In chapter 2.6, we used inducible CRISPRi to show that the changes in tRNA transcription during differentiation are not due to loss of the Pol III subunit RPC7α. Instead, we identified mTORC1 activity changes upon differentiation activate the Pol III repressor MAF1, which restricts Pol III to highly occupied “housekeeping” tRNA genes in differentiated cells.

Chapter 3 presents a summary of the work in this thesis, compares to previous studies and offers a comprehensive discussion about impact and future insights of this research. Chapter 4 provides the detailed information of the methods in this work, and chapter 5 lists the abbreviations and supplementary tables.

Chapter 2 - Results

The results described in this chapter have been accepted for publication:

L. Gao[*]**,** A. Behrens[*], G. Rodschinka, S. Forcelloni, S. Wani, K. Strasser, D. D. Nedialkova. Selective gene expression maintains human tRNA anticodon pools during differentiation. *Nature Cell Biology*, *accepted in principle.*

[*]Equal contribution

Contributions:

L.G. planned experiments and performed cell maintenance, molecular cloning, CRISPRi knockdown, CRISPR/Cas9 genome editing, RNA and protein experiments, and prepared sequencing libraries for ChIP-Seq, ATAC-Seq, and RNA-Seq; A.B. analysed RNA-Seq, mim-tRNAseq, ATAC-Seq, ChIP-Seq, performed sequence motif searches, and developed the convolutional neural network; G.R. and S.W. established hiPSC differentiation protocols; G.R. provided the inducible CRISPRi hiPSC line, performed immunostainings, and constructed ribosome profiling libraries; K.S. prepared mim-tRNAseq libraries; S.F. performed ribosome profiling data analysis. D. D. N. conceptualized and supervised the project.

2.1 Human tRNA pools are extensively remodeled at transcript level but remain largely stable at anticodon level during differentiation

2.1.1 Derivation of homogeneous cultures of cardiomyocytes, neuronal progenitor cells, and neurons by directed hiPSC differentiation

To define the repertoires of human tRNA pools in physiological settings across differentiation, we created culture models of cell types with vastly diverse proteomes from neuronal and cardiac lineages by establishing a workflow using a reference hiPSC line (*kucg-2*) that is karyotypically normal and obtained from a healthy individual (Kilpinen et al. 2017). With small molecule-based protocols, we differentiate hiPSC into CM (Zhang, Guo, et al. 2015; Tohyama et al. 2013), and into proliferating neuronal progenitor cells (NPC), which were then further derived into mature neurons (Reinhardt et al. 2013; Marrone et al. 2019). This workflow yields cell types from the central nervous system and the heart that are particularly sensitive to tRNA defects and protein misfolding, and are selectively damaged in diseases linked to tRNA dysregulation (e.g. familial dysautonomia, amyotrophic lateral sclerosis, Parkinson's disease, and diverse cardiomyopathies) (Henning and Brundel 2017; Labbadia and Morimoto 2015; Sarin and Leidel 2014).

NPC derivation from hiPSC was initiated through embryoid bodies (EBs) formation with small molecules that stimulate Wnt and Hedgehog signaling pathways to promote dorsal and ventral brain development (**Figure 2.1a)**. After seven days of priming, EBs were dissociated to obtain ventral NPC that are capable of differentiating into cells of the neural tube and the neural crest. At this stage, the NPC culture is still a mixture of different cell types and must be purified by sequential digestion of the different cell types for two more passages to get more homogenous cultures. Once purified, the resulting homogeneous NPC culture can be maintained as the NPC line, or further directed towards differentiation into motor neuron-like cells. For this, NPC are patterned by inhibiting proliferation with retinoid acid (RA) while enhancing hedgehog signaling by adding PMA and neuronal survival with neutrophins (BDNF. GDNF). After six days, patterned neurons are matured by inhibiting gliogenesis with TGF-B3 and supplemented with compounds that enhance survival and growth of neurons (dbcAMP, BDNF, GDNF).

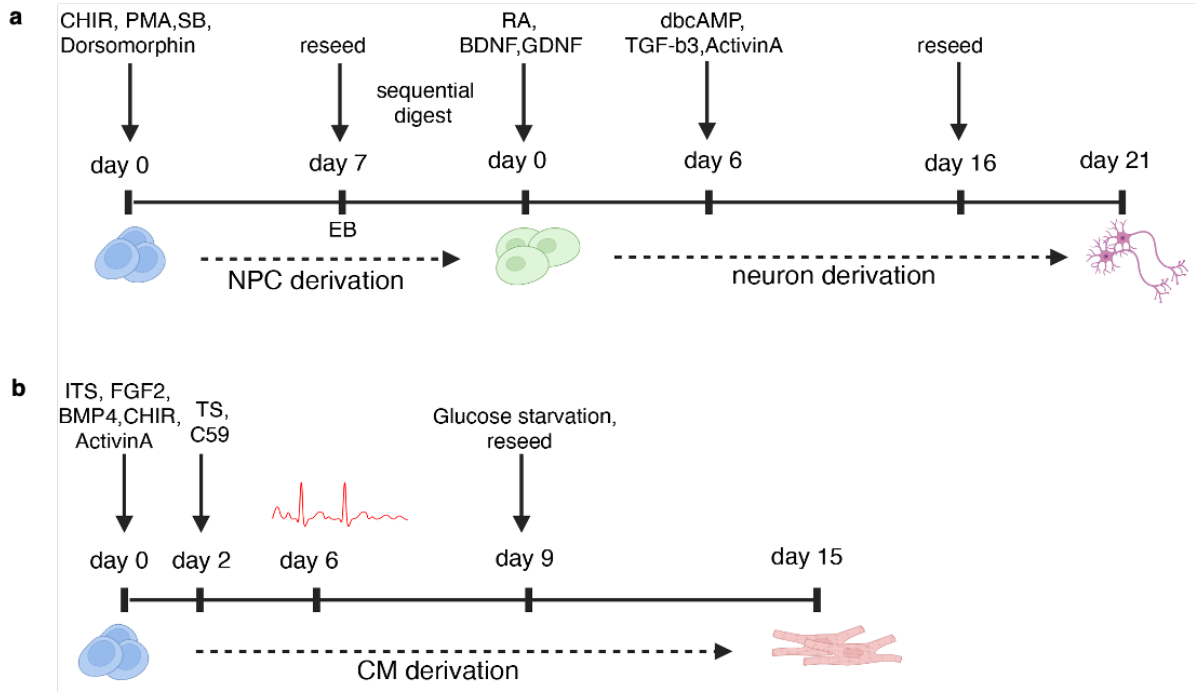

Figure 2.1. Schematic representation of differentiation protocols. Schematic workflow of (**a**) NPC derivation from hiPSC, neurons derivation from NPC, and (**b**) CM derivation from hiPSC.

hiPSC differentiation into CM was initiated in medium containing CHIR99021, which activates Wnt signaling to induce mesodermal commitment, as well as growth factors that induce lateral mesoderm (Activin A, FGF2b, BMP4) and a combination of insulin/transferrin/selenium (ITS) that boosts cell metabolism and protein synthesis and reduces excessive toxic oxygen radicals (**Figure 2.1b)**. After one day of priming, the stimulation of Wnt signaling was discontinued by substituting the growth factors with ascorbic acid (AA), which enhances proliferation of cardiac progenitor cells. One day later, Wnt signaling was actively inhibited with C59 to promote cardiac mesoderm formation. First beating was observed between day 5 and 6 after the start of differentiation. 9 days after starting CM derivation, cells were deprived of glucose and supplemented with lactate for 24 hours, since CM but not other cells are able to metabolize lactate in the absence of glucose (Fuerstenau-Sharp et al. 2015). Cells were further matured in the presence of FCS supplemented for another 5 days.

Immunostaining for known protein markers of specific cell types demonstrated the successful differentiation of homogenous populations of NPC, neurons and CM from hiPSC. The pluripotency marker proteins POU5F1 and SOX2 were expressed uniformly in hiPSC, while NPC were positive for the neural progenitor markers PAX6 and NESTIN. Neurons stained at

day 21 of derivation were positive for the neuronal markers MAP2 and CHAT, and CM showed high levels of cardiac troponin T (CTNT) and cardiac-specific alpha-actinin-2 (ACTN2) at day 15 (**Figure 2.2**).

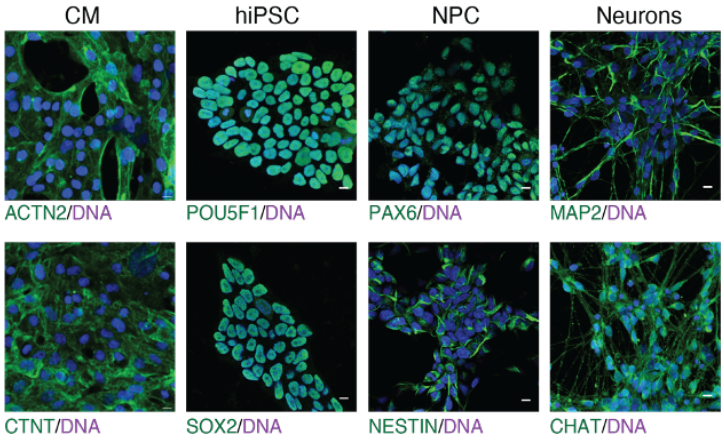

Figure 2.2. Successful derivation of homogenous population of NPC, neurons and CM from hiPSC. Fluorescence microscopy images depicting immunostaining of cell type-specific protein markers (green) in CM, hiPSC, NPC and neurons. DAPI (blue) is utilized as a nuclear counterstain. The scale bar represents 10 µm.

We next generated RNA samples in biological duplicates from hiPSC and NPC, as well as neurons at day 21 and CM at day 15. RNA sequencing (RNA-Seq) analysis showed distinct transcriptomic profiles in these cell lines (**Figure 2.3a**), as represented in the heatmap by z score, which measures how much the expression level of a gene deviates from the average expression level across all samples, and log2 fold change (log2FC) calculated with DESeq2 (Love, Huber, and Anders 2014), which measures the relative difference in gene expression between two samples.

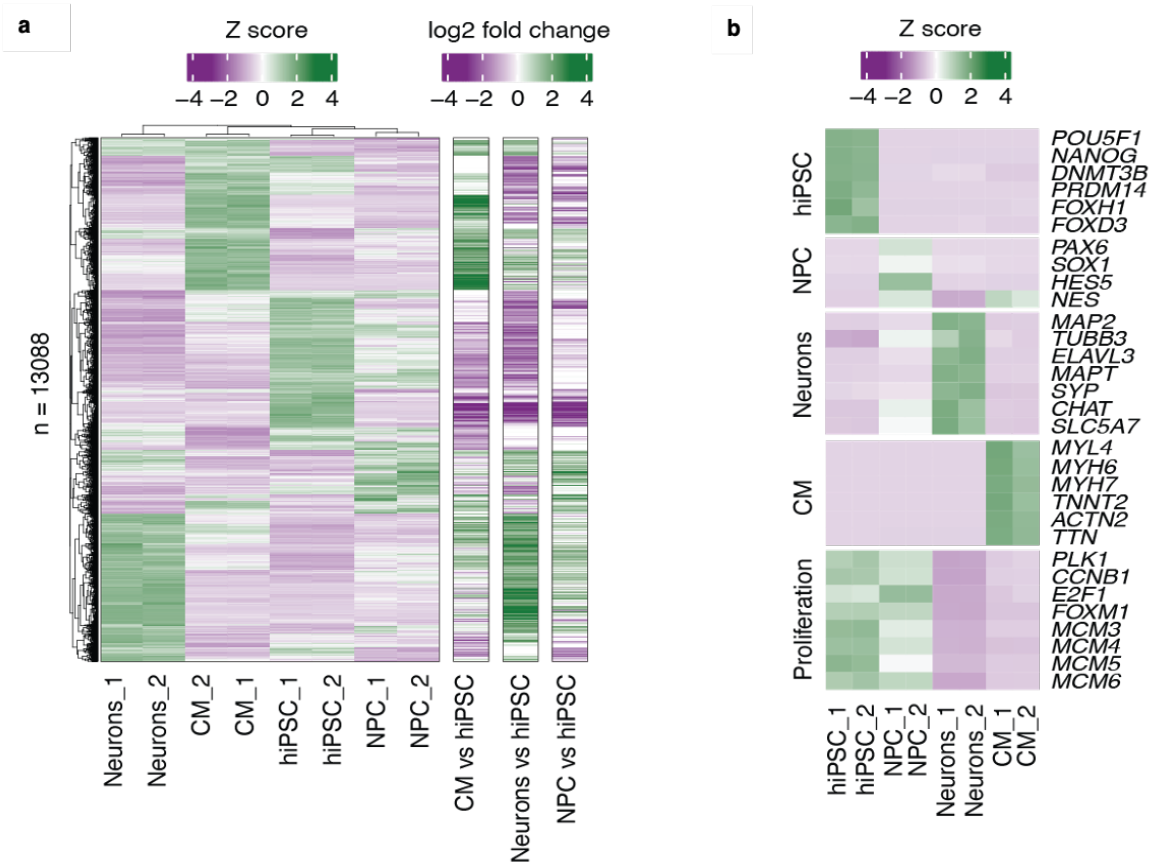

Figure 2.3. Cell type-specific mRNA transcript profiles in hiPSC, NPC, neurons and CM. a, Heatmap of the dynamic expression patterns of mRNA transcripts highlighting only those differentially expressed (Wald test; FDR ≤ 0.05) in at least one cell line compared to hiPSC. Left panel: heatmap of hierarchically clustered expression presenting scaled Z scores of normalized mRNA transcript counts in neurons, CM, hiPSC and NPC (n = 2). Right panel: differential expression in CM, neurons and NPC relative to hiPSC, represented as log2 fold changes. **b,** Heatmaps of gene expression patterns for known markers specific to each cell type and proliferative state in hiPSC, NPC, neurons, and CM, with 2 biological replicates for each cell line. The scale represents the standardized Z score based on DESeq2 normalized RNA-Seq raw gene counts across all samples.

The pluripotency-associated *POU5F1*, *NANOG, DNMT3B*, *PRDM14*, *FOXH1* and *FOXD3* were strongly downregulated in all differentiated cells (**Figure 2.3b**). Common markers of cell proliferation such as polo-like kinase 1 (*PLK1*), cyclin B1 (*CCNB1*), the cell cycle regulator *E2F1*, and replication-initiation complex genes (*MCM3-MCM6*) (Whitfield et al. 2006) were expressed in hiPSC and NPC and strongly downregulated in neurons and CM. NPC expressed neuronal progenitor markers (*PAX6*, *SOX1*, *HES5*and *NES*), while *NES* was also upregulated in CM, consistent with its high expression in heart (Karlsson et al. 2021). Cardiac markers such as sarcomere component-encoding genes (*MYL2, MYH4, MYH7, TNNT2, ACTN2*) and titin (*TTN*) were highly expressed in CM, while genes encoding neuron-specific cytoskeletal proteins (*MAP2*, *TUBB3, MAPT*) and other markers of mature neurons (*ELAVL3*, *SYP, CHAT*

and *SLC5A7)* were specifically upregulated in neurons (**Figure 2.3b**). Collectively, these data demonstrate a robust and successful derivation of highly homogeneous populations of NPC, neurons, and CM from hiPSC.

2.1.2 Analysis of mature tRNA abundance in hiPSC-derived models with mim-tRNAseq

We next profiled mature tRNA abundance in the four isogenic cell types using mim-tRNAseq (Behrens, Rodschinka, and Nedialkova 2021). We generated an alignment reference of 435 mature tRNA transcripts based on a curated set of 600 predicted nuclear-encoded and 22 mitochondrial tRNA genes (Methods) (Chan et al. 2021; Jühling et al. 2009). Unique transcripts within each anticodon family were then clustered by a sequence identity threshold of 97%, followed by indexing of known misincorporation-inducing modified sites, which generates a reference of modified sites that can cause errors during reverse transcription. We then aligned the tRNA-derived sequencing reads to this reference with GSNAP in SNP-tolerant mode, which substantially increases accuracy and limits multi-mapping (Behrens, Rodschinka, and Nedialkova 2021). We obtained ~80% uniquely mapped reads and minimal multi-mapped reads (≤ 2%) for all samples (**Figure 2.4a**). A large proportion of all tRNA-mapped reads were full-length (median of 79%–81%) (**Figure 2.4b**). More than 95% of reads originate from transcripts containing the 3’ CCA tail, a stretch of ubiquitous nucleotides added post-transcriptionally to the 3′ end of tRNA molecules prior to their export from the nucleus for aminoacylation (**Figure 2.4c**), indicating that they are from translationally competent and mature tRNAs. 96.2%–97.3% of the uniquely mapped reads were from nuclear-encoded tRNAs (**Figure 2.4d**), on which we focused the rest of our analyses.

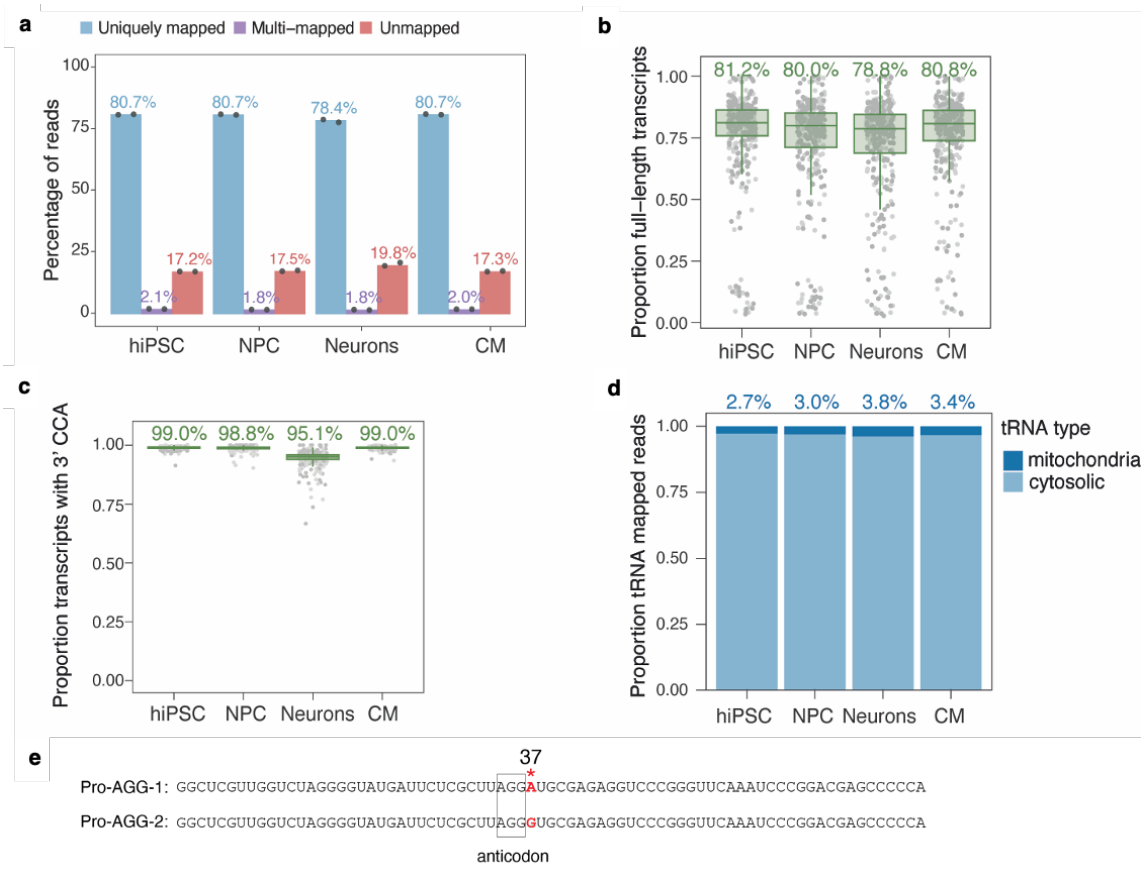

Figure 2.4. mim-tRNAseq generates full length reads from mature tRNA transcripts. a, The alignment statistics for reads from mim-tRNAseq in hiPSC, NPC, neurons and CM. The bars and percentages represent mean values in each cell type. The dots indicate the individual sample values, with two biological replicates for each cell line. **b**, Boxplot of full-length fraction per tRNA transcript in datasets (center line and label: median; box limits: upper and lower quartiles; whiskers: 1.5×interquartile range). Boxplots displaying the distribution of full-length proportion per tRNA transcript in the mim-tRNAseq datasets. The center line and label represent the median value, while the box limits represent the upper and lower quartiles. The whiskers extend to 1.5x the interquartile range. **c,** Boxplot illustrating the distribution of full 3'-CCA end fraction for each tRNA transcript. **d,** Barplot depicting the fractions of cytosolic and mitochondrial tRNA reads per cell type. The bars represent the mean values for each cell type, while the percentages indicate the mean mitochondrial proportion for 2 biological replicates. **e,** Full transcript sequences for human hg38 tRNA-Pro-AGG-1 and tRNA-Pro-AGG-2. The box indicates the anticodon, and the single mismatch is highlighted in bold. The mismatch coincides with the modified m^1G37 position of tRNA-Pro-AGG-2.

Cluster-aligned reads were deconvoluted and assigned to individual tRNA transcripts based on unique mismatch patterns to the parent reference (Behrens, Rodschinka, and Nedialkova 2021; Behrens and Nedialkova 2022). With this, mismatches between the reads and the reference sequence are identified and used to assign the read to the appropriate tRNA transcript, ensuring identification and quantification of individual tRNA transcripts. With this workflow, we could

analyse 373 out of the 413 predicted human nuclear-encoded tRNA transcripts (90%) at single-transcript resolution. Some of the remaining 40 transcripts (n=7) had low coverage with less than 10 reads, and most others differ from the parent reference only at sites with misincorporation-inducing nucleotide modifications, precluding accurate deconvolution (Behrens and Nedialkova 2022). For example, tRNA-Pro-AGG-1 and tRNA-Pro-AGG-2 differ only by one nucleotide at position 37 (adenine for tRNA-Pro-AGG-1, guanine for tRNA-Pro-AGG-2), and either of these two nucleotides could be modified in a way that would introduce a mismatched nucleotide during RT (**Figure 2.4e**).

To validate the capability of our workflow to detect known instances of tRNA abundance variation, we measured the levels of tRNA-Arg-UCU-4 during differentiation in the four cell lines. As one of the 6 nuclear-encoded human tRNA-Arg-UCU isodecoders, tRNA-Arg-UCU-4 is highly abundant in brain tissues (Torres et al. 2019). The expression of *n-Tr20* (mouse homolog of *tRNA-Arg-UCU-4-1*) is constrained specifically to the mouse central nervous system, while the other four isodecoders are expressed in all tissues (Ishimura et al. 2014). This strong cell type-dependent isodecoder expression pattern was successfully recapitulated with mim-tRNAseq in our experimental system, in which the number of reads mapped to tRNA-Arg-UCU-4 was 64-fold higher in neurons compared to all the other cell types, hiPSC, NPC, and CM (**Figure 2.5**).

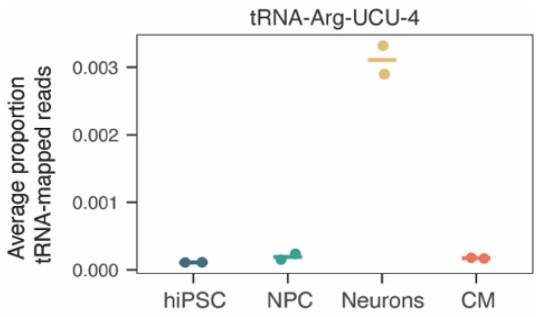

Figure 2.5. mim-tRNAseq detects the upregulation of tRNA-Arg-UCU-4 specifically in neurons. The expression of neuron-specific tRNA-Arg-UCU-4 in four human cell lines was assessed by examining the proportions of tRNA-aligned reads from mim-tRNAseq. The line in the graph represents the mean value from 2 biological replicates, while the dots display individual sample values.

2.1.3 tRNA transcript levels vary greatly across differentiation

We next analyzed the variation in tRNA transcript levels across differentiation. The high reproducibility among biological replicates was evidenced by the principal component (PC) analysis (**Figure 2.6a**), which identifies the main axes of variance and the key variables within

a data set. The first PC that reflects cell differentiation comprises 89% of the variation, indicating the distinct composition of tRNA transcripts pools in proliferating hiPSC and NPC, as well as in NPC and neurons. Cardiomyocytes were also reproducibly distinguished from hiPSC and differentiated neuronal cell lines, with 6% variation across the PC2, indicating that variation in tRNA transcript abundance can faithfully discriminate different human cell types and individual stages of cell differentiation (**Figure 2.6a**).

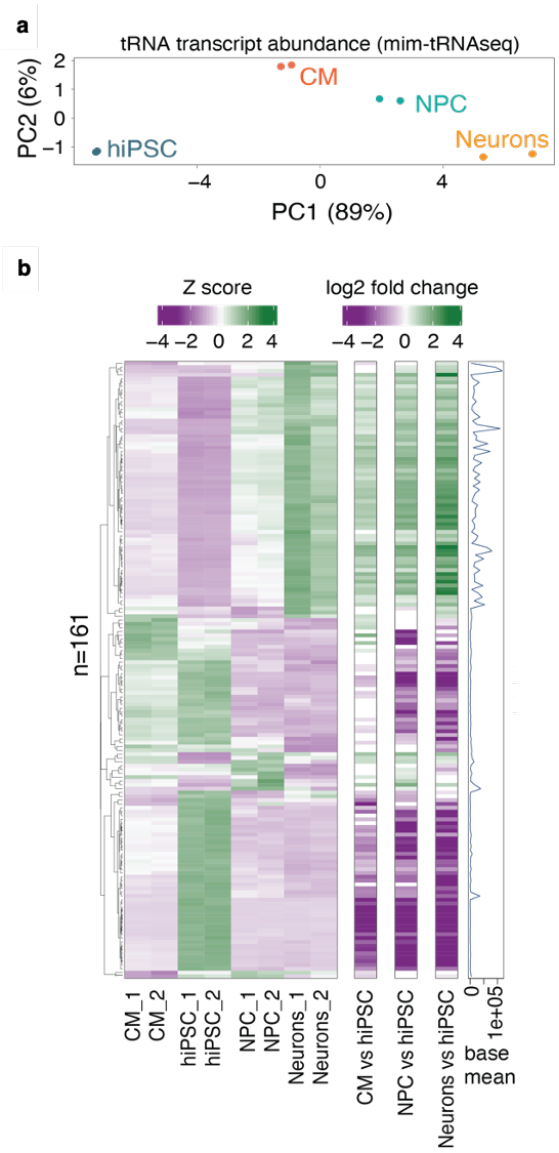

Figure 2.6. tRNA transcript pools are highly dynamic across differentiation. a, Principal component analysis (PCA) performed on count data transformed with variance stabilization for tRNA transcripts in DESeq2 from each cell line with 2 biological replicates. The variance explained by principal components is indicated in parentheses within the axis titles. **b,** Heatmap of the dynamic expression patterns of tRNA transcripts, showing only the tRNA transcripts with differential expression in at least one of differentiated cell types compared to hiPSC. Differential expression was determined using the Wald test with a false discovery rate (FDR) threshold of ≤ 0.05. Left panel: expression heatmap with hierarchically clustered data, showing the scaled Z scores of normalized transcript counts in CM, hiPSC, NPC and neurons, each with two biological replicates. Middle panels: differential tRNA transcript expressions of CM, NPC and neurons relative to hiPSC, presented as log2 fold changes. Right panel: base mean values normalized for each tRNA transcript across all of the samples.

We then analysed the differential expression of tRNA transcripts in NPC, neurons, and CM compared to hiPSC with DESeq2. Of the 373 nuclear-encoded tRNA transcripts we could resolve by mim-tRNAseq, 161 showed significantly differential expression (up to ~70-fold) in differentiated cells compared to hiPSC (*p-adj* ≤ 0.05, **Figure 2.6b, Table S1**). From the

remaining 212 tRNA transcripts, 205 had zero or very low counts (<0.005% of tRNA-mapped reads). Besides the pronounced increase of tRNA-Arg-UCU-4 in neurons (**Figure 2.5**), the transcripts with low expression (low base mean in **Figure 2.6b**, right panel**)** exhibit the strongest magnitude changes. These transcripts were significantly downregulated upon differentiation in both neuronal and cardiac cultures (**Figure 2.6b**). The alteration of tRNA abundance identified by mim-tRNAseq were highly concordant with the levels of three tRNA transcripts in Northern blotting analysis (tRNA-Arg-UCU-4, tRNA-Asn-GUU-1 and tRNA-Gly-CCC-2; **Figure 2.7**), validating the quantitative nature of our mim-tRNAseq measurements. Collectively, these data show that human tRNA transcript pools are extensively remodeled during differentiation.

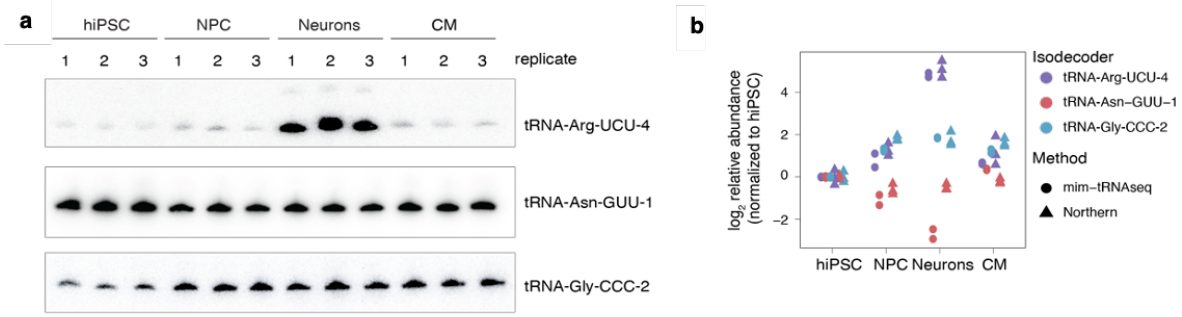

Figure 2.7. mim-tRNAseq accurately quantifies changes in tRNA abundance during differentiation. a, Northern blot analysis for tRNA-Arg-UCU-4, tRNA-Asn-GUU-1, and tRNA-Gly-CCC-2 across all cell types, each with 3 biological replicates. Matched samples that corresponded to those for mim-tRNAseq were used. **b,** Relative levels of tRNA-Arg-UCU-4, tRNA-Asn-GUU-1, and tRNA-Gly-CCC-2 quantified with mim-tRNAseq (**Figure 2.6b,** 2 biological replicates) and Northern blotting (**a**) from matched samples, with values normalized to the mean in hiPSC.

2.1.4 tRNA anticodon and isotype pools vary to a much lesser extent

To define how this extensive reprogramming of tRNA transcripts impacts anticodon pools, uniquely mapped tRNA reads were summed within each anticodon family prior to differential expression analysis by DESeq2. Out of the 57 anticodon families encoded by the full set of predicted human tRNA genes, 9 were not expressed in any of the cell types we profiled (**Table S2**). 47 of the remaining 48 anticodon families were shown to be robustly expressed in all cell types, and tRNA-Ile-GAU was only detectable at very low levels in hiPSC (0.002% of uniquely mapped reads, compared to 2.9% and 0.8% for tRNA-Ile-AAU and tRNA-Ile-UAU, respectively; **Table S2**). PC analysis showed that different cell types can be well resolved by anticodon-based tRNA abundance, while maintaining high reproducibility between duplicates

(**Figure 2.8a)**. DESeq2 analysis revelaed that 46 tRNA anticodon families were regulated differentially in at least one of the differentiated cell types compared to hiPSC (*p-adj* ≤ 0.05, **Figure 2.8b**, **Table S2**).

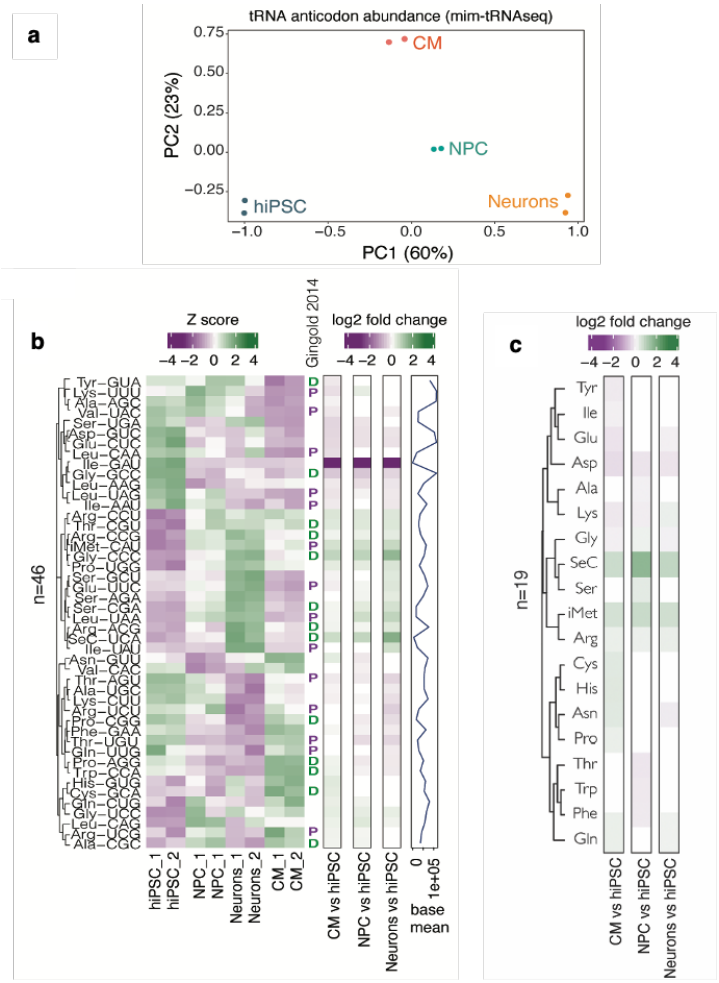

Figure 2.8. tRNA anticodon and isotype pools are largely stable during differentiation. a, PCA as conducted in **Figure 2.6a** using variance stabilizing-transformed counts aggregated by tRNA anticodon. **b,** Heatmap as in **Figure 2.6b** for count data aggregated by tRNA anticodon. Anticodon families linked to proliferating ("P") or differentiated ("D") cells, as presented in Gingold *et al.* 2014, are labeled. **c,** Differential expression as in **Figure 2.6b** and **(b)** middle, count data summed by tRNA isotype for CM, neurons and NPC relative to hiPSC, reported as $\log_2$ fold changes.

In contrast to the large fold changes we found for individual tRNA transcripts, the differences for tRNA abundance at the anticodon level were of a much smaller magnitude. A strong decrease was observed for tRNA-Ile-GAU, which was only detectable in hiPSC. Besides this, the largest differences in differentiated cells relative to hiPSC were for tRNA-Gly-CCC that was upregulated by 1.5 to 2.5-fold, and the selenocysteine-inserting tRNA-SeC-UCA, with a 3-fold increase. Changes of the remaining tRNA anticodons were to a markedly smaller extent, only up to 0.7 to 1.7-fold (**Figure 2.8b**, **Table S2**). Moreover, we did not find a distinct segregation of anticodon pools between actively dividing cells (hiPSC and NPC) and non-dividing post-mitotic cells (neurons and CM). Likewise, there was no substantial overlap among the tRNA anticodon families that exhibited significant changes in abundance in NPC,

neurons or CM lines, whether they were associated with differentiation ("D") or proliferation ("P") tRNAs identified in prior studies (**Figure 2.8b**, **Table S2**). When tRNA-mapped reads were summed based on their isotypes (tRNAs recognizing one or more codons but carrying the same amino acid), the differences in tRNA abundance between cell types were even less pronounced (**Table S3**). Thus, despite extensive remodeling of tRNA transcript pools, human cells maintain largely unchanged tRNA anticodon availability during differentiation.

2.2 tRNA anticodon availability correlates with a stable codon usage and decoding rate across cell types.

We asked whether the modest differences of tRNA abundance at anticodon level are associated with differences in codon demand in the highly distinct transcriptomes of the four cell types **(Figure 2.3a**). To determine the codon demand in each cell line, we calculated codon frequency by counting the number of each codon and dividing it by the total number of codons in the coding sequence. Then we weighted codon frequencies by multiplying the codon frequency with normalized expression of transcripts from RNA-Seq data, and summed the weighted codon usages from all transcripts to get the overall weighted codon usage. Examination for all 61 sense codons revealed a striking lack of variance in codon demand among all four cell types (coefficient of variation 0.77 - 13.22%; **Figure 2.9**), in line with prior studies showing relatively stable codon demand in different mammalian tissues and developmental stages (Kutter et al. 2011a; Schmitt et al. 2014).

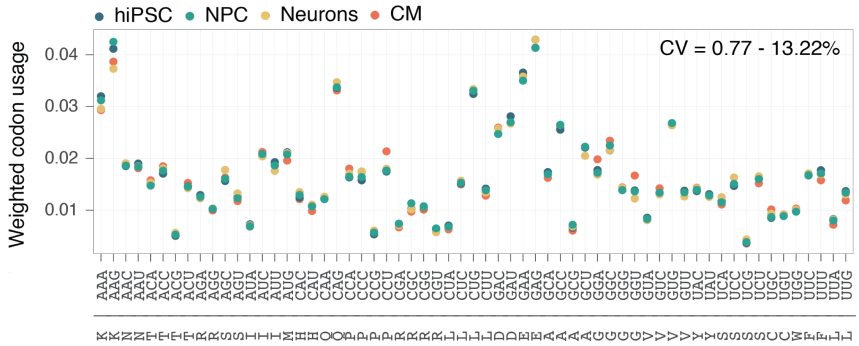

Figure 2.9. Codon usage is stable across differentiation. Codon usage aggregated and weighted by transcript expression (TPM) using RNA-Seq data across all transcripts. The values displayed per codon represent the mean weighted codon frequencies from two biological replicates per cell type, shown as proportions out of the total codon usage values. The range of coefficient of variation (CV) for each codon is shown in the top right corner. The x-axis labels the codon sequence. The corresponding amino acids are represented in single-letter codes.

Across different cell types, we observed robust positive correlations between mRNA codon usage and the abundance of tRNA anticodons, with similar magnitude (Pearson's r= 0.57 - 0.63; **Figure 2.10a**). Interestingly, the codon usage of mRNAs with universally high abundance across all four cell types exhibited a stronger correlation with tRNA anticodon levels compared to the codon usage observed in highly abundant transcripts specific to individual cell types (median Pearson's median Pearson's r=0.39 - 0.45 vs r=0.36 - 0.42; **Figure 2.10, b-c**). This could be due to the fact that mRNAs that are commonly abundant across different cell types may be under stronger selection pressure to optimize their codon usage to match the available tRNA anticodon pools. We conclude that across different human cell types, tRNA anticodon abundance is equally well adjusted to the relatively stable codon demand.

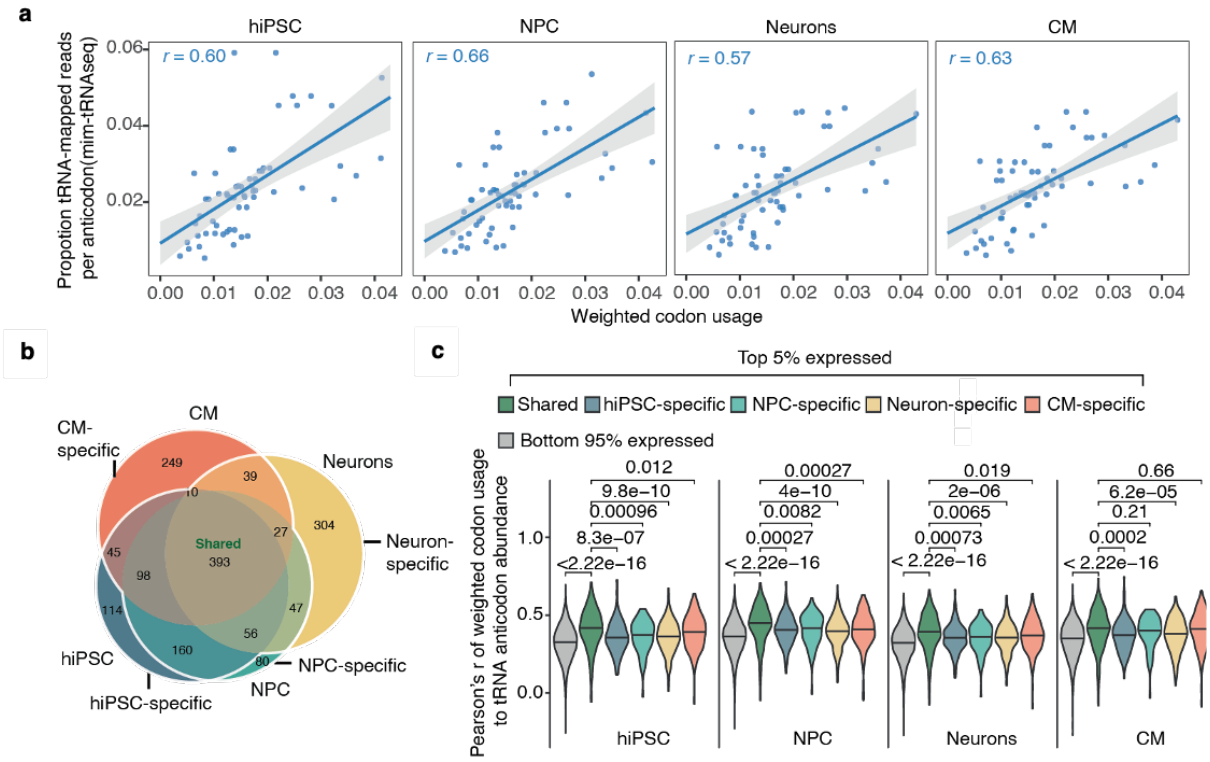

Figure 2.10. tRNA abundance correlates with codon usage in human cells, showing optimization in specific transcript sets. a, The correlation between the mean weighted codon usage and the mean tRNA anticodon abundance measured with mim-tRNAseq method scaled to proportions of the total tRNA-mapping reads from two biological replicates for each cell line. The solid blue lines represent the linear regression model. The shaded gray area indicates the 95% confidence interval (CI). **b,** The size and overlap of the gene sets with the highest expression (top 5%) examined using mean TPM values from two biological replicates for each cell type. The categorized cell-type or state-specific gene sets are indicated, as well as shared sets showing overlap between different cells. **c,** Violin plots illustrating the Pearson's correlation coefficient distributions between the mean weighted codon usage and mean tRNA anticodon abundance for each transcript, as determined in (**b**). The center lines represent the median values. P-values were computed using the Kruskal-Wallis test based on ranks.

The ratio of codon demand to tRNA supply should remain constant in different cell types if both variables change concordantly during differentiation. However, with a stable usage of different codons across differentiation, the small but significant changes of tRNA anticodon levels we detected upon differentiation led to divergent supply to demand ratios between cell types (**Figure 2.11**). For example, with an invariant usage of its cognate GGG codon (**Figure 2.9**), the most strongly up-regulated anticodon family tRNA-Gly-CCC (1.8 - 2.5-fold; **Table S2)** resulted in a higher tRNA supply to codon demand ratio in differentiated cells than hiPSC (**Figure 2.11**). To test whether these variations in tRNA anticodon abundance impact decoding rates, we measured codon dwell times of the 61 sense codons in hiPSC and NPC with ribosome profiling.

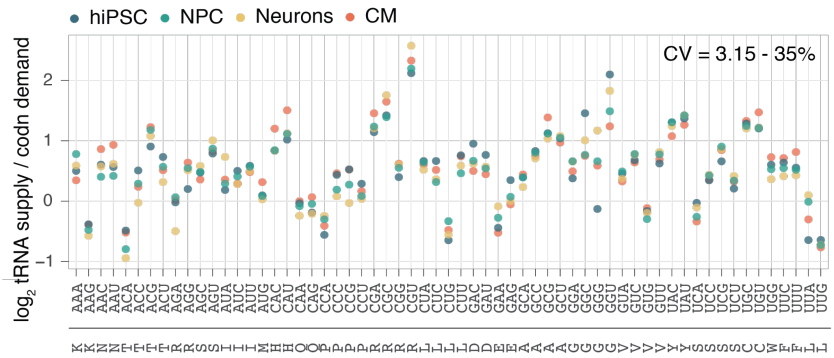

Figure 2.11. tRNA supply to demand ratios across cell types. Log_2 tRNA supply to codon demand ratios per codon. Mean tRNA anticodon abundance as a proportion of all tRNA-mapped reads from mim-tRNAseq for each cell type (n = 2) were divided by proportional mean weighted codon usages for corresponding codons (as in **Figure 2.9**). X-axis labels: codon sequence and corresponding amino acid in single-letter code.

Codon dwell time refers to the time that a ribosome spends at a particular codon during translation of mRNA into protein. It is influenced by various factors, such as the codon usage patterns in the mRNA, the abundance and availability of tRNA molecules, and the interactions between the ribosome and mRNA (Gobet et al. 2020a; Weinberg et al. 2016). Codon dwell time can be measured *in vivo* with ribosome profiling, which relies on the protection of a short segment of mRNA by a translating ribosome from nuclease digestion (Ingolia et al. 2009), generating ribosome-protected fragments (RPFs). If a particular codon is translated slowly, the ribosome will remain at that position for a longer period, and footprints generated by ribosomes at this position would be more prevalent in sequencing libraries. Therefore, the number of ribosome footprints generated along an mRNA can provide insight into the rates of translation of individual codons in living cells.

In ribosome profiling, two widely used translation inhibitors for eukaryotic cells are cycloheximide (CHX) and tigecycline (TIG). CHX binds to the exit (E)-site of the large ribosomal subunit (Klinge et al. 2011). This inhibits elongation by preventing the release of deacylated tRNA from the E-site and trapping peptidyl-tRNA in the 40S A site (aminoacyl-tRNA site or acceptor site), impeding subsequent ribosomal translocation (Schneider-Poetsch et al. 2010). Tigecycline (TIG) is an antibiotic similar to tetracycline that has been shown to obstruct tRNA accommodation by binding to and inhibit GTPases, such as eEF1A and eIF5A, thereby reducing aminoacyl-tRNAs binding at A site (Jenner et al. 2013). To avoid disrupting ribosome dynamics (Hussmann et al. 2015), translation inhibitors were not used to pre-treat the cells prior to lysis, but were rather directly added to the lysates during sample preparation (Wu et al. 2019). In yeast, compared to samples supplemented with only CHX, a cocktail of CHX and tigecycline (TIG) enriches short footprints from ribosomes in the process of decoding (Wu et al. 2019). Therefore, we compared the effect of CHX alone and CHX together with TIG on codon dwell time measurements by ribosome profiling in human cells. Both treatments generated ribosome footprints with two predominant sizes in human cells: 20-23 nt (short) and 28-33 nt (long) (**Figure 2.12a,b)**, which likely represent ribosomes with two distinct elongation states, open and occupied ribosomal A sites, respectively (Lareau et al. 2014; Wu et al. 2019). Interestingly, the inclusion of CHX and TIG in lysates did not alter the ratio of short to long footprints in comparison to CHX only.

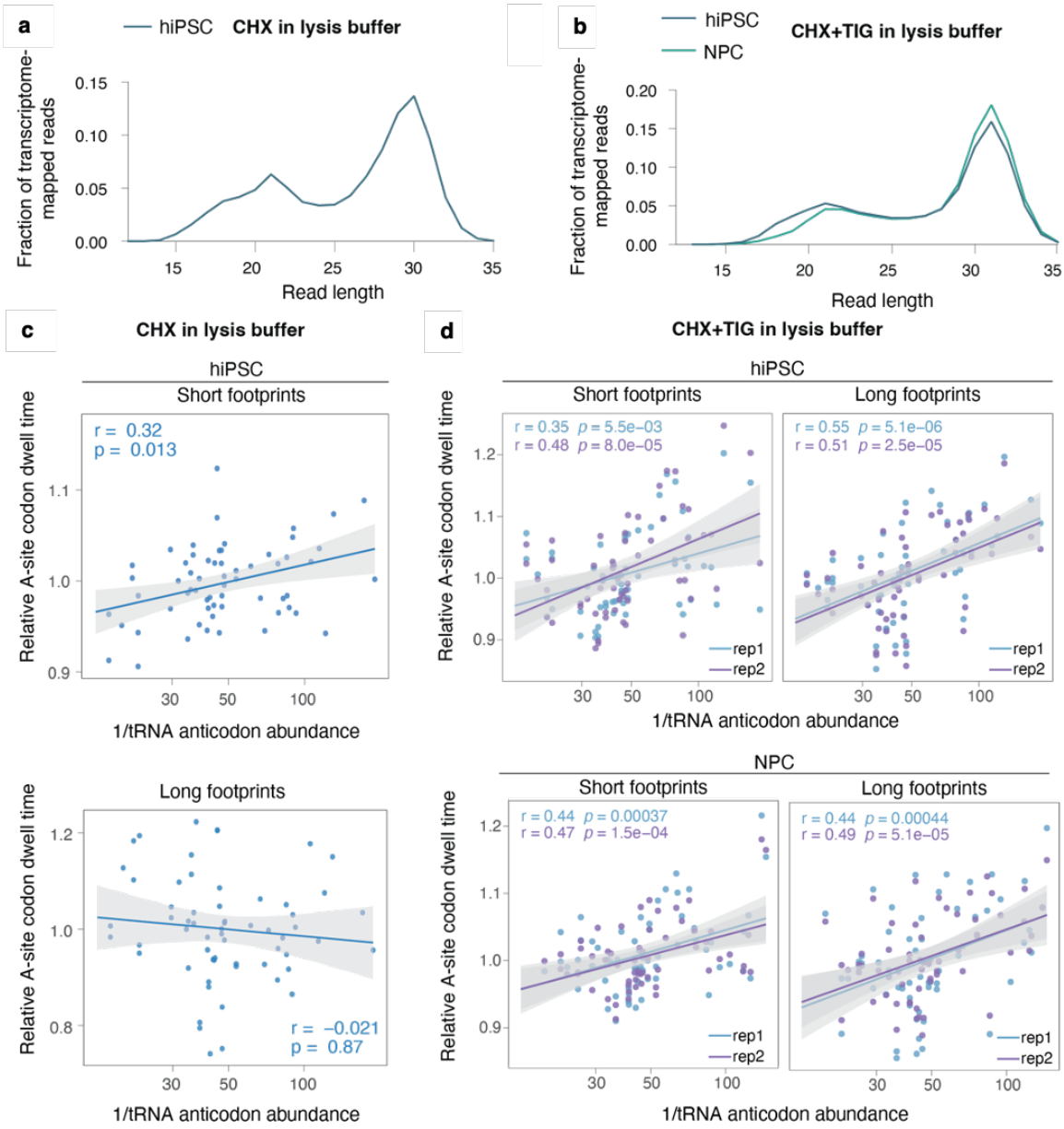

Figure 2.12. tRNA anticodon levels correlate with decoding rates across cell types. a-b, Representative distributions of read lengths in (**a**) ribosome footprints derived from extracts of hiPSC supplemented with CHX only, and (**b**) ribosome footprints obtained from extracts of hiPSC and NPC supplemented with both CHX and TIG. **c-d**, The correlation between codon dwell time assessed with Scikit-ribo and the reciprocal of tRNA anticodon abundance for short (20-22 nt) and long (28-32 nt) footprints obtained from (**c**) hiPSC libraries (single replicate) prepared with only CHX, as well as (**d**) hiPSC and NPC extracts (two biological replicates shown as rep1 and rep2) supplemented with both CHX and TIG. The solid blue lines represent the linear regression models. The shaded gray area indicates 95% confidence interval (CI). The Pearson's correlation coefficients are provided.

Codon dwell times were then calculated with Scikit-ribo, an analysis tool for predicting ribosome A-site locations with a random forest classifier (Fang et al. 2018). We found that in hiPSC with CHX treatment alone, codon dwell times were only modestly correlated with the

reciprocal of tRNA anticodon levels (1/tRNA) for short footprints (Pearson's r=0.32; p=0.01), and no significant correlation was detected for long footprints (Pearson's r=-0.047; p=0.72; **Figure 2.12c**). However, when treated with CHX and TIG together, both hiPSC and NPC show strong anti-correlation between codon dwell times and the cognate tRNA anticodon abundance, with a Pearson's r of 0.44-0.55 for long footprints and 0.38-0.48 for short footprints (**Figure 2.12d**). These findings demonstrate the importance of tRNA anticodon availability in driving ribosome decoding rates in human cells.

However, individual codon dwell times in hiPSC and NPC were strongly correlated (Pearson's r=0.9, p=2.6e-23) and showed no clear dependence on the differences of cognate tRNA abundance between these cell types (**Figure 2.13a**). For example, tRNA-Gly-CCC is upregulated by 1.7-fold in NPC but the ribosome dwell time at the matching GGG codon increases by only 5%. Ribosome dwell times at codons GGC and GGU remain identical in hiPSC and NPC despite a 1.6-fold decrease in the abundance of their cognate tRNA-Gly-GCC in NPC (**Figure 2.13b, Table S4**). These data suggest that the variation in tRNA anticodon pools between NPC and hiPSC is insufficient to cause a substantial change in decoding speed.

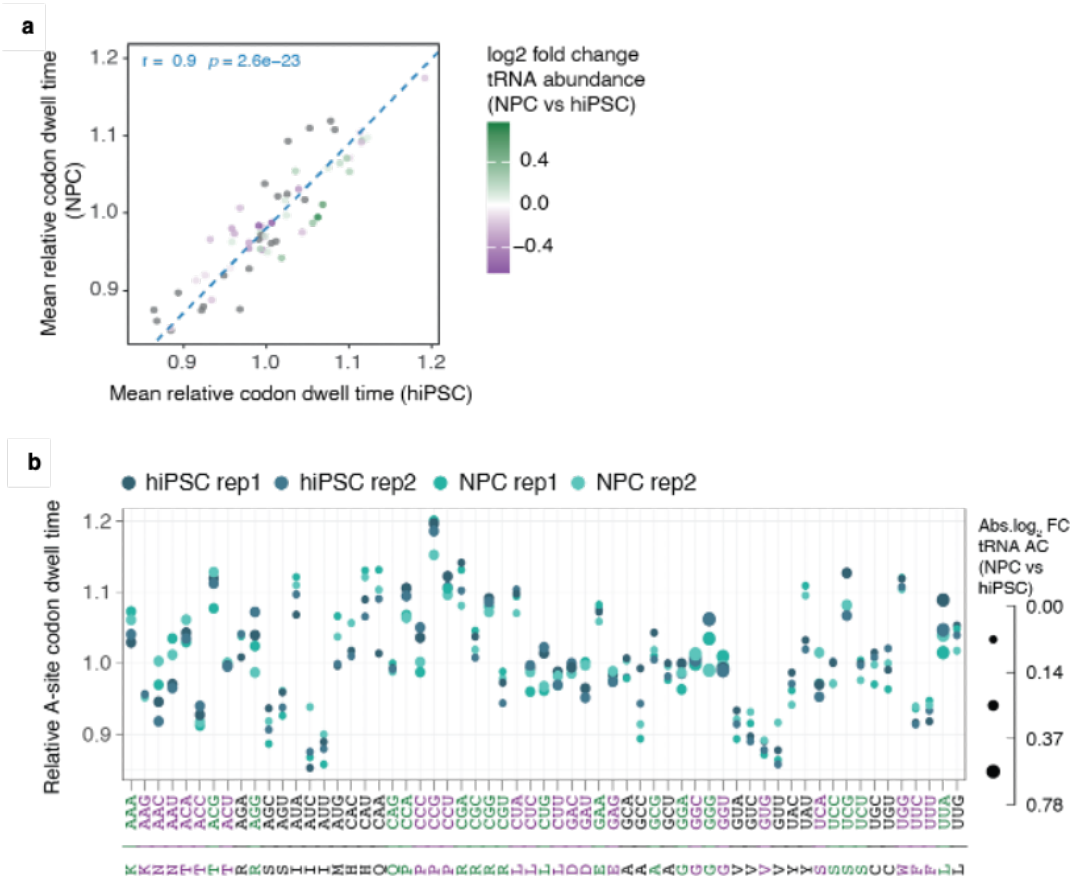

Figure 2.13. Divergence in tRNA anticodon abundance does not substantially alter the decoding rate. a, The correlation between the mean codon dwell time (long footprints in Fig. 12d) in hiPSC and NPC. The data points were colored based on the log2 fold changes in tRNA anticodon abundance measured in NPC compared to hiPSC. Gray dots indicate non-significant changes (adjusted p-value ≤ 0.05). **b,** The codon dwell times assessed using long footprint fragments (28-33 nt) obtained from two biological replicates of hiPSC and NPC extracts supplemented with both CHX and TIG. The size of each dot indicates the absolute log2 fold change of tRNA abundance aggregated at anticodon level in NPC compared to hiPSC (FDR ≤ 0.05). The direction of change is represented by the color of the codon label, where green indicates upregulation of the matched tRNA anticodon in NPC, and purple indicates anticodon levels downregulated.

2.3 tRNA anticodon levels are buffered through the stable expression of major isodecoders

Next, we sought to elucidate the molecular mechanisms underlying the differences in magnitude that we observed between alterations in tRNA transcript abundance and anticodon levels (**Figure 2.6b, 8b**). We hypothesized that this may be due to the uneven contribution of various isodecoders to the mature tRNA pools. In order to test this, we first determined the count of isodecoders within each anticodon family using all predicted human tRNA genes (Chan et al. 2021). Subsequently, we counted the isodecoders that collectively accounted for 90% or more of the total reads mapped to mature tRNAs for each anticodon family, which we referred to as "major isodecoders". Although the number of isodecoders for predicted human tRNA genes exhibit a range of 1 to 26 per anticodon family, the majority of mature tRNA anticodon families in hiPSC consists of one to four major isodecoders (**Figure 2.14a, b; Table S5**). This number declines upon differentiation, resulting in most anticodon families being composed of just one to two major isodecoders in NPC and neurons (**Figure 2.14c**). For example, a total of nine isodecoders for tRNA-Ala-UGC are encoded by the human genome, and six of them are identified in mature hiPSC tRNA pools with varying levels of abundance. Two of the most abundant ones tRNA-Ala-UGC-3 and tRNA-Ala-UGC-4 are preferentially used and become the major isodecoders for this anticodon family in CM, NPC, and neurons (**Figure 2.14c**). Likewise, out of the five predicted isodecoders for tRNA-Pro-UGG, three are expressed in hiPSC and the two most abundant isodecoders dominate the mature tRNA-Pro-UGG population following differentiation (**Figure 2.14c**).

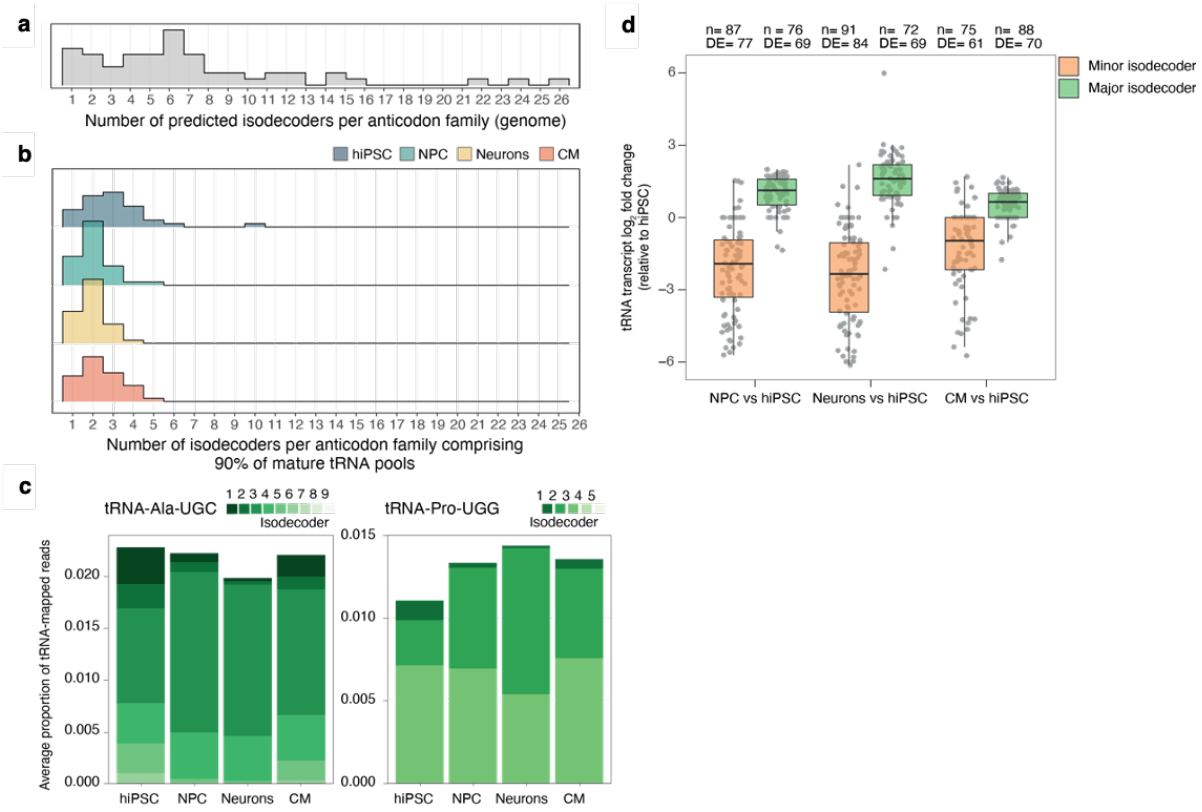

Figure 2.14. Human anticodon pools are buffered via stable expression of major tRNA isodecoders. a, The distribution of tRNA gene copy numbers per isodecoder within each anticodon family across all predicted tRNA genes in the human hg38 genome. **b,** The distribution of isodecoder count per tRNA anticodon family accumulatively comprising at least 90% of each anticodon in each of the four cell types. The isodecoder abundance represents the average proportions of reads per unique transcript obtained from mim-tRNAseq (n = 2) for anticodon families where unique transcripts have been fully resolved. **c,** The changes in proportional isodecoder composition for tRNA-Ala-UGC (left) and tRNA-Pro-UGG (right) during the differentiation. The values represent the mean proportions of tRNA-mapped reads for each isodecoder obtained with mim-tRNAseq from two biological replicate samples. The isodecoders are ordered from top to bottom in ascending order based on the unique isodecoder number in its gene name. **d**, Box plots representing the log2 fold change in tRNA transcript expression between differentiated cells and hiPSC (p-adj ≤ 0.05) for transcripts that exhibited measurable expression in at least one cell line (≥0.005% of tRNA-mapped reads). The transcripts were further categorized based on their major or minor occupancy in the anticodon pools in each cell type. The labels include the total count of transcripts ("n") and the number of transcripts that exhibit significant differential expression ("DE") in each group. The center line and label represent the median value, while the box limits represent the upper and lower quartiles. The whiskers extend to 1.5x the interquartile range.

Globally, in differentiated cell types, the vast majority of minor isodecoders (71 - 87%) exhibited significant downregulation compared to hiPSC, with fold changes of up to 70-fold (**Figure 2.14d**). By contrast, the abundance of most major isodecoders shows an increase in differentiated cells compared to hiPSC, although the magnitude of this increase is relatively

modest, ranging from approximately 1.2 to 4-fold (excluding the exceptional 63-fold upregulation of tRNA-Arg-UCU-4 in neurons). These data show that isodecoders contribute unevenly to the pool of translationally competent tRNAs in human cells.

2.4 Pol III transcription is restricted to housekeeping tRNA genes during differentiation

2.4.1 Optimization of Pol III ChIP-Seq

To elucidate the mechanisms underlying the stable expression of major isodecoders, we asked whether mature tRNA abundance in human cells is driven by the transcriptional activity of tRNA genes. To test this, we analysed genome-wide Pol III occupancy landscapes by chromatin immunoprecipitation sequencing (ChIP-Seq). Although being extensively used as a powerful tool to map DNA-binding protein profiles and histone modifications across the genome, ChIP-Seq is still hindered by the lack of standardization in the first chromatin shearing step of the experimental workflow. The traditional nuclei extraction and chromatin shearing processes face three major challenges:

1. Large input material requirements, which makes ChIP cost-ineffective and labor-intensive, especially for differentiated cells.

2. Lysis of cell membrane with hypotonic buffers and homogenization with mechanical dounces often fail to effectively extract the nuclei of fixed cells.

3. Depending on the variable extent of nuclei extraction by the traditional workflow, the chromatin shearing steps (e.g., buffer composition and shearing strength) often need to be optimized for individual input materials to ensure the quality of chromatin and guarantee the sequencing results. Shearing conditions also vary largely among distinct samples, such as different types of cultured cell lines and primary tissues.

Together, these issues undermine ChIP reproducibility and make data comparison among different cell types challenging.

Nuclei extraction optimization with NEXSON

To avoid these drawbacks, we used Nuclei EXtraction by SONication (NEXSON) (Arrigoni et al. 2016). Instead of the typical chemical and mechanical treatment in the nuclei extraction step,

this method introduces a brief sonication to disrupt the cell membrane and release the nuclei. This ensures nuclei isolation with high quality and purity from a wide range of formaldehyde-fixed cells, tissues, and organisms. For efficient nuclei isolation and complete removal of cytoplasm, we first tried a range of sonication period of 60 seconds, 90 seconds and 120 seconds in mESC cells (**Figure 2.15a**), one of the model cell lines included in the recommended NEXSON protocol (Arrigoni et al. 2016). We found that 120 seconds of sonication gave the cleanest nuclei isolation (**Figure 2.15a**). To exclude a negative effect of cell clustering on nuclei isolation, given the large cell cluster patches in the untreated sample without sonication (**Figure 2.15a,** left panel), we also compared the sonication with and without prior cell singularization by accutase. The cells were either crosslinked in culture plate in monolayer, named as " plates" (**Figure 2.15b,** upper panels), or first singularized by accutase then crosslinked by resuspension in tubes, named as "singularized" (**Figure 2.15b,** lower panels). Surprisingly, singularization did not enhance the nuclei isolation efficacy, but instead decreased the sheared chromatin quality by leaving fragments > 1000 bp, above the optimal 100-1000 bp length for ChIP (**Figure 2.15c**). Therefore, we used crosslinking in plates with 120 seconds sonication for nuclei extraction throughout the rest of this work. With this optimised NEXSON protocol, we were able to substantially scale down the number of cells required to ~ 10,000 per histone mark ChIP reaction, and ~100,000 per Pol III ChIP reaction.

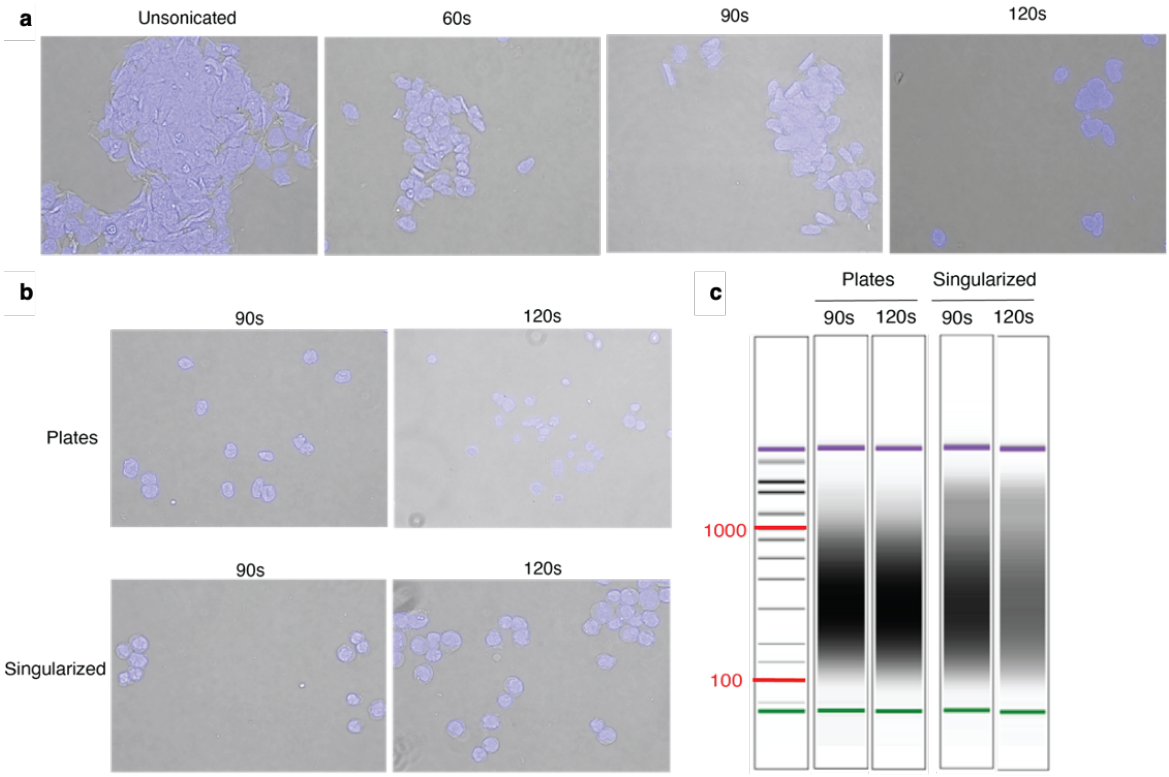

Figure 2.15. Nuclei extraction by sonication (NEXSON) from cells fixed with formaldehyde. a, Formaldehyde-fixed mESCs were sonicated in nuclei extraction buffer for 60s, 90s and 120s. Images in the DAPI (blue, nuclei) channel and differential interference contrast (DIC) channel were captured before (untreated) and after sonication. **b,** hiPSC were crosslinked with formaldehyde in plates (upper) or singularized with accutase before crosslinking (lower), followed by sonication for 90s and 120s. Images were captured in DAPI (blue, nuclei) and differential interference contrast (DIC). **c**, Size distribution determined by Agilent 2100 Bioanalyzer for hiPSC with treatment in (**b**). 100bp and 1000bp were highlighted and labeled in red.

Crosslinking and chromatin shearing optimization

To achieve the 100-1000 bp DNA fragment size that is recommended for ChIP-Seq (Landt et al. 2012), we tested different combinations of formaldehyde concentration and chromatin shearing time. Using 0.5% and 0.8% of formaldehyde (FA), with 10 minutes crosslinking in "plate" and 120 seconds sonication for nuclei isolation, 10 minutes shearing results in a left-shifted size distribution for 0.8% formaldehyde (**Figure 2.16a,** right panel) compared to 0.5% (**Figure 2.16a,** left panel). This indicates that the lower concentration of formaldehyde (0.5%) is less efficient in crosslinking, and 10 minutes is insufficient for chromatin shearing to the required fragment size. With 15 minutes shearing, a left shifting of fragment size was shown in 0.8% and 1% FA (**Figure 2.16b,** middle and right panels) compared to 0.5% FA (**Figure 2.16b,** left panel), with reduced proportion of large fragments. Therefore, we used 10 minutes crosslinking with 0.8% PA, and 18 minutes of sonication for chromatin shearing to generate the desired DNA fragment size for ChIP-Seq. Combined with an identical shearing buffer composition and sonication power, this greatly enhanced reproducibility across different input samples.

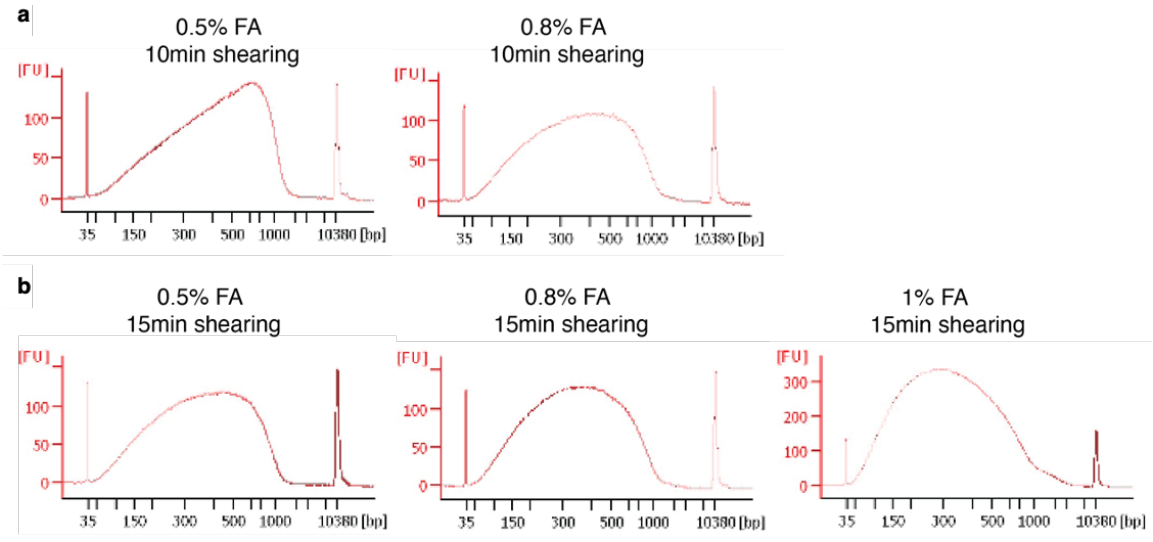

Figure 2.16. Optimization of formaldehyde concentration and chromatin shearing time for ChIP. Size distribution using different formaldehyde concentrations at 0.5%, 0.8% and 1% (left to right panels) and chromatin sheared with 10 min (**a**) and 15 min (**b**), with the same time of 10 minutes crosslinking and 120 seconds sonication for nuclei isolation. DNA size distribution was analyzed using capillary electrophoresis and generated with Agilent expert 2100 software. The x-axis represents base pairs (bp), and the y-axis represents fluorescence units (FU).

ChIP-Seq normalization with spike-in

Normalization is a critical step that accounts for systematic biases and technical variability that can arise during sample preparation, sequencing, and data processing of ChIP-Seq (Angelini et al. 2015). One commonly used normalization method is reads per million mapped reads (RPM). This method normalizes the read counts by dividing the number of reads mapping to a specific genomic location with the total number of mapped reads in the sample, and then multiplying by a scaling factor of one million. This adjusts for differences in sequencing depth between samples. However, this normalization method assumes that the number of protein-DNA interactions is proportional to the total number of reads in the sample. If there are differences in the number of peaks between samples, this assumption may not hold true, leading to inaccurate normalization. Normalization can also be done using internal control regions, which involves using regions of the genome that are known to be devoid of protein-DNA interactions. However, although processed in the same manner as the ChIP-enriched DNA, the non-enriched DNA lack specific antibodies binding in the ChIP reaction, indicating that input DNA may not reflect the same chromatin structure as the ChIP-enriched DNA, thus cannot represent the binding proportionally.

To circumvent these disadvantages, we opted for using spike-in normalization. For this, we added a small amount of *Drosophila melanogaster* chromatin and antibody at the same ratio in all chromatin samples from human cell lines at the beginning of the ChIP. *Drosophila melanogaster* chromatin is the most well-studied spike-in source for ChIP-Seq because of the high quality of its sequence assembly and the minimal overlapping of *Drosophila* genome to mouse and human genomes (~0.05%). This reduces cross-reactivity and background signals in downstream ChIP-Seq mapping (Orlando et al. 2014). Moreover, high-quality spike-in chromatin and antibodies of *Drosophila* are commercially available, eliminating the batch-to-batch variations that can arise from culturing cells and cell number estimation (Orlando et al. 2014). After library generation and sequencing, the reads are mapped to the human and *Drosophila* genomes, and the number of *Drosophila*-mapped reads can be used to correct for

technical variation and to identify global changes in protein-DNA interactions (Greulich et al. 2021). Generally, a spike-in concentration of 0.5-5% of the total experimental chromatin input is recommended. We used a ratio of 0.5% in this work and it ensures the detectability of spike-in in ChIP while maintaining a high signal-to-noise ratio. The resulting sequencing reads from spike-in were also sufficient for mapping and statistical analysis, while accounting for minimal proportion in the total sequencing reads.

Antibodies for ChIP-Seq of endogenous Pol III

For ChIP with RNA polymerase III (pol III), we tried various antibodies for different Pol III subunit proteins, including RPC4 (a gift from Nouria Hernandez), RPC7 (Santa Cruz, #21754) and RPC1 (Abcam; #ab96328). However, although some of the antibodies were validated by immunoblotting following immunoprecipitation and mass spectrometry, none of these antibodies gave specific ChIP-Seq signals, as shown by the random and even distribution of the example RPC4 ChIP-Seq reads in human genome, and detected peaks are not associated with annotated genes, similar to the input libraries without ChIP pull down (**Figure 2.17a,b**). This discrepancy of antibody efficacy could be derived from the difference of ChIP workflows used. In contrast to the non-specific signal from these antibodies in our workflow, the Pol III antibody we used for ChIP-Seq throughout this work (Cell signaling technology, #12825) recognizes the largest DNA-interacting Pol III subunit RPC1, and yields strong and specific ChIP-Seq signal at known Pol III target genes (**Figure 2.17c)**. Our chromatin shearing and sequencing protocol also yielded exceptionally high resolution even at closely spaced tRNA genes (**Figure 2.17d)**.

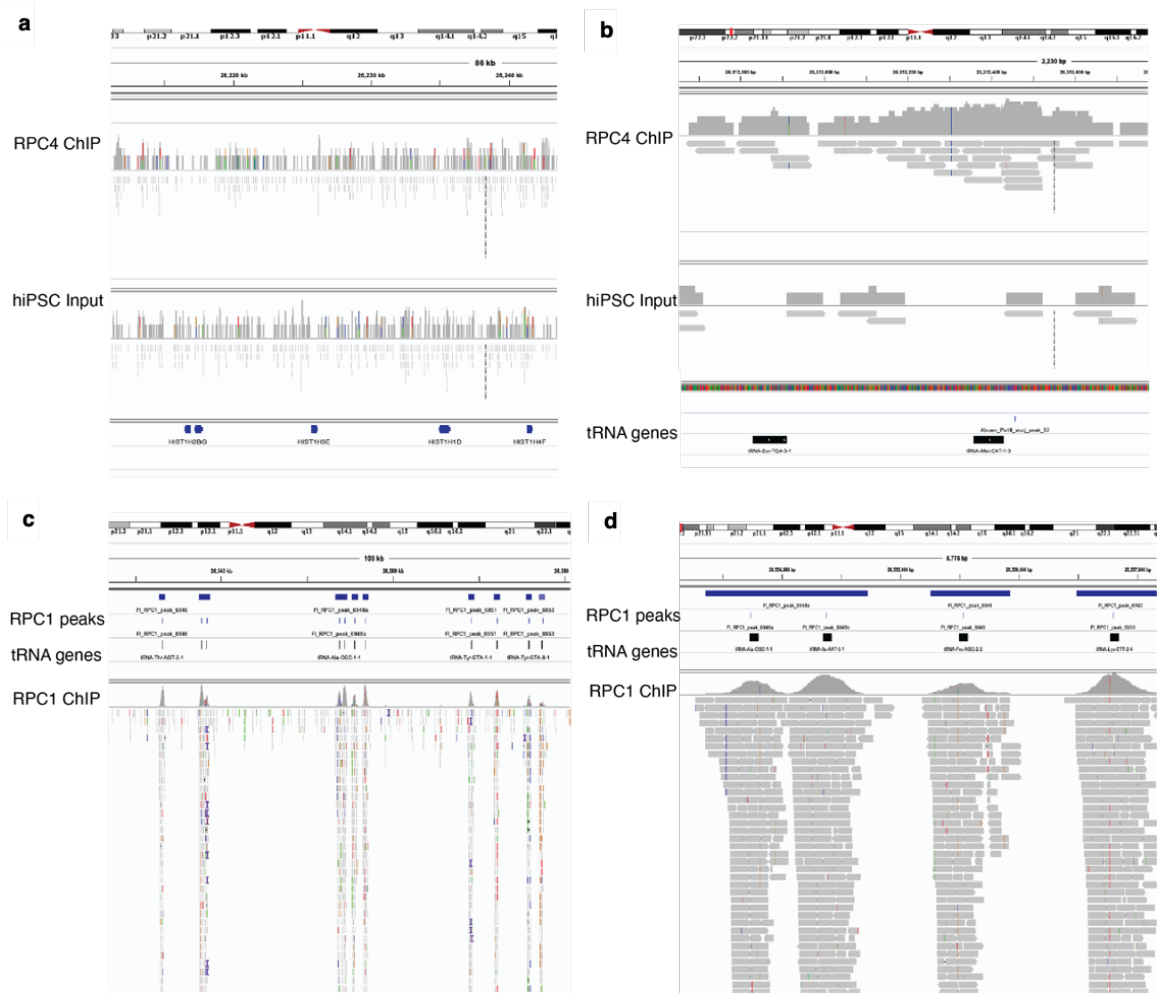

Figure 2.17. Endogenous Pol III ChIP-Seq optimization. Example IGV views with (right) or without zooming (left) for ChIP-Seq or input libraries with nonspecific RPC7 (Santa Cruz, #21754; **a,b**) and specific RPC1 (Cell signaling technology, #12825; **c,d**) antibodies. The corresponding annotated coding genes and tRNA genes are shown overlapped. All ChIP-Seq libraries were prepared with the TECAN library preparation kit.

Endogenous BRF1 ChIP-Seq optimization

Despite the strong enrichment of RPC1 at tRNA genes, the same chromatin shearing and ChIP protocol didn't yield specific peaks with a BRF1 antibody (Abcam, #ab264191). Since extended crosslinking could mask the target epitopes, or their integrity could be compromised by extensive sonication, we compared shorter crosslinking and chromatin shearing (5 minutes crosslinking and 9 minutes shearing versus 10 minutes crosslinking and 15 minutes shearing). All these variations still produce sheared fragments in the desired size range (100-1000 bp; **Figure 2.18**). Therefore, for BRF1 ChIP, we used 10 minutes crosslinking and 9 minutes chromatin shearing, which dramatically improved ChIP signal.

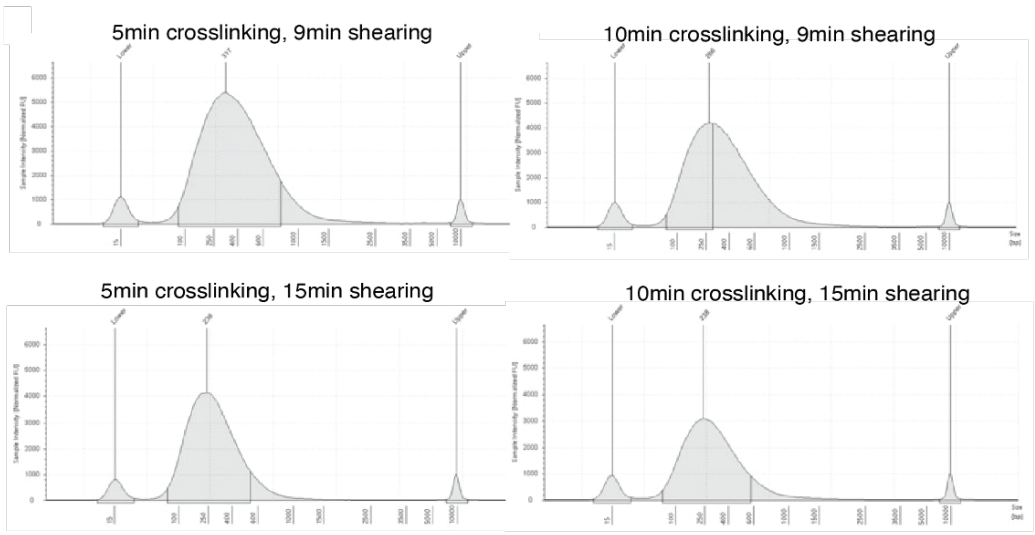

Figure 2.18. Optimization of crosslinking and chromatin shearing time for BRF1 ChIP. hiPSCs were crosslinked for 5min (left panels) and 10min (right panels), and sheared for 9min (top panels) and 15min (bottom panels), respectively. The size distribution of sheared chromatin fragments was analyzed using capillary electrophoresis and generated with 4200 TapeStation System. The x-axis represents base pairs (bp), and the y-axis represents fluorescence units (FU).

ChIP-Seq library construction optimization

We tested two kits for ChIP-Seq library construction: Ovation® Ultralow V2 DNA-Seq Library Preparation Kit from TECAN ("TECAN"; **Figure 2.19a**) and NEB Ultra II DNA library prep kit ("NEB"; **Figure 2.19b**) using the same amount of starting material from either ChIP DNA (**Figure 2.19a,b** left panel) or input chromatin samples (**Figure 2.19a,b** right panel**)**. The TECAN kit yielded libraries with a single peak for both ChIP DNA and input (**Figure 2.19a)**, while the NEB kit gave an extra peak indicative of primer dimers (**Figure 2.19b)**. In addition, the same starting amount of DNA produced higher library yields with the TECAN kit than the NEB kit (**Figure 2.19)**. Therefore, we used the TECAN kit for constructing ChIP-Seq libraries throughout this work.

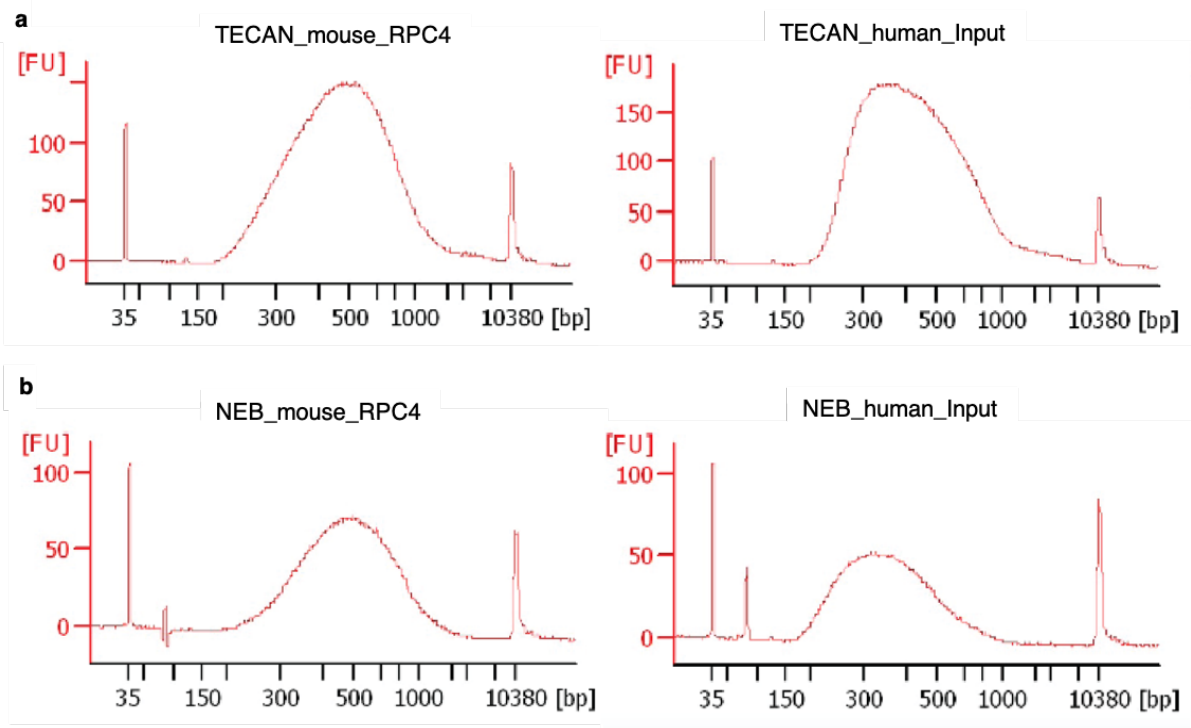

Figure 2.19. Comparison of TECAN and NEB library preparation kits. Size distribution of libraries using TECAN (**a**) and NEB (**b**) preparation kits. Same amount of material was used for library preparation, with either mouse RPC4 ChIP DNA (left) or human input (right). DNA size distribution was analyzed using capillary electrophoresis and generated with Agilent expert 2100 software. The x-axis represents base pairs (bp), and the y-axis represents fluorescence units (FU).

2.4.2 Pol III occupancy at tRNA genes predicts mature tRNA levels in human cells

We then performed ChIP-Seq for the Pol III catalytic core subunit RPC1 (Sepehri and Hernandez 1997) and the TFIIIB subunit BRF1, which recruits Pol III to tRNA genes. We performed 110-bp paired-end sequencing to maximize alignment accuracy due to the repetitive nature of tRNA genes. We found both RPC1 and BRF1 to be highly enriched at predicted tRNA genes (**Figure 2.20a**). As expected, BRF1 ChIP signal was absent from *RNAU6-1,* the spliceosomal snRNA gene that recruits Pol III through a BRF2-containing TFIIIB (**Figure 2.20b)** (Schramm and Hernandez 2002).

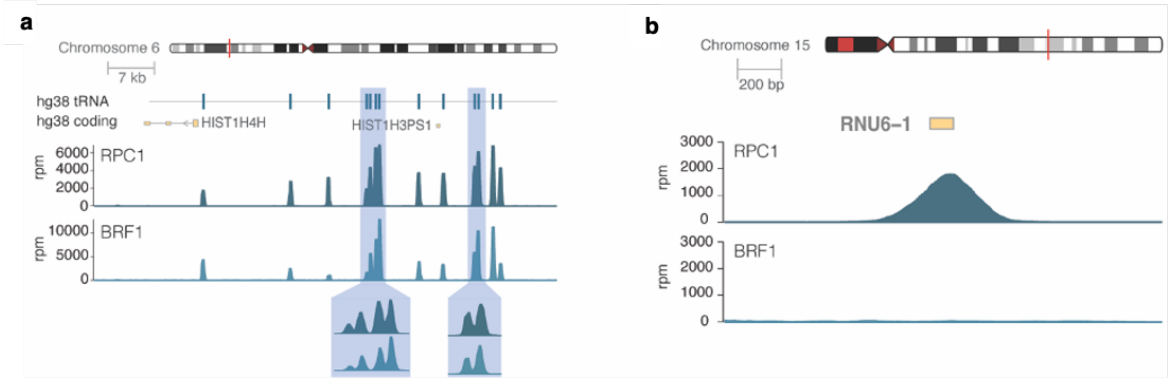

Figure 2.20. RPC1 and BRF1 are specifically enriched at predicted tRNA genes. a, The ChIP-Seq signal for RPC1 and BRF1 at predicted tRNA genes (represented by blue tick marks) is shown at a genomic locus (indicated by a red line) on human chromosome 6. The data is representatively shown from one biological replicate of hiPSC and has been normalized for estimated library sizes based on counts over extended tRNA features (±125 bp). The ChIP signal is scaled to reads-per-million (rpm). The insets highlighted in blue shadow display enlarged regions focusing on closely spaced tRNA genes. **b**, Representative view of normalized ChIP-Seq enrichment of RPC1 and BRF1 at the U6 RNA gene (*RNU6-1*) on human chromosome 15 from single biological replicate of hiPSC. The y-axis values represent the ChIP signal normalized and scaled similarly as in (**a**).

Unlike Pol II, Pol III is generally not found in an arrested state, as its occupancy at tRNA genes strongly correlates with ongoing pre-tRNA transcription (Orioli et al. 2016). To test whether Pol III enrichment at tRNA genes is a good predictor for the levels of mature tRNAs in different cellular contexts, we determined the proportion of RPC1 ChIP-Seq reads at tRNA genes, and compared it to ttRNA transcript abundances measured by mim-tRNAseq. We obtained an almost perfect linear correlation between the strength of RPC1 ChIP-Seq signal and the levels of tRNA in all four cell types (R^2=0.88 - 0.9, **Figure 2.21**). These data indicate that nearly all the variations in human mature tRNA levels can be explained by differences in Pol III occupancy, and post-transcriptional regulation has minimal impact on controlling individual tRNA levels in hiPSC and across their differentiation.

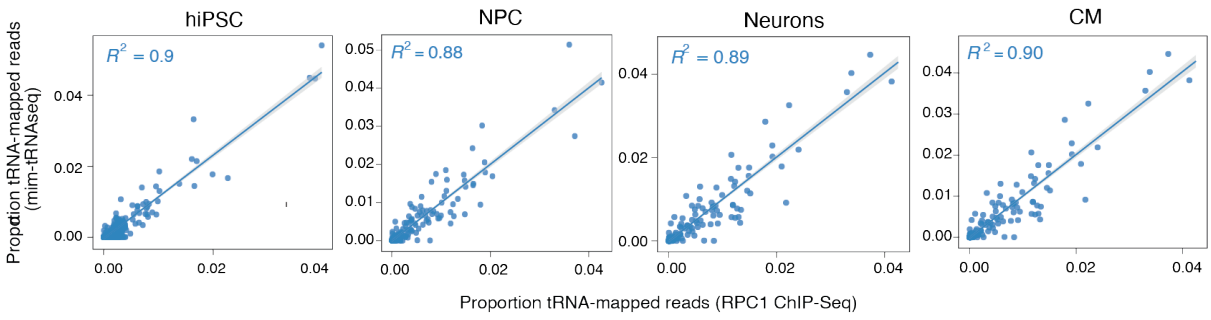

Figure 2.21. RPC1 occupancy is highly correlated with tRNA levels in all cell types. The correlation between the mean tRNA abundance per deconvoluted transcript determined with mim-tRNAseq analysis (total of 373

unique transcripts) and the average reads of RPC1 ChIP-Seq aligned to tRNA features extended by ±125 bp in two biological replicates of hiPSC, NPC, neurons and CM. Measurements are scaled to the proportions of total tRNA-mapping reads for all datasets and methods. The solid blue lines represent the linear regression models, The shaded gray area indicates the 95% confidence interval (CI). The correlation coefficients are calculated using Pearson's correlation.

2.4.3 Pol III binding is restricted to housekeeping tRNA genes during differentiation

In order to gain insights into the changes of tRNA repertoires during differentiation, we determined RPC1 and BRF1 enrichment at predicted tRNA genes by peak calling. tRNA genes with ≥25% of multimapped reads were excluded from further analysis, which enabled us to analyze the occupancy of Pol III during differentiation across 558 out of the predicted 619 human tRNA genes (90%) at single-gene resolution. With two biological replicates for each cell line, we then identified consensus peaks at the predicted tRNA genes by considering the overlap between peak sets in the ChIP-Seq libraries. We found a substantial overlap between ChIP-Seq peaks at tRNA genes for the same protein target RPC1 in biological replicates (**Figure 2.22a**). Moreover, consensus peaks for RPC1 and BRF1 almost completely overlap in the same cell line (**Figure 2.22b**), consistent with prior study suggesting that TFIIIB is necessary and sufficient for Pol III recruitment (Kassavetis et al. 1990).

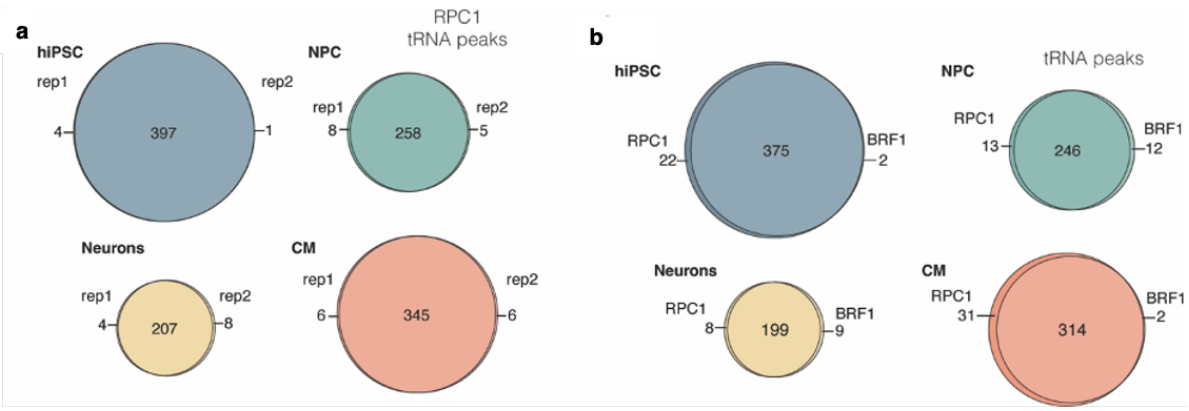

Figure 2.22. Highly reproducible ChIP-Seq data show RPC1 and BRF1 overlap at tRNA genes. a, The Venn diagram illustrating the overlap of tRNA peaks in the two replicates of RPC1 ChIP-Seq datasets. The shared peaks indicate the number of consensus peaks in each cell type. **b,** The Venn diagram displaying the overlap of tRNA peaks between two replicates of RPC1 and BRF1 ChIP-Seq consensus peak sets for each cell type.

We found that RPC1 accumulates in the vicinity of the transcription start sites (TSS) for a subset of predicted tRNA genes (**Figure 2.23a**). Moreover, we found a remarkable decrease of Pol III peak numbers at tRNA genes during differentiation. Based on this, we categorized tRNA

genes into three distinct classes. We defined the first class of tRNA genes (n=205) as "housekeeping", as they exhibited Pol III occupancy in all cell populations. Transcripts encoded by this set of genes correspond to the same 47 tRNA anticodon families that exhibited measurable expression with mim-tRNAseq (**Table S2**). When examining the isodecoder level, these housekeeping tRNA genes comprised 70% of the major isodecoders in hiPSC, and in neurons, they constituted 94% (**Figure 2.23b**). The second set consisted of tRNA genes (n=159) that did not display Pol III binding across any cell type, and we referred to them as "inactive". The third set (n=194) comprised tRNA genes where a notable RPC1 ChIP peak observed in hiPSC that was absent in one or more differentiated cell types. These genes were labeled as "repressed" (**Figure 2.23a**).

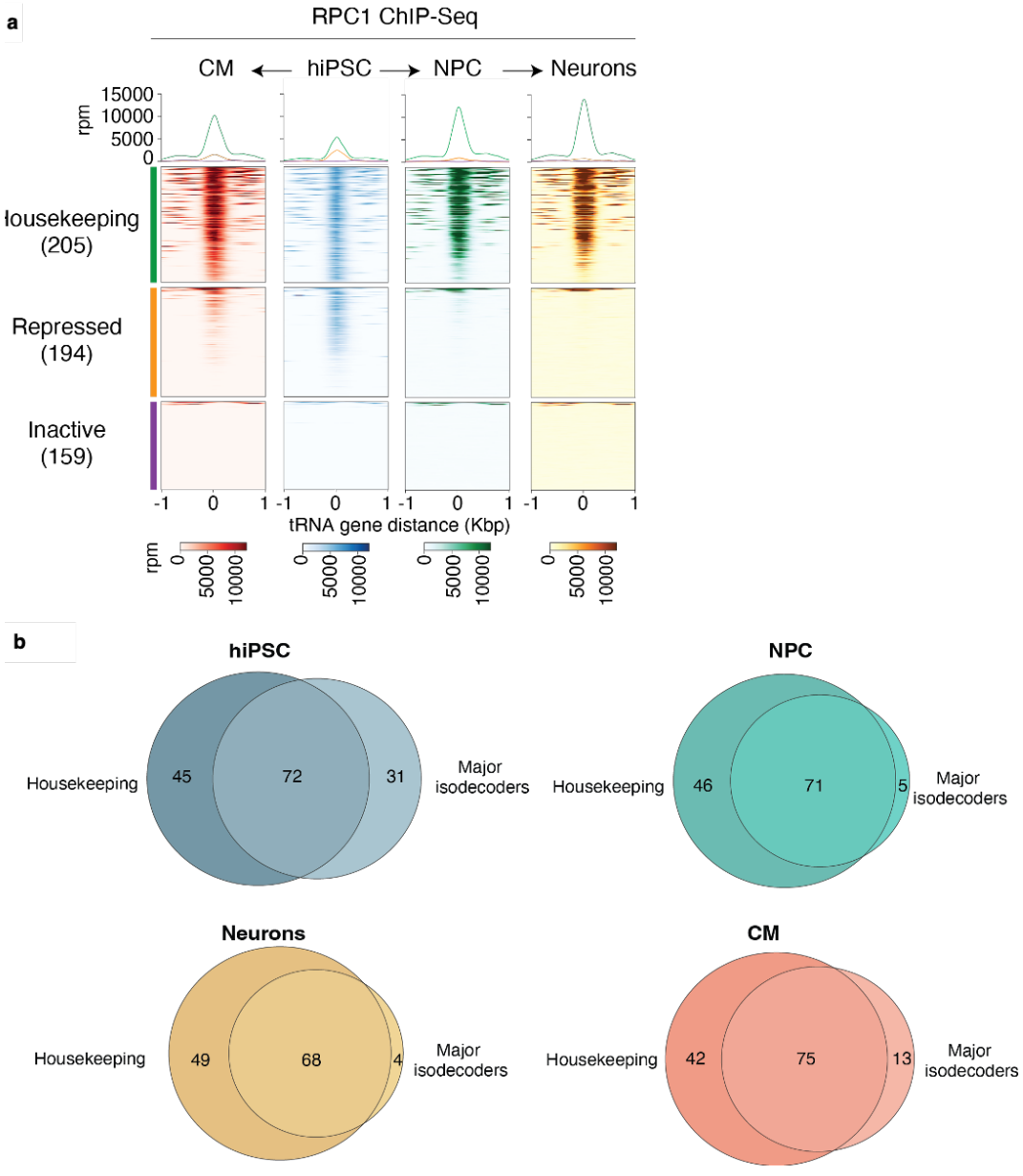

Figure 2.23. RPC1 ChIP-Seq reveals Pol III restriction at housekeeping tRNA genes which constitute major isodecoders during differentiation. a, The RPC1 ChIP-Seq heatmaps showing normalized signal surrounding the start sites of tRNA genes (±1 Kbp) in each cell type with single replicate. The tRNA genes are categorized as housekeeping, repressed, or inactive based on significant peaks in the RPC1 ChIP-Seq data (FDR ≤0.05). tRNA genes are sorted in descending order within each group according to the mean value for the respective region across all cell lines. **b**, Venn diagrams illustrating the overlap between the housekeeping tRNA gene sets determined by consensus RPC1 tRNA peaks in all four cell lines, and the major isodecoders comprising 90% of the anticodon pools measured with mim-tRNAseq data in hiPSC, NPC, neurons and CM. Housekeeping tRNA genes were consolidated based on identical transcripts to facilitate alignment with data for major isodecoders at transcript-level.

We observed the largest number of RPC1 peaks overlapping with tRNA genes in hiPSC (n=397), whereas subsets of these peaks are present in differentiated cells (**Figure 2.24a**). We did not identify any tRNA genes that gained extra RPC1 ChIP peaks in CM. However, from NPC and neurons, each peak set contained an additional gene with one peak that was not detected in all the other cell types (**Figure 2.24a**). Consistently, no mature tRNA transcripts were found to be absent in hiPSC (<0.005% of tRNA-mapped reads) but present in any of the differentiated cell types.

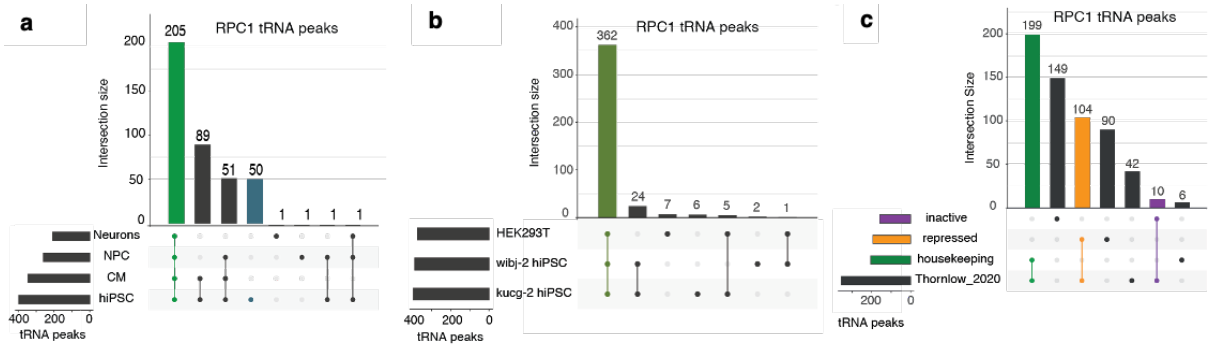

Figure 2.24. Comparison of RPC1 ChIP-Seq peaks at tRNA genes among datasets. UpSet plots of (**a**) the number of significant consensus RPC1 peaks located within 125 bp for annotated tRNA genes in each cell type (FDR ≤ 0.05), with the green set representing housekeeping tRNAs and the blue set representing hiPSC-specific tRNAs; (**b**) the significant consensus RPC1 peaks of annotated tRNA genes (located within 125 bp) from two replicates in each cell type (FDR ≤ 0.05); and (**c**) the numbers of tRNA genes in three tRNA activity groups and the active tRNA genes predicted in (Thornlow et al. 2020). Bar plots on the lower left shows the total count number of detected consensus tRNA peaks per cell type/group/publication. Bar plots on the right depict the size of consensus peaks (upper) for specific intersection sets (lower).

To rule out cell line-specific effects, we conducted RPC1 ChIP-Seq in two additional human cell lines. Out of the 397 RPC1 tRNA peaks identified in the *kucg-2* hiPSC line, 362 were observed in another reference hiPSC line, *wijb-2*, and also in HEK293T cells (**Figure 2.24b**).

In the RPC1 ChIP-Seq datasets obtained from *kucg-2* and *wibj-2* hiPSC, we identified 24 tRNA peaks that were not detected in HEK293T cells. Conversely, only 10 tRNA genes met the peak calling threshold in *wibj-2* hiPSC or HEK293T but not in the *kucg-2* hiPSC line (**Figure 2.24b**). Around one third of all predicted tRNA genes are therefore not occupied by Pol III in two distinct hiPSC lines or the immortalized HEK293T cell line. Notably, 97% of the housekeeping tRNA genes (199 out of 205) were suggested to be active based on predictions with a random forest classifier that determines the gene activity by training on gene body sequence and genomic context of tRNA genes (Thornlow et al. 2020) (**Figure 2.24c)**. However, nearly half of the tRNA genes detected with Pol III binding in hiPSC and were repressed upon differentiation were not predicted to be active with this method, emphasizing the limitations of relying solely on computational methods to define tRNA gene expression.

We reasoned that during differentiation, changes in Pol III occupancy at tRNA genes can occur both in a gene-specific manner and at a global level. Due to the limitations of standard ChIP-Seq workflows in capturing global changes, we employed DiffBind analysis to assess differential occupancy of RPC1 at tRNA genes after spike-in normalization (Ross-Innes et al. 2012). This analysis discovered that a considerable number of tRNA genes exhibited a significant reduction of Pol III occupancy in differentiated cells compared to hiPSC. More specifically, Pol III enrichment decreased at 197 genes in CM, 397 genes in NPC, and 403 genes in neurons, respectively (FDR ≤ 0.05; **Figure 2.25a; Table S6-8**). The most prominent effect size was observed in genes with relatively low to medium RPC1 enrichment, which mirrored the substantial decrease in the tRNA transcripts with low abundance in differentiated cells (**Figure 2.6b**). This reduction is not attributed to an overall reduction in Pol III abundance, as the levels of its core subunits RPC1 and RPC2 were stable in hiPSC and NPC, with only a modest decrease observed in neurons and CM (**Figure 2.25b**). In CM, RPC1 enrichment was found to be increased at 117 tRNA genes that exhibited mid- to high-occupancy, mainly by a small magnitude (less than three-fold). In contrast, there were only two tRNA genes that show significantly higher occupancy in neurons when compared to hiPSC. One of these genes did not pass the peak calling threshold due to low read counts, and the other gene, *tRNA-Arg-TCT-4-1*, encodes the neuron-specific isodecoder tRNA-Arg-UCU-4 (Ishimura et al. 2014) (**Figure 2.5**, **Table S7**). Taken together, these data suggest that differentiation is accompanied by a general decrease of Pol III occupancy at tRNA genes, primarily affecting the genes with lower occupancy.

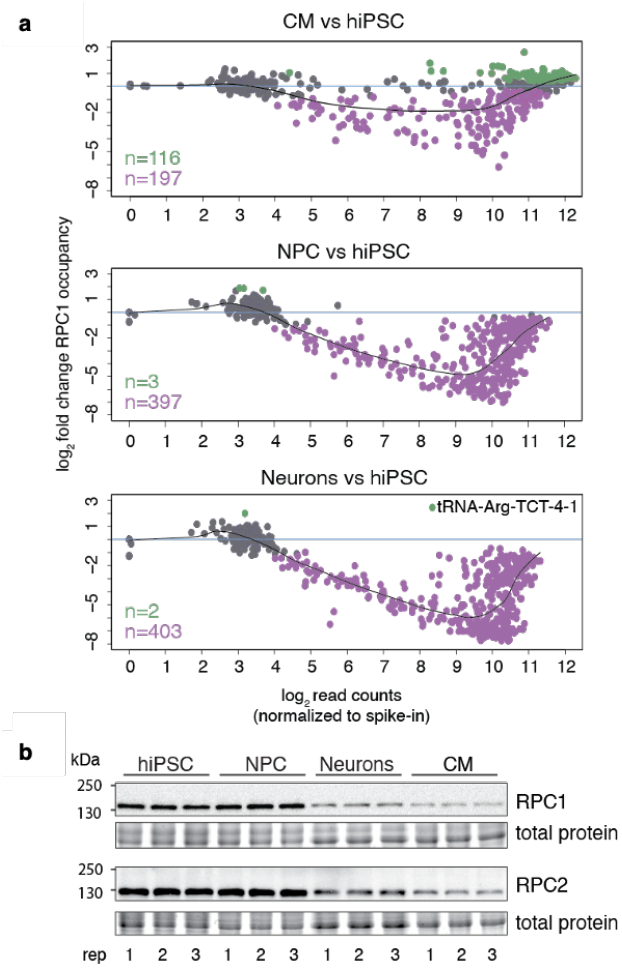

Figure 2.25. Global RPC1 occupancy is reduced at the tRNA genes upon differentiation. a, The MA plots generated with DiffBind depicting the log2 fold-change in RPC1 occupancy against the spike-in normalized RPC1 ChIP-Seq read counts over tRNA features (±125bp) from two biological replicates of CM, NPC and neurons relative to hiPSC (from top to bottom). Occupancies that are significantly higher and lower (FDR ≤ 0.05) are highlighted in green and purple, respectively. **b**, Immunoblot analysis for RPC1 and RPC2 proteins in three biological replicates of hiPSC, NPC, neurons, and CM.

2.4.4 Optimization of the ATAC-Seq experimental workflow

We then asked whether chromatin states correlate with the Pol III activity loss at specific tRNA genes upon differentiation. For this, we wanted to analyze chromatin accessibility the Assay for Transposase-Accessible Chromatin using sequencing (ATAC-Seq) (Buenrostro et al. 2013). In this assay, the insertion of sequencing adapters into open chromatin regions by the Tn5 transposase enzyme generates DNA fragments that can be sequenced to identify accessible regions. We found that the widely used Illumina TDE1 enzyme efficiently tagmented chromatin in hiPSC when using directly upon arrival, generating clear nucleosome patterns with the majority enriched in the regions of nucleosome-free, one and two nucleosomes ("early"; (**Figure 2.26a,** left panel). However, digestion with the same batch of enzyme after storage (-25°C to -15°C without aliquoting, according to manufacturer's instructions) led to very poor transposition, as shown by the exceptional high signal corresponding to multiple nucleosomes ("late"; **Figure 2.26a,** right panel). By contrast, the ATAC-Seq kit from Active

Motif consistently produced libraries with clear nucleosomal patterns in both hiPSC and differentiated cells such as neurons, without yielding fragments > 1000bp, irrespective of the reaction time (**Figure 2.26b**). Therefore, we opted for the Active Motif ATAC-Seq kit for generating libraries from all cell lines, and obtained comprehensive genome-wide profiles of nucleosome-free regions (NFRs) and chromatin accessibility at high resolution. The ATAC-Seq signals generally overlap with RPC1 ChIP-Seq signals at tRNA genes, and simultaneously disappear with RPC1 signals at selected loci upon differentiation (**Figure 2.26c**).

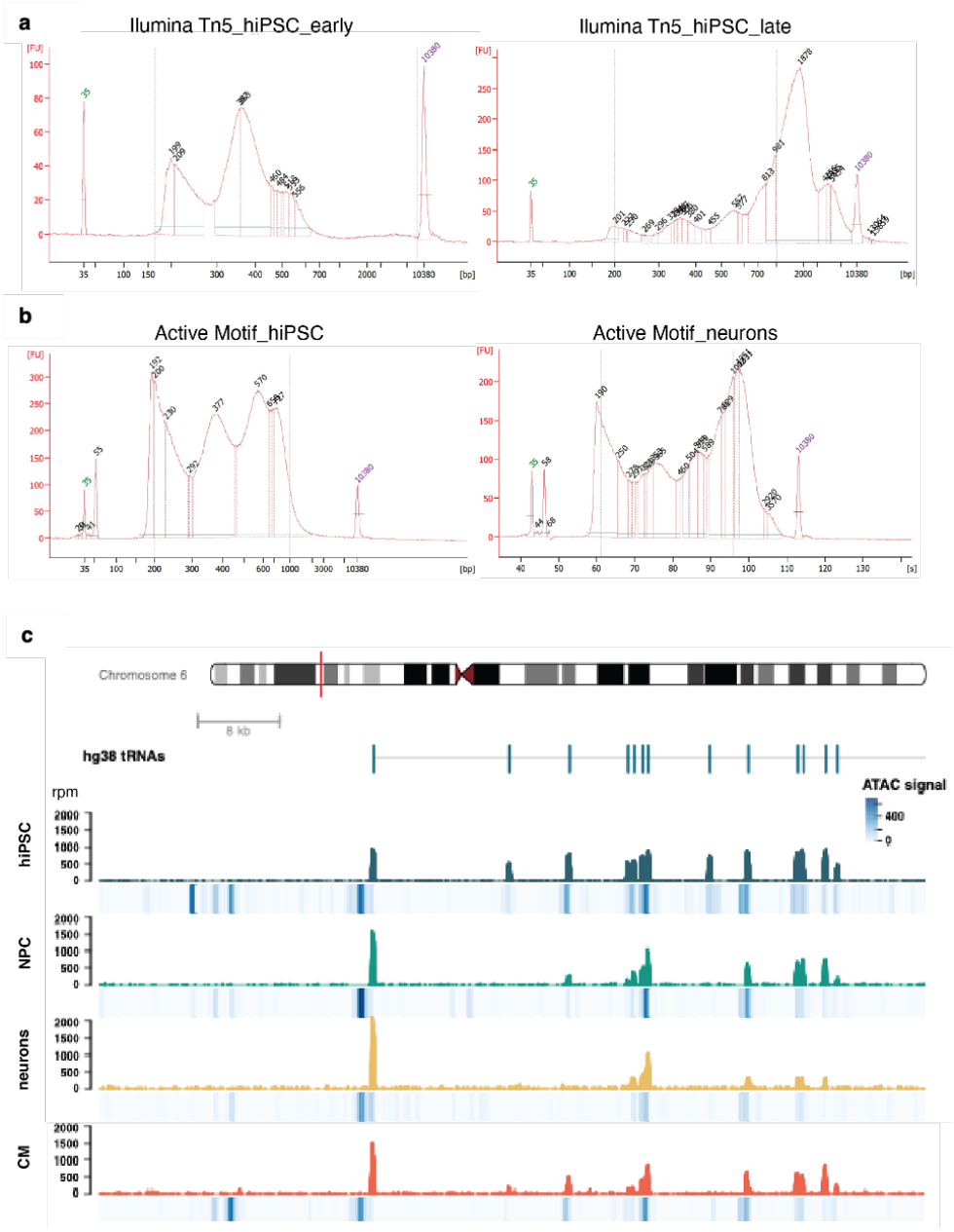

Figure 2.26. Active Motif ATAC-Seq kit generates genome-wide profiles of nucleosome-free regions (NFRs) and chromatin accessibility at high resolution. a-b, Size distribution of ATAC-Seq libraries prepared with Illumina Tn5 transpose for hiPSC directly upon arrival (**a,** left) or after storage (**a,** right), and Active Motif kit for

hiPSC and neurons (**b**). DNA size distribution was analyzed using capillary electrophoresis and generated with Agilent expert 2100 software. The x-axis represents base pairs (bp), and the y-axis represents fluorescence units (FU). **c**,The ATAC-Seq signal (shaded blue squares) is depicted below the corresponding RPC1 ChIP-Seq signals (normalized and scaled to rpm) at genomic regions (indicated by a red line) on human chromosome 6 including predicted tRNA genes (represented by blue tick marks) from one biological replicate of hiPSC, NPC, neurons and CM.

2.4.5 Remodeling of chromatin at tRNA genes during differentiation

Due to the previously reported co-localization of Pol II-associated histone marks with active tRNA genes (Moqtaderi et al. 2010b; Barski et al. 2010a; Van Bortle, Phanstiel, and Snyder 2017), we performed ChIP-Seq in hiPSC, NPC, neurons and CM for H3K4me3, which is positioned adjacent to the transcription start sites (TSS) of actively transcribed Pol II genes (Barski et al. 2007). We also profiled H3K27me3, which serves as a marker for Pol II genes that are repressed under specific cellular states (Bernstein et al. 2006). We observed a significant correlation between the presence of H3K4me3 and RPC1 enrichment at tRNA genes, consistent with previous studies in transformed human cell lines (Barski et al. 2010b; Moqtaderi et al. 2010b). The NFR (Nucleosome-Free Region) signal obtained from ATAC-Seq also coincided with tRNA genes bound by RPC1 (**Figure 2.27a**), but these measurements demonstrated lower predictive accuracy for mature tRNA levels compared to RPC1 ChIP occupancy, especially in differentiated cells (R^2 of 0.56 for NFR ATAC-Seq in neurons versus 0.9 for RPC1 ChIP-Seq, **Figure 2.21** and **2.27b**). Upon differentiation, the selective loss of RPC1 at repressed tRNA loci was accompanied by the loss of H3K4me3 and NFR ChIP signal, and the acquisition of H3K27me3, suggesting the occurrence of chromatin condensation and the establishment of facultative heterochromatin. In contrast, permanently inactive tRNA genes were within closed chromatin regions that lacked the presence of both H3K4me3 and H3K27me3 marks (**Figure 2.27a**).

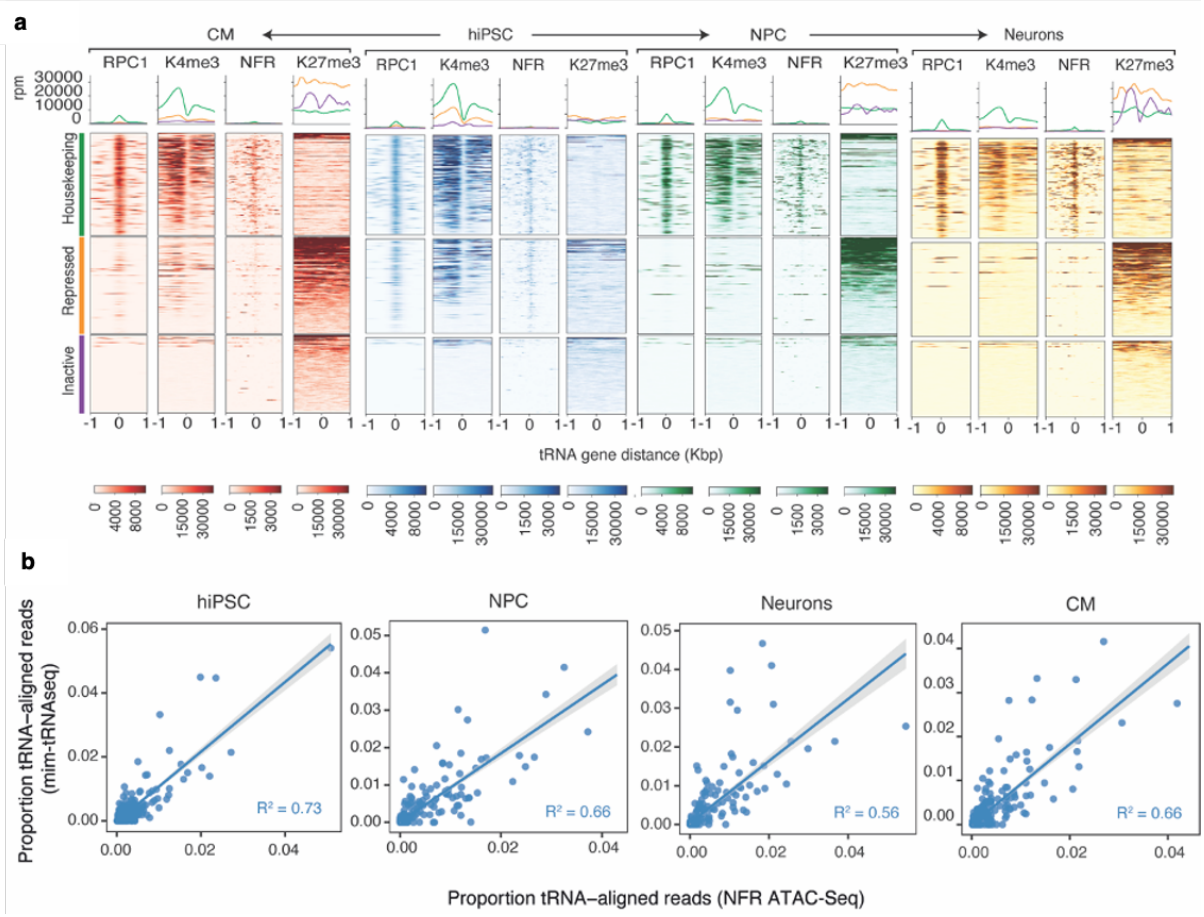

Figure 2.27. Pol III occupancy at tRNA genes is coupled with chromatin status. a, Heatmaps and metagene profile plots displaying the ChIP-Seq occupancy signal for RPC1, H3K4me3, nucleosome-free regions (NFR) obtained from ATAC-Seq data and H3K27me3 surrounding tRNA gene start sites (±1 Kbp) from for single biological replicate of CM, hiPSC, NPC and neurons, The tRNA genes are categorized based on tRNA activity. The signal is normalized for estimated library sizes based on counts over extended tRNA features (±125 bp) and is scaled to reads-per-million (rpm). The tRNA genes (n=558) were categorized into housekeeping, repressed, and inactive according to significant RPC1 ChIP-Seq peaks (FDR ≤ 0.05), and were arranged in a descending order based on the mean value per region. **b**, The correlation (depicted as Pearson's correlation coefficients) between the tRNA abundance per transcript (n=373) measured by mim-tRNAseq and the mean ATAC-Seq NFR read counts aligned to extended tRNA features (±125 bp) in two biological replicates of each cell type. Both values are scaled proportionally to the total number of tRNA-mapped reads. The solid blue lines represent the linear regression models. The shaded gray area indicates 95% confidence interval (CI).

Most human tRNA genes are found in multiple clusters on six different chromosomes, and almost half localize on chromosomes 1 and 6. The clusters typically contain multiple copies of the same tRNA gene or related tRNA genes with slight sequence variations, which has been suggested to allow for the coordinated expression and regulation of the tRNA genes, as well as efficient processing of precursor tRNA transcripts into mature tRNAs (Bermudez-Santana et al. 2010; Pai and Engelke 2010). Given this non-random clustering and the association of

H3K4me3 with Pol II activity, we wondered whether the presence of neighboring tRNA or Pol II genes affects RPC1 occupancy. Approximately 80% of housekeeping (166/204) and repressed (151/194) tRNA genes were found to be located near other active tRNA genes based on the presence of RPC1 ChIP peaks, with median distances of 0.96 Kbp and 3.69 Kbp, respectively (**Figure 2.28a**). The close spatial arrangement of active tRNA genes may facilitate the formation of transcription "factories" where active Pol III molecules are concentrated, as revealed in HeLa cells, which enables the efficient Pol III recycling during transcription processes (Pombo et al. 1999). By contrast, inactive tRNAs tended to be located at greater distances from their nearest tRNA neighbors (median distance of 380.5 kbp), and also showed no preference for clustering with other active or inactive tRNAs (**Figure 2.28b**).

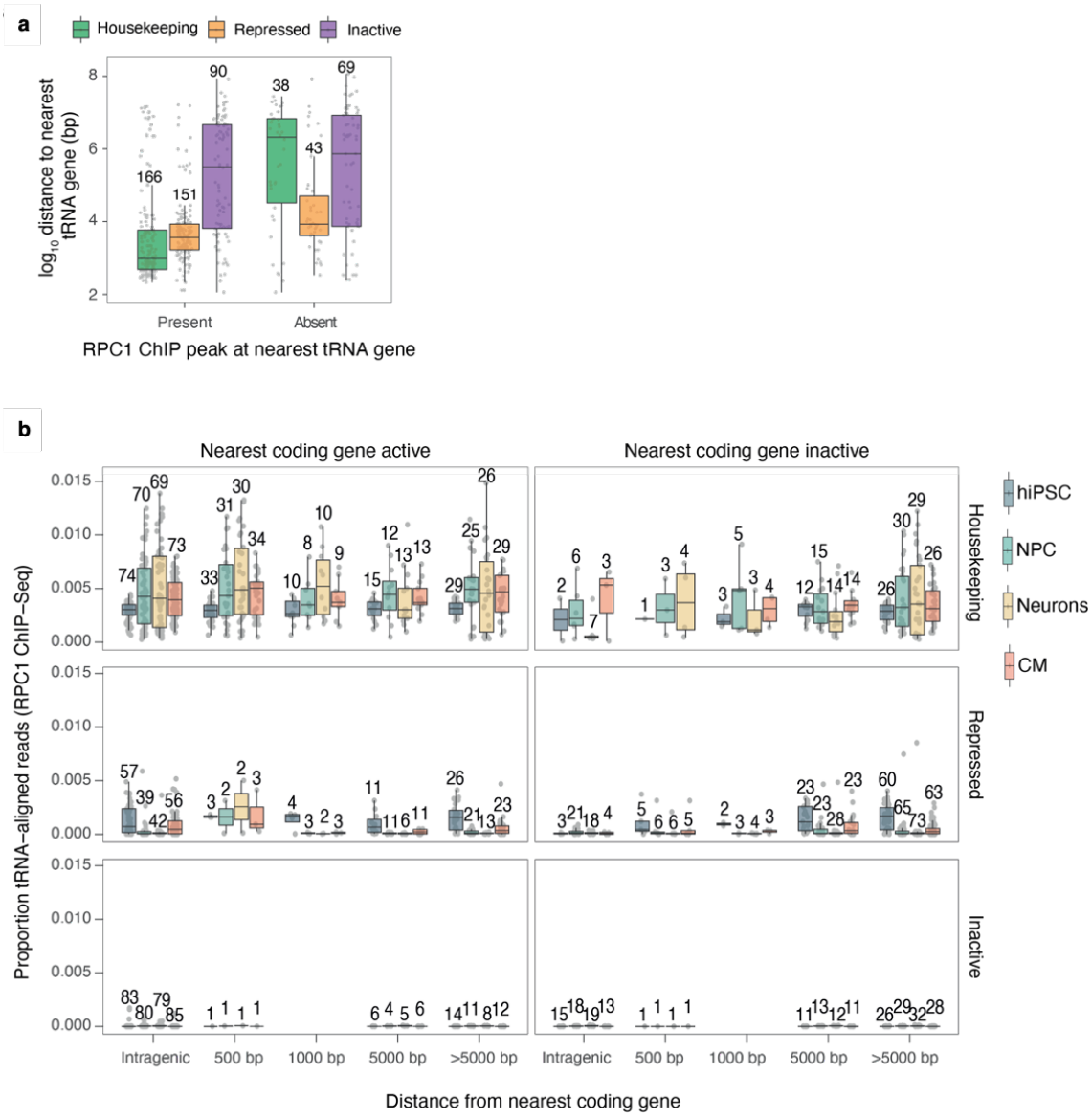

Figure 2.28. Pol III occupancy at tRNA genes is related to activity of nearby tRNA genes but not Pol II genes. a, Boxplot illustrating the distribution of distances (represented as log10) between tRNA genes in distinct activity classes and their closest neighboring tRNA gene. The data is divided into groups based on whether the closest neighboring tRNA gene aligns with a RPC1 ChIP-Seq peak from two biological replicates of one or more cell types. The numbers represent the sample size in each respective group. **b**, Boxplot illustrating the distribution for mean counts of RPC1 ChIP-Seq reads mapped to extended tRNA features (±125 bp) based on the distance between tRNA genes with different activities and their closest neighboring coding gene. The data is categorized based on tRNA activity and whether the closest coding gene is predicted active by the presence of ATAC-Seq NFR peaks and upstream H3K4me3. Single replicate was included for H3K4me3 in NPC. Two biological replicates were used for all other cell types. **a-b**, The center line and label represent the median. The box limits indicate the upper and lower quartiles. The whiskers extend to 1.5x the interquartile range.

To determine the potential influence of nearby Pol II transcription on the activity of tRNA genes, we evaluated RPC1 occupancy at tRNA genes based on their proximity to the nearest coding genes. Potentially active coding genes were defined by the presence of upstream H3K4me3 and NFR peaks in our H3K4me3 ChIP-Seq and ATAC-Seq datasets. Despite half of the tRNA genes with gene-specific RPC1 ChIP data being either intragenic (234 out of 558, 42%) or near the coding genes (≤500 bp; 44 out of 558, 8%), the linear distance of these tRNAs to active or inactive Pol II genes did not show any association with RPC1 occupancy (**Figure 2.28b**). Therefore, while active human tRNA genes often localize in close proximity to one another, Pol III occupancy strengths are not globally associated with nearby Pol II gene activity.

2.5 tRNA gene body and upstream sequences regulate differential Pol III recruitment

2.5.1 tRNAScan-SE scores alone are not sufficient to predict tRNA gene transcription

We next investigated whether sequence-dependent regulatory mechanisms drive the selective expression of tRNA genes we observed during differentiation. To this end, we first assessed the correlation between RPC1 occupancy and the overall bit scores from tRNAScan-SE, the most widely used tRNA gene prediction tool (Chan et al. 2021). The bit score is calculated based on the sequence and secondary structure of the predicted tRNA gene, and it reflects how well the predicted gene matches the known characteristics of tRNA genes. Higher bit scores reflect a greater degree of conservation in consensus tRNA features, including congruence between the anticodon and isotype, matching of A- and B-box consensus sequences, and

preservation of secondary structures, and thereby a higher confidence in the prediction. All housekeeping tRNA genes surpassed the 55 bit-score threshold suggested to distinguish functional tRNA genes from pseudogenes. By contrast, out of the 159 inactive genes, 131 (82%) had bit scores that fell below this threshold (**Figure 2.29**). However, 45 tRNA genes with detectable RPC1 occupancy in hiPSC fell below the 55-bit threshold and conversely, at 28 loci with bit scores exceeding 55, we did not detect any noticeable RPC1 peaks (**Figure 2.29a)**. Therefore, the tRNAScan-SE score alone does not accurately predict the potential for tRNA gene expression in different human cell types (Thornlow et al. 2020).

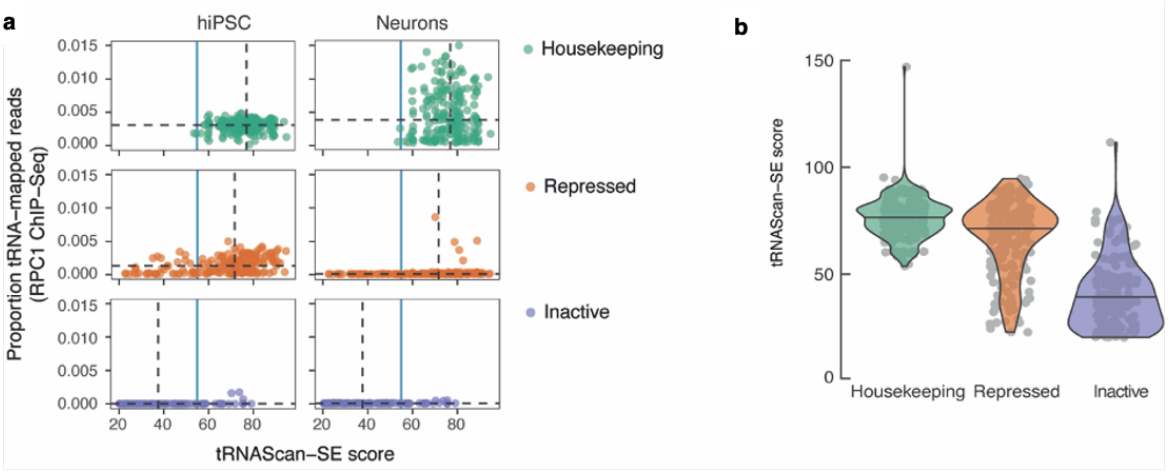

Figure 2.29. tRNAScan-SE alone is not sufficient to predict tRNA gene transcription. a, The correlation between mean RPC1 enrichment at tRNA genes and predicted tRNAScan-SE scores, categorized by tRNA gene activity in two biological replicates of hiPSC and neurons. Dashed black horizontal and vertical lines represent the median RPC1 occupancy and tRNAScan-SE scores for each cell line and gene group, respectively. Solid blue lines represent the 55-bit score threshold employed for the prediction of functional tRNAs. **b**, The violin plot displaying the distribution of tRNAScan-SE scores for tRNA genes (n = 558) categorized by tRNA activity. The center line represents the median value.

2.5.2 A- and B-box sequences within tRNA gene body are linked to Pol III occupancy

To quantify the impact of the known intragenic promoters A- and B-boxes on differential RPC1 occupancy at tRNA genes, we compared sequence logos of the promoters, segregating them by tRNA activity status - housekeeping, repressed and active, based on RPC1 ChIP-Seq datasets (**Figure 2.30a**). Consistent with previous analyses in mouse liver (Canella et al. 2012), we observed high sequence similarity among the three tRNA gene groups, with only minor variations in the internal promoter sequences. Compared to repressed or inactive genes, housekeeping tRNA genes exhibited lower levels of variation at A-box positions 3 and 7, as

well as positions 4, 5, and 7 in B-box. To quantify this, a consensus sequence, which represents the most commonly occurring nucleotide sequence pattern at these two promoters, was then defined for each promoter with the online prediction tool MEME (Bailey et al. 2009), based on all 619 predicted tRNAs in the hg38 genome from GtRNAdb (Chan and Lowe 2009) (**Figure 2.30b).** We then quantified the occurrence of each predicted consensus pattern in tRNA gene sequences. This analysis unveiled a significantly higher density of both A-box and B-box consensus sequences in housekeeping tRNAs compared to repressed and inactive tRNA genes (**Figure 2.30c**). These findings indicate that subtle differences in A- and B-box promoters can contribute to the variation in Pol III occupancy of tRNA genes across different human cell types.

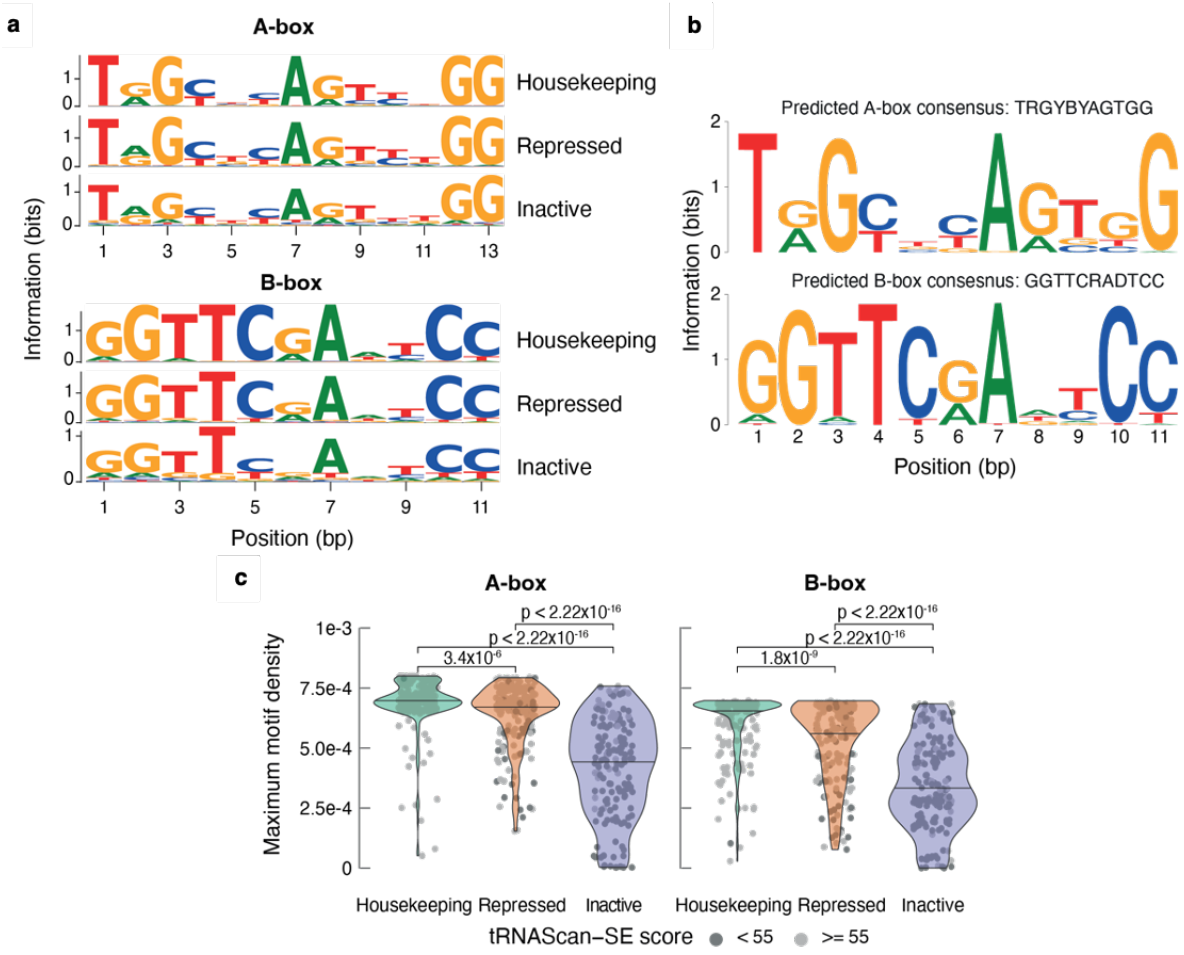

Figure 2.30. A- and B-box sequences contribute to differential Pol III recruitment. a, The sequence logos depicting the promoter sequences of A- and B-boxes from aligned mature hg38 tRNA, categorized by tRNA activity. **b**, MEME analysis prediction of human A- and B-box consensus sequences throughout the entire hg38 tRNA gene set consisting of 619 genes. **c**, Violin plots displaying the maximum density distribution of A- and B-box motifs for tRNA genes (a total of 558 genes) categorized by tRNA activity. The center line represents the

median. The color of the dots differentiates tRNAs based on whether the tRNAScan-SE score exceeds the threshold for predicting functionality. P-values were calculated with the Kruskal-Wallis test by rank.

To experimentally validate the importance of tRNA gene body sequences for expression, we chose to genetically modify the hiPSC cell line by replacing the *tRNA-Pro-TGG-2-1* gene on chromosome 11 with the *tRNA-Pro-TGG-1-1* gene sequence. These two genes differ only by three nucleotides, one of which resides in the A-box (**Figure 2.32a**). Genome editing was enabled by the CRISPR/Cas9 technology, which is based on the naturally occurring clustered regularly interspaced short palindromic repeats (CRISPR) RNA system in *Streptococcus pyogenes*. CRISPR/Cas9 depends on the nuclease activity of the Cas9 protein together with its associated guide RNAs (gRNAs), which specifically binds to the target genomic location directly upstream of a protospacer adjacent motif (PAM) sequence of "NGG". DNA cleavage then generates double-strand DNA breaks, which activate endogenous DNA repair pathways. Precise genome editing can be achieved with homology-directed repair (HDR) when supplying cells with a repair DNA template (**Figure 2.31**).

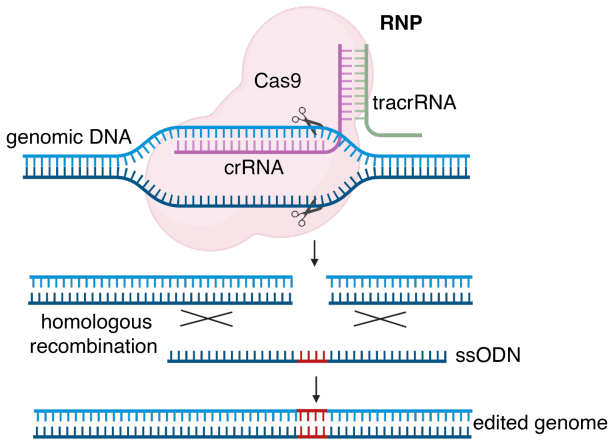

Figure 2.31. Schematic representation of genome editing with Alt-R CRISPR-Cas9. Specific sgRNA containing crRNA and tracrRNA forms a ribonucleoprotein (RNP) complex with Cas9 endonuclease and generates double-stranded breaks at genomic DNA. The cleavage is then repaired by homology-directed recombination (HDR) with oligodeoxynucleotides (ssODN), resulting in a modified sequence.

The Alt-R CRISPR-Cas9 System is more efficient than plasmid-based CRISPR-Cas9 as it exhibits enhanced genome editing potency, low off-target effects and low toxicity. With Alt-R, research-optimized CRISPR RNA (crRNA) that is complementary to the target sequence is annealed with the uniform transactivating crRNAs (tracrRNAs) that stabilize and guide the crRNA. This annealed oligo is mixed with the Alt-R HiFi Cas9 nuclease to form ribonucleoprotein (RNP) complex, which is then delivered to the cells by nucleofection, together with a short single-stranded oligodeoxynucleotides (ssODNs, 75-100 nt) harboring the desired mutations within the sequence homologous to the target sequence that serves as template for HDR (**Figure 2.31**). ssODNs were designed from both sense and antisense strands to increase the chances of finding a complementary strand. The nucleofected single cells were

maintained until colonies were ready to be picked. Single colonies were then picked for further culturing and evaluation of mutations by PCR on the genomic DNA. For this, screening primer pairs include one primer annealing to the expected mutation sequence, and another binding the intact regions outside the mutation site **(Table 4.4)**. Heterozygous clones were further ruled out by PCR amplifying with one primer binding outside of the mutation site and one binding to the target sequence region, which gives a PCR product with at least one of the alleles unmutated. Potential homozygous clones were validated by Sanger sequencing on the PCR products. The homozygous hiPSC colonies with the desired mutations were preserved and differentiated to NPC harboring the edits, followed by further culturing for 8 passages.

ChIP-Seq analysis of CRISPR edited hiPSC and the corresponding derived NPC demonstrated a significant decrease in RPC1 occupancy at the edited *tRNA-Pro-TGG-2-1* genomic locus in hiPSC and NPC. By contrast, the strength of ChIP occupancy at the adjacent non-edited *tRNA-Pro-AGG-2-4*, which is also upregulated during differentiation, was similiar in both the wild-type and edited hiPSC and NPC samples. The signal at the unedited *tRNA-Pro-TGG-1-1* also remained unchanged (**Figure 2.32b**). These data confirm the importance of tRNA gene body sequences for Pol III occupancy.

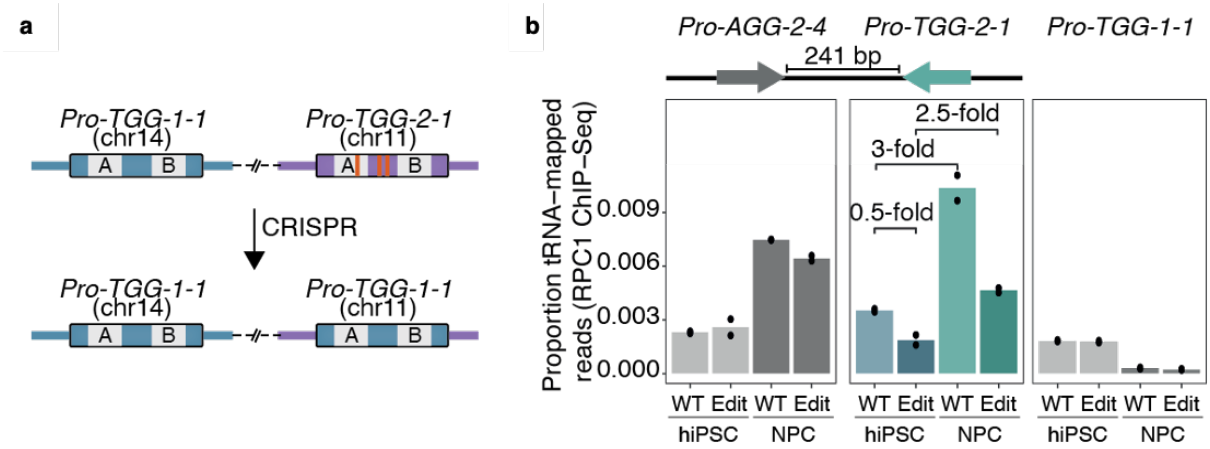

Figure 2.32. CRISPR editing validates the importance of the tRNA gene body sequence for Pol III recruitment. a, Schematic illustration of CRISPR-Cas9 editing to substitute the gene body sequence of *tRNA-Pro-TGG-2-1* with *tRNA-Pro-TGG-1-1*, which exhibits a difference of three nucleotides represented by vertical orange lines. **b**, The RPC1 enrichment at *tRNA-Pro-TGG-2-1* locus of wild-type ("WT") and CRISPR-edited ("Edit") in two biological replicates of hiPSC and NPC. Bars represent the median. The RPC1 signal of the neighboring *tRNA-Pro-AGG-2-4* gene (from chromosome 11) and the unedited *tRNA-Pro-TGG-1-1* (from chromosome 14) are presented for comparison.

2.5.3 5' flanking regions contribute to differential Pol III occupancy at tRNA genes

A modest increase in RPC1 occupancy was still detected at the edited *tRNA-Pro-TGG-2-1* locus in NPC compared to hiPSC (**Figure 2.32b**), suggesting that tRNA gene body sequences are not the exclusive factor influencing transcriptional activity. Indeed, we found numerous instances where identical tRNA genes with distinct flanking sequences exhibited selective occupancy by Pol III during differentiation, which are categorized into different activity classes. For example, while all the 5 gene copies of *Tyr-GTA-5* share the same sequence, their Pol III occupancies are highly variable within cells and among cell types (**Figure 2.33**). We reasoned that differences in upstream 5' flanking sequence might account for differential RPC1 recruitment to tRNA genes by TFIIIB.

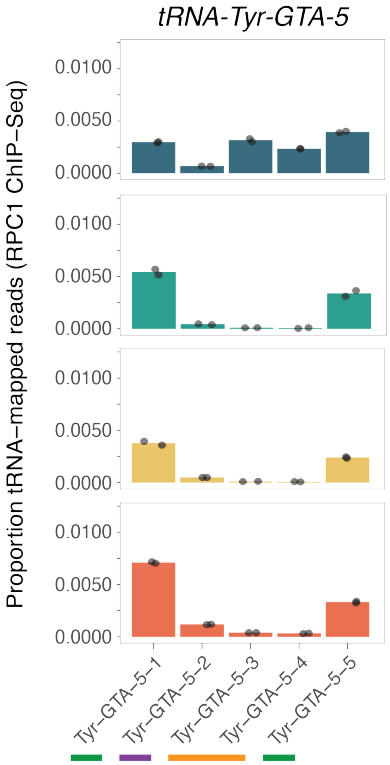

Figure 2.33. RPC1 occupancy at identical tRNA bodies varies dramatically among different cell types. The mean RPC1 ChIP-Seq reads mapped to extended tRNA features (±125 bp) for five tRNA-Tyr-GTA-5 isodecoders in all cell types. The sequences of all *tRNA-Tyr-GTA-5* genes are identical. The color bars below the gene names indicate tRNA activity class, with green representing housekeeping, orange for repressed and purple for inactive. Bars indicate the mean values from two biological replicates. Dots represent values for individual samples.

Due to the variability in the distance at which transcription initiates from tRNA gene TSS, traditional position weight matrix models like MEME are inappropriate for accurately identifying overrepresented sequence motifs associated with TSS. Deep convolutional neural networks (CNNs) can predict the sequence preferences and specificity of DNA-binding factors using the genome wide binding sites data from ChIP-Seq as an input for training the model. It has been used to predict the sequence preferences of a wide range of DNA-binding factors,

including transcription factors, chromatin regulators, and epigenetic marks. Novel DNA-binding motifs can also be identified. To predict BRF1 binding directly from sequences upstream of tRNA genes, we developed a CNN called tRNet by modifying the Binding and Expression Prediction Network (BPNet) architecture (Avsec et al. 2021), which models and predicts TF binding and gene expression from DNA sequence data (**Figure 2.34**). For this, tRNet was built with an initial convolutional layer with filter width of 20 bp to learn local sequence motifs. An additional eight convolutional layers with filter width of 10 bp combining residual skip connections and exponential dilation in every layer allowed for progressively more complex sequence features and motifs in a ~250 bp receptive field to be learned. Max pooling and two fully-connected layers combine learned sequence features for the separate prediction of tRNA activity status (**Figure 2.34**).

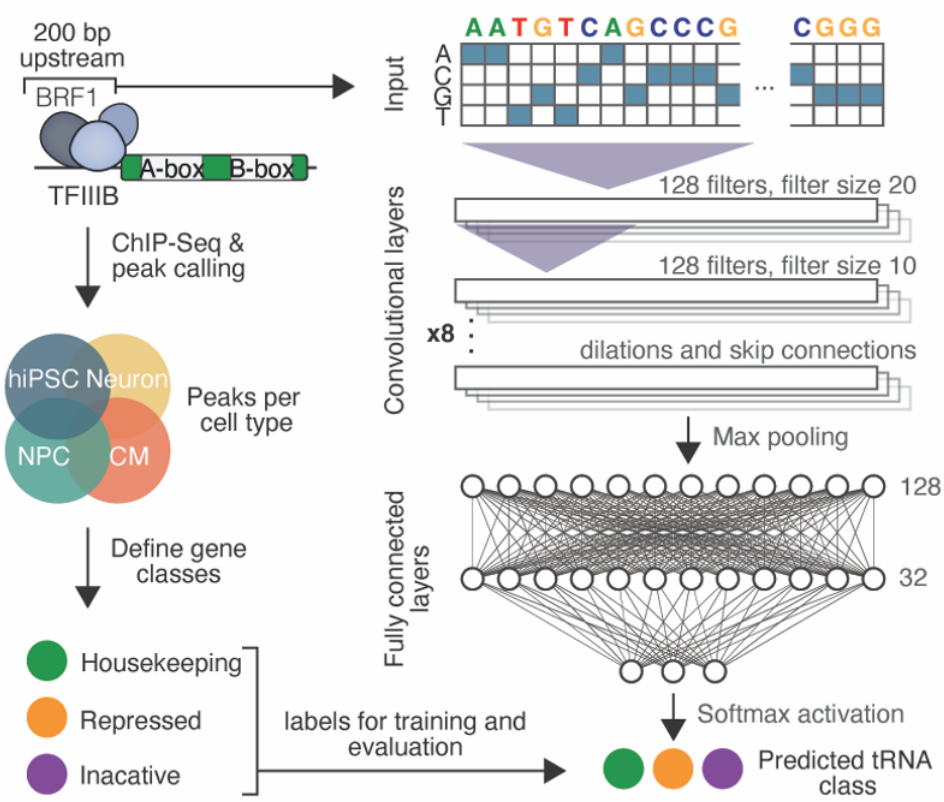

Figure 2.34. Schematic representation of tRNet architecture and training.

Next, we trained tRNet with the 200-bp sequence upstream of tRNA genes, incorporating their respective activity status (housekeeping, repressed or inactive) based on the BRF1 ChIP-Seq enrichment. Upon evaluation using 5-fold cross-validation, tRNet exhibited excellent accuracy in predicting tRNA activity, achieving a high level of precision ranging from 75% to 78% across all folds. The evaluation of tRNet using the area under the receiver operating

characteristic curve (AUROC) demonstrated its ability to effectively differentiate genes with different activity classes. Specifically, tRNet confidently distinguished housekeeping (AUROC = 0.91) and inactive (AUROC = 0.92) genes from other classes. However, the classification of repressed tRNAs based on the BRF1 upstream sequence alone was relatively more challenging (AUROC = 0.81) (**Figure 2.35a**).

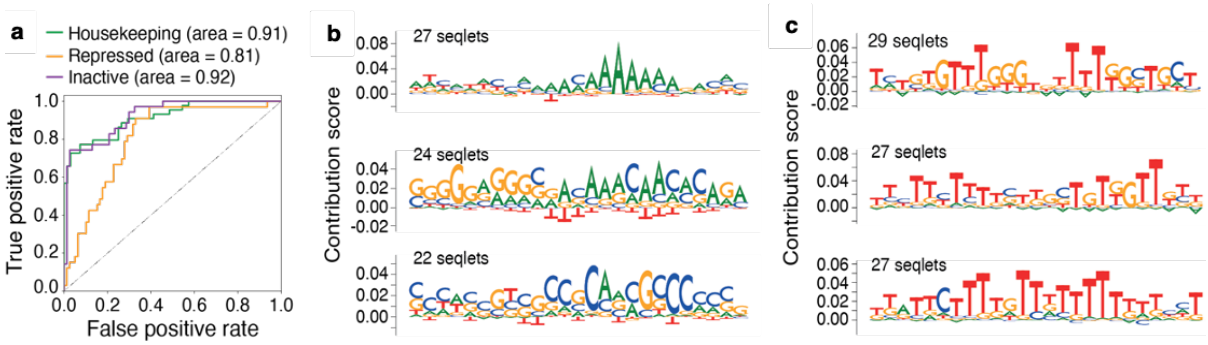

Figure 2.35. tRNet identified upstream GC and polyA sequences contributing to Pol III occupancy. a, The receiver operating characteristic (ROC) curve illustrating the performance of tRNet for the test data in each task. The curves for each task were generated with the One vs Rest macro-average scores. **b-c**, The top three sequence motif patterns generated by TF-Modisco for prediction in the housekeeping tRNA task (**b**) and inactive tRNA task (**c**). The number of seqlets contributing to each motif pattern is shown.

We found that the predictive capability of tRNet for housekeeping tRNAs is primarily driven by the presence of GC-rich and polyA stretches in the BRF1 upstream regions using TF-Modisco (**Figure 2.35b**), which detects sequence motifs and their associated cis-regulatory elements (CREs) through learning a set of motif grammars that best explain the variation in the activity scores across the BRF1 ChIP-Seq sequences (**Figure 2.34**). In line with this, predictions for tRNA gene activity based on chromatin states identified a potential role of GC content near tRNA loci (Thornlow et al. 2020), whereas a polyA stretch potentially enhances TFIIIB recruitment with the TATA-box binding protein (TBP) subunit. In contrast, the regions upstream of inactive tRNA genes exhibited significant enrichment of polyT stretches (**Figure 2.35c**). polyT stretches also serve as Pol III termination signals and impede tRNA transcription *in vitro* (Girbig et al. 2022). To test if tRNA upstream sequences can alter Pol III binding, we used CRISPR-Cas9 to insert the 100-bp sequence upstream of *tRNA-Pro-TGG-1-1* to the region directly preceding *tRNA-Pro-TGG-2-1* in hiPSC (**Figure 2.36a)**. This editing decreased the GC content of the *tRNA-Pro-TGG-2-1* upstream region from 60% (GC content for 100bp sequence upstream of *tRNA-Pro-TGG-2-1*) to 30% (GC content for 100bp sequence upstream of *tRNA-Pro-TGG-1-1*). Accordingly, this editing reproducibly reduced the RPC1 ChIP

occupancy at *tRNA-Pro-TGG-2-1* in NPC carrying this edit, while not affecting the signal of ChIP occupancy at the adjacent non-edited *tRNA-Pro-AGG-2-4* or the unedited *tRNA-Pro-TGG-1-1* (**Figure 2.36b**). These experimental results corroborate the predictions from tRNet. Taken together, our data indicate that the combination of intragenic and upstream sequence features plays a crucial role in determining Pol III occupancy at human tRNA genes.

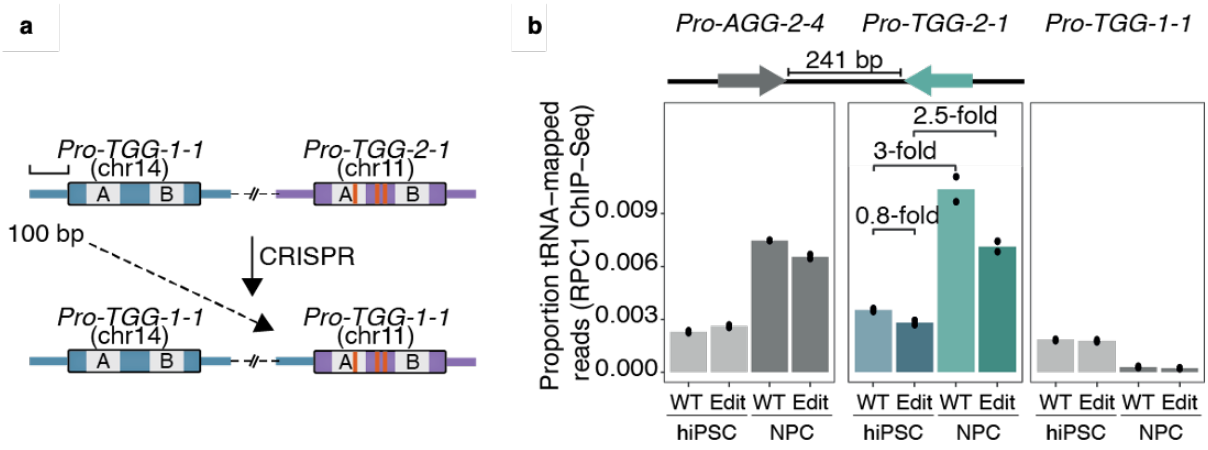

Figure 2.36. CRISPR editing verified upstream sequence modifies Pol III transcription. a, The schematic illustration showing CRISPR-Cas9 genome editing to introduce 100-bp sequence upstream of *tRNA-Pro-TGG-1-1* gene to upstream of *tRNA-Pro-TGG-2-1* gene. **b**, The RPC1 enrichment at *tRNA-Pro-TGG-2-1* locus of wild-type ("WT") and CRISPR-edited ("Edit") in two biological replicates of hiPSC and NPC. Bars represent the median. The RPC1 signal of the neighboring *tRNA-Pro-AGG-2-4* gene (from chromosome 11) and the unedited *tRNA-Pro-TGG-1-1* (from chromosome 14) are presented for comparison.

2.5.4 The expression of *tRNA-Arg-TCT-4-1* mirrors that of its neighbouring *CADM3* gene in neurons

We next investigated the mechanism underlying the specific upregulation of *tRNA-Arg-TCT-4-1* in neurons, which stood out as a rare instance of pronounced selectivity despite the marked reduction of RPC1 enrichment at all other tRNA genes (**Figure 2.25a**). *tRNA-Arg-TCT-4-1* was categorized as a housekeeping gene given that a substantial RPC1 peak is consistently present in consensus sets across all cell types, suggesting that it is not inactive in non-neuronal cells. Its A-box and B-box sequences are also the same as *tRNA-Arg-TCT-1-1*, *tRNA-Arg-TCT-3-1* and *tRNA-Arg-TCT-3-2*. We therefore asked whether the genomic context contributes to its enhanced expression in neurons. The *tRNA-Arg-TCT-4-1* locus is notably distant from other human tRNA genes at a distance of more than 2.25 Mbp, whereas there are two coding genes in its vicinity: *AIM2* (TSS 9.4 kbp distance) and *CADM3* (TSS 30 kbp away). While *AIM2* shows expression in B cells and plasma cells, *CADM3* (Cell Adhesion Molecule 3) expression

is remarkably high in neuronal cells within the brain and eye (Human Protein Atlas proteinatlas.org) (Karlsson et al. 2021), facilitating the formation and maintenance of synapses and the proper function of retinal pigment epithelium (RPE). Moreover, *CADM3* and *tRNA-Arg-TCT-4-1* consistently colocalize in the genome of various vertebrate species. We found a remarkable correspondence between the mRNA levels of the well conserved *CADM3* and the observed expression pattern of *tRNA-Arg-TCT-4-1* by mim-tRNAseq during hiPSC differentiation, both of which were specifically upregulated in neurons (**Figure 2.37**).

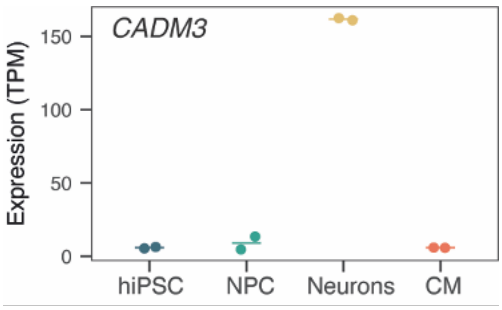

Figure 2.37. *CADM3* is specifically expressed in neurons. Transcript abundances are represented as TPM (transcripts per million) values calculated using RSEM. The line represents the mean abundance from two biological replicates. The dots indicate individual sample values.

We therefore wonder whether *tRNA-Arg-TCT-4-1* gene overlaps with a distally located *cis*-regulatory sequence element of *CADM3*. Enhancers are specific DNA sequences that play a crucial role in driving cell type- and tissue- specific gene expression and undergo Pol II transcription upon activation. These elements, which are evolutionarily conserved, are positioned between 5 Kbp and 1 Mbp away from the Pol II promoters they control (Panigrahi and O'Malley 2021; Heinz et al. 2015). In contrast, tRNA loci exhibit high mutation rates, with the gene body but not flanking regions subject to purifying selection (Thornlow et al. 2018). The location of tRNA genes is also prone to rapid turnover and the majority of tRNA genes exhibit divergent genomic positions, while only very few tRNA genes, such as *tRNA-Arg-TCT-4-1*, maintain conserved synteny between mice and humans (Bermudez-Santana et al. 2010; Kutter et al. 2011b). Alignment of the *tRNA-Arg-TCT-4-1* locus in mice and humans demonstrated a remarkable conservation not only in the tRNA gene body sequence, but also in the 140 bp upstream region, with a sequence identity of 99% (**Figure 2.38a**).

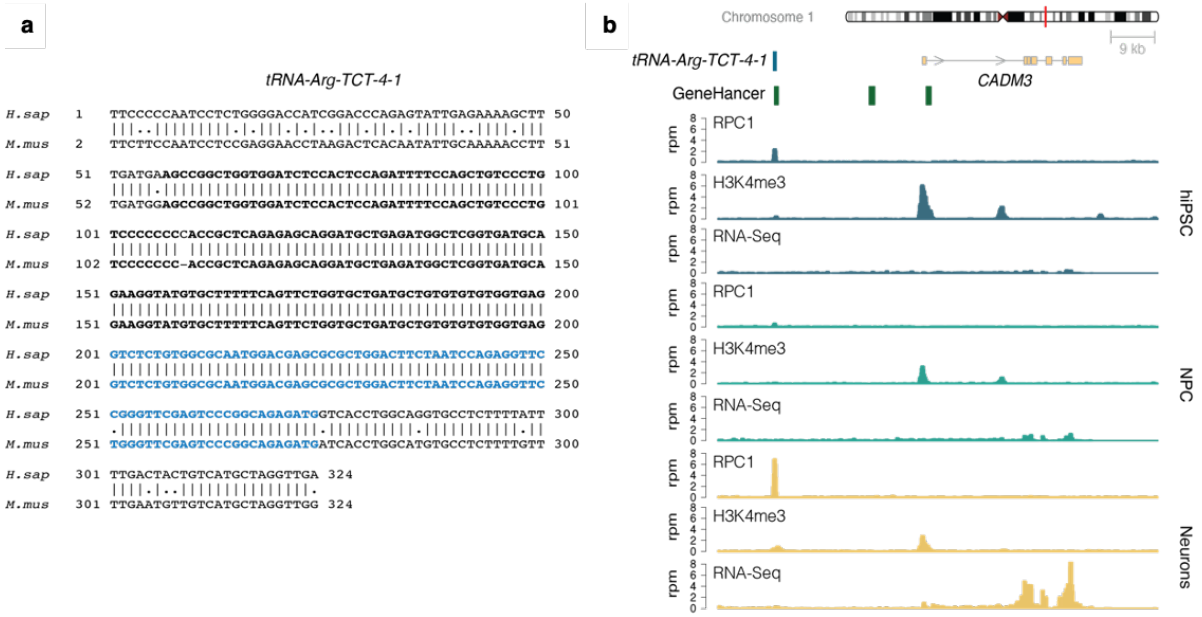

Figure 2.38. The *tRNA-Arg-TCT-4-1* gene overlaps with a predicted enhancer of *CADM3*. **a**, Pairwise sequence alignment for *tRNA-Arg-TCT-4-1* loci from the human (hg38) and mouse (mm39), encompassing 200 bp upstream of the tRNA gene start site and 150 bp downstream. The *tRNA-Arg-TCT-4-1* gene sequences are highlighted in blue. The bold black region represents approximately 140 bp of upstream sequences with nearly identical sequence composition. **b**, Representative normalized ChIP-Seq occupancy of RPC1 and H3K4me3, and RNA-Seq peaks around *tRNA-Arg-TCT-4-1* and *CADM3* genes on chromosome 1 from single replicate of hiPSC, NPC, and neurons. Values in y-axis represent the genome-wide signal normalized with library sizes estimated with read counts at extended tRNA features (±125 bp). The values are scaled to reads-per-million (rpm). Coding genes, annotated tRNA genes, and enhancers sourced from the GeneHancer database are shown.

In the GeneHancer database, we discovered the presence of an enhancer that overlaps with the human *tRNA-Arg-TCT-4-1* gene, annotated by FANTOM5 CAGE data. The enhancer is specifically transcribed in neurons *in vivo*, with *CADM3* identified as one of its potential target genes (Andersson et al. 2014; Fishilevich et al. 2017) (**Figure 2.38b**). Overall, we found 55 annotated enhancers overlapping with predicted human tRNA genes, although only 27 of these enhancers demonstrate *in vivo* transcriptional activity according to FANTOM5 CAGE data. Remarkably, 37 of these (67%) are housekeeping tRNA genes, and only 4 (7%) are inactive tRNA genes based on the lack of RPC1 peaks in our ChIP-Seq datasets.

Consistent with the regulatory role of enhancers, very low levels of *CADM3* mRNA expression were detected in RNA-Seq datasets of hiPSC and NPC, despite the presence of a strong H3K4me3 ChIP signal at the TSS of the *CADM3* gene (**Figure 2.37, 38b**). We deduced that this could be attributed to the Pol II pausing at the *CADM3* promoter region, which potentially protects it from the accumulation of repressive histone marks until its activation becomes

necessary in neurons. Pol II pauses near the promoter region, where it can await further signals to either resume transcription or terminate and release the RNA transcript. This allows for rapid and precise control over the timing and level of gene expression. Indeed, analysis of publicly available ChIP-Seq data in NPC isolated from the cortical region of developing mice identified paused Pol II at the *CADM3* promoter, and this pausing was relieved in the subsequent daughter neurons (Liu et al. 2017). This suggests that the activation of a neuron-specific *CADM3* enhancer facilitates the Pol III transcription of the overlapping *tRNA-Arg-TCT-4-1* gene by establishing a chromatin state permissive for transcription. This rare regulatory mechanism would explain the remarkable high levels of tRNA-Arg-UCU-4 in neurons. Similar to *tRNA-Arg-TCT-4-1* that overlaps with *CADM3* enhancer in neurons (**Figure 2.39a**), two other genes *tRNA-Lys-TTT-3-1* and *tRNA-Lys-TTT-3-2* within the tRNA genes that overlap with transcribed enhancers might also be co-regulated with specific enhancers in NPC and neurons (**Figure 2.39b**), but this regulatory mechanism appears to be rare based on our dataset.

Figure 2.39. Heatmaps showing the proportion of RPC1 ChIP reads mapped to tRNA genes and the scaled Z scores from normalized transcript read counts (DESeq2) for enhancer target genes with RNA-Seq data from two biological replicates of hiPSC, NPC, neurons and CM for *tRNA-Arg-TCT-4-1* (**a**), *tRNA-Lys-TTT-3-1* and *tRNA-Lys-TTT-3-2* (**b**).

2.6 Reduced mTORC1 signaling triggers MAF1-dependent repression of a tRNA gene subset upon differentiation

2.6.1 The repression of specific tRNA genes upon hiPSC differentiation is not caused by the loss of RPC7α

We next investigated whether variations in Pol III composition are linked to the selective repression of a subset of tRNA genes upon differentiation. The human Pol III complex consists of 17 subunits. Among these subunits, RPC7 that mediates transcription initiation in complex

with RPC3 and RPC6 (Wang and Roeder 1997; Lefèvre et al. 2011) is noteworthy as it has two isoforms, RPC7α and RPC7β, which are encoded by two gene paralogs, *POLR3G* and *POLR3GL*, respectively. High levels of RPC7α are characteristic of cancer cells, embryonic stem cells as well as early developmental stages, while in differentiated cells, RPC7α is largely substituted by RPC7β (Haurie et al. 2010; Lund et al. 2017; Wang et al. 2020; Wong et al. 2011). Our experimental workflow also faithfully recapitulated the differentiation-induced switch of expression from *POLR3G* to *POLR3GL*. We observed markedly high levels of *POLR3G* mRNA and RPC7α protein in hiPSC, which exhibited a significant decrease in NPC and were almost undetectable in CM and neurons (**Figure 2.40**). In contrast, mRNA level of *POLR3GL* remains relatively low in hiPSC, NPC and neurons, with a subtle increase upon neuronal differentiation, while it substantially increases in CM (**Figure 2.40a**).

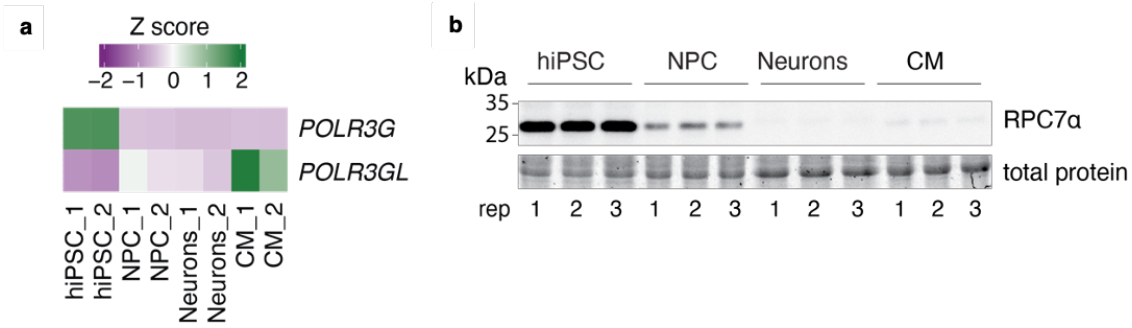

Figure 2.40. RPC7α is lost during hiPSC differentiation. a, Heatmaps representing gene expression levels of *POLR3G* and *POLR3GL* in two biological replicates of hiPSC, NPC, neurons, and CM. The scale represents the standardized Z score determined with raw gene counts across all samples from RNA-Seq. **b**, Immunoblots for RPC7α in three biological replicates of hiPSC, NPC, neurons, and CM.

We therefore wondered whether the temporal switch from RPC7α to RPC7β in the Pol III complex is associated with the selective repression of Pol III transcription during differentiation (**Figure 2.23a**), as these two processes coincide. Due to the poor performance of commercial RPC7β antibodies in immunoblotting and ChIP experiments (Van Bortle et al. 2022), our focus was on analyzing the repertoire of tRNA genes bound by RPC7α in hiPSC.

Recent structural studies of Pol III bound to a DNA template revealed that RPC7α makes limited contacts with the DNA, primarily through interactions with the minor groove, suggesting that the role of RPC7α in Pol III may be more focused on stabilizing the overall structure of the enzyme and assembly of the subunits, rather than directly interacting with the DNA template (Girbig et al. 2021b; Wang et al. 2021; Ramsay et al. 2020). Due to the limited contacts between RPC7α and DNA in Pol III, we were able to identify a total of 294 consensus

peaks that overlapped with tRNA genes from the RPC7α ChIP-Seq datasets. Remarkably, 292 of these peaks were found to be shared with the RPC1 consensus peaks (**Figure 2.41a**). While 98% (200 out of 205) of the housekeeping tRNA genes showed significant RPC7α peaks in hiPSC, only 48% (93 out of 194) of the repressed tRNA loci are enriched with RPC7α (**Figure 2.41b,c**). This discrepancy is likely due to factors such as reduced epitope accessibility or lower affinity to the RPC7α antibody, given that many repressed tRNA loci generally exhibit lower Pol III enrichment (**Figure 2.25a**). Nevertheless, these findings indicate that RPC7α-containing Pol III does not preferentially occupy tRNA genes that undergo selective repression during differentiation.

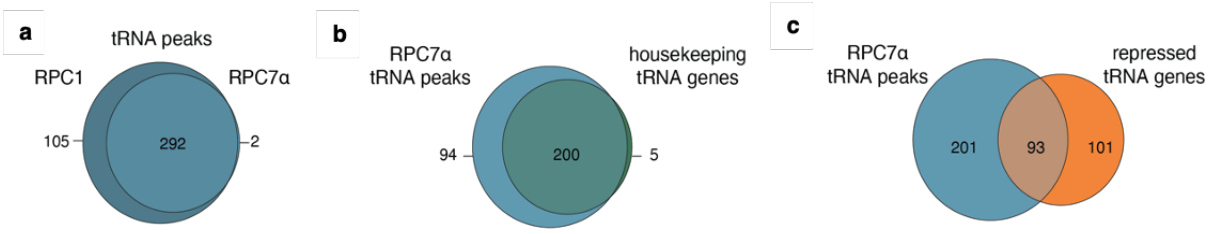

Figure 2.41. RPC7α does not preferentially occupy repressed tRNA genes. Venn diagrams depicting overlap between consensus RPC7α ChIP-Seq peaks at tRNA genes in *kucg-2* hiPSC and (**a**) consensus RPC1 ChIP-Seq peaks at tRNA genes in *kucg-2* hiPSC, (**b**) housekeeping tRNA genes across all cell types, and (**c**) repressed tRNA genes during differentiation.

To directly examine the impact of RPC7α loss on Pol III occupancy at tRNA genes, we repressed *POLR3G* transcription with inducible CRISPR interference (CRISPRi), in which the catalytically dead Cas9 (dCas9) fused with a Krüppel-associated box (KRAB) domain sterically blocks transcription initiation and interferes with gene expression under the guidance of a specific sgRNA targeting the gene promoter regions (Mandegar et al. 2016).

We used a CRISPRi hiPSC line that was previously generated in the lab by stably integrating the inducible TetO promoter-driven KRAB-dCas9-2A-mCherry cassette into the human *AAVS1* "safe harbor" locus in the *kucg-2* line **(Figure 2.42)**. sgRNAs were chosen near the transcription start site (TSS) and selected based on ATAC-Seq data for the nucleosome free region which allows binding of TFs, as well as dCas9. sgRNAs were then expressed from a U6 promoter in a lentiviral vector containing EGFP an a pruromycin resistance gene. sgRNA plasmids were packaged into lentivirus, which were then used to transduce the CRISPRi hiPSC. The transduction efficiency was evaluated by determining the percentage of GFP-positive cells and a GFP percentage of 80% is aimed after puromycin selection. Transduced cells were

induced with or without 2 µM doxycycline for desired time. RNA, protein and chromatin samples were harvested and compared between doxycycline-induced and uninduced cells.

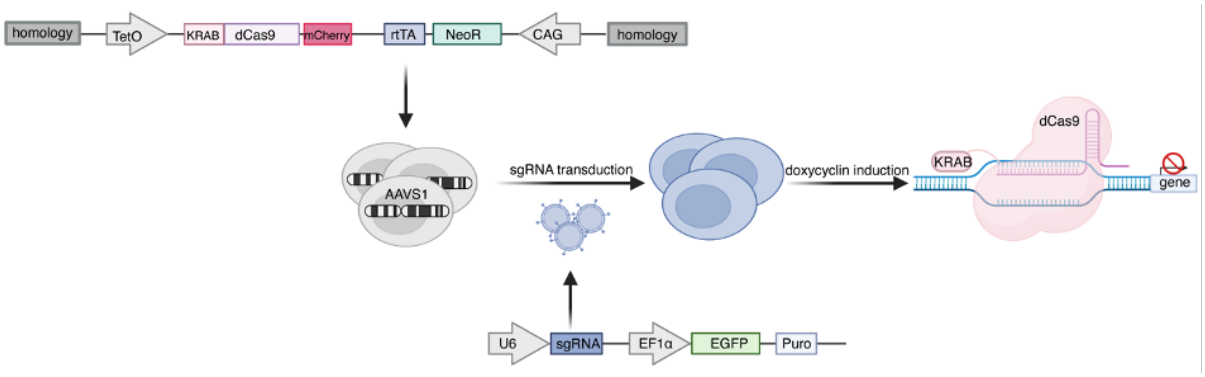

Figure 2.42. Schematic representation of inducible CRISPRi for gene knockdown. The inducible CRISPRi expression cassette contains a constitutive CAG promoter controlling the activity of the doxycycline-inducible transcriptional activator (rtTA), KRAB-dCas9-mCherry (CRISPRi) driven by the doxycycline-response element (TetO) positioned in the opposite direction of the transactivator to avoid unintended expression without doxycycline, Neomycin resistance cassette for stable selection, left and right homology arms of human *AAVS1* locus. This cassette is stably integrated into hiPSC or NPC by TALENs engineering to produce CRISPRi lines. The sgRNA construct contains U6 promoter-driven sgRNA, which can be visualized by *EGFP* expression under EF1α promoter and Puromycin resistance cassette for stable selection. Individual sgRNAs are introduced into CRISPRi cells by lentiviral transduction, followed by antibiotic selection of transduced cells. Supplementation of doxycycline triggers the expression of KRAB-dCas9, repressing the transcription of the target gene.

For *POLR3G* knockdown in hiPSC, to avoid prolonged silencing of this gene, which can result in a loss of pluripotency and spontaneous differentiation (Wong et al. 2011), we obtained samples following a 2-day induction of KRAB-dCas9. The knockdown was highly efficient, demonstrated by a drastic decrease in *POLR3G* expression but an unperturbed *POLR3GL* mRNA level (**Figure 2.43a)**. Stable *NANOG* expression was also maintained, indicating that knockdown did not impact stem cell pluripotency. Despite efficient RPC7α depletion at the protein levels, we did not detect any significant changes in Pol III occupancy at tRNA loci (**Figure 2.43b,c**). By contrast, the depletion of the core catalytic Pol III subunits RPC2 results in a substantial number of tRNA genes (n=400) with significantly decreased RPC1 occupancy (**Figure 2.43d,e**), validating our ability to detect global changes in Pol III signal. Taken together, we conclude that the selective repression of tRNA genes during differentiation is not primarily driven by the loss of RPC7α.

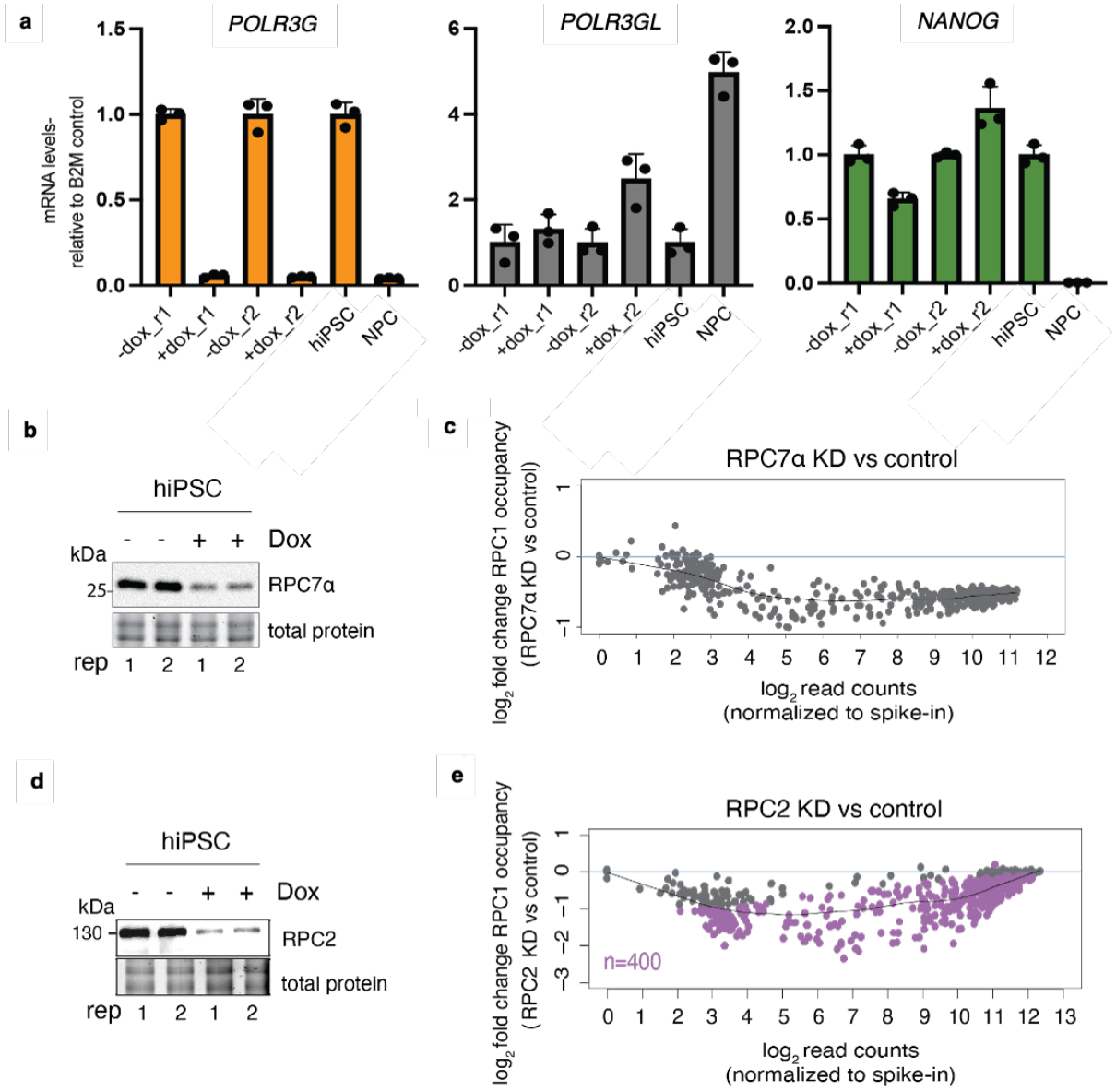

Figure 2.43. RPC7α depletion does not direct Pol III transcription repression. a, RT-qPCR showing mRNA levels of *POLR3G, POLR3GL* and *NANOG* in two biological replicates of hiPSC CRISPRi cells carrying sgRNA targeting *POLR3G*. Gene knockdown was induced by addition of 2 µM doxycycline for 2 days. Single replicate of hiPSC and NPC were used as controls. Each sample was normalized to the reference gene *B2M* in three technical replicates for relative mRNA quantification. **b** and **d**, Immunoblot analysis of RPC7α (**b**) or RPC2 (**d**) from on two biological replicates of hiPSC CRISPRi cells carrying a single-guide RNA (sgRNA) targeting *POLR3G* (**b**) or *POLR3B* (**d**). Gene knockdown was achieved by treating the cells with 2 µM doxycycline for a duration of 2 days. **c** and **e**, MA plots generated with DiffBind depicting spike-in normalized RPC1 ChIP-seq counts over tRNA features (±125 bp) on the x-axis versus log2 fold-change on the y-axis for doxycycline-induced hiPSC targeting (**c**) *POLR3G*/RPC7α or (**e**) *POLR3B*/RPC2 compared to uninduced controls. Two biological replicates are included. Gray dots indicate non-significant tRNA genes (FDR>0.05).

Recent structural work has suggested that RPC7α, but not RPC7β, may bind to a surface on RPC1 that overlaps with the docking site of MAF1, which would prevent it from binding and

inhibiting Pol III transcription (Girbig et al. 2021b). To experimentally test this hypothesis, we treated control and RPC7α-depleted hiPSC with the mTORC1 inhibitor rapamycin, which represses tRNA transcription via MAF1 (Orioli et al. 2016) (**Figure 2.44a**). With this, in RPC7α-depleted hiPSC, the binding site on RPC1 that is shared between MAF1 and RPC7α is released for potential binding of dephosphorylated MAF1 under rapamycin treatment. In treated cells, Thr389 phosphorylation in ribosomal protein S6 kinase beta-1 (S6K1) phosphorylation was lost, reflecting a decreased activity of mTORC1. A downward shift in gel migration of MAF1 indicated its dephosphorylation (**Figure 2.44a**). We identified 341 tRNA loci with significantly reduced RPC1 binding in rapamycin-treated control hiPSC, where RPC7α is highly abundant and RPC7β is not expressed (**Figure 2.44b,** upper panel**)**. RPC7α depletion marginally increased this number (n=399) without changing effect sizes (**Figure 2.44b,** lower panel). MAF1 can thus efficiently repress Pol III transcription in the presence of RPC7α.

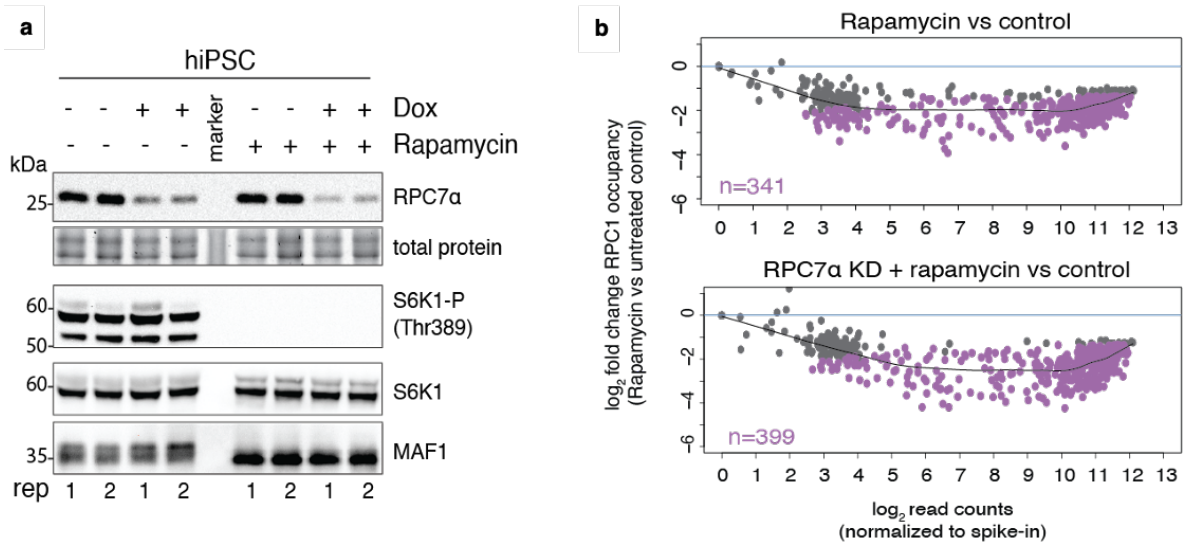

Figure 2.44. RPC7α does not interfere with MAF1-directed Pol III transcription repression. a, Immunoblots of RPC7α, MAF1, S6K1 and phospho-S6K1 in two biological replicates of hiPSC CRISPRi cells targeting *POLR3G*. Gene knockdown was induced by addition of 2 µM doxycycline for 1.5 days, followed by treatment with 10 nM rapamycin or a DMSO-only control for 8 hours. **b**, MA plots generated with DiffBind depicting spike-in normalized RPC1 ChIP-Seq counts over tRNA features (±125 bp) on the x-axis versus log2 fold-change on the y-axis for (upper) uninduced hiPSC carrying a sgRNA against *POLR3G* and treated with 10 nM rapamycin for 8 hours relative to untreated controls (n=2), (lower) doxycycline-induced hiPSC targeting *POLR3G* and treated with 10 nM rapamycin for 8 hours relative to untreated controls (n=2). Green and gray dots represent significantly higher (FDR ≤ 0.05) and non-significant (FDR > 0.05) tRNA genes, respectively.

2.6.2 Decreased mTORC1 signaling activates MAF1 in differentiated cells

In search of an alternative mechanism for the selective tRNA gene repression during differentiation, we next focused on Pol III repressor MAF1. The gel migration pattern of MAF1 shows that it is predominantly present as phosphorylated in hiPSC (**Figure 2.44a**), which impairs its ability to repress Pol III (Michels et al. 2010). This is consistent with high mTORC1 activity as it is required for the expression of key pluripotency genes, such as *SOX2*, *NANOG*, and *POU5F1*, and thus the maintenance of pluripotency for human embryonic stem cells (hESC) (Zhou, Su, et al. 2009). mTORC1 signaling was reported to be suppressed upon differentiation of hESC into NPC and neurons (Blair et al. 2017). Similar downregulation of mTORC1 activity has also been reported at later neurogenesis stages in the mouse cortex (Harnett et al. 2022b). In line with these reports, examination of the phosphorylation status of direct mTORC1 substrates S6K1, and 4E-BP1 (Michels et al. 2010; Battaglioni et al. 2022) revealed a significant reduction in mTORC1 activity across all differentiated cell types compared to hiPSC, shown by the dephosphorylation of these targets (**Figure 2.45a**).

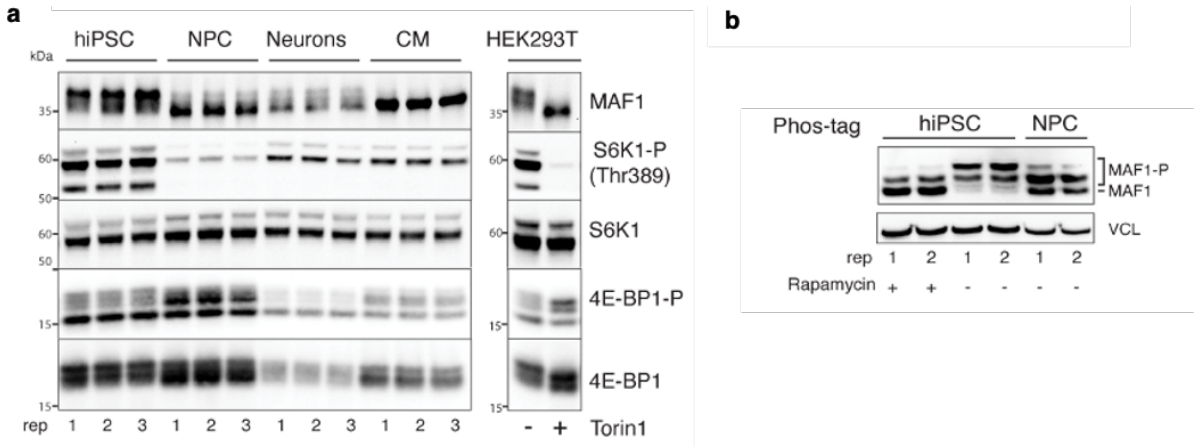

Figure 2.45. mTORC1 activity decreases during differentiation. a, Immunoblots for the protein levels of MAF1, phospho-S6K1, S6K1 and phospho-4E-BP1 and 4E-BP1 in three biological replicates of hiPSC, NPC, neurons, and CM. Samples from untreated HEK293T cells and HEK293T cells treated with Torin 1 at 250 nM for 1 hour were used as positive controls for mTOR inhibition. **b,** Immunoblot analysis of MAF1 on Phos-tag gel from two biological replicates of hiPSC, NPC, and hiPSC subjected to 10 nM rapamycin treatment for 8 hours. Vinculin (VCL) is used as the loading control.

Notably, with a reduced mTORC1 activity, the downstream mTORC1 target MAF1 was dephosphorylated upon differentiation, represented by the downward shifted single band **(Figure 2.45a)**. Interestingly, while Thr389 S6K1 phosphorylation was completely abolished in rapamycin-treated hiPSC (**Figure 2.44a**), this treatment resulted in partial MAF1

dephosphorylation and a small portion of MAF1 remained partially phosphorylated, which was also observed for MAF1 from NPC (**Figure 2.45b**). This may be related to the fact that MAF1 phosphorylation at one or more of the specific target sites (Ser60, Ser68, and Ser75) exhibit low sensitivity to mTORC1 suppression. This incomplete dephosphorylation, however, does not interfere with MAF1's ability to inhibit Pol III transcription upon rapamycin treatment (**Figure 2.44b**). We conclude that reduced mTORC1 activity during differentiation activates MAF1 by modifying its phosphorylation status.

2.6.3 MAF1 depletion relieves selective tRNA gene repression in differentiated cells

To experimentally examine the role of MAF1 activation in mediating selective tRNA gene repression during differentiation, we repressed *MAF1* with inducible CRISPRi in hiPSC and NPC. MAF1 was also depleted in hiPSC preceding NPC derivation, followed by differentiation into NPC in the absence of MAF1 (**Figure 2.46a,b**). Depletion of MAF1 did not result in changes in RPC1 levels in any of the cell lines (**Figure 2.46b)**. In hiPSC, *MAF1* knockdown led to a slight increase in Pol III occupancy at 39 tRNA genes (**Figure 2.46c**, top panel). In contrast, NPC derived without MAF1 or depleted of MAF1 after its derivation showed significantly higher RPC1 occupancy strength at 109 and 110 tRNA genes, respectively, with effect sizes predominantly >4-fold and up to approximately 30-fold (**Figure 2.46c**, middle and bottom panel). Importantly, nearly all these loci belong to the subset of tRNA genes that are repressed upon differentiation (**Figure 2.46d,** left panel). In MAF1-depleted NPC, no inactive tRNA loci showed significant increase in RPC1 ChIP signal, and only 8 gained RPC1 ChIP peaks in hiPSC (**Figure 2.46d)**. MAF1 depletion also had minimal impact on the strength of RPC1 ChIP signal at housekeeping tRNA genes.

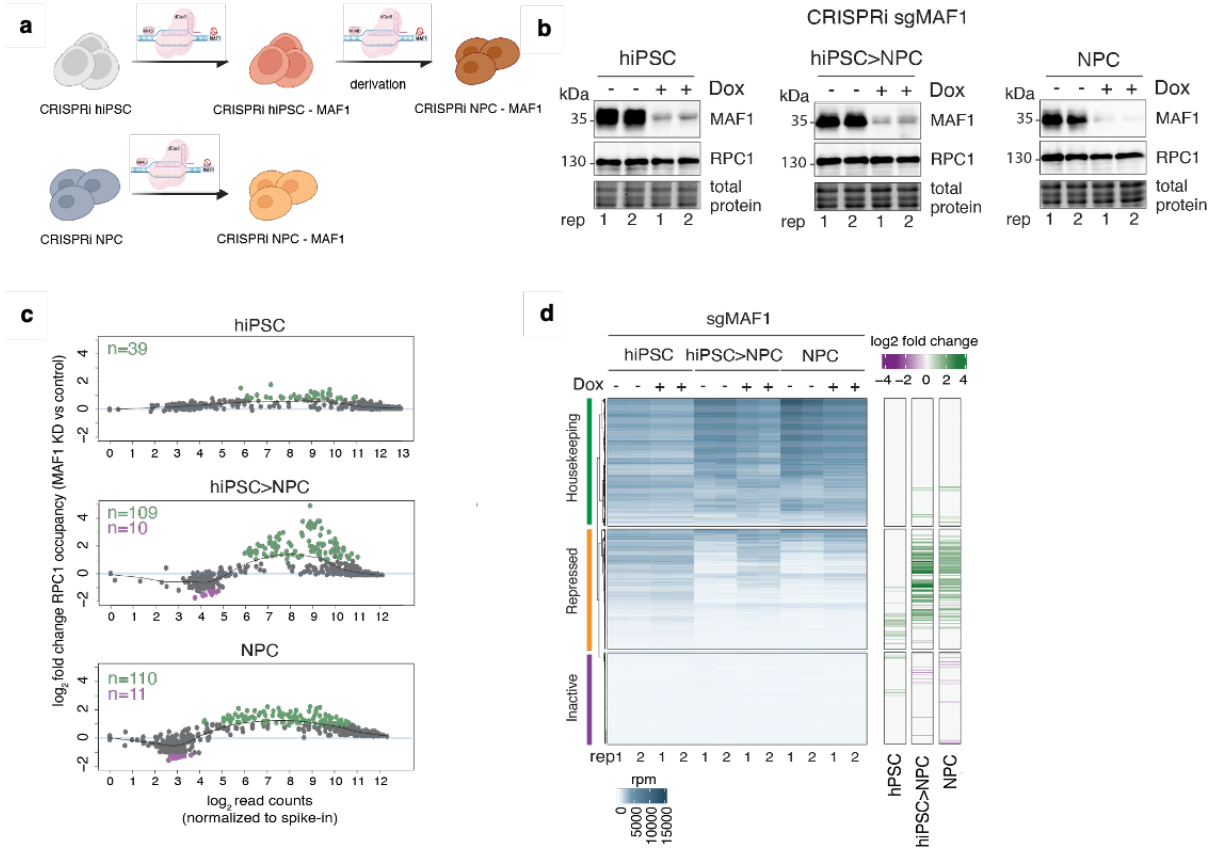

Figure 2.46. MAF1 depletion relieves selective tRNA gene repression in NPC differentiation. a, Schematic representation for CRISPRi mediated *MAF1* knockdown in hiPSC, NPC and derived CRISPRi NPC-MAF1. **b**, Immunoblots of MAF1 and RPC1 in two biological replicates of CRISPRi cell lines targeting *MAF1*. Gene knockdown was achieved by treating cells with 2 µM doxycycline (Dox) for three cell doubling times (left: 3 days for hiPSC; right: 6 days for NPC). For derived NPC-MAF1 (hiPSC>NPC) samples (middle), hiPSC harboring *MAF1* sgRNA was treated with 2 µM Dox for 3 days, NPC derivation was subsequently carried out under continuous Dox treatment. **c**, MA plots displaying spike-in normalized RPC1 ChIP-Seq counts over tRNA features (±125 bp) on the x axis versus log2 fold-change on the y axis for doxycycline-treated hiPSC, hiPSC>NPC and NPC (from top to bottom) targeting *MAF1* compared to uninduced controls generated by DiffBind. Two biological replicates are included for each cell type. Green and purple dots indicate significantly higher or lower occupancies (FDR ≤ 0.05), respectively. **d**, The RPC1 ChIP-Seq heatmaps showing normalized signal changes for two biological replicates of *MAF1* knockdown by inducible CRISPRi (+ Dox) compared to uninduced CM controls (-Dox). Left panel depicts ChIP-Seq counts of RPC1 over extended tRNA features (±125 bp). The normalized signal that takes into account estimated library sizes was calculated from these read counts and scaled proportionally to one million reads (rpm). Right panel illustrates differential occupancy analysis by DiffBind with spike-in normalization for 2 biological replicates of induced (+ Dox) samples relative to corresponding uninduced controls (-Dox) represented as log2 fold changes (FDR ≤ 0.05). tRNA genes were categorized into housekeeping, repressed, and inactive according to significant RPC1 ChIP-Seq peaks (FDR ≤ 0.05), and were arranged in a descending order based on the mean value per region.

Collectively, these data demonstrate that human cell type-specific tRNA repertoires during differentiation are established through a process dependent on MAF1 and mTORC1 (**Figure 2.47**).

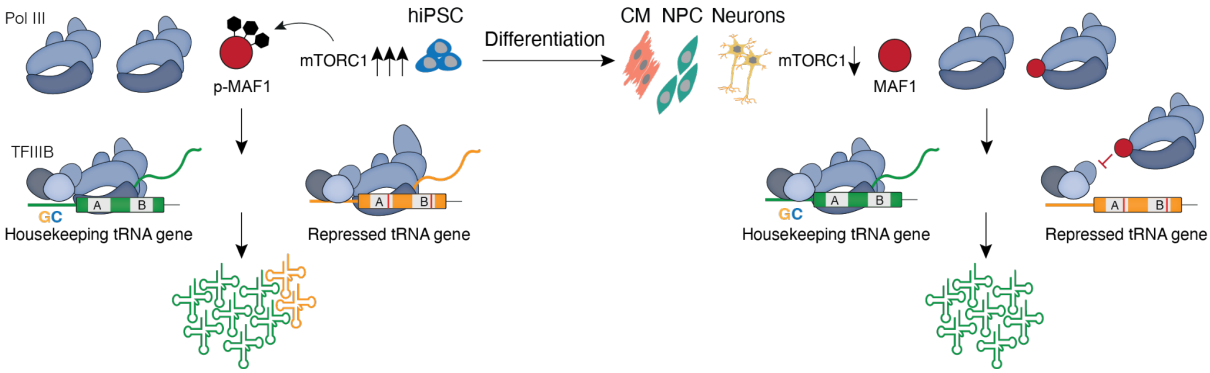

Figure 2.47. Model illustrating the selective expression of tRNA genes during hiPSC differentiation.

Chapter 3 - Discussion

Previous research has demonstrated significant diversity in the position and intensity of Pol III occupancy at tRNA genes among different mammalian tissues and immortalized human cell lines (Orioli 2017). However, the mechanisms responsible for this variability and the resulting implications for mature tRNA populations remained unclear. By the integration of Pol III ChIP-Seq data with accurate quantification of mature tRNAs in isogenic, non-transformed human cell types, here we discovered that differences in Pol III occupancy strength account for nearly all of the variations observed in mature tRNA levels (R^2=0.9). Our findings also provide compelling evidence that during normal growth, post-transcriptional regulation, the potential difference in tRNA stability among isodecoders (Guy et al. 2014) or mechanisms downstream of polymerase recruitment such as those known for Pol II (Guenther et al. 2007) play only a minor role in controlling mature tRNA levels. The remarkable consistency between the two entirely distinct approaches (Pol III ChIP-Seq and mim-tRNAseq) further emphasizes the accuracy and quantitative nature of mim-tRNAseq. While Pol III ChIP-Seq relies on specific antibodies that are often not available for many organisms, the use of mim-tRNAseq for profiling mature tRNA repertoires is much more widely applicable. We expect that this method will contribute to the discovery of essential elements regarding tRNA regulation in diverse biological contexts.

We found that 205 out of the 619 predicted human tRNA genes, which we refer to as "housekeeping", exhibited detectable Pol III ChIP peaks across all four cell types we examined. "Housekeeping" genes of Pol II are characterized by highly abundant and stable transcription across cell states and types (Joshi et al. 2022). The robust expression we observed of housekeeping tRNA genes implies the existence of a basal tRNA gene subset that represents each isotype and may be resistant to shutdown in stress conditions, such as nutrient deprivation, similarly to what has been observed for some tRNA genes in yeast (Turowski and Tollervey 2016). It is also reflected in early Pol III ChIP-Seq studies showing that a set of 120 tRNA genes are consistently expressed in various immortalized cell lines and fibroblasts, whereas varying number of other genes exhibited cell type-specific expression, potentially matching the distinct translational demand in each particular cell type (Oler et al. 2010b). It is also in line with a study in the livers of mice, which showed stable Pol III binding at high-occupancy tRNA genes in fasted or fed animals (Bonhoure et al. 2020). High-resolution mapping of Pol III in mouse liver and brain tissues across various developmental stages also identified one group of tRNA genes that remained consistent in expression during development and another group that

exhibited changes, but did not reveal any specific sequence features or regulatory mechanisms that could explain this difference (Schmitt et al. 2014).

Here, we discovered that the robust binding of Pol III at housekeeping tRNA genes is accounted for by their distinct internal promoters (A- and B-boxes), as well as GC-rich and polyA stretches present in their 5' flanking sequence regions. Consistent with the notion that TFIIIC binding to the B-box with higher specificity (Stillman and Geiduschek 1984), we found that B-box sequences display clearer separations among three tRNA gene groups in their density of consensus sequence. *In vitro* studies also show that mutations within the variable positions in the A- and B-boxes alter Pol III binding, with a stronger influence of the B-box (Canella et al. 2012). Similarly, it has been reported that a substantial portion of the sequence variations observed among human tRNA isodecoders is in the intragenic A- and B-box promoters (Goodenbour and Pan 2006). In line with our findings, high GC content has been associated with human Pol III occupancy given that Pol III-occupied tRNA loci reside in CpG islands and contain high CpG promoters (HCPs) (Oler et al. 2010b; Canella et al. 2012), potentially due to the DNA hypomethylation in the CpG island. Moreover, blocks of A-rich motif were also identified 22 bp upstream of tRNA genes with striking evolutionary conservation ranging from insects to mammals, suggesting its potential role in transcription (Giuliodori et al. 2003), corroborating the polyA stretch we identified upstream of human housekeeping tRNA genes.

In the future, it will be important to determine whether tRNA gene body and upstream regions function independently or synergistically. However, the edit in the tRNA gene body in hiPSC already leads to a a 2-fold reduction in the occupancy of *tRNA-Pro-TGG-2-1*, which encodes a major isodecoder. It is possible that an additional decrease in its expression, which might be caused by simultaneously editing its upstream region, would have a detrimental impact on cell viability. Therefore, instead of editing endogenous tRNA genes, future research to elucidate the regulatory interplay between gene body and upstream regions could avoid such cellular tRNA pool perturbations by inserting "designer tRNA genes" containing different combinations of gene body and upstream regions to the vicinity of active tRNA genes.

The sequence determinants of tRNA transcription discovered here will boost the development of therapeutics based on suppressor tRNAs for treating human diseases characterized by nonsense mutations that introduce premature termination codons in mRNA (Dolgin 2022). So far, the design of suppressor tRNAs has primarily focused on identifying transcripts capable of being effectively charged *in vivo* while not causing readthrough of normal stop codons (Porter,

Heil, and Lueck 2021; Wang et al. 2022). Our findings demonstrate that the effectiveness of DNA-based suppressor tRNA therapeutics will be strongly influenced by the selection of intragenic promoters, 5' flanking sequence, and the insertion site of the transgene. Incorporating A- and B-boxes, as well as 5′ flanking elements of housekeeping tRNAs, along with precise targeting of the transgene near active tRNA loci, will potentially enhance the expression of a therapeutic tRNA in various cell types. On the other hand, incorporating sequence features of repressed tRNA genes could enable the design of transgenes that exhibit lower expression levels or that can be turned off upon differentiation in diseases where such regulation is desirable.

All these sequence determinants could maintain the observed high Pol III occupancy at housekeeping tRNA loci irrespective of the cellular context, potentially allowing them to escape from MAF1-mediated repression. Similar mechanisms could also explain the safeguarding of a subset of extensively transcribed tRNA genes against stress-mediated MAF1 inhibition during nutrient deficiency in yeast and mice (Bonhoure et al. 2020; Turowski et al. 2016). It also aligns with the pattern of MAF1-mediated repression of in human cells exposed to serum starvation, which dislocate Pol III from majority of tRNA genes through a MAF1-dependent manner while leaving stable Pol III occupancy at a selective subset (Orioli et al. 2016). Interestingly, of the 39 tRNA genes that did not exhibit a decrease in Pol III occupancy in serum-starved fibroblasts (Orioli et al. 2016), we found that 37 of them fall into the housekeeping tRNA set in our classification. Apart from the sequence determinants, the lower sensitivity of housekeeping tRNA genes to MAF1 repression in differentiated cells can be attributed to the relatively high Pol III levels compared to MAF1, which exhibits a four- to ten-fold lower abundance compared to most of the Pol III-specific subunits (Beck et al. 2011; Kulak et al. 2014). The Pol III occupancy at these genes under differentiation could also be stabilized by the facilitated recycling, during which the elongation of transcriptionally engaged Pol III is not affected by its association with MAF1 (Cabart, Lee, and Willis 2008).

In cells with high mTORC1 activity, including hiPSC and HEK293T, we observed notable Pol III ChIP-Seq peaks at a second subgroup of "repressed" tRNA genes. We find the intragenic promoters and 5' flanking sequences of these genes render their lower favorability to Pol III recruitment or retention. This leads to reduced Pol III occupancy, which likely explains their MAF1-mediated suppression during differentiation. Previous structural and *in vitro* studies have indicated that MAF1 impedes the recruitment of Pol III by competing with TFIIIB (Vorländer et al. 2020); however, it is unable to obstruct transcription reinitiation (Cabart, Lee,

and Willis 2008). Indeed, we find that most of these repressed tRNA sites yield mature tRNAs when bound by Pol III, albeit with generally lower abundance compared to housekeeping tRNAs. This mechanism of more promiscuous transcription generates tRNA pools with a broader range of isodecoder composition in cells with high mTORC1 activity, such as pluripotent stem cells and cancers (Saxton and Sabatini 2017). Therefore, loss of MAF1 activity, in addition to tRNA gene copy number variations, may be potentially involved in the restructuring of tRNA repertoires within cancer cells (Goodarzi et al. 2016).

Besides mTORC1-mediated MAF1 inactivation, the high occurrence of open chromatin, coupled with abundant Pol III, could help explain the promiscuous transcription of tRNA genes observed in hiPSC. In line with this notion, the genome of mouse embryonic stem cells exhibits a globally pervasive state of highly transcriptional activity, which undergoes substantial silencing as the cells differentiate (Efroni et al. 2008). Although H3K4me3 and RPC1 ChIP signals at tRNA genes strongly correlate with each other, both in our datasets and previous studies (Moqtaderi et al. 2010a), we did not find a clear association between tRNA gene activity and Pol II transcription of neighboring coding genes.

Why do active tRNA gene sets get restricted upon differentiation? Given that the synthesis of highly abundant tRNA is energetically costly, and considering the central role of Pol III repressor MAF1 in growth and nutrient consumption, the MAF1-dependent Pol III transcription restriction to housekeeping tRNA genes and expression of minimal isodecoder pools in differentiated cells likely serves to preserve unaltered tRNA anticodon pools while saving cellular resources. Consistently, mice lacking Maf1 are viable but display a lean phenotype and high levels of energy expenditure (Bonhoure et al. 2015). In support of this idea, we found that levels of Pol III subunits, including core subunits RPC1 and RPC2, are lower in neurons and CM, as compared to hiPSC and NPC. Given that Pol III is also responsible for the synthesis of 5S ribosomal rRNA, and ribosome levels decrease during neurogenesis due to a combination of reduced Pol I rRNA transcription and decreased synthesis of ribosomal proteins (Chau et al. 2018; Harnett et al. 2022a), one could envision that this coupling through Pol III might assist in regulating the total levels of ribosomes and tRNAs in response to growth signals while preserving their balance and overall stoichiometry under differentiated status with unique global translation demands. However, it will be a challenge to decipher whether dysregulated differentiation is attributed to alternations of tRNA repertoires, given that MAF1 also prevents Pol III recruitment to non-tRNA genes, such as 5S ribosomal RNA (Schramm and Hernandez 2002).

Notably, we show that the remodeling of tRNA repertoires across differentiation does not involve Pol III recruitment to tRNA loci that are inactive in hiPSC. Their remarkably degenerate intragenic A- and B-box sequences found in both hiPSC and differentiated cells, coupled with the upstream polyT sequences, may impede Pol III recruitment irrespective of the cellular contexts. These tRNA loci lack essential sequence motifs necessary for Pol III transcription, but they still possess certain tRNA-like characteristics that facilitate their recognition by tRNA gene prediction tools (Chan et al. 2021). Moreover, their longer distance from adjacent tRNA genes may also play a part in their inactivation, as we found that the proximity to active tRNA loci is critical in determining the tRNA transcriptional activity. It would be interesting to further investigate whether inactive tRNA genes have a high degree of DNA methylation, given its important role in regulating Pol II target genes (Moore, Le, and Fan 2013).

The tRNA gene *tRNA-Arg-TCT-4-1* has been discovered as a prominent example of tissue-specific expression among tRNA isodecoders in the field (Ishimura et al. 2014). Following revealing of its central role in central neural system, subsequent studies found that the phenotypes induced by the processing deficiency in *tRNA-Arg-TCT-4-1* can be rescued by the overexpression of other tRNA-Arg-UCU isodecoders, implying that the phenotypes are caused by a reduction in the tRNA-Arg-UCU anticodon levels, and not due to isodecoder-specific functions unique to *tRNA-Arg-TCT-4-1* (Kapur et al. 2020). We find that tRNA genes with highly cell context-specific expression, like *tRNA-Arg-TCT-4-1* (Ishimura et al. 2014), are very rare. The overlap of this gene with a neuron-specific enhancer element we discovered here may lead to an increased Pol III occupancy in neurons despite the general trend of decreased expression for all other tRNA genes. Therefore, instead of the physical proximity to Pol II genes (Gerber et al. 2020), long-range interactions of regulatory DNA sequences may modify the expression of specific tRNA genes. It is possible that the remaining tRNA genes we identified to overlap with enhancers may potentially exhibit differential expression in cells where the respective enhancers are active, and this enhancer-driven regulation may occur for other tRNA genes in cellular contexts beyond those analysed in our work.

Our ribosome profiling data suggest that the variations in the composition of isodecoders between hiPSC and NPC have minimal impact on decoding speed. Instead, translation elongation rates at individual codons in human cells are determined by the relative abundance of the corresponding tRNA anticodon families, which remains relatively consistent across various cell types. In physiological conditions, the stable tRNA anticodon availability mediated

through housekeeping tRNA gene transcription ensures consistent decoding rates and accuracy during development. This stability minimizes the risk of ribosome errors and protein misfolding that could arise from fluctuations in codon translation rates (Nedialkova and Leidel 2015; Mordret et al. 2019). In the future, our discovery of the outsized significance of housekeeping tRNA genes for determining mature tRNA pools in human cells will help elucidate the mechanisms through which tRNA dysregulation causes neurological disorders and cancers.

Chapter 4 - Materials and Methods

4.1 Materials

Table 4.1. Cell lines used in this study.

Cell line	Source	Identifier
cDN003_*kucg*_wt_ips	HipSci	HPSI0214i-*kucg-2*
cDN001_*wibj*_wt_ips	HipSci	HPSI0214i-*wibj-2*
cDN013_CRISPRi_kp6c2_ips	This study; genetically modified from cDN003 to express doxycylcine-inducible KRAB-dCas9 (Mandegar et al. 2016)	N/A
cDN057_Lenti-X™_293T	Takara	#632180
HEK 293T/17	ATCC	CRL-11268
ES-E14TG2a	ECACC	#08021401

Table 4.2. Antibodies used in this study.

Antibody	Source	Identifier
rabbit anti-*POLR3A*/RPC1	Abcam	#ab96328
Mouse anti-Pol III RPC32/RPC4	Santa Cruz	#sc-21754
rabbit anti-*POLR3A*/RPC1	Cell Signaling	#12825
mouse anti-*POLR3B*/RPC2	Santa Cruz	#sc-515362
mouse anti-Pol III RPC32/RPC7α	Santa Cruz	#sc-21754
mouse anti-MAF1	Santa Cruz	#sc-515614 X
anti-phospho-p70 S6 Kinase	Cell Signaling	#9206S
anti-phospho-S6	Santa Cruz	sc-293144
rabbit anti-phospho-4E-BP1	Cell Signaling	#2855T
rabbit anti-vinculin	Cell Signaling	#13901

anti-rabbit IgG-HRP	Dianova	#111-035-003
anti-mouse IgG-HRP	Dianova	#115-035-003
anti-4E-BP1	Cell Signaling	#9644
anti-S6 Ribosomal Protein (5G10)	Cell Signaling	2217T
anti-p70 S6 Kinase	Cell Signaling	#2708T
POU5F1 C-10	Santa Cruz	#sc-5279
SOX2 E-4	Santa Cruz	#sc-365823
Nanog P1-2D8	Millipore	#MABD24
PAX6	Abcam	#ab5790
Nestin	R&D Systems	#MAB1259
goat anti-mouse Alexa Fluor 488	Thermo Scientific	#A-11001
goat anti-rabbit Alexa Fluor 488	Thermo Scientific	#A-11034
goat anti-mouse Alexa Fluor 633	Thermo Scientific	#A-21052
MAP2	Abcam	#ab92434
CHAT	Abcam	#ab6168
goat anti-rabbit A633	Thermo Scientific	#A-21070
goat anti-chicken A488	Thermo Scientific	#A-11039
ACTN2	Sigma-Aldrich	#A7811
cTNT	DSHB	CT3
TSC2 (D93F12)	Cell Signaling	#4308
anti-BRF1	Abcam	#ab264191
anti-POLR3G/RPC7α	Santa Cruz	#sc21754
anti-H3K4me3	Active Motif	39159
anti-H3K27me3	Millipore	07-449

Spike-in Antibody	Active Motif	61686

Table 4.3. Plasmids used in this study.

Plasmids	Source	Identifier
pAAVS1-PDi-CRISPRn	Mandegar et al. 2016	Addgene #73500
pAAVS1-TALEN-F	Mandegar et al. 2016	N/A
pAAVS1-TALEN-R	Mandegar et al. 2016	N/A
pMDLg/pRRE	Didier Trono Lab	Addgene #12251
pMD2.G	Didier Trono Lab	Addgene #12259
pRSV-Rev	Didier Trono Lab	Addgene #12253
pU6-sgRNA-EF1α-Puro-T2A-BFP	Jonathan Weissman Lab	pDN064; Addgene plasmid #60955
pU6-sgRNA-EF1α-Puro-GFP	This study; from pDN064	pDN115
pU6-sgRNA(*POLR3G*)-EF1α-Puro-GFP	This study; from pDN115	pDN307
pU6-sgRNA(*POLR3B*)-EF1α-Puro-GFP	This study; from pDN115	pDN416
pU6-sgRNA(*MAF1*)-EF1α-Puro-GFP	This study; from pDN115	pDN160

Table 4.4. Oligonucleotides used in this study.

Purpose	Source	Sequence (or Identifier)
RT-qPCR (NANOG)	This study	5’-CCTGTGATTTGTGGGCCTG-3’; 5’-GACAGTCTCCGTGTGAGGCAT-3’
RT-qPCR (POLR3G)	This study	5’-CACTTCGGCTGCAGAGTTTT-3’; 5’-AGTGGGCAAATTCTGAAAG-3’
RT-qPCR (POLR3GL)	This study	5’-AGAGCTACGAGGAGCCATGA-3’; 5’-TTGTCTGAATAACGCTCCACA-3’
RT-qPCR (B2M)	This study	5’-TGCTGTCTCCATGTTTGATGTATCT-3’; 5’-TCTCTGCTCCCCACCTCTAAGT-3’
PCR screening for heterozygous insertion at AAVS1 locus	This study	5′-CGAGAGCTCAGCTAGTCTTC-3′; 5′-CTCTCCCTCCCAGGATCC-3′; 5′-GTTCATTCAGGGCACCGGAC-3′

crRNA for tRNA-Pro-TGG-2-1 gene body swap	This study; Synthesized at IDT	5′-UGUGGGCCAAGGCUAGGGAGGUUUUAGAGCUAUGCU
crRNA for tRNA-Pro-TGG-2-1 upstream sequence edit	This study; Synthesized at IDT	5′-UUGCUCAGCAGAUGGCUCGUGUUUUAGAGCUAUGCU-3′
tracrRNA	IDT Alt-R®	N/A
HDR donor ssODN_1 for tRNA-Pro-TGG-2-1 gene body swap	This study; Synthesized at IDT	G*C*T CTG TGC ATA GGG GCC ATT TGT TCT TGA CCG ACT TCA CTC CAA GGA TCT GGT GTG GGC CAA GGC TAG ACT ACA AGG ACC ACG ACG GCG ATT ATA AGG ATC ACG ACA TCG ACT ACA AAG ACG ACG ATG ACA AGG GGA GTG GGC AGA AGG CGA TGG CTG GTT GGA GAG AAG CCA GGC CGT CTA GTG GGG GAG GAT GG*T* T
HDR donor ssODN_2 for tRNA-Pro-TGG-2-1 gene body swap	This study; Synthesized at IDT	A*A*C CAT CCT CCC CCA CTA GAC GGC CTG GCT TCT CTC CAA CCA GCC ATC GCC TTC TGC CCA CTC CCC TTG TCA TCG TCG TCT TTG TAG TCG ATG TCG TGA TCC TTA TAA TCG CCG TCG TGG TCC TTG TAG TCT AGC CTT GGC CCA CAC CAG ATC CTT GGA GTG AAG TCG GTC AAG AAC AAA TGG CCC CTA TGC ACA GA*G* C
HDR donor ssODN_1 for tRNA-Pro-TGG-2-1 upstream sequence edit	This study; Synthesized at IDT	A*T*C GCC TCT AGT AAA TTC GAG GAG ACC TTG CTC AGC AGA TGA AAA TCA CTA GAT TCT AAA GGA ATC AAA ACT GTT CAA GTG TTG TGC TAC AAC TAA AAA AAT AAA TGA ACA CTC TTA AAG AAT AGA ATC TCT CCA GTT CTG GCT CGT TGG TCT AGG GGT ATG ATT CTC GGT TTG GGT CCG AG*A* G
HDR donor ssODN_2 for tRNA-Pro-TGG-2-1 upstream sequence edit	This study; Synthesized at IDT	C*T*C TCG GAC CCA AAC CGA GAA TCA TAC CCC TAG ACC AAC GAG CCA GAA CTG GAG AGA TTC TAT TCT TTA AGA GTG TTC ATT TAT TTT TTT AGT TGT AGC ACA ACA CTT GAA CAG TTT TGA TTC CTT TAG AAT CTA GTG ATT TTC ATC TGC TGA GCA AGG TCT CCT CGA ATT TAC TAG AGG CG*A* T
PCR screening for tRNA-Pro-TGG-2-1 gene body swap	This study	5′-CAGCCAGGGTGCAAAAACCG-3′; 5′-GCACTTGCTGTATGCCGAGC-3′

PCR screening for tRNA-Pro-TGG-2-1 upstream sequence edit	This study	5′-GGATCAGGGATTCCAAGGCG-3′; 5′-GGTGCAAAAACCGCTTGCTC-3′
sgRNAs (POLR3G)	This study;insert into pDN115	5′- GGACTCGCCGGAGCGCTCTG-3′
sgRNAs (MAF1)	This study; insert into pDN115	5′-GGTGCCGGCCGGCAAGGAAA-3′
sgRNAs (POLR3B)	This study; insert into pDN115	5’-GAGGCACGCAGGGAGCGTCA-3′
Northern blotting (tRNA-Arg-UCU-4)	This study;labeled with 32P at the 5' end	5′-CGGAACCTCTGGATTAGAAGTCCAGCGCGCTCGTCC-3′
Northern blotting (tRNA-Gly-CCC-2)	This study;labeled with 32P at the 5' end	5′-CGGGTCGCAAGAATGGGAATCTTGCATGATAC-3′
Northern blotting (tRNA-Asn-GUU-1)	This study;labeled with 32P at the 5' end	5′-CGTCCCTGGGTGGGATCGAACC-3′

tRNA sequencing and ribosome profiling (RT primer)	This study	5′-pRNAGATCGGAAGAGCGTCGTGTAGGGAAAGAG/iSp18/GTGACTGGAGTTCAGACGTGTGCTC-3′
tRNA sequencing and ribosome profiling (library construction PCR)	This study	Forward: 5′-AATGATACGGCGACCACCGAGATCTACACTCTTTCCCTACACGACGCT∗C-3′; Reverse: 5′-CAAGCAGAAGACGGCATACGAGATNNNNNNGTGACTGGAGTTCAGACGTGT∗G-3′

4.2 Methods

4.2.1 Cell culture

Cell culture and maintenance

hiPSC were cultured in mTeSR Plus medium on plates coated with Geltrex at 37°C/5% CO2. To maintain the cells, the medium was replaced every other day, and every five days the cells were passaged as clusters using 0.5 mM EDTA/PBS solution at a ratio of 1:20. To perform single-cell splitting, the cells were detached with Accutase and then resuspended in mTeSR Plus containing 10 µM of Y-27632 ROCK inhibitor. Cells were counted using the Cell Countess II system and then centrifuged at 200g for 5 minutes. Cells were resuspended in mTeSR Plus medium containing 10 µM of Y-27632. On the following day, the medium was replaced with Y-27632-free mTeSR Plus medium.

mESCs (ES-E14TG2a) were cultured in mESC medium with freshly added inhibitors (CHIR: GSK3β inhibitor; PD: MEK/ERK-pathway inhibitor) and LIF (leukemia inhibitory factor) on plates coated with 0.2% Gelatine solution (Sigma-Aldrich) at 5.0% CO2 and 37°C. Medium was changed every day and the cells were passaged with accutase (Gibco) every 2 - 3 days as single cells.

Lenti-X™ 293T cells (#632180, Takara) and HEK 293T/17 cells (ATCC® CRL-11268™) were maintained in DMEM high glucose medium with 10% FCS, cultured at 37°C/5% CO2. Cell passaging was carried out every two days using 0.25% Trypsin/EDTA, with a ratio of 1:20 to 1:10.

hiPSC differentiation

NPC and neurons were differentiated from HPSI0214i-*kucg-2* by adding small molecules, following established protocols (Reinhardt et al. 2013; Marrone et al. 2019). To derive NPC, hiPSC were cultivated until they reached 90% confluency. A checkered pattern was created on the dish by scratching it with a cannula, after which the cells were incubated with Collagenase IV at 37°C for 10-15 minutes. The cell clusters were gently scraped from the plate and transferred to a 15-ml tube containing N2B27 medium consisting of a mixture of Neurobasal medium (Gibco, #21103049) and DMEM/F12 (Gibco, #21331020) in a 50:50 ratio, supplemented with N2 Supplement (0.5x; Thermo Fisher Scientific, #17502048), B27 Supplement (0.5x; Thermo Fisher Scientific, #12587010), and GlutaMAX™ (2 mM; Gibco, #35050061). The cell suspension was then pelleted by centrifugation. The cell clusters were rinsed once with N2B27 medium and subsequently transferred to a sterile dish without coating. They were then resuspended in NPC-induction medium (NPC-IM; N2B27 supplemented with ascorbic acid (200 µM; AA; Sigma Aldrich, #A4403), CHIR99021 (3 µM; Axon Medchem, #Axon1386), PMA (0.5 µM; Santa Cruz Biotechnology, #sc-202785A), Dorsomorphin (150 nM; Absource, #S7306), and SB431542 (10 µM; Biomol, #Cay12031), along with Y-27632 (5 µM). This was incubated at 37°C/5% CO2, allowing embryoid bodies (EBs) formation. the medium was replaced every other day with NPC-IM without ROCK inhibitor Y-27632. On day six, the embryoid bodies were dissociated into individual cells by pipetting and then seeded onto a Geltrex-coated well containing NPC expansion medium (NPC-EM; N2B27 supplemented with ascorbic acid (200 µM; AA), CHIR99021 (3 µM), and PMA (0.5 µM)). The medium was replaced every two days. In order to eliminate non-NPC cells, a sequential digestion process was conducted during the initial passages using Accutase. For regular passaging, the cells were treated similarly to single-cell passaging of hiPSC, carried out every 5 days at a 1:10 ratio.

To induce the differentiation of neurons from NPC (Marrone et al. 2019), the cells were first singularized using Accutase. Subsequently, one million cells were plated into a 6-well containing the patterning medium (PM; N2B27 supplemented with AA (200 µM), retinoic acid (1 µM; Sigma Aldrich, #R2625), PMA (0.5 µM), and GDNF/BDNF (10 ng/ml; Peprotech, #450-10 and #450-02). The cells were cultured for six days, with the medium being replaced every two days. On the sixth day, the medium was replaced with maturation medium (MM; N2B27 supplemented with AA (200 µM), dbcAMP (100 µM; Sigma Aldrich, #D0627),

GDNF/BDNF (5 ng/ml), TGF-β3 (1 ng/ml; Peprotech, #AF-100-36E), and Activin A (5 ng/µl; Life Technologies, #PHG9014). Two days later, the medium was changed to MM excluding Activin A. The cells were maintained for additional ten days, with regular medium changes every two or three days. On day 16, the cells were dissociated using Accutase and resuspended in MM, then centrifuged for 5 minutes at 200g. The cell pellets were transferred to a fresh plate. On day 19, the medium was supplemented with CompE (0.1 µM; Merck, #565790) to promote neuronal maturation. The cells were harvested on day 21.

Cardiomyocytes were differentiated from hiPSC line using a previously described method with some modifications (Zhang, Schulte, et al. 2015). hiPSC were singularized using Accutase, and then seeded on Matrigel-coated plates containing day 0 differentiation medium (KO-DMEM (Gibco #10829-018) supplemented with L-Glutamine (2 mM; Gibco #25030-024), each insulin/transferrin/selenious acid (5 µg/ml, ITS - Corning#354351), FGF2 (10 ng/ml; Peprotech #100-18B-250), CHIR 99201 (1 µM; Axon #Axon 1386), BMP-4 (1 ng/ml; R&D #314-BP-010), Activin A (5 ng/ml; Life Technologies #PHG9014), ROCK inhibitor (10 µM; Y-27632; Stemcell Technologies #72305)). After one day, medium was replaced with transferrin/selenium (TS) medium (KO-DMEM supplemented with L-Glutamine (2 mM), human transferrin (5.5 µg/ml; Sigma-Aldrich #TS8158-100mg), sodium selenite (6.7 ng/ml; Sigma-Aldrich #214485), ascorbic acid (250µM; Sigma #A4403-100mg)). On both day 2 and 3, the medium was changed to TS medium containing WNT-inhibitor C59 (0.2 µM; Tocris #5148). Daily medium exchanges were performed until day 9. To enrich the population of cardiomyocytes, cells were subjected to glucose deprivation for one day with TS-minus glucose medium (DMEM w/o Glucose (Gibco #A13320-01)supplemented with L-Glutamine (2 mM), human transferrin (5.5 µg/ml), sodium selenite (6.7 ng/µl) , ascorbic acid (250 µM), Lactic Acid (4 mM; Sigma L4263-100ml)). On day 10, the cells were detached using Accutase and seeded on Matrigel-coated wells in CM-Maturation medium (KO-DMEM supplemented with FCS (2%; Gibco #16000-044), L-Glutamine (2 mM), ROCK inhibitor (10 µM). On the following day, the medium was changed with fresh CM-MMwithout the ROCK inhibitor. Subsequent medium exchanges were performed every other day until the cells were harvested on day 15.

4.2.2 Molecular cloning

DNA Digestion and fragments clean-up

1 µg plasmids were digested with 2-5 units of enzyme (NEB)at 37°C for 2 hours, Backbone dephosphorylation was performed by adding 5 units of Antarctic phosphatase 30 minutes prior to the end of the incubation. PCR products were purified with the Zymo DNA Clean & Concentrator kit. plasmid digestions were purified through agarose gel size selection, gel excision, and subsequent gel extraction using the Gel Extraction Kit from Analytics Jena.

Ligation and Gibson Assembly

Ligation of the backbone to the insert was conducted at a molar ratio of 1:3 with T4 Ligase (M0202S) following the manufacturer's instruction. Subsequently, 2 µl of the ligation mix was used for the transformation step.

Gibson assembly was performed using a custom-made Gibson Master Mix obtained from the Core Facility at MPI Biochemistry. Assembly of backbone with the insert was conducted at a molar ratio of 1:3, incubated for 2 hours at 50°C. 2 µl of the assembly mix was used for the transformation step.

Bacterial transformation, purification and Sanger sequencing

Top10 competent bacteria were thawed while being kept on ice. 50 µl of the thawed competent bacteria cells was mixed with plasmid DNA and incubated on ice for 30 minutes. The cells were incubated at 42°C for 45 seconds for heat shock, and immediately placed on ice for 5 minutes. The cells were supplemented with 200 µl of SOB medium and incubated at 37°C for at least one hour. The cells were spread onto LB plates containing Carbenicillin antibiotics and then incubated overnight at 37°C. Next day, colonies were picked for culturing overnight and DNA was purified with innuPREP Plasmid Mini Kit (Analytik Jena) and sent for Sanger sequencing at Eurofins Genomics using Tube-to-Seq service, with plasmid diluted to 50 ng/µl in 15 µl and 2 µl 10 µM sequencing primer combined.

Plasmid construction

The vector plasmid for single guide RNA knockdown (pDN115 pU6-sgRNA-EF1α-Puro-GFP) was cloned from pDN064_pU6-sgRNA EF1α-Puro-T2A-BFP by replacing the BFP with a GFP cassette. To insert the sgRNA, the expression vectors pDN115 were digested using BstXI and BlpI, then assembled by Gibson assembly using sgRNA oligos harboring 30bp overhangs Successful insertion was confirmed through Sanger sequencing. All primers used were listed in **Table 4.4.**

4.2.3 CRISPRi workflows

Generation of inducible CRISPRi hiPSC line

HPSI0214i-*kucg-2* cells were genetically modified by Geradline Rodschinka to incorporate a doxycycline-inducible promoter-driven KRAB-dCas9 construct at the human *AAVS1* locus. The plasmid pAAVS1-PDi-CRISPRn was generously provided as a gift from Bruce Conklin (Addgene plasmid #73500; RRID: Addgene_73500). After nucleofection together with forward and reverse TALEN arms, cultures were subjected to antibiotic selection using G418 (100 µg/ml) until stable colonies emerged from single cells. Following the selection, individual colonies were picked and subjected to PCR screening for heterozygous insertion with two primers flanking the human *AAVS1* locus (5′-CGAGAGCTCAGCTAGTCTTC-3′ and 5′-CTCTCCCTCCCAGGATCC-3′) along with an extra primer that binds to the insert (5′-GTTCATTCAGGGCACCGGAC-3′). Flow cytometry and immunoblotting analyses were performed to assess the expression of KRAB-dCas9 in positive clones, following the addition of doxycycline (2 µM). Expanded clones were subjected to G-band analysis to confirm the integrity of the genome.

CRISPRi library design

An adapted workflow for the CRISPRiaDesign protocol was utilized to design sgRNAs that specifically target the transcription start sites (TSS) of genes with the GENCODE v19 annotation. For incorporating SNPs information in the genome of HPSI0214i-*kucg-2*, GATK haplotype calls were used for the cell line, and variant sites were extractedexclusively using the gvcftools *extract_variants v0.17.0*. The generated genomic variant call format (GVCF) file was then indexed and the genotypes were called with GATK *GenotypeGVCFs v4.1.0.0*. To preserve the genomic context and theposition information in GRCh37 and our customized genome, only SNPs were retained. GATK *SelectVariants v4.1.0.0*was used for this with the parameter "-select-type SNP". To replace nucleotides in the GRCh37 reference genome usingthe called genotype SNPs, a sequence dictionary was first created from the reference genome with Picard *CreateSequenceDictionary* v2.17.10. The SNP VCF file was then supplied to GATK *FastaAlternateReferenceMaker*v4.1.0.0 in order to generate the altered reference genome. For training a linear regression model using elastic net to predict sgRNA activity, the custom genome was combined with additional training data obtained from the CRISPRia pipeline, including TSS predictions and sgRNA activity scores, as well as our own ATAC-Seq

data obtained from the HPSI0214i-*kucg-2* cells as a representative measure for chromatin accessibility. Following the prediction of activity scores, the identification of off-targets per sgRNA was performed as described.

CRISPRi knockdown

Single guide RNAs were cloned into pU6-sgRNA EF1α-Puro-T2A-GFP using Gibson assembly. This construct was generated by replacing BFP (Blue Fluorescent Protein) with GFP (Green Fluorescent Protein) in pU6-sgRNA EF1α-Puro-T2A-BFP, a gift from Jonathan Weissman (Addgene plasmid #60955), and verified with Sanger sequencing. Lentivirus stocks containing sgRNAs were generated by co-transfecting the resulting plasmid with three lentiviral packaging plasmids, pRSV-Rev (Addgene plasmid #12253), pMDLg/pRRE (Addgene plasmid #12251;), and pMD2.G (Addgene plasmid #12259), using TransIT®-Lenti Transfection Reagent (Mirus, # MIR6603) into Lenti-X™ 293T cells, according to the manufacturer's instructions. The viral supernatant was collected 48-72 hours post-transfection and filtered using a PVDF syringe filter (0.45 μm). The supernatant was then precipitated overnight at 4°C using Lentivirus precipitation solution (Alstembio, #VC125). The virus stocks were concentrated by ten fold using cold PBS, divided into smaller aliquots, and then stored at -80°C.

hiPSC were transduced by mixing thawed lentivirus stock and fresh medium onto the plates, incubated for 10 minutes at 37°C/5% CO2, followed by adding the trypsinized cells to the plates containing lentivirus. The hiPSC were cultured with lentivirus for two days, after which they were split and selected with puromycin (2.5 μg/ml) for 2-3 days until the proportion of GFP-positive cells surpassed 80%. NPC transduction was similar to hiPSC, except that lentivirus incubation was shortened to one day, and was carried out without doxycycline. Transduced cells were subjected to antibioticselection with puromycin (2.5 μg/ml) in the absence or presence of doxycycline, respectively, until the proportion of GFP-positive cells exceeded 80%.

4.2.4 Genome editing with CRISPR-Cas9 RNP

The tracrRNA, crRNA and ssODN templates were acquired from IDT. The gRNAs were generated by annealing the crRNA (5′-UGUGGGCCAAGGCUAGGGAGGUUUUAGAGCUAUGCU-3′ for the *tRNA-Pro-TGG-2-1* gene body swap; 5′- UUGCUCAGCAGAUGGCUCGUGUUUUAGAGCUAUGCU-3′ for

the *tRNA-Pro-TGG-2-1* upstream sequence edit) with tracrRNA in equal molar ratios at 95°C for 5 minutes following the manufacturer's instructions. The Ribonucleoprotein (RNP) complex was formed by combining gRNA (100 pmol) with Alt-R HiFi Cas9 (50 pmol; IDT), followed by incubation for 20 minutes at room temperature. HPSI0214i-*kucg-2* cultures were singularized using Accutase and then nucleofected with the preassembled RNP and HDR donor oligo using the CA137 program with P3 solution (Lonza) in Nucleocuvette™ Strips. The cells were subsequently transferred to new culture plates and replated in mTeSR Plus medium, supplemented with CloneR™ (1:10 dilution; Stem Cell, #05888). Medium was replaced with mTeSR™ Plus every other day until colonies are ready to be picked. Colonies were individually picked and expanded. Homozygously edited clones were screened out by PCR amplifying genomic DNA with primers that flank the target region. Sanger sequencing was then carried out to confirm the sequence modifications.

4.2.5 RNA workflows

RNA isolation

The cells were lysed using LiDS/LET buffer (5% LiDS in solution containing 20 mM Tris; 2 mM EDTA; 100 mM LiCl; 5 mM DTT, pH 7.4). Proteinase K was supplemented at 100 µg/ml fresh in the buffer prior to lysis reaction. The lysates were incubated for 10 minutes at 60°C, followed by pushing 10 times through a 26G needle fitted in 1ml syringe andvortexing. Two volumes of ice-cold acid phenol (pH 4.3) were added to the lysates, along with 1/10 volume of 1-Bromo-3-chloropropane, as well as 50 µg glycogen (Thermo Fisher Scientific #AM9510). The samples were thoroughly mixed by vigorous vortexing, and centrifuged at 10,000g, 4°C. The upper aqueous phase was carefully transferred to a fresh tube. The phenol/BCP extraction was then repeated to ensure efficient separation and purification. For RNA precipitation,3 volumes of 100% ice-cold ethanol were added to the aqueous phase, and incubated at -20°C for at least 30 minutes. The RNA pellets were carefully washed with 80% ethanol, followed by gentle air-drying. Finally, the pellets were reconstituted in RNase-free water. The concentration of RNA was determined using a Nanodrop spectrophotometer, and the samples were subsequently stored at a temperature of -80°C for long-term preservation.

DNase treatment

10 µg RNA was digested with Turbo DNase (Thermo Scientific) for 30 minutes at 37°C/1500rpm. For RNA extraction, acid phenol (pH 4.3) of one volume, BCP and 3M NaOAc

(pH 4.5) at one-tenth of the volume and 10µl of Glycogen were added and thoroughly mixed. The samples were then centrifugated at 10,000xg for five minutes at 4°C. The aqueous phase was then transferred to a fresh tube and washed with an equal volume of BCP by mixing, followed by centrifugation at 10,000xg/4°C for 5 minutes. The RNA was then precipitated by adding three volumes of 100% ice-cold ethanol, and the resulting pellets were subsequently resuspended in water.

Quantitative RT-PCR

For reverse transcription, 1 µg of the DNase-treated RNA was reverse transcribed to cDNA with the Protoscript II First Strand cDNA Synthesis Kit from NEB, with the 20 µl reaction volume diluted to 50 µl by adding water and then stored at -20°C. The KAPA SYBR Fast qPCR Mix from Roche was utilized for quantitative RT-PCR, with primers listed in **Table 4.4**. ΔΔCt values relative to the control samples were calculated.

Northern blotting

0.5 µg total RNA was separated on 10% denaturing polyacrylamide/7M urea/1×TBE gels. RNA was then transferred onto the Immobilon-Ny+ membranes (Millipore) using 1×TBE buffer at a constant current of 4mA/cm2 for 40 minutes in the TransBlot Turbo transfer system (Bio-Rad). The transferred RNA was crosslinked using a Stratalinker UV crosslinker at 0.04 J. The membranes were incubated for one hour at 80°C, followed by pre-hybridization for 4 hours at 55°C in hybridization buffer (Na2HPO4 (20 mM; pH 7.2), 5× SSC, 7% SDS, 2× Denhardt solution, sheared salmon sperm DNA (40 µg/ml)). The membranes were incubated overnight with 10 pmol of probes labeled with ^{32}P at the 5' end (tRNA-Arg-UCU-4: 5′-CGGAACCTCTGGATTAGAAGTCCAGCGCGCTCGTCC-3′; tRNA-Gly-CCC-2: 5′-CGGGTCGCAAGAATGGGAATCTTGCATGATAC-3′; tRNA-Asn-GUU-1: 5′-CGTCCCTGGGTGGGATCGAACC-3′). The membranes were subjected to three washes with solution containing Na2HPO4 (25 mM; pH 7.5), 5% SDS, 3×SSC and 10×Denhardt, followed by one time wash in 1×SSC and 10% SDS. The membranes were then exposed to Phosphor screens and scanned using a Typhoon FLA 9000 (GE Healthcare). Intensity of the bands was quantified using ImageJ software.

RNA-Seq library construction

250 ng total RNA (same samples as used for preparing mim-tRNAseq library) was used to construct mRNA-Seq library using Zymo-Seq RiboFree Total RNA Library Kit (Zymo Research, #R3000). Libraries were quantified using the Qubit dsDNA HS assay and the fragment size was determined using an Agilent TapeStation. Subsequently, Sequencing of the libraries was performed on the Illumina NovaSeq platform with120 cycles, generating at least 21 million reads for each library.

RNA-Seq data analysis

The preprocessing of RNA-Seq datasets involved removal of potential 3' adapters with Trim Galore v0.6.4 using default settings, and only reads with a length of 20 or more were retained. Alignment of reads to the human GRCh38 genome was carried out using STAR v2.6.1c with the following settings, only retaining uniquely mapped reads containinga maximum of one mismatch as well as gene-level quantification of the sequencing reads: *--outSAMtype BAM SortedByCoordinate --outFilterMultimapNmax 1 --outFilterMismatchNmax 1 --quantMode TranscriptomeSAM GeneCounts.* In addition, featureCounts v1.6.2 was employed to count reads that overlapped with a filtered subset of protein-coding gene annotations obtained from the basic gene annotation database GENCODE. Differential gene expression analysis was conducted with DESeq2 v1.38.1 using default settings and the gene counts obtained fromfeatureCounts. The gene expression heatmaps were created with standardized gene read counts and the values of significant log2 fold-change (p-adj ≤ 0.05) obtained from DESeq2 were combined using ComplexHeatmap v2.14.0116.Using the same scaled read counts matrix, heatmaps for specific gene subsets were created by subsetting specific gene lists before plotting.

Construction of tRNA sequencing libraries

The preparation of tRNA-Seq libraries was carried out with the mim-tRNAseq workflow. In brief, total RNA samples from two biological replicates of each cell line was combined with synthetic *E.coli* tRNAs (tRNA-Lys-UUU-CCA and tRNA-Lys-UUU-CC) in a ratio of 3:1, dephosphorylated using T4 PNK (NEB, #M0201S) and precipitated with ethanol.RNA was separated on denaturing gels consisting of 10% polyacrylamide, 7M urea, and 1× TBE buffer. RNA with length of 60 -100 nt was extracted by gel excision and elution, followed by ethanol precipitation. Next, preadenylated, barcoded 3'-adapters was ligated to the gel-purified tRNA in 1× T4 RNA ligase buffer, 20 U Superase In (Thermo Scientific, #AM2696), 25% PEG-8000, and 1 µl T4 RNA Ligase 2, truncated KQ (NEB, #M0373S). The mix was incubated at 25°C

for 3 hours, and the resulting ligation products were then purified by size selection using a 10% polyacrylamide gel containing 7M urea and 1× TBE buffer. 100 ng of the adapter-ligated tRNA was then annealed by combining with 1 µl 1.25 µM RT primer (5′-pRNAGATCGGAAGAGCGTCGTGTAGGGAAAGAG/iSp18/GTGACTGGAGTTCAGAC GTGTGCTC-3′) and incubating for 2 minutes at 82°C, followed by 5 minutes incubation at 25°C. Reverse transcription was carried out with TGIRT (500 nM; InGex, #TGIRT50) in a reaction mixture containing Tris-HCl (50 mM; pH 8.3), KCl (75 mM), MgCl2(3 mM), DTT (5 mM; prepared from a freshly made 100 mM stock), dNTPs (1.25 mM) and Superase In (20 U) for 16h at 42°C. Following reverse transcription, the RNA samples were added with NaOH (0.1 M) and hydrolyzed by incubating at 90°C for 5 minutes. The cDNA products were separated from the unextended primer by resolving on a 10% polyacrylamide gel containing 7M urea and 1× TBE buffer. Following staining with SYBR Gold, the gel regions containing cDNAs that were at least 10 nucleotides longer than the RT primer were carefully excised. The gel slices were then crushed using a pestle, and the DNA was eluted in 1× TE buffer at 1500 rpm and 70°C for 60 minutes. Gel debris was eliminated by centrifugation through a Spin-X filter and the cDNA was purified with ethanol precipitation. For cDNA circularization, the gel-purified cDNA samples were incubated with CircLigase ssDNA ligase (Lucigen) in 1× reaction buffer containing1 mM ATP, 50 mM MgCl2 and 1M betaine at 60°C for 3 hours. After 10 minutes incubation at 80°C for enzymeinactivation, 1/5 of the circularized cDNA was utilized for library construction PCR using a common forward primer (5′-AATGATACGGCGACCACCGAGATCTACACTCTTTCCCTACACGACGCT∗C-3′) and reverse primers with unique indexes (5′-CAAGCAGAAGACGGCATACGAGATNNNNNNGTGACTGGAGTTCAGACGTGT∗G-3′, NNNNNN represents the reverse complement for Illumina index sequence; phosphorothioate bonds are denoted by asterisks) in 1× GC buffer with KAPA HiFi DNA Polymerase (Roche). The PCR reaction was initiated with an denaturation step of 3 minutes at 95°C, followed by five cycles of 20 seconds at 98°C, 30 seconds at 62°C, and 30 seconds at 72°C, with a ramp rate of 3°C per second. The PCR products were purified using the DNA Clean&Concentrator 5 kit (Zymo Research), followed by quantification using Qubit dsDNA HS kit (Thermo Scientific, #Q32851). The libraries were sequenced on the Illumina NextSeq 550 platform for 150 cycles, generating at least 2.5 million reads for each library.

tRNA sequencing data analysis

For demultiplexing and removal of 3' sequencing adapters, cutadapt v3.5 was utilized. During the process, indels were not allowed (--no-indels), and quality trimming with a minimum score of 30 (-q 30,30) was applied to both read ends.Considering that the sequencing was conducted with more cycles compared to the length of any fragment sequenced, all reads should contain adapters and only the trimmed reads were retained using the "--trimmed-only" option. Subsequently, reads were trimmed further to eliminate the two 5'-RN nucleotides resulting from circularization by the RT primer, using the parameter *-u* 2. During both processing steps, reads < 10 nt were excluded from further analysis using the parameter *-m* 10. Analysis of tRNA expression and modification was performed using the computational package v 1.2 of mim-tRNAseq (https://mim-trnaseq.readthedocs.io/en/latest/index.html). In brief, the analysis used the pre-compiled GtRNAdb human hg38 reference with the species parameter set to Hsap (*--species Hsap*). The clustering was performed with a cluster ID of 0.97, allowing a maximum mismatch tolerance at a proportion of 7.5% of the read length for the first round of alignment and 5% of the read length for realignment. The deconvolution coverage ratio was set to 0.4 at mismatch sites to enable accurate cluster deconvolution. A minimum coverage threshold was set to 0.05% of the total reads per transcript for filtering the low coverage transcripts (*mimseq --species Hsap --cluster-id 0.97 --threads 40 --min-cov 0.0005 --max-mismatches 0.075 --control-condition kiPSC --deconv-cov-ratio 0.4 -n hg38_diff --out-dir hg38_WTdiff_2rep_deconv0.4_ID0.97_0.075_remap0.05_v12/ --max-multi 6 --remap --remap-mismatches 0.05 sampleData_ht_diff_2rep.txt.).*

4.2.6 Protein workflows

Immunoblotting

Cell lysis was performed using RIPA buffer containing 20 mM Tris pH 7.5, 1% NP-40, 0.5% sodium deoxycholate, 150 mM NaCl, 0.1% SDS, 20 µM leupeptin, 10 µg/ml aprotinin, 0.5 mM AEBSF, 2.5 µM pepstatin A and 1x Phosphatase Inhibitor Cocktail (Cell Signaling, #5870). The protein concentration was determined using the Pierce™ BCA Protein Assay Kit (Thermo Scientific, #23225). 20 µg of total protein was separated by 10% homemade SDS-PAGE gel supplemented with 2,2,2-Trichloroethanol (TCE; 0.5%; Sigma, #T54801), or 4%–12% precast Bis-Tris gels (Life Technologies) using Bolt™ MES SDS Running Buffer (1x; Invitrogen, #B0002). TCE-stained total protein was visualized by UV illumination using a ChemiDoc system (Bio-Rad). The proteins were subsequently transferred onto the nitrocellulose membrane (Amersham, #10600015). To visualize total protein in the precast gels,

the membranes were gently shaken in Ponceau S solution (0.5% Ponceau S, 1% acetic acid) for 3 minutes at room temperature to stain the total protein. After rinsing with distilled water and PBST (0.1% Tween-20), the membranes were imaged on BioRad. The membranes were incubated in a blocking solution of 5% milk/PBST (0.1% Tween-20) for 1 hour, followed by overnight incubation at 4°C with primary antibodies. Primary antibodies used in immunoblotting include rabbit anti-*POLR3A*/RPC1 (1:1000 diluted; Cell Signaling; #12825), mouse anti-*POLR3B*/RPC2 (1:1000 diluted; Santa Cruz; #sc-515362), mouse anti-Pol III RPC32/RPC7α (1:1000 diluted; Santa Cruz; #sc-21754), mouse anti-MAF1 (1:1000 diluted; Santa Cruz; #sc-515614 X), anti-phospho-p70 S6 Kinase (1:1000 diluted; Cell Signaling, #9206S), rabbit anti-phospho-4E-BP1 (1:1000 diluted; Cell Signaling, #2855T), and rabbit anti-vinculin (1:1000 diluted; Cell Signaling; #13901). HRP-conjugated secondary antibodies were then added to the membranes and incubated for 1 hour at room temperature. The secondary antibodies used include anti-rabbit IgG-HRP (1:4000 diluted; Dianova, #111-035-003) or anti-mouse IgG-HRP (1:4000 diluted; Dianova, #115-035-003). Proteins were detected using chemiluminescence with SuperSignal West Pico Plus substrate (Thermo Scientific, #34577) and captured using iBright imaging system (Thermo Scientific).

For immunoblotting of S6K1 and 4EBP1, the membranes were first incubated with phospho antibodies including anti-phospho-4E-BP1 (1:1000 diluted; Cell Signaling, #2855T), anti-phospho-p70 S6 Kinase (T389), (1:1000 diluted; Cell Signaling, #9206S). The membranes were stripped by gently shaking at at room temperature in Restore Western Blot stripping buffer (Thermo Scientific, #21059) for twice of 15 minutes. After blocking again, the membranes were re-probed with primary antibodies against total proteins including anti-4E-BP1 (1:2000 diluted; Cell Signaling, #9644) and anti-p70 S6 Kinase (1:2000 diluted; Cell Signaling, #2708T).

To perform Phos-tag immunoblotting, 20 µg of total protein was combined with 4x Laemmli Sample Buffer (1x; Biorad #161-0747) containing 25 mM DTT. The mixture was then heated at 95°C for 10 minutes. The denatured samples were loaded onto Phos-tag gels (8% Acrylamide/Bis solution 29:1; 20 µM Phostag (Wako #AAL-107); 0.375 M Tris-Cl, pH 8.8; 40 µM MnCl2) and the electrophoresis was performed in Tris/Glycine/SDS running buffer (1x; Biorad, #1610732). The gels were subject to two times of 10 minutes gentle shaking in transfer buffer (25 mM Tris, 192 mM glycine, 10% methanol) supplemented with 1 mM EDTA, followed by two additional 10-minute washes in the transfer buffer lacking EDTA.

Transferring of protein to PVDF membranes (Amersham, #10600021) was carried out overnight at room temperature intransfer buffer (25 mM Tris, 192 mM glycine, 10% methanol) at 35V. The membrane was blocked with 5% milk/PBST solution (0.1% Tween-20) for 1 hour at room temperature, and then incubated overnight at 4°C with primary mouse anti-MAF1 antibody (1:1000 diluted; Santa Cruz; #sc-515614 X) and secondary anti-mouse IgG-HRP antibody (1:4000diluted; Dianova, #115-035-003) for 1 hour at room temperature. Protein visualization was performed with SuperSignal West Femto Maximum Sensitivity Substrate (Thermo Scientific, #34094) and captured using iBright system.

Immunostaining

Cells were cultured on µ-Slide 8 Well glass bottom (ibidi, #80827). Cultured cells were rinsed with PBS and then fixed with 3.7% formaldehyde by gently shaking at room temperature for 10 minutes. Formaldehyde was gradually replaced with PBST (0.02% Tween-20), and this was followed by three complete rinses with PBS to ensure complete removal. hiPSC and NPC were subsequently subjected to permeabilization for 10 minutes using 0.5% Triton-X100/PBST, followed by one hour incubation in blocking solution (PBS containing 3% BSA and 0.1% Triton-X100). Cells were then incubated overnight at 4°C with primary antibodies diluted in the blocking solution (POU5F1 C-10, 1:400 diluted, Santa Cruz, #sc-5279; SOX2 E-4, 1:200 diluted, Santa Cruz, #sc-365823; Nanog P1-2D8, 1:200 diluted, Millipore #MABD24; PAX6, 1:200 diluted, Abcam #ab5790; Nestin, 1:200 diluted, R&D Systems, #MAB1259). Following three washes with PBST, cells were exposed to secondary antibody diluted with blocking solution at room temperature for one hour (goat anti-mouse Alexa Fluor 488, 1:2000 diluted, Thermo Scientific, #A-11001; goat anti-rabbit Alexa Fluor 488, 1:2000 diluted, Thermo Scientific, #A-11034; goat anti-mouse Alexa Fluor 633, 1:500 diluted, Thermo Scientific, #A-21052). Cells were subjected to three washes with PBST prior to imaging, with DAPI added at 1:1000 dilution during the second washingstep. Neurons were permeabilized with 0.7% Tween-20/PBS for 10-minute, followed by blocking in neurons blocking solution (PBS supplemented with 1% BSA, 0.1% Triton-X100, and 10% FCS) for one hour. After washing in 0.1% BSA/PBS, cells were incubated overnight at 4°C with the primary antibodies in 1% BSA/PBS (MAP2, 1:1000 diluted, Abcam, #ab92434; CHAT, 1:200 diluted, Abcam, #ab6168). Following three times of wash with 0.1% BSA/PBS solution, the cells were incubated with secondary antibodies diluted in 1% BSA/PBS at room temperature for one hour (goat anti-rabbit A633, 1:500 diluted, Thermo Scientific #A-21070; goat anti-chicken A488, 1:2000

diluted, Thermo Scientific, #A-11039). Cells were then washed again for three times with 0.1% BSA/PBST solution (containing 0.05% Tween-20), with DAPI added at 1:1000 during the second wash. The cardiomyocytes were blocked and permeabilized by incubating in blocking solution (3% BSA and 0.1% Triton-X in PBS) at room temperature for one hour. Following three washes in PBS-T (PBS with 0.1% Tween), cells were incubated together with primary antibodies (ACTN2, 1:800 diluted, Sigma-Aldrich #A7811; cTNT, CT3, 1:5 diluted, DSHB) diluted with staining solution (1 % BSA and 0.1 % Tween in PBS) overnight at 4°C. Following three times wash with PBST (PBS with Tween-20), cells were incubated with secondary(goat anti-mouse Alexa Fluor 488, 1:2000 diluted, Thermo Scientific, #A-11001) and DAPI (1:1000) diluted with staining solution at room temperature for one hour in the dark. After three times wash with PBS containing 0.1% Tween, cells were then imaged in PBS.

4.2.7 ChIP-Seq and ATAC-Seq workflows

ChIP-Seq library construction

Cultured cells in 6-wells were fixed using 0.8% methanol-free formaldehyde solution (Thermo Scientific, #28906) in DMEM at room temperature for 10 minutes with gentle shaking. The crosslinking was then quenched by adding 0.125 M glycine and shaking at room temperature for 5 minutes. After two washes with ice-cold PBS, cells were resuspended using Farnham buffer (5 mM PIPES, pH=8.0; 85 mM KCl; 0.5% IGEPAL-CA 630) and snap-frozen in liquid nitrogen. Before use, all buffers were added with cOmplete™ EDTA-free Protease Inhibitor Cocktail (Roche, #1187358000). Isolation and shearing of chromatin were carried out following the NEXSON protocol. Frozen cell pellets were gently thawed on ice and sonicated in 1 ml tubes (Covaris, #520130) for 2 minutes on Covaris S220 sonicator with the following parameters: peak power = 75W, duty factor = 2%, and cycles/burst = 200. The resulting isolated nuclei were rinsed once with Farnham buffer and then resuspended with shearing buffer (10 mM Tris-HCl, pH 8.0; 0.1% SDS; 1 mM EDTA). All chromatin was sheared using a Covaris S220 sonicator in 1ml tubes for 18 minutes with the following parameters: peak power = 140W; duty factor = 5%; cycles/burst = 200, except that chromatin used for BRF1 ChIP was sheared for 9 minutes with the same settings. The sheared chromatin was clarified through centrifugation at 16,000g for 10 minutes. 10 µl of the sheared chromatin was utilized for quality control analysis on the Agilent TapeStation system. Size distribution of DNA fragments ranging from 100 to 800 bp was regarded as appropriate for ChIP reaction. After shearing, the chromatin was rapidly frozen in liquid nitrogen, divided into aliquots, and then stored at -80°C.

10µl aliquot was used for DNA concentration determination. For this, the samples were decrosslinked by incubating with 0.2 M NaCl at 65 °C overnight, then incubated with 50 µg/ml RNaseA (Thermo Scientific, #EN0531) for 30 minutes at 37 °C, followed by incubation with 200 µg/ml Proteinase K (Sigma-Aldrich, #P2308) for 1 hour at 65 °C. DNA purification was carried out using the DNA ChIP Clean & Concentrator kit (Zymo Research, #D5205), eluting in 10 µl of the Elution buffer (10 mM Tris, pH 8.5 and 0.1 mM EDTA.

Sheared chromatin was placed on ice after thawing. For RPC1 ChIP, 5 µg of chromatin was diluted at a 1:8 ratio using ChIP Dilution buffer (23 mM Tris-HCl, pH=8.0; 200 mM NaCl; 2.3 mM EDTA;1.3% Triton X). Magna ChIP™ Protein A+G Magnetic Beads (Merck, #16-663) were blocked in 5 mg/ml BSA in PBS at room temperature for 2 hours on a rotating platform, followed by resuspending in ChIP Dilution buffer. Chromatin was supplemented with 0.5% *D. melanogaster* chromatin (Active Motif, #53083) as spike-in and pre-cleared by incubating with 10 µl BSA blocked magnetic beads at 4°C for 1 hour on a rotating platform. Following the removal of beads, pre-cleared chromatin was incubated with 5 µg *POLR3A*/RPC1 antibody (Cell Signaling Technology, #12825) and 0.2 µg of spike-in *Drosophila* antibody (Active Motif, #61686) on a rotating platform overnight at 4°C. For H3K4me3 and H3K27me3, each ChIP was performed with 2 µg of pre-cleared chromatin and 5 µl of H3K4me3 antibody (Active Motif, #39159) or H3K27me3 antibody (Millipore, #07-449). The spike-in chromatin or antibody was not included in these experiments. The samples were incubated with 60 µl of BSA-blocked magnetic beads at 4 °C for 2 hours on a rotating platform. The chromatin-antibody-beads complexes were sequentially washing using low-salt buffer (0.1% SDS, 1% Triton X-100, 2 mM EDTA pH=8.0, 20 mM Tris-HCl pH=8.0, 150 mM NaCl), high-salt buffer (0.1% SDS, 1% Triton X-100, 2 mM EDTA pH=8.0, 20 mM Tris-HCl pH=8.0, 500 mM NaCl), lithium chloride buffer (0.25 M LiCl, 1% IGEPAL-CA 630, 1% sodium deoxycholate, 1 mM EDTA, 10 mM Tris-HCl, pH=8.0) and Tris-EDTA buffer (10 mM Tris-HCl, 1 mM EDTA pH=8.0).Each wash step was repeated twice, 10 minutes each, on a rotating platform at 4°C. DNA was then eluted from the beads in ChIP elution buffer (1% SDS, 50mM NaHCO3) for two times of 30 minutes on a rotating platform at room temperature. Reverse crosslinking and DNA purification was following the same procedure as for the input chromatin.

For BRF1 and *POLR3G*/RPC7α ChIP, 5 µg of sheared chromatin was diluted with ChIP RIPA buffer (50 mM Tris-HCl pH=8.0, 150 mM NaCl, 2 mM EDTA pH=8.0, 1% NP-40, 0.5%

sodium deoxycholate, 0.1% SDS) at a ratio of 1:8 and pre-cleared as mentioned above. The magnetic beads were blocked with 5 mg/ml BSA in PBS as described for RPC1 ChIP, but then resuspended with ChIP RIPA buffer. 5 µg of precleared chromatin was incubated with 10 µl of anti-BRF1 antibody (Abcam, #ab264191) or 20 µl of anti-*POLR3G*/RPC7α antibody (Santa Cruz, #sc21754) on a rotating platformovernight at 4°C. Then the chromatin-antibody complexes were incubated with 60 µl of BSA-blocked magnetic beads while rotating at 4 °C for 6 hours. The beads were washed three times in low salt buffer buffer (0.1% SDS, 1% Triton X-100, 2 mM EDTA pH=8.0, 20 mM Tris-HCL pH=8.0, 150 mM NaCl) and one time in high salt buffer (0.1% SDS, 1% Triton X-100, 2 mM EDTA pH=8.0, 20 mM Tris-HCl pH=8.0, 500 mM NaCl) by rotating at 4°C for 10 minutes each time. DNA was eluted with two consecutive incubations in RIPA elution buffer (1% SDS, 100mM NaHCO3) while rotating at room temperature for 30 minutes. Reversal of crosslinking and DNA purification was carried out following the same procedure as that for input chromatin.

Eluted DNA samples were used to prepare sequencing libraries using the Ovation® Ultralow V2 DNA-Seq Library Preparation Kit (Tecan, #0344NB) and SPRIselect beads (Beckman Coulter, #B23318) following the manufacturer's instructions. The concentration of the library was measured using the Qubit dsDNA HS assay (Thermo Scientific), and the distribution of fragment size was evaluated using the Agilent TapeStation system. Sequencing was conducted on Illumina NovaSeq platform with 110-bp paired-end, generating at least 30 million reads for each library.

ATAC-Seq library construction

ATAC-Seq was conducted using ATAC-Seq Kit (Active Motif, #53150), following the manufacturer's instructions. In brief, 50,000 cells of each cell type (n=2 biological replicates) were tagmented for 60 minutes at 37°C. Once a nucleosomal banding pattern was verified with an Agilent Tapestation, the libraries were quantified using the KAPA Library Quantification Kit (Kapa, # KK4854). The sequencing was on Illumina NextSeq 550 platform with 75bp paired-end, generating read counts ranging from 21.5 to 46 million reads for each library.

ChIP-Seq read alignment and analysis of multimapping

The ChIP-Seq and ATAC-Seq datasets were first preprocessed to eliminate potential 3' adapters with Trim Galore v0.6.4 using default settings, and only reads with a length ≥ 20 were retained. Considering the high occurrence of tRNA gene duplication that can also include

flanking sequences, we first focused on evaluating the extent of multi-mapping in RPC1 ChIP-Seq reads aligned to predicted tRNA genes. Paired-end reads with 2x 110 bp from the RPC1 ChIP-Seq libraries were aligned to the human reference genome GRCh38 with STAR v2.6.1c, allowing a maximum of one mismatch per read (*--outFilterMismatchNmax 1*), and up to 10 alignment positions (*--outFilterMultimapNmax 10*). The alignment was performed in end-to-end mode, with introns in reads being explicitly prohibited (*--alignEndsType EndToEnd --alignIntronMax 1*). To eliminate read duplicates, Picard Tools MarkDuplicates v2.17.10 was used, with the parameter REMOVE_DUPLICATES=true to directly filter the duplicates in the resulting BAM (Binary Alignment Map) file. For read counting, we used *mmquant* v1.3, which assessed the overlap of reads with the 619 predicted human tRNA genes and each gene was extended by 125 bp of both upstream and downstream sequences. With a custom Python script, we parsed the *mmquant* output to generate library-specific outputstRNA genes represented as rows, and columns for uniquely mapped read counts, multi-mapped read counts, and proportion of the total reads per tRNA that were accounted for by multi-mapping reads. To identify tRNA genes that cannot be distinguished in ChIP-Seq data, we defined a consensus tRNA gene list using those with at least 25% multi-mapping reads and a minimum of 50 aligned reads in the RPC1 ChIP-Seq libraries (in total 61 tRNA genes from 16 anticodon families and 27 isodecoders; **Supplementary Table 4).** As anticipated, 20 out of the 23 tRNA genes fall into the this group. These genes, including Glu-CTC, Gly-TCC, Asp-GTC, Leu-CAG, are present in four tandem repeats of a tRNA gene cluster on chromosome 1. All gene-level analysis forChIP-Seq and ATAC-Seq excluded this set of 61 tRNA genes identified. Since the majority of multi-mapped reads were aligned to the same gene copies that encode identical tRNA transcripts, a random alignment position was selected and reported for these reads in the analysis of tRNA transcript-aggregated Pol III occupancy and chromatin accessibility.

Peak calling and annotation for ChIP-Seq and ATAC-Seq

After adapter trimming, ChIP-Seq libraries and ATAC-Seq libraries were aligned to the GRCh38 human reference genome with the STAR aligner using the following settings: allowing a maximum of one mismatch per read and up to 10 alignment positions, performing end-to-end alignment and prohibiting introns, and reporting only one alignment per read(outFilterMismatchNmax 1, --outFilterMultimapNmax 10, --alignEndsType EndToEnd, --alignIntronMax 1, and --outSAMmultNmax 1). The reads originating from libraries containing spike-in were also aligned to the r6.39 D. melanogaster genome using the same

alignment settings, except that only uniquely-mapped reads were kept (*--outFilterMultimapNmax 1*). Subsequently, read duplicates were eliminated with Picard Tools MarkDuplicates v2.17.10, following the same procedure as described earlier, alignments to mitochondrial genome were also filtered out for the ATAC-Seq libraries. To accommodate the transposon dimerization before insertion, we additionally shifted the filtered ATAC-Seq reads by +4 bp for positive strand alignments, and -5 bp for negative strand alignments using the deepTools alignmentSieve v3.4.0. Simultaneously, alignmentSieve was utilized to split fragments into segments representing nucleosome-free regions (NFRs) with a maximum of 100 nt in length. Both operations, namely the shifting of reads and the splitting of fragments into NFRs, were carried out concurrently using the parameters *--ATACshift and --maxFragmentLength 100*. The ATAC-Seq alignments for NFR were converted to BEDPE format using alignmentSieve with the parameter *--BED* for peak calling.

Peaks calling was performed with MACS callpeak v2.2.6, using the HPSI0214i-*kucg-2* input samples for the *kucg-2* hiPSC and CM datasets, HPSI0214i-*wibj-2* input sample for the *wibj-2* hiPSC datasets, HPSI0214i-*kucg-2*-derived NPC input samples for the NPC and neuron datasets, with the fragment sizes specified *(--extsize*) and the building of shifting model disabled *(--nomodel*). The calculation of dynamic lambda uses a small region size of 500 bp (*--slocal 500*), with peak summits reported (*--call-summits)*. Peak calling with MACS was performed on all reads without removingduplicates (--keep-dup all) since these were previously filtered with Picard Tools for duplicates. Peak calling for ATAC-Seq was performed using the BEDPE files generated as mentioned above (*-f BEDPE*), without including the corresponding input control samples, and not disabling the shifting model building or specifying the fragment sizes. In addition, for all peak calling analyses, normalized signal to per million reads was saved in bedgraph format to visually inspect the datasets (*-B and -SMPR*). Significant peaks were called for both types of data with FDR-adjusted Poisson distribution p-values less than or equal to 0.05. To further filter the set of predicted peaks, the bed file (https://www.encodeproject.org/files/ENCFF356LFX/) containing unified GRCh38 blacklist regions in the ENCODE project was used to identify overlaps with bedtools intersect v2.29.2.

To annotate the peak region summits that passed the blacklist filter, we searched for the nearest predicted tRNA locus using bedtools closest in the filtered tRNA gene set, excluding those tRNA genes that exhibited significant "within isodecoder" multi-mapped reads in hiPSC, as defined previously. For each sample, peaks with tRNA "hits" were identified as those located

within 125 bp from annotated tRNA genes. tRNA hits that were shared by both replicates for each cell type or experiment condition were utilized to define the consensus tRNA peaks for the corresponding condition. With the RPC1 tRNA peak datasets, we designated housekeeping tRNAs as those present in the consensus sets across all cell types. The tRNAs that were absent from all consensus gene lists were identified as persistently inactive tRNAs.Repressed tRNA genes were characterized with occupancy in any cell type but were not included in the housekeeping tRNA set. This was determined by taking the difference between the union of all tRNA gene peaks across all cell types and the set of housekeeping tRNAs.

Normalization and visualization of ChIP-Seq coverage

To visually analyze the ChIP-Seq datasets, the BAM files with duplicate filtered were transformed into normalized bigWig tracks with deepTools v3.5.1. For calculating the normalization factors for each individual library, *mmquant* was utilized to count the ChIP-Seq reads that overlapped with the annotated hg38 human tRNA genes, extending by 125 bp at both ends to ensure comprehensive coverage of the regions of interest. Normalization factors were computed using the obtained counts as input with the "calcNormFactors" function from the edgeR v3.34.1 package, with the "RLE" method. The relative library sizes were determined by summing the reads that were assigned to tRNA features and scaling them per million reads, allowing for a normalized comparison across samples. The library size factors were then multiplied with the edgeR normalization factors, then the reciprocal of the resulting product was used for generating normalized signals. To generate the normalized signal files, deepTools bamCoverage was implemented with a normalization bin size set to 1 bp (*--binSize 1*), the previously calculated scale factors (*--scaleFactor*), and read extension based on the fragment lengths estimated by Phantompeakqualtools (*--extendReads*). The plotting of the signal was carried out using deepTools computeMatrix, specifically in the reference-point mode and the plotHeatmap function, with tRNA gene start as the reference point (*--referencePoint TSS*), and the regions of interest (-R) defined using BED files of housekeeping, repressed, and inactive tRNAs, including either 500 bp or 1000 bp upstream and downstream flanking the tRNA gene start (*-a 500 -b 500* or *-a 1000 -b 1000*, respectively).

DiffBind analysis

To perform the differential occupancy analysis, we used DiffBind v3.2.7 and specifically included 560 filtered human tRNA genes, excluding the 49 tRNA genes that were identified in

the above-mentioned multi-mapping analysis. With this, we obtained occupancy results for all tRNA genes irrespective of whether a ChIP peak was present or absent. In brief, we first created a BED file including all 560 tRNA genes, with each gene extended by 200 bp on both ends to capture the complete ChIP signal surrounding each tRNA gene. To prevent peak merging during the DiffBind analysis, we identified the overlapping regions within the extended features with bedtools intersect for tRNAs that were separated by no more than 200 bp, The overlapping regions were subsequently removed from the extended features with bedtools subtract. DiffBind analysis were provided with sample sheets containing the duplicate-filtered bam files specifically used for aligning reads to the human genome and the D. melanogaster genome (the "BamReads" column and "SpikeIn" column, respectively), the tRNA regions extended and processed ("Peaks" column), as well as metadata including condition and replicate. Following read counting (dba.count), the filtering of blacklisted regions was not performed since it had already been conducted after peak calling, while non-redundant greylist regions were identified and excluded in the analysis using the *dba.blacklist* function with *blacklist* set to *FALSE*. Analysis of normalization and differential occupancy was carried out using the *dba.normalize* function using RLE normalization in DESeq2 which used the Benjamini-Hochberg-adjusted Wald test p-value in combination with spike-in normalization (normalize=DBA_NORM_RLE and spikein=TRUE) and *dba.analyze* function. Finally, the results for each individual contrast were obtained using the *dba.report* function inDiffBind. To restore the annotation information, such as the tRNA gene name, the *annotatePeakInBatch* function from ChIPpeakAnno v3.26.4 was used, allowing for associating the identified peaks with specific tRNA genes.

4.2.8 Ribosome profiling and codon usage analysis

Construction of ribosome profiling libraries

Ribosome footprint libraries were generated following the previously described protocol with minor modifications. Cell culture medium was replaced 2 hours before harvesting. Cells were rapidly rinsed with ice-cold PBS containing cycloheximide (CHX, 100 µg/ml, Sigma Aldrich, #C1988) and immediately frozen in liquid nitrogen.

For libraries prepared in the lysis buffer with cycloheximide (CHX), plates were thawed and kept on ice, and cells were harvested by scraping them off the plate using 400 µl of polysome lysis buffer (20 mM Tris pH=7.4, 5 mM $MgCl_2$, 150 mM NaCl, 1 mM DTT, 1% Triton-X100,

100 µg/ml CHX, 0.1% NP-40, 25 U/ml Turbo DNase (Thermo Scientific, #AM2238), 20 µM leupeptin, 10 µg/ml aprotinin, 0.5 mM AEBSF, 2.5 µM pepstatin A, and 1x Phosphatase Inhibitor Cocktail (Cell Signaling, #5870)). The samples were vigorously vortexed, followed by trituration through a 26G needle, and centrifuged at 16,000xg for 7 minutes at 4°C. The resulting supernatant was carefully transferred to a fresh tube, and the concentration of RNA was quantified using the Qubit RNA HS Kit. Aliquoted samples containing 20 µg of RNA in 200 µl of polysome lysis buffer were rapidly frozen and preserved at -80°C. 20 µg of RNA in 200 µl of polysome lysis buffer was subjected to digestion using 50 U of RNase I (Thermo Scientific, #AM2295) at 2,000 rpm, 22°C for 45 minutes.

For libraries prepared in the lysis buffer containing both CHX and tigecycline (TIG), upon thawing the plates, cells in 10-cm dish were added with 15 ml of polysome lysis buffer containing 0.1% NP-40 and 100 µg/ml of TIG (Sigma Aldrich, #PZ0021). After 5 minutes incubation on ice, the extracts were centrifuged at 3,000 g for 5 minutes at 4°C. Ribosomes were separated by pelleting through a 3 ml sucrose cushion (1 M sucrose, 20 mM Tris pH=8.0, 140 mM KCl, 5 mM MgCl2, 1 mM DTT) by centrifuging the layered solutions with Type 70 Ti rotor at 50,000 rpm for 120 minutes at 4°C.Ribosome pellets were washed once and resuspended in 200 µl of polysome lysis buffer without drugs, followed by incubation with 200 U of RNase I for hiPSC or 300 U RNase I for NPC, at 2,000 rpm for 45 minutes at 22°C.

100 U of Superase In (Thermo Scientific, #AM2694) was added to stop the RNase I digestion. The extracts were then loaded to a sucrose cushion. For this, 0.9 ml of 1 M sucrose in the polysome lysis buffer was layered below the digested extract (200 µl), and then centrifuged at 120,000 rpm for 75 minutes at 4°C using a S120AT2 rotor (Thermo Scientific).The pellet was resuspended in 400 µl of LiDS/LET lysis buffer, and RNA extraction was performed following the protocol for total RNA isolation. 3 µg RNA were combined with the loading dye, boiled at 90°C for 3 minutes, and then loaded on 15% polyacrylamide gels containing 7M urea and 1×TBE. Fragments with lengths ranging from 19 to 32 nt were carefully excised from the gel and then crushed using a pestle. RNA was extracted by incubating in 400 µl of gel elution buffer (containing 0.3 M NaOAc pH=4.5, 0.25% SDS, 1 mM EDTA pH=8.0) at 65°C for 10 minutes. The eluted RNA was snap-frozen on dry ice for 10 minutes, then thawed at 65°C for 5 minutes, and incubated overnight at room temperature on a rotating wheel. The gel debris was eliminated by centrifuging through a Spin-X filter (Corning), and the RNA was purified with ethanol precipitation. The size-selected RNA was then dephosphorylated using T4 PNK

(NEB, #M0201S) at 37°C for 45 minutes.The dephosphorylated RNA was combined with pre-adenylated adapters harboring 5 random nucleotides at the 5' ends in a mixture containing 25% PEG-8000, 1x T4 RNA ligase buffer, Superase In and 1 µl T4 RNA Ligase 2, truncated KQ (NEB, #M0373S), incubated at 25°C for 3 h. The ligation products were separated by size selection on a 12% polyacrylamide gel containing 7M urea and 1×TBE. The concentration of the purified RNA ligated with adapters was determined using a Nanodrop spectrophotometer. For samples treated with CHX only, 50 ng linker-ligated samples weresubjected to rRNA depletion with the Ribo-Seq riboPOOL h/m/r depletion kit from siTOOLs, according to the manufacturer's instructions. For CHX+TIG treated samples, the legacy RiboZero Gold kit from Illumina was used for rRNA depletion. rRNA-depleted footprints were then annealed with the RT primer for 5 minutes at 65°C(5′-pRNAGATCGGAAGAGCGTCGTGTAGGGAAAGAG/iSp18/GTGACTGGAGTTCAGACGTGTGCTC-3′), followed by reverse transcription at 50°C for 30 minutes with RT master mix (0.5 mM dNTPs, 1x Protoscript II Buffer, 10 mM DTT, 20 U Superase In and 200 U Protoscript II (NEB, #E6560S)). Following reverse transcription, samples was treated with 0.1 M NaOH at 90°C for 5 minutes for RNA hydrolysis. The cDNA products were separated by size selection using a 12% polyacrylamide gel containing 7M urea and 1×TBE. The excised gel slices were thoroughly crushed using a pestle, the DNA was then eluted in 1x TE buffer at 1500 rpm for 60 minutes at 70°C. The removal of gel debris was achieved by centrifuging through a Spin-X filter, followed by the purification of cDNA with ethanol precipitation. To perform cDNA circularization, the gel-purified reverese transcription (RT) product was combined with 3 µM of recombinant TS2126 RNA ligase 1 (also known as CircLigase) in circularization buffer (50 µM ATP, 50 mM MOPS (pH=7.5), 2.5 mM MnCl2, 5 mM MgCl2, 10 mM KCl, 1 mM DTT and 1 mM Betaine) for a reaction mix of in total 20 µl, incubated at 60°C for 3 hours, followed by 10 minutes heat inactivation at 80°C.

Libraries were generated from the circularized cDNA using a universal forward primer (5′-AATGATACGGCGACCACCGAGATCTACACTCTTTCCCTACACGACGCT*C-3′) and a reverse primer containing index sequence (5′-CAAGCAGAAGACGGCATACGAGATNNNNNNGTGACTGGAGTTCAGACGTGT*G-3′).Amplification was performed in 1× HiFi buffer using KAPA HiFi DNA Polymerase (Roche) with an initial denaturation step for 3 minutes at 95°C, followed by six to ten cycles of 20 seconds at 98°C, 30 seconds at 62°C, and 15 seconds at 72°C with a ramp rate of 3°C per second. The PCR products were separated by size selection on an 8% polyacrylamide gel in 1×

TBE. After excision, gel slices were crushed using a pestle, and DNA was eluted in 300 µl of DNA elution buffer (300 nM NaCl, 10 mM Tris-Cl pH=7.5, 0.2% Triton-X 100) with overnight rotation. On the following day, the removal of gel debris was achieved by centrifuging through a Spin-X filter, and the DNA was ethanol precipitated.Libraries were quantified using the Qubit dsDNA High Sensitivity kit, and sequencing was performed on Illumina NextSeq 550 platform with single-end 75 - 86 bp, generating at least 19 million reads for each library.

Codon usage analysis

For the calculation of transcripts per million (TPM) for coding-gene expression, RSEM v1.3.1 was used. A customized reference transcriptome annotation was first constructed, based on the APPRIS annotations. From these, we extracted the MANE-annotated transcript for each coding gene, representing a precise match for the exonic regions between transcripts in the RefSeq and the corresponding counterparts in the Ensembl/GENCODE annotation. We retained only MANE-annotated transcripts that met specific criteria: they must have a coding sequence (CDS) that starts with an AUG codon, and end with a UAG, UAA, or UGA stop codon, with a length that is a multiple of three, and do not contain any unidentified bases. Out of these, each coding sequence (CDS) was translated into its corresponding amino acid sequence. And sequences that did not have a perfect match to protein sequences in UniProtKB/SwissProt were excluded, resulting in a reference dataset with 16,731 transcripts.

To create an RSEM reference with STAR for read alignment, the RSEM tool "*rsem-prepare-reference*" was used, enabling the "*--star*" option. We specified the human GRCh38 reference genome along with the custom transcriptome that was described earlier. To calculate transcripts per million (TPM) for each sample, we used the reference generated previously and adapter-trimmed RNA-Seq reads using "*rsem-calculate-expression*". From each isoform results file obtained, the transcript ID and TPM columns was extracted and then merged into the final table with transcript-level TPM values for all the samples.

For calculating the codon usage within each sample, we employed a weighting approach. Specifically, we multiplied the frequencies of the 61 sense codons for each transcript in our customized annotation by the corresponding transcript's TPM expression level in that specific sample. To distinguish between dynamics at start codons and the coding methionine codons, we separately counted the occurrence of start AUG codons and coding AUG codons. Furthermore, the raw codon usages were aggregated by summing them across all transcripts,

generating an aggregated codon usage value for each codon. To normalize the codon usage values, we divided them by the sum of all codon usages within each sample, reflecting proportional codon usage. To perform gene subset analysis, we first subsetted the raw values per transcript and then summed the values per codon and converted them to proportional codon usage within the specific gene subset.

To compare with tRNA anticodon abundance, we used raw read counts from mim-tRNAseq that were summed based on the anticodon and converted into proportions of the total tRNA-aligned reads, similar to the process used for codon usage analysis. Each codon usage value was then matched to the corresponding abundance for the cognate anticodon. In cases where a perfect match between the codon and anticodon was not available because of wobble pairing, we replicated the anticodon abundance of the tRNAs known to wobble pair with such codons, to ensure that all 61 sense codons had the corresponding values for tRNA anticodon abundance.

Ribosome profiling data analysis

The sequencing libraries were first demultiplexed and adapters were trimmed with Cutadapt v2. To prevent indels during the alignment to the adapter sequence, the option *--no-indels* was used, and low-quality bases were eliminated from both the 5' and 3' ends using *-q 30,30*. Reads lacking adapters were excluded from further analysis using the *--trimmed-only* option. After demultiplexing, additional trimming was performed on the reads using the *-u 2* option to eliminate the two 5'-RN nucleotides generated by circularization with the RT primer. Trimmed reads with a length greater than 10 nt were aligned to a reference of human ribosomal RNA with Bowtie v1.2.2. using option *-p 40 -S --best*.

The reads filtered for ribosomal RNA (rRNA) were aligned to the GRCh38 human genome using STAR v2.6.1c with the following options: *--outFilterMultimapNmax 1 --outSAMtype BAM SortedByCoordinate --outFilterMismatchNmax 0 --outFilterMatchNmin 20 --alignEndsType Local --seedSearchStartLmax 14 --alignIntronMax 10000 --sjdbOverhang 28 --outFilterIntronMotifs RemoveNoncanonicalUnannotated --quantMode TranscriptomeSAM --outSAMattributes NH HI AS nM NM MD*. Approximately 5.3 to 21.9 million of preprocessed reads were aligned to the coding regions in the human GRCh38 transcriptome.

To determine the A-site location within each mapped read, we used Scikit-ribo that utilizes a random forest algorithm with recursive feature selection as well as a generalized linear model for accurately predicting the A-site position using matched datasets of ribosome profiling and

RNA-Seq. To calculate Transcripts Per Million (TPM) for transcript abundances in RNA-Seq data, we used Kallisto 0.44.0 with the following parameters: *-b 100 --single -l 180 -s 20 -t 40*, with a reference MANE-annotated transcripts set, as described in the Codon usage analysis section. To prevent memory errors caused by the large human genome size and the existence of multiple transcript isoforms, we omitted RNAfold dependencies from Scikit-ribo and we built separate indexes for each chromosome. To ensure the compatibility of hg38 GTF (Gene Transfer Format) file with Scikit-ribo, transcript and UTR (Untranslated Region) annotations were removed from the file. To accurately represent the start and end coordinates of each transcript, adjustments were made to the start codon of the first exon and the stop codon of the last exon by taking into consideration the gene strand information. To assess codon dwell times, ribosome footprints of different lengths (20-22 nucleotides shorter footprints and 29-32 nucleotides longer footprints) were analyzed separately.

4.2.9 Motif analysis and convolutional neural network

Sequence motif analysis

For comparing the sequences of A- and B-box in three activity groups of tRNAs identified from the RPC1 ChIP-Seq data, we performed multiple sequence alignments for all hg38 human tRNA genes with the *cmalign* command ofInfernal v1.1.2, based on tRNA covariance models. We next extracted the A- and B-box sequences from the generated alignments (positions 9-21 and 75-85 for A- and B-box, respectively). We created sequence logos for the extracted subsequences, which were categorized based on the tRNA activity class, with the logomaker v0.8 package from Python.

To characterize the motifs present in A- and B-box promoter sequences throughout the genome, we utilized the MEME prediction tool available online and uploaded the predicted tRNA sequences of all 619 tRNAs in the hg38 humangenome from GtRNAdb. Motif was predicted in classic mode, allowing for One Occurrence Per Sequence (oops) foe eachmotif, which is anticipated for A- and B-boxes in the tRNA sequences. The search was restricted to two motifs with a length of 9-11 nucleotides, as determined from previous predictions of the consensus motif lengths for A- and B-boxes.Finally, motif searching was restricted to the specified strand only, as the provided sequences were mature tRNA instead of DNA. MEME identified exactly a total of two motifs from the input sequences, and the consensus sequence for each motif matched the known consensus sequences of A- and B-box.

The XML format results were downloaded and imported to R v4.2.2 with *read_meme,* and visualized using the *view_motifs* function in the universalmotif package v1.16.0. The motif instances were converted to position weight matrices (PWMs) with the *convert_type* function from the universalmotif package. Motif densities in each sequence were computed using a customized version of the seqPattern function, called plotMotifDensityMap. In brief, motifScanHits is utilized with the imported PWMs to identify motif hits with motif counting score at a minimum of 90% (minScore = 90%). Next, 2D binned kernel density estimates were computed on these motif hits with the *bkde2D* function from the KernSmooth v2.23 package, with a bandwidth of 1 bp applied in both coordinate directions. The maximum density score was obtained for each sequence and used to compare the distributions of motif densities among each tRNA activity group.

tRNet architecture

tRNet is a convolutional neural network (CNN) developed in Keras v2.2.4 (with a Tensorflow v1.15.5 backend) for predicting the tRNA gene classes (housekeeping, repressed, or inactive) based on genomic input sequences provided in a one-hot-encoded format (A = [1,0,0,0], C = [0,1,0,0], G = [0,0,1,0], T = [0,0,0,1]). Conceptually, the tRNet architecture is inspired by the BPNet model, with slight modifications to the receptive field size and the output (**Extended Data Fig. 5f**). In summary, tRNet comprises an initial convolutional layer with a total of 128 filters and a width of 20bp, which is followed by eight sequential dilated layers with 128 filters and a width of 10bp, with the dilation rate doubled at each layer. By employing exponential dilation rates, the number of skip positions within the convolutional filter is doubled,resulting in an increased complexity for pattern learning and receptive field in the sequence space visible to the network.Following each convolutional layer, a rectified linear activation (ReLU) function is applied (f(x) = max(0, x)). A global max pooling operation is then performed, followed by a fully-connected hidden layer with 32 neurons. The final tRNet output is generated by a fully-connected layer with activated softmax, producing three outputs representing the probabilities of input tRNA gene sequences belonging to each tRNA gene class.

tRNet transfer learning approach

During the training of tRNet, a transfer learning approach was employed by leveraging a pre-trained network that was initially trained for a binary classification task. In this network, the

architecture is exactly the same as that of tRNet, with the only difference being the final output layer, which consists of a single sigmoid activation to predict whether the input sequences belong to housekeeping tRNAs. Inputs for this model were limited to sequences from tRNA genes in the housekeeping and inactive groups. Due to the more pronounced sequence differences between these two groups, the classification problem becomes simpler, allowing for learned features to be effectively utilized in the resulting multi-class model with improved generalization. Transfer learning was done by training the modified model using input sequences obtained from the housekeeping and inactive genes, along with their respective gene group labels derived from the called peaks in the ChIP-Seq data. Subsequently, all layers were frozen to avoid retraining of the previously trained layers, and the model architecture was modified by replacing the output layer with a new layer that generates three outputs with softmax activation, as mentioned earlier. Following that, the model was retrained using one-hot-encoded sequence from all the three groups along with their respective tRNA gene group labels. The last convolutional layer in the network was then unfrozen and the model was trained again to optimize the weights in this layer specifically for new multi-class model.

CNN training and evaluation

All networks were trained using the same approach with 80% of the input data, and 20% was held out for validation. To assess the performance of the models, a K-fold cross-validation with k = 5 was conducted on the training data. The validation accuracy and loss were measured for each fold, allowing for a comparison of performance across the five folds. The initial binary classification model that transferred learning was trained using the Adam optimizer with a learning rate of 0.00025, determined with parameter hypertuning. The model utilized a loss function of binary cross-entropy and implemented early stopping using a patience of ten epochs. For the final model training, following transfer learning, identical training setting were used, with the only difference being the use of a categorical cross-entropy loss function that is specifically designed for the multi-class output for this model. Performance of the final model was assessed using held-out testing data. The model's prediction accuracy for each class was evaluated by calculating the area under the receiver operating characteristic curve (auROC) and plotting the macro-average scores One vs Rest (OvR).

Calculation of nucleotide contribution score and TF-Modisco motif analysis

To determine the contribution scores for each nucleotide in the input sequences towards the final prediction, we utilized the SHAP DeepExplainer module, which is an extension of DeepLift and allows for the calculation of SHAP contribution scores. The contribution scores, which are calculated in every input sequence for each nucleotide, are derived from the difference in the output between the model when provided with shuffled input sequences and when provided with the actual sequences upstream to tRNA genes. Ten dinucleotide-shuffled sequences were provided for each input sequence to calculate the contribution scores. The generated hypothetical DeepExplainer contribution scores were multiplied by the one-hot encoded matrix for individual sequence, resulting in a final contribution scores for everysequence. The hypothetical as well as the final contribution scores were then separately calculated for each output or task in the model, corresponding to the sequence classification as housekeeping, repressed, or inactive tRNAs. TF-Modisco v0.5.14.1 was then utilized to calculate the contribution scores from SHAP DeepExplainer individually for each task to identify the enriched sequence or motifs among nucleotides with high contributions to the model output. Significant high-importance windows, referred to as seqlets, were identified by applying a sliding window with a size of 15bp, incorporating a 5bp flanking sequence, and applying a seqlet FDR threshold at 0.01(*TfModiscoWorkflow(sliding_window_size=15, flank_size=5, target_seqlet_fdr=0.01*). The final patterns were generated by assembling the detected seqlets, using a 20bp window size, a 10bp flanking sequence, and requiring at least 20 seqlets per cluster (*TfModiscoSeqletsToPatternsFactory(trim_to_window_size=20, initial_flank_to_add=10, final_min_cluster_size=20)*.

Chapter 5 - Supplemental Data

5.1 Abbreviations

4EBP1	eukaryotic translation initiation factor 4E binding protein 1
5S rRNA	5S ribosomal RNA
AA	ascorbic acid
ACTN2	alpha-actinin-2
aaRS	aminoacyl-tRNA synthetases
A site	aminoacyl site
ATAC-Seq	Assay for Transposase-Accessible Chromatin sequencing
AUROC	area under the receiver operating characteristic curve
BDNF	Brain-derived neurotrophic factor
BDP1	B double prime 1
BFP	Blue Fluorescent Protein
BMP4	bone morphogenetic protein 4
bp	base pairs
BPNet	Binding and Expression Prediction Network
BRF1 or BRF2	TFIIB-related factor 1 or 2
CADM3	Cell Adhesion Molecule 3
CCNB1	cyclin B1
CDS	coding sequence
ChIP-Seq	chromatin immunoprecipitation sequencing
CHX	cycloheximide
CI	confidence interval
CK2	Casein kinase II
CM	cardiomyocytes
CNNs	convolutional neural networks
CNS	central nervous system
CpG	Cytosine-phosphate-Guanine
CREs	cis-regulatory elements
CRISPR	clustered regularly interspaced short palindromic repeats
CRISPRa	CRISPR activation
CRISPRi	CRISPR interference
crRNA	CRISPR RNA
CTNT	cardiac troponin T
CV	coefficient of variation
dbcAMP	dibutyryl cyclic adenosine monophosphate
DIC	differential interference contrast
DNMTs	DNA methyltransferases
Dox	doxycycline
Dr1	down-regulator of transcription 1
E site	exit site
EBs	embryoid bodies

EGF	epidermal growth factor
eIF4E	Eukaryotic Translation Initiation Factor 4E
ERK	extracellular signal-regulated kinase
FA	formaldehyde
FDR	false discovery rate
FGF2b	fibroblast growth factor 2
FU	fluorescence units
GDNF	glial cell line-derived neurotrophic factor
GFP	Green Fluorescent Protein
GTPBP2	GTP-binding protein 2
GVCF	genomic variant call format
HAT	Histone Acetyltransferase
HCPs	high CpG promoters
HDGC	hereditary diffuse gastric cancer
HDR	homology-directed repair
hESC	human embryonic stem cells
HipSci	Human Induced Pluripotent Stem Cells Initiative
hiPSC	human pluripotent stem cells
IFNs	interferons
ITS	insulin/transferrin/selenium
KRAB	Krüppel-associated box
log2FC	log2 fold change
MM	maturation medium
MM	multiple myeloma
MPS1	mucopolysaccharidosis type 1
mRNA	messenger RNA
mt tRNA	mitochondria tRNAs
ncRNA	non-coding RNA
NEXSON	Nuclei EXtraction by SONication
NFR	nucleosome free regions
NLS	nuclear localization sequences
NPC-EM	NPC expansion medium
NPC-IM	NPC-induction medium
oops	One Occurrence Per Sequence
OPP	O-propargyl-puromycin
P site	peptidyl site
PAM	protospacer adjacent motif
PCA	principal component analysis
Phe	phenylalanine
PLK1	polo-like kinase 1
PM	patterning medium
Pol III	RNA polymerase III
Pro	Proline

PSE	proximal sequence element
PTC	premature termination codon
PWMs	position weight matrices
RA	retinoid acid
rAAV	recombinant adeno-associated virus
RB	retinoblastoma tumour-suppressor protein
ReLU	rectified linear unit
RNAi	RNA interference
RNA-Seq	RNA sequencing
RNase P	ribonuclease P
RNP	ribonucleoprotein
RPE	retinal pigment epithelium
RPFs	ribosome-protected fragments
RPM	reads per million
rpS6	ribosomal protein S6
rRNA	ribosomal RNA
RT	reverse transcription
rtTA	reverse tetracycline-controlled transactivator
S6K1	ribosomal protein S6 kinase 1
SARS-CoV-2	severe acute respiratory syndrome coronavirus 2
sgRNA	single-guide RNA
SRP	signal recognition particle
ssODN	single-stranded oligodeoxynucleotides
sup-tRNAs	suppressor tRNAs
SNAPc	snRNA activator protein complex
TBP	TATA-box binding protein
TCE	2,2,2-Trichloroethanol
TetO	tetracycline operator
TPM	transcripts per million
tRNAScan-SE	tRNAScan-Search Engine
tRNA-Seq	tRNA sequencing
TGF-β	transforming growth factor-β
TIG	tigecycline
TSC2	tuberous sclerosis complex 2
TSS	transcription start site
TTN	titin
tracrRNAs	transactivating crRNAs
UTR	untranslated region
VCL	Vinculin
WT	wild type

5.2 Supplementary tables

Table S1. Differential expression analysis at tRNA transcript level using DESeq2 in differentiated cell lines relative to hiPSC.

		NPC vs hiPSC		Neurons vs hiPSC		CM vs hiPSC	
Unique tRNA	**Base mean**	**log2FoldChange**	**Adjusted p-value**	**log2FoldChange**	**Adjusted p-value**	**log2FoldChange**	**Adjusted p-value**
Homo_sapiens_tRNA-Asp-GTC-1	12209,92759	1,666397205	9,81E-131	2,398474373	4,7122E-269	1,209683816	1,26884E-69
Homo_sapiens_tRNA-Glu-TTC-2	37195,12218	1,681249398	3,51E-114	1,998683895	3,2656E-161	0,962550133	4,18831E-38
Homo_sapiens_tRNA-Leu-CAA-4	7889,884106	1,422613867	1,47E-76	2,098125163	7,0844E-165	0,791412975	9,59656E-25
Homo_sapiens_tRNA-Trp-CCA-2	13213,94031	1,841949822	2,24E-74	2,310203228	6,413E-117	1,262355822	1,42018E-35
Homo_sapiens_tRNA-Ser-TGA-1	21175,0473	1,905167386	2,58E-70	2,752392022	1,3746E-146	1,178331494	1,3781E-27
Homo_sapiens_tRNA-Leu-CAG-2	25687,74651	1,46684462	1,89E-69	1,870938082	8,6288E-113	0,697581704	1,24788E-16
Homo_sapiens_tRNA-Leu-CAG-1	36474,21661	0,816674776	4,77E-68	0,925704169	1,37448E-86	0,623639833	2,68039E-40
Homo_sapiens_tRNA-Glu-TTC-1	30725,76213	1,663357259	6,00E-68	2,901317509	2,1954E-205	1,076454813	5,02448E-29
Homo_sapiens_tRNA-Gly-CCC-2	61219,41342	2,000005782	5,09E-64	3,024359353	7,2957E-146	1,662927697	2,64992E-44
Homo_sapiens_tRNA-Ala-TGC-5	2758,454969	-2,264836486	3,01E-63	-2,69736234	1,14337E-79	-0,105753961	0,552199588
Homo_sapiens_tRNA-Gly-GCC-1	36107,38699	-1,356319619	4,09E-62	-2,14850092	7,6983E-152	-1,755689579	4,3571E-103
Homo_sapiens_tRNA-Ala-AGC-8	42332,92675	1,722212533	8,47E-62	2,143023245	1,49532E-95	1,151296184	4,29489E-28
Homo_sapiens_tRNA-Leu-CAA-1	10301,47975	1,147757303	2,14E-60	1,432071121	2,86526E-92	0,451300325	2,22286E-10
Homo_sapiens_tRNA-Leu-TAA-1	16493,6109	1,85567546	5,38E-60	2,598928701	6,413E-117	1,036222366	1,94974E-19
Homo_sapiens_tRNA-Arg-TCG-1	18855,57289	1,690144453	1,69E-58	2,194505097	4,98405E-98	1,094698405	3,81201E-25
Homo_sapiens_tRNA-Lys-CTT-1	34606,22052	1,694908257	4,85E-58	2,19151242	1,36424E-96	1,154319403	2,21205E-27
Homo_sapiens_tRNA-Pro-TGG-2	16944,08225	1,883160417	1,86E-57	2,877693379	5,8996E-133	1,432530075	1,57823E-33
Homo_sapiens_tRNA-Tyr-GTA-4	812,5581737	-4,519068797	7,88E-57	-4,39021803	1,04212E-48	-4,198014929	5,80052E-53
Homo_sapiens_tRNA-Glu-TTC-4	7974,263643	-1,978668347	8,56E-57	-2,548038104	1,00664E-89	-1,029106992	2,29558E-16
Homo_sapiens_tRNA-Cys-GCA-13	717,273401	-5,706070486	2,62E-56	-5,553073798	5,6235E-47	-5,368472557	4,16407E-56
Homo_sapiens_tRNA-Ala-AGC-4	27803,58283	1,806712694	2,67E-54	2,542260323	1,2238E-106	1,125693632	1,18623E-21
Homo_sapiens_tRNA-Lys-TTT-6	3491,402313	-2,05902552	4,49E-53	-3,19678157	4,2109E-112	-1,820435187	3,26857E-42
Homo_sapiens_tRNA-Gly-GCC-2	79439,31533	1,657056587	1,18E-51	2,619271196	1,4079E-127	1,485759783	2,23514E-41
Homo_sapiens_tRNA-Cys-GCA-9	2768,304901	-2,966375411	2,85E-51	-2,544149367	1,57616E-36	1,225636224	1,82568E-10
Homo_sapiens_tRNA-Ile-TAT-3	1183,114786	-5,591195553	5,09E-50	-4,907857635	9,524E-38	-2,74534187	2,70483E-14
Homo_sapiens_tRNA-Gln-CTG-3	2631,664182	-3,81443047	2,17E-49	-3,750750026	5,89205E-46	-0,894806241	0,000708956
Homo_sapiens_tRNA-Ala-TGC-3	35487,28689	1,477452522	1,38E-46	1,856067509	4,18203E-73	0,852546692	3,1336E-16
Homo_sapiens_tRNA-Trp-CCA-4	11849,29485	1,452328893	1,43E-46	1,981341843	1,69062E-85	1,413090081	7,32622E-44
Homo_sapiens_tRNA-Val-CAC-3	11495,98034	1,623062839	7,44E-46	2,115167466	4,96095E-77	0,942986836	3,27167E-16
Homo_sapiens_tRNA-Ile-AAT-1	823,1841166	-4,676139331	2,67E-45	-4,325806636	8,69981E-37	-4,640707742	1,11883E-46
Homo_sapiens_tRNA-Arg-TCG-3	17671,59146	1,394552901	8,95E-44	1,764596789	2,09311E-69	0,960421244	3,04235E-21
Homo_sapiens_tRNA-Lys-CTT-4	1849,141406	-2,374958353	9,86E-44	-2,802461466	1,77842E-54	-0,534449383	0,002224259
Homo_sapiens_tRNA-Arg-CCT-4	19323,05659	1,739603641	2,44E-42	2,573109003	2,20953E-91	1,451775183	1,67421E-29
Homo_sapiens_tRNA-Pro-CGG-2	1920,650468	-1,718518515	1,31E-41	-1,615014598	1,72622E-34	-0,36309724	0,004981199
Homo_sapiens_tRNA-Ala-CGC-3	14022,76117	1,463774811	2,63E-41	2,204551319	3,94966E-92	1,148754118	1,0564E-25
Homo_sapiens_tRNA-Ile-TAT-2	17527,92876	1,294976743	7,43E-41	2,224035706	5,1482E-118	0,93578165	9,79288E-22

Homo_sapiens_tRNA-Leu-TAG-3	16692,05255	1,672533956	1,99E-39	2,323974304	3,81027E-75	0,825422164	1,93809E-10
Homo_sapiens_tRNA-Ser-GCT-5	1585,702805	-2,177690112	2,10E-39	-1,456983028	3,84645E-18	-0,263338413	0,145414793
Homo_sapiens_tRNA-Met-CAT-6	19165,01042	1,666699471	1,87E-38	2,358402806	6,3332E-76	1,103326954	2,32437E-17
Homo_sapiens_tRNA-Arg-TCT-1	17439,85197	1,71247034	6,33E-38	0,834241493	4,49157E-10	1,077235983	1,26468E-15
Homo_sapiens_tRNA-Gln-CTG-1	73095,33807	1,335561499	7,35E-35	1,769462146	1,55922E-60	1,034329073	3,41155E-21
Homo_sapiens_tRNA-Arg-CCG-2	19189,63084	1,579452598	1,49E-34	2,160552661	9,31829E-64	0,976323694	7,17012E-14
Homo_sapiens_tRNA-Leu-AAG-1	4675,068436	-4,135922107	1,49E-34	-4,232079552	1,11527E-35	-1,853553012	5,98316E-08
Homo_sapiens_tRNA-Arg-CCT-2	6498,689878	1,245973713	1,08E-32	1,403830806	8,66841E-41	1,131320838	4,48388E-27
Homo_sapiens_tRNA-Met-CAT-1	15261,56667	1,641498721	1,08E-32	2,752002557	7,2425E-90	1,445727961	2,02826E-25
Homo_sapiens_tRNA-Asn-GTT-5	397,8984804	-3,1969003	1,30E-32	-2,540064588	2,87264E-20	-1,213107163	1,67576E-06
Homo_sapiens_tRNA-Ser-CGA-4	7926,112094	1,455144077	4,71E-32	2,186863824	7,71925E-71	0,8288311	3,80082E-11
Homo_sapiens_tRNA-Arg-TCG-5	4621,453872	-1,219636913	2,32E-31	-1,602092409	2,07872E-49	0,329602693	0,002206991
Homo_sapiens_tRNA-Ser-TGA-4	1820,362424	-3,171088747	4,83E-29	-3,696347236	5,05915E-37	-2,044394922	5,79803E-13
Homo_sapiens_tRNA-Ile-AAT-6	1590,649993	-1,542216457	5,52E-29	-2,195027174	3,06961E-50	-0,84773326	5,82931E-10
Homo_sapiens_tRNA-Ala-AGC-13	862,1992748	-5,082228937	7,34E-29	-5,785293849	2,72223E-32	-4,215072131	4,81329E-21
Homo_sapiens_tRNA-Ile-AAT-4	5317,215455	1,507388417	1,58E-28	1,288729605	4,1563E-21	1,192978885	3,50266E-18
Homo_sapiens_tRNA-Leu-AAG-2	49165,76648	1,039830856	1,58E-28	1,597996948	7,98978E-66	0,827193339	2,70099E-18
Homo_sapiens_tRNA-Arg-ACG-1	46865,66693	1,0883475	2,23E-28	1,85907265	1,62373E-80	0,763813831	1,7626E-14
Homo_sapiens_tRNA-Gln-TTG-1	18163,75574	1,423042299	1,38E-27	1,910068796	8,04906E-49	0,941001417	1,15166E-12
Homo_sapiens_tRNA-Thr-AGT-1	33661,36024	1,21360101	2,87E-27	1,487845473	1,64395E-40	0,823129222	4,24841E-13
Homo_sapiens_tRNA-Cys-GCA-6	844,1444102	-2,452013663	4,95E-27	-1,166239413	2,36653E-07	1,696452312	2,4639E-16
Homo_sapiens_tRNA-Arg-TCG-4	733,3985424	-4,444805095	7,66E-25	-4,706988034	3,17007E-25	-1,478901328	0,000646028
Homo_sapiens_tRNA-Lys-TTT-3	109445,9166	1,343884738	2,15E-24	1,605360772	1,53712E-34	0,485950027	0,000384849
Homo_sapiens_tRNA-Thr-CGT-4	10261,83794	1,364060496	2,39E-24	1,620149378	6,25843E-34	0,959028541	1,38789E-12
Homo_sapiens_tRNA-Thr-AGT-4	971,1748998	-4,998852654	2,61E-24	-4,476415191	1,93544E-19	-2,878782581	3,5463E-09
Homo_sapiens_tRNA-Cys-GCA-2	23741,93952	1,235206657	1,16E-23	1,77636941	9,40026E-48	1,019252809	2,44036E-16
Homo_sapiens_tRNA-Thr-CGT-2	17517,22359	1,109490615	1,86E-23	1,788531281	4,92668E-59	0,829824445	1,43245E-13
Homo_sapiens_tRNA-Cys-GCA-4	21379,09502	1,371481056	2,50E-23	1,964228055	1,04783E-46	1,076371148	1,04876E-14
Homo_sapiens_tRNA-Ala-AGC-6	721,4821788	-3,429681597	1,75E-22	-3,980088619	1,15317E-26	-1,095254769	0,002166567
Homo_sapiens_tRNA-Ala-AGC-2	22633,24825	0,896190359	3,51E-22	1,000092383	2,23414E-27	0,586158063	4,08201E-10
Homo_sapiens_tRNA-Ala-AGC-5	2581,12528	-1,402358265	6,25E-22	-2,783001895	3,6333E-73	-1,638204089	2,11201E-29
Homo_sapiens_tRNA-Ala-AGC-24	546,0179784	-5,403210585	8,99E-22	-4,87425102	1,77378E-17	-4,373980657	1,5766E-15
Homo_sapiens_tRNA-Val-TAC-1	16220,58272	1,158285353	3,28E-21	1,555660575	2,42677E-37	0,55853683	8,64611E-06
Homo_sapiens_tRNA-Gln-TTG-2	807,5343777	-1,878532916	5,98E-21	-1,499904011	2,50388E-13	-0,456903362	0,027672266
Homo_sapiens_tRNA-Ala-AGC-10	191,5053916	-5,397982677	6,27E-21	-5,458988085	7,27738E-18	-5,734914866	1,58054E-25
Homo_sapiens_tRNA-Arg-TCT-3	4397,474778	-1,359677021	2,10E-20	-1,295667791	1,91963E-18	-0,804656181	5,94132E-08
Homo_sapiens_tRNA-Pro-CGG-1	16147,43556	0,889279651	5,10E-20	1,14968757	1,28731E-32	0,621614884	2,55371E-10
Homo_sapiens_tRNA-Ser-GCT-1	1578,01671	-2,742343224	8,36E-20	-2,969208629	3,01592E-22	-0,792880605	0,011842889
Homo_sapiens_tRNA-Ala-CGC-1	11953,84689	0,981230141	1,29E-19	1,085281826	9,37039E-24	0,318980916	0,004979598
Homo_sapiens_tRNA-Ala-CGC-2	9528,72087	0,995984908	3,03E-19	1,01096558	8,56544E-20	0,583306138	2,42036E-07
Homo_sapiens_tRNA-Ala-TGC-4	11410,90528	0,932522847	7,22E-19	1,354855124	2,3996E-38	0,625173878	4,38378E-09

Homo_sapiens_tRNA-Ile-AAT-8	1714,591257	-1,203747527	8,55E-19	-1,739550076	5,01769E-34	-0,399044228	0,004188725
Homo_sapiens_tRNA-Ala-TGC-1	3586,189988	-1,357270868	2,55E-18	-2,357403012	4,76706E-49	-0,345391613	0,038660735
Homo_sapiens_tRNA-SeC-TCA-1	6648,603081	1,450532677	5,83E-18	2,714495573	6,60791E-60	1,067034891	3,42E-10
Homo_sapiens_tRNA-Thr-AGT-3	1547,801396	-4,760997465	2,00E-17	-4,811547834	1,70405E-17	-2,33385873	4,07319E-05
Homo_sapiens_tRNA-Gln-CTG-4	1190,140116	-1,627641956	4,07E-17	-1,731496293	2,77001E-18	-0,903464469	3,30957E-06
Homo_sapiens_tRNA-Thr-TGT-5	14799,21951	0,901265508	1,14E-16	1,254541774	3,59911E-31	0,642516148	5,30224E-09
Homo_sapiens_tRNA-Glu-TTC-14	337,7935002	-2,399859413	1,43E-16	-1,866910775	3,26586E-10	-1,501538907	1,09919E-07
Homo_sapiens_tRNA-Ala-CGC-4	3865,161428	-1,399139119	1,51E-16	-1,922818015	5,81176E-29	0,210751463	0,2933793
Homo_sapiens_tRNA-Ile-AAT-12	1194,479816	-2,066249478	2,38E-15	-3,086381558	3,06184E-30	-2,206408677	2,66841E-17
Homo_sapiens_tRNA-Met-CAT-3	14883,54805	0,767005156	4,39E-15	0,312764824	0,001718196	0,642962117	7,43106E-11
Homo_sapiens_tRNA-Cys-GCA-14	416,4530054	-1,918893582	5,63E-15	-2,212383503	1,34794E-17	-2,158699967	4,65602E-19
Homo_sapiens_tRNA-Ala-TGC-6	689,5766148	-2,711398382	9,61E-15	-3,424897433	6,24641E-21	-1,470031666	3,02032E-05
Homo_sapiens_tRNA-Ala-AGC-9	446,6675805	-5,130537498	2,47E-14	-5,753527166	8,00007E-16	-3,353324329	4,52565E-07
Homo_sapiens_tRNA-Pro-TGG-3	17317,09556	0,676224376	2,62E-14	0,770624084	2,96014E-18	0,527532212	4,18296E-09
Homo_sapiens_tRNA-Ser-GCT-2	4014,776031	-0,987390215	6,43E-14	-1,423942375	1,41483E-26	-0,662556634	6,19151E-07
Homo_sapiens_tRNA-Arg-TCT-4	3230,8158	1,5322649	1,45E-13	5,986600688	9,8069E-199	1,084185289	1,90457E-07
Homo_sapiens_tRNA-Asn-GTT-2	53450,66063	0,778179344	2,40E-13	1,523126508	1,02879E-47	0,885044834	1,15629E-16
Homo_sapiens_tRNA-Leu-TAA-2	678,7619781	-4,28718568	3,11E-13	-4,403311655	1,94017E-13	-1,831340067	0,002306863
Homo_sapiens_tRNA-Leu-AAG-3	970,9759366	-1,552714666	5,16E-13	-2,344730773	2,18379E-25	-0,968638876	7,35794E-06
Homo_sapiens_tRNA-Val-TAC-3	636,4073503	-1,607894773	7,89E-13	-2,221471922	5,19173E-21	-1,769290414	1,66184E-15
Homo_sapiens_tRNA-Val-TAC-2	11220,15369	0,83204724	9,25E-13	1,029083779	6,27508E-19	0,491814799	3,55839E-05
Homo_sapiens_tRNA-Gly-CCC-1	2401,242874	-2,925639137	2,19E-12	-4,456577266	4,92652E-26	-1,587280626	0,000205935
Homo_sapiens_tRNA-Asp-GTC-2	91968,51576	0,325878724	2,70E-12	0,763517994	1,16199E-61	-0,029911468	0,661855977
Homo_sapiens_tRNA-Thr-CGT-1	353,7153173	-3,410261161	1,20E-11	-3,631366686	6,10463E-12	-0,067287603	0,942733647
Homo_sapiens_tRNA-Ala-AGC-14	136,8280867	-4,381208562	2,21E-11	-4,869008507	1,3909E-11	-4,821264506	5,05651E-14
Homo_sapiens_tRNA-Arg-TCG-2	3150,760915	-0,813004669	3,77E-11	-1,342357755	1,40059E-26	-0,348692194	0,006014556
Homo_sapiens_tRX-Ala-AGC-5	100,36175	-4,604038605	4,11E-11	-5,976008772	2,39204E-11	-3,535625553	5,94132E-08
Homo_sapiens_tRNA-Val-TAC-4	828,1772754	-4,494843932	1,10E-10	-5,519986627	1,24551E-14	-2,594839148	0,000254122
Homo_sapiens_tRNA-Ser-AGA-4	150,7763646	-2,504410686	2,58E-10	-2,412954473	6,02593E-09	-2,430100782	2,59962E-10
Homo_sapiens_tRNA-Cys-GCA-8	1323,308124	-1,173553567	3,56E-10	-0,853214469	7,00502E-06	-0,340491972	0,092000912
Homo_sapiens_tRNA-His-GTG-1	64519,29391	0,784363324	3,96E-10	1,306850495	4,10209E-26	0,776060734	7,78734E-10
Homo_sapiens_tRNA-Leu-TAG-2	3060,113061	-1,886715809	5,40E-10	-2,854821813	7,33316E-21	-0,443285319	0,200372697
Homo_sapiens_tRNA-Leu-CAA-3	1004,684409	-3,145543532	6,15E-10	-4,126795401	1,1779E-15	-2,170158943	2,56997E-05
Homo_sapiens_tRNA-Val-CAC-1	44068,87192	0,459489902	1,63E-09	1,10026818	1,04212E-48	0,442805086	7,52523E-09
Homo_sapiens_tRNA-Ile-AAT-3	1539,810773	-0,858277791	1,82E-09	-0,330985228	0,025592475	-0,623421659	1,23478E-05
Homo_sapiens_tRNA-Glu-TTC-3	1653,440435	-3,206025052	2,06E-09	-4,527058296	4,78718E-17	-1,455881949	0,009089984
Homo_sapiens_tRNA-Arg-ACG-2	35561,64241	0,542174763	4,17E-09	1,062087015	1,47548E-31	0,408516766	1,29997E-05
Homo_sapiens_tRNA-Ser-CGA-3	340,1637886	-2,645288811	1,05E-08	-3,178474273	2,67401E-11	-2,172592366	2,5145E-06
Homo_sapiens_tRNA-Ile-TAT-1	6849,595183	1,024127649	7,04E-08	1,991946285	1,22392E-26	0,993455393	1,95334E-07
Homo_sapiens_tRNA-Thr-TGT-1	2481,479975	-1,051058486	2,31E-07	-2,120879461	7,60478E-25	0,216045641	0,381927171
Homo_sapiens_tRNA-Glu-CTC-1	116642,4631	0,44202607	2,86E-07	0,879642733	1,83526E-25	0,095006182	0,364571333

Homo_sapiens_tRNA-Leu-TAA-3	2255,431132	0,858674424	3,48E-07	0,175597695	0,340959692	0,322334738	0,077710768
Homo_sapiens_tRNA-Ala-TGC-2	2702,91058	-0,581611701	6,20E-07	-1,525764417	1,07597E-36	-0,490720071	2,64017E-05
Homo_sapiens_tRNA-Tyr-GTA-1	28545,34593	0,702442211	8,84E-07	1,245042497	5,61573E-19	0,468280743	0,001416727
Homo_sapiens_tRNA-Ala-AGC-15	981,0059408	-1,022295465	1,16E-06	-1,03129133	1,24072E-06	-0,698328084	0,00102688
Homo_sapiens_tRNA-Thr-AGT-2	13613,28501	0,455427619	1,37E-06	0,568742196	1,01143E-09	0,297218991	0,002166567
Homo_sapiens_tRNA-Pro-TGG-1	1184,933445	-1,343326532	1,85E-06	-1,725337615	9,69068E-10	-0,616953452	0,038660735
Homo_sapiens_tRNA-Ala-AGC-19	48,44180073	-5,237388001	2,12E-06	-6,122144671	6,15496E-06	-4,247578306	2,64114E-05
Homo_sapiens_tRNA-Ala-AGC-1	4461,762946	-0,768525067	2,34E-06	-3,054096962	4,75195E-74	-0,327719264	0,060336272
Homo_sapiens_tRNA-Cys-GCA-1	73,41348635	-3,115278792	2,59E-06	-0,903790806	0,155089601	0,580975257	0,406743788
Homo_sapiens_tRNA-Arg-CCT-1	7914,751008	0,64230983	3,11E-06	0,531601832	0,000108738	0,652618168	2,38953E-06
Homo_sapiens_tRNA-Asn-GTT-9	45,97642863	-4,016010346	4,55E-06	-5,961186181	4,3405E-06	-0,877755444	0,339289245
Homo_sapiens_tRNA-Leu-CAA-2	1582,791749	-1,845796225	3,24E-05	-2,493642974	1,2498E-08	-0,569828187	0,267109552
Homo_sapiens_tRNA-Arg-CCG-1	22013,48918	0,448815459	5,01E-05	0,870568452	5,60015E-16	0,404204661	0,000295139
Homo_sapiens_tRNA-Cys-GCA-10	33,67660077	-4,083123682	7,61E-05	-3,872394296	0,000402489	-1,597290849	0,106262934
Homo_sapiens_tRNA-Gln-CTG-6	198,0151258	-1,576898714	0,000102987	-2,402966734	1,74316E-08	-1,230510011	0,002309001
Homo_sapiens_tRNA-Val-CAC-4	69,89747512	-2,132160378	0,000654018	-1,483117371	0,019469834	-0,463722033	0,548017098
Homo_sapiens_tRNA-Lys-TTT-1	573,2548718	-0,874586267	0,000762057	-1,058376981	4,87096E-05	-0,224122609	0,485806176
Homo_sapiens_tRNA-Asn-GTT-3	15644,84366	0,287327173	0,001396576	0,881464453	8,798E-25	0,477319687	4,59763E-08
Homo_sapiens_tRNA-Cys-GCA-11	5952,130529	0,415341188	0,002348221	0,761371777	5,52872E-09	0,237945469	0,097836445
Homo_sapiens_tRNA-Leu-TAG-1	6984,441389	0,255136728	0,003515556	-0,330952825	0,000115757	0,005143634	0,980580662
Homo_sapiens_tRNA-Lys-CTT-2	38705,02169	0,229157495	0,003773462	0,032344101	0,700775628	0,007790025	0,954846643
Homo_sapiens_tRNA-Cys-GCA-5	834,3517306	-0,633581657	0,003881402	-0,946599746	1,23689E-05	-0,353890791	0,12410949
Homo_sapiens_tRNA-Gln-CTG-5	51,07060156	-2,625874255	0,011016142	-4,499879813	7,87312E-05	-2,096733923	0,04046494
Homo_sapiens_tRNA-Tyr-GTA-7	138,8631056	-1,11036927	0,011772411	-0,870368397	0,048368195	-1,744477014	3,02032E-05
Homo_sapiens_tRNA-Val-AAC-3	1422,606864	0,386884499	0,018166234	-1,121033089	3,90251E-12	-0,193533981	0,282297256
Homo_sapiens_tRNA-Asn-GTT-4	2056,568048	-0,381616089	0,019411916	0,536439251	0,000467546	0,277558053	0,092000912
Homo_sapiens_tRNA-Ser-AGA-3	106,8018068	-1,080297579	0,024979745	-0,243166151	0,624466972	-0,960891034	0,039761304
Homo_sapiens_tRNA-Thr-CGT-3	2437,645903	0,410247494	0,033822373	-0,155977909	0,427908259	0,443139535	0,018131541
Homo_sapiens_tRNA-Cys-GCA-12	17,42920862	-2,526669518	0,04210655	-2,980255701	0,020733056	-1,675993541	0,166862516
Homo_sapiens_tRNA-Cys-GCA-18	14,68350071	-3,055056943	0,047243492	-2,569080088	0,096056967	0,90138879	0,579305151
Homo_sapiens_tRNA-Thr-AGT-5	2840,793208	0,207929294	0,053916722	-0,45522468	8,41735E-06	-0,126644005	0,267109552
Homo_sapiens_tRX-Lys-CTT-3	40,9970552	1,513664864	0,057298122	1,804342206	0,016385178	0,632192359	0,501272112
Homo_sapiens_tRNA-Ala-AGC-12	755,112747	-1,36428037	0,059146758	-2,446109154	0,000218258	-4,771398947	5,81393E-13
Homo_sapiens_tRNA-Leu-TAA-4	14,33395359	-2,763640207	0,059146758	-4,077826056	0,012353138	-2,376632779	0,08924896
Homo_sapiens_tRNA-Ile-GAT-1	8,390042589	-5,701209591	0,060317276	-3,105148363	0,255069937	-5,238036215	0,055738605
Homo_sapiens_tRNA-Thr-AGT-6	1940,385772	-0,264559555	0,060362028	-0,35592704	0,007978809	0,255122173	0,061542383
Homo_sapiens_tRNA-Asn-GTT-1	4142,187352	-0,357434392	0,062853335	-1,525100453	5,68806E-18	0,800282006	5,66491E-06
Homo_sapiens_tRNA-Cys-GCA-3	6,755936546	-5,294863315	0,084046327	-0,886608855	0,743447614	0,72343129	0,867991381
Homo_sapiens_tRNA-Asn-GTT-8	6,116766732	-4,4926215	0,092736735	-3,620376435	0,135848126	-0,269300199	0,942733647
Homo_sapiens_tRNA-Thr-TGT-2	4231,89799	-0,339029107	0,145978737	0,890213916	9,16109E-06	0,315475166	0,162683667
Homo_sapiens_tRNA-Asn-GTT-27	6,029676281	-4,345524112	0,169088766	-4,724772295	0,097771973	0,082722213	0,98872343

Homo_sapiens_tRNA-Cys-GCA-19	8,515594854	-2,961503334	0,175199552	-3,156602271	0,132197222	1,299007332	0,529593503
Homo_sapiens_tRNA-Asp-GTC-3	1824,923537	0,210036772	0,196711417	0,126244569	0,406402101	-0,413694564	0,003488256
Homo_sapiens_tRNA-iMet-CAT-3	17,43726556	1,665446981	0,20588917	1,677630116	0,158727844	1,343206822	0,301149116
Homo_sapiens_tRNA-Glu-CTC-2	139,2358039	0,590459807	0,250853224	0,847411907	0,056098167	-0,083696064	0,922245391
Homo_sapiens_tRNA-Lys-TTT-5	34,2744664	1,056731908	0,250908062	1,315395558	0,102353465	0,377893297	0,739059623
Homo_sapiens_tRNA-Cys-GCA-15	12,17144801	-1,673825869	0,379086356	-2,680573059	0,126873975	0,767818512	0,701486964
Homo_sapiens_tRNA-Arg-CCT-3	4551,473952	0,113460692	0,383718001	-0,241852568	0,018066304	-0,558979189	1,23474E-08
Homo_sapiens_tRNA-Val-AAC-5	98,07815835	0,612053838	0,399092722	1,079350194	0,056098167	0,305149686	0,701486964
Homo_sapiens_tRNA-Arg-TCT-5	4,669160311	-2,009201118	0,431674287	-0,540413607	0,782265182	-0,357124835	0,917739776
Homo_sapiens_tRNA-Ala-AGC-3	6361,180167	-0,118539382	0,448784414	0,578383873	2,36653E-07	0,654302965	5,30224E-09
Homo_sapiens_tRNA-Gln-TTG-3	11299,97615	-0,108274614	0,482938971	-0,022971623	0,841119695	0,097906893	0,482748018
Homo_sapiens_tRNA-Gln-CTG-2	6454,568665	-0,193122229	0,493579714	-1,668966517	1,10646E-17	-0,020788955	0,954846643
Homo_sapiens_tRNA-Thr-TGT-6	16,6053634	1,00432099	0,505653929	1,20891531	0,293383536	0,46024471	0,779196873
Homo_sapiens_tRNA-Asn-GTT-6	2,981433004	-2,236658965	0,521549688	-2,457719901	0,359334076	-0,382674035	0,922245391
Homo_sapiens_tRNA-Thr-TGT-3	2810,415471	0,151485489	0,532114865	-0,113249552	0,527019478	0,336020273	0,055738605
Homo_sapiens_tRNA-Gly-CCC-4	2,348439919	-3,322858145	0,533004715	-4,012834288	0,309900433	-2,125552978	0,665473345
Homo_sapiens_tRNA-Gln-CTG-9	1,546584744	2,925681567	0,589884319	1,418031397	0,722321295	2,525415275	0,591825734
Homo_sapiens_tRNA-Gly-TCC-5	0,781369952	4,051373109	0,615632525	3,083933087	NA	2,091084185	0,791204113
Homo_sapiens_tRNA-Lys-CTT-11	0,790114391	4,051372993	0,615632525	3,083932977	NA	2,177104652	0,784024112
Homo_sapiens_tRNA-Arg-CCT-6	0,593143339	3,941052051	0,629079037	0	NA	2,177089211	NA
Homo_sapiens_tRNA-Cys-GCA-16	2,320809475	-2,363270711	0,629079037	-2,285946278	0,490147288	-0,864196978	0,867991381
Homo_sapiens_tRX-Trp-CCA-1	0,748698486	3,665426639	0,677684933	3,083932192	NA	2,790806188	0,702016233
Homo_sapiens_tRNA-Gln-TTG-4	9,625399988	-0,988144427	0,684806301	0,686310112	0,639548244	-0,249433893	0,922245391
Homo_sapiens_tRNA-Asn-GTT-11	1,486587731	-2,875283582	0,691287053	-3,237914177	0,466876911	-1,567210764	0,79481645
Homo_sapiens_tRNA-Asn-GTT-24	3,610538211	1,619487231	0,72466744	1,390975373	0,615778277	1,379369922	0,701486964
Homo_sapiens_tRNA-Leu-TAA-5	0,373565808	3,348278186	0,72466744	0	NA	1,148170801	NA
Homo_sapiens_tRNA-Cys-GCA-20	0,524344752	-3,032277048	0,773431115	-2,049616498	NA	-2,653769543	NA
Homo_sapiens_tRNA-Arg-TCT-2	4881,028175	-0,068130811	0,777016392	-0,847918639	2,50388E-13	0,193097123	0,124640699
Homo_sapiens_tRNA-Asn-GTT-10	0,827373786	-2,932726587	0,777016392	-1,950066037	NA	-0,033534858	1
Homo_sapiens_tRNA-Gly-GCC-3	3,889631333	1,447630273	0,777016392	3,524714316	0,154319911	2,242784375	0,450690175
Homo_sapiens_tRNA-Leu-AAG-4	54,67956392	0,378522762	0,777016392	1,121762111	0,088985809	0,133290958	0,917739776
Homo_sapiens_tRNA-His-GTG-2	6,231644108	0,984980544	0,779254682	1,808697008	0,325670488	0,928118577	0,702016233
Homo_sapiens_tRNA-Gly-CCC-5	0,604346263	-2,875821775	0,780268596	-1,893161225	NA	-1,005869042	NA
Homo_sapiens_tRNA-Ala-AGC-20	0,355805399	-2,702024135	0,804868567	-1,719363585	NA	-3,833019463	NA
Homo_sapiens_tRNA-Asn-GTT-7	1,93149785	1,572023835	0,804868567	2,037168136	0,525470041	0,015222748	1
Homo_sapiens_tRNA-Val-CAC-6	8,63805006	0,773898477	0,804868567	0,511661848	0,748891292	0,539048417	0,807643068
Homo_sapiens_tRNA-Ala-AGC-11	6337,892297	-0,057419491	0,809877311	-0,115316144	0,326838174	0,019283769	0,922245391
Homo_sapiens_tRNA-Val-CAC-9	0,19548629	2,597609731	0,827631276	0	NA	0	NA
Homo_sapiens_tRNA-Trp-CCA-1	3004,893955	0,063894618	0,853019629	-0,310653753	0,025570197	0,609814613	4,93521E-06
Homo_sapiens_tRNA-Asp-GTC-4	24,46653729	0,437104028	0,858758747	0,698938468	0,50028406	0,265408624	0,878530542
Homo_sapiens_tRNA-Lys-TTT-9	2,074436623	-1,289162969	0,873125274	-3,25882094	0,326838174	-0,767093156	0,878530542

Homo_sapiens_tRNA-Gln-CTG-7	1,217107604	1,34009376	0,88060964	0,619531308	NA	1,497084881	0,739059623
Homo_sapiens_tRNA-Glu-TTC-12	0,242039106	2,203619583	0,88060964	0	NA	2,091048859	NA
Homo_sapiens_tRNA-Thr-TGT-4	0,451406745	2,203615587	0,88060964	0	NA	3,48137656	NA
Homo_sapiens_tRNA-Leu-CAA-6	1,116577652	-2,083649807	0,883097018	1,901907406	NA	-3,214615358	0,661219211
Homo_sapiens_tRNA-Val-CAC-2	5513,91191	0,051746629	0,883097018	-0,39618153	0,001489307	0,413820178	0,000958498
Homo_sapiens_tRNA-Val-CAC-8	0,661140537	2,056287485	0,883097018	0,089972756	NA	0,335273287	NA
Homo_sapiens_tRX-Val-AAC-1	7,122116095	0,729160067	0,917807505	1,368063681	0,521827944	0,414640741	0,917739776
Homo_sapiens_tRNA-Lys-CTT-3	16,82223533	0,398640057	0,923378509	0,054917731	0,961000668	-0,112105033	0,954846643
Homo_sapiens_tRX-Cys-GCA-3	1,698563063	1,321814469	0,923378509	3,401135306	0,370864936	1,770172307	0,739059623
Homo_sapiens_tRX-Glu-CTC-1	15,2021508	0,431290791	0,927989868	0,965683993	0,475771144	0,088107969	0,975581723
Homo_sapiens_tRNA-Glu-CTC-7	0,714750874	1,59083282	0,942897888	-0,228813465	NA	0,658491356	NA
Homo_sapiens_tRNA-Gly-GCC-4	0,419101432	1,592488021	0,942897888	0,089995297	NA	-2,023652142	NA
Homo_sapiens_tRNA-Lys-CTT-13	0,680107147	-1,628082072	0,942897888	1,579524637	NA	-1,343017786	NA
Homo_sapiens_tRX-Asp-ATC-1	0,171072758	-1,628084072	0,942897888	-0,645423522	NA	-2,75909281	NA
Homo_sapiens_tRNA-Ser-GCT-6	30,66751906	-0,247560864	0,945381821	0,283462116	0,747621134	-0,48725217	0,665473345
Homo_sapiens_tRNA-Lys-CTT-6	2,62039431	1,16120456	0,948802344	3,568439252	0,375039679	-2,752320656	0,623921982
Homo_sapiens_tRNA-Ala-CGC-5	0,123155094	-1,211477106	0,995389799	-0,228816555	NA	-2,342491046	NA
Homo_sapiens_tRNA-Cys-GCA-17	2,194670707	0,68587068	0,995389799	1,317154078	0,669726557	0,754898569	0,878530542
Homo_sapiens_tRNA-Tyr-ATA-1	0,123155094	-1,211477106	0,995389799	-0,228816555	NA	-2,342491046	NA
Homo_sapiens_tRNA-Val-AAC-6	0,123155094	-1,211477106	0,995389799	-0,228816555	NA	-2,342491046	NA
Homo_sapiens_tRNA-Ala-AGC-16	0,366559047	0,106399417	1	-0,645422889	NA	-2,759070518	NA
Homo_sapiens_tRNA-Ala-AGC-17	1,141465879	-0,345130603	1	-2,550720582	NA	-4,664326265	0,462247129
Homo_sapiens_tRNA-Ala-TGC-7	0,134281573	-0,471232944	1	0,511427607	NA	-0,092780336	NA
Homo_sapiens_tRNA-Arg-CCT-5	1,468579239	0,665072466	1	1,442454928	NA	1,458108388	0,785339492
Homo_sapiens_tRNA-Arg-TCG-6	0,063959587	0	1	0	NA	1,148148088	NA
Homo_sapiens_tRNA-Asn-GTT-14	0,061577547	-0,471237391	1	0,511423159	NA	-1,602260576	NA
Homo_sapiens_tRNA-Asn-GTT-17	0,145408052	0	1	0	NA	2,259072129	NA
Homo_sapiens_tRNA-Asn-GTT-25	0,109495211	-0,892665633	1	0,089994917	NA	-2,023683555	NA
Homo_sapiens_tRNA-Asp-GTC-10	2,543956558	0,38884176	1	1,3394776	0,606205522	-1,773026484	0,601973887
Homo_sapiens_tRNA-Asp-GTC-5	0,148358267	0	1	3,083936103	NA	0	NA
Homo_sapiens_tRNA-Asp-GTC-9	0,433380148	0	1	3,685532867	NA	2,177075033	NA
Homo_sapiens_tRNA-Cys-GCA-21	1,151302703	0,842638146	1	2,335784661	NA	1,989780351	0,784024112
Homo_sapiens_tRNA-Cys-GCA-24	0,997694288	-0,274148608	1	0,604402166	NA	1,736580393	0,766511825
Homo_sapiens_tRNA-Cys-GCA-7	0,072704026	0	1	0	NA	1,241550036	NA
Homo_sapiens_tRNA-Gln-CTG-11	0,212317854	0	1	3,083934498	NA	1,148159589	NA
Homo_sapiens_tRNA-Glu-CTC-3	0,357896715	-0,287586526	1	-0,645421432	NA	-1,249575855	NA
Homo_sapiens_tRNA-Glu-CTC-5	0,072704026	0	1	0	NA	1,241550036	NA
Homo_sapiens_tRNA-Glu-TTC-7	0,713069774	-0,471226647	1	2,35117477	NA	2,217281458	NA
Homo_sapiens_tRNA-Gly-CCC-3	0,109495211	-0,892665633	1	0,089994917	NA	-2,023683555	NA
Homo_sapiens_tRNA-Gly-GCC-5	0,072704026	0	1	0	NA	1,241550036	NA
Homo_sapiens_tRNA-Gly-TCC-4	5,637245803	-0,170206971	1	-0,459364724	0,813248536	-0,184031043	0,954846643

Homo_sapiens_tRNA-Gly-TCC-6	0,588809342	0,014208837	1	-1,100986122	NA	-0,855681702	NA
Homo_sapiens_tRNA-Ile-AAT-10	0,670825982	-0,32858672	1	-0,20563099	NA	-3,557397911	NA
Homo_sapiens_tRNA-Ile-AAT-2	4331,566086	-0,009775968	1	0,411696207	0,000694623	-0,399625676	0,001225359
Homo_sapiens_tRNA-Leu-AAG-5	0,670086999	0,869262448	1	1,749578433	NA	2,182565782	NA
Homo_sapiens_tRNA-Leu-AAG-6	0,721492386	-0,471232942	1	2,752518152	NA	-0,09273149	0,998658404
Homo_sapiens_tRNA-Leu-AAG-8	0,567182248	0,106431855	1	-0,645419993	NA	0,241877599	NA
Homo_sapiens_tRNA-Leu-TAG-4	0,6511704	0	1	4,086876356	NA	1,14816834	NA
Homo_sapiens_tRNA-Lys-CTT-10	0,061577547	-0,471237391	1	0,511423159	NA	-1,602260576	NA
Homo_sapiens_tRNA-Lys-CTT-12	0,273895402	-0,47123322	1	1,749574986	NA	-0,186187926	NA
Homo_sapiens_tRNA-Lys-CTT-16	0,148358267	0	1	3,083936103	NA	0	NA
Homo_sapiens_tRNA-Lys-CTT-5	1,132714845	-0,980593625	1	-0,861298241	NA	-0,683646095	0,940409857
Homo_sapiens_tRNA-Lys-CTT-8	0,134281573	-0,471232944	1	0,511427607	NA	-0,092780336	NA
Homo_sapiens_tRNA-Lys-TTT-11	0,148358267	0	1	3,083936103	NA	0	NA
Homo_sapiens_tRNA-Lys-TTT-14	0,109495211	-0,892665633	1	0,089994917	NA	-2,023683555	NA
Homo_sapiens_tRNA-Lys-TTT-7	0,865744097	0,865557285	1	-1,101978011	NA	-0,158303773	0,988346679
Homo_sapiens_tRNA-Phe-GAA-10	3,196693377	0,164380425	1	-0,542605242	0,841119695	0,439187665	0,922245391
Homo_sapiens_tRNA-Phe-GAA-4	83,9635361	0,067224141	1	0,039029887	0,945398355	0,146310373	0,878530542
Homo_sapiens_tRNA-Phe-GAA-5	0,212317854	0	1	3,083934498	NA	1,148159589	NA
Homo_sapiens_tRNA-Pro-AGG-3	1,470583147	0,534563324	1	1,167637614	NA	0,742065656	0,922245391
Homo_sapiens_tRNA-Ser-ACT-1	0,223615142	0,447834547	1	0,089995297	NA	-2,023666435	NA
Homo_sapiens_tRNA-Ser-AGA-5	0,189496721	-0,471230756	1	0,511429794	NA	0,756691741	NA
Homo_sapiens_tRNA-Sup-TTA-1	0,063959587	0	1	0	NA	1,148148088	NA
Homo_sapiens_tRNA-Thr-AGT-7	0,587210813	0	1	4,086861088	NA	0	NA
Homo_sapiens_tRNA-Val-AAC-4	2,969944448	0,419538132	1	0,173384597	0,945398355	0,488924682	0,917739776
Homo_sapiens_tRX-Ala-AGC-6	0,063959587	0	1	0	NA	1,148148088	NA
Homo_sapiens_tRX-Arg-ACG-1	0,063959587	0	1	0	NA	1,148148088	NA
Homo_sapiens_tRX-Leu-CAG-1	0,388015333	0,869262531	1	1,749574986	NA	-0,186175873	NA
Homo_sapiens_tRX-Lys-CTT-1	0,109495211	-0,892665633	1	0,089994917	NA	-2,023683555	NA
Homo_sapiens_tRX-Lys-TTT-2	0,73556908	0	1	4,556870116	NA	0	1
Homo_sapiens_tRX-Met-CAT-1	0,349152276	-0,287586321	1	-0,645421522	NA	-1,343025456	NA
Homo_sapiens_tRX-Val-TAC-2	0,941120887	0,048559881	1	-1,447762873	NA	0,188255552	0,984558654
Homo_sapiens_tRNA-Ala-AGC-18	0	NA	NA	NA	NA	NA	NA
Homo_sapiens_tRNA-Ala-AGC-21	0	NA	NA	NA	NA	NA	NA
Homo_sapiens_tRNA-Ala-AGC-23	0	NA	NA	NA	NA	NA	NA
Homo_sapiens_tRNA-Ala-TGC-8	0	NA	NA	NA	NA	NA	NA
Homo_sapiens_tRNA-Ala-TGC-9	0	NA	NA	NA	NA	NA	NA
Homo_sapiens_tRNA-Arg-CCT-7	0	NA	NA	NA	NA	NA	NA
Homo_sapiens_tRNA-Asn-ATT-1	0	NA	NA	NA	NA	NA	NA
Homo_sapiens_tRNA-Asn-GTT-12	0	NA	NA	NA	NA	NA	NA
Homo_sapiens_tRNA-Asn-GTT-13	0	NA	NA	NA	NA	NA	NA
Homo_sapiens_tRNA-Asn-GTT-16	0	NA	NA	NA	NA	NA	NA

Homo_sapiens_tRNA-Asn-GTT-18	0	NA	NA	NA	NA	NA	NA
Homo_sapiens_tRNA-Asn-GTT-21	0	NA	NA	NA	NA	NA	NA
Homo_sapiens_tRNA-Asn-GTT-22	0	NA	NA	NA	NA	NA	NA
Homo_sapiens_tRNA-Asn-GTT-26	0	NA	NA	NA	NA	NA	NA
Homo_sapiens_tRNA-Asn-GTT-28	0	NA	NA	NA	NA	NA	NA
Homo_sapiens_tRNA-Asp-GTC-6	0	NA	NA	NA	NA	NA	NA
Homo_sapiens_tRNA-Asp-GTC-8	0	NA	NA	NA	NA	NA	NA
Homo_sapiens_tRNA-Cys-ACA-1	0	NA	NA	NA	NA	NA	NA
Homo_sapiens_tRNA-Cys-GCA-22	0	NA	NA	NA	NA	NA	NA
Homo_sapiens_tRNA-Cys-GCA-23	0	NA	NA	NA	NA	NA	NA
Homo_sapiens_tRNA-Gln-CTG-10	0	NA	NA	NA	NA	NA	NA
Homo_sapiens_tRNA-Gln-CTG-12	0	NA	NA	NA	NA	NA	NA
Homo_sapiens_tRNA-Gln-CTG-13	0	NA	NA	NA	NA	NA	NA
Homo_sapiens_tRNA-Gln-CTG-16	0	NA	NA	NA	NA	NA	NA
Homo_sapiens_tRNA-Gln-CTG-17	0	NA	NA	NA	NA	NA	NA
Homo_sapiens_tRNA-Gln-CTG-8	0	NA	NA	NA	NA	NA	NA
Homo_sapiens_tRNA-Gln-TTG-10	0	NA	NA	NA	NA	NA	NA
Homo_sapiens_tRNA-Gln-TTG-5	0	NA	NA	NA	NA	NA	NA
Homo_sapiens_tRNA-Gln-TTG-6	0	NA	NA	NA	NA	NA	NA
Homo_sapiens_tRNA-Glu-CTC-16	0	NA	NA	NA	NA	NA	NA
Homo_sapiens_tRNA-Glu-TTC-11	0	NA	NA	NA	NA	NA	NA
Homo_sapiens_tRNA-Glu-TTC-5	0	NA	NA	NA	NA	NA	NA
Homo_sapiens_tRNA-Glu-TTC-6	0	NA	NA	NA	NA	NA	NA
Homo_sapiens_tRNA-Glu-TTC-9	0	NA	NA	NA	NA	NA	NA
Homo_sapiens_tRNA-Gly-CCC-6	0	NA	NA	NA	NA	NA	NA
Homo_sapiens_tRNA-Gly-CCC-7	0	NA	NA	NA	NA	NA	NA
Homo_sapiens_tRNA-Gly-CCC-8	0	NA	NA	NA	NA	NA	NA
Homo_sapiens_tRNA-Gly-GCC-6	0	NA	NA	NA	NA	NA	NA
Homo_sapiens_tRNA-Ile-AAT-11	0	NA	NA	NA	NA	NA	NA
Homo_sapiens_tRNA-Ile-AAT-9	0	NA	NA	NA	NA	NA	NA
Homo_sapiens_tRNA-Leu-AAG-7	0	NA	NA	NA	NA	NA	NA
Homo_sapiens_tRNA-Leu-CAA-5	0	NA	NA	NA	NA	NA	NA
Homo_sapiens_tRNA-Lys-CTT-14	0	NA	NA	NA	NA	NA	NA
Homo_sapiens_tRNA-Lys-CTT-15	0	NA	NA	NA	NA	NA	NA
Homo_sapiens_tRNA-Lys-CTT-7	0	NA	NA	NA	NA	NA	NA
Homo_sapiens_tRNA-Lys-CTT-9	0	NA	NA	NA	NA	NA	NA
Homo_sapiens_tRNA-Lys-TTT-10	0	NA	NA	NA	NA	NA	NA
Homo_sapiens_tRNA-Lys-TTT-12	0	NA	NA	NA	NA	NA	NA
Homo_sapiens_tRNA-Lys-TTT-13	0	NA	NA	NA	NA	NA	NA
Homo_sapiens_tRNA-Lys-TTT-15	0	NA	NA	NA	NA	NA	NA
Homo_sapiens_tRNA-Lys-TTT-8	0	NA	NA	NA	NA	NA	NA

Homo_sapiens_tRNA-Met-CAT-7	0	NA	NA	NA	NA	NA	NA
Homo_sapiens_tRNA-Phe-GAA-11	0	NA	NA	NA	NA	NA	NA
Homo_sapiens_tRNA-Phe-GAA-12	0	NA	NA	NA	NA	NA	NA
Homo_sapiens_tRNA-Phe-GAA-2	0	NA	NA	NA	NA	NA	NA
Homo_sapiens_tRNA-Phe-GAA-6	0	NA	NA	NA	NA	NA	NA
Homo_sapiens_tRNA-Phe-GAA-7	0	NA	NA	NA	NA	NA	NA
Homo_sapiens_tRNA-Phe-GAA-8	0	NA	NA	NA	NA	NA	NA
Homo_sapiens_tRNA-Pro-AGG-4	0	NA	NA	NA	NA	NA	NA
Homo_sapiens_tRNA-Pro-GGG-1	0	NA	NA	NA	NA	NA	NA
Homo_sapiens_tRNA-Pro-TGG-4	0	NA	NA	NA	NA	NA	NA
Homo_sapiens_tRNA-Pro-TGG-5	0	NA	NA	NA	NA	NA	NA
Homo_sapiens_tRNA-SeC-TCA-2	0	NA	NA	NA	NA	NA	NA
Homo_sapiens_tRNA-SeC-TCA-3	0	NA	NA	NA	NA	NA	NA
Homo_sapiens_tRNA-Ser-AGA-6	0	NA	NA	NA	NA	NA	NA
Homo_sapiens_tRNA-Thr-CGT-5	0	NA	NA	NA	NA	NA	NA
Homo_sapiens_tRNA-Thr-CGT-6	0	NA	NA	NA	NA	NA	NA
Homo_sapiens_tRNA-Tyr-GTA-10	0	NA	NA	NA	NA	NA	NA
Homo_sapiens_tRNA-Tyr-GTA-9	0	NA	NA	NA	NA	NA	NA
Homo_sapiens_tRNA-Val-AAC-7	0	NA	NA	NA	NA	NA	NA
Homo_sapiens_tRNA-Val-CAC-10	0	NA	NA	NA	NA	NA	NA
Homo_sapiens_tRNA-Val-CAC-11	0	NA	NA	NA	NA	NA	NA
Homo_sapiens_tRNA-Val-CAC-13	0	NA	NA	NA	NA	NA	NA
Homo_sapiens_tRNA-Val-CAC-14	0	NA	NA	NA	NA	NA	NA
Homo_sapiens_tRNA-Val-CAC-7	0	NA	NA	NA	NA	NA	NA
Homo_sapiens_tRX-Ala-GGC-3	0	NA	NA	NA	NA	NA	NA
Homo_sapiens_tRX-Ala-GGC-4	0	NA	NA	NA	NA	NA	NA
Homo_sapiens_tRX-Asn-GTT-1	0	NA	NA	NA	NA	NA	NA
Homo_sapiens_tRX-Asn-GTT-2	0	NA	NA	NA	NA	NA	NA
Homo_sapiens_tRX-Cys-GCA-1	0	NA	NA	NA	NA	NA	NA
Homo_sapiens_tRX-Cys-GCA-2	0	NA	NA	NA	NA	NA	NA
Homo_sapiens_tRX-Gln-CTG-2	0	NA	NA	NA	NA	NA	NA
Homo_sapiens_tRX-Gln-CTG-3	0	NA	NA	NA	NA	NA	NA
Homo_sapiens_tRX-Gln-TTG-1	0	NA	NA	NA	NA	NA	NA
Homo_sapiens_tRX-Gly-CCC-1	0	NA	NA	NA	NA	NA	NA
Homo_sapiens_tRX-Gly-CCC-2	0	NA	NA	NA	NA	NA	NA
Homo_sapiens_tRX-Gly-CCC-3	0	NA	NA	NA	NA	NA	NA
Homo_sapiens_tRX-Ile-AAT-3	0	NA	NA	NA	NA	NA	NA
Homo_sapiens_tRX-Ile-GAT-1	0	NA	NA	NA	NA	NA	NA
Homo_sapiens_tRX-Ile-GAT-2	0	NA	NA	NA	NA	NA	NA
Homo_sapiens_tRX-Leu-CAA-3	0	NA	NA	NA	NA	NA	NA
Homo_sapiens_tRX-Leu-TAA-2	0	NA	NA	NA	NA	NA	NA

Homo_sapiens_tRX-Lys-CTT-6	0	NA	NA	NA	NA	NA	NA
Homo_sapiens_tRX-Met-CAT-2	0	NA	NA	NA	NA	NA	NA
Homo_sapiens_tRX-Pro-GGG-1	0	NA	NA	NA	NA	NA	NA
Homo_sapiens_tRX-Pro-GGG-2	0	NA	NA	NA	NA	NA	NA
Homo_sapiens_tRX-Ser-GCT-1	0	NA	NA	NA	NA	NA	NA
Homo_sapiens_tRX-Ser-GGA-2	0	NA	NA	NA	NA	NA	NA
Homo_sapiens_tRX-Tyr-GTA-1	0	NA	NA	NA	NA	NA	NA
Homo_sapiens_tRX-Val-CAC-4	0	NA	NA	NA	NA	NA	NA
Homo_sapiens_tRX-Val-TAC-3	0	NA	NA	NA	NA	NA	NA

Table S2. Differential expression analysis at tRNA anticodon level using DESeq2 in differentiated cell lines relative to hiPSC.

		NPC vs hiPSC		Neurons vs hiPSC		CM vs hiPSC	
Anticodon	**baseMean**	**log2FoldChange**	**Adjusted p-value**	**log2FoldChange**	**Adjusted p-value**	**log2FoldChange**	**Adjusted p-value**
Homo_sapiens_tRNA-Thr-TGT	23995,80452	-0,361361627	7,01E-50	-0,429181404	2,39578E-66	-0,009600269	0,713499633
Homo_sapiens_tRNA-Gly-GCC	113315,7933	-0,641940147	2,87E-40	-0,429470272	7,21332E-19	-0,620975357	1,70227E-37
Homo_sapiens_tRNA-Leu-TAA	17488,04397	0,570693717	4,19E-29	0,741834768	2,65097E-48	0,10548503	0,0458904
Homo_sapiens_tRNA-iMet-CAT	64256,96807	0,525618053	3,25E-27	0,653823455	9,20374E-42	0,466911417	1,57973E-21
Homo_sapiens_tRNA-Gly-CCC	55580,89025	0,778184978	9,82E-26	1,356213354	6,19626E-76	0,739054898	6,49163E-23
Homo_sapiens_tRNA-Leu-AAG	53171,27147	-0,343619913	1,15E-15	-0,234310215	4,98174E-08	-0,195242569	7,88973E-06
Homo_sapiens_tRNA-Pro-TGG	32894,81896	0,25656079	4,38E-13	0,392892092	2,77248E-29	0,259803794	1,95287E-13
Homo_sapiens_tRNA-Ser-CGA	17156,16676	0,28286318	3,10E-11	0,457942691	9,83014E-28	0,098995654	0,021121811
Homo_sapiens_tRNA-Arg-CCG	38564,25489	0,178991403	8,24E-10	0,248576142	5,26101E-18	0,134079306	4,42756E-06
Homo_sapiens_tRNA-Thr-CGT	28483,7479	0,32898137	5,26E-09	0,351121317	2,43287E-10	0,320438414	1,14038E-08
Homo_sapiens_tRNA-SeC-TCA	5680,092923	0,718645941	8,38E-09	1,543421665	2,41485E-37	0,590349989	2,64659E-06
Homo_sapiens_tRNA-Ser-TGA	26120,37066	-0,272649497	2,19E-08	0,02869919	0,650770047	-0,425819617	5,9853E-19
Homo_sapiens_tRNA-Pro-AGG	51703,34215	-0,198438616	1,36E-07	-0,189932994	3,42005E-07	0,134787714	0,000329612
Homo_sapiens_tRNA-Arg-CCT	35761,62237	0,338253956	2,29E-07	0,339629679	1,35861E-07	0,365054711	2,06848E-08
Homo_sapiens_tRNA-Leu-CAG	58684,10582	0,332220235	2,50E-07	0,147672029	0,027098674	0,171714602	0,008263653
Homo_sapiens_tRNA-Asn-GTT	72550,16343	-0,207907208	1,91E-06	0,025549576	0,650770047	0,264577712	1,31137E-09
Homo_sapiens_tRNA-Glu-CTC	113222,7594	-0,290392861	4,54E-06	-0,280762525	6,23577E-06	-0,382012286	1,51438E-09
Homo_sapiens_tRNA-Pro-CGG	17667,93151	-0,173953555	4,56E-05	-0,355575765	1,65495E-17	-0,04176857	0,371314896
Homo_sapiens_tRNA-Asp-GTC	102662,1987	-0,296413061	5,63E-05	-0,25619769	0,000424519	-0,415361367	1,14038E-08
Homo_sapiens_tRNA-Ala-CGC	37564,39161	0,10734464	0,000173496	-0,015942948	0,659989633	0,108613566	0,000109264
Homo_sapiens_tRNA-Phe-GAA	63370,37867	-0,099220229	0,000501709	-0,175981203	2,02717E-10	0,056584015	0,045515785
Homo_sapiens_tRNA-Ser-AGA	50239,50389	0,107585088	0,000512205	0,259917615	2,87287E-18	-0,004132796	0,893673331
Homo_sapiens_tRNA-Trp-CCA	37043,52299	-0,104072342	0,000917861	-0,183826962	1,98392E-09	0,160664139	1,3399E-07
Homo_sapiens_tRNA-Thr-AGT	53536,84417	-0,181507322	0,001848646	-0,435421178	4,89976E-15	-0,187624657	0,000992209
Homo_sapiens_tRNA-Gly-TCC	65740,22338	0,228469668	0,003498061	0,218926589	0,004447305	0,242836488	0,001441375
Homo_sapiens_tRNA-Ile-GAT	11,77424134	-6,406200053	0,004026106	-4,217710335	0,027258614	-5,710190325	0,002074417
Homo_sapiens_tRNA-Lys-TTT	113426,2562	0,230816623	0,005359065	-0,011710457	0,896174061	-0,315012723	0,000108705

Homo_sapiens_tRNA-Glu-TTC	72038,67868	0,092243982	0,009125398	0,340420202	1,79449E-24	-0,135525575	8,6952E-05
Homo_sapiens_tRNA-Lys-CTT	73127,20848	-0,057923946	0,010667407	-0,315292186	4,26854E-48	-0,128768807	3,89247E-09
Homo_sapiens_tRNA-Val-CAC	58490,12547	-0,130032754	0,01152939	-0,025554344	0,684570874	0,02566093	0,673228733
Homo_sapiens_tRNA-Arg-ACG	76652,28865	0,100265234	0,030151071	0,332189194	1,85891E-14	0,113159432	0,011467146
Homo_sapiens_tRNA-Leu-TAG	25720,62424	-0,090776663	0,030151071	-0,192789512	1,48693E-06	-0,248333824	6,87937E-10
Homo_sapiens_tRNA-Arg-TCG	42919,23505	0,081664948	0,037992635	0,014226419	0,78490768	0,13732341	0,000278611
Homo_sapiens_tRNA-Gln-CTG	79585,70335	0,138690431	0,039275345	0,043603799	0,608710571	0,200848119	0,002011456
Homo_sapiens_tRNA-Ile-AAT	67384,06509	-0,075759847	0,104384455	-0,206215437	1,63754E-06	-0,189075283	1,58971E-05
Homo_sapiens_tRNA-Gln-TTG	29189,60063	-0,099020182	0,122554241	-0,171734556	0,004661379	-0,022996196	0,713499633
Homo_sapiens_tRNA-Leu-CAA	19927,92617	-0,127089898	0,188672505	-0,138281787	0,142462372	-0,359656953	5,39859E-05
Homo_sapiens_tRNA-Val-AAC	55616,29825	0,104470924	0,189992235	0,082552804	0,325978325	0,033145871	0,688018576
Homo_sapiens_tRNA-Ala-TGC	54576,14644	-0,049264372	0,190629413	-0,184354021	1,08938E-07	-0,081960992	0,020226829
Homo_sapiens_tRNA-Ser-GCT	57622,5449	0,040032725	0,232532415	0,308241429	1,78972E-24	-0,089261959	0,00385517
Homo_sapiens_tRNA-Met-CAT	56755,59113	-0,053676031	0,540857861	-0,062513549	0,47370256	0,072401865	0,368509811
Homo_sapiens_tRNA-His-GTG	61115,73739	0,056736536	0,55531386	0,138487069	0,094359925	0,29986703	0,000144876
Homo_sapiens_tRNA-Ile-TAT	23387,03052	0,016363282	0,680249658	0,520336813	2,27519E-72	0,042922571	0,165295706
Homo_sapiens_tRNA-Asp-ATC	0,257011699	-2,361798241	0,741142181	-1,809317344	0,785628821	-3,239510879	0,611737167
Homo_sapiens_tRNA-Ala-AGC	111863,0067	0,011221995	0,773913733	-0,052979605	0,081431064	-0,095761246	0,000898959
Homo_sapiens_tRNA-Tyr-ATA	0,182312516	-1,927002267	0,773913733	-1,37452137	0,844064307	-2,804720335	0,670567423
Homo_sapiens_tRNA-Val-TAC	27695,19729	-0,018667775	0,773913733	-0,149941338	0,003908553	-0,227668726	8,12767E-06
Homo_sapiens_tRNA-Cys-GCA	55378,53292	-0,025158259	0,784020495	0,06328088	0,487000273	0,26143101	0,000490894
Homo_sapiens_tRNA-Arg-TCT	29551,93077	0,030515829	0,814522042	-0,537855718	4,8294E-07	-0,05475422	0,673228733
Homo_sapiens_tRNA-Tyr-GTA	83024,73111	0,011743833	0,842147211	0,011005617	0,859336747	-0,195713353	0,00014402
Homo_sapiens_tRNA-Ser-ACT	0,272221586	-0,284386934	0,972405529	-1,083133964	0,859336747	-2,513319694	0,675599085
Homo_sapiens_tRNA-Sup-TTA	0,068080391	0	1	0	1	0,667213479	0,893673331
Homo_sapiens_tRNA-Ala-GGC	0	NA	NA	NA	NA	NA	NA
Homo_sapiens_tRNA-Asn-ATT	0	NA	NA	NA	NA	NA	NA
Homo_sapiens_tRNA-Cys-ACA	0	NA	NA	NA	NA	NA	NA
Homo_sapiens_tRNA-Pro-GGG	0	NA	NA	NA	NA	NA	NA
Homo_sapiens_tRNA-Ser-GGA	0	NA	NA	NA	NA	NA	NA

Table S3. Differential expression analysis at tRNA isotype level using DESeq2 in differentiated cell lines relative to hiPSC.

		NPC vs hiPSC		Neurons vs hiPSC		CM vs hiPSC	
Gene	**baseMean**	**log2FoldChange**	**Adjusted p-value**	**log2FoldChange**	**Adjusted p-value**	**log2FoldChange**	**Adjusted p-value**
Homo_sapiens_tRNA-iMet	64368,09128	0,571745284	1,90E-24	0,657135101	4,43775E-32	0,497790351	1,24063E-18
Homo_sapiens_tRNA-Arg	223752,3907	0,182397495	2,14E-07	0,153829838	1,02406E-05	0,167708739	1,04149E-06
Homo_sapiens_tRNA-Asp	102668,3407	-0,250183901	0,000110848	-0,253299044	5,96518E-05	-0,383683503	3,95657E-10
Homo_sapiens_tRNA-SeC	5681,097979	0,763872916	0,000110848	1,544791253	3,9033E-17	0,620887037	0,001103109
Homo_sapiens_tRNA-Lys	186820,7183	0,165459516	0,000945815	-0,124967505	0,012137889	-0,204367034	1,44697E-05
Homo_sapiens_tRNA-Asn	72604,58078	-0,161537377	0,006647977	0,029134973	0,761800765	0,296063341	4,57822E-08

Homo_sapiens_tRNA-Glu	185308,6799	-0,103182692	0,026016654	-0,036190495	0,559645619	-0,262371255	1,30088E-10
Homo_sapiens_tRNA-Gly	234669,571	-0,084662178	0,042727557	0,124655584	0,001071975	-0,09592913	0,009313774
Homo_sapiens_tRNA-Gln	108930,7434	0,119577908	0,049603631	-0,012704133	0,963525597	0,170183296	0,00174584
Homo_sapiens_tRNA-Ser	151210,0442	0,07949299	0,065547623	0,260876995	3,84875E-12	-0,068840904	0,08349234
Homo_sapiens_tRNA-Leu	175164,8487	0,07543829	0,093733842	0,003434572	0,967017077	-0,047574628	0,254327558
Homo_sapiens_tRNA-Ala	204244,0484	0,058314563	0,138981061	-0,078806312	0,02882485	-0,022973366	0,541732039
Homo_sapiens_tRNA-His	61196,7882	0,10305607	0,248484077	0,142198164	0,072504807	0,331086859	5,96386E-06
Homo_sapiens_tRNA-Thr	106137,3567	-0,048804883	0,371649166	-0,223876397	9,8776E-08	0,009197938	0,851086933
Homo_sapiens_tRNA-Tyr	83089,32909	0,057948011	0,415861581	0,014430026	0,963525597	-0,164591482	0,002719708
Homo_sapiens_tRNA-Phe	63444,94022	-0,05313488	0,449154722	-0,173768905	0,002158058	0,087933955	0,120496451
Homo_sapiens_tRNA-Trp	37091,20295	-0,058077209	0,513690793	-0,179975115	0,012137889	0,192138867	0,004810189
Homo_sapiens_tRNA-Val	141931,5385	0,030860849	0,57323982	-0,005214221	0,967017077	0,01081054	0,851086933
Homo_sapiens_tRNA-Cys	55449,05224	0,021095168	0,917640325	0,066867014	0,559645619	0,292977233	9,13748E-05
Homo_sapiens_tRNA-Ile	90850,5092	-0,009116006	0,946829749	-0,00724064	0,967017077	-0,103066183	0,040383455
Homo_sapiens_tRNA-Pro	102382,4442	-0,006864905	0,946829749	-0,027036344	0,725226947	0,170718316	9,13748E-05
Homo_sapiens_tRNA-Met	56818,95476	-0,007394672	0,952481704	-0,058942038	0,575456408	0,103753458	0,165272468
Homo_sapiens_tRNA-Sup	0,06809663	0	1	0	1	0,695177087	0,889231945

Table S4. Codon dwell times estimated from ribosome profiling data in hiPSC and NPC.

	codon dwell time: long footprints (28 - 33nt)				**codon dwell time: short footprints (22 -23nt)**					
codon	**hiPSC CHX+TIG rep1**	**hiPSC CHX+TIG rep2**	**NPC CHX+TIG rep1**	**NPC CHX+TIG rep2**	**hiPSC CHX rep1**	**hiPSC CHX+TIG rep1**	**hiPSC CHX+TIG rep2**	**NPC CHX+TIG rep1**	**NPC CHX+TIG rep2**	**hiPSC CHX rep1**
AAA	1,0294	1,0407	1,0728	1,061	1,1941	0,9499	0,9278	0,9841	0,9991	0,9837
AAC	0,9458	0,9184	0,9698	1,003	1,1543	0,9209	0,8987	0,939	0,9429	0,9903
AAG	0,9567	0,9562	0,9526	0,9517	1,0977	0,9866	0,9664	0,9701	1,001	1
AAT	0,9706	0,9653	1,0349	1,012	1,1138	0,9057	0,8946	0,9591	0,9637	1,0088
ACA	1,0429	1,0349	1,0297	1,0613	1,0041	0,9651	0,9664	0,9848	0,9839	0,9646
ACC	0,9276	0,9399	0,9124	0,9175	0,9834	1,0029	1,0163	1,0041	1,0132	0,9456
ACG	1,1191	1,1121	1,0773	1,1282	1,1774	1,0198	1,0697	1,0162	1,0277	1,0211
ACT	0,9965	0,9953	1,0003	1,0004	0,9571	0,9615	1,0263	0,9854	0,982	0,9793
AGA	1,0086	1,0412	1,038	1,0414	0,8947	1,023	1,0294	1,0292	1,02	1,0189
AGC	0,9366	0,9066	0,8867	0,9186	1,0476	0,978	0,9703	0,9685	0,9808	0,943
AGG	1,0396	1,0721	1,0243	0,9871	1,0508	1,1085	1,1166	1,066	1,0588	1,0258
AGT	0,9593	0,9379	0,9264	0,9611	1,0857	0,9595	0,9284	0,9817	0,9847	1,0333
ATA	1,0682	1,0969	1,1213	1,1097	1,0754	0,9572	0,9828	1,0429	0,9917	0,9424
ATC	0,8528	0,8755	0,8678	0,9385	1,0167	0,9035	0,9425	0,9467	0,9338	0,9362
ATG	0,9965	0,9993	1,0662	1,0373	0,9403	0,9647	0,965	0,9906	0,9798	1,0196
ATT	0,8895	0,8796	0,8578	0,9	0,9193	0,913	0,8864	0,91	0,9128	0,9868

CAA	1,0138	1,0906	1,1313	1,1033	0,9821	0,9573	0,996	1,027	1,0434	0,9807
CAC	1,0176	1,01	1,0177	1,0565	1,2056	0,9901	1,0051	0,9887	0,982	1,0694
CAG	0,9931	0,9918	1	0,988	1	1,016	1,0203	1,0189	1,0486	1,0197
CAT	1,0896	1,0656	1,1305	1,121	1,205	0,9795	0,9742	1,0287	1	1,1234
CCA	1,1057	1,0946	1,0679	1,0641	1,0299	1,0666	1,1117	1,0482	1,0441	1,0577
CCC	1,0361	1,0503	0,9875	1,0018	0,9904	1,063	1,0731	1,0063	0,9865	1,0192
CCG	1,1966	1,1859	1,2002	1,1524	1,1503	1,2024	1,247	1,1542	1,1646	1,0734
CCT	1,1223	1,1067	1,1051	1,0962	1,0008	1,0694	1,0601	1,0893	1,074	1,0336
CGA	1,1414	1,1022	1,1312	1,081	1,0075	1,0827	1,0609	1,1061	1,0337	1,016
CGC	1,0374	1,008	1,0458	1,0191	1,0342	1,0544	1,0683	1,0016	1,0132	1,0393
CGG	1,0913	1,0861	1,08	1,0721	0,998	1,1685	1,1739	1,1295	1,0784	1,029
CGT	0,9727	0,9439	0,9883	0,9785	1,0121	0,953	0,984	0,9276	0,9425	1,0285
CTA	1,0979	1,1036	1,0941	1,0704	0,8651	1,0189	1,0643	0,99	1,0022	1,0479
CTC	0,9936	0,997	0,9601	0,9876	0,8906	1,0216	1,0195	0,9909	0,9486	0,97
CTG	1,0141	1,0224	0,9615	0,9677	1,0163	1,0714	1,1021	1,043	1,0508	1,0407
CTT	0,988	0,9695	0,969	0,9821	0,8802	0,9431	0,9838	0,9731	0,9601	1,0223
GAA	1,0724	1,0762	1,0822	1,0587	1,2228	1,0037	0,9956	0,9972	1,0103	0,9896
GAC	0,9942	1	0,993	0,9857	1,1833	0,9671	0,9806	1,0007	0,9822	1,0171
GAG	0,9842	0,9738	0,9761	0,9888	1,1272	1,0062	0,9983	0,99	0,9798	0,9512
GAT	0,9647	0,9517	1,0012	0,997	1,1023	0,9376	0,9367	0,9575	0,9799	1,0031
GCA	1,0071	0,9803	0,9787	1,0038	0,9357	0,9932	1,0033	1,0146	1,0186	0,9732
GCC	0,9927	0,9433	0,8939	0,9142	0,9502	1,0415	1,0611	0,9982	0,9873	0,9061
GCG	1,0431	1,0051	1,0104	1,0187	0,9271	1,0961	1,0968	1,101	1,023	0,9452
GCT	1	0,9816	0,9764	0,9962	0,9675	1,0321	1,0294	1,0423	1,0093	0,9432
GGA	0,9997	0,9854	0,9633	0,9867	0,9372	1	1	1,0011	0,9931	0,961
GGC	1,0079	1,005	0,9988	1,013	0,9838	1,0729	1,0547	1,0645	1,0179	0,9127
GGG	1,0618	1,0623	1,0346	0,9901	0,9599	1,1564	1,173	1,0643	1,0796	0,965
GGT	0,992	0,9895	1,0096	0,9953	1,0067	1,0309	1,0235	1,0301	1,0293	0,9634
GTA	0,9336	0,9144	0,8935	0,921	0,9478	0,9415	0,9074	0,9485	0,9852	0,9838
GTC	0,897	0,8901	0,9155	0,9315	0,8385	1,0149	0,9804	0,9893	0,9606	0,9837
GTG	0,8905	0,878	0,8714	0,8917	0,7416	0,9628	0,9481	0,9413	0,9655	0,9819
GTT	0,8776	0,8578	0,8641	0,9166	0,7523	0,941	0,9244	0,9297	0,9715	0,9717
TAC	0,9868	0,9713	0,9619	0,9415	1,0461	0,9458	0,9543	0,9919	0,956	1,0344
TAT	1,0325	1,0195	1,1089	1,0953	1,0239	0,9066	0,9591	1,0284	1,0064	0,9695
TCA	0,97	0,9529	0,9712	1,015	0,9169	1,0315	0,9967	0,9947	1,0089	0,9707
TCC	1,0002	1,0023	0,971	0,972	0,9231	1,0775	1,0993	1,0547	1,0898	1,0111
TCG	1,1269	1,067	1,0815	1,0822	1,0345	1,1547	1,2029	1,2159	1,1803	1,0883
TCT	0,9998	0,9969	1,0041	0,9761	0,9281	1,0036	1,0364	1,046	1,0459	1,0021
TGC	1,0149	1,0082	0,9704	0,998	1,013	0,9676	0,9915	1	1,0035	0,9954
TGG	1,1188	1,1075	1,12	1,1041	1,0627	1,1347	1,1497	1,1061	1,0895	0,981

TGT	0,9907	1,0208	0,9635	1	0,9776	0,9817	0,9636	0,9725	0,9752	1,0051
TTA	1,089	1,0471	1,015	1,0397	0,9566	0,9492	1,0245	0,9735	0,9829	1,0018
TTC	0,9163	0,914	0,9362	0,9392	0,795	0,96	0,9443	0,9503	0,969	0,9519
TTG	1,0532	1,0394	1,0484	1,0177	0,9752	1,0179	1,0709	1,0672	1,0382	1,0356
TTT	0,9184	0,9335	0,9473	0,9408	0,8065	0,9543	0,9362	0,9344	0,9536	1,0025

Table S5. Read proportion of cytosolic tRNA-mapped reads in hiPSC and differentiated cells.

Anticodon	WT_k_hiPSC_rep1	WT_k_hiPSC_rep2	WT_k_NPC_rep1	WT_k_NPC_rep2	WT_k_neurons_rep1	WT_k_neurons_rep2	WT_k_CM_rep1	WT_k_CM_rep2
Homo_sapiens_tRNA-Ala-AGC	0,045251973	0,045482819	0,046369472	0,04583226	0,043955401	0,042537534	0,043320617	0,043567294
Homo_sapiens_tRNA-Ala-CGC	0,014538664	0,014196315	0,015393352	0,015818845	0,014156302	0,013928113	0,015970907	0,015725234
Homo_sapiens_tRNA-Ala-GGC	0	0	0	0	0	0	0	0
Homo_sapiens_tRNA-Ala-TGC	0,022805366	0,022825114	0,022397649	0,022063907	0,020232018	0,019462164	0,022358191	0,021758949
Homo_sapiens_tRNA-Arg-ACG	0,027283009	0,027771773	0,030500215	0,028999203	0,034761609	0,033803404	0,030994009	0,029945844
Homo_sapiens_tRNA-Arg-CCG	0,014079958	0,01360028	0,015786389	0,01579743	0,016376632	0,016123933	0,015509847	0,015561607
Homo_sapiens_tRNA-Arg-CCT	0,012058916	0,011464945	0,014165875	0,015831475	0,014439237	0,015022702	0,01580061	0,015198847
Homo_sapiens_tRNA-Arg-TCG	0,015964229	0,016658965	0,017223913	0,017601266	0,016204612	0,016412192	0,018724167	0,018004995
Homo_sapiens_tRNA-Arg-TCT	0,012633877	0,012858772	0,011972382	0,014298352	0,00812113	0,009269468	0,013142902	0,011974589
Homo_sapiens_tRNA-Asn-ATT	0	0	0	0	0	0	0	0
Homo_sapiens_tRNA-Asn-GTT	0,027530773	0,028740726	0,023787482	0,025360232	0,027893849	0,028808678	0,03473463	0,034448251
Homo_sapiens_tRNA-Asp-ATC	5,26039E-07	2,88637E-07	0	0	0	0	0	0
Homo_sapiens_tRNA-Asp-GTC	0,048328774	0,047313354	0,039769035	0,038753096	0,036967749	0,042311708	0,037796632	0,035591659
Homo_sapiens_tRNA-Cys-ACA	0	0	0	0	0	0	0	0
Homo_sapiens_tRNA-Cys-GCA	0,02094424	0,020588756	0,021415735	0,019727431	0,02262292	0,02028709	0,025927231	0,025017168
Homo_sapiens_tRNA-Gln-CTG	0,028280905	0,030630143	0,033822419	0,031567954	0,030353964	0,029726592	0,033789907	0,035504774
Homo_sapiens_tRNA-Gln-TTG	0,011657023	0,012650088	0,011499183	0,01139025	0,010978859	0,010358744	0,012101344	0,012385422
Homo_sapiens_tRNA-Glu-CTC	0,054135718	0,051138369	0,041526198	0,045291933	0,041058576	0,044716084	0,041619704	0,041042533
Homo_sapiens_tRNA-Glu-TTC	0,027032614	0,026775975	0,029222002	0,028607686	0,033270192	0,034164725	0,025566089	0,024560025
Homo_sapiens_tRNA-Gly-CCC	0,01245555	0,012906108	0,020870829	0,023005086	0,031583297	0,032678263	0,020433042	0,022884054
Homo_sapiens_tRNA-Gly-GCC	0,059349816	0,05902999	0,039040464	0,03744456	0,04383435	0,04313265	0,037996725	0,040766439
Homo_sapiens_tRNA-Gly-TCC	0,023133088	0,022975205	0,028954115	0,025494764	0,027322767	0,025761364	0,027521034	0,028309568
Homo_sapiens_tRNA-His-GTG	0,021421883	0,022880821	0,02422246	0,022233583	0,025345408	0,022888068	0,027536189	0,02827693
Homo_sapiens_tRNA-Ile-AAT	0,029588638	0,028247446	0,027256144	0,028079439	0,025101568	0,024479472	0,026622545	0,025287528
Homo_sapiens_tRNA-Ile-GAT	1,84114E-05	1,64523E-05	3,38241E-07	0	1,44798E-06	0	0	6,61567E-07
Homo_sapiens_tRNA-Ile-TAT	0,008146765	0,008405394	0,008461439	0,008426138	0,011742233	0,011760189	0,008738561	0,008721662
Homo_sapiens_tRNA-Leu-AAG	0,024285113	0,023693622	0,01846289	0,019673069	0,019748683	0,020632471	0,021201047	0,021676914
Homo_sapiens_tRNA-Leu-CAA	0,008842714	0,008675558	0,008173258	0,007999477	0,007196741	0,008581365	0,007037391	0,006933225
Homo_sapiens_tRNA-Leu-CAG	0,02075434	0,020628588	0,026344246	0,026188294	0,021236046	0,024167302	0,023890348	0,023809146
Homo_sapiens_tRNA-Leu-TAA	0,00529353	0,005296198	0,007626322	0,008242734	0,008801969	0,008715532	0,005696336	0,005961383
Homo_sapiens_tRNA-Leu-TAG	0,011289847	0,011006878	0,010210484	0,010909227	0,009626448	0,009673297	0,009647324	0,009557663
Homo_sapiens_tRNA-Lys-CTT	0,031738559	0,031259949	0,030339888	0,030680038	0,025023378	0,025063962	0,029842515	0,029114695

Homo_sapiens_tRNA-Lys-TTT	0,046146239	0,044422656	0,055147843	0,052002093	0,047638189	0,041211806	0,037057909	0,037438976
Homo_sapiens_tRNA-Met-CAT	0,022433456	0,022848205	0,022986527	0,020993137	0,022431786	0,020449153	0,024348326	0,024374786
Homo_sapiens_tRNA-Phe-GAA	0,026226723	0,025834731	0,024461596	0,024539857	0,023122472	0,022420476	0,02792764	0,027474008
Homo_sapiens_tRNA-Pro-AGG	0,021108364	0,021496807	0,019120769	0,01831072	0,01861926	0,018325066	0,024061673	0,02381113
Homo_sapiens_tRNA-Pro-CGG	0,007621778	0,007755961	0,006759072	0,006992953	0,005883714	0,006022896	0,0078411	0,007450571
Homo_sapiens_tRNA-Pro-GGG	0	0	0	0	0	0	0	0
Homo_sapiens_tRNA-Pro-TGG	0,010819043	0,01133044	0,013155888	0,013543871	0,014445608	0,014334599	0,013645316	0,013505897
Homo_sapiens_tRNA-SeC-TCA	0,001394003	0,001157722	0,002057182	0,00217284	0,003915333	0,003423247	0,00201017	0,00191634
Homo_sapiens_tRNA-Ser-ACT	5,26039E-07	0	3,38241E-07	0	0	0	0	0
Homo_sapiens_tRNA-Ser-AGA	0,018464492	0,01880065	0,019868959	0,020634566	0,02214248	0,022004692	0,019276925	0,018755433
Homo_sapiens_tRNA-Ser-CGA	0,005789584	0,005874626	0,0069999	0,007318577	0,008001237	0,007840126	0,006537546	0,006250267
Homo_sapiens_tRNA-Ser-GCT	0,021539716	0,021862799	0,022632727	0,022362624	0,026219118	0,026995433	0,021188461	0,020567466
Homo_sapiens_tRNA-Ser-GGA	0	0	0	0	0	0	0	0
Homo_sapiens_tRNA-Ser-TGA	0,011166754	0,011864707	0,009375029	0,009862617	0,011423968	0,011847863	0,008830773	0,008719898
Homo_sapiens_tRNA-Sup-TTA	0	0	0	0	0	0	0	2,20522E-07
Homo_sapiens_tRNA-Thr-AGT	0,024234613	0,024255598	0,022476459	0,020623035	0,018087273	0,0173766	0,021919221	0,021650452
Homo_sapiens_tRNA-Thr-CGT	0,009257233	0,009621132	0,011425108	0,012502752	0,011885293	0,011947492	0,011817002	0,012309562
Homo_sapiens_tRNA-Thr-TGT	0,010747501	0,010879012	0,008394806	0,008591421	0,007895824	0,008019458	0,010961922	0,011027445
Homo_sapiens_tRNA-Trp-CCA	0,014854813	0,015024703	0,014225406	0,013798659	0,012952164	0,013087246	0,017071543	0,017110336
Homo_sapiens_tRNA-Tyr-ATA	0	5,77274E-07	0	0	0	0	0	0
Homo_sapiens_tRNA-Tyr-GTA	0,033855865	0,03380486	0,033163863	0,035637979	0,034672703	0,032759294	0,029707922	0,030744356
Homo_sapiens_tRNA-Val-AAC	0,020820621	0,021566369	0,022056702	0,023909475	0,020857255	0,023589455	0,021840109	0,022544229
Homo_sapiens_tRNA-Val-CAC	0,023634403	0,023710075	0,021478648	0,022152863	0,022048072	0,024019851	0,024262792	0,025053554
Homo_sapiens_tRNA-Val-TAC	0,011619674	0,011840461	0,011842159	0,011507211	0,010826242	0,010062514	0,010283561	0,010220774
Homo_sapiens_tRNA-iMet-CAT	0,019419779	0,018329018	0,027556841	0,027225019	0,02897462	0,029795668	0,025890244	0,027487239

Table S6. RPC1 ChIP-Seq peaks at annotated hg38 tRNA genes in human cell lines, and differential RPC1 occupancy in NPC relative to hiPSC.

Gene	chr	start	end	length	hiPSC log2 read counts	NPC log2 read counts	log2 FoldChange	FDR
Homo_sapiens_tRNA-Ile-AAT-5-3	chr6	27237445	27237769	325	11,46631593	6,044916264	5,399056209	3,20E-136
Homo_sapiens_tRNA-Tyr-GTA-5-3	chr14	20652973	20653317	345	11,34405971	4,765459374	6,528091082	9,82E-131
Homo_sapiens_tRNA-Lys-CTT-2-5	chr16	3175565	3175888	324	11,31009693	6,397251597	4,89283255	2,55E-128
Homo_sapiens_tRNA-Ser-AGA-4-1	chr6	27553287	27553619	333	11,25105268	5,663460431	5,561051894	2,76E-127
Homo_sapiens_tRNA-Ile-AAT-8-1	chr6	27668457	27668781	325	11,47107249	6,805221696	4,652338589	3,55E-127
Homo_sapiens_tRNA-Ser-TGA-2-1	chr6	27545563	27545895	333	11,42773114	4,993818319	6,384411867	3,55E-127
Homo_sapiens_tRNA-Val-TAC-4-1	chr6	27290500	27290823	324	11,27988443	4,602747273	6,610614325	8,89E-127
Homo_sapiens_tRNA-Ser-GCT-2-1	chr6	27297870	27298202	333	11,53640612	6,820705217	4,696846796	5,99E-126
Homo_sapiens_tRNA-Thr-AGT-3-1	chr6	28725892	28726216	325	11,24002219	4,608248819	6,56917861	1,21E-122
Homo_sapiens_tRNA-Gln-CTG-5-1	chr6	27295307	27295629	323	11,0845295	5,815067616	5,249699347	1,08E-116
Homo_sapiens_tRNA-Ser-GCT-4-1	chr6	28597214	28597546	333	10,99375456	5,80312403	5,165133804	1,28E-115

Homo_sapiens_tRNA-Leu-AAG-1-3	chr5	181173918	181174250	333	11,22695381	4,642164432	6,523737804	5,84E-115
Homo_sapiens_tRNA-Glu-TTC-6-1	chr1	148308796	148309118	323	10,95827429	4,77159989	6,123025863	1,92E-114
Homo_sapiens_tRX-Ala-AGC-5-1	chr6	57813364	57813687	324	11,29707539	4,18540947	7,006029489	7,62E-114
Homo_sapiens_tRNA-Asn-GTT-1-1	chr1	161540115	161540439	325	11,30501984	6,967308422	4,325547076	9,05E-113
Homo_sapiens_tRNA-Ser-TGA-4-1	chr6	27505702	27506034	333	11,62494725	6,15096222	5,449245265	1,28E-112
Homo_sapiens_tRNA-Lys-TTT-7-1	chr6	28747618	28747941	324	11,33599014	4,826910083	6,442548525	1,45E-112
Homo_sapiens_tRNA-Ile-AAT-1-1	chr6	57822847	57823171	325	11,15085368	4,647517975	6,446216224	1,21E-111
Homo_sapiens_tRNA-Asn-GTT-4-1	chr1	168895551	168898875	325	10,86473047	4,411479804	6,3889789	2,72E-111
Homo_sapiens_tRNA-Thr-CGT-1-1	chr6	28488867	28489191	325	10,85341767	5,489567588	5,348410585	3,35E-111
Homo_sapiens_tRNA-Phe-GAA-3-1	chr6	28807707	28808030	324	11,26108215	7,012092154	4,240635366	4,66E-111
Homo_sapiens_tRNA-Gly-CCC-1-2	chr1	168617955	168621166	322	11,07198632	5,323082664	5,702697769	3,12E-108
Homo_sapiens_tRNA-iMet-CAT-1-5	chr6	27332859	27333181	323	11,38205713	6,870483555	4,49393238	2,22E-107
Homo_sapiens_tRNA-Ala-TGC-6-1	chr6	28758238	28758560	323	10,67157485	5,523445594	5,134611574	3,73E-107
Homo_sapiens_tRNA-Ala-AGC-5-1	chr6	28710463	28710785	323	10,7854138	4,330589556	6,381993672	5,24E-107
Homo_sapiens_tRNA-Ala-TGC-7-1	chr6	28802674	28802995	322	10,75663401	4,205514212	6,499631299	6,58E-107
Homo_sapiens_tRNA-Asn-GTT-2-2	chr1	161427951	161428275	325	11,4654014	6,56328769	4,881259965	1,59E-106
Homo_sapiens_tRNA-Arg-ACG-2-4	chr6	27670439	27670762	324	11,30021925	6,013645695	5,251130004	1,89E-104
Homo_sapiens_tRNA-Pro-CGG-1-2	chr16	3171922	3172244	323	10,82882506	5,567175684	5,223449025	3,13E-104
Homo_sapiens_tRNA-Ser-ACT-1-1	chr6	27293766	27294090	325	11,35807014	6,578782633	4,765424956	3,60E-104
Homo_sapiens_tRNA-Ala-AGC-6-1	chr6	28811946	28812268	323	10,61066504	5,45944589	5,118316093	5,05E-104
Homo_sapiens_tRNA-Tyr-GTA-5-4	chr14	20663066	20663410	345	10,95509218	3,923846539	6,91996615	3,50E-103
Homo_sapiens_tRNA-Leu-TAA-2-1	chr6	27720993	27721326	334	10,68033116	4,547983784	6,097040171	2,33E-102
Homo_sapiens_tRNA-Arg-CCG-1-1	chr6	28742826	28743149	324	10,76551409	4,724253791	5,982228207	3,21E-102
Homo_sapiens_tRNA-Thr-CGT-6-1	chr6	27303663	27303985	323	11,08941946	5,035250508	6,028434472	2,21E-101
Homo_sapiens_tRNA-Trp-CCA-3-1	chr6	26318976	26319298	323	10,67464343	4,13675565	6,462722366	4,23E-101
Homo_sapiens_tRNA-Thr-CGT-5-1	chr6	27618230	27618554	325	11,19228625	6,854081874	4,327264114	4,33E-100
Homo_sapiens_tRNA-Lys-TTT-9-1	chr6	27575941	27576264	324	10,70530601	4,308794541	6,333740625	2,05E-99
Homo_sapiens_tRNA-Lys-CTT-4-1	chr16	3191375	3191698	324	10,41658736	5,380471316	5,009092828	4,12E-99
Homo_sapiens_tRNA-Leu-TAA-4-1	chr6	27230429	27230762	334	11,74568185	7,135567074	4,590169668	5,23E-98
Homo_sapiens_tRNA-Ser-GCT-1-1	chr6	27097180	27097512	333	10,49500167	4,505868403	5,948114908	6,14E-98
Homo_sapiens_tRNA-Val-AAC-6-1	chr6	28735303	28735625	323	10,64106583	4,258951933	6,310176309	7,44E-98
Homo_sapiens_tRNA-Ser-GCT-5-1	chr6	28212911	28213243	333	11,10473372	6,363493562	4,719921105	1,63E-97
Homo_sapiens_tRNA-Asn-GTT-14-1	chr1	148048390	148048714	325	10,36115535	4,805520671	5,520861763	2,67E-97
Homo_sapiens_tRNA-Tyr-GTA-6-1	chr6	26594748	26595087	340	10,65855322	4,652851726	5,956146777	3,95E-97
Homo_sapiens_tRNA-Lys-TTT-6-1	chr6	27334864	27335187	324	11,17153125	5,935384376	5,202054775	7,98E-97
Homo_sapiens_tRNA-Thr-AGT-4-1	chr6	27726568	27726892	325	10,72892584	4,036269899	6,637578545	1,11E-96
Homo_sapiens_tRNA-Ala-AGC-19-1	chr6	57793419	57793742	324	10,7754319	4,151903069	6,556904674	1,69E-96
Homo_sapiens_tRNA-Phe-GAA-1-1	chr6	28790596	28790919	324	10,59970043	5,712809803	4,857679519	1,75E-96
Homo_sapiens_tRNA-Leu-CAA-2-1	chr6	27605512	27605870	359	11,27097963	6,093284389	5,147267974	2,86E-96
Homo_sapiens_tRNA-Gln-CTG-9-1	chr1	148353435	148353757	323	10,99914889	4,054517692	6,862750186	3,30E-96
Homo_sapiens_tRNA-Val-AAC-4-1	chr6	27680980	27681303	324	10,45869062	4,975844209	5,443085065	5,45E-96

Homo_sapiens_tRNA-Ser-AGA-2-3	chr6	27495688	27496020	333	11,35895271	7,450478537	3,898608752	7,17E-96
Homo_sapiens_tRNA-Ala-TGC-5-1	chr6	28817109	28817431	323	10,74044802	6,175718493	4,534369297	8,52E-96
Homo_sapiens_tRNA-Glu-TTC-3-1	chr1	16872457	16872779	323	11,46120211	5,738748675	5,68685394	1,01E-95
Homo_sapiens_tRNA-Ala-AGC-2-3	chr6	28719578	28719900	323	10,46429853	4,343841348	6,059378655	1,61E-95
Homo_sapiens_tRNA-Lys-CTT-5-1	chr16	3180428	3180751	324	10,57868976	4,524898856	6,000328857	1,50E-94
Homo_sapiens_tRNA-Trp-CCA-3-2	chr6	26331318	26331640	323	10,77517817	5,458685716	5,288993071	1,68E-94
Homo_sapiens_tRNA-Asn-GTT-9-1	chr1	145475255	145475579	325	10,32035276	5,19823663	5,087850044	1,94E-94
Homo_sapiens_tRNA-Ser-AGA-2-4	chr6	27502913	27503245	333	11,06886145	7,146242631	3,90988948	1,67E-93
Homo_sapiens_tRNA-Tyr-GTA-4-1	chr14	20657338	20657682	345	10,53292946	4,424012158	6,053812881	3,73E-92
Homo_sapiens_tRNA-Arg-TCT-3-1	chr9	128339950	128340291	342	10,39826207	4,390881708	5,955439742	1,27E-91
Homo_sapiens_tRNA-Ser-CGA-3-1	chr6	27672324	27672656	333	11,59264317	6,769762385	4,801210057	1,56E-91
Homo_sapiens_tRNA-Glu-TTC-4-2	chr1	161421967	161422289	323	11,18267114	6,889529816	4,283859912	6,02E-91
Homo_sapiens_tRNA-Glu-TTC-4-1	chr1	16535153	16535475	323	11,86403445	7,108406838	4,732451984	1,98E-90
Homo_sapiens_tRNA-Val-CAC-1-4	chr5	181173524	181173847	324	10,62205708	5,668735673	4,929888132	1,08E-89
Homo_sapiens_tRNA-His-GTG-1-5	chr6	27158001	27158323	323	10,24232297	4,791080741	5,405628249	2,17E-89
Homo_sapiens_tRNA-Leu-TAG-2-1	chr14	20625244	20625576	333	11,82810828	7,063558352	4,743497466	1,32E-87
Homo_sapiens_tRNA-Asn-GTT-26-1	KI270713.1	28630	28953	324	10,72683758	5,087387469	5,592834417	5,13E-87
Homo_sapiens_tRNA-Gly-CCC-6-1	chr1	121016719	121017040	322	10,96977989	6,442993297	4,505147962	2,38E-86
Homo_sapiens_tRNA-Asn-GTT-2-1	chr1	148529131	148529455	325	11,22067244	6,696439386	4,501962618	1,67E-85
Homo_sapiens_tRNA-Asn-GTT-2-7	chr1	145287640	145287964	325	11,38241783	6,941118876	4,424723672	5,81E-85
Homo_sapiens_tRNA-Arg-ACG-2-3	chr6	27215047	27215370	324	10,55173649	6,879895426	3,65923264	3,52E-84
Homo_sapiens_tRNA-Ala-AGC-24-1	chr6	57815848	57816171	324	10,35966868	4,086403577	6,223926383	1,19E-83
Homo_sapiens_tRNA-Val-CAC-1-8	chr1	121020603	121020926	324	10,0697121	5,048462449	5,002068876	2,64E-83
Homo_sapiens_tRNA-Lys-TTT-13-1	chr6	28693084	28693408	325	10,4988134	3,806715951	6,603784654	6,04E-82
Homo_sapiens_tRNA-Arg-TCG-4-1	chr6	26299551	26299874	324	10,13591864	4,302020921	5,769688625	1,42E-81
Homo_sapiens_tRNA-Gln-TTG-2-1	chr6	28589253	28589575	323	11,39185801	7,758210232	3,621804593	2,79E-80
Homo_sapiens_tRNA-Tyr-GTA-8-1	chr6	26575444	26575784	341	10,52425615	5,204607694	5,293537315	4,00E-80
Homo_sapiens_tRNA-Val-AAC-1-3	chr5	181169484	181169807	324	10,59823787	6,917770593	3,664601488	2,46E-78
Homo_sapiens_tRNA-Thr-TGT-4-1	chr14	20631034	20631357	324	11,37118824	7,287951851	4,068546464	2,22E-77
Homo_sapiens_tRNA-Asn-GTT-24-1	chr1	146369975	146370299	325	10,71305381	6,021913787	4,660535504	3,65E-76
Homo_sapiens_tRX-Ala-AGC-6-1	chr6	57792707	57793030	324	9,993800593	4,102086082	5,857985825	1,42E-74
Homo_sapiens_tRX-Met-CAT-2-1	chr6	57808519	57808843	325	9,958108113	4,019851202	5,875293801	1,48E-74
Homo_sapiens_tRNA-Gly-CCC-1-1	chr1	16545813	16546134	322	11,33589704	7,174793053	4,141386583	3,85E-72
Homo_sapiens_tRNA-Val-TAC-3-1	chr10	5853585	5853908	324	10,07312871	5,103059341	4,937727601	3,75E-70
Homo_sapiens_tRNA-Cys-GCA-17-1	chr7	149691055	149691377	323	10,74447054	6,426739663	4,295079545	8,33E-70
Homo_sapiens_tRNA-Gln-CTG-4-1	chr1	148264982	148265304	323	10,06074333	3,865322863	6,115983409	2,24E-69
Homo_sapiens_tRNA-Gln-TTG-3-1	chr6	26311070	26311392	323	9,70481235	4,436436583	5,228556941	2,45E-69
Homo_sapiens_tRNA-Met-CAT-2-1	chr16	71426367	71426690	324	11,34274382	7,2170378	4,109572678	3,17E-69
Homo_sapiens_tRNA-Ile-TAT-3-1	chr6	28537464	28537808	345	11,35411352	4,39883763	6,849043254	5,57E-69
Homo_sapiens_tRNA-Ala-TGC-1-1	chr6	28789644	28789966	323	11,11248879	7,511200553	3,587638099	5,91E-69
Homo_sapiens_tRNA-Ser-GCT-6-1	chr6	26305364	26305698	335	10,1134541	6,240474872	3,860881236	2,53E-68

Homo_sapiens_tRNA-Pro-AGG-1-1	chr16	3191863	3192185	323	9,86734284	5,764844521	4,081508451	1,07E-67
Homo_sapiens_tRNA-Pro-TGG-3-4	chr16	3184007	3184329	323	10,39043164	7,044916264	3,332995112	1,24E-67
Homo_sapiens_tRNA-Ala-CGC-4-1	chr6	28729189	28729511	323	11,3078745	7,678901464	3,616085324	1,30E-67
Homo_sapiens_tRNA-Ser-TGA-3-1	chr6	26312470	26312802	333	11,58425353	8,272226859	3,301658261	1,54E-67
Homo_sapiens_tRNA-Gln-CTG-6-1	chr6	27791230	27791552	323	11,4228457	8,238701845	3,173193159	2,06E-67
Homo_sapiens_tRNA-Ala-AGC-15-1	chr14	88978972	88979295	324	10,63791206	6,773745446	3,847190886	5,66E-67
Homo_sapiens_tRNA-Ser-AGA-1-1	chr6	27541649	27541981	333	9,877519804	4,1668931	5,658933746	6,84E-67
Homo_sapiens_tRNA-Gln-TTG-3-2	chr6	26311621	26311943	323	10,92879976	7,644510352	3,272831194	4,36E-66
Homo_sapiens_tRNA-Val-AAC-5-1	chr6	27235383	27235706	324	10,54455343	6,60722021	3,917651531	1,18E-65
Homo_sapiens_tRNA-Pro-CGG-2-1	chr6	27091616	27091938	323	11,45473207	7,552983824	3,883717751	1,23E-65
Homo_sapiens_tRNA-Val-CAC-11-2	chr1	16860072	16860395	324	9,608102898	4,12720959	5,434991716	8,01E-64
Homo_sapiens_tRNA-Asn-GTT-25-1	chr1	149558293	149558618	326	9,91469095	4,56647022	5,300099405	2,97E-63
Homo_sapiens_tRNA-Pro-AGG-2-3	chr7	128783324	128783646	323	11,0358941	6,93975619	4,079143076	3,28E-63
Homo_sapiens_tRNA-Gly-CCC-5-1	chr1	167271579	167274820	322	10,19707335	5,889247756	4,295209121	1,80E-61
Homo_sapiens_tRNA-Pro-AGG-2-8	chr16	3189508	3189830	323	11,21614669	8,094756129	3,113005304	1,83E-61
Homo_sapiens_tRNA-Leu-AAG-3-1	chr6	28988876	28989208	333	9,84012252	5,420889261	4,383510948	5,53E-61
Homo_sapiens_tRNA-Phe-GAA-1-3	chr11	59557371	59557694	324	10,90634776	7,618679042	3,273657669	2,55E-60
Homo_sapiens_tRNA-Arg-TCG-5-1	chr6	28542988	28543311	324	11,38521814	8,089110214	3,281783449	4,20E-60
Homo_sapiens_tRNA-Glu-TTC-14-1	KI270713.1	31510	31831	322	9,821791222	3,403593485	6,338903224	1,40E-59
Homo_sapiens_tRNA-Asn-GTT-3-1	chr1	144419141	144419465	325	10,90296156	7,12768914	3,761126962	1,44E-59
Homo_sapiens_tRNA-Arg-ACG-2-2	chr6	27213718	27214041	324	10,08398454	6,239145163	3,825222315	2,20E-59
Homo_sapiens_tRNA-Leu-AAG-2-1	chr5	181187575	181187907	333	11,20869103	7,980757328	3,215774631	1,58E-58
Homo_sapiens_tRNA-Thr-TGT-1-1	chr6	28474426	28474750	325	11,32225339	7,676284774	3,630055005	1,86E-58
Homo_sapiens_tRNA-Pro-AGG-2-5	chr14	20609210	20609532	323	11,42060441	7,933879519	3,470549631	2,39E-58
Homo_sapiens_tRNA-Gly-CCC-4-1	chr1	166781455	166784666	322	11,23831067	7,567882631	3,652406334	2,88E-57
Homo_sapiens_tRNA-Asn-GTT-5-1	chr1	165204559	165207883	325	9,473140649	4,212755266	5,215060657	1,55E-56
Homo_sapiens_tRNA-Lys-TTT-2-1	chr11	122559821	122560144	324	10,99232721	5,349602012	5,586168312	1,91E-56
Homo_sapiens_tRNA-Leu-AAG-2-2	chr6	28943496	28943828	333	10,54679443	7,625308043	2,911727459	3,52E-55
Homo_sapiens_tRNA-Val-CAC-14-1	chr1	145157031	145157354	324	9,014819471	4,81030204	4,18013047	3,86E-55
Homo_sapiens_tRNA-Pro-AGG-2-7	chr16	3182509	3182831	323	11,23556866	8,262338139	2,962483995	1,53E-54
Homo_sapiens_tRNA-Lys-CTT-2-4	chr6	26556420	26556743	324	11,64969125	8,225674893	3,408257675	5,28E-54
Homo_sapiens_tRNA-Gln-CTG-2-1	chr6	27547626	27547948	323	10,61226895	7,475338169	3,124197592	7,13E-53
Homo_sapiens_tRNA-Ala-AGC-1-1	chr6	28795838	28796160	323	11,54296807	8,237926142	3,291058854	1,19E-52
Homo_sapiens_tRNA-Tyr-GTA-3-1	chr6	26576978	26577317	340	9,644187278	5,454112287	4,180269093	3,38E-52
Homo_sapiens_tRNA-Ala-AGC-3-1	chr6	28607030	28607352	323	10,91361688	8,053007568	2,850658464	9,35E-52
Homo_sapiens_tRNA-Asp-GTC-3-1	chr6	27583331	27583653	323	11,23128633	7,918877867	3,295985561	2,05E-51
Homo_sapiens_tRNA-Lys-TTT-4-1	chr6	27591688	27592011	324	11,40297223	8,360134964	3,029403175	2,72E-51
Homo_sapiens_tRNA-Ile-AAT-12-1	chr6	57800085	57800409	325	11,31151842	7,783351712	3,510313672	1,41E-50
Homo_sapiens_tRNA-Val-CAC-2-1	chr6	27280144	27280467	324	11,56186555	8,545745718	3,004211717	4,82E-50
Homo_sapiens_tRNA-Lys-CTT-3-1	chr16	3157279	3157602	324	11,27144681	8,048082824	3,209837186	2,09E-48
Homo_sapiens_tRNA-Ala-AGC-11-1	chr6	26571738	26572061	324	11,35971841	8,430723367	2,916262187	2,65E-48

Homo_sapiens_tRNA-Thr-AGT-2-2	chr6	27684569	27684893	325	11,63981075	8,392775835	3,230364726	1,86E-47
Homo_sapiens_tRNA-iMet-CAT-1-4	chr6	26330175	26330497	323	11,40269651	8,188630533	3,200075693	2,57E-47
Homo_sapiens_tRNA-Asn-GTT-8-1	chr1	149740122	149740446	325	9,063857344	3,322247112	5,663696338	2,60E-47
Homo_sapiens_tRNA-Und-TTA-3-1	chr1	161420745	161421068	324	9,338109806	3,53070481	5,722989544	6,19E-46
Homo_sapiens_tRNA-His-GTG-1-9	chr15	45201025	45201347	323	10,87443043	8,181843541	2,68123227	2,78E-45
Homo_sapiens_tRNA-Val-CAC-11-1	chr1	165475391	165478622	324	9,240786165	3,278064092	5,898678223	3,54E-45
Homo_sapiens_tRNA-Asp-GTC-2-7	chr6	27503618	27503940	323	9,978780476	7,227575556	2,74100131	7,30E-45
Homo_sapiens_tRNA-Arg-ACG-1-2	chr6	26537372	26537695	324	11,94519832	9,058669229	2,873572387	1,32E-44
Homo_sapiens_tRNA-Pro-AGG-2-2	chr6	26555144	26555466	323	10,90605226	7,903998551	2,987490312	6,26E-44
Homo_sapiens_tRNA-Cys-GCA-11-1	chr7	149415012	149415334	323	9,295579556	4,988555985	4,273043582	6,26E-44
Homo_sapiens_tRNA-Trp-CCA-1-1	chr17	8220743	8221065	323	11,26021573	8,553697296	2,695093692	6,26E-44
Homo_sapiens_tRNA-Met-CAT-4-2	chr6	26743137	26743460	324	8,802657643	5,227129247	3,564172317	8,75E-43
Homo_sapiens_tRNA-Ala-TGC-2-1	chr6	28643319	28643641	323	10,56491647	7,795910907	2,755911052	1,83E-42
Homo_sapiens_tRNA-Arg-ACG-1-1	chr6	26328014	26328337	324	11,48520609	8,517518574	2,953365473	5,04E-42
Homo_sapiens_tRNA-Cys-GCA-5-1	chr15	79744529	79744852	324	9,369784295	5,888116033	3,459854612	3,59E-41
Homo_sapiens_tRNA-Cys-GCA-13-1	chr7	149355549	149355871	323	10,69087464	4,219960158	6,356482955	5,37E-41
Homo_sapiens_tRNA-Trp-CCA-5-1	chr7	99469558	99469880	323	8,76745567	4,444145872	4,265686895	9,10E-41
Homo_sapiens_tRNA-Ala-AGC-21-1	chr6	26749786	26750109	324	9,07796108	3,189090098	5,813032746	1,35E-40
Homo_sapiens_tRNA-Phe-GAA-5-1	chr6	28764261	28764588	328	8,765488316	3,956566826	4,771067188	1,63E-40
Homo_sapiens_tRNA-Asn-GTT-7-1	chr1	120844136	120844460	325	9,345366437	5,684443271	3,617730507	2,55E-40
Homo_sapiens_tRNA-Arg-TCT-3-2	chr11	59551184	59551504	321	9,26264572	5,94411198	3,295847076	3,14E-40
Homo_sapiens_tRNA-Arg-TCG-2-1	chr6	26322692	26323015	324	10,80317611	8,067557089	2,721785249	4,17E-40
Homo_sapiens_tRNA-iMet-CAT-2-1	chr6	27777759	27778081	323	10,32036877	4,499961426	5,728781758	5,63E-40
Homo_sapiens_tRNA-Phe-GAA-2-1	chr11	59566254	59566577	324	11,71416544	8,800949505	2,898789507	8,11E-40
Homo_sapiens_tRNA-Val-CAC-4-1	chr1	143803868	143804191	324	8,44390711	3,348781682	5,051161036	3,10E-39
Homo_sapiens_tRNA-Trp-CCA-3-3	chr17	8186232	8186554	323	10,39983332	7,905256659	2,484906402	4,83E-39
Homo_sapiens_tRNA-Lys-CTT-14-1	chr16	3196027	3196350	324	8,730441903	4,300324735	4,393892426	4,98E-39
Homo_sapiens_tRNA-Thr-TGT-3-1	chr14	20613664	20613987	324	11,28255179	8,520803571	2,747455719	5,90E-39
Homo_sapiens_tRNA-Thr-TGT-2-1	chr1	222464879	222465202	324	10,7029728	8,269625308	2,422420023	7,28E-39
Homo_sapiens_tRNA-Pro-TGG-1-1	chr14	20632880	20633202	323	10,87769332	6,437208568	4,394864063	1,43E-38
Homo_sapiens_tRNA-Val-CAC-1-7	chr1	149712426	149712749	324	10,17522705	7,326426524	2,837480362	6,09E-38
Homo_sapiens_tRNA-Cys-GCA-8-1	chr14	72962845	72963167	323	9,977397001	4,992768476	4,926937328	6,09E-38
Homo_sapiens_tRNA-Arg-TCT-5-1	chr6	27562058	27562395	338	8,537897192	3,975844209	4,506899068	3,57E-37
Homo_sapiens_tRNA-Cys-GCA-9-3	chr7	149635561	149635883	323	10,18668869	4,597224667	5,488870379	1,49E-36
Homo_sapiens_tRNA-Pro-AGG-2-6	chr14	20613275	20613597	323	11,5774206	8,826396066	2,736281555	1,52E-36
Homo_sapiens_tRNA-Cys-GCA-9-2	chr7	149331003	149331325	323	8,765938122	4,422453576	4,309993482	6,13E-35
Homo_sapiens_tRNA-Ile-TAT-2-3	chr6	27631295	27631639	345	11,50343328	9,050988665	2,43884788	8,78E-34
Homo_sapiens_tRNA-Cys-GCA-12-1	chr7	149646829	149647151	323	8,38858823	3,772829937	4,594241721	1,13E-33
Homo_sapiens_tRNA-Gln-TTG-3-3	chr6	27795735	27796057	323	10,73648599	8,366844884	2,357888577	2,81E-33
Homo_sapiens_tRNA-Leu-CAG-1-6	chr1	161530216	161530549	334	10,93776355	8,64082424	2,283938601	1,39E-32
Homo_sapiens_tRNA-Gln-CTG-1-2	chr6	27519403	27519725	323	10,70233627	8,268105848	2,421357418	2,79E-32

Homo_sapiens_tRNA-Asn-GTT-17-1	chr1	161621549	161621873	325	9,535007018	3,625983566	5,770107235	2,30E-31
Homo_sapiens_tRNA-Val-AAC-1-4	chr5	181218144	181218467	324	11,79784577	9,234539896	2,548100283	4,54E-31
Homo_sapiens_tRNA-Ala-CGC-5-1	chr6	28695806	28696128	323	8,442136781	3,25018349	5,109177228	4,86E-31
Homo_sapiens_tRNA-Met-CAT-3-1	chr6	28944449	28944772	324	11,41753942	9,223716374	2,181565444	5,74E-31
Homo_sapiens_tRNA-Asn-GTT-6-1	chr1	143735794	143736118	325	7,937588783	4,17433011	3,73193143	1,02E-30
Homo_sapiens_tRNA-Val-AAC-1-2	chr5	181164028	181164351	324	8,283982677	4,22175345	4,002003844	1,27E-30
Homo_sapiens_tRNA-Thr-AGT-6-1	chr6	27162145	27162469	325	10,2390924	7,56999957	2,654102521	4,93E-30
Homo_sapiens_tRNA-Ser-AGA-2-1	chr6	26327463	26327795	333	10,92698823	8,399732601	2,511549715	1,29E-29
Homo_sapiens_tRNA-Lys-CTT-2-2	chr5	181207629	181207952	324	11,43834995	9,110347021	2,313674137	4,16E-29
Homo_sapiens_tRNA-Val-CAC-6-1	chr6	27205962	27206285	324	8,165237853	3,835145991	4,275893574	1,07E-28
Homo_sapiens_tRNA-Ser-AGA-2-2	chr6	27478686	27479018	333	11,59124344	9,337232544	2,240390941	1,19E-28
Homo_sapiens_tRNA-Asn-GTT-2-6	chr19	1383559	1383761	203	10,41102439	8,445396937	1,955642405	3,38E-28
Homo_sapiens_tRNA-Ile-AAT-3-1	chr6	27275085	27275409	325	8,117290647	3,113732085	4,881922163	5,21E-28
Homo_sapiens_tRNA-Lys-CTT-2-3	chr5	181221853	181222176	324	11,56439924	9,088741455	2,458452261	7,41E-28
Homo_sapiens_tRNA-iMet-CAT-1-6	chr6	27592695	27593017	323	11,52979622	9,211117969	2,303676089	1,51E-27
Homo_sapiens_tRNA-Tyr-GTA-5-5	chr14	20683147	20683486	340	11,65839295	9,385937126	2,258292	3,37E-27
Homo_sapiens_tRNA-Thr-AGT-5-1	chr17	8139326	8139650	325	11,02617414	8,805670522	2,206177092	3,78E-27
Homo_sapiens_tRNA-Ala-AGC-16-1	chr6	57870219	57870542	324	8,263044186	4,189090098	4,03732611	8,06E-27
Homo_sapiens_tRNA-Thr-TGT-5-1	chr14	20681564	20681887	324	11,41973635	9,427420734	1,980262473	8,06E-27
Homo_sapiens_tRNA-Asn-GTT-10-1	chr1	145129113	145129437	325	9,015205905	3,973717406	4,969443544	9,82E-27
Homo_sapiens_tRNA-Lys-TTT-5-1	chr11	59556303	59556626	324	10,25699504	7,977706032	2,265075533	3,16E-26
Homo_sapiens_tRNA-Leu-TAA-3-1	chr11	59551629	59551962	334	11,10445947	8,919086192	2,171502895	3,83E-26
Homo_sapiens_tRNA-Gly-TCC-2-6	chr1	161530987	161531309	323	11,32333018	9,290145924	2,02053903	6,98E-26
Homo_sapiens_tRNA-Glu-TTC-5-1	chr1	161612592	161612914	323	10,38398817	8,428684872	1,944698531	8,96E-26
Homo_sapiens_tRNA-Ser-CGA-2-1	chr6	27209723	27210055	333	7,853538898	3,84449952	3,965654886	1,76E-25
Homo_sapiens_tRNA-Tyr-GTA-1-1	chr6	26568732	26569073	342	11,23896076	9,222203457	2,003455343	1,96E-25
Homo_sapiens_tRNA-Ala-AGC-8-2	chr8	66114201	66114386	186	9,339609439	7,354111863	1,977511198	2,61E-25
Homo_sapiens_tRNA-Pro-CGG-1-3	chr17	8222707	8223029	323	11,22019199	9,282908249	1,925583691	2,73E-25
Homo_sapiens_tRNA-Thr-AGT-1-1	chr17	8187072	8187358	287	10,84484225	8,569911122	2,259767982	2,90E-25
Homo_sapiens_tRNA-Val-AAC-3-1	chr6	27650802	27651125	324	11,42552864	9,232759844	2,177308273	1,45E-24
Homo_sapiens_tRNA-Leu-CAA-3-1	chr6	27602443	27602800	358	11,29753246	5,975844209	5,204768331	7,86E-24
Homo_sapiens_tRNA-Ile-AAT-2-1	chr6	27688062	27688386	325	11,75854303	9,580532032	2,162042041	8,59E-24
Homo_sapiens_tRNA-Pro-TGG-3-3	chr16	3158796	3159118	323	8,193889404	5,269406895	2,885482829	1,27E-23
Homo_sapiens_tRNA-Ser-GCT-4-3	chr17	8186740	8187034	295	11,21291021	9,214108635	1,983947883	2,64E-22
Homo_sapiens_tRNA-Cys-GCA-2-1	chr4	123508724	123509046	323	7,886345464	3,692235076	4,107632343	3,39E-22
Homo_sapiens_tRNA-Thr-CGT-3-1	chr6	28648081	28648405	325	10,85607255	9,021528111	1,821911786	3,86E-22
Homo_sapiens_tRNA-Arg-TCT-2-1	chr17	8120799	8121137	339	7,902021681	4,664779343	3,186592087	7,04E-22
Homo_sapiens_tRNA-iMet-CAT-1-3	chr6	26312998	26313320	323	11,38573669	9,408479554	1,963050495	7,23E-22
Homo_sapiens_tRNA-Met-CAT-3-2	chr6	28953139	28953462	324	11,73346955	9,645722979	2,071504118	8,87E-22
Homo_sapiens_tRNA-Tyr-GTA-5-2	chr8	66113862	66114063	202	8,481149765	5,954947758	2,504957655	9,09E-22
Homo_sapiens_tRNA-Cys-GCA-9-1	chr3	132231672	132231994	323	8,977846057	4,988555985	3,930977722	1,85E-21

Homo_sapiens_tRNA-Cys-GCA-21-1	chr7	149664698	149665020	323	7,930983215	4,046434877	3,809023299	3,12E-21
Homo_sapiens_tRX-Val-CAC-4-1	chr1	149708534	149708855	322	10,49016466	8,343945867	2,128853594	4,56E-21
Homo_sapiens_tRNA-Thr-CGT-2-1	chr16	1428576	1428609	323	11,13526756	9,504947508	1,620074418	7,36E-21
Homo_sapiens_tRNA-Leu-AAG-2-3	chr14	20610006	20610338	333	11,90447689	9,823221083	2,063921525	2,39E-20
Homo_sapiens_tRNA-Val-CAC-1-6	chr6	26537928	26538251	324	10,81737979	8,936684017	1,865872229	3,18E-20
Homo_sapiens_tRNA-Val-TAC-2-1	chr11	59550861	59551168	308	10,41599627	8,458210404	1,943718216	3,59E-20
Homo_sapiens_tRNA-Ile-TAT-2-2	chr6	27020220	27020564	345	9,39736391	7,445492363	1,934857528	4,63E-20
Homo_sapiens_tRNA-Lys-TTT-3-3	chr6	28950903	28951226	324	11,49607566	9,448897975	2,029885794	4,73E-20
Homo_sapiens_tRNA-Ser-CGA-1-1	chr17	8138755	8139087	333	10,05626691	8,318162503	1,7268279	5,60E-20
Homo_sapiens_tRNA-Cys-GCA-9-4	chr7	149707543	149707865	323	7,883566767	4,759292611	3,09242905	5,68E-20
Homo_sapiens_tRNA-Val-TAC-1-1	chr11	59550503	59550826	324	11,32063037	9,450526083	1,855244503	1,28E-19
Homo_sapiens_tRNA-Gln-CTG-1-3	chr6	28941475	28941797	323	11,15871886	9,211851827	1,930142736	2,97E-19
Homo_sapiens_tRNA-Cys-GCA-6-1	chr3	132228974	132229296	323	7,531130032	3,865322863	3,598498217	3,06E-19
Homo_sapiens_tRNA-His-GTG-1-2	chr1	147073099	147073421	323	7,835789017	4,243128331	3,535507167	4,42E-19
Homo_sapiens_tRNA-Arg-CCT-1-1	chr17	75033780	75034103	324	10,8323539	9,114521242	1,70549745	8,77E-19
Homo_sapiens_tRNA-Cys-GCA-14-1	chr17	38861558	38861880	323	10,10269242	6,39566176	3,649297096	1,78E-18
Homo_sapiens_tRNA-Phe-GAA-1-2	chr6	28981546	28981869	324	10,06549944	8,144706201	1,905619009	3,52E-18
Homo_sapiens_tRNA-His-GTG-1-8	chr15	45200287	45200609	323	11,59384096	9,865755051	1,714268106	3,80E-18
Homo_sapiens_tRNA-Leu-CAA-1-2	chr6	28940927	28941282	356	11,39587927	9,561250546	1,818842039	3,89E-18
Homo_sapiens_tRNA-Gly-GCC-2-5	chr16	70789381	70789702	322	7,796889716	4,943568753	2,82065494	9,65E-18
Homo_sapiens_tRNA-His-GTG-1-1	chr1	146037918	146038240	323	10,35935821	8,799672842	1,549333364	1,74E-17
Homo_sapiens_tRNA-Gly-TCC-4-1	chr1	161440045	161440367	323	7,515494406	3,456398839	3,972427233	3,60E-17
Homo_sapiens_tRNA-Gly-CCC-3-1	chr17	19860736	19861057	322	7,370061767	3,804324399	3,521532422	5,68E-17
Homo_sapiens_tRNA-Asn-GTT-2-4	chr13	30673838	30674162	325	11,17367003	9,633298201	1,5290425	6,99E-17
Homo_sapiens_tRNA-Leu-CAA-4-1	chr1	248873729	248874085	357	11,44279206	9,80484789	1,625030289	7,06E-17
Homo_sapiens_tRNA-Lys-TTT-8-1	chr1	205474017	205474340	324	7,254705888	3,144349239	4,011559263	1,32E-16
Homo_sapiens_tRNA-Trp-CCA-4-1	chr12	98504126	98504448	323	10,6583185	9,042061918	1,604352769	1,52E-16
Homo_sapiens_tRNA-Leu-AAG-4-1	chr6	28478497	28478829	333	7,362593829	4,028083907	3,276497811	2,01E-16
Homo_sapiens_tRNA-Arg-CCT-2-1	chr17	75034305	75034628	324	11,3226007	9,694057459	1,615018444	2,72E-16
Homo_sapiens_tRNA-Phe-GAA-4-1	chr6	28823190	28823514	325	7,427670251	3,785022757	3,579310862	3,19E-16
Homo_sapiens_tRNA-Tyr-GTA-7-1	chr14	20659832	20660176	345	7,227547731	3,579130598	3,565979481	1,52E-15
Homo_sapiens_tRNA-Gln-CTG-1-5	chr17	8119626	8119948	323	11,22725853	9,685909759	1,528402521	1,60E-15
Homo_sapiens_tRNA-Ala-CGC-1-1	chr6	26553377	26553699	323	11,10201507	9,401416604	1,684119142	3,38E-15
Homo_sapiens_tRNA-Arg-CCG-2-1	chr17	68019771	68020094	324	11,30601443	9,880286687	1,414517986	4,56E-15
Homo_sapiens_tRNA-Lys-TTT-1-1	chr16	73478191	73478514	324	8,420471885	6,105006408	2,286589652	7,98E-15
Homo_sapiens_tRNA-Gly-GCC-1-5	chr21	17454663	17454984	322	11,533754	9,790174603	1,725704816	1,25E-14
Homo_sapiens_tRNA-Asp-GTC-2-6	chr6	27479548	27479870	323	11,4811426	9,882487757	1,583403595	3,32E-14
Homo_sapiens_tRX-Ile-AAT-3-1	chr6	27260805	27261130	326	6,883030837	2,992768476	3,805911113	3,72E-14
Homo_sapiens_tRNA-Val-CAC-7-1	chr6	27728422	27728745	324	7,112167985	3,835145991	3,216457115	4,46E-14
Homo_sapiens_tRNA-Leu-TAG-1-1	chr17	8120188	8120520	333	11,39118072	9,722710756	1,650863139	6,09E-14
Homo_sapiens_tRNA-Phe-GAA-1-5	chr13	94549524	94549847	324	11,1367651	9,636498633	1,486538165	9,57E-14

Homo_sapiens_tRNA-Ile-AAT-6-1	chr6	26756426	26756750	325	6,512637396	3,144349239	3,291544114	1,14E-13
Homo_sapiens_tRNA-Ala-CGC-2-1	chr6	28673710	28674032	323	11,41865171	9,925882986	1,479123781	1,26E-13
Homo_sapiens_tRNA-Cys-GCA-2-2	chr17	38867519	38867841	323	11,06596011	9,553162571	1,498645905	1,39E-13
Homo_sapiens_tRNA-Asn-GTT-11-2	chr1	149646325	149646649	325	7,122687381	3,816255016	3,228175068	4,05E-13
Homo_sapiens_tRNA-Thr-AGT-2-1	chr6	26532791	26533115	325	11,63840873	10,10083592	1,52127364	1,90E-12
Homo_sapiens_tRNA-Arg-TCG-3-1	chr17	75034987	75035310	324	11,49970136	10,12735954	1,359248923	3,87E-12
Homo_sapiens_tRNA-Gly-GCC-2-6	chr17	8125620	8125941	322	11,50659893	10,16829061	1,32543858	7,49E-12
Homo_sapiens_tRNA-Val-CAC-1-5	chr5	181222269	181222592	324	11,58441432	10,04206142	1,524783909	7,91E-12
Homo_sapiens_tRNA-Gly-TCC-3-1	chr17	8221422	8221744	323	11,22330981	9,697448486	1,5086125	9,90E-12
Homo_sapiens_tRNA-Arg-CCT-3-1	chr16	3152774	3153097	324	11,57086222	9,928943028	1,621542679	1,41E-11
Homo_sapiens_tRNA-Und-NNN-1-1	chr6	26749073	26749397	325	6,609080097	1,44107029	4,96367486	1,61E-11
Homo_sapiens_tRNA-Ile-AAT-5-4	chr14	102316966	102317290	325	11,51351531	10,12208181	1,377120172	1,95E-11
Homo_sapiens_tRNA-Cys-GCA-1-1	chr7	149310064	149310386	323	6,95089119	4,1668931	2,72696285	2,09E-11
Homo_sapiens_tRNA-Phe-GAA-11-1	chr6	28726952	28727275	324	7,051391538	4,019851202	2,955679692	2,53E-11
Homo_sapiens_tRX-Phe-GAA-2-1	chr1	121009418	121009748	331	6,650283164	3,567880804	2,996958488	4,20E-11
Homo_sapiens_tRNA-Ser-AGA-2-6	chr17	8226484	8226816	333	10,44306022	8,922263883	1,502244214	4,32E-11
Homo_sapiens_tRNA-Val-AAC-2-1	chr5	181188290	181188613	324	10,89411698	9,481908144	1,396243674	5,61E-11
Homo_sapiens_tRNA-Ile-AAT-5-2	chr6	27177089	27177413	325	10,59530278	9,143818228	1,434526671	8,31E-11
Homo_sapiens_tRNA-Met-CAT-6-1	chr16	87383896	87384219	324	11,50652176	10,28621017	1,208909384	1,01E-10
Homo_sapiens_tRNA-Asp-GTC-2-11	chr17	8222112	8222434	323	11,66296012	10,08661902	1,555743343	1,02E-10
Homo_sapiens_tRNA-Ile-AAT-5-1	chr6	26553996	26554320	325	11,73882416	10,23922845	1,480592508	1,58E-10
Homo_sapiens_tRNA-Cys-GCA-10-1	chr7	149377384	149377706	323	6,895113617	4,190922151	2,638016205	1,73E-10
Homo_sapiens_tRNA-Cys-GCA-2-3	chr17	39153608	39153930	323	11,33006399	9,995100181	1,320628801	2,51E-10
Homo_sapiens_tRNA-Ser-CGA-4-1	chr12	56190238	56190570	333	10,13137511	8,837490443	1,281176586	2,52E-10
Homo_sapiens_tRNA-Thr-AGT-1-2	chr17	8226109	8226433	325	10,90119185	9,420841487	1,46112358	3,90E-10
Homo_sapiens_tRNA-Phe-GAA-1-6	chr19	1383236	1383437	202	9,812551172	8,538290771	1,262650182	5,68E-10
Homo_sapiens_tRNA-Val-CAC-1-1	chr1	161399574	161399897	324	11,64885037	10,35108993	1,283247996	7,51E-10
Homo_sapiens_tRNA-Ala-TGC-3-2	chr12	124921629	124921951	323	11,35353828	10,01549204	1,322054158	9,35E-10
Homo_sapiens_tRNA-Ser-AGA-3-1	chr6	27532082	27532414	333	6,72036836	3,975844209	2,672089271	9,64E-10
Homo_sapiens_tRNA-Ile-AAT-9-1	chr6	27273834	27274158	325	6,633162001	3,901621061	2,674080184	1,58E-09
Homo_sapiens_tRNA-Phe-GAA-1-4	chr12	124927717	124928040	324	10,70859648	9,429072995	1,264556742	1,82E-09
Homo_sapiens_tRNA-Leu-CAG-2-1	chr16	57299825	57300158	334	11,50207082	10,13693585	1,347530271	2,07E-09
Homo_sapiens_tRNA-Arg-CCG-1-3	chr16	3150548	3150871	324	11,39581711	10,04877785	1,32957463	3,05E-09
Homo_sapiens_tRNA-Ile-AAT-5-5	chr17	8187467	8187791	325	11,41556167	10,0424106	1,35504962	3,20E-09
Homo_sapiens_tRNA-Arg-ACG-1-3	chr14	22929575	22929898	324	11,22630002	9,928461979	1,28192226	4,27E-09
Homo_sapiens_tRNA-Ala-AGC-2-1	chr6	28838318	28838640	323	11,3133971	10,06315142	1,235518943	4,48E-09
Homo_sapiens_tRNA-Pro-TGG-3-2	chr14	20683890	20684212	323	11,49535649	10,31382892	1,168325111	8,37E-09
Homo_sapiens_tRNA-Gly-GCC-3-1	chr16	70778085	70778406	322	7,065716255	5,06555943	1,959851122	8,40E-09
Homo_sapiens_tRNA-Cys-GCA-4-1	chr17	38869166	38869488	323	10,71027783	9,54045015	1,157249692	9,35E-09
Homo_sapiens_tRNA-Glu-TTC-8-1	chr1	149692679	149693002	324	6,817438699	4,094266139	2,658734635	1,09E-08
Homo_sapiens_tRNA-His-GTG-1-6	chr9	144338114	144341316	323	6,890581582	4,770375147	2,069084084	1,26E-08

Homo_sapiens_tRNA-Val-CAC-9-1	chr6	27150117	27150440	324	6,361750631	3,612363026	2,675479687	1,62E-08
Homo_sapiens_tRNA-Ile-AAT-4-1	chr17	8226865	8227189	325	10,68555561	9,376145715	1,292321926	1,66E-08
Homo_sapiens_tRNA-Gly-GCC-2-4	chr16	70778913	70779234	322	9,140263626	7,816553252	1,30588667	1,77E-08
Homo_sapiens_tRNA-Arg-CCG-1-2	chr6	28881262	28881585	324	11,51896319	10,29878364	1,204844872	2,29E-08
Homo_sapiens_tRNA-Asn-GTT-2-5	chr17	38751655	38751979	325	10,72310352	9,670133779	1,042635045	2,36E-08
Homo_sapiens_tRNA-Asp-GTC-2-10	chr12	124939521	124939840	320	11,24620992	9,983835551	1,245541306	2,42E-08
Homo_sapiens_tRNA-Leu-CAA-1-1	chr6	28896097	28896453	357	11,45995859	10,23587285	1,20812998	3,60E-08
Homo_sapiens_tRNA-Cys-GCA-7-1	chr1	93516151	93516474	324	7,002812123	4,462486518	2,468051592	3,63E-08
Homo_sapiens_tRNA-Ala-CGC-3-1	chr2	156400643	156400965	323	10,56232298	9,293297693	1,251379698	4,40E-08
Homo_sapiens_tRNA-Lys-CTT-2-1	chr1	146039275	146039598	324	10,98294741	9,787184734	1,180918355	4,86E-08
Homo_sapiens_tRNA-Pro-TGG-4-1	chr16	3170834	3171155	322	5,96229001	2,804324399	3,06521328	6,02E-08
Homo_sapiens_tRNA-Glu-CTC-3-1	chr13	41455799	41456122	324	6,621026399	4,417759589	2,138273628	1,01E-07
Homo_sapiens_tRNA-Val-CAC-3-1	chr19	4724509	4724832	324	10,27892425	9,334227484	0,936822306	1,20E-07
Homo_sapiens_tRNA-iMet-CAT-1-7	chr6	27902367	27902689	323	10,86672903	9,68964479	1,161476164	1,52E-07
Homo_sapiens_tRNA-Glu-CTC-2-1	chr1	248874122	248874444	323	10,99861657	9,919431722	1,066202956	2,08E-07
Homo_sapiens_tRNA-iMet-CAT-1-8	chr17	82494595	82494917	323	11,98070698	10,76110695	1,201561358	2,53E-07
Homo_sapiens_tRNA-Ala-AGC-2-2	chr6	28863559	28863881	323	11,30835566	10,21875258	1,076286638	2,65E-07
Homo_sapiens_tRNA-Tyr-GTA-5-1	chr8	66113241	66113584	344	11,07890264	9,885464381	1,176434314	3,44E-07
Homo_sapiens_tRNA-Pro-TGG-3-1	chr5	181188728	181189050	323	11,41399102	10,25909036	1,138473295	4,30E-07
Homo_sapiens_tRNA-Asn-GTT-11-1	chr1	120952165	120952489	325	6,516163159	3,910554687	2,530828921	4,60E-07
Homo_sapiens_tRNA-Asn-GTT-2-3	chr10	222293833	222297077	325	11,54482658	10,44133311	1,088695266	4,91E-07
Homo_sapiens_tRNA-Ala-AGC-23-1	chr6	28778641	28778963	323	6,299243202	3,842169838	2,407976753	5,24E-07
Homo_sapiens_tRNA-Arg-TCG-6-1	chr9	110198397	110198720	324	5,925304435	3,25018349	2,584747902	6,04E-07
Homo_sapiens_tRX-Glu-TTC-2-1	chr1	121000862	121001185	324	5,735035922	2,785022757	2,841089979	6,31E-07
Homo_sapiens_tRNA-Asp-GTC-2-9	chr12	124927219	124927541	323	9,984128314	8,936069009	1,035067225	6,61E-07
Homo_sapiens_tRNA-Gly-GCC-2-1	chr1	161523721	161524042	322	11,45051472	10,30631248	1,127621272	6,85E-07
Homo_sapiens_tRNA-His-GTG-1-7	chr15	45198480	45198802	323	11,58796416	10,53391578	1,039479453	1,81E-06
Homo_sapiens_tRNA-Leu-CAG-1-7	chr6	26521082	26521415	334	10,53670561	9,426058774	1,094110133	2,18E-06
Homo_sapiens_tRNA-Pro-AGG-2-1	chr1	167715362	167715684	323	11,36053174	10,28749625	1,05737226	2,62E-06
Homo_sapiens_tRNA-Ala-TGC-4-1	chr12	124939843	124940162	320	10,79409828	9,779052228	1,001239973	3,54E-06
Homo_sapiens_tRNA-iMet-CAT-1-2	chr6	26286400	26286722	323	9,356544582	8,295749709	1,044331612	5,14E-06
Homo_sapiens_tRNA-Ser-TGA-1-1	chr10	67764377	67764709	333	11,52514109	10,55456583	0,957590365	6,16E-06
Homo_sapiens_tRNA-Thr-TGT-6-1	chr5	181191561	181191883	323	11,53171582	10,5877947	0,93113616	1,06E-05
Homo_sapiens_tRNA-Arg-CCT-5-1	chr16	3193792	3194115	324	5,724888494	3,444145872	2,172054617	1,60E-05
Homo_sapiens_tRNA-Glu-CTC-1-7	chr6	125780121	125780443	323	11,47070305	10,48069042	0,974801486	1,79E-05
Homo_sapiens_tRNA-Glu-TTC-2-2	chr15	26082108	26082430	323	11,33352746	10,42284275	0,897962591	2,63E-05
Homo_sapiens_tRNA-Gly-GCC-4-1	chr1	161480440	161480761	322	5,634558926	3,144349239	2,366139629	2,75E-05
Homo_sapiens_tRNA-Ala-TGC-3-1	chr5	181206742	181207064	323	11,78889452	10,78261078	0,989532887	2,96E-05
Homo_sapiens_tRNA-Thr-CGT-4-1	chr17	31549948	31550270	323	11,08312912	10,22570354	0,846637389	3,48E-05
Homo_sapiens_tRNA-Asp-GTC-1-1	chr12	98503377	98503699	323	11,60515253	10,59035965	0,997094629	4,29E-05
Homo_sapiens_tRNA-Leu-TAA-1-1	chr6	144216421	144216754	334	11,22592527	10,34849826	0,865242306	4,47E-05

Homo_sapiens_tRNA-Val-AAC-1-5	chr6	27753274	27753597	324	11,01997068	10,04637409	0,957865385	4,53E-05
Homo_sapiens_tRNA-Arg-CCT-4-1	chr7	139340574	139340897	324	11,17085713	10,23011435	0,92618689	4,63E-05
Homo_sapiens_tRNA-Cys-GCA-18-1	chr7	149375633	149375955	323	5,728663643	3,456398839	2,158297927	6,00E-05
Homo_sapiens_tRNA-Glu-CTC-1-6	chr6	289820733	289823955	323	11,741416	10,73851352	0,984855155	6,40E-05
Homo_sapiens_tRNA-Glu-TTC-1-1	chr2	130337002	130337324	323	10,8954842	9,986181385	0,895288134	7,39E-05
Homo_sapiens_tRNA-Glu-TTC-2-1	chr13	449178001	449181203	323	11,59017722	10,71556104	0,861825239	7,66E-05
Homo_sapiens_tRNA-Thr-AGT-1-3	chr19	331769311	331772555	325	11,68948929	10,86864081	0,809633653	0,00010008
Homo_sapiens_tRNA-Ala-TGC-9-1	chr6	286339556	286342709	324	5,07612512	3,026032791	1,974885829	0,00011672
Homo_sapiens_tRNA-Ala-AGC-4-1	chr6	286581111	286584333	323	10,98135196	10,11621081	0,851792214	0,00013014
Homo_sapiens_tRNA-Ser-AGA-2-5	chr8	95269531	95269863	333	11,27047261	10,47291384	0,786570306	0,00016153
Homo_sapiens_tRNA-Pro-AGG-3-1	chr16	3160259	3160604	346	5,82896848	3,623272539	2,098621061	0,00018215
Homo_sapiens_tRNA-Lys-TTT-3-2	chr1	204506904	204507227	324	11,68719223	10,81517888	0,857781423	0,00018905
Homo_sapiens_tRNA-Gly-TCC-2-1	chr1	146036935	146037257	323	11,35811992	10,48816887	0,85563085	0,00021658
Homo_sapiens_tRNA-Cys-GCA-2-4	chr17	39154365	39154687	323	11,59533973	10,71350894	0,867072439	0,00021658
Homo_sapiens_tRNA-Gln-TTG-1-1	chr17	49192402	49192724	323	11,58315019	10,77077832	0,800053292	0,00025249
Homo_sapiens_tRNA-Ile-TAT-1-1	chr19	39412042	39412385	344	9,014914203	8,330799977	0,678974471	0,0003377
Homo_sapiens_tRNA-Ser-AGA-5-1	chr7	149608250	149608572	323	6,004592316	4,3355754	1,593912043	0,00042371
Homo_sapiens_tRNA-Lys-TTT-3-5	chr17	8119029	8119352	324	11,29747744	10,51227869	0,773317325	0,00043361
Homo_sapiens_tRNA-Arg-TCT-1-1	chr1	93847447	93847782	336	10,86694746	10,00835826	0,843448886	0,00043644
Homo_sapiens_tRNA-Cys-GCA-23-1	chr7	149595088	149595410	323	5,524519028	3,634100175	1,79886585	0,00060499
Homo_sapiens_tRNA-Arg-TCG-1-1	chr15	89334947	89335270	324	11,44097634	10,65135446	0,77653931	0,0006831
Homo_sapiens_tRNA-Gly-GCC-2-3	chr6	27902782	27903103	322	11,52341788	10,70661323	0,802394247	0,00073109
Homo_sapiens_tRNA-Lys-CTT-1-1	chr14	58239769	58240092	324	11,37446992	10,56357576	0,796625272	0,00080042
Homo_sapiens_tRNA-Val-AAC-1-1	chr3	169772104	169772427	324	10,88905479	10,07809584	0,79658544	0,00087562
Homo_sapiens_tRNA-Leu-TAG-3-1	chr16	22195585	22195917	333	10,86380681	10,11331216	0,738671306	0,00090933
Homo_sapiens_tRNA-Glu-TTC-1-2	chr13	41060612	41060934	323	10,32867024	9,652311616	0,667428386	0,00091976
Homo_sapiens_tRNA-Lys-CTT-1-2	chr15	78860436	78860759	324	11,17969288	10,40497758	0,761805701	0,00104598
Homo_sapiens_tRNA-Met-CAT-1-1	chr8	123157104	123157427	324	11,25236453	10,48366293	0,755532947	0,00109452
Homo_sapiens_tRNA-Ala-AGC-8-1	chr2	27051088	27051411	324	11,58601317	10,80383658	0,768258271	0,00125456
Homo_sapiens_tRNA-Leu-CAG-2-2	chr16	57300354	57300687	334	11,60718904	10,80456679	0,787337408	0,00144403
Homo_sapiens_tRNA-Arg-ACG-2-1	chr3	45688873	45689196	324	11,68273225	10,9244535	0,744684682	0,0017283
Homo_sapiens_tRNA-Trp-CCA-2-1	chr17	19508055	19508377	323	11,48694706	10,77332508	0,70192343	0,00200826
Homo_sapiens_tRNA-Gly-CCC-2-1	chr2	70248865	70249186	322	11,44077384	10,72217639	0,706428453	0,0023284
Homo_sapiens_tRNA-Lys-TTT-3-4	chr11	59560209	59560532	324	11,63005012	10,87189613	0,743647207	0,00253472
Homo_sapiens_tRNA-Pro-CGG-1-1	chr1	167714599	167714921	323	11,44178475	10,74685725	0,68336991	0,00267122
Homo_sapiens_tRX-Tyr-GTA-1-1	chr14	20669048	20669384	337	5,804137073	4,315536506	1,406235597	0,00296904
Homo_sapiens_tRNA-Leu-AAG-2-4	chr16	22297014	22297346	333	11,9258603	11,12214143	0,785769836	0,00335841
Homo_sapiens_tRNA-Lys-TTT-3-1	chr1	204506401	204506724	324	10,86433659	10,22304463	0,630639323	0,00617169
Homo_sapiens_tRNA-Leu-AAG-7-1	chr5	181164435	181164770	336	4,910050822	3,159417553	1,623863468	0,00760378
Homo_sapiens_tRNA-Gly-GCC-2-2	chr2	156401021	156401342	322	11,38974595	10,7447322	0,633164574	0,00822712
Homo_sapiens_tRX-Lys-CTT-1-1	chr16	2927535	2927858	324	5,268453056	3,722988169	1,44480083	0,00864187

Homo_sapiens_tRNA-SeC-TCA-1-1	chr19	45478475	45478812	338	9,935590468	9,456400073	0,475525915	0,0086432
Homo_sapiens_tRNA-Arg-TCT-4-1	chr1	159141485	159141809	325	6,658505107	5,945200634	0,700705351	0,00931702
Homo_sapiens_tRNA-Gln-CTG-1-1	chr6	18836045	18836367	323	5,134670404	3,625983566	1,384168312	0,01035813
Homo_sapiens_tRNA-Phe-GAA-12-1	chr8	123258356	123258682	327	2,434927987	4,355339765	-1,71790054	0,01192632
Homo_sapiens_tRNA-Glu-CTC-1-1	chr1	146035566	146035888	323	11,85630917	11,20398259	0,638603508	0,01283198
Homo_sapiens_tRNA-Cys-GCA-16-1	chr7	149546414	149546736	323	5,097852661	3,69998836	1,310595173	0,01552231
Homo_sapiens_tRNA-Lys-CTT-7-1	chr1	54957743	54958066	324	5,11749609	3,556542596	1,419953948	0,015920 2
Homo_sapiens_tRNA-Glu-CTC-5-1	chr8	58592113	58592434	322	1,766481845	3,856103799	-1,865305233	0,01669187
Homo_sapiens_tRNA-Leu-TAA-2-1	chr11	113562147	113562481	335	1,663343235	3,733095228	-1,87986495	0,01791468
Homo_sapiens_tRNA-Ser-GCT-4-2	chr15	405936 99	405940 31	333	11,35849603	10,7674787	0,579644366	0,01855982
Homo_sapiens_tRNA-Glu-TTC-9-1	chr2	203364280	203364603	324	5,312856569	4,070548724	1,157145647	0,02190839
Homo_sapiens_tRNA-Asp-GTC-2-8	chr12	96035895	96036217	323	11,47272147	10,90900486	0,552590997	0,02577868
Homo_sapiens_tRNA-Cys-GCA-15-1	chr7	149584599	149584921	323	5,054065344	3,67922864	1,267955457	0,02827425
Homo_sapiens_tRNA-Pro-TGG-2-1	chr11	762357 09	762360 21	313	10,98466191	10,45432594	0,520968823	0,02827425
Homo_sapiens_tRNA-Tyr-GTA-2-1	chr2	270506 56	270509 95	340	11,52661748	10,98736917	0,528621569	0,03276382
Homo_sapiens_tRNA-Gly-TCC-1-1	chr19	4723944	4724266	323	11,08817937	10,57902243	0,499929067	0,03467687
Homo_sapiens_tRNA-Gln-CTG-1-4	chr15	658689 36	658692 58	323	11,3582831	10,86178435	0,487841793	0,03673608
Homo_sapiens_tRNA-Gln-CTG-8-2	chr1	146055486	146055808	323	4,556254832	3,129121881	1,273841799	0,03827117
Homo_sapiens_tRNA-Ile-TAT-2-1	chr2	428104 0	428107 53	344	10,52927028	10,11666376	0,407401052	0,03947004
Homo_sapiens_tRNA-Pro-AGG-2-4	chr11	762353 87	762356 99	313	10,70612688	10,20616674	0,490204383	0,04838159
Homo_sapiens_tRNA-Glu-TTC-13-1	chr2	748967 93	748971 16	324	2,471434702	4,001156734	-1,353964835	0,05498622
Homo_sapiens_tRNA-Val-CAC-10-1	chr1	166798 80	166802 03	324	1,725118974	3,590293347	-1,667369108	0,05508451
Homo_sapiens_tRNA-iMet-CAT-1-1	chr1	153671124	153671446	323	11,54398924	11,05214054	0,481864992	0,05786081
Homo_sapiens_tRNA-Val-TAC-1-2	chrX	186747 83	186751 06	324	10,2629545	9,835805741	0,419573505	0,07642643
Homo_sapiens_tRNA-Ser-GCT-3-1	chr11	663479 94	663483 26	333	10,25981977	9,842859779	0,410000247	0,07976172
Homo_sapiens_tRNA-Gln-TTG-5-1	chr2	457101 76	457104 99	324	2,608870289	4,028083907	-1,29255967	0,08578161
Homo_sapiens_tRNX-Val-AAC-1-1	chr6	158403490	158403813	324	2,575719225	3,941388155	-1,2414975	0,0987494
Homo_sapiens_tRNA-Lys-TTT-14-1	chr14	735886 99	735890 28	330	3,123243608	4,295215349	-1,067287571	0,10053809
Homo_sapiens_tRNA-Sup-TTA-1-1	chr17	607861 06	607864 27	322	2,663343235	3,956566826	-1,167521167	0,10142993
Homo_sapiens_tRNA-Lys-TTT-11-1	chr12	276902 47	276905 70	324	2,706488921	4,068557143	-1,163052497	0,10577177
Homo_sapiens_tRNA-Gly-CCC-7-1	chr2	115515 81	115518 92	312	5,010806691	4,009496503	0,917709208	0,10757228
Homo_sapiens_tRNA-Glu-TTC-12-1	chr1	172188272	172188598	327	4,743666219	3,702559117	0,932021379	0,12048067
Homo_sapiens_tRNA-Asn-GTT-13-1	chr1	168753 37	168756 61	325	5,257614961	4,480596929	0,724286609	0,14365 69
Homo_sapiens_tRNA-Ala-TGC-8-1	chr11	502745 82	502749 04	323	2,694561732	3,932644008	-1,121953447	0,14365 69
Homo_sapiens_tRNA-Ser-AGA-6-1	chr11	109165185	109165518	334	4,660926199	3,775274226	0,798264662	0,15719123
Homo_sapiens_tRNA-Tyr-GTA-9-1	chr8	656971 71	656975 09	339	2,898195222	3,994867399	-0,989165728	0,15731141
Homo_sapiens_tRX-Gln-TTG-1-1	chr8	881328 81	881332 05	325	2,48242714	3,692235076	-1,092863745	0,16441319
Homo_sapiens_tRX-Val-TAC-3-1	chr17	400825 54	400828 77	324	2,052714365	3,365117123	-1,111228464	0,16818419
Homo_sapiens_tRX-Lys-CTT-4-1	chr7	971414 47	971417 70	324	2,598803483	3,823371213	-1,052115073	0,17161332
Homo_sapiens_tRNA-Glu-TTC-7-1	chr1	143666862	143667184	323	3,018883166	4,030132111	-0,92900116	0,18268069
Homo_sapiens_tRNA-Pro-TGG-5-1	chr1	207004683	207005010	328	2,496234592	3,743131973	-1,034069104	0,18569167

Homo_sapiens_tRX-Pro-GGG-2-1	chr3	124141746	124142069	324	3,018883166	4,052503842	-0,928141336	0,18795412
Homo_sapiens_tRX-Cys-GCA-2-1	chr8	100816887	100820088	322	3,001665336	4,070548724	-0,968034364	0,19996212
Homo_sapiens_tRNA-Leu-TAA-5-1	chr6	69204360	69204693	334	2,795567995	3,813879238	-0,886544813	0,2193274
Homo_sapiens_tRNA-Leu-AAG-8-1	chr3	148503315	148503647	333	2,190484987	3,25018349	-0,937141049	0,25162049
Homo_sapiens_tRNA-Lys-CTT-12-1	chr1	39504394	39504720	327	3,395922435	4,227129247	-0,763986701	0,25205089
Homo_sapiens_tRX-Und-NNN-9-1	chr22	30308043	30308372	330	3,130249777	4,003243498	-0,80895347	0,25205089
Homo_sapiens_tRX-Und-NNN-6-1	chr9	2959214	2959543	330	2,663343235	3,67922864	-0,893859794	0,25402212
Homo_sapiens_tRX-Gly-CCC-3-1	chr1	145437472	145437793	322	2,832695108	3,785022757	-0,869348876	0,25421814
Homo_sapiens_tRX-Ala-GGC-3-1	chr19	12188435	12188759	325	2,565417583	3,54224709	-0,838425723	0,25421814
Homo_sapiens_tRNA-Und-GCA-5-1	chr17	68394690	68395015	326	2,745948642	3,68964584	-0,829596362	0,27367965
Homo_sapiens_tRNA-Asn-GTT-18-1	chr1	165322712	165325916	325	3,076609276	3,947914469	-0,755220533	0,27402293
Homo_sapiens_tRNA-Gln-CTG-11-1	chr1	143584575	143584897	323	3,220561489	4,07253756	-0,755922765	0,27840163
Homo_sapiens_tRNA-Ala-AGC-17-1	chr6	57861040	57861363	324	5,435964652	6,013130718	-0,534246272	0,27859278
Homo_sapiens_tRNA-Gln-TTG-10-1	chr6	37320093	37320416	324	2,775447487	3,668735673	-0,804603008	0,28170517
Homo_sapiens_tRNA-Lys-TTT-15-1	chr2	223321471	223321794	324	3,227111676	4,0765173	-0,748157114	0,29985453
Homo_sapiens_tRNA-Glu-TTC-11-1	chr14	31767483	31767808	326	3,139077526	4,001156734	-0,738038918	0,30537514
Homo_sapiens_tRX-Lys-CTT-3-1	chr15	95784519	95784842	324	3,123243608	3,930452507	-0,717491345	0,30735373
Homo_sapiens_tRNA-Thr-AGT-7-1	chr17	64530674	64530998	325	2,795567995	3,681836623	-0,779108183	0,30755817
Homo_sapiens_tRNA-Und-NNN-4-1	chr1	7930153	7930473	321	2,795567995	3,65816583	-0,752407797	0,31658792
Homo_sapiens_tRNA-Cys-GCA-3-1	chr7	149588947	149589269	323	4,470698157	3,755577293	0,619065383	0,31658792
Homo_sapiens_tRNA-Phe-GAA-6-1	chr6	28763471	28763795	325	4,123243608	3,37805693	0,648975969	0,32889128
Homo_sapiens_tRNA-Phe-GAA-7-1	chr6	27664640	27664966	327	3,865816856	2,958719044	0,753534966	0,3289527
Homo_sapiens_tRX-Ala-GGC-4-1	chr16	80445429	80445756	328	2,986302388	3,823371213	-0,702188858	0,33088116
Homo_sapiens_tRNA-Gly-CCC-2-2	chr16	636610	636931	322	11,19517252	10,98070769	0,211347326	0,34427763
Homo_sapiens_tRNA-Val-AAC-7-1	chr1	180215015	180215338	324	2,804355235	3,623272539	-0,72619581	0,36840515
Homo_sapiens_tRNA-SeC-TCA-3-1	chr17	40117174	40117498	325	2,745948642	3,54224709	-0,699214782	0,37454733
Homo_sapiens_tRX-Lys-TTT-2-1	chr3	152113410	152113666	327	3,324001282	4,028083907	-0,639055134	0,37961813
Homo_sapiens_tRX-Arg-ACG-1-1	chr8	66112815	66113138	324	2,052714365	2,975844209	-0,751950429	0,37989302
Homo_sapiens_tRNA-Pro-GGG-1-1	chr10	22563524	22563847	324	2,916685105	3,692235076	-0,663712749	0,38570189
Homo_sapiens_tRX-Met-CAT-1-1	chr6	28480600	28480923	324	2,986302388	3,743131973	-0,634973108	0,39422012
Homo_sapiens_tRX-Leu-CAG-1-1	chr9	120354949	120355282	334	3,043340255	3,712809803	-0,610156366	0,42217197
Homo_sapiens_tRX-Ser-GGA-2-1	chrX	25261846	25262168	323	1,100114862	2,155670067	-0,80403438	0,42217197
Homo_sapiens_tRNA-SeC-TCA-2-1	chr22	44150531	44150865	335	3,212219919	3,874483389	-0,605788023	0,42441525
Homo_sapiens_tRX-Lys-CTT-5-1	chr7	126018318	126021702	335	3,553651389	4,13675565	-0,529752325	0,43536345
Homo_sapiens_tRX-Cys-GCA-1-1	chr7	149405938	149406260	323	3,310081475	3,975844209	-0,605009751	0,44196118
Homo_sapiens_tRX-Cys-GCA-4-1	chr7	149628027	149628360	334	3,524519028	4,046434877	-0,491585127	0,45158576
Homo_sapiens_tRNA-Asn-GTT-20-1	chr1	146049072	146049398	327	4,249165002	3,722988169	0,477823422	0,46167735
Homo_sapiens_tRNA-Cys-GCA-24-1	chr17	38833596	38833918	323	4,43058169	3,872201665	0,487541353	0,48226969
Homo_sapiens_tRX-Leu-CAA-3-1	chr2	151831012	151831330	319	2,924766734	3,53070481	-0,540687324	0,49074591
Homo_sapiens_tRX-Pro-GGG-1-1	chrX	119603772	119604091	320	1,409041811	2,22175345	-0,677547575	0,49347463
Homo_sapiens_tRNA-Asn-GTT-16-1	chr1	148405258	148405582	325	3,114318136	3,68964584	-0,533928873	0,49805026

Homo_sapiens_tRNA-Asn-GTT-21-1	chr1	148378790	148379114	325	4,216396733	3,712809803	0,436564181	0,50566188
Homo_sapiens_tRNA-His-GTG-2-1	chr1	143661056	143661378	323	3,343828134	3,881318755	-0,481817988	0,52981 03
Homo_sapiens_tRNA-Cys-GCA-22-1	chr7	149556585	149556905	321	3,809894083	3,295215349	0,434333405	0,53139176
Homo_sapiens_tRNA-Lys-CTT-10-1	chr19	355757 22	355760 45	324	3,018883166	3,545114576	-0,490487759	0,53200 44
Homo_sapiens_tRNA-Gly-TCC-6-1	chr18	576788 19	576791 41	323	1,331722604	2,22175345	-0,670346208	0,55122242
Homo_sapiens_tRX-Lys-CTT-6-1	chr5	168389513	168389835	323	2,420518146	3,013643012	-0,554645908	0,55304825
Homo_sapiens_tRX-Asn-GTT-1-1	chr1	148317243	148317563	321	2,852038071	3,365117123	-0,47312412	0,55773505
Homo_sapiens_tRNA-Cys-GCA-20-1	chr7	149597829	149598151	323	3,938936676	3,553697757	0,370706642	0,57090542
Homo_sapiens_tRX-Und-NNN-8-1	chr10	623437 15	623440 39	325	2,994004311	3,480596929	-0,432347515	0,57641 85
Homo_sapiens_tRNA-Leu-AAG-5-1	chr2	300545 76	300548 99	324	3,130249777	3,567880804	-0,420036003	0,59283 89
Homo_sapiens_tRX-Trp-CCA-1-1	chr7	673994 34	673997 56	323	3,390097011	2,919433333	0,414382218	0,59343353
Homo_sapiens_tRNA-Gly-CCC-8-1	chr1	146488740	146489061	322	2,843537356	3,352060206	-0,437953555	0,59400106
Homo_sapiens_tRNA-Gln-CTG-7-1	chr1	148328686	148329008	323	3,409041811	3,835145991	-0,386895938	0,59400106
Homo_sapiens_tRX-Glu-CTC-1-1	chr8	119131 65	119134 87	323	2,898195222	3,390881708	-0,432457883	0,59400106
Homo_sapiens_tRX-Ser-GCT-1-1	chr13	114241213	114241539	327	3,289782062	3,722988169	-0,407476119	0,59918236
Homo_sapiens_tRX-Ile-AAT-4-1	chr17	8205947	8206284	338	2,95085769	3,416194234	-0,418359864	0,60665904
Homo_sapiens_tRNA-Cys-GCA-25-1	chr3	176997 67	177000 97	331	3,227111676	2,67922864	0,448081118	0,61452982
Homo_sapiens_tRX-Ala-AGC-2-1	chr6	578300 46	578303 69	324	3,060070663	3,516149666	-0,389657583	0,61495686
Homo_sapiens_tRNA-Lys-TTT-10-1	chr19	412421 11	412424 34	324	3,035897931	3,504395834	-0,394139419	0,61712906
Homo_sapiens_tRNA-Gly-TCC-5-1	chr18	576784 96	576788 18	323	0,48242714	0	0,779657609	0,62277258
Homo_sapiens_tRNA-Asp-GTC-6-1	chr3	184648181	184648502	322	3,401724432	3,818626889	-0,400540478	0,63426569
Homo_sapiens_tRNA-Asn-GTT-28-1	chr1	149639327	149639651	325	2,745948642	3,17433011	-0,382886505	0,63948267
Homo_sapiens_tRNA-Asp-GTC-4-1	chr9	749029 48	749032 70	323	2,598803483	3,062555475	-0,398536421	0,63948267
Homo_sapiens_tRNA-Ile-GAT-1-1	chrX	3838251	3838575	325	0	0	0,698309111	0,651429
Homo_sapiens_tRNA-Asp-GTC-8-1	chr12	122376251	122376572	322	3,297688209	3,668735673	-0,321396799	0,65585123
Homo_sapiens_tRNA-Asp-GTC-9-1	chr1	161604672	161604994	323	1,82407931	2,365117123	-0,453544036	0,65585123
Homo_sapiens_tRNA-Cys-GCA-19-1	chr7	149612939	149613261	323	3,409041811	3,755577293	-0,323882647	0,659241 6
Homo_sapiens_tRNA-Und-NNN-2-1	chr8	981411 08	981414 27	320	3,363386197	2,919433333	0,357017224	0,66462805
Homo_sapiens_tRNA-Lys-CTT-11-1	chr19	519220 14	519223 38	325	3,674251227	4,038306522	-0,332167037	0,66462805
Homo_sapiens_tRNA-Gln-TTG-6-1	chr4	409066 00	409069 23	324	3,78109822	4,104031943	-0,29208879	0,67005478
Homo_sapiens_tRX-Gln-CTG-2-1	chr11	480657 06	480660 34	329	3,760773459	4,054517692	-0,287002768	0,68396289
Homo_sapiens_tRNA-Arg-CCT-6-1	chr1	148010933	148011254	322	3,363386197	3,68964584	-0,31103892	0,68454618
Homo_sapiens_tRX-Cys-GCA-3-1	chr1	161605370	161605691	322	2,994004311	3,37805693	-0,341105695	0,68703975
Homo_sapiens_tRX-Arg-CCT-2-1	chr11	118241246	118241575	330	3,395922435	3,722988169	-0,307565601	0,69032016
Homo_sapiens_tRNA-Cys-ACA-1-1	chr5	152608910	152609336	427	3,212219919	3,53070481	-0,306643244	0,70095493
Homo_sapiens_tRNA-Tyr-GTA-10-1	chr7	149557916	149558239	324	3,695822864	4,01778834	-0,263049352	0,710340 4
Homo_sapiens_tRNA-Gln-CTG-17-1	chr20	178743 72	178747 00	329	3,78109822	3,468548617	0,273148602	0,71120644
Homo_sapiens_tRNA-Leu-CAA-5-1	chr11	9275117	9275441	325	3,81425098	3,480596929	0,274742221	0,71311402
Homo_sapiens_tRNA-Asn-GTT-16-3	chr1	120945163	120945487	325	2,725118974	3,078497931	-0,32965418	0,71325948
Homo_sapiens_tRNA-Met-CAT-7-1	chr6	578420 88	578424 11	324	4,169325765	3,919433333	0,244744633	0,71325948
Homo_sapiens_tRX-Asn-GTT-3-1	chr1	146394069	146394393	325	3,123243608	2,765459374	0,292818307	0,71638321

Homo_sapiens_tRNA-Asp-GTC-10-1	chr1	161523019	161523341	323	3,190484987	3,468548617	-0,271816199	0,71638321
Homo_sapiens_tRNA-Gln-CTG-16-1	chr2	218626291	218626609	319	3,884723661	4,144349239	-0,241138395	0,72122806
Homo_sapiens_tRNA-Gly-GCC-5-1	chr16	707885688	707888889	322	3,587307524	3,835145991	-0,235866011	0,73123349
Homo_sapiens_tRNA-Leu-AAG-6-1	chr20	503356679	503360111	333	3,41479139	3,668735673	-0,249802231	0,74255869
Homo_sapiens_tRNA-Gln-CTG-10-1	chr1	147005075	147005397	323	2,631434232	2,901621061	-0,239199171	0,77710126
Homo_sapiens_tRNA-Asp-GTC-5-1	chr5	142394297	142394619	323	3,107233978	3,3355754	-0,220396899	0,78077586
Homo_sapiens_tRX-Asp-ATC-1-1	chr6	28827287	28827609	323	3,494786252	3,722988169	-0,216252736	0,78077586
Homo_sapiens_tRX-Gln-CTG-3-1	chr1	145563120	145563442	323	3,986302388	4,205514212	-0,184101218	0,7850697
Homo_sapiens_tRNA-Gln-CTG-8-1	chr1	149044811	149045133	323	3,36497257	3,644847152	-0,211202085	0,78549215
Homo_sapiens_tRNA-Lys-CTT-6-1	chr18	46089179	46089502	324	3,427741057	3,113732085	0,234567583	0,78549215
Homo_sapiens_tRNA-Gly-GCC-6-1	chr6	142257513	142257834	322	3,233632257	3,44107029	-0,204036792	0,79945606
Homo_sapiens_tRX-Val-TAC-2-1	chr2	84858626	84858949	324	3,471434702	3,25018349	0,195766886	0,79969474
Homo_sapiens_tRNA-Lys-CTT-13-1	chr1	165596787	165597110	324	3,489347384	3,681836623	-0,181332723	0,81311074
Homo_sapiens_tRNA-Ala-AGC-20-1	chr1	150045280	150045601	322	2,994004311	3,207325539	-0,20043407	0,82164842
Homo_sapiens_tRX-Phe-GAA-1-1	chr1	145168278	145168608	331	3,471434702	3,291804911	0,173158041	0,826971
Homo_sapiens_tRNA-Pro-AGG-4-1	chr2	87112324	87112646	323	2,986302388	3,22175345	-0,191854969	0,826971
Homo_sapiens_tRNA-Tyr-GTA-11-1	chr7	149356527	149356854	328	3,083845039	3,25018349	-0,156719205	0,8562471
Homo_sapiens_tRNA-Ile-AAT-11-1	chr12	129231527	129231852	326	3,587307524	3,416194234	0,140023228	0,86074986
Homo_sapiens_tRNA-Lys-TTT-12-1	chr19	495345 0	495348 7 3	324	3,558853585	3,352060206	0,142863173	0,86272976
Homo_sapiens_tRNA-Leu-CAA-6-1	chr1	161611820	161612154	335	3,664631942	3,53070481	0,132092927	0,86881651
Homo_sapiens_tRNA-Asn-GTT-22-1	chr1	143717166	143717490	325	2,631434232	2,785022757	-0,14315621	0,86881651
Homo_sapiens_tRNA-Ile-AAT-10-1	chr6	272839 5	272842 8 3	325	3,397473451	3,278064092	0,135669108	0,86881651
Homo_sapiens_tRX-Und-NNN-7-1	chr3	111349530	111349855	326	3,799968305	3,625983566	0,123618726	0,86906738
Homo_sapiens_tRNA-Gln-CTG-8-3	chr1	120476726	120477048	323	3,756251773	3,623272539	0,118800944	0,87004237
Homo_sapiens_tRNA-Glu-CTC-16-1	chr12	113948614	113948935	322	3,494786252	3,623272539	-0,124429191	0,87013458
Homo_sapiens_tRNA-Lys-CTT-8-1	chr16	3164812	3165135	324	3,7355714	3,565058256	0,132746432	0,8719206
Homo_sapiens_tRNA-Gln-TTG-4-1	chr6	145182597	145182919	323	3,637676866	3,519069442	0,113434037	0,87355432
Homo_sapiens_tRX-Gly-CCC-2-1	chr1	148244341	148244663	323	2,71583402	2,846825445	-0,132748664	0,87456262
Homo_sapiens_tRNA-Arg-CCT-7-1	chr1	143848388	143848709	322	2,745948642	2,865322863	-0,122606235	0,88929075
Homo_sapiens_tRNA-Glu-TTC-10-1	chr1	143784019	143784342	324	0,331722604	0	0,200257718	0,89081008
Homo_sapiens_tRNA-iMet-CAT-3-1	chr9	194038 7	194041 7	326	3,620196373	3,492545455	0,095343259	0,89706277
Homo_sapiens_tRX-Asn-GTT-2-1	chr1	144539524	144539848	325	3,608870289	3,468548617	0,089716246	0,90911528
Homo_sapiens_tRX-Gly-CCC-1-2	chr1	148020348	148020669	322	2,994004311	3,078497931	-0,084865235	0,91616914
Homo_sapiens_tRNA-Lys-CTT-9-1	chr5	26198304	26198627	324	3,139077526	3,25018349	-0,083004779	0,91616914
Homo_sapiens_tRNA-Glu-TTC-10-2	chr1	145176813	145177136	324	3,865816856	3,755577293	0,065756208	0,92249872
Homo_sapiens_tRNA-Gln-CTG-4-2	chr1	143691348	143691670	323	3,745948642	3,647517975	0,060330772	0,92270402
Homo_sapiens_tRNA-Lys-CTT-16-1	chr15	763822958	763826262	325	2,815411748	2,705125302	0,080834244	0,92920785
Homo_sapiens_tRNA-Gln-CTG-13-1	chr5	151868387	151868709	323	3,598803483	3,53070481	0,054486295	0,93659181
Homo_sapiens_tRNA-Tyr-ATA-1-1	chr2	218245700	218246043	344	3,241851286	3,295215349	-0,055213717	0,9412111
Homo_sapiens_tRNA-Glu-CTC-7-1	chr2	158881533	158881856	324	3,107233978	3,129121881	-0,054663544	0,9412111
Homo_sapiens_tRNA-Phe-GAA-8-1	chr6	78958167	78958490	324	3,541788444	3,492545455	0,031538673	0,96103777

Homo_sapiens_tRNA-Leu-TAG-4-1	chr14	20676893	20677225	333	3,955862623	3,939209907	0,014797585	0,98240425
Homo_sapiens_tRNA-Gln-CTG-12-1	chr12	74457276	74457599	324	3,575719225	3,54224709	0,005111278	0,99520797
Homo_sapiens_tRNA-Phe-GAA-9-1	chr1	143792598	143792928	331	0	0	0	1
Homo_sapiens_tRNA-Lys-CTT-15-1	chr11	54759182	54759505	324	0	0	0	1
Homo_sapiens_tRX-Ala-AGC-1-1	chr6	26713543	26713866	324	0	0	0	1
Homo_sapiens_tRX-Ala-AGC-1-2	chr6	26787820	26788143	324	0	0	0	1
Homo_sapiens_tRX-Ile-GAT-2-1	chrX	3838665	3838989	325	0	0	0	1
Homo_sapiens_tRNA-Ile-GAT-1-2	chrX	3876675	3876999	325	0	0	0	1
Homo_sapiens_tRX-Ile-GAT-1-2	chrX	3877089	3877413	325	0	0	0	1
Homo_sapiens_tRNA-Ile-GAT-1-3	chrX	3915104	3915428	325	0	0	0	1
Homo_sapiens_tRX-Ile-GAT-1-1	chrX	3915518	3915842	325	0	0	0	1

Table S7. RPC1 ChIP-Seq peaks at annotated hg38 tRNA genes in human cell lines, and differential RPC1 occupancy in neurons relative to hiPSC.

Gene	chr	start	end	length	hiPSC log2 read counts	Neurons log2 read counts	log2FoldChange	FDR
Homo_sapiens_tRNA-Ser-GCT-2-1	chr6	27297870	27298202	333	11,53640612	4,695053205	6,825597587	1,05E-172
Homo_sapiens_tRNA-Ile-AAT-8-1	chr6	27668457	27668781	325	11,47107249	4,587219488	6,835500196	1,05E-172
Homo_sapiens_tRNA-Asn-GTT-1-1	chr1	161540115	161540439	325	11,30501984	5,005382975	6,278026685	5,77E-166
Homo_sapiens_tRNA-Phe-GAA-3-1	chr6	28807707	28808030	324	11,26108215	4,824523047	6,419811018	3,49E-165
Homo_sapiens_tRNA-Ser-AGA-2-3	chr6	27495688	27496020	333	11,35895271	5,440981735	5,908972075	1,26E-162
Homo_sapiens_tRNA-Lys-CTT-2-5	chr16	3175565	3175888	324	11,31009693	4,318981614	6,985920795	1,14E-159
Homo_sapiens_tRNA-Ser-TGA-3-1	chr6	26312470	26312802	333	11,58425353	5,71045087	5,855701702	8,89E-158
Homo_sapiens_tRNA-iMet-CAT-1-5	chr6	27332859	27333181	323	11,38205713	5,25942749	6,118339704	1,85E-155
Homo_sapiens_tRNA-Leu-TAA-4-1	chr6	27230429	27230762	334	11,74568185	4,928464052	6,832220583	1,38E-154
Homo_sapiens_tRNA-Ile-AAT-5-3	chr6	27237445	27237769	325	11,46631593	3,781711525	7,674706324	5,04E-149
Homo_sapiens_tRNA-Ser-AGA-2-4	chr6	27502913	27503245	333	11,06886145	4,394989813	6,6690201	1,13E-148
Homo_sapiens_tRNA-Tyr-GTA-5-3	chr14	20652973	20653317	345	11,34405971	3,942824268	7,377610511	1,93E-146
Homo_sapiens_tRNA-Gln-CTG-6-1	chr6	27791230	27791552	323	11,4228457	6,224272762	5,185314123	4,48E-146
Homo_sapiens_tRNA-Ser-AGA-4-1	chr6	27553287	27553619	333	11,25105268	4,174004409	7,108592305	7,16E-146
Homo_sapiens_tRNA-Pro-AGG-2-8	chr16	3189508	3189830	323	11,21614669	5,568495127	5,656405634	9,14E-146
Homo_sapiens_tRNA-Lys-TTT-4-1	chr6	27591688	27592011	324	11,40297223	5,02966616	6,343070403	3,16E-145
Homo_sapiens_tRNA-Pro-AGG-2-7	chr16	3182509	3182831	323	11,23556866	5,517893153	5,735635174	7,35E-144
Homo_sapiens_tRNA-Ser-TGA-4-1	chr6	27505702	27506034	333	11,62494725	4,520243773	7,062928033	1,10E-143
Homo_sapiens_tRNA-Gln-CTG-5-1	chr6	27295307	27295629	323	11,0845295	4,765078977	6,377024846	6,98E-143
Homo_sapiens_tRNA-Thr-CGT-5-1	chr6	27618230	27618554	325	11,19228625	4,086832664	7,094428073	2,07E-142
Homo_sapiens_tRNA-Val-CAC-2-1	chr6	27280144	27280467	324	11,56186555	5,6877405	5,857305729	6,93E-142
Homo_sapiens_tRNA-Ser-ACT-1-1	chr6	27293766	27294090	325	11,35807014	4,216934128	7,155340376	1,07E-141
Homo_sapiens_tRNA-Ser-GCT-4-1	chr6	28597214	28597546	333	10,99375456	4,630521781	6,42153413	2,69E-141
Homo_sapiens_tRNA-Val-TAC-4-1	chr6	27290500	27290823	324	11,27988443	3,696835545	7,504600943	1,39E-139
Homo_sapiens_tRNA-Leu-TAG-2-1	chr14	20625244	20625576	333	11,82810828	4,954065327	6,875274099	4,14E-139

Homo_sapiens_tRNA-Glu-TTC-4-1	chr1	165351533	165354755	323	11,86403445	5,412117045	6,457956644	6,20E-139
Homo_sapiens_tRNA-Asn-GTT-2-2	chr1	161427951	161428275	325	11,4654014	5,656587729	5,801803389	3,46E-138
Homo_sapiens_tRNA-Thr-TGT-4-1	chr14	20631034	20631357	324	11,37118824	4,916001165	6,463886311	5,68E-137
Homo_sapiens_tRNA-Ala-TGC-1-1	chr6	28789644	28789966	323	11,11248879	4,836720671	6,286378894	8,01E-137
Homo_sapiens_tRNA-Ser-CGA-3-1	chr6	27672324	27672656	333	11,59264317	4,498921961	7,139691247	1,46E-136
Homo_sapiens_tRNA-Ser-TGA-2-1	chr6	27545563	27545895	333	11,42773114	3,749397898	7,764680771	7,99E-135
Homo_sapiens_tRX-Ala-AGC-5-1	chr6	57813364	57813687	324	11,29707539	3,940820198	7,379632296	2,36E-134
Homo_sapiens_tRNA-Ala-CGC-4-1	chr6	28729189	28729511	323	11,3078745	5,502662882	5,787599314	2,07E-133
Homo_sapiens_tRNA-Arg-ACG-2-4	chr6	27670439	27670762	324	11,30021925	4,434750821	6,784041824	3,41E-133
Homo_sapiens_tRNA-Arg-ACG-2-3	chr6	27215047	27215370	324	10,55173649	4,413562892	6,132618653	1,70E-132
Homo_sapiens_tRNA-Ser-GCT-5-1	chr6	28212911	28213243	333	11,10473372	5,01567285	6,099110931	3,07E-132
Homo_sapiens_tRNA-Glu-TTC-4-2	chr1	161421967	161422289	323	11,18267114	5,692375559	5,523182188	5,04E-131
Homo_sapiens_tRNA-Ala-AGC-1-1	chr6	28795838	28796160	323	11,54296807	5,653837662	5,920563418	7,37E-131
Homo_sapiens_tRNA-Leu-AAG-1-3	chr5	181173918	181174250	333	11,22695381	3,989212957	7,296192821	1,81E-130
Homo_sapiens_tRNA-Glu-TTC-6-1	chr1	148308796	148309118	323	10,95827429	3,99211899	6,956263914	1,83E-130
Homo_sapiens_tRNA-Arg-TCG-5-1	chr6	28542988	28543311	324	11,38521814	6,028487125	5,352697063	2,52E-130
Homo_sapiens_tRNA-Tyr-GTA-5-4	chr14	20663066	20663410	345	10,95509218	4,016624567	6,922075787	8,95E-130
Homo_sapiens_tRNA-Ala-TGC-7-1	chr6	28802674	28802995	322	10,75663401	3,990182286	6,812598187	1,68E-129
Homo_sapiens_tRNA-Lys-TTT-7-1	chr6	28747618	28747941	324	11,33599014	4,150317447	7,253794536	1,04E-128
Homo_sapiens_tRNA-Phe-GAA-1-3	chr11	59557371	59557694	324	10,90634776	5,226647609	5,714179304	1,19E-128
Homo_sapiens_tRNA-Thr-AGT-3-1	chr6	28725892	28726216	325	11,24002219	3,432613157	7,751004818	1,78E-128
Homo_sapiens_tRNA-Val-AAC-1-3	chr5	181169484	181169807	324	10,59823787	5,132833449	5,449325847	1,36E-127
Homo_sapiens_tRNA-Thr-AGT-2-2	chr6	27684569	27684893	325	11,63981075	5,60063535	6,039501846	1,39E-127
Homo_sapiens_tRNA-Pro-CGG-1-2	chr16	3171922	3172244	323	10,82882506	4,793719863	6,082241888	6,82E-127
Homo_sapiens_tRNA-Gln-TTG-2-1	chr6	28589253	28589575	323	11,39185801	6,62583927	4,758438511	1,05E-126
Homo_sapiens_tRNA-Ala-TGC-5-1	chr6	28817109	28817431	323	10,74044802	4,279817532	6,445881336	1,83E-126
Homo_sapiens_tRNA-Gly-CCC-1-1	chr1	16545813	16546134	322	11,33589704	4,088643953	7,186414152	1,85E-126
Homo_sapiens_tRNA-Leu-CAA-2-1	chr6	27605512	27605870	359	11,27097963	4,2967929	7,015316608	1,45E-125
Homo_sapiens_tRNA-Leu-AAG-2-2	chr6	28943496	28943828	333	10,54679443	5,184857192	5,396702886	1,61E-125
Homo_sapiens_tRNA-Ile-AAT-1-1	chr6	57822847	57823171	325	11,15085368	3,637344052	7,386917897	2,51E-124
Homo_sapiens_tRNA-Thr-CGT-1-1	chr6	28488867	28489191	325	10,85341767	3,860810829	7,078424333	8,61E-124
Homo_sapiens_tRNA-Gly-CCC-1-2	chr1	16861795	16862116	322	11,07198632	3,865044258	7,173146244	2,01E-123
Homo_sapiens_tRNA-Lys-TTT-6-1	chr6	27334864	27335187	324	11,17153125	4,215277042	7,004160332	7,14E-123
Homo_sapiens_tRNA-Asp-GTC-3-1	chr6	27583331	27583653	323	11,23128633	5,279024564	5,951801795	8,86E-123
Homo_sapiens_tRNA-Gly-CCC-6-1	chr1	121016719	121017040	322	10,96977989	4,216105823	6,787366466	1,87E-122
Homo_sapiens_tRNA-Gly-CCC-4-1	chr1	16678145	16678466	322	11,23831067	4,156375114	7,009941166	4,08E-122
Homo_sapiens_tRNA-Leu-TAA-2-1	chr6	27720993	27721326	334	10,68033116	4,195628943	6,51142084	1,43E-121
Homo_sapiens_tRNA-Thr-TGT-1-1	chr6	28474426	28474750	325	11,32225339	5,393525223	5,942201908	6,67E-121
Homo_sapiens_tRNA-Ala-AGC-6-1	chr6	28811946	28812268	323	10,61066504	3,919058315	6,627263867	8,48E-121
Homo_sapiens_tRNA-Lys-CTT-2-4	chr6	26556420	26556743	324	11,64969125	6,076811586	5,54668915	3,12E-120
Homo_sapiens_tRNA-Asn-GTT-4-1	chr1	16889551	16889875	325	10,86473047	3,467193154	7,374289266	3,15E-120

Homo_sapiens_tRNA-Ile-AAT-12-1	chr6	57800085	57800409	325	11,31151842	4,55543063	6,683238618	5,17E-120
Homo_sapiens_tRNA-Lys-TTT-9-1	chr6	27575941	27576264	324	10,70530601	4,040720836	6,642815859	3,77E-119
Homo_sapiens_tRNA-Glu-TTC-3-1	chr1	16872457	16872779	323	11,46120211	4,275848329	7,23826618	4,04E-119
Homo_sapiens_tRNA-Ala-TGC-6-1	chr6	28758238	28758560	323	10,67157485	3,634866957	6,975104249	1,01E-118
Homo_sapiens_tRNA-Ala-AGC-5-1	chr6	28710463	28710785	323	10,7854138	3,500963666	7,289716406	3,21E-117
Homo_sapiens_tRNA-Ala-AGC-19-1	chr6	57793419	57793742	324	10,7754319	4,108008521	6,692724957	3,25E-117
Homo_sapiens_tRNA-Asn-GTT-2-7	chr1	145287640	145287964	325	11,38241783	6,045284182	5,342133872	1,17E-115
Homo_sapiens_tRNA-Asn-GTT-14-1	chr1	148048390	148048714	325	10,36115535	4,258623233	6,115969419	1,29E-115
Homo_sapiens_tRNA-Gln-CTG-2-1	chr6	27547626	27547948	323	10,61226895	4,064421246	6,52091004	1,95E-115
Homo_sapiens_tRNA-Ser-GCT-1-1	chr6	27097180	27097512	333	10,49500167	4,105327004	6,49489482	2,05E-115
Homo_sapiens_tRNA-Trp-CCA-3-2	chr6	26331318	26331640	323	10,77517817	4,596503969	6,280601546	4,47E-115
Homo_sapiens_tRNA-Thr-AGT-4-1	chr6	27726568	27726892	325	10,72892584	3,633626813	7,063230232	1,79E-114
Homo_sapiens_tRNA-Gln-TTG-3-2	chr6	26311621	26311943	323	10,92879976	6,348239519	4,577965064	3,78E-114
Homo_sapiens_tRNA-Ala-TGC-2-1	chr6	28643319	28643641	323	10,56491647	4,918039984	5,621498996	7,30E-114
Homo_sapiens_tRNA-iMet-CAT-1-6	chr6	27592695	27593017	323	11,52979622	6,308512885	5,222098968	1,53E-113
Homo_sapiens_tRNA-Pro-AGG-2-5	chr14	20609210	20609532	323	11,42060441	6,239764327	5,164051579	1,72E-112
Homo_sapiens_tRNA-Asn-GTT-9-1	chr1	145475255	145475579	325	10,32035276	4,131516187	6,19367322	6,81E-112
Homo_sapiens_tRNA-Ala-AGC-2-3	chr6	28719578	28719900	323	10,46429853	3,861870352	6,660235487	2,20E-111
Homo_sapiens_tRNA-Val-CAC-1-4	chr5	181173524	181173847	324	10,62205708	4,927452342	5,736683507	2,40E-111
Homo_sapiens_tRNA-Thr-CGT-6-1	chr6	27303663	27303985	323	11,08941946	3,567521319	7,529065551	2,46E-111
Homo_sapiens_tRNA-iMet-CAT-1-4	chr6	26330175	26330497	323	11,40269651	6,039082527	5,370290321	5,71E-111
Homo_sapiens_tRNA-Gln-CTG-9-1	chr1	148353435	148353757	323	10,99914889	3,46858487	7,463045968	5,85E-110
Homo_sapiens_tRNA-Pro-TGG-3-4	chr16	3184007	3184329	323	10,39043164	5,782271239	4,60784437	8,93E-110
Homo_sapiens_tRNA-Val-AAC-3-1	chr6	27650802	27651125	324	11,42552864	6,248718419	5,174248687	9,19E-110
Homo_sapiens_tRNA-Tyr-GTA-4-1	chr14	20657338	20657682	345	10,53292946	3,939817119	6,646917381	1,38E-107
Homo_sapiens_tRNA-Lys-CTT-5-1	chr16	3180428	3180751	324	10,57868976	3,779470492	6,848648277	1,46E-107
Homo_sapiens_tRNA-His-GTG-1-5	chr6	27158001	27158323	323	10,24232297	4,376174506	5,866555922	4,82E-107
Homo_sapiens_tRNA-Val-AAC-5-1	chr6	27235383	27235706	324	10,54455343	4,340834227	6,140485578	1,28E-106
Homo_sapiens_tRNA-Phe-GAA-1-1	chr6	28790596	28790919	324	10,59970043	3,357861767	7,207400381	1,49E-106
Homo_sapiens_tRNA-Arg-TCT-3-1	chr9	128339950	128340291	342	10,39826207	3,753970673	6,616038669	2,11E-106
Homo_sapiens_tRNA-Cys-GCA-17-1	chr7	149691055	149691377	323	10,74447054	4,466496791	6,277610471	2,62E-106
Homo_sapiens_tRNA-Pro-CGG-2-1	chr6	27091616	27091938	323	11,45473207	6,289511828	5,15650737	2,02E-105
Homo_sapiens_tRNA-Arg-CCG-1-1	chr6	28742826	28743149	324	10,76551409	3,315892233	7,508322995	4,54E-105
Homo_sapiens_tRNA-Pro-AGG-2-2	chr6	26555144	26555466	323	10,90605226	5,753399868	5,148248679	2,83E-104
Homo_sapiens_tRNA-Asn-GTT-26-1	KI270713.1	28630	28953	324	10,72683758	4,516211792	6,254229083	1,60E-103
Homo_sapiens_tRNA-Lys-TTT-3-3	chr6	28950903	28951226	324	11,49607566	6,337981707	5,152932649	1,07E-102
Homo_sapiens_tRNA-His-GTG-1-9	chr15	45201025	45201347	323	10,87443043	6,536452232	4,331204581	7,12E-102
Homo_sapiens_tRNA-Ala-AGC-24-1	chr6	57815848	57816171	324	10,35966868	3,940820198	6,446402051	2,34E-101
Homo_sapiens_tRNA-Lys-TTT-13-1	chr6	28693084	28693408	325	10,4988134	3,962258694	6,656309392	3,05E-101
Homo_sapiens_tRNA-Lys-CTT-3-1	chr16	3157279	3157602	324	11,27144681	6,289511828	4,974693698	3,45E-101
Homo_sapiens_tRNA-Lys-CTT-4-1	chr16	3191375	3191698	324	10,41658736	3,155511288	7,190891782	3,63E-101

Homo_sapiens_tRNA-Leu-AAG-2-1	chr5	181187575	181187907	333	11,20869103	6,787374171	4,400603703	6,25E-101
Homo_sapiens_tRNA-Val-AAC-6-1	chr6	28735303	28735625	323	10,64106583	2,971122871	7,536162018	1,99E-100
Homo_sapiens_tRNA-Lys-CTT-2-2	chr5	181207629	181207952	324	11,43834995	6,778974228	4,648983413	5,31E-100
Homo_sapiens_tRNA-Trp-CCA-3-1	chr6	26318976	26319298	323	10,67464343	3,012813923	7,734901813	7,88E-100
Homo_sapiens_tRNA-Val-AAC-4-1	chr6	27680980	27681303	324	10,45869062	3,155511288	7,231100807	1,02E-98
Homo_sapiens_tRNA-Tyr-GTA-6-1	chr6	26594748	26595087	340	10,65855322	3,193947189	7,518658566	1,02E-98
Homo_sapiens_tRNA-Ser-GCT-6-1	chr6	26305364	26305698	335	10,1134541	5,065341353	5,017865429	1,48E-97
Homo_sapiens_tRNA-Ala-AGC-15-1	chr14	88978972	88979295	324	10,63791206	5,761523877	4,860469151	4,13E-97
Homo_sapiens_tRNA-Pro-AGG-2-3	chr7	128783324	128783646	323	11,0358941	5,730780913	5,306170176	7,55E-96
Homo_sapiens_tRNA-Arg-ACG-1-1	chr6	26328014	26328337	324	11,48520609	6,763727719	4,71827947	9,94E-96
Homo_sapiens_tRNA-Tyr-GTA-8-1	chr6	26575444	26575784	341	10,52425615	3,833483767	6,7681261	1,70E-95
Homo_sapiens_tRNA-Asn-GTT-24-1	chr1	146369975	146370299	325	10,71305381	5,465451618	5,265591181	1,64E-94
Homo_sapiens_tRNA-Val-CAC-1-8	chr1	121020603	121020926	324	10,0697121	3,567521319	6,527044324	4,12E-94
Homo_sapiens_tRNA-Arg-TCT-1-1	chr1	93847447	93847782	336	10,86694746	5,183586604	5,713733385	1,79E-93
Homo_sapiens_tRNA-Ala-AGC-11-1	chr6	26571738	26572061	324	11,35971841	7,135413962	4,21503317	3,50E-93
Homo_sapiens_tRNA-Asp-GTC-2-7	chr6	27503618	27503940	323	9,978780476	5,503002485	4,459454374	2,78E-92
Homo_sapiens_tRNA-Arg-ACG-2-2	chr6	27213718	27214041	324	10,08398454	4,012813923	6,150891102	3,18E-91
Homo_sapiens_tRX-Met-CAT-2-1	chr6	57808519	57808843	325	9,958108113	3,807829869	6,19519438	2,11E-90
Homo_sapiens_tRNA-Met-CAT-3-2	chr6	28953139	28953462	324	11,73346955	7,19257095	4,526735082	7,63E-90
Homo_sapiens_tRX-Ala-AGC-6-1	chr6	57792707	57793030	324	9,993800593	3,807829869	6,229183496	1,03E-89
Homo_sapiens_tRNA-Asn-GTT-2-1	chr1	148529131	148529455	325	11,22067244	6,748604798	4,477472362	1,17E-89
Homo_sapiens_tRNA-Phe-GAA-2-1	chr11	59566254	59566577	324	11,71416544	7,170365763	4,534593792	3,19E-89
Homo_sapiens_tRNA-Arg-TCG-4-1	chr6	26299551	26299874	324	10,13591864	3,275848329	6,938689295	6,16E-88
Homo_sapiens_tRNA-Val-CAC-1-7	chr1	149712426	149712749	324	10,17522705	5,067639056	5,03592604	6,32E-88
Homo_sapiens_tRNA-Pro-AGG-1-1	chr16	3191863	3192185	323	9,86734284	3,629899972	6,312798219	1,61E-87
Homo_sapiens_tRNA-Arg-TCG-2-1	chr6	26322692	26323015	324	10,80317611	6,522513479	4,286021295	2,58E-87
Homo_sapiens_tRNA-Gly-CCC-5-1	chr1	167271579	167274880	322	10,19707335	4,278231161	5,932861516	3,23E-87
Homo_sapiens_tRX-Val-CAC-4-1	chr1	149708534	149708855	322	10,49016466	5,429400711	5,086167736	1,51E-86
Homo_sapiens_tRNA-Val-TAC-3-1	chr10	5853585	5853908	324	10,07312871	3,694458602	6,360393084	4,10E-85
Homo_sapiens_tRNA-Leu-TAA-3-1	chr11	59551629	59551962	334	11,10445947	6,887949796	4,209670621	1,27E-84
Homo_sapiens_tRNA-Gln-TTG-3-1	chr6	26311070	26311392	323	9,70481235	4,257818527	5,478306819	5,81E-84
Homo_sapiens_tRNA-Ala-AGC-3-1	chr6	28607030	28607352	323	10,91361688	7,180339489	3,715549681	1,43E-83
Homo_sapiens_tRNA-Thr-TGT-3-1	chr14	20613664	20613987	324	11,28255179	7,143672528	4,128523285	6,41E-81
Homo_sapiens_tRNA-Met-CAT-2-1	chr16	71426367	71426690	324	11,34274382	6,916893503	4,418031621	8,05E-81
Homo_sapiens_tRNA-Ile-TAT-3-1	chr6	28537464	28537808	345	11,35411352	3,806729891	7,546699088	2,35E-79
Homo_sapiens_tRNA-Leu-AAG-3-1	chr6	28988876	28989208	333	9,84012252	3,535290531	6,297394051	1,67E-78
Homo_sapiens_tRNA-Ser-AGA-1-1	chr6	27541649	27541981	333	9,877519804	3,687304184	6,366314312	3,33E-78
Homo_sapiens_tRNA-Pro-AGG-2-6	chr14	20613275	20613597	323	11,5774206	7,455686399	4,116732006	5,35E-77
Homo_sapiens_tRNA-Gln-CTG-4-1	chr1	148264982	148265304	323	10,06074333	3,105327004	7,036944435	9,37E-77
Homo_sapiens_tRNA-Val-CAC-11-2	chr1	168600702	168603995	324	9,608102898	3,572707382	5,927985105	1,50E-76
Homo_sapiens_tRNA-Asn-GTT-3-1	chr1	144419141	144419465	325	10,90296156	6,640755397	4,258082663	1,43E-75

Homo_sapiens_tRNA-Ile-TAT-2-3	chr6	27631295	27631639	345	11,50343328	7,720432676	3,779195253	1,76E-75
Homo_sapiens_tRNA-Asn-GTT-25-1	chr1	149558293	149558618	326	9,91469095	4,482111603	5,47036491	4,18E-74
Homo_sapiens_tRNA-Lys-TTT-2-1	chr11	122559821	122560144	324	10,99232721	3,751686097	7,217025874	4,23E-74
Homo_sapiens_tRNA-Trp-CCA-3-3	chr17	8186232	8186554	323	10,39983332	6,850017887	3,562532184	1,61E-73
Homo_sapiens_tRNA-Met-CAT-3-1	chr6	28944449	28944772	324	11,41753942	7,948297409	3,460408207	1,85E-72
Homo_sapiens_tRNA-Tyr-GTA-3-1	chr6	26576978	26577317	340	9,644187278	3,567521319	6,091957062	8,91E-71
Homo_sapiens_tRNA-Lys-CTT-2-3	chr5	181221853	181222176	324	11,56439924	7,498489472	4,052320814	1,70E-69
Homo_sapiens_tRNA-Thr-TGT-5-1	chr14	20681564	20681887	324	11,41973635	8,122133412	3,288317037	2,10E-68
Homo_sapiens_tRNA-Thr-AGT-1-1	chr17	8187072	8187358	287	10,84484225	6,921357034	3,934583848	9,77E-68
Homo_sapiens_tRNA-Glu-TTC-14-1	KI270713.1	31510	31831	322	9,821791222	2,807829869	7,027803577	1,14E-67
Homo_sapiens_tRNA-Pro-TGG-1-1	chr14	20632880	20633202	323	10,87769332	4,316665199	6,55081135	1,51E-67
Homo_sapiens_tRNA-Thr-CGT-3-1	chr6	28648081	28648405	325	10,85607255	7,48266791	3,370770373	2,85E-67
Homo_sapiens_tRNA-Thr-AGT-5-1	chr17	8139326	8139650	325	11,02617414	7,427247986	3,593483159	9,23E-66
Homo_sapiens_tRNA-Arg-TCT-3-2	chr11	59551184	59551504	321	9,26264572	4,376174506	4,886494651	1,42E-65
Homo_sapiens_tRNA-Tyr-GTA-5-5	chr14	20683147	20683486	340	11,65839295	8,028636901	3,629223577	2,04E-65
Homo_sapiens_tRNA-Asn-GTT-5-1	chr1	165204519	165207833	325	9,473140649	3,275848329	6,268273686	2,29E-65
Homo_sapiens_tRNA-Ser-AGA-2-1	chr6	26327463	26327795	333	10,92698823	7,0231601	3,89272416	5,42E-65
Homo_sapiens_tRNA-Trp-CCA-1-1	chr17	8220743	8221065	323	11,26021573	7,947299517	3,309606519	9,34E-65
Homo_sapiens_tRNA-Cys-GCA-5-1	chr15	79744529	79744852	324	9,369784295	4,48417722	4,888194225	1,46E-64
Homo_sapiens_tRNA-Arg-ACG-1-2	chr6	26537372	26537695	324	11,94519832	8,472652233	3,466341104	8,22E-64
Homo_sapiens_tRNA-Ser-AGA-2-2	chr6	27478686	27479018	333	11,59124344	8,135578241	3,44680103	1,06E-63
Homo_sapiens_tRNA-Gly-GCC-1-5	chr21	17454663	17454984	322	11,533754	7,66390779	3,862587859	1,93E-63
Homo_sapiens_tRNA-Gln-CTG-1-2	chr6	27519403	27519725	323	10,70233627	7,208565126	3,504417186	6,98E-63
Homo_sapiens_tRNA-Val-CAC-14-1	chr1	145157031	145157354	324	9,014819471	2,965219475	6,095373833	1,08E-61
Homo_sapiens_tRNA-Lys-TTT-5-1	chr11	59556303	59556626	324	10,25699504	6,59737258	3,658053065	1,50E-60
Homo_sapiens_tRNA-Met-CAT-4-2	chr6	26743137	26743460	324	8,802657643	3,778348669	5,117231352	9,43E-60
Homo_sapiens_tRNA-Leu-CAG-1-6	chr1	161530216	161530549	334	10,93776355	7,771018665	3,167087722	1,53E-59
Homo_sapiens_tRNA-Cys-GCA-11-1	chr7	149415012	149415334	323	9,295579556	3,502323199	5,757577517	2,62E-58
Homo_sapiens_tRNA-Leu-CAA-1-2	chr6	28940927	28941282	356	11,39587927	7,953845498	3,434809466	4,10E-58
Homo_sapiens_tRNA-Asn-GTT-7-1	chr1	120844136	120844460	325	9,345366437	4,903429677	4,445381354	6,58E-56
Homo_sapiens_tRNA-Val-CAC-11-1	chr1	165475389	165478602	324	9,240786165	3,193947189	6,092188317	2,65E-55
Homo_sapiens_tRNA-Thr-AGT-6-1	chr6	27162145	27162469	325	10,2390924	6,484349221	3,752433986	3,81E-55
Homo_sapiens_tRNA-Tyr-GTA-1-1	chr6	26568732	26569073	342	11,23896076	8,196283259	3,037280571	6,69E-55
Homo_sapiens_tRNA-iMet-CAT-1-3	chr6	26312998	26313320	323	11,38573669	8,153998348	3,226910128	1,13E-54
Homo_sapiens_tRNA-Gln-CTG-1-3	chr6	28941475	28941797	323	11,15871886	7,746736236	3,403572132	3,48E-54
Homo_sapiens_tRNA-Und-TTA-3-1	chr1	161420745	161421068	324	9,338109806	4,191420877	5,242861859	1,09E-53
Homo_sapiens_tRNA-Thr-TGT-2-1	chr1	222464879	222465202	324	10,7029728	7,827274361	2,864489574	1,26E-53
Homo_sapiens_tRNA-Val-TAC-1-1	chr11	59550503	59550826	324	11,32063037	8,121886876	3,195419279	2,84E-53
Homo_sapiens_tRNA-Ile-TAT-2-2	chr6	27020220	27020564	345	9,39736391	5,90497244	3,481462181	3,50E-53
Homo_sapiens_tRNA-Thr-AGT-1-2	chr17	8226109	8226433	325	10,90119185	7,201137628	3,683358989	1,33E-52
Homo_sapiens_tRNA-Leu-TAG-1-1	chr17	8120188	8120520	333	11,39118072	7,989086927	3,395311202	7,31E-52

Homo_sapiens_tRNA-Asn-GTT-8-1	chr1	149740122	149740446	325	9,063857344	2,429758003	6,630545142	1,06E-51
Homo_sapiens_tRNA-Gln-TTG-3-3	chr6	27795735	27796057	323	10,73648599	7,757396426	2,975451938	2,06E-51
Homo_sapiens_tRNA-Trp-CCA-5-1	chr7	99469558	99469880	323	8,76745567	3,280610064	5,435881673	2,65E-51
Homo_sapiens_tRNA-Cys-GCA-2-2	chr17	38867519	38867841	323	11,06596011	7,947764885	3,104192068	6,33E-51
Homo_sapiens_tRNA-Pro-CGG-1-3	chr17	8222707	8223029	323	11,22019199	8,410641725	2,804526887	7,65E-51
Homo_sapiens_tRNA-Ala-CGC-1-1	chr6	26553377	26553699	323	11,10201507	7,847438059	3,242433367	5,52E-50
Homo_sapiens_tRNA-iMet-CAT-2-1	chr6	27777759	27778081	323	10,32036877	3,350332109	7,025338393	6,27E-50
Homo_sapiens_tRNA-His-GTG-1-1	chr1	14603791	14603824	323	10,35935821	7,594261798	2,760326567	1,67E-49
Homo_sapiens_tRNA-Val-CAC-4-1	chr1	14380368	14380491	324	8,44390711	3,195628943	5,272992499	1,82E-49
Homo_sapiens_tRNA-Phe-GAA-5-1	chr6	28764261	28764588	328	8,765488316	3,564921281	5,285025053	2,00E-49
Homo_sapiens_tRNA-Lys-CTT-14-1	chr16	3196027	3196350	324	8,730441903	3,837798027	4,871371055	4,18E-48
Homo_sapiens_tRNA-Ala-AGC-21-1	chr6	26749786	26750109	324	9,07796108	2,568819584	6,454299929	2,77E-47
Homo_sapiens_tRNA-Cys-GCA-9-3	chr7	14963556	14963583	323	10,18668869	2,924139212	7,035961251	2,83E-47
Homo_sapiens_tRNA-Ser-GCT-4-3	chr17	8186740	8187034	295	11,21291021	8,232913803	2,979096298	2,89E-47
Homo_sapiens_tRNA-Cys-GCA-13-1	chr7	14935549	14935571	323	10,69087464	3,778348669	6,875063143	2,95E-47
Homo_sapiens_tRNA-Ile-AAT-2-1	chr6	27688062	27688386	325	11,75854303	8,626717625	3,123828735	3,13E-47
Homo_sapiens_tRNA-Ser-AGA-2-6	chr17	8226484	8226816	333	10,44306022	7,04779324	3,399073268	5,01E-47
Homo_sapiens_tRNA-Ser-CGA-1-1	chr17	8138755	8139087	333	10,05626691	7,288231669	2,781216495	6,33E-47
Homo_sapiens_tRNA-Ile-AAT-5-1	chr6	26553996	26554320	325	11,73882416	8,363889987	3,364381355	1,04E-46
Homo_sapiens_tRNA-Cys-GCA-8-1	chr14	72962845	72963167	323	9,977397001	4,481422406	5,4992952	4,37E-46
Homo_sapiens_tRNA-Ala-TGC-3-2	chr12	124921629	124921951	323	11,35353828	8,228497073	3,11898293	6,63E-46
Homo_sapiens_tRNA-Arg-TCT-5-1	chr6	27562058	27562395	338	8,537897192	3,317437751	5,240792234	8,47E-46
Homo_sapiens_tRNA-Val-TAC-2-1	chr11	59550861	59551168	308	10,41599627	7,380531787	3,03627996	4,03E-45
Homo_sapiens_tRNA-Cys-GCA-9-2	chr7	14931003	14931325	323	8,765938122	3,153782085	5,5817022	7,55E-45
Homo_sapiens_tRNA-Gly-TCC-2-6	chr1	16153098	16153409	323	11,32333018	8,60564936	2,710392032	7,84E-45
Homo_sapiens_tRNA-Leu-AAG-2-3	chr14	20610006	20610338	333	11,90447689	8,737207484	3,15687459	8,30E-45
Homo_sapiens_tRNA-Asn-GTT-2-6	chr19	1383559	1383761	203	10,41102439	7,926498186	2,486943756	2,72E-44
Homo_sapiens_tRNA-Ala-AGC-8-2	chr8	66114201	66114386	186	9,339609439	6,649076914	2,69211317	5,52E-44
Homo_sapiens_tRNA-Arg-CCT-2-1	chr17	75034305	75034628	324	11,3226007	8,65220733	2,671416299	4,62E-41
Homo_sapiens_tRNA-Glu-TTC-5-1	chr1	161612592	161612914	323	10,38398817	7,897102613	2,490268711	6,75E-41
Homo_sapiens_tRNA-Pro-TGG-3-3	chr16	3158796	3159118	323	8,193889404	3,360862661	4,735197822	1,30E-40
Homo_sapiens_tRNA-Ile-AAT-4-1	chr17	8226865	8227189	325	10,68555561	7,547499499	3,125904183	1,33E-40
Homo_sapiens_tRNA-Cys-GCA-12-1	chr7	14964682	14964751	323	8,38858823	3,723356087	4,670297358	1,59E-40
Homo_sapiens_tRNA-Ala-CGC-2-1	chr6	28673710	28674032	323	11,41865171	8,753578269	2,660706006	7,19E-40
Homo_sapiens_tRNA-Tyr-GTA-5-2	chr8	66113862	66114063	202	8,481149765	4,739321217	3,733688132	8,96E-40
Homo_sapiens_tRNA-Asn-GTT-6-1	chr1	143735794	143736118	325	7,937588783	3,601587068	4,326200007	1,21E-39
Homo_sapiens_tRNA-Asp-GTC-2-6	chr6	27479548	27479870	323	11,4811426	8,711005095	2,765946701	1,94E-39
Homo_sapiens_tRNA-Asn-GTT-2-4	chr13	30673838	30674162	325	11,17367003	8,765536221	2,408188877	5,86E-39
Homo_sapiens_tRNA-Val-CAC-1-6	chr6	26537928	26538251	324	10,81737979	8,145443238	2,664394954	6,03E-39
Homo_sapiens_tRNA-Val-AAC-1-2	chr5	181164028	181164351	324	8,283982677	2,571412613	5,60655313	1,31E-38
Homo_sapiens_tRNA-Lys-CTT-2-1	chr1	146039275	146039598	324	10,98294741	8,132778587	2,841909703	2,68E-38

Homo_sapiens_tRNA-Val-AAC-1-4	chr5	181218144	181218467	324	11,79784577	8,953955417	2,83796069	2,89E-38
Homo_sapiens_tRNA-Pro-TGG-3-2	chr14	20683890	20684212	323	11,49535649	8,862129849	2,626137021	8,00E-38
Homo_sapiens_tRNA-Ala-CGC-5-1	chr6	28695806	28696128	323	8,442136781	3,564921281	4,942792473	6,17E-37
Homo_sapiens_tRNA-Leu-CAA-3-1	chr6	27602443	27602800	358	11,29753246	4,442235958	6,78941765	1,03E-36
Homo_sapiens_tRNA-Gln-CTG-1-5	chr17	8119626	8119948	323	11,22725853	8,788038974	2,434360944	1,87E-36
Homo_sapiens_tRNA-Val-AAC-2-1	chr5	181188290	181188613	324	10,89411698	8,173466895	2,714411634	2,65E-36
Homo_sapiens_tRNA-Arg-CCG-2-1	chr17	68019771	68020094	324	11,30601443	9,027881324	2,275779949	4,25E-36
Homo_sapiens_tRNA-Val-CAC-6-1	chr6	27205962	27206285	324	8,165237853	2,810027313	5,316482932	8,33E-36
Homo_sapiens_tRNA-Arg-CCT-1-1	chr17	75033780	75034103	324	10,8323539	8,422311728	2,409005439	1,78E-35
Homo_sapiens_tRNA-Asn-GTT-17-1	chr1	161621549	161621873	325	9,535007018	3,626163478	5,948830564	1,80E-35
Homo_sapiens_tRNA-Leu-CAG-2-1	chr16	57299825	57300158	334	11,50207082	8,67834196	2,817201742	1,89E-35
Homo_sapiens_tRNA-Ala-AGC-16-1	chr6	57870219	57870542	324	8,263044186	3,277437321	5,003132972	4,74E-35
Homo_sapiens_tRNA-iMet-CAT-1-8	chr17	82494595	82494917	323	11,98070698	9,089905395	2,880662508	9,42E-35
Homo_sapiens_tRNA-Phe-GAA-1-5	chr13	94549524	94549847	324	11,1367651	8,662174774	2,468470529	1,21E-34
Homo_sapiens_tRNA-Ile-AAT-3-1	chr6	27275085	27275409	325	8,117290647	2,865044258	5,201151785	2,86E-34
Homo_sapiens_tRNA-Cys-GCA-14-1	chr17	38861558	38861880	323	10,10269242	4,874807607	5,198089118	3,25E-33
Homo_sapiens_tRNA-Thr-CGT-2-1	chr16	14285767	14286089	323	11,13526756	9,066667546	2,068015291	6,19E-33
Homo_sapiens_tRNA-Asp-GTC-2-11	chr17	8222112	8222434	323	11,66296012	8,776547792	2,874086658	1,92E-32
Homo_sapiens_tRNA-Phe-GAA-1-2	chr6	28981546	28981869	324	10,06549944	7,453619986	2,611447812	3,40E-32
Homo_sapiens_tRNA-Tyr-GTA-5-1	chr8	66113241	66113584	344	11,07890264	8,352754392	2,723123972	1,56E-31
Homo_sapiens_tRNA-Ser-CGA-2-1	chr6	27209723	27210055	333	7,853538898	3,631143322	4,254582253	2,28E-31
Homo_sapiens_tRNA-Lys-CTT-1-2	chr15	78860436	78860759	324	11,17969288	8,478977465	2,6946049	4,61E-31
Homo_sapiens_tRNA-Asn-GTT-10-1	chr1	145129113	145129437	325	9,015205905	3,776102403	5,277810804	5,14E-31
Homo_sapiens_tRNA-Arg-CCG-1-2	chr6	28881262	28881585	324	11,51896319	9,005442902	2,50577804	6,46E-31
Homo_sapiens_tRNA-Gly-GCC-2-4	chr16	70778913	70779234	322	9,140263626	6,325628296	2,797126883	7,76E-31
Homo_sapiens_tRNA-SeC-TCA-1-1	chr19	45478475	45478812	338	9,935590468	7,839986605	2,093756071	7,76E-31
Homo_sapiens_tRNA-His-GTG-1-8	chr15	45200287	45200609	323	11,59384096	9,31335647	2,277339542	1,09E-30
Homo_sapiens_tRNA-Arg-TCT-2-1	chr17	8120799	8121137	339	7,902021681	4,013767528	3,939422138	1,66E-30
Homo_sapiens_tRNA-Gly-GCC-2-6	chr17	8125620	8125941	322	11,50659893	9,296076857	2,206565414	6,07E-30
Homo_sapiens_tRNA-Gly-TCC-3-1	chr17	8221422	8221744	323	11,22330981	8,686973263	2,528444335	8,11E-30
Homo_sapiens_tRNA-Cys-GCA-9-4	chr7	149707543	149707865	323	7,883566767	3,863987065	4,017936406	2,78E-29
Homo_sapiens_tRNA-Ala-AGC-2-1	chr6	28838318	28838640	323	11,3133971	8,96488981	2,341306976	1,94E-28
Homo_sapiens_tRNA-Arg-CCT-3-1	chr16	3152774	3153097	324	11,57086222	8,896130735	2,665988974	2,10E-28
Homo_sapiens_tRNA-Leu-CAA-4-1	chr1	248873729	248874085	357	11,44279206	9,291322278	2,148590323	3,13E-28
Homo_sapiens_tRNA-Lys-TTT-1-1	chr16	73478191	73478514	324	8,420471885	5,050297941	3,389613098	5,08E-28
Homo_sapiens_tRNA-Cys-GCA-4-1	chr17	38869166	38869488	323	10,71027783	8,495525538	2,216211489	9,35E-28
Homo_sapiens_tRNA-Cys-GCA-2-1	chr4	123508724	123509046	323	7,886345464	3,351841188	4,629746667	1,11E-27
Homo_sapiens_tRNA-Cys-GCA-9-1	chr3	132231672	132231994	323	8,977846057	4,412117045	4,540462164	1,41E-27
Homo_sapiens_tRNA-Asp-GTC-2-9	chr12	124927219	124927541	323	9,984128314	7,707722162	2,265016329	8,33E-27
Homo_sapiens_tRNA-Val-CAC-1-5	chr5	181222269	181222592	324	11,58441432	9,202489538	2,376956042	2,19E-26
Homo_sapiens_tRNA-Arg-TCT-4-1	chr1	159141485	159141809	325	6,658505107	9,103357455	-2,439789343	3,80E-26

Homo_sapiens_tRNA-Cys-GCA-21-1	chr7	149664698	149665020	323	7,930983215	3,751686097	4,188437904	3,96E-26
Homo_sapiens_tRNA-Arg-TCG-3-1	chr17	75034987	75035310	324	11,49970136	9,426408095	2,070222983	4,81E-26
Homo_sapiens_tRNA-His-GTG-1-2	chr1	147073099	147073421	323	7,835789017	3,563619502	4,357486919	5,81E-26
Homo_sapiens_tRNA-Ile-AAT-5-5	chr17	8187467	8187791	325	11,41556167	9,000696229	2,409929581	1,03E-25
Homo_sapiens_tRNA-Ile-AAT-5-4	chr14	102316966	102317290	325	11,51351531	9,361583311	2,148153035	1,57E-25
Homo_sapiens_tRNA-Cys-GCA-6-1	chr3	132228974	132229296	323	7,531130032	3,110685062	4,367745381	1,74E-25
Homo_sapiens_tRNA-Gly-GCC-2-5	chr16	70789381	70789702	322	7,796889716	4,337029612	3,478056716	3,25E-25
Homo_sapiens_tRNA-Asp-GTC-2-10	chr12	124939521	124939840	320	11,24620992	8,916910699	2,325770082	3,44E-25
Homo_sapiens_tRNA-Phe-GAA-1-4	chr12	124927717	124928040	324	10,70859648	8,553240808	2,153525417	2,28E-24
Homo_sapiens_tRNA-iMet-CAT-1-7	chr6	27902367	27902689	323	10,86672903	8,60150463	2,255179966	3,79E-24
Homo_sapiens_tRNA-Met-CAT-6-1	chr16	87383896	87384219	324	11,50652176	9,62174478	1,882589286	8,06E-24
Homo_sapiens_tRNA-Thr-CGT-4-1	chr17	31549948	31550270	323	11,08312912	9,04334115	2,03845887	1,90E-23
Homo_sapiens_tRNA-Thr-AGT-2-1	chr6	26532791	26533115	325	11,63840873	9,483897674	2,150793851	2,85E-23
Homo_sapiens_tRNA-Asn-GTT-2-3	chr10	22229383	22229707	325	11,54482658	9,391480584	2,14863584	3,79E-23
Homo_sapiens_tRNA-Ala-TGC-4-1	chr12	124939843	124940162	320	10,79409828	8,710233212	2,083575042	6,86E-22
Homo_sapiens_tRNA-Pro-AGG-2-1	chr1	167715362	167715684	323	11,36053174	9,19666488	2,158119003	1,05E-21
Homo_sapiens_tRNA-Gly-TCC-4-1	chr1	161440045	161440367	323	7,515494406	3,105327004	4,459661636	2,36E-21
Homo_sapiens_tRNA-Trp-CCA-4-1	chr12	98504126	98504448	323	10,6583185	8,826207427	1,831728246	3,53E-21
Homo_sapiens_tRNA-Cys-GCA-2-3	chr17	39153608	39153930	323	11,33006399	9,368553323	1,95829213	7,49E-21
Homo_sapiens_tRNA-Gly-CCC-3-1	chr17	19860736	19861057	322	7,370061767	3,599047757	3,798111286	9,96E-21
Homo_sapiens_tRNA-Pro-TGG-3-1	chr5	181188728	181189050	323	11,41399102	9,347434134	2,060405454	6,82E-20
Homo_sapiens_tRNA-Phe-GAA-4-1	chr6	28823190	28823514	325	7,427670251	3,692077736	3,7542164	4,13E-19
Homo_sapiens_tRNA-Tyr-GTA-7-1	chr14	20659832	20660176	345	7,227547731	3,286934694	3,773146693	1,26E-18
Homo_sapiens_tRNA-Ser-CGA-4-1	chr12	56190238	56190570	333	10,13137511	8,353507863	1,779383718	1,75E-18
Homo_sapiens_tRNA-Glu-TTC-2-1	chr13	44917801	44918123	323	11,59017722	9,683198738	1,90201264	1,96E-18
Homo_sapiens_tRNA-Thr-TGT-6-1	chr5	181191561	181191883	323	11,53171582	9,690039767	1,837630309	3,05E-18
Homo_sapiens_tRNA-Gly-GCC-2-1	chr1	161523721	161524042	322	11,45051472	9,463417499	1,980952569	3,18E-18
Homo_sapiens_tRNA-Leu-AAG-4-1	chr6	28478497	28478829	333	7,362593829	4,153782085	3,198159538	6,23E-18
Homo_sapiens_tRNA-Leu-CAG-1-7	chr6	26521082	26521415	334	10,53670561	8,538632841	1,995069509	7,90E-18
Homo_sapiens_tRNA-Val-CAC-3-1	chr19	4724509	4724832	324	10,27892425	8,767040639	1,512774654	1,21E-17
Homo_sapiens_tRNA-Ala-CGC-3-1	chr2	156400643	156400965	323	10,56232298	8,610158197	1,948778572	2,03E-17
Homo_sapiens_tRNA-Asn-GTT-2-5	chr17	38751655	38751979	325	10,72310352	9,143018977	1,57939782	2,67E-17
Homo_sapiens_tRNA-Ala-TGC-3-1	chr5	181206742	181207064	323	11,78889452	9,782902049	1,999852786	2,78E-17
Homo_sapiens_tRNA-Ile-AAT-5-2	chr6	27177089	27177413	325	10,59530278	8,725722305	1,862652838	3,66E-17
Homo_sapiens_tRNA-Ala-AGC-4-1	chr6	28658111	28658433	323	10,98135196	9,122341755	1,8535733	6,93E-17
Homo_sapiens_tRNA-Glu-CTC-2-1	chr1	248874122	248874444	323	10,99861657	9,280884364	1,715078446	6,93E-17
Homo_sapiens_tRNA-Gly-GCC-3-1	chr16	70778085	70778406	322	7,065716255	4,085019099	3,006952848	1,11E-16
Homo_sapiens_tRNA-His-GTG-1-7	chr15	45198480	45198802	323	11,58796416	9,781964477	1,801310174	1,29E-16
Homo_sapiens_tRNA-Ala-AGC-2-2	chr6	28863559	28863881	323	11,30835566	9,576868989	1,728031467	1,44E-16
Homo_sapiens_tRNA-Val-CAC-7-1	chr6	27728422	27728745	324	7,112167985	3,782830737	3,295714378	3,15E-16
Homo_sapiens_tRNA-Val-CAC-1-1	chr1	161399574	161399897	324	11,64885037	9,949360629	1,696340044	4,18E-16

Homo_sapiens_tRNA-Cys-GCA-10-1	chr7	149377384	149377706	323	6,895113617	3,356358976	3,539365466	4,56E-16
Homo_sapiens_tRNA-Arg-CCG-1-3	chr16	3150548	3150871	324	11,39581711	9,578041198	1,814208327	6,47E-16
Homo_sapiens_tRNA-Phe-GAA-1-6	chr19	1383236	1383437	202	9,812551172	8,184987377	1,62867887	1,19E-15
Homo_sapiens_tRNA-Asn-GTT-11-2	chr1	149646325	149646649	325	7,122687381	3,777225973	3,406146911	1,81E-15
Homo_sapiens_tRNA-Lys-TTT-3-2	chr1	204506904	204507227	324	11,68719223	9,880687559	1,801072783	3,39E-15
Homo_sapiens_tRNA-Cys-GCA-1-1	chr7	149310064	149310386	323	6,95089119	3,752828838	3,191817137	3,71E-15
Homo_sapiens_tRNA-Gly-TCC-2-1	chr1	146036935	146037257	323	11,35811992	9,555742457	1,79753502	6,09E-15
Homo_sapiens_tRNA-Lys-CTT-1-1	chr14	582397689	582400902	324	11,37446992	9,531749929	1,835876942	7,47E-15
Homo_sapiens_tRNA-Leu-TAA-1-1	chr6	144216421	144216754	334	11,22592527	9,587623	1,634795501	9,77E-15
Homo_sapiens_tRNA-Ile-AAT-9-1	chr6	27273834	27274158	325	6,633162001	3,06257927	3,566101539	2,54E-14
Homo_sapiens_tRNA-Ser-TGA-1-1	chr10	67764377	67764709	333	11,52514109	9,911721493	1,60901719	2,71E-14
Homo_sapiens_tRNA-Ser-AGA-2-5	chr8	95269531	95269863	333	11,27047261	9,696560151	1,570879269	3,44E-14
Homo_sapiens_tRX-Ile-AAT-3-1	chr6	27260805	27261130	326	6,883030837	3,692077736	3,215061135	4,34E-14
Homo_sapiens_tRNA-Gln-TTG-1-1	chr17	49192402	49192724	323	11,58315019	9,939914663	1,639156388	4,54E-14
Homo_sapiens_tRNA-Asp-GTC-1-1	chr12	98503377	98503699	323	11,60515253	9,768623637	1,830143353	5,36E-14
Homo_sapiens_tRNA-Gly-CCC-2-1	chr2	70248865	70249186	322	11,44077384	9,718136399	1,718304347	7,16E-14
Homo_sapiens_tRNA-Glu-TTC-2-2	chr15	26082108	26082430	323	11,33352746	9,742178956	1,588187036	8,46E-14
Homo_sapiens_tRNA-Und-NNN-1-1	chr6	26749073	26749397	325	6,609080097	0,916001165	5,534667917	8,46E-14
Homo_sapiens_tRNA-Cys-GCA-7-1	chr1	93516151	93516474	324	7,002812123	3,464405686	3,550239515	8,92E-14
Homo_sapiens_tRNA-Leu-CAA-1-1	chr6	28896097	28896453	357	11,45995859	9,837713888	1,61830878	1,64E-13
Homo_sapiens_tRNA-Lys-TTT-3-5	chr17	8119029	8119352	324	11,29747744	9,685804431	1,607898641	1,72E-13
Homo_sapiens_tRNA-Lys-TTT-3-1	chr1	204506401	204506724	324	10,86433659	9,207192848	1,653213198	3,15E-13
Homo_sapiens_tRNA-Ser-AGA-3-1	chr6	27532082	27532414	333	6,72036836	3,400104202	3,202228781	3,16E-13
Homo_sapiens_tRNA-Phe-GAA-11-1	chr6	28726952	28727275	324	7,051391538	4,082294469	3,015930952	1,18E-12
Homo_sapiens_tRNA-Lys-TTT-8-1	chr1	205474017	205474340	324	7,254705888	4,516884572	2,752749287	1,60E-12
Homo_sapiens_tRNA-Glu-CTC-3-1	chr13	41455799	41456122	324	6,621026399	3,664970443	2,928464445	2,18E-12
Homo_sapiens_tRNA-Lys-TTT-3-4	chr11	59560209	59560532	324	11,63005012	9,921312913	1,702457743	2,98E-12
Homo_sapiens_tRNA-Ala-AGC-8-1	chr2	27051088	27051411	324	11,58601317	9,941657553	1,639901544	3,91E-12
Homo_sapiens_tRNA-Gly-GCC-2-3	chr6	27902782	27903103	322	11,52341788	9,883858163	1,634437223	4,28E-12
Homo_sapiens_tRNA-Thr-AGT-1-3	chr19	33176931	33177255	325	11,68948929	10,26743918	1,419014222	6,90E-12
Homo_sapiens_tRNA-Val-AAC-1-5	chr6	27753274	27753597	324	11,01997068	9,409802528	1,604526894	7,65E-12
Homo_sapiens_tRNA-Arg-TCG-1-1	chr15	89334947	89335270	324	11,44097634	9,888853465	1,548183878	8,89E-12
Homo_sapiens_tRNA-Glu-CTC-1-6	chr6	28982073	28982395	323	11,741416	10,05833702	1,676770374	9,16E-12
Homo_sapiens_tRNA-Pro-CGG-1-1	chr1	167714599	167714921	323	11,44178475	9,90983126	1,527510516	1,11E-11
Homo_sapiens_tRNA-Glu-TTC-8-1	chr1	149692679	149693002	324	6,817438699	3,661323798	3,174278436	1,15E-11
Homo_sapiens_tRNA-Arg-ACG-1-3	chr14	22929575	22929898	324	11,22630002	9,76044127	1,463085719	2,04E-11
Homo_sapiens_tRNA-Glu-CTC-1-1	chr1	146035566	146035888	323	11,85630917	10,18075399	1,669193771	3,40E-11
Homo_sapiens_tRX-Phe-GAA-2-1	chr1	121009418	121009748	331	6,650283164	3,89178545	2,73546851	3,52E-11
Homo_sapiens_tRNA-Glu-CTC-1-7	chr6	125780121	125780443	323	11,47070305	9,966433503	1,499945475	3,67E-11
Homo_sapiens_tRNA-Arg-CCT-4-1	chr7	139340574	139340897	324	11,17085713	9,669050534	1,498147943	3,88E-11
Homo_sapiens_tRNA-Ile-AAT-6-1	chr6	26756426	26756750	325	6,512637396	0,096352447	6,49875939	5,29E-11

Homo_sapiens_tRNA-Ala-AGC-23-1	chr6	28778641	28778963	323	6,299243202	3,105327004	3,244144531	1,06E-10
Homo_sapiens_tRNA-Cys-GCA-2-4	chr17	39154365	39154687	323	11,59533973	10,08912156	1,502188661	1,22E-10
Homo_sapiens_tRNA-Ile-TAT-1-1	chr19	39412042	39412385	344	9,014914203	7,817088552	1,202711239	1,57E-10
Homo_sapiens_tRNA-Met-CAT-1-1	chr8	123157104	123157427	324	11,25236453	9,785026394	1,462572783	1,89E-10
Homo_sapiens_tRNA-iMet-CAT-1-2	chr6	26286400	26286722	323	9,356544582	7,921034338	1,432014	3,84E-10
Homo_sapiens_tRNA-Leu-TAG-3-1	chr16	22195585	22195917	333	10,86380681	9,479483626	1,380383267	4,11E-10
Homo_sapiens_tRNA-Leu-AAG-2-4	chr16	22297014	22297346	333	11,9258603	10,25998215	1,659360355	4,20E-10
Homo_sapiens_tRNA-Val-CAC-9-1	chr6	27150117	27150440	324	6,361750631	3,533961727	2,83776425	4,65E-10
Homo_sapiens_tRNA-Leu-CAG-2-2	chr16	57300354	57300687	334	11,60718904	10,08763415	1,514812947	6,64E-10
Homo_sapiens_tRNA-Val-AAC-1-1	chr3	169772104	169772427	324	10,88905479	9,417479695	1,465901047	7,10E-10
Homo_sapiens_tRNA-Trp-CCA-2-1	chr17	19508055	19508377	323	11,48694706	10,10984918	1,373411697	1,00E-09
Homo_sapiens_tRNA-Arg-ACG-2-1	chr3	45688873	45689196	324	11,68273225	10,24037752	1,437868498	1,02E-09
Homo_sapiens_tRNA-Asn-GTT-11-1	chr1	120952165	120952489	325	6,516163159	3,529967955	3,04663424	1,71E-09
Homo_sapiens_tRX-Glu-TTC-2-1	chr1	121000862	121001185	324	5,735035922	2,020425173	3,561707816	1,74E-09
Homo_sapiens_tRNA-Arg-TCG-6-1	chr9	110198397	110198720	324	5,925304435	2,860810829	3,109658664	2,43E-09
Homo_sapiens_tRNA-Tyr-GTA-2-1	chr2	27050656	27050995	340	11,52661748	10,09736752	1,425305628	3,10E-09
Homo_sapiens_tRNA-Arg-CCT-5-1	chr16	3193792	3194115	324	5,724888494	2,360862661	3,244603289	3,45E-09
Homo_sapiens_tRNA-Ser-GCT-4-2	chr15	40593699	40594031	333	11,35849603	9,952819127	1,401442219	5,92E-09
Homo_sapiens_tRNA-His-GTG-1-6	chr9	144338114	144338436	323	6,890581582	4,876905438	2,023910627	6,40E-09
Homo_sapiens_tRNA-Glu-TTC-1-1	chr2	130337002	130337324	323	10,8954842	9,589275571	1,302916547	7,07E-09
Homo_sapiens_tRNA-Gln-CTG-1-4	chr15	65868936	65869258	323	11,3582831	10,11744149	1,236700166	4,73E-08
Homo_sapiens_tRNA-Gly-TCC-1-1	chr19	4723944	4724266	323	11,08817937	9,846611077	1,238440972	7,10E-08
Homo_sapiens_tRNA-Pro-TGG-4-1	chr16	3170834	3171155	322	5,96229001	3,198986581	2,700201527	8,18E-08
Homo_sapiens_tRNA-iMet-CAT-1-1	chr1	153671124	153671446	323	11,54398924	10,22742238	1,311990568	8,73E-08
Homo_sapiens_tRNA-Gly-GCC-2-2	chr2	156401021	156401342	322	11,38974595	10,13555195	1,250492859	1,12E-07
Homo_sapiens_tRNA-Glu-TTC-1-2	chr13	41060612	41060934	323	10,32867024	9,271120254	1,057894209	1,12E-07
Homo_sapiens_tRNA-Pro-TGG-2-1	chr11	76235709	76236021	313	10,98466191	9,781991409	1,199762686	2,15E-07
Homo_sapiens_tRNA-Ser-AGA-5-1	chr7	149608250	149608572	323	6,004592316	3,689692934	2,374459187	4,31E-07
Homo_sapiens_tRNA-Asp-GTC-2-8	chr12	96035895	96036217	323	11,47272147	10,28777869	1,180902744	1,07E-06
Homo_sapiens_tRNA-Pro-AGG-2-4	chr11	76235387	76235699	313	10,70612688	9,540838703	1,161974712	1,38E-06
Homo_sapiens_tRNA-Val-TAC-1-2	chrX	18674783	18675106	324	10,2629545	9,181537597	1,078873415	2,03E-06
Homo_sapiens_tRNA-Cys-GCA-18-1	chr7	149375633	149375955	323	5,728663643	3,193947189	2,55435928	2,05E-06
Homo_sapiens_tRNA-Gly-GCC-4-1	chr1	161480440	161480761	322	5,634558926	3,275848329	2,391172134	9,94E-06
Homo_sapiens_tRNA-Pro-AGG-3-1	chr16	3160259	3160604	346	5,82896848	3,461612822	2,4079772	1,77E-05
Homo_sapiens_tRNA-Ala-TGC-9-1	chr6	28633956	28634279	324	5,07612512	3,014720503	2,08308571	1,82E-05
Homo_sapiens_tRX-Tyr-GTA-1-1	chr14	20669048	20669384	337	5,804137073	3,779470492	2,045917853	2,69E-05
Homo_sapiens_tRNA-Gly-CCC-2-2	chr16	636610	636931	322	11,19517252	10,3504624	0,843429559	2,95E-05
Homo_sapiens_tRNA-Glu-TTC-9-1	chr2	203364280	203364603	324	5,312856569	3,066260873	2,178680331	5,10E-05
Homo_sapiens_tRNA-Ile-TAT-2-1	chr2	42810410	42810753	344	10,52927028	9,798495177	0,730077391	0,000145 58
Homo_sapiens_tRNA-Ala-AGC-17-1	chr6	57861040	57861363	324	5,435964652	3,533961727	1,909845158	0,000273 17
Homo_sapiens_tRNA-Leu-AAG-7-1	chr5	181164435	181164770	336	4,910050822	2,856564941	2,166263432	0,000556 08

Homo_sapiens_tRNA-Cys-GCA-23-1	chr7	149595088	149595410	323	5,524519028	3,753970673	1,739880155	0,000662 65
Homo_sapiens_tRX-Lys-CTT-1-1	chr16	2927535	2927858	324	5,268453056	3,429758003	1,844424261	0,001003 11
Homo_sapiens_tRNA-Lys-CTT-7-1	chr1	54957743	54958066	324	5,11749609	3,275848329	1,859912657	0,002125 11
Homo_sapiens_tRNA-Ser-GCT-3-1	chr11	66347994	66348326	333	10,25981977	9,570188388	0,686193993	0,00244
Homo_sapiens_tRNA-Cys-GCA-16-1	chr7	149546414	149546736	323	5,097852661	3,360862661	1,662435093	0,002490 98
Homo_sapiens_tRNA-Gly-CCC-7-1	chr2	115515851	115518912	312	5,010806691	3,434038619	1,511043284	0,009972 26
Homo_sapiens_tRNA-Glu-CTC-5-1	chr8	58592113	58592434	322	1,766481845	3,889709161	-1,996206717	0,014255 15
Homo_sapiens_tRNA-Gln-CTG-1-1	chr6	188360445	188363667	323	5,134670404	3,887629879	1,264917348	0,017849 91
Homo_sapiens_tRNA-Gln-CTG-8-2	chr1	146055486	146055808	323	4,556254832	3,148582002	1,451739287	0,019610 97
Homo_sapiens_tRNA-Glu-TTC-12-1	chr1	172188272	172188598	327	4,743666219	3,279024564	1,43463234	0,019837 93
Homo_sapiens_tRNA-Asn-GTT-13-1	chr1	168753377	168756661	325	5,257614961	4,277437321	0,982436276	0,045131 56
Homo_sapiens_tRNA-Cys-GCA-15-1	chr7	149584599	149584921	323	5,054065344	3,985329119	1,108201741	0,056215 36
Homo_sapiens_tRNA-Cys-GCA-3-1	chr7	149588947	149589269	323	4,470698157	3,356358976	1,07547989	0,082763 68
Homo_sapiens_tRNA-Leu-TAG-4-1	chr14	20676893	20677225	333	3,955862623	2,69802255	1,159117197	0,088646 14
Homo_sapiens_tRNA-Ser-AGA-6-1	chr11	109165185	109165518	334	4,660926199	3,722189752	0,924006456	0,099333 95
Homo_sapiens_tRX-Leu-TAA-2-1	chr11	113562147	113562481	335	1,663343235	3,107115235	-1,347518853	0,121677 6
Homo_sapiens_tRNA-Phe-GAA-7-1	chr6	27664640	27664966	327	3,865816856	2,628655549	1,21222975	0,132574 29
Homo_sapiens_tRNA-Lys-TTT-11-1	chr12	27690247	27690570	324	2,706488921	3,986301059	-1,115772362	0,144656 44
Homo_sapiens_tRX-Val-AAC-1-1	chr6	158403490	158403813	324	2,575719225	3,694458602	-1,066720836	0,191148 45
Homo_sapiens_tRNA-Gly-GCC-6-1	chr6	142257513	142257834	322	3,233632257	4,219416195	-0,961767898	0,192884 31
Homo_sapiens_tRX-Pro-GGG-1-1	chrX	119603772	119604091	320	1,409041811	2,860810829	-1,300192417	0,195509 72
Homo_sapiens_tRX-Phe-GAA-1-1	chr1	145168278	145168608	331	3,471434702	2,429758003	1,01468565	0,197076 52
Homo_sapiens_tRX-Lys-CTT-4-1	chr7	97141447	97141770	324	2,598803483	3,750542452	-1,040672125	0,206957 39
Homo_sapiens_tRNA-Gln-CTG-10-1	chr1	147005075	147005397	323	2,631434232	3,663755918	-0,962786836	0,208876 5
Homo_sapiens_tRNA-Tyr-GTA-9-1	chr8	65697171	65697509	339	2,898195222	3,866100677	-0,913697187	0,216781 81
Homo_sapiens_tRNA-Asn-GTT-21-1	chr1	148378790	148379114	325	4,216396733	3,359362994	0,777137001	0,222483 36
Homo_sapiens_tRNA-Asn-GTT-28-1	chr1	149639327	149639651	325	2,745948642	3,749397898	-0,907038975	0,242930 92
Homo_sapiens_tRNA-Cys-GCA-24-1	chr17	38833596	38833918	323	4,43058169	3,571412613	0,763703924	0,267801 1
Homo_sapiens_tRNA-Asn-GTT-22-1	chr1	143717166	143717490	325	2,631434232	3,568819584	-0,868953386	0,267801 1
Homo_sapiens_tRNA-Phe-GAA-12-1	chr8	123258356	123258682	327	2,434927987	3,428328304	-0,843467115	0,271745 36
Homo_sapiens_tRNA-Phe-GAA-8-1	chr6	78958167	78958490	324	3,541788444	2,695647563	0,759033406	0,274116 9
Homo_sapiens_tRX-Ser-GGA-2-1	chrX	25261846	25262168	323	1,100114862	2,360862661	-1,158765115	0,275521 19
Homo_sapiens_tRX-Asn-GTT-1-1	chr1	148317243	148317563	321	2,852038071	3,778348669	-0,839608461	0,286861 84
Homo_sapiens_tRNA-Leu-AAG-8-1	chr3	148503315	148503647	333	2,190484987	3,155511288	-0,92546256	0,288948 9
Homo_sapiens_tRNA-Glu-TTC-10-2	chr1	145176813	145177136	324	3,865816856	3,107115235	0,721639571	0,289466 49
Homo_sapiens_tRX-Gln-TTG-1-1	chr8	88132881	88133205	325	2,48242714	3,461612822	-0,884853569	0,304017 98
Homo_sapiens_tRX-Ala-AGC-2-1	chr6	57830046	57830369	324	3,060070663	3,889709161	-0,752994266	0,310813 66
Homo_sapiens_tRNA-SeC-TCA-3-1	chr17	40117174	40117498	325	2,745948642	3,65888757	-0,804280031	0,328509 95
Homo_sapiens_tRNA-Lys-CTT-10-1	chr19	35575722	35576045	324	3,018883166	3,786183173	-0,745728121	0,338794 96
Homo_sapiens_tRNA-Glu-TTC-7-1	chr1	143666862	143667184	323	3,018883166	3,806729891	-0,707213878	0,345893 35
Homo_sapiens_tRX-Und-NNN-6-1	chr9	2959214	2959543	330	2,663343235	3,563619502	-0,795105906	0,346460 08

Homo_sapiens_tRNA-Asn-GTT-20-1	chr1	146049072	146049398	327	4,249165002	3,661323798	0,585376681	0,35828068
Homo_sapiens_tRNA-Gln-TTG-6-1	chr4	40906600	40906923	324	3,78109822	3,108901253	0,636810605	0,35828068
Homo_sapiens_tRNA-Gln-CTG-17-1	chr20	17874372	17874700	329	3,78109822	3,190577789	0,630132353	0,38611628
Homo_sapiens_tRNA-Val-CAC-10-1	chr1	16679880	16680203	324	1,725118974	2,690885828	-0,880748623	0,38643903
Homo_sapiens_tRX-Arg-ACG-1-1	chr8	66112815	66113138	324	2,052714365	3,012813923	-0,795927288	0,38699846
Homo_sapiens_tRNA-Lys-CTT-8-1	chr16	3164812	3165135	324	3,7355714	2,963246296	0,7347634	0,38712299
Homo_sapiens_tRX-Ala-GGC-3-1	chr19	12188435	12188759	325	2,565417583	3,318981614	-0,659552514	0,40459701
Homo_sapiens_tRX-Cys-GCA-1-1	chr7	149405938	149406260	323	3,310081475	2,563619502	0,718898066	0,41808339
Homo_sapiens_tRNA-Cys-GCA-25-1	chr3	176997677	176997707	331	3,227111676	2,429758003	0,739219192	0,42159051
Homo_sapiens_tRNA-Met-CAT-7-1	chr6	57842088	57842411	324	4,169325765	3,60285505	0,519569843	0,42159051
Homo_sapiens_tRX-Gly-CCC-1-2	chr1	148020348	148020669	322	2,994004311	3,721022474	-0,637776459	0,42244523
Homo_sapiens_tRNA-Gly-CCC-8-1	chr1	146488740	146489061	322	2,843537356	3,627410051	-0,643769681	0,43383446
Homo_sapiens_tRX-Lys-CTT-6-1	chr5	168389513	168389835	323	2,420518146	3,234661144	-0,750380789	0,44505365
Homo_sapiens_tRNA-Cys-ACA-1-1	chr5	152608910	152609336	427	3,212219919	3,861870352	-0,592969705	0,45030804
Homo_sapiens_tRNA-Gln-CTG-8-3	chr1	120476726	120477048	323	3,756251773	3,234661144	0,529867188	0,45456245
Homo_sapiens_tRX-Und-NNN-8-1	chr10	62343715	62344039	325	2,994004311	3,60285505	-0,567026932	0,45785528
Homo_sapiens_tRNA-Gly-TCC-5-1	chr18	57678496	57678818	323	0,48242714	0	1,294860037	0,50670355
Homo_sapiens_tRX-Gly-CCC-2-1	chr1	148244341	148244663	323	2,71583402	3,356358976	-0,564220308	0,51378096
Homo_sapiens_tRX-Gln-CTG-2-1	chr11	48065706	48066034	329	3,760773459	3,23792926	0,472232437	0,5147222
Homo_sapiens_tRNA-Ile-GAT-1-1	chrX	3838251	3838575	325	0	0	1,230372688	0,51760983
Homo_sapiens_tRX-Lys-CTT-3-1	chr15	95784519	95784842	324	3,123243608	3,719854251	-0,492420251	0,51760983
Homo_sapiens_tRNA-Pro-AGG-4-1	chr2	87112324	87112646	323	2,986302388	3,688499054	-0,568094381	0,51846226
Homo_sapiens_tRNA-Pro-TGG-5-1	chr1	207004683	207005010	328	2,496234592	3,234661144	-0,576653023	0,51853752
Homo_sapiens_tRNA-Und-GCA-5-1	chr17	68394690	68395015	326	2,745948642	3,354854618	-0,531733915	0,52648158
Homo_sapiens_tRNA-Tyr-ATA-1-1	chr2	218245700	218246043	344	3,241851286	2,69326866	0,520162041	0,54264918
Homo_sapiens_tRX-Trp-CCA-1-1	chr7	67399434	67399756	323	3,390097011	2,814412184	0,466863823	0,54591627
Homo_sapiens_tRNA-Gln-TTG-5-1	chr2	45710176	45710499	324	2,608870289	3,193947189	-0,530511593	0,54857168
Homo_sapiens_tRNA-Tyr-GTA-10-1	chr7	149557916	149558239	324	3,695822864	3,239560546	0,424716678	0,55794517
Homo_sapiens_tRX-Pro-GGG-2-1	chr3	124141746	124142069	324	3,018883166	3,564921281	-0,464451333	0,55918216
Homo_sapiens_tRX-Val-TAC-3-1	chr17	40082554	40082877	324	2,052714365	2,69326866	-0,517562799	0,58999623
Homo_sapiens_tRNA-Arg-CCT-7-1	chr1	143848388	143848709	322	2,745948642	3,350332109	-0,489038395	0,59751256
Homo_sapiens_tRNA-Glu-CTC-7-1	chr2	158881533	158881856	324	3,107233978	3,599047757	-0,434318058	0,59871699
Homo_sapiens_tRNA-Thr-AGT-7-1	chr17	64530674	64530998	325	2,795567995	3,35334869	-0,453540913	0,59871699
Homo_sapiens_tRX-Gln-CTG-3-1	chr1	145563120	145563442	323	3,986302388	3,572707382	0,353255869	0,59871699
Homo_sapiens_tRNA-Asn-GTT-16-1	chr1	148405258	148405582	325	3,114318136	3,597776424	-0,442727669	0,59887958
Homo_sapiens_tRNA-Phe-GAA-6-1	chr6	28763471	28763795	325	4,123243608	3,72452148	0,357808725	0,60008319
Homo_sapiens_tRNA-Asn-GTT-18-1	chr1	165322712	165325916	325	3,076609276	3,536618113	-0,395232305	0,60295351
Homo_sapiens_tRNA-Lys-CTT-9-1	chr5	26198304	26198627	324	3,139077526	3,688499054	-0,420327506	0,60386859
Homo_sapiens_tRNA-Asp-GTC-4-1	chr9	74902948	74903270	323	2,598803483	3,190577789	-0,455058342	0,60542276
Homo_sapiens_tRNA-SeC-TCA-2-1	chr22	44150531	44150865	335	3,212219919	3,690885828	-0,421899587	0,60542276
Homo_sapiens_tRNA-Gln-CTG-8-1	chr1	149044811	149045133	323	3,36497257	2,965219475	0,41475387	0,60542276

Homo_sapiens_tRNA-Gln-CTG-11-1	chr1	143584575	143584897	323	3,220561489	3,663755918	-0,373152921	0,62899657
Homo_sapiens_tRNA-Gln-TTG-10-1	chr6	37320093	37320416	324	2,775447487	3,236296127	-0,405019362	0,63045449
Homo_sapiens_tRNA-Gln-CTG-16-1	chr2	218626291	218626609	319	3,884723661	3,503681452	0,326608392	0,64050616
Homo_sapiens_tRNA-Asp-GTC-10-1	chr1	161523019	161523341	323	3,190484987	3,568819584	-0,353382359	0,64218729
Homo_sapiens_tRNA-Gln-TTG-4-1	chr6	145182597	145182919	323	3,637676866	3,280610064	0,332810535	0,64491204
Homo_sapiens_tRNA-Cys-GCA-20-1	chr7	149597829	149598151	323	3,938936676	3,663755918	0,277295479	0,66036599
Homo_sapiens_tRX-Leu-CAG-1-1	chr9	120354949	120355282	334	3,043340255	3,46300993	-0,355439519	0,67082602
Homo_sapiens_tRNA-Tyr-GTA-11-1	chr7	149356527	149356854	328	3,083845039	3,49960285	-0,356941783	0,67208774
Homo_sapiens_tRNA-Ile-AAT-10-1	chr6	27283959	27284283	325	3,397473451	3,06257927	0,345664678	0,67706886
Homo_sapiens_tRX-Ser-GCT-1-1	chr13	114241213	114241539	327	3,289782062	3,661323798	-0,331398627	0,68203888
Homo_sapiens_tRX-Glu-CTC-1-1	chr8	119131615	119134847	323	2,898195222	3,351841188	-0,348272122	0,68369805
Homo_sapiens_tRNA-His-GTG-2-1	chr1	143661056	143661378	323	3,343828134	3,010904819	0,340120377	0,68545014
Homo_sapiens_tRNA-Gly-TCC-6-1	chr18	57678819	57679141	323	1,331722604	2,012813923	-0,528714761	0,68589106
Homo_sapiens_tRNA-Leu-AAG-5-1	chr2	300545776	300548989	324	3,130249777	3,467193154	-0,321464992	0,69009085
Homo_sapiens_tRNA-Asp-GTC-5-1	chr5	142394297	142394619	323	3,107233978	3,398644798	-0,308891119	0,69178514
Homo_sapiens_tRNA-Asp-GTC-9-1	chr1	161604672	161604994	323	1,82407931	2,282193823	-0,433140565	0,70106814
Homo_sapiens_tRNA-Gln-CTG-13-1	chr5	151868387	151868709	323	3,598803483	3,280610064	0,278333104	0,70314325
Homo_sapiens_tRX-Gly-CCC-3-1	chr1	145437472	145437793	322	2,832695108	3,193947189	-0,328628971	0,70706575
Homo_sapiens_tRNA-Sup-TTA-1-1	chr17	60786106	60786427	322	2,663343235	3,012813923	-0,282505832	0,74691504
Homo_sapiens_tRNA-Asp-GTC-6-1	chr3	184648181	184648502	322	3,401724432	3,060734939	0,301039073	0,74999944
Homo_sapiens_tRX-Und-NNN-9-1	chr22	30308043	30308372	330	3,130249777	3,428328304	-0,255106448	0,75652334
Homo_sapiens_tRNA-Glu-TTC-11-1	chr14	31767483	31767808	326	3,139077526	2,865044258	0,259938995	0,76185684
Homo_sapiens_tRNA-Lys-CTT-11-1	chr19	51922014	51922338	325	3,674251227	4,008993186	-0,246675886	0,76185684
Homo_sapiens_tRX-Asn-GTT-3-1	chr1	146394069	146394393	325	3,123243608	3,429758003	-0,249585403	0,76185684
Homo_sapiens_tRNA-Lys-TTT-14-1	chr14	73588699	73589028	330	3,123243608	3,461612822	-0,232971117	0,76261534
Homo_sapiens_tRNA-Lys-CTT-12-1	chr1	39504394	39504720	327	3,395922435	3,661323798	-0,225563424	0,76474823
Homo_sapiens_tRNA-Ala-TGC-8-1	chr11	50274582	50274904	323	2,694561732	2,922109	-0,274992417	0,76715708
Homo_sapiens_tRNA-Arg-CCT-6-1	chr1	148010933	148011254	322	3,363386197	3,064421246	0,232023939	0,7783195
Homo_sapiens_tRX-Cys-GCA-4-1	chr7	149628027	149628360	334	3,524519028	3,280610064	0,199760015	0,77982282
Homo_sapiens_tRNA-Lys-CTT-16-1	chr15	76382298	76382622	325	2,815411748	3,229745047	-0,280348233	0,79029441
Homo_sapiens_tRNA-Val-AAC-7-1	chr1	180215015	180215338	324	2,804355235	3,103536553	-0,233687044	0,80835295
Homo_sapiens_tRNA-Gln-CTG-4-2	chr1	143691348	143691670	323	3,745948642	3,628655549	0,152710219	0,81729904
Homo_sapiens_tRX-Arg-CCT-2-1	chr11	118241246	118241575	330	3,395922435	3,193947189	0,194824322	0,82014049
Homo_sapiens_tRX-Val-TAC-2-1	chr2	84858626	84858949	324	3,471434702	3,721022474	-0,177626375	0,82159923
Homo_sapiens_tRNA-Gly-GCC-5-1	chr16	70788568	70788889	322	3,587307524	3,753970673	-0,156240135	0,82880368
Homo_sapiens_tRNA-Leu-CAA-5-1	chr11	9275117	9275441	325	3,81425098	4,012813923	-0,158480392	0,83884492
Homo_sapiens_tRX-Cys-GCA-3-1	chr1	161605370	161605691	322	2,994004311	2,755111606	0,192225771	0,84443393
Homo_sapiens_tRNA-Lys-TTT-10-1	chr19	41242111	41242434	324	3,035897931	3,200662474	-0,170068964	0,84607709
Homo_sapiens_tRNA-Pro-GGG-1-1	chr10	22563524	22563847	324	2,916685105	2,805629074	0,174263176	0,85259112
Homo_sapiens_tRNA-Leu-TAA-5-1	chr6	69204360	69204693	334	2,795567995	2,922109	-0,160608764	0,85679283
Homo_sapiens_tRNA-Leu-AAG-6-1	chr20	50335679	50336011	333	3,41479139	3,198986581	0,149552844	0,85872136

Homo_sapiens_tRNA-Lys-CTT-6-1	chr18	46089179	46089502	324	3,427741057	3,657667912	-0,16539878	0,85872136
Homo_sapiens_tRNA-Glu-TTC-10-1	chr1	143784019	143784342	324	0,331722604	0	0,336770676	0,86170705
Homo_sapiens_tRNA-Lys-TTT-12-1	chr19	49534550	49534873	324	3,558853585	3,428328304	0,133191501	0,87742266
Homo_sapiens_tRNA-Asp-GTC-8-1	chr12	122376251	122376572	322	3,297688209	3,465800093	-0,117519998	0,88031138
Homo_sapiens_tRX-Asn-GTT-2-1	chr1	144539524	144539848	325	3,608870289	3,464405686	0,128565337	0,88225957
Homo_sapiens_tRNA-Gln-CTG-7-1	chr1	148328686	148329008	323	3,409041811	3,505038427	-0,116009862	0,88281628
Homo_sapiens_tRNA-Glu-CTC-16-1	chr12	113948614	113948935	322	3,494786252	3,601587068	-0,104711666	0,90099459
Homo_sapiens_tRX-Ile-AAT-4-1	chr17	8205947	8206284	338	2,95085769	3,146844468	-0,113866335	0,90371356
Homo_sapiens_tRNA-Lys-CTT-13-1	chr1	165596787	165597110	324	3,489347384	3,631143322	-0,098829106	0,90489271
Homo_sapiens_tRX-Met-CAT-1-1	chr6	28480600	28480923	324	2,986302388	3,192263472	-0,103899367	0,90781271
Homo_sapiens_tRNA-Cys-GCA-22-1	chr7	149556585	149556905	321	3,809894083	3,72452148	0,074980788	0,91740424
Homo_sapiens_tRX-Lys-CTT-5-1	chr7	126018338	126021702	335	3,553651389	3,467193154	0,081375601	0,91740424
Homo_sapiens_tRNA-Asn-GTT-16-3	chr1	120945163	120945487	325	2,725118974	2,568819584	0,109716734	0,91740424
Homo_sapiens_tRNA-Leu-CAA-6-1	chr1	161611820	161612154	335	3,664631942	3,65888757	0,077050361	0,92708681
Homo_sapiens_tRNA-Und-NNN-2-1	chr8	98141108	98141427	320	3,363386197	3,431186286	-0,08033889	0,92789886
Homo_sapiens_tRNA-Lys-TTT-15-1	chr2	223321471	223321794	324	3,227111676	3,35334869	-0,076816817	0,92924512
Homo_sapiens_tRX-Ala-GGC-4-1	chr16	80445429	80445756	328	2,986302388	3,066260873	-0,068295616	0,93821725
Homo_sapiens_tRX-Lys-TTT-2-1	chr3	152113400	152116606	327	3,324001282	3,275848329	0,064811532	0,94058188
Homo_sapiens_tRNA-Glu-TTC-13-1	chr2	74896793	74897116	324	2,471434702	2,568819584	-0,061694761	0,94757748
Homo_sapiens_tRNA-Gln-CTG-12-1	chr12	74457276	74457599	324	3,575719225	3,563619502	0,04449392	0,95753812
Homo_sapiens_tRNA-Cys-GCA-19-1	chr7	149612939	149613261	323	3,409041811	3,400104202	-0,043393859	0,95753812
Homo_sapiens_tRNA-iMet-CAT-3-1	chr9	194038732	194041907	326	3,620196373	3,597776424	0,040247583	0,96001528
Homo_sapiens_tRNA-Und-NNN-4-1	chr1	7930153	7930473	321	2,795567995	2,862929097	-0,033043057	0,97351115
Homo_sapiens_tRX-Leu-CAA-3-1	chr2	151831012	151831330	319	2,924766734	2,8713712	-0,031649595	0,97351115
Homo_sapiens_tRNA-Ala-AGC-20-1	chr1	150045280	150045601	322	2,994004311	3,058888247	-0,014754764	0,99302992
Homo_sapiens_tRNA-Ile-AAT-11-1	chr12	129231527	129231852	326	3,587307524	3,539269616	0,00803497	0,99483986
Homo_sapiens_tRX-Asp-ATC-1-1	chr6	28827287	28827609	323	3,494786252	3,562316547	-0,008263967	0,99483986
Homo_sapiens_tRX-Und-NNN-7-1	chr3	111349530	111349855	326	3,799968305	3,808929009	-0,00604219	0,99525477
Homo_sapiens_tRX-Cys-GCA-2-1	chr8	100816887	100820088	322	3,001665336	3,012813923	-0,002621147	0,99887386
Homo_sapiens_tRNA-Phe-GAA-9-1	chr1	143792598	143792928	331	0	0	0	1
Homo_sapiens_tRNA-Lys-CTT-15-1	chr11	54759182	54759505	324	0	0	0	1
Homo_sapiens_tRX-Ala-AGC-1-1	chr6	26713543	26713866	324	0	0	0	1
Homo_sapiens_tRX-Ala-AGC-1-2	chr6	26787820	26788143	324	0	0	0	1
Homo_sapiens_tRX-Ile-GAT-2-1	chrX	3838665	3838989	325	0	0	0	1
Homo_sapiens_tRNA-Ile-GAT-1-2	chrX	3876675	3876999	325	0	0	0	1
Homo_sapiens_tRX-Ile-GAT-1-2	chrX	3877089	3877413	325	0	0	0	1
Homo_sapiens_tRNA-Ile-GAT-1-3	chrX	3915104	3915428	325	0	0	0	1
Homo_sapiens_tRX-Ile-GAT-1-1	chrX	3915518	3915842	325	0	0	0	1

Table S8. RPC1 ChIP-Seq peaks at annotated hg38 tRNA genes in human cell lines, and differential RPC1 occupancy in CM relative to hiPSC.

Gene	chr	start	end	length	hiPSC log2 read counts	CM log2 read counts	log2FoldChange	FDR
Homo_sapiens_tRX-Ala-AGC-5-1	chr6	57813364	57813687	324	11,29707539	5,95782317	5,276422959	2,33E-103
Homo_sapiens_tRNA-Ile-AAT-1-1	chr6	57822847	57823171	325	11,15085368	4,856257136	6,183286281	2,14E-98
Homo_sapiens_tRNA-Lys-TTT-9-1	chr6	27575941	27576264	324	10,70530601	5,734863805	4,90866522	9,93E-88
Homo_sapiens_tRNA-Tyr-GTA-4-1	chr14	20657338	20657682	345	10,53292946	5,537939354	4,925489001	8,92E-80
Homo_sapiens_tRNA-Val-AAC-4-1	chr6	27680980	27681303	324	10,45869062	5,875655814	4,530030064	2,63E-79
Homo_sapiens_tRNA-Ala-AGC-19-1	chr6	57793419	57793742	324	10,7754319	6,387945668	4,34004491	1,16E-76
Homo_sapiens_tRNA-Ala-AGC-24-1	chr6	57815848	57816171	324	10,35966868	5,774440393	4,527314325	3,06E-71
Homo_sapiens_tRNA-Thr-AGT-4-1	chr6	27726568	27726892	325	10,72892584	6,948353577	3,745769819	5,10E-68
Homo_sapiens_tRNA-Trp-CCA-3-1	chr6	26318976	26319298	323	10,67464343	7,186984287	3,4591618	2,08E-66
Homo_sapiens_tRX-Ala-AGC-6-1	chr6	57792707	57793030	324	9,993800593	5,365767513	4,56271453	1,34E-64
Homo_sapiens_tRNA-Tyr-GTA-5-3	chr14	20652973	20653317	345	11,34405971	8,167155174	3,153333057	4,11E-61
Homo_sapiens_tRNA-Ala-TGC-6-1	chr6	28758238	28758560	323	10,67157485	7,437965585	3,208317964	7,35E-60
Homo_sapiens_tRNA-Lys-TTT-13-1	chr6	28693084	28693408	325	10,4988134	6,552077498	3,901798379	8,43E-60
Homo_sapiens_tRNA-Thr-AGT-3-1	chr6	28725892	28726216	325	11,24002219	8,050882315	3,164012275	3,57E-58
Homo_sapiens_tRX-Met-CAT-2-1	chr6	57808519	57808843	325	9,958108113	6,13309019	3,781556692	1,14E-56
Homo_sapiens_tRNA-Thr-CGT-6-1	chr6	27303663	27303985	323	11,08941946	7,421688186	3,628187937	6,75E-55
Homo_sapiens_tRNA-Ala-AGC-2-3	chr6	28719578	28719900	323	10,46429853	7,296166747	3,140898996	7,97E-54
Homo_sapiens_tRNA-Tyr-GTA-8-1	chr6	26575444	26575784	341	10,52425615	6,660201126	3,815597856	5,41E-53
Homo_sapiens_tRNA-Lys-CTT-5-1	chr16	3180428	3180751	324	10,57868976	7,277792158	3,269810876	1,12E-51
Homo_sapiens_tRNA-Tyr-GTA-5-4	chr14	20663066	20663410	345	10,95509218	8,020791972	2,909821377	6,42E-49
Homo_sapiens_tRNA-Asn-GTT-26-1	KI270713.1	28630	28953	324	10,72683758	7,175005604	3,510803107	3,38E-48
Homo_sapiens_tRNA-Tyr-GTA-6-1	chr6	26594748	26595087	340	10,65855322	7,56772983	3,061983916	1,00E-46
Homo_sapiens_tRNA-Pro-CGG-1-2	chr16	3171922	3172244	323	10,82882506	7,899799949	2,903019725	1,62E-46
Homo_sapiens_tRNA-Ala-TGC-7-1	chr6	28802674	28802995	322	10,75663401	8,154200115	2,581141671	3,27E-45
Homo_sapiens_tRNA-Val-TAC-4-1	chr6	27290500	27290823	324	11,27988443	8,628849311	2,628474232	1,74E-44
Homo_sapiens_tRNA-Ala-AGC-5-1	chr6	28710463	28710785	323	10,7854138	8,112349286	2,650555068	3,84E-44
Homo_sapiens_tRNA-Lys-CTT-2-5	chr16	3175565	3175888	324	11,31009693	8,877527209	2,411364906	1,19E-42
Homo_sapiens_tRNA-Leu-AAG-1-3	chr5	181173918	181174250	333	11,22695381	8,401511767	2,798842741	9,54E-42
Homo_sapiens_tRNA-Lys-TTT-6-1	chr6	27334864	27335187	324	11,17153125	8,28183745	2,859151317	3,98E-38
Homo_sapiens_tRNA-Ser-AGA-4-1	chr6	27553287	27553619	333	11,25105268	8,816394144	2,410785279	5,56E-38
Homo_sapiens_tRNA-Gly-CCC-1-2	chr1	16861795	16862116	322	11,07198632	8,347872418	2,696407591	6,85E-38
Homo_sapiens_tRNA-Arg-TCT-3-1	chr9	128339950	128340291	342	10,39826207	7,814904117	2,556721849	1,06E-36
Homo_sapiens_tRNA-Und-TTA-3-1	chr1	161420745	161421068	324	9,338109806	5,104149408	4,141132018	2,95E-36
Homo_sapiens_tRNA-Lys-TTT-2-1	chr11	122559821	122560144	324	10,99232721	6,748962385	4,150356705	6,73E-36
Homo_sapiens_tRNA-Trp-CCA-5-1	chr7	99469558	99469880	323	8,76745567	4,383931647	4,277217274	9,14E-36
Homo_sapiens_tRNA-Ala-AGC-21-1	chr6	26749786	26750109	324	9,07796108	4,379906426	4,565734549	1,79E-35
Homo_sapiens_tRNA-Val-AAC-6-1	chr6	28735303	28735625	323	10,64106583	8,17094014	2,443804397	6,00E-35
Homo_sapiens_tRNA-Lys-TTT-7-1	chr6	28747618	28747941	324	11,33599014	8,661704304	2,64420388	4,92E-34
Homo_sapiens_tRNA-Ser-AGA-1-1	chr6	27541649	27541981	333	9,877519804	6,891973383	2,948302572	5,13E-34
Homo_sapiens_tRNA-Phe-GAA-5-1	chr6	28764261	28764588	328	8,765488316	4,791936707	3,890137304	1,33E-32

Homo_sapiens_tRNA-Gly-CCC-5-1	chr1	167271590	167274800	322	10,19707335	7,32532135	2,834958265	4,20E-32
Homo_sapiens_tRNA-Cys-GCA-13-1	chr7	149355549	149355871	323	10,69087464	5,261496597	5,209809105	8,61E-32
Homo_sapiens_tRNA-Ser-TGA-4-1	chr6	27505702	27506034	333	11,62494725	9,141830711	2,45239303	1,33E-30
Homo_sapiens_tRNA-Glu-TTC-6-1	chr1	148308796	148309118	323	10,95827429	8,747836637	2,182141676	2,05E-30
Homo_sapiens_tRNA-Thr-CGT-5-1	chr6	27618230	27618554	325	11,19228625	9,064170525	2,09937976	1,59E-29
Homo_sapiens_tRNA-Glu-TTC-14-1	KI270713.1	31510	31831	322	9,821791222	7,016753282	2,766505367	2,84E-29
Homo_sapiens_tRNA-Arg-TCT-5-1	chr6	27562058	27562395	338	8,537897192	4,955458398	3,510464429	2,29E-28
Homo_sapiens_tRNA-Ile-AAT-5-3	chr6	27237445	27237769	325	11,46631593	9,467884233	1,968943517	4,33E-28
Homo_sapiens_tRNA-Leu-TAA-2-1	chr6	27720993	27721326	334	10,68033116	8,52787807	2,121887111	4,89E-28
Homo_sapiens_tRNA-Val-TAC-3-1	chr10	5853585	5853908	324	10,07312871	7,510524127	2,527346466	1,27E-27
Homo_sapiens_tRNA-Arg-CCG-1-1	chr6	28742826	28743149	324	10,76551409	8,584686269	2,148301952	1,30E-26
Homo_sapiens_tRNA-Ile-AAT-12-1	chr6	57800085	57800409	325	11,31151842	8,819780499	2,45532289	2,39E-26
Homo_sapiens_tRNA-Phe-GAA-1-1	chr6	28790596	28790919	324	10,59970043	8,533655808	2,033399359	5,74E-26
Homo_sapiens_tRNA-Ile-TAT-3-1	chr6	28537464	28537808	345	11,35411352	7,884548113	3,393855356	5,19E-25
Homo_sapiens_tRNA-His-GTG-1-5	chr6	27158001	27158323	323	10,24232297	8,235744549	1,971397851	5,90E-24
Homo_sapiens_tRNA-Ser-AGA-2-4	chr6	27502913	27503245	333	11,06886145	9,31648121	1,718771917	9,76E-23
Homo_sapiens_tRNA-Asn-GTT-5-1	chr1	165204599	165207833	325	9,473140649	7,052378754	2,377374281	3,83E-22
Homo_sapiens_tRNA-Ala-AGC-16-1	chr6	57870219	57870542	324	8,263044186	4,60230973	3,559486118	8,48E-22
Homo_sapiens_tRNA-Pro-TGG-3-4	chr16	3184007	3184329	323	10,39043164	8,646887056	1,708529107	9,94E-22
Homo_sapiens_tRNA-Ala-CGC-5-1	chr6	28695806	28696128	323	8,442136781	4,992128453	3,365860909	1,59E-21
Homo_sapiens_tRNA-Val-CAC-11-2	chr1	168600072	168600395	324	9,608102898	7,483741598	2,082634641	6,38E-21
Homo_sapiens_tRNA-Arg-TCG-4-1	chr6	26299551	26299874	324	10,13591864	8,238659565	1,856022836	4,54E-20
Homo_sapiens_tRNA-iMet-CAT-2-1	chr6	27777759	27778081	323	10,32036877	6,65126917	3,555729866	1,03E-19
Homo_sapiens_tRNA-Cys-GCA-11-1	chr7	149415012	149415334	323	9,295579556	6,805664377	2,438687401	1,59E-19
Homo_sapiens_tRNA-Ala-AGC-6-1	chr6	28811946	28812268	323	10,61066504	8,91632596	1,655852125	1,74E-19
Homo_sapiens_tRNA-Ser-GCT-1-1	chr6	27097180	27097512	333	10,49500167	8,788338342	1,666999914	4,83E-19
Homo_sapiens_tRNA-Ser-CGA-3-1	chr6	27672324	27672656	333	11,59264317	9,607851271	1,939558203	6,13E-19
Homo_sapiens_tRNA-Lys-CTT-14-1	chr16	3196027	3196350	324	8,730441903	6,230600733	2,447521345	7,89E-19
Homo_sapiens_tRNA-Ser-GCT-2-1	chr6	27297870	27298202	333	11,53640612	9,982690776	1,517062395	1,98E-18
Homo_sapiens_tRNA-Ile-TAT-1-1	chr19	39412042	39412385	344	9,014914203	10,59424234	-1,538285777	8,03E-18
Homo_sapiens_tRNA-Lys-CTT-4-1	chr16	3191375	3191698	324	10,41658736	8,833575897	1,543267278	1,29E-17
Homo_sapiens_tRNA-Ala-AGC-8-2	chr8	66114201	66114386	186	9,339609439	10,8378043	-1,460332684	3,26E-17
Homo_sapiens_tRNA-Asn-GTT-10-1	chr1	145129113	145129437	325	9,015205905	5,311935479	3,567989647	3,46E-17
Homo_sapiens_tRNA-Gly-CCC-1-1	chr1	165458133	165461344	322	11,33589704	9,505832144	1,779895319	2,43E-16
Homo_sapiens_tRNA-Pro-AGG-1-1	chr16	3191863	3192185	323	9,86734284	8,21517284	1,606480039	5,15E-16
Homo_sapiens_tRNA-Val-CAC-1-4	chr5	181173524	181173847	324	10,62205708	8,938525347	1,635987824	7,39E-16
Homo_sapiens_tRNA-Cys-GCA-9-3	chr7	149635561	149635883	323	10,18668869	6,971571402	3,109265144	3,58E-15
Homo_sapiens_tRNA-Leu-AAG-3-1	chr6	28988876	28989208	333	9,84012252	8,024899944	1,76130603	3,95E-15
Homo_sapiens_tRNA-Gly-CCC-3-1	chr17	19860736	19861057	322	7,370061767	4,015618704	3,225882489	4,08E-14
Homo_sapiens_tRNA-Glu-TTC-3-1	chr1	168724577	168727799	323	11,46120211	9,618788831	1,782874907	4,54E-14
Homo_sapiens_tRNA-Phe-GAA-4-1	chr6	28823190	28823514	325	7,427670251	3,894091698	3,385779587	5,88E-14

Homo_sapiens_tRNA-Ser-CGA-2-1	chr6	27209723	27210055	333	7,853538898	5,387444525	2,392884628	5,97E-14
Homo_sapiens_tRNA-Leu-TAA-4-1	chr6	27230429	27230762	334	11,74568185	10,21886661	1,47647443	2,32E-13
Homo_sapiens_tRNA-Gln-CTG-4-1	chr1	148264982	148265304	323	10,06074333	8,35594906	1,645723649	2,65E-13
Homo_sapiens_tRNA-Ser-TGA-2-1	chr6	27545563	27545895	333	11,42773114	9,973364241	1,406918796	3,33E-13
Homo_sapiens_tRNA-Ile-TAT-2-1	chr2	42810410	42810753	344	10,52927028	11,93091037	-1,35701245	3,63E-13
Homo_sapiens_tRNA-Tyr-GTA-7-1	chr14	20659832	20660176	345	7,227547731	3,824825538	3,257624275	6,02E-13
Homo_sapiens_tRNA-Gln-TTG-3-1	chr6	26311070	26311392	323	9,70481235	8,187560117	1,465328503	8,81E-13
Homo_sapiens_tRNA-Val-CAC-7-1	chr6	27728422	27728745	324	7,112167985	3,827783662	3,145663784	2,10E-12
Homo_sapiens_tRNA-Cys-GCA-9-1	chr3	132231672	132231994	323	8,977846057	11,66644146	-2,593721821	2,27E-12
Homo_sapiens_tRNA-Gly-GCC-2-4	chr16	70778913	70779234	322	9,140263626	10,74689685	-1,546678286	2,32E-12
Homo_sapiens_tRNA-Cys-GCA-17-1	chr7	149691055	149691377	323	10,74447054	9,160838813	1,524865657	3,43E-12
Homo_sapiens_tRNA-Asn-GTT-6-1	chr1	143735794	143736118	325	7,937588783	6,145865012	1,721354578	6,17E-12
Homo_sapiens_tRNA-Val-CAC-6-1	chr6	27205962	27206285	324	8,165237853	6,062133906	2,0192906	2,46E-11
Homo_sapiens_tRNA-Cys-GCA-9-2	chr7	149331003	149331325	323	8,765938122	6,773290034	1,91102458	2,75E-11
Homo_sapiens_tRNA-Cys-GCA-2-1	chr4	123508724	123509046	323	7,886345464	5,455855056	2,330336016	7,00E-11
Homo_sapiens_tRNA-Lys-TTT-8-1	chr1	205474017	205474340	324	7,254705888	4,384936199	2,744812009	9,42E-11
Homo_sapiens_tRNA-Trp-CCA-4-1	chr12	98504126	98504448	323	10,6583185	11,92481829	-1,219967369	1,03E-10
Homo_sapiens_tRNA-Glu-TTC-4-1	chr1	165351453	165354775	323	11,86403445	10,40056643	1,403199316	1,12E-10
Homo_sapiens_tRNA-Asn-GTT-2-6	chr19	1383559	1383761	203	10,41102439	11,53789476	-1,089706368	1,32E-10
Homo_sapiens_tRNA-Asn-GTT-4-1	chr1	168895551	168898875	325	10,86473047	9,6974615	1,126737427	2,73E-10
Homo_sapiens_tRNA-Gln-CTG-5-1	chr6	27295307	27295629	323	11,0845295	9,896440757	1,144855794	4,41E-10
Homo_sapiens_tRNA-Cys-GCA-12-1	chr7	149646829	149647151	323	8,38858823	6,594531416	1,709180918	4,90E-10
Homo_sapiens_tRNA-Und-NNN-1-1	chr6	26749073	26749397	325	6,609080097	2,028532444	4,156770266	5,48E-10
Homo_sapiens_tRNA-Pro-AGG-2-7	chr16	3182509	3182831	323	11,23556866	10,05252154	1,139967718	5,48E-10
Homo_sapiens_tRNA-Ile-AAT-9-1	chr6	27273834	27274158	325	6,633162001	3,341174313	3,112319628	5,99E-10
Homo_sapiens_tRNA-Leu-AAG-4-1	chr6	28478497	28478829	333	7,362593829	4,987506431	2,264624942	5,99E-10
Homo_sapiens_tRNA-Asn-GTT-14-1	chr1	148048390	148048714	325	10,36115535	9,206085507	1,113856139	6,38E-10
Homo_sapiens_tRNA-Phe-GAA-3-1	chr6	28807707	28808030	324	11,26108215	10,19104075	1,034871025	7,91E-10
Homo_sapiens_tRNA-Ser-AGA-3-1	chr6	27532082	27532414	333	6,72036836	3,604898641	2,951797151	7,93E-10
Homo_sapiens_tRNA-Ile-AAT-3-1	chr6	27275085	27275409	325	8,117290647	6,146753633	1,87580877	1,01E-09
Homo_sapiens_tRNA-Gly-GCC-3-1	chr16	70778085	70778406	322	7,065716255	8,920265663	-1,764524705	1,07E-09
Homo_sapiens_tRNA-Phe-GAA-11-1	chr6	28726952	28727275	324	7,051391538	4,185255416	2,717222539	1,44E-09
Homo_sapiens_tRNA-Ala-TGC-1-1	chr6	28789644	28789966	323	11,11248879	9,914286839	1,151032182	1,89E-09
Homo_sapiens_tRNA-Cys-GCA-14-1	chr17	38861558	38861880	323	10,10269242	7,549055909	2,427710439	2,11E-09
Homo_sapiens_tRNA-Asn-GTT-2-5	chr17	38751655	38751979	325	10,72310352	11,84914096	-1,083579684	2,82E-09
Homo_sapiens_tRNA-Cys-GCA-5-1	chr15	79744529	79744852	324	9,369784295	7,965217484	1,337667205	4,25E-09
Homo_sapiens_tRNA-SeC-TCA-1-1	chr19	45478475	45478812	338	9,935590468	10,98815496	-1,014218173	4,33E-09
Homo_sapiens_tRNA-Gly-CCC-2-2	chr16	636610	636931	322	11,19517252	12,40038675	-1,155177895	4,35E-09
Homo_sapiens_tRNA-His-GTG-1-1	chr1	146037918	146038240	323	10,35935821	11,41806961	-1,019528046	6,90E-09
Homo_sapiens_tRNA-Arg-ACG-2-2	chr6	27213718	27214041	324	10,08398454	8,83527299	1,192860021	8,89E-09
Homo_sapiens_tRNA-Val-CAC-14-1	chr1	145157031	145157354	324	9,014819471	10,10032009	-1,042869867	1,07E-08

Homo_sapiens_tRNA-Asp-GTC-3-1	chr6	27583331	27583653	323	11,23128633	10,00599791	1,168820127	2,24E-08
Homo_sapiens_tRNA-Phe-GAA-1-6	chr19	1383236	1383437	202	9,812551172	10,9527135	-1,090363349	2,68E-08
Homo_sapiens_tRNA-Cys-GCA-10-1	chr7	149377384	149377706	323	6,895113617	4,476229087	2,279317921	2,84E-08
Homo_sapiens_tRNA-Leu-CAA-3-1	chr6	27602443	27602800	358	11,29753246	8,351019519	2,763436764	2,91E-08
Homo_sapiens_tRNA-Trp-CCA-3-2	chr6	26331318	26331640	323	10,77517817	9,601285709	1,120415713	4,34E-08
Homo_sapiens_tRNA-Asn-GTT-25-1	chr1	149558293	149558618	326	9,91469095	8,568996847	1,273019407	6,88E-08
Homo_sapiens_tRNA-His-GTG-1-2	chr1	147073099	147073421	323	7,835789017	5,860596617	1,849521394	7,37E-08
Homo_sapiens_tRNA-Thr-AGT-2-2	chr6	27684569	27684893	325	11,63981075	10,4233369	1,156345261	8,11E-08
Homo_sapiens_tRNA-Ala-AGC-15-1	chr14	88978972	88979295	324	10,63791206	9,519196438	1,067281046	1,23E-07
Homo_sapiens_tRNA-Gln-TTG-3-2	chr6	26311621	26311943	323	10,92879976	9,944062411	0,946064898	1,33E-07
Homo_sapiens_tRNA-Ser-AGA-2-5	chr8	95269531	95269863	333	11,27047261	12,38621383	-1,063564795	1,61E-07
Homo_sapiens_tRNA-Glu-TTC-8-1	chr1	149692679	149693002	324	6,817438699	4,184101684	2,457822306	1,61E-07
Homo_sapiens_tRX-Ile-AAT-3-1	chr6	27260805	27261130	326	6,883030837	4,60230973	2,126650428	1,94E-07
Homo_sapiens_tRNA-Ile-TAT-2-3	chr6	27631295	27631639	345	11,50343328	10,43338363	1,021629222	2,25E-07
Homo_sapiens_tRNA-Ser-ACT-1-1	chr6	27293766	27294090	325	11,35807014	10,31197348	1,000031495	2,31E-07
Homo_sapiens_tRNA-Ser-GCT-4-1	chr6	28597214	28597546	333	10,99375456	10,03250014	0,92298918	2,99E-07
Homo_sapiens_tRNA-Ser-CGA-1-1	chr17	8138755	8139087	333	10,05626691	11,01611749	-0,920289683	3,59E-07
Homo_sapiens_tRNA-Cys-GCA-21-1	chr7	149664698	149665020	323	7,930983215	6,108108851	1,694854982	3,59E-07
Homo_sapiens_tRNA-Val-CAC-11-1	chr1	165475339	165478662	324	9,240786165	7,871457831	1,284095296	5,01E-07
Homo_sapiens_tRNA-Asn-GTT-9-1	chr1	145475255	145475579	325	10,32035276	9,366843541	0,914660761	5,12E-07
Homo_sapiens_tRNA-Pro-AGG-2-8	chr16	3189508	3189830	323	11,21614669	10,27623905	0,902042571	5,50E-07
Homo_sapiens_tRNA-Val-CAC-9-1	chr6	27150117	27150440	324	6,361750631	3,824825538	2,345862757	6,26E-07
Homo_sapiens_tRNA-Arg-ACG-2-3	chr6	27215047	27215370	324	10,55173649	9,695165905	0,826131346	7,83E-07
Homo_sapiens_tRNA-Glu-TTC-5-1	chr1	161612592	161612914	323	10,38398817	11,29325644	-0,872378069	9,55E-07
Homo_sapiens_tRNA-Val-AAC-1-3	chr5	181169484	181169807	324	10,59823787	9,705989147	0,857740426	1,06E-06
Homo_sapiens_tRNA-Lys-TTT-4-1	chr6	27591688	27592011	324	11,40297223	10,42775168	0,930183514	1,71E-06
Homo_sapiens_tRNA-Tyr-GTA-3-1	chr6	26576978	26577317	340	9,644187278	8,502055428	1,075686085	2,69E-06
Homo_sapiens_tRNA-Ala-TGC-5-1	chr6	28817109	28817431	323	10,74044802	9,841314962	0,860578078	3,18E-06
Homo_sapiens_tRNA-Arg-CCT-4-1	chr7	139340574	139340897	324	11,17085713	12,2475483	-1,015374182	4,51E-06
Homo_sapiens_tRNA-Gln-CTG-6-1	chr6	27791230	27791552	323	11,4228457	10,5886492	0,800866063	5,47E-06
Homo_sapiens_tRNA-Val-TAC-1-2	chrX	186747783	186751066	324	10,2629545	11,32228336	-0,999008015	5,83E-06
Homo_sapiens_tRNA-Ser-CGA-4-1	chr12	56190238	56190570	333	10,13137511	11,06799841	-0,890878421	6,10E-06
Homo_sapiens_tRNA-Arg-CCT-1-1	chr17	75033780	75034103	324	10,8323539	11,72356875	-0,850846132	6,38E-06
Homo_sapiens_tRNA-iMet-CAT-1-2	chr6	26286400	26286722	323	9,356544582	10,40802878	-0,99092753	6,45E-06
Homo_sapiens_tRNA-Tyr-GTA-5-1	chr8	66113241	66113584	344	11,07890264	12,14932785	-1,00715762	7,65E-06
Homo_sapiens_tRNA-Ser-GCT-3-1	chr11	66347994	66348326	333	10,25981977	11,26364138	-0,946392916	1,42E-05
Homo_sapiens_tRNA-Ser-TGA-3-1	chr6	26312470	26312802	333	11,58425353	10,75220191	0,795828697	1,45E-05
Homo_sapiens_tRNA-Cys-GCA-8-1	chr14	72962845	72963167	323	9,977397001	8,417342205	1,419812647	1,48E-05
Homo_sapiens_tRNA-Cys-GCA-9-4	chr7	149707543	149707865	323	7,883566767	9,139712119	-1,159535136	1,56E-05
Homo_sapiens_tRNA-Val-CAC-3-1	chr19	4724509	4724832	324	10,27892425	11,06015262	-0,749358201	1,67E-05
Homo_sapiens_tRNA-Ala-AGC-17-1	chr6	57861040	57861363	324	5,435964652	2,233928531	2,822127016	1,72E-05

Homo_sapiens_tRNA-Gln-CTG-9-1	chr1	148353435	148353757	323	10,99914889	10,03944411	0,907059143	1,83E-05
Homo_sapiens_tRNA-Glu-TTC-4-2	chr1	161421967	161422289	323	11,18267114	10,32672823	0,815707928	2,05E-05
Homo_sapiens_tRNA-Arg-TCG-6-1	chr9	110198397	110198720	324	5,925304435	3,603173216	2,076433281	2,65E-05
Homo_sapiens_tRNA-Arg-ACG-2-4	chr6	27670439	27670762	324	11,30021925	10,39634543	0,855963218	3,11E-05
Homo_sapiens_tRNA-Val-AAC-1-2	chr5	181164028	181164351	324	8,283982677	7,095442475	1,098943928	3,11E-05
Homo_sapiens_tRNA-Pro-AGG-3-1	chr16	3160259	3160604	346	5,82896848	3,020798079	2,48116559	3,35E-05
Homo_sapiens_tRNA-Ala-TGC-2-1	chr6	28643319	28643641	323	10,56491647	9,725617537	0,798768694	3,67E-05
Homo_sapiens_tRNA-Lys-CTT-3-1	chr16	3157279	3157602	324	11,27144681	10,35186944	0,868497747	3,84E-05
Homo_sapiens_tRNA-Phe-GAA-1-2	chr6	28981546	28981869	324	10,06549944	10,9683843	-0,852042013	5,21E-05
Homo_sapiens_tRNA-Cys-GCA-6-1	chr3	132228974	132229296	323	7,531130032	8,805152076	-1,161400393	6,15E-05
Homo_sapiens_tRNA-Gln-CTG-1-4	chr15	65868936	65869258	323	11,3582831	12,30375567	-0,887949476	6,15E-05
Homo_sapiens_tRNA-Leu-CAA-2-1	chr6	27605512	27605870	359	11,27097963	10,36922008	0,850156642	6,83E-05
Homo_sapiens_tRNA-Ile-AAT-8-1	chr6	27668457	27668781	325	11,47107249	10,76700387	0,676702405	7,07E-05
Homo_sapiens_tRNA-Glu-TTC-1-1	chr2	130337002	130337324	323	10,8954842	11,79989143	-0,849048159	0,000118886
Homo_sapiens_tRNA-Gly-CCC-2-1	chr2	70248865	70249186	322	11,44077384	12,36449528	-0,865386017	0,000120062
Homo_sapiens_tRNA-Asp-GTC-2-8	chr12	96035895	96036217	323	11,47272147	12,44378911	-0,905254515	0,000121658
Homo_sapiens_tRNA-Glu-CTC-1-7	chr6	125780121	125780443	323	11,47070305	12,3746439	-0,847697581	0,000139409
Homo_sapiens_tRNA-Pro-TGG-4-1	chr16	3170834	3171155	322	5,96229001	3,889851953	1,803589396	0,000147554
Homo_sapiens_tRNA-Lys-CTT-2-4	chr6	26556420	26556743	324	11,64969125	10,79789794	0,802412759	0,000163472
Homo_sapiens_tRNA-Ile-AAT-5-4	chr14	102316966	102317290	325	11,51351531	12,32086766	-0,763912181	0,00016942
Homo_sapiens_tRNA-Leu-TAG-3-1	chr16	22195585	22195917	333	10,86380681	11,730913	-0,815024894	0,00016942
Homo_sapiens_tRNA-Asn-GTT-11-1	chr1	120952165	120952489	325	6,516163159	4,561198779	1,699986011	0,000187151
Homo_sapiens_tRNA-Val-AAC-5-1	chr6	27235383	27235706	324	10,54455343	9,733660521	0,766135361	0,000210156
Homo_sapiens_tRNA-Glu-CTC-2-1	chr1	248874122	248874444	323	10,99861657	11,78897568	-0,747589689	0,000227072
Homo_sapiens_tRNA-Pro-CGG-1-1	chr1	167714599	167714921	323	11,44178475	12,30903641	-0,813213964	0,000232986
Homo_sapiens_tRNA-Thr-AGT-1-3	chr19	33176931	33177255	325	11,68948929	12,48467798	-0,7514992	0,000244586
Homo_sapiens_tRNA-Ile-AAT-6-1	chr6	26756426	26756750	325	6,512637396	5,212063086	1,168647026	0,00025912
Homo_sapiens_tRNA-Glu-TTC-2-2	chr15	26082108	26082430	323	11,33352746	12,14217247	-0,762050846	0,000285492
Homo_sapiens_tRNA-Met-CAT-1-1	chr8	123157104	123157427	324	11,25236453	12,1243839	-0,815815874	0,000287294
Homo_sapiens_tRNA-Ser-TGA-1-1	chr10	67764377	67764709	333	11,52514109	12,32722456	-0,75637138	0,000291538
Homo_sapiens_tRNA-Cys-GCA-2-3	chr17	39153608	39153930	323	11,33006399	12,12068772	-0,746415813	0,000292893
Homo_sapiens_tRNA-Ser-GCT-5-1	chr6	28212911	28213243	333	11,10473372	10,35464056	0,711797595	0,000292893
Homo_sapiens_tRNA-Thr-CGT-4-1	chr17	31549948	31550270	323	11,08312912	11,84384668	-0,719737238	0,000351625
Homo_sapiens_tRNA-Ile-AAT-5-2	chr6	27177089	27177413	325	10,59530278	11,41514951	-0,770012429	0,000364848
Homo_sapiens_tRNA-Lys-CTT-2-3	chr5	181221853	181222176	324	11,56439924	10,7270151	0,784952998	0,000366329
Homo_sapiens_tRNA-Phe-GAA-1-5	chr13	94549524	94549847	324	11,1367651	11,87463972	-0,699409099	0,000397306
Homo_sapiens_tRNA-Lys-TTT-3-1	chr1	204506401	204506724	324	10,86433659	11,69367235	-0,776167863	0,000474979
Homo_sapiens_tRNA-Asn-GTT-2-4	chr13	30673838	30674162	325	11,17367003	11,83929161	-0,635369169	0,000490255
Homo_sapiens_tRNA-Leu-TAA-1-1	chr6	144216421	144216754	334	11,22592527	11,99627309	-0,726105305	0,000492554
Homo_sapiens_tRNA-Leu-CAA-4-1	chr1	248873729	248874085	357	11,44279206	12,15074757	-0,672236938	0,000505436
Homo_sapiens_tRNA-Glu-CTC-3-1	chr13	41455799	41456122	324	6,621026399	5,212063086	1,232280284	0,000611533

Homo_sapiens_tRNA-Gly-CCC-4-1	chr1	16678145	16678466	322	11,23831067	10,44875107	0,740821496	0,000651483
Homo_sapiens_tRNA-Arg-CCT-5-1	chr16	3193792	3194115	324	5,724888494	3,892679834	1,552994123	0,000653757
Homo_sapiens_tRNA-Cys-GCA-2-4	chr17	39154365	39154687	323	11,59533973	12,43070606	-0,778791391	0,000657409
Homo_sapiens_tRNA-Gln-TTG-1-1	chr17	49192402	49192724	323	11,58315019	12,35620148	-0,726187911	0,000703052
Homo_sapiens_tRNA-Val-AAC-1-1	chr3	169772104	169772427	324	10,88905479	11,73098753	-0,783376364	0,000731088
Homo_sapiens_tRNA-Gly-TCC-1-1	chr19	4723944	4724266	323	11,08817937	11,89871323	-0,756855879	0,000765613
Homo_sapiens_tRNA-Thr-CGT-2-1	chr16	14285767	14286089	323	11,13526756	11,73783727	-0,577715486	0,000800661
Homo_sapiens_tRNA-Phe-GAA-1-3	chr11	59557371	59557694	324	10,90634776	10,23767336	0,636150774	0,000805429
Homo_sapiens_tRNA-Arg-ACG-1-3	chr14	22929575	22929898	324	11,22630002	11,99216983	-0,71889306	0,00081942
Homo_sapiens_tRNA-Glu-TTC-2-1	chr13	44917801	44918123	323	11,59017722	12,35079832	-0,714337251	0,000838676
Homo_sapiens_tRNA-Pro-TGG-2-1	chr11	76235709	76236021	313	10,98466191	11,79228084	-0,753620815	0,000850022
Homo_sapiens_tRX-Glu-TTC-2-1	chr1	121000862	121001185	324	5,735035922	3,887018519	1,550743028	0,000850022
Homo_sapiens_tRNA-Pro-AGG-2-4	chr11	76235387	76235699	313	10,70612688	11,541757	-0,776336166	0,000886715
Homo_sapiens_tRNA-Arg-TCT-3-2	chr11	59551184	59551504	321	9,26264572	8,502629628	0,713087354	0,001011494
Homo_sapiens_tRX-Tyr-GTA-1-1	chr14	20669048	20669384	337	5,804137073	4,013022026	1,50150877	0,001011786
Homo_sapiens_tRNA-Val-CAC-1-8	chr1	121020603	121020926	324	10,0697121	10,71435336	-0,613350572	0,001038276
Homo_sapiens_tRNA-Arg-TCG-1-1	chr15	89334947	89335270	324	11,44097634	12,22039783	-0,728325468	0,001060327
Homo_sapiens_tRNA-Ala-CGC-3-1	chr2	156400643	156400965	323	10,56232298	11,33944954	-0,725873272	0,001144135
Homo_sapiens_tRNA-Lys-TTT-3-5	chr17	8119029	8119352	324	11,29747744	12,04141119	-0,69799849	0,001145046
Homo_sapiens_tRNA-Arg-CCG-2-1	chr17	68019771	68020094	324	11,30601443	11,91588622	-0,58247158	0,001212103
Homo_sapiens_tRNA-Leu-TAG-2-1	chr14	20625244	20625576	333	11,82810828	11,06708096	0,711692384	0,001272262
Homo_sapiens_tRNA-Trp-CCA-2-1	chr17	19508055	19508377	323	11,48694706	12,24690594	-0,710598225	0,001275609
Homo_sapiens_tRNA-Asn-GTT-2-1	chr1	148529131	148529455	325	11,22067244	10,51369266	0,66595234	0,001318554
Homo_sapiens_tRNA-Asn-GTT-2-3	chr10	22229383	22229707	325	11,54482658	12,27257242	-0,683118899	0,001352624
Homo_sapiens_tRNA-Asn-GTT-13-1	chr1	16875337	16875661	325	5,257614961	3,341174313	1,573381455	0,001524646
Homo_sapiens_tRNA-Gln-CTG-1-5	chr17	8119626	8119948	323	11,22725853	11,85379461	-0,59491833	0,001801899
Homo_sapiens_tRNA-Ala-TGC-9-1	chr6	28633956	28634279	324	5,07612512	3,341174313	1,427255961	0,001881824
Homo_sapiens_tRNA-Gly-GCC-2-2	chr2	156401021	156401342	322	11,38974595	12,15770982	-0,713900571	0,001918453
Homo_sapiens_tRNA-Leu-CAG-1-7	chr6	26521082	26521415	334	10,53670561	11,28593484	-0,698023587	0,001949921
Homo_sapiens_tRNA-Glu-TTC-9-1	chr2	203364280	203364603	324	5,312856569	3,435189172	1,531793752	0,001980877
Homo_sapiens_tRNA-Gly-GCC-4-1	chr1	161480440	161480761	322	5,634558926	3,818891032	1,482888784	0,002076444
Homo_sapiens_tRNA-Met-CAT-6-1	chr16	87383896	87384219	324	11,50652176	12,10982434	-0,574195976	0,002079924
Homo_sapiens_tRNA-Leu-CAG-2-2	chr16	57300354	57300687	334	11,60718904	12,400813	-0,733801932	0,002096886
Homo_sapiens_tRNA-Ala-AGC-2-2	chr6	28863559	28863881	323	11,30835566	11,98226444	-0,634520984	0,002112904
Homo_sapiens_tRNA-Asn-GTT-2-2	chr1	161427951	161428275	325	11,4654014	10,82921888	0,602163284	0,002264791
Homo_sapiens_tRNA-Met-CAT-2-1	chr16	71426367	71426690	324	11,34274382	10,63623934	0,661225099	0,002391316
Homo_sapiens_tRNA-Ile-AAT-4-1	chr17	8226865	8227189	325	10,68555561	11,41358603	-0,678707043	0,002393057
Homo_sapiens_tRNA-Gln-CTG-2-1	chr6	27547626	27547948	323	10,61226895	9,995427425	0,585191699	0,002418977
Homo_sapiens_tRNA-Asp-GTC-2-9	chr12	124927219	124927541	323	9,984128314	10,6391832	-0,61715163	0,002440719
Homo_sapiens_tRNA-His-GTG-1-7	chr15	45198480	45198802	323	11,58796416	12,28016414	-0,648837648	0,002441501
Homo_sapiens_tRNA-Gly-GCC-2-1	chr1	161523721	161524042	322	11,45051472	12,17308968	-0,674049096	0,002445268

Homo_sapiens_tRNA-Ser-GCT-4-2	chr15	40593699	40594031	333	11,35849603	12,12388172	-0,709045036	0,00244611
Homo_sapiens_tRNA-Cys-GCA-18-1	chr7	149375633	149375955	323	5,728663643	4,013022026	1,395527731	0,00264092 5
Homo_sapiens_tRNA-Thr-TGT-6-1	chr5	181191561	181191883	323	11,53171582	12,1958429	-0,624544131	0,00266184 4
Homo_sapiens_tRNA-Asp-GTC-1-1	chr12	985033777	985036999	323	11,60515253	12,36537369	-0,70317108	0,00293420 6
Homo_sapiens_tRNA-Pro-CGG-2-1	chr6	27091616	27091938	323	11,45473207	10,77892542	0,63342331	0,00310140 7
Homo_sapiens_tRNA-iMet-CAT-1-1	chr1	153671124	153671446	323	11,54398924	12,29141922	-0,690289843	0,00374459 3
Homo_sapiens_tRNA-Gly-TCC-2-1	chr1	146036935	146037257	323	11,35811992	12,05942039	-0,652701315	0,00376721 9
Homo_sapiens_tRNA-Val-CAC-1-1	chr1	161399574	161399897	324	11,64885037	12,28283635	-0,596576973	0,00383020 6
Homo_sapiens_tRNA-Lys-CTT-1-1	chr14	582397679	582400912	324	11,37446992	12,08854999	-0,662654728	0,00399554 9
Homo_sapiens_tRNA-Arg-ACG-2-1	chr3	456888733	456891966	324	11,68273225	12,39473451	-0,660775755	0,00405869 7
Homo_sapiens_tRNA-Arg-TCG-3-1	chr17	750349877	750353100	324	11,49970136	12,0895887	-0,558659296	0,00407407 4
Homo_sapiens_tRNA-Arg-ACG-1-1	chr6	26328014	26328337	324	11,48520609	10,83969106	0,605878959	0,00411721
Homo_sapiens_tRNA-Leu-CAG-1-6	chr1	161530216	161530549	334	10,93776355	11,5022847	-0,536549254	0,00421450 7
Homo_sapiens_tRNA-Pro-AGG-2-2	chr6	26555144	26555466	323	10,90605226	10,28094269	0,588402579	0,00431471 1
Homo_sapiens_tRNA-Leu-CAA-1-1	chr6	28896097	28896453	357	11,45995859	12,11455947	-0,612439789	0,00450697 4
Homo_sapiens_tRNA-Thr-AGT-5-1	chr17	8139326	8139650	325	11,02617414	10,42696171	0,565582578	0,00490861 9
Homo_sapiens_tRNA-Glu-CTC-1-6	chr6	28982073	28982395	323	11,741416	12,4681512	-0,670382743	0,00499060 9
Homo_sapiens_tRNA-Val-AAC-1-5	chr6	27753274	27753597	324	11,01997068	11,70714765	-0,637934845	0,00521060 9
Homo_sapiens_tRNA-Asn-GTT-3-1	chr1	144419141	144419465	325	10,90296156	10,2631404	0,599222634	0,00521796
Homo_sapiens_tRNA-Cys-GCA-4-1	chr17	38869166	38869488	323	10,71027783	11,29802357	-0,554919445	0,00522678 2
Homo_sapiens_tRNA-Gly-GCC-2-3	chr6	27902782	27903103	322	11,52341788	12,20953716	-0,636197697	0,00568089
Homo_sapiens_tRNA-Pro-AGG-2-1	chr1	167715362	167715684	323	11,36053174	12,01071973	-0,60633721	0,00595571 7
Homo_sapiens_tRNA-Phe-GAA-1-4	chr12	124927717	124928040	324	10,70859648	11,31024896	-0,565450732	0,00624239 7
Homo_sapiens_tRNA-Thr-CGT-1-1	chr6	28488867	28489191	325	10,85341767	10,32687525	0,501699934	0,00646335 3
Homo_sapiens_tRNA-Lys-CTT-2-1	chr1	146039275	146039598	324	10,98294741	11,60073085	-0,578703665	0,00650362 7
Homo_sapiens_tRNA-Ala-AGC-4-1	chr6	28658111	28658433	323	10,98135196	11,61157584	-0,588669162	0,00672188 3
Homo_sapiens_tRNA-Gln-CTG-1-1	chr6	18836045	18836367	323	5,134670404	3,435189172	1,323756138	0,00676115 1
Homo_sapiens_tRNA-Gln-TTG-2-1	chr6	28589253	28589575	323	11,39185801	10,88071759	0,48722583	0,00714236 3
Homo_sapiens_tRX-Phe-GAA-2-1	chr1	121009418	121009748	331	6,650283164	5,560309793	0,932910467	0,00727948 7
Homo_sapiens_tRNA-Glu-TTC-12-1	chr1	172188272	172188598	327	4,743666219	2,752065336	1,488805141	0,00781181 5
Homo_sapiens_tRNA-Lys-TTT-3-2	chr1	204506904	204507227	324	11,68719223	12,32410628	-0,592442972	0,00814076
Homo_sapiens_tRNA-His-GTG-1-8	chr15	45200287	45200609	323	11,59384096	12,13370951	-0,510425246	0,00924602 1
Homo_sapiens_tRNA-Val-CAC-2-1	chr6	27280144	27280467	324	11,56186555	11,01931922	0,512798941	0,00927205 4
Homo_sapiens_tRNA-Arg-TCT-1-1	chr1	93847447	93847782	336	10,86694746	11,5132251	-0,597843381	0,01003632 4
Homo_sapiens_tRNA-Ala-AGC-23-1	chr6	28778641	28778963	323	6,299243202	5,074616163	1,004725186	0,01003632 4
Homo_sapiens_tRNA-Ala-AGC-1-1	chr6	28795838	28796160	323	11,54296807	10,9726978	0,535565298	0,01006932 5
Homo_sapiens_tRNA-Gln-TTG-3-3	chr6	27795735	27796057	323	10,73648599	11,23929194	-0,476682532	0,01253812 9
Homo_sapiens_tRNA-Thr-AGT-6-1	chr6	27162145	27162469	325	10,2390924	9,643694649	0,554392329	0,01267947 1
Homo_sapiens_tRNA-Glu-CTC-1-1	chr1	146035566	146035888	323	11,85630917	12,51809709	-0,607108252	0,01297009 6
Homo_sapiens_tRNA-Asn-GTT-11-2	chr1	149646325	149646649	325	7,122687381	6,132492199	0,838966454	0,01442072 6
Homo_sapiens_tRNA-Lys-CTT-1-2	chr15	78860436	78860759	324	11,17969288	11,76895451	-0,546973153	0,01566507 7

Homo_sapiens_tRNA-Met-CAT-3-1	chr6	28944449	28944772	324	11,41753942	11,88542552	-0,444421785	0,017778671
Homo_sapiens_tRNA-Arg-TCG-2-1	chr6	26322692	26323015	324	10,80317611	10,30279802	0,47247952	0,017960052
Homo_sapiens_tRNA-Val-CAC-1-7	chr1	149712426	149712749	324	10,17522705	10,69698226	-0,48999773	0,017960052
Homo_sapiens_tRNA-Leu-AAG-2-4	chr16	22297014	22297346	333	11,9258603	12,59077259	-0,604510913	0,018398981
Homo_sapiens_tRNA-Asn-GTT-24-1	chr1	146369975	146370299	325	10,71305381	10,16133218	0,514742287	0,018555579
Homo_sapiens_tRNA-Asn-GTT-2-7	chr1	145287640	145287964	325	11,38241783	10,86069561	0,489884926	0,018643272
Homo_sapiens_tRNA-iMet-CAT-1-5	chr6	27332859	27333181	323	11,38205713	10,92775756	0,432549222	0,018811058
Homo_sapiens_tRX-Lys-CTT-1-1	chr16	2927535	2927858	324	5,268453056	3,820376948	1,100984951	0,018811058
Homo_sapiens_tRNA-Ala-AGC-2-1	chr6	28838318	28838640	323	11,3133971	11,83066149	-0,485133155	0,020228581
Homo_sapiens_tRNA-Ser-AGA-2-3	chr6	27495688	27496020	333	11,35895271	10,93814044	0,402321186	0,022064264
Homo_sapiens_tRNA-Thr-AGT-2-1	chr6	26532791	26533115	325	11,63840873	12,16041618	-0,488133726	0,022671561
Homo_sapiens_tRNA-Arg-CCG-1-3	chr16	3150548	3150871	324	11,39581711	11,93693816	-0,503788085	0,022755792
Homo_sapiens_tRNA-Ala-TGC-4-1	chr12	124939843	124940162	320	10,79409828	11,31066201	-0,48311787	0,023356031
Homo_sapiens_tRNA-Ala-AGC-11-1	chr6	26571738	26572061	324	11,35971841	10,89680394	0,437926553	0,025212923
Homo_sapiens_tRNA-iMet-CAT-1-7	chr6	27902367	27902689	323	10,86672903	11,38572111	-0,483799857	0,026702703
Homo_sapiens_tRNA-Cys-GCA-23-1	chr7	149595088	149595410	323	5,524519028	4,287473748	0,951729467	0,027222045
Homo_sapiens_tRNA-Phe-GAA-8-1	chr6	78958167	78958490	324	3,541788444	4,928205591	-1,040784627	0,029010979
Homo_sapiens_tRNA-Gly-TCC-2-6	chr1	161530987	161531309	323	11,32333018	11,75980852	-0,413570559	0,030808138
Homo_sapiens_tRNA-Lys-TTT-3-4	chr11	59560209	59560532	324	11,63005012	12,18618798	-0,51153372	0,032192187
Homo_sapiens_tRNA-Ala-AGC-8-1	chr2	27051088	27051411	324	11,58601317	12,12319232	-0,496334521	0,032552893
Homo_sapiens_tRNA-Leu-AAG-2-2	chr6	28943496	28943828	333	10,54679443	10,16237473	0,367198669	0,039985184
Homo_sapiens_tRNA-Gly-CCC-6-1	chr1	121016719	121017040	322	10,96977989	10,52442614	0,419217516	0,040187575
Homo_sapiens_tRNA-Cys-GCA-2-2	chr17	38867519	38867841	323	11,06596011	11,50490278	-0,41313086	0,041629202
Homo_sapiens_tRNA-Ser-GCT-6-1	chr6	26305364	26305698	335	10,1134541	9,709470968	0,382914253	0,048232568
Homo_sapiens_tRNA-Val-AAC-2-1	chr5	181188290	181188613	324	10,89411698	11,34243852	-0,41966675	0,0484778
Homo_sapiens_tRNA-Pro-TGG-3-1	chr5	181188728	181189050	323	11,41399102	11,88948994	-0,441841107	0,048568019
Homo_sapiens_tRNA-Gly-TCC-3-1	chr17	8221422	8221744	323	11,22330981	11,68930887	-0,433982697	0,049017451
Homo_sapiens_tRNA-Cys-GCA-7-1	chr1	93516151	93516474	324	7,002812123	6,130397275	0,712144541	0,053832276
Homo_sapiens_tRNA-Thr-AGT-1-1	chr17	8187072	8187358	287	10,84484225	10,40054974	0,415513561	0,053832276
Homo_sapiens_tRNA-Cys-GCA-20-1	chr7	149597829	149598151	323	3,938936676	5,106587274	-0,854510528	0,055125663
Homo_sapiens_tRNA-Thr-CGT-3-1	chr6	28648081	28648405	325	10,85607255	11,23250976	-0,357284145	0,058881491
Homo_sapiens_tRNA-Lys-CTT-2-2	chr5	181207629	181207952	324	11,43834995	11,02360196	0,389826842	0,059390155
Homo_sapiens_tRNA-Lys-TTT-14-1	chr14	73588699	73589028	330	3,123243608	4,475286152	-0,937050043	0,062830688
Homo_sapiens_tRNA-Gly-GCC-2-6	chr17	8125620	8125941	322	11,50659893	11,89133839	-0,363792255	0,063558226
Homo_sapiens_tRNA-Ile-AAT-2-1	chr6	27688062	27688386	325	11,75854303	11,33195295	0,398774556	0,064163091
Homo_sapiens_tRNA-Arg-CCT-2-1	chr17	75034305	75034628	324	11,3226007	11,70816917	-0,363933082	0,067887336
Homo_sapiens_tRNA-Asn-GTT-8-1	chr1	149740122	149740446	325	9,063857344	8,6273155	0,40607454	0,070052977
Homo_sapiens_tRNA-Ala-TGC-3-1	chr5	181206742	181207064	323	11,78889452	12,24852575	-0,424012017	0,070718575
Homo_sapiens_tRNA-Asn-GTT-20-1	chr1	146049072	146049398	327	4,249165002	2,894091698	0,923049796	0,070981996
Homo_sapiens_tRNA-Phe-GAA-2-1	chr11	59566254	59566577	324	11,71416544	11,2936982	0,392505697	0,070981996
Homo_sapiens_tRNA-Val-CAC-4-1	chr1	143803868	143804191	324	8,44390711	8,851460715	-0,379698245	0,073724881

Homo_sapiens_tRNA-Arg-ACG-1-2	chr6	26537372	26537695	324	11,94519832	11,56109515	0,361387389	0,078195874
Homo_sapiens_tRNA-Asp-GTC-2-7	chr6	27503618	27503940	323	9,978780476	10,3162496	-0,321246546	0,080831278
Homo_sapiens_tRX-Cys-GCA-4-1	chr7	149628027	149628360	334	3,524519028	4,643121468	-0,798421763	0,091131912
Homo_sapiens_tRNA-Cys-GCA-1-1	chr7	149310064	149310386	323	6,95089119	7,565073291	-0,529704029	0,093741508
Homo_sapiens_tRNA-Trp-CCA-3-3	chr17	8186232	8186554	323	10,39983332	10,72630936	-0,310417277	0,095839954
Homo_sapiens_tRNA-Pro-CGG-1-3	chr17	8222707	8223029	323	11,22019199	11,54792595	-0,311261049	0,098146041
Homo_sapiens_tRNA-Tyr-GTA-5-5	chr14	20683147	20683486	340	11,65839295	11,28674063	0,348590166	0,098237655
Homo_sapiens_tRNA-Lys-TTT-3-3	chr6	28950903	28951226	324	11,49607566	11,10229328	0,366586174	0,098990201
Homo_sapiens_tRNA-Tyr-GTA-1-1	chr6	26568732	26569073	342	11,23896076	11,56394836	-0,307490531	0,115770713
Homo_sapiens_tRNA-His-GTG-1-9	chr15	45201025	45201347	323	10,87443043	11,18546535	-0,295179465	0,117475772
Homo_sapiens_tRNA-Leu-AAG-7-1	chr5	181164435	181164770	336	4,910050822	3,889851953	0,722368367	0,122024009
Homo_sapiens_tRNA-Asn-GTT-1-1	chr1	161540115	161540439	325	11,30501984	11,58852028	-0,271104013	0,123618294
Homo_sapiens_tRNA-Lys-CTT-7-1	chr1	54957743	54958066	324	5,11749609	4,133687933	0,692285687	0,135055145
Homo_sapiens_tRNA-Met-CAT-4-2	chr6	26743137	26743460	324	8,802657643	8,471635384	0,311422376	0,140986652
Homo_sapiens_tRNA-Tyr-GTA-5-2	chr8	66113862	66114063	202	8,481149765	8,856396365	-0,346050041	0,141205268
Homo_sapiens_tRNA-Trp-CCA-1-1	chr17	8220743	8221065	323	11,26021573	11,56245283	-0,286236085	0,142637652
Homo_sapiens_tRNA-Ala-AGC-3-1	chr6	28607030	28607352	323	10,91361688	10,62689099	0,273001462	0,146007682
Homo_sapiens_tRX-Val-CAC-4-1	chr1	149708534	149708855	322	10,49016466	10,8422155	-0,327139841	0,146147422
Homo_sapiens_tRNA-Asp-GTC-2-11	chr17	8222112	8222434	323	11,66296012	12,04261791	-0,348733187	0,149204595
Homo_sapiens_tRNA-iMet-CAT-1-6	chr6	27592695	27593017	323	11,52979622	11,20217738	0,3066923	0,154014707
Homo_sapiens_tRNA-Pro-TGG-3-2	chr14	20683890	20684212	323	11,49535649	11,80465951	-0,29064724	0,163009253
Homo_sapiens_tRNA-Leu-CAA-1-2	chr6	28940927	28941282	356	11,39587927	11,71359283	-0,297476745	0,164250954
Homo_sapiens_tRNA-Ser-AGA-2-2	chr6	27478686	27479018	333	11,59124344	11,28703389	0,286393888	0,165052769
Homo_sapiens_tRNA-Asp-GTC-2-10	chr12	124939521	124939840	320	11,24620992	11,57694478	-0,307107325	0,176499775
Homo_sapiens_tRNA-Ile-AAT-5-5	chr17	8187467	8187791	325	11,41556167	11,75472526	-0,313827028	0,176499775
Homo_sapiens_tRNA-Gly-CCC-7-1	chr2	115515851	115518952	312	5,010806691	4,131295472	0,615275317	0,176634366
Homo_sapiens_tRNA-iMet-CAT-1-8	chr17	82494595	82494917	323	11,98070698	12,32094179	-0,313902714	0,184183211
Homo_sapiens_tRNA-Asn-GTT-21-1	chr1	148378790	148379114	325	4,216396733	3,236156833	0,639740665	0,189976814
Homo_sapiens_tRNA-Cys-GCA-22-1	chr7	149556585	149556905	321	3,809894083	4,677080947	-0,605594536	0,192613002
Homo_sapiens_tRNA-Ser-AGA-2-6	chr17	8226484	8226816	333	10,44306022	10,75992906	-0,293613581	0,203256272
Homo_sapiens_tRNA-Cys-GCA-24-1	chr17	38833596	38833918	323	4,43058169	3,439063271	0,625890645	0,211154834
Homo_sapiens_tRNA-Arg-CCG-1-2	chr6	28881262	28881585	324	11,51896319	11,81542813	-0,276450078	0,211953379
Homo_sapiens_tRNA-Ser-AGA-6-1	chr11	109165185	109165518	334	4,660926199	5,359137678	-0,526097646	0,216468987
Homo_sapiens_tRNA-Leu-TAG-4-1	chr14	20676893	20677225	333	3,955862623	3,015618704	0,599182968	0,231979026
Homo_sapiens_tRNA-Pro-TGG-1-1	chr14	20632880	20633202	323	10,87769332	10,45011309	0,370266267	0,233919003
Homo_sapiens_tRNA-Lys-CTT-11-1	chr19	51922014	51922338	325	3,674251227	2,597984527	0,61653759	0,253536105
Homo_sapiens_tRNA-Phe-GAA-6-1	chr6	28763471	28763795	325	4,123243608	3,236156833	0,566355274	0,253980162
Homo_sapiens_tRNA-Met-CAT-7-1	chr6	57842088	57842411	324	4,169325765	3,341174313	0,551488489	0,258112889
Homo_sapiens_tRNA-Thr-TGT-2-1	chr1	222464879	222465202	324	10,7029728	10,47783138	0,214303216	0,260138396
Homo_sapiens_tRNA-Gly-GCC-1-5	chr21	17454663	17454984	322	11,533754	11,25731585	0,256602318	0,267029705
Homo_sapiens_tRNA-Asp-GTC-10-1	chr1	161523019	161523341	323	3,190484987	4,022090023	-0,54618554	0,275010661

Homo_sapiens_tRNA-His-GTG-1-6	chr9	144338114	144341316	323	6,890581582	7,284122552	-0,339602069	0,27501061
Homo_sapiens_tRNA-Gln-CTG-1-2	chr6	275194003	275197255	323	10,70233627	10,94272318	-0,226184266	0,27811136 9
Homo_sapiens_tRNA-Glu-TTC-1-2	chr13	410606 12	410609 34	323	10,32867024	10,56618078	-0,223405189	0,28265486 7
Homo_sapiens_tRX-Lys-CTT-4-1	chr7	971414 47	971417 70	324	2,598803483	3,591037118	-0,573715906	0,28367669 9
Homo_sapiens_tRNA-Pro-AGG-2-6	chr14	206132 75	206135 97	323	11,5774206	11,32687401	0,233937382	0,29329862 7
Homo_sapiens_tRNA-Leu-TAA-3-1	chr11	595516 29	595519 62	334	11,10445947	10,86873727	0,221497695	0,29743038 2
Homo_sapiens_tRNA-Phe-GAA-12-1	chr8	123258 356	123258 682	327	2,434927987	3,34324309	-0,523723308	0,31447028 1
Homo_sapiens_tRNA-Leu-CAG-2-1	chr16	572998 25	573001 58	334	11,50207082	11,75240214	-0,231970231	0,32078788 6
Homo_sapiens_tRNA-Gln-CTG-1-3	chr6	289414 75	289417 97	323	11,15871886	11,39499884	-0,220396558	0,32392356 1
Homo_sapiens_tRNA-iMet-CAT-1-4	chr6	263301 75	263304 97	323	11,40269651	11,16501228	0,221646727	0,32496204 7
Homo_sapiens_tRNA-Ala-CGC-2-1	chr6	286737 10	286740 32	323	11,41865171	11,63524423	-0,203752739	0,33171448 3
Homo_sapiens_tRNA-Gly-GCC-2-5	chr16	707893 81	707897 02	322	7,796889716	7,493303858	0,270502741	0,34377963 7
Homo_sapiens_tRNA-Val-CAC-1-5	chr5	181222 269	181222 592	324	11,58441432	11,8198854	-0,218482115	0,34684095 1
Homo_sapiens_tRNA-Ala-TGC-3-2	chr12	124921 629	124921 951	323	11,35353828	11,57997879	-0,210962107	0,34992620 9
Homo_sapiens_tRNA-Val-AAC-1-4	chr5	181218 144	181218 467	324	11,79784577	12,02524615	-0,211603187	0,35262148 6
Homo_sapiens_tRNA-Asn-GTT-7-1	chr1	120844 136	120844 460	325	9,345366437	9,101713189	0,223978134	0,36126734 6
Homo_sapiens_tRNA-Cys-GCA-3-1	chr7	149588 947	149589 269	323	4,470698157	3,826305358	0,421347845	0,37172480 2
Homo_sapiens_tRNA-Lys-TTT-11-1	chr12	276902 47	276905 70	324	2,706488921	3,523450473	-0,455060288	0,38509331 3
Homo_sapiens_tRNA-Arg-TCT-2-1	chr17	8120799	8121137	339	7,902021681	8,170211974	-0,238409296	0,38509331 3
Homo_sapiens_tRNA-Arg-CCT-3-1	chr16	3152774	3153097	324	11,57086222	11,34192071	0,210083831	0,40045647
Homo_sapiens_tRNA-Arg-TCT-4-1	chr1	159141485	159141809	325	6,658505107	6,410281481	0,2209261	0,41348161 2
Homo_sapiens_tRNA-Ser-GCT-4-3	chr17	8186740	8187034	295	11,21291021	11,39585439	-0,171712367	0,42836207 5
Homo_sapiens_tRNA-Lys-TTT-1-1	chr16	734781 91	734785 14	324	8,420471885	8,658284928	-0,212536683	0,45306967 8
Homo_sapiens_tRNA-Leu-TAG-1-1	chr17	8120188	8120520	333	11,39118072	11,57886283	-0,174413628	0,45748645 9
Homo_sapiens_tRNA-Thr-AGT-1-2	chr17	8226109	8226433	325	10,90119185	11,09494813	-0,178457104	0,47173771 7
Homo_sapiens_tRNA-Gln-CTG-12-1	chr12	744572 76	744575 99	324	3,575719225	4,133687933	-0,363648033	0,47297748 5
Homo_sapiens_tRNA-Ile-AAT-5-1	chr6	265539 96	265543 20	325	11,73882416	11,92993369	-0,176240611	0,47388538 6
Homo_sapiens_tRNA-Gln-CTG-16-1	chr2	218626 291	218626 609	319	3,884723661	3,339102565	0,340649941	0,49950049 9
Homo_sapiens_tRNA-Ser-AGA-5-1	chr7	149608 250	149608 572	323	6,004592316	5,662274065	0,266782961	0,49950049 9
Homo_sapiens_tRNA-Tyr-GTA-2-1	chr2	270506 56	270509 95	340	11,52661748	11,706321	-0,164780381	0,52296713 7
Homo_sapiens_tRX-Und-NNN-7-1	chr3	111349530	111349855	326	3,799968305	3,238381698	0,329917774	0,52408146 3
Homo_sapiens_tRNA-Gly-GCC-6-1	chr6	142257513	142257834	322	3,233632257	3,75050733	-0,333317304	0,52462228 7
Homo_sapiens_tRNA-Ser-AGA-2-1	chr6	263274 63	263277 95	333	10,92698823	10,77250972	0,143894297	0,54624208 5
Homo_sapiens_tRNA-Gln-CTG-4-2	chr1	143691348	143691670	323	3,745948642	4,133687933	-0,280756518	0,55404828 8
Homo_sapiens_tRNA-Thr-TGT-4-1	chr14	206310 34	206313 57	324	11,37118824	11,23014004	0,132388544	0,55733549 3
Homo_sapiens_tRNA-iMet-CAT-1-3	chr6	263129 98	263133 20	323	11,38573669	11,52315176	-0,128843952	0,56422752 9
Homo_sapiens_tRX-Gln-CTG-2-1	chr11	480657 06	480660 34	329	3,760773459	4,185255416	-0,286902969	0,56422752 9
Homo_sapiens_tRX-Und-NNN-9-1	chr22	303080 43	303083 72	330	3,130249777	3,599716165	-0,301596929	0,56422752 9
Homo_sapiens_tRNA-Gln-CTG-7-1	chr1	148328686	148329008	323	3,409041811	2,891266586	0,296416049	0,57386015 9
Homo_sapiens_tRX-Trp-CCA-1-1	chr7	673994 34	673997 56	323	3,390097011	3,824825538	-0,272638313	0,59694705 5
Homo_sapiens_tRNA-Leu-CAA-6-1	chr1	161611820	161612154	335	3,664631942	4,134882677	-0,27353396	0,59694705 5

Homo_sapiens_tRNA-Asn-GTT-18-1	chr1	165322712	165325956	325	3,076609276	2,594515005	0,278337059	0,607067199
Homo_sapiens_tRNA-Val-CAC-1-6	chr6	26537928	26538251	324	10,81737979	10,69956613	0,110840149	0,620524122
Homo_sapiens_tRNA-Ile-AAT-11-1	chr12	129231527	129231852	326	3,587307524	3,127699325	0,261872698	0,620524122
Homo_sapiens_tRNA-Lys-TTT-12-1	chr19	49534550	49534873	324	3,558853585	3,964222367	-0,253514544	0,629587892
Homo_sapiens_tRNA-Asn-GTT-17-1	chr1	161621549	161621873	325	9,535007018	9,76887726	-0,187868032	0,629587892
Homo_sapiens_tRNA-Arg-TCG-5-1	chr6	28542988	28543311	324	11,38521814	11,28621987	0,093597974	0,672707004
Homo_sapiens_tRNA-Gln-CTG-8-2	chr1	146055486	146055808	323	4,556254832	4,825565638	-0,192466002	0,695074037
Homo_sapiens_tRNA-iMet-CAT-3-1	chr9	194038732	194041907	326	3,620196373	3,242821161	0,210827931	0,698043801
Homo_sapiens_tRNA-Asp-GTC-2-6	chr6	27479548	27479870	323	11,4811426	11,57970567	-0,092204341	0,698043801
Homo_sapiens_tRNA-Val-TAC-1-1	chr11	59550503	59550826	324	11,32063037	11,22442732	0,090372628	0,698043801
Homo_sapiens_tRNA-Tyr-GTA-9-1	chr8	65697171	65697509	339	2,898195222	3,247247005	-0,204951548	0,709863965
Homo_sapiens_tRNA-Gln-TTG-4-1	chr6	145182597	145182919	323	3,637676866	3,339102565	0,195903879	0,711183844
Homo_sapiens_tRNA-Gln-CTG-8-3	chr1	120476726	120477048	323	3,756251773	4,019504977	-0,170194512	0,749566292
Homo_sapiens_tRNA-Leu-AAG-2-3	chr14	20610006	20610338	333	11,90447689	11,99078136	-0,079909749	0,760571133
Homo_sapiens_tRNA-Gly-GCC-5-1	chr16	70788568	70788889	322	3,587307524	3,821861336	-0,161632104	0,761480911
Homo_sapiens_tRX-Ala-AGC-2-1	chr6	57830046	57830369	324	3,060070663	3,34324309	-0,16906245	0,763484133
Homo_sapiens_tRNA-Glu-TTC-10-2	chr1	145176813	145177136	324	3,865816856	4,081448528	-0,154906281	0,767916608
Homo_sapiens_tRNA-Thr-TGT-5-1	chr14	20681564	20681887	324	11,41973635	11,48639807	-0,063124131	0,771985536
Homo_sapiens_tRNA-Pro-AGG-2-5	chr14	20609210	20609532	323	11,42060441	11,34691482	0,06917978	0,775567313
Homo_sapiens_tRNA-Leu-AAG-2-1	chr5	181187575	181187907	333	11,20869103	11,27660147	-0,064019904	0,775567313
Homo_sapiens_tRNA-Cys-GCA-19-1	chr7	149612939	149613261	323	3,409041811	3,134882677	0,154853013	0,777293594
Homo_sapiens_tRNA-Ala-CGC-1-1	chr6	26553377	26553699	323	11,10201507	11,17515711	-0,068025586	0,781958975
Homo_sapiens_tRNA-Cys-GCA-15-1	chr7	149584599	149584921	323	5,054065344	4,859874276	0,132985046	0,783972749
Homo_sapiens_tRNA-Gln-CTG-13-1	chr5	151868387	151868709	323	3,598803483	3,826305358	-0,143140562	0,784056195
Homo_sapiens_tRNA-SeC-TCA-2-1	chr22	44150531	44150865	335	3,212219919	3,439063271	-0,146516152	0,790997679
Homo_sapiens_tRNA-Ile-GAT-1-1	chrX	3838251	3838575	325	0	0	-0,163757639	0,802721254
Homo_sapiens_tRNA-Pro-AGG-2-3	chr7	128783324	128783646	323	11,0358941	10,96725611	0,063556206	0,805333367
Homo_sapiens_tRX-Lys-CTT-3-1	chr15	95784519	95784842	324	3,123243608	3,341174313	-0,13047668	0,810166417
Homo_sapiens_tRNA-Cys-GCA-16-1	chr7	149546414	149546736	323	5,097852661	5,239492845	-0,10757793	0,813978551
Homo_sapiens_tRNA-Ile-TAT-2-2	chr6	27020220	27020564	345	9,39736391	9,453911806	-0,05234277	0,821244528
Homo_sapiens_tRNA-Gln-TTG-6-1	chr4	40906600	40906923	324	3,78109822	3,604898641	0,112829028	0,826948407
Homo_sapiens_tRNA-Leu-CAA-5-1	chr11	9275117	9275441	325	3,81425098	3,604898641	0,115004313	0,826948407
Homo_sapiens_tRNA-Val-TAC-2-1	chr11	59550861	59551168	308	10,41599627	10,46890268	-0,049282664	0,833963174
Homo_sapiens_tRNA-Val-AAC-3-1	chr6	27650802	27651125	324	11,42552864	11,37265948	0,049551004	0,834150525
Homo_sapiens_tRNA-Pro-TGG-3-3	chr16	3158796	3159118	323	8,193889404	8,252464318	-0,054101235	0,840223805
Homo_sapiens_tRNA-Lys-CTT-8-1	chr16	3164812	3165135	324	3,7355714	3,523450473	0,107170346	0,842765314
Homo_sapiens_tRNA-Lys-TTT-5-1	chr11	59556303	59556626	324	10,25699504	10,20920146	0,044909418	0,844768179
Homo_sapiens_tRNA-His-GTG-2-1	chr1	143661056	143661378	323	3,343828134	3,132492199	0,101452118	0,847797093
Homo_sapiens_tRNA-Lys-CTT-12-1	chr1	39504394	39504720	327	3,395922435	3,517966428	-0,093570729	0,853797626
Homo_sapiens_tRNA-Met-CAT-3-2	chr6	28953139	28953462	324	11,73346955	11,77738095	-0,040857571	0,861289523
Homo_sapiens_tRNA-Glu-TTC-7-1	chr1	143666862	143667184	323	3,018883166	3,132492199	-0,079441717	0,880714811

Homo_sapiens_tRNA-Tyr-GTA-10-1	chr7	149557916	149558239	324	3,695822864	3,824825538	-0,071226766	0,886842025
Homo_sapiens_tRNA-Gln-CTG-17-1	chr20	178743772	178747000	329	3,78109822	3,677080947	0,064374629	0,899365582
Homo_sapiens_tRNA-Gly-TCC-4-1	chr1	161440045	161440367	323	7,515494406	7,552636358	-0,029446671	0,940974367
Homo_sapiens_tRNA-Asp-GTC-8-1	chr12	122376251	122376572	322	3,297688209	3,240603137	0,038054051	0,945952088
Homo_sapiens_tRX-Gln-CTG-3-1	chr1	145563120	145563442	323	3,986302388	3,952073414	0,031531598	0,951626724
Homo_sapiens_tRNA-Lys-CTT-13-1	chr1	165596787	165597110	324	3,489347384	3,433248215	0,033150651	0,951626724
Homo_sapiens_tRNA-Thr-TGT-1-1	chr6	28474426	28474750	325	11,32225339	11,30901987	0,012398363	0,958657332
Homo_sapiens_tRX-Asp-ATC-1-1	chr6	28827287	28827609	323	3,494786252	3,521624773	-0,027201931	0,958657332
Homo_sapiens_tRNA-Ala-CGC-4-1	chr6	28729189	28729511	323	11,3078745	11,31652172	-0,008038331	0,971504479
Homo_sapiens_tRX-Lys-CTT-5-1	chr7	12601838	12602172	335	3,553651389	3,525273865	0,016416142	0,973582094
Homo_sapiens_tRNA-Thr-TGT-3-1	chr14	20613664	20613987	324	11,28255179	11,28528833	-0,002453888	0,990977438
Homo_sapiens_tRNA-Gln-CTG-11-1	chr1	143584575	143584897	323	3,220561489	3,238381698	-0,00497086	0,990977438
Homo_sapiens_tRX-Leu-TAA-2-1	chr11	113562147	113562481	335	1,663343235	3,51979676	-1,212491424	1
Homo_sapiens_tRX-Ser-GGA-2-1	chrX	252618466	252621688	323	1,100114862	3,34324309	-1,329300372	1
Homo_sapiens_tRNA-Glu-TTC-13-1	chr2	74896793	74897116	324	2,471434702	3,894091698	-0,912999704	1
Homo_sapiens_tRX-Pro-GGG-1-1	chrX	119603772	119604091	320	1,409041811	3,236156833	-1,043437465	1
Homo_sapiens_tRNA-Asp-GTC-4-1	chr9	74902948	74903270	323	2,598803483	3,826305358	-0,739842586	1
Homo_sapiens_tRNA-Asn-GTT-22-1	chr1	143717166	143717490	325	2,631434232	3,759830228	-0,702945775	1
Homo_sapiens_tRNA-Glu-CTC-5-1	chr8	58592113	58592434	322	1,766481845	3,020798079	-0,698877452	1
Homo_sapiens_tRNA-Sup-TTA-1-1	chr17	60786106	60786427	322	2,663343235	3,680357701	-0,638474461	1
Homo_sapiens_tRNA-Leu-TAA-5-1	chr6	69204360	69204693	334	2,795567995	3,75050733	-0,5862136	1
Homo_sapiens_tRNA-Cys-GCA-25-1	chr3	176997677	177000097	331	3,227111676	2,018210716	0,625527511	1
Homo_sapiens_tRX-Val-TAC-3-1	chr17	40082554	40082877	324	2,052714365	3,134882677	-0,580461708	1
Homo_sapiens_tRNA-Gln-CTG-10-1	chr1	147005075	147005397	323	2,631434232	3,523450473	-0,541630055	1
Homo_sapiens_tRX-Asn-GTT-2-1	chr1	144539524	144539848	325	3,608870289	2,601445726	0,555647463	1
Homo_sapiens_tRX-Leu-CAA-3-1	chr2	151831012	151831330	319	2,924766734	3,686888968	-0,458708274	1
Homo_sapiens_tRNA-Ile-AAT-10-1	chr6	27283959	27284283	325	3,397473451	2,604898641	0,465315479	1
Homo_sapiens_tRX-Ala-GGC-3-1	chr19	12188435	12188759	325	2,565417583	3,341174313	-0,446096111	1
Homo_sapiens_tRNA-Ala-TGC-8-1	chr11	50274582	50274904	323	2,694561732	3,439063271	-0,43569232	1
Homo_sapiens_tRNA-Val-CAC-10-1	chr1	166798870	166802033	324	1,725118974	2,601445726	-0,463350657	1
Homo_sapiens_tRNA-Lys-CTT-6-1	chr18	46089179	46089502	324	3,427741057	2,594515005	0,435957889	1
Homo_sapiens_tRNA-Asn-GTT-28-1	chr1	149639327	149639651	325	2,745948642	3,437127522	-0,413062058	1
Homo_sapiens_tRX-Arg-ACG-1-1	chr8	66112815	66113138	324	2,052714365	2,888435931	-0,424198748	1
Homo_sapiens_tRNA-Gln-TTG-10-1	chr6	37320093	37320416	324	2,775447487	3,427409625	-0,397896382	1
Homo_sapiens_tRNA-Pro-TGG-5-1	chr1	207004683	207005010	328	2,496234592	3,238381698	-0,382238531	1
Homo_sapiens_tRX-Lys-CTT-6-1	chr5	168389513	168389835	323	2,420518146	3,134882677	-0,393041561	1
Homo_sapiens_tRX-Ala-GGC-4-1	chr16	80445429	80445756	328	2,986302388	3,599716165	-0,352994175	1
Homo_sapiens_tRNA-Phe-GAA-7-1	chr6	27664640	27664966	327	3,865816856	3,24503578	0,346729604	1
Homo_sapiens_tRX-Asn-GTT-3-1	chr1	146394069	146394393	325	3,123243608	3,685258921	-0,336464372	1
Homo_sapiens_tRNA-Glu-CTC-16-1	chr12	113948614	113948935	322	3,494786252	2,896911288	0,336734245	1
Homo_sapiens_tRNA-Pro-GGG-1-1	chr10	22563524	22563847	324	2,916685105	3,51613377	-0,334688781	1

Homo_sapiens_tRNA-Cys-ACA-1-1	chr5	152608910	152609336	427	3,212219919	2,597984527	0,316352249	1
Homo_sapiens_tRX-Lys-TTT-2-1	chr3	152113410	152116606	327	3,324001282	2,74894764	0,306444326	1
Homo_sapiens_tRX-Ile-AAT-4-1	chr17	8205947	8206284	338	2,95085769	3,433248215	-0,290304941	1
Homo_sapiens_tRNA-Pro-AGG-4-1	chr2	87112324	87112646	323	2,986302388	3,528913751	-0,286308249	1
Homo_sapiens_tRX-Arg-CCT-2-1	chr11	118241246	118241575	330	3,395922435	2,896911288	0,268474661	1
Homo_sapiens_tRNA-Asp-GTC-9-1	chr1	161604672	161604994	323	1,82407931	2,437127522	-0,28798217	1
Homo_sapiens_tRX-Val-AAC-1-1	chr6	158403490	158403813	324	2,575719225	3,018210716	-0,259797249	1
Homo_sapiens_tRNA-Val-AAC-7-1	chr1	180215015	180215338	324	2,804355235	2,242821161	0,263857129	1
Homo_sapiens_tRNA-Gln-TTG-5-1	chr2	45710176	45710499	324	2,608870289	3,025958927	-0,250099221	1
Homo_sapiens_tRX-Gly-CCC-2-1	chr1	148244341	148244663	323	2,71583402	2,238381698	0,240194435	1
Homo_sapiens_tRNA-Leu-AAG-8-1	chr3	148503315	148503647	333	2,190484987	2,604898641	-0,232861772	1
Homo_sapiens_tRNA-Glu-TTC-11-1	chr14	31767483	31767808	326	3,139077526	2,75517631	0,222546009	1
Homo_sapiens_tRNA-SeC-TCA-3-1	chr17	40117174	40117498	325	2,745948642	3,134882677	-0,223300025	1
Homo_sapiens_tRX-Met-CAT-1-1	chr6	28480600	28480923	324	2,986302388	2,608343311	0,218892049	1
Homo_sapiens_tRX-Und-NNN-6-1	chr9	2959214	2959543	330	2,663343235	3,018210716	-0,204552994	1
Homo_sapiens_tRX-Glu-CTC-1-1	chr8	119131615	119134847	323	2,898195222	3,238381698	-0,195395068	1
Homo_sapiens_tRX-Gly-CCC-3-1	chr1	145437472	145437793	322	2,832695108	3,127699325	-0,192134163	1
Homo_sapiens_tRNA-Ala-AGC-20-1	chr1	150045280	150045601	322	2,994004311	2,604898641	0,194462054	1
Homo_sapiens_tRNA-Und-NNN-4-1	chr1	7930153	7930473	321	2,795567995	2,433248215	0,190874982	1
Homo_sapiens_tRNA-Lys-TTT-15-1	chr2	223321471	223321794	324	3,227111676	2,894091698	0,177489043	1
Homo_sapiens_tRNA-Glu-CTC-7-1	chr2	158881533	158881856	324	3,107233978	2,761378204	0,177075843	1
Homo_sapiens_tRX-Asn-GTT-1-1	chr1	148317243	148317563	321	2,852038071	3,134882677	-0,171009132	1
Homo_sapiens_tRNA-Lys-TTT-10-1	chr19	41242111	41242434	324	3,035897931	2,75517631	0,154768053	1
Homo_sapiens_tRX-Und-NNN-8-1	chr10	62343715	62344039	325	2,994004311	3,238381698	-0,150255156	1
Homo_sapiens_tRX-Cys-GCA-2-1	chr8	100816887	100820008	322	3,001665336	3,233928531	-0,151725617	1
Homo_sapiens_tRNA-Gly-CCC-8-1	chr1	146488740	146489061	322	2,843537356	3,130097752	-0,151193658	1
Homo_sapiens_tRNA-Und-GCA-5-1	chr17	68394690	68395015	326	2,745948642	2,433248215	0,153120885	1
Homo_sapiens_tRX-Val-TAC-2-1	chr2	84858626	84858949	324	3,471434702	3,238381698	0,140693368	1
Homo_sapiens_tRX-Phe-GAA-1-1	chr1	145168278	145168608	331	3,471434702	3,240603137	0,137951871	1
Homo_sapiens_tRNA-Gln-CTG-8-1	chr1	149044811	149045133	323	3,36497257	3,597984527	-0,125047645	1
Homo_sapiens_tRNA-Asp-GTC-6-1	chr3	184648181	184648502	322	3,401724432	3,132492199	0,12207078	1
Homo_sapiens_tRNA-Und-NNN-2-1	chr8	98141108	98141427	320	3,363386197	3,132492199	0,108844514	1
Homo_sapiens_tRNA-Lys-CTT-16-1	chr15	76382298	76382622	325	2,815411748	2,597984527	0,111028895	1
Homo_sapiens_tRX-Ser-GCT-1-1	chr13	114241213	114241539	327	3,289782062	3,429358449	-0,102555294	1
Homo_sapiens_tRNA-Thr-AGT-7-1	chr17	64530674	64530998	325	2,795567995	2,604898641	0,099846784	1
Homo_sapiens_tRNA-Tyr-GTA-11-1	chr7	149356527	149356854	328	3,083845039	3,238381698	-0,096213335	1
Homo_sapiens_tRNA-Asp-GTC-5-1	chr5	142394297	142394619	323	3,107233978	3,238381698	-0,093540226	1
Homo_sapiens_tRNA-Asn-GTT-16-1	chr1	148405258	148405582	325	3,114318136	2,891266586	0,091725572	1
Homo_sapiens_tRX-Gly-CCC-1-2	chr1	148020348	148020669	322	2,994004311	3,132492199	-0,084910416	1
Homo_sapiens_tRNA-Arg-CCT-7-1	chr1	143848388	143848709	322	2,745948642	2,891266586	-0,085335493	1
Homo_sapiens_tRNA-Leu-AAG-6-1	chr20	50335679	50336011	333	3,41479139	3,240603137	0,081115582	1

Homo_sapiens_tRX-Leu-CAG-1-1	chr9	120354949	120355282	334	3,043340255	3,139651785	-0,070046562	1
Homo_sapiens_tRX-Pro-GGG-2-1	chr3	124141746	124142069	324	3,018883166	2,891266586	0,057354168	1
Homo_sapiens_tRNA-Tyr-ATA-1-1	chr2	218245700	218246043	344	3,241851286	3,334950121	-0,052734771	1
Homo_sapiens_tRNA-Arg-CCT-6-1	chr1	148010933	148011254	322	3,363386197	3,240603137	0,048191954	1
Homo_sapiens_tRNA-Lys-CTT-9-1	chr5	261983004	261986207	324	3,139077526	3,238381698	-0,048091398	1
Homo_sapiens_tRNA-Asn-GTT-16-3	chr1	120945163	120945487	325	2,725118974	2,75828059	-0,038222777	1
Homo_sapiens_tRNA-Gly-TCC-6-1	chr18	57678819	57679141	323	1,331722604	1,433248215	-0,031315561	1
Homo_sapiens_tRNA-Leu-AAG-5-1	chr2	300545776	300548899	324	3,130249777	3,134882677	-0,022166838	1
Homo_sapiens_tRX-Cys-GCA-3-1	chr1	161605370	161605691	322	2,994004311	3,028532444	-0,022368476	1
Homo_sapiens_tRNA-Glu-TTC-10-1	chr1	143784019	143784342	324	0,331722604	0,417625826	-0,020659229	1
Homo_sapiens_tRX-Cys-GCA-1-1	chr7	149405938	149406260	323	3,310081475	3,24503578	0,016119348	1
Homo_sapiens_tRNA-Lys-CTT-10-1	chr19	35575722	35576045	324	3,018883166	3,020798079	-0,013071986	1
Homo_sapiens_tRNA-Gly-TCC-5-1	chr18	57678496	57678818	323	0,48242714	0,433248215	0,002426769	1
Homo_sapiens_tRX-Gln-TTG-1-1	chr8	88132881	88133205	325	2,48242714	2,437127522	0,000126091	1
Homo_sapiens_tRNA-Phe-GAA-9-1	chr1	143792598	143792928	331	0	0	0	1
Homo_sapiens_tRNA-Lys-CTT-15-1	chr11	54759182	54759505	324	0	0	0	1
Homo_sapiens_tRX-Ala-AGC-1-1	chr6	26713543	26713866	324	0	0	0	1
Homo_sapiens_tRX-Ala-AGC-1-2	chr6	26787820	26788143	324	0	0	0	1
Homo_sapiens_tRX-Ile-GAT-2-1	chrX	3838665	3838989	325	0	0	0	1
Homo_sapiens_tRNA-Ile-GAT-1-2	chrX	3876675	3876999	325	0	0	0	1
Homo_sapiens_tRX-Ile-GAT-1-2	chrX	3877089	3877413	325	0	0	0	1
Homo_sapiens_tRNA-Ile-GAT-1-3	chrX	3915104	3915428	325	0	0	0	1
Homo_sapiens_tRX-Ile-GAT-1-1	chrX	3915518	3915842	325	0	0	0	1

References

Ablasser, A., F. Bauernfeind, G. Hartmann, E. Latz, K. A. Fitzgerald, and V. Hornung. 2009. 'RIG-I-dependent sensing of poly(dA:dT) through the induction of an RNA polymerase III-transcribed RNA intermediate', *Nat Immunol*, 10: 1065-72.

Agris, P. F., E. R. Eruysal, A. Narendran, V. Y. P. Väre, S. Vangaveti, and S. V. Ranganathan. 2018. 'Celebrating wobble decoding: Half a century and still much is new', *RNA Biol*, 15: 537-53.

Alamos, P., M. Tello, P. Bustamante, F. Gutiérrez, A. Shmaryahu, J. Maldonado, G. Levicán, and O. Orellana. 2018. 'Functionality of tRNAs encoded in a mobile genetic element from an acidophilic bacterium', *RNA Biol*, 15: 518-27.

Alla, R. K., and B. R. Cairns. 2014. 'RNA polymerase III transcriptomes in human embryonic stem cells and induced pluripotent stem cells, and relationships with pluripotency transcription factors', *PLOS ONE*, 9: e85648.

Allison, D. S., S. H. Goh, and B. D. Hall. 1983. 'The promoter sequence of a yeast tRNAtyr gene', *Cell*, 34: 655-64.

Andersson, Robin, Claudia Gebhard, Irene Miguel-Escalada, Ilka Hoof, Jette Bornholdt, Mette Boyd, Yun Chen, Xiaobei Zhao, Christian Schmidl, Takahiro Suzuki, Evgenia Ntini, Erik Arner, Eivind Valen, Kang Li, Lucia Schwarzfischer, Dagmar Glatz, Johanna Raithel, Berit Lilje, Nicolas Rapin, Frederik Otzen Bagger, Mette Jørgensen, Peter Refsing Andersen, Nicolas Bertin, Owen Rackham, A. Maxwell Burroughs, J. Kenneth Baillie, Yuri Ishizu, Yuri Shimizu, Erina Furuhata, Shiori Maeda, Yutaka Negishi, Christopher J. Mungall, Terrence F. Meehan, Timo Lassmann, Masayoshi Itoh, Hideya Kawaji, Naoto Kondo, Jun Kawai, Andreas Lennartsson, Carsten O. Daub, Peter Heutink, David A. Hume, Torben Heick Jensen, Harukazu Suzuki, Yoshihide Hayashizaki, Ferenc Müller, Alistair R. R. Forrest, Piero Carninci, Michael Rehli, Albin Sandelin, and Fantom Consortium The. 2014. 'An atlas of active enhancers across human cell types and tissues', *Nature*, 507: 455-61.

Angelini, Claudia, Ruth Heller, Rita Volkinshtein, and Daniel Yekutieli. 2015. 'Is this the right normalization? A diagnostic tool for ChIP-seq normalization', *BMC Bioinformatics*, 16: 150.

Antequera, Francisco, and Adrian Bird. 1999. 'CpG islands as genomic footprints of promoters that are associated with replication origins', *Current Biology*, 9: R661-R67.

Arnold, G. J., C. Schmutzler, U. Thomann, H. van Tol, and H. J. Gross. 1986. 'The human tRNAVal gene family: organization, nucleotide sequences and homologous transcription of three single-copy genes', *Gene*, 44: 287-97.

Arrigoni, L., A. S. Richter, E. Betancourt, K. Bruder, S. Diehl, T. Manke, and U. Bönisch. 2016. 'Standardizing chromatin research: a simple and universal method for ChIP-seq', *Nucleic Acids Res*, 44: e67.

Avsec, Žiga, Melanie Weilert, Avanti Shrikumar, Sabrina Krueger, Amr Alexandari, Khyati Dalal, Robin Fropf, Charles McAnany, Julien Gagneur, Anshul Kundaje, and Julia Zeitlinger. 2021. 'Base-resolution models of transcription-factor binding reveal soft motif syntax', *Nature Genetics*, 53: 354-66.

Bailey, T. L., M. Boden, F. A. Buske, M. Frith, C. E. Grant, L. Clementi, J. Ren, W. W. Li, and W. S. Noble. 2009. 'MEME SUITE: tools for motif discovery and searching', *Nucleic Acids Res*, 37: W202-8.

Barski, A., I. Chepelev, D. Liko, S. Cuddapah, A. B. Fleming, J. Birch, K. Cui, R. J. White, and K. Zhao. 2010a. 'Pol II and its associated epigenetic marks are present at Pol III-transcribed noncoding RNA genes', *Nat Struct Mol Biol*, 17: 629-34.

Barski, A., S. Cuddapah, K. Cui, T. Y. Roh, D. E. Schones, Z. Wang, G. Wei, I. Chepelev, and K. Zhao. 2007. 'High-resolution profiling of histone methylations in the human genome', *Cell*, 129: 823-37.

Barski, Artem, Iouri Chepelev, Dritan Liko, Suresh Cuddapah, Alastair B. Fleming, Joanna Birch, Kairong Cui, Robert J. White, and Keji Zhao. 2010b. 'Pol II and its associated

epigenetic marks are present at Pol III–transcribed noncoding RNA genes', *Nature Structural & Molecular Biology*, 17: 629-34.

Battaglioni, S., D. Benjamin, M. Wälchli, T. Maier, and M. N. Hall. 2022. 'mTOR substrate phosphorylation in growth control', *Cell*, 185: 1814-36.

Beck, M., A. Schmidt, J. Malmstroem, M. Claassen, A. Ori, A. Szymborska, F. Herzog, O. Rinner, J. Ellenberg, and R. Aebersold. 2011. 'The quantitative proteome of a human cell line', *Mol Syst Biol*, 7: 549.

Behrens, A., and D. D. Nedialkova. 2022. 'Experimental and computational workflow for the analysis of tRNA pools from eukaryotic cells by mim-tRNAseq', *STAR Protoc*, 3: 101579.

Behrens, A., G. Rodschinka, and D. D. Nedialkova. 2021. 'High-resolution quantitative profiling of tRNA abundance and modification status in eukaryotes by mim-tRNAseq', *Mol Cell*, 81: 1802-15.e7.

Bermudez-Santana, C., C. S. Attolini, T. Kirsten, J. Engelhardt, S. J. Prohaska, S. Steigele, and P. F. Stadler. 2010. 'Genomic organization of eukaryotic tRNAs', *BMC Genomics*, 11: 270.

Bernard, G., E. Chouery, M. L. Putorti, M. Tétreault, A. Takanohashi, G. Carosso, I. Clément, O. Boespflug-Tanguy, D. Rodriguez, V. Delague, J. Abou Ghoch, N. Jalkh, I. Dorboz, S. Fribourg, M. Teichmann, A. Megarbane, R. Schiffmann, A. Vanderver, and B. Brais. 2011. 'Mutations of POLR3A encoding a catalytic subunit of RNA polymerase Pol III cause a recessive hypomyelinating leukodystrophy', *Am J Hum Genet*, 89: 415-23.

Bernstein, B. E., T. S. Mikkelsen, X. Xie, M. Kamal, D. J. Huebert, J. Cuff, B. Fry, A. Meissner, M. Wernig, K. Plath, R. Jaenisch, A. Wagschal, R. Feil, S. L. Schreiber, and E. S. Lander. 2006. 'A bivalent chromatin structure marks key developmental genes in embryonic stem cells', *Cell*, 125: 315-26.

Betat, H., and M. Mörl. 2015. 'The CCA-adding enzyme: A central scrutinizer in tRNA quality control', *Bioessays*, 37: 975-82.

Bhargava, P. 2013. 'Epigenetic regulation of transcription by RNA polymerase III', *Biochimica et biophysica acta*, 1829: 1015-25.

Bhaskar, P. T., and N. Hay. 2007. 'The two TORCs and Akt', *Dev Cell*, 12: 487-502.

Blair, J. D., D. Hockemeyer, J. A. Doudna, H. S. Bateup, and S. N. Floor. 2017. 'Widespread Translational Remodeling during Human Neuronal Differentiation', *Cell reports*, 21: 2005-16.

Boccaletto, Pietro, Filip Stefaniak, Angana Ray, Andrea Cappannini, Sunandan Mukherjee, Elżbieta Purta, Małgorzata Kurkowska, Niloofar Shirvanizadeh, Eliana Destefanis, Paula Groza, Gülben Avşar, Antonia Romitelli, Pınar Pir, Erik Dassi, Silvestro G Conticello, Francesca Aguilo, and Janusz M Bujnicki. 2021. 'MODOMICS: a database of RNA modification pathways. 2021 update', *Nucleic Acids Research*, 50: D231-D35.

Boisnard, Stéphanie, Gilles Lagniel, Cecilia Garmendia-Torres, Mikael Molin, Emmanuelle Boy-Marcotte, Michel Jacquet, Michel B. Toledano, Jean Labarre, and Stéphane Chédin. 2009. 'H₂O₂ Activates the Nuclear Localization of Msn2 and Maf1 through Thioredoxins in Saccharomyces cerevisiae', *Eukaryotic Cell*, 8: 1429-38.

Bonhoure, N., A. Byrnes, R. D. Moir, W. Hodroj, F. Preitner, V. Praz, G. Marcelin, S. C. Chua, Jr., N. Martinez-Lopez, R. Singh, N. Moullan, J. Auwerx, G. Willemin, H. Shah, K. Hartil, B. Vaitheesvaran, I. Kurland, N. Hernandez, and I. M. Willis. 2015. 'Loss of the RNA polymerase III repressor MAF1 confers obesity resistance', *Genes Dev*, 29: 934-47.

Bonhoure, Nicolas, Viviane Praz, Robyn D. Moir, Gilles Willemin, François Mange, Catherine Moret, Ian M. Willis, and Nouria Hernandez. 2020. 'MAF1 is a chronic repressor of RNA polymerase III transcription in the mouse', *Scientific Reports*, 10: 11956.

Borck, G., F. Hög, M. L. Dentici, P. L. Tan, N. Sowada, A. Medeira, L. Gueneau, H. Thiele, M. Kousi, F. Lepri, L. Wenzeck, I. Blumenthal, A. Radicioni, T. L. Schwarzenberg, B. Mandriani, R. Fischetto, D. J. Morris-Rosendahl, J. Altmüller, A. Reymond, P. Nürnberg, G. Merla, B. Dallapiccola, N. Katsanis, P. Cramer, and C. Kubisch. 2015.

'BRF1 mutations alter RNA polymerase III-dependent transcription and cause neurodevelopmental anomalies', *Genome Res*, 25: 155-66.

Braglia, P., R. Percudani, and G. Dieci. 2005. 'Sequence context effects on oligo(dT) termination signal recognition by Saccharomyces cerevisiae RNA polymerase III', *J Biol Chem*, 280: 19551-62.

Buenrostro, Jason D., Paul G. Giresi, Lisa C. Zaba, Howard Y. Chang, and William J. Greenleaf. 2013. 'Transposition of native chromatin for fast and sensitive epigenomic profiling of open chromatin, DNA-binding proteins and nucleosome position', *Nature Methods*, 10: 1213-18.

Bulmer, Michael. 1987. 'Coevolution of codon usage and transfer RNA abundance', *Nature*, 325: 728-30.

Cabart, P., J. Lee, and I. M. Willis. 2008. 'Facilitated recycling protects human RNA polymerase III from repression by Maf1 in vitro', *J Biol Chem*, 283: 36108-17.

Cai, Y., and Y. H. Wei. 2016. 'Stress resistance and lifespan are increased in C. elegans but decreased in S. cerevisiae by mafr-1/maf1 deletion', *Oncotarget*, 7: 10812-26.

Campbell, Kirsteen J., and Robert J. White. 2014. 'MYC Regulation of Cell Growth through Control of Transcription by RNA Polymerases I and III', *Cold Spring Harbor Perspectives in Medicine*, 4.

Canella, D., V. Praz, J. H. Reina, P. Cousin, and N. Hernandez. 2010. 'Defining the RNA polymerase III transcriptome: Genome-wide localization of the RNA polymerase III transcription machinery in human cells', *Genome Res*, 20: 710-21.

Canella, Donatella, David Bernasconi, Federica Gilardi, Gwendal LeMartelot, Eugenia Migliavacca, Viviane Praz, Pascal Cousin, Mauro Delorenzi, Nouria Hernandez, and X. Consortium Cycli. 2012. 'A multiplicity of factors contributes to selective RNA polymerase III occupancy of a subset of RNA polymerase III genes in mouse liver', *Genome Research*, 22: 666-80.

Carlson, B. A., S. Y. Kwon, M. Chamorro, S. Oroszlan, D. L. Hatfield, and B. J. Lee. 1999. 'Transfer RNA modification status influences retroviral ribosomal frameshifting', *Virology*, 255: 2-8.

Chan, P. P., B. Y. Lin, A. J. Mak, and T. M. Lowe. 2021. 'tRNAscan-SE 2.0: improved detection and functional classification of transfer RNA genes', *Nucleic Acids Res*, 49: 9077-96.

Chan, P. P., and T. M. Lowe. 2009. 'GtRNAdb: a database of transfer RNA genes detected in genomic sequence', *Nucleic Acids Res*, 37: D93-7.

Chau, K. F., M. L. Shannon, R. M. Fame, E. Fonseca, H. Mullan, M. B. Johnson, A. K. Sendamarai, M. W. Springel, B. Laurent, and M. K. Lehtinen. 2018. 'Downregulation of ribosome biogenesis during early forebrain development', *eLife*, 7.

Chédin, S., M. Riva, P. Schultz, A. Sentenac, and C. Carles. 1998. 'The RNA cleavage activity of RNA polymerase III is mediated by an essential TFIIS-like subunit and is important for transcription termination', *Genes Dev*, 12: 3857-71.

Chen, Chun-Yuan, Rainer B. Lanz, Christopher J. Walkey, Wen-Hsuan Chang, Wange Lu, and Deborah L. Johnson. 2018. 'Maf1 and Repression of RNA Polymerase III-Mediated Transcription Drive Adipocyte Differentiation', *Cell reports*, 24: 1852-64.

Chiu, Y. H., J. B. Macmillan, and Z. J. Chen. 2009. 'RNA polymerase III detects cytosolic DNA and induces type I interferons through the RIG-I pathway', *Cell*, 138: 576-91.

Choe, Byung K., and Milton W. Taylor. 1972. 'Kinetics of synthesis and characterization of transfer RNA precursors in mammalian cells', *Biochimica et Biophysica Acta (BBA) - Nucleic Acids and Protein Synthesis*, 272: 275-87.

Ciliberto, G., G. Raugei, F. Costanzo, L. Dente, and R. Cortese. 1983. 'Common and interchangeable elements in the promoters of genes transcribed by RNA polymerase III', *Cell*, 32: 725-33.

Cloutier, T. E., M. D. Librizzi, A. K. Mollah, M. Brenowitz, and I. M. Willis. 2001. 'Kinetic trapping of DNA by transcription factor IIIB', *Proc Natl Acad Sci U S A*, 98: 9581-6.

Cormack, B. P., and K. Struhl. 1992. 'The TATA-binding protein is required for transcription by all three nuclear RNA polymerases in yeast cells', *Cell*, 69: 685-96.

Cozen, Aaron E., Erin Quartley, Andrew D. Holmes, Eva Hrabeta-Robinson, Eric M. Phizicky, and Todd M. Lowe. 2015. 'ARM-seq: AlkB-facilitated RNA methylation sequencing reveals a complex landscape of modified tRNA fragments', *Nature Methods*, 12: 879-84.

Crick, F. H. 1966. 'Codon--anticodon pairing: the wobble hypothesis', *J Mol Biol*, 19: 548-55.

Cudny, H, and M P Deutscher. 1980. 'Apparent involvement of ribonuclease D in the 3' processing of tRNA precursors', *Proceedings of the National Academy of Sciences*, 77: 837-41.

Darnell, A. M., A. R. Subramaniam, and E. K. O'Shea. 2018. 'Translational Control through Differential Ribosome Pausing during Amino Acid Limitation in Mammalian Cells', *Mol Cell*, 71: 229-43.e11.

Dekker, Job, and Tom Misteli. 2015. 'Long-Range Chromatin Interactions', *Cold Spring Harbor Perspectives in Biology*, 7.

Desai, Neelam, JaeHoon Lee, Rajendra Upadhya, Yaya Chu, Robyn D. Moir, and Ian M. Willis. 2005. 'Two Steps in Maf1-dependent Repression of Transcription by RNA Polymerase III*', *Journal of Biological Chemistry*, 280: 6455-62.

Deutscher, M P, C W Marlor, and R Zaniewski. 1984. 'Ribonuclease T: new exoribonuclease possibly involved in end-turnover of tRNA', *Proceedings of the National Academy of Sciences*, 81: 4290-93.

Dieci, G., and A. Sentenac. 1996. 'Facilitated recycling pathway for RNA polymerase III', *Cell*, 84: 245-52.

Dingermann, T., D. J. Burke, S. Sharp, J. Schaack, and D. Söll. 1982. 'The 5- flanking sequences of Drosophila tRNAArg genes control their in vitro transcription in a Drosophila cell extract', *J Biol Chem*, 257: 14738-44.

Dittmar, K. A., E. M. Mobley, A. J. Radek, and T. Pan. 2004. 'Exploring the regulation of tRNA distribution on the genomic scale', *J Mol Biol*, 337: 31-47.

Dittmar, Kimberly A., Jeffrey M. Goodenbour, and Tao Pan. 2006. 'Tissue-Specific Differences in Human Transfer RNA Expression', *PLOS Genetics*, 2: e221.

Dixon, Jesse R., Siddarth Selvaraj, Feng Yue, Audrey Kim, Yan Li, Yin Shen, Ming Hu, Jun S. Liu, and Bing Ren. 2012. 'Topological domains in mammalian genomes identified by analysis of chromatin interactions', *Nature*, 485: 376-80.

Dolgin, Elie. 2022. 'tRNA therapeutics burst onto startup scene', *Nature Biotechnology*, 40: 283-86.

Donze, David, and Rohinton T. Kamakaka. 2001. 'RNA polymerase III and RNA polymerase II promoter complexes are heterochromatin barriers in Saccharomyces cerevisiae', *The EMBO Journal*, 20: 520-31.

dos Reis, M., R. Savva, and L. Wernisch. 2004. 'Solving the riddle of codon usage preferences: a test for translational selection', *Nucleic Acids Res*, 32: 5036-44.

Downward, J. 2003. 'Targeting RAS signalling pathways in cancer therapy', *Nat Rev Cancer*, 3: 11-22.

Drubin, D. G., and A. A. Hyman. 2017. 'Stem cells: the new "model organism"', *Mol Biol Cell*, 28: 1409-11.

Drummond, D. A., and C. O. Wilke. 2008. 'Mistranslation-induced protein misfolding as a dominant constraint on coding-sequence evolution', *Cell*, 134: 341-52.

Durrieu-Gaillard, S., H. Dumay-Odelot, G. Boldina, N. J. Tourasse, D. Allard, F. André, F. Macari, A. Choquet, P. Lagarde, G. Drutel, T. Leste-Lasserre, M. Petitet, T. Lesluyes, L. Lartigue-Faustin, J. W. Dupuy, F. Chibon, R. G. Roeder, D. Joubert, S. Vagner, and M. Teichmann. 2018. 'Regulation of RNA polymerase III transcription during transformation of human IMR90 fibroblasts with defined genetic elements', *Cell cycle (Georgetown, Tex.)*, 17: 605-15.

Efroni, S., R. Duttagupta, J. Cheng, H. Dehghani, D. J. Hoeppner, C. Dash, D. P. Bazett-Jones, S. Le Grice, R. D. McKay, K. H. Buetow, T. R. Gingeras, T. Misteli, and E. Meshorer. 2008. 'Global transcription in pluripotent embryonic stem cells', *Cell Stem Cell*, 2: 437-47.

Elf, Johan, Daniel Nilsson, Tanel Tenson, and Måns Ehrenberg. 2003. 'Selective Charging of tRNA Isoacceptors Explains Patterns of Codon Usage', *Science*, 300: 1718-22.

Engelke, D. R., S. Y. Ng, B. S. Shastry, and R. G. Roeder. 1980. 'Specific interaction of a purified transcription factor with an internal control region of 5S RNA genes', *Cell*, 19: 717-28.

Enver, T., S. Soneji, C. Joshi, J. Brown, F. Iborra, T. Orntoft, T. Thykjaer, E. Maltby, K. Smith, R. Abu Dawud, M. Jones, M. Matin, P. Gokhale, J. Draper, and P. W. Andrews. 2005. 'Cellular differentiation hierarchies in normal and culture-adapted human embryonic stem cells', *Hum Mol Genet*, 14: 3129-40.

Fang, H., Y. F. Huang, A. Radhakrishnan, A. Siepel, G. J. Lyon, and M. C. Schatz. 2018. 'Scikit-ribo Enables Accurate Estimation and Robust Modeling of Translation Dynamics at Codon Resolution', *Cell Syst*, 6: 180-91.e4.

Fang, Z., Y. Yi, G. Shi, S. Li, S. Chen, Y. Lin, Z. Li, Z. He, W. Li, and S. Zhong. 2017. 'Role of Brf1 interaction with ERα, and significance of its overexpression, in human breast cancer', *Mol Oncol*, 11: 1752-67.

Faust, Russell A., Markus Gapany, Payam Tristani, Alan Davis, George L. Adams, and Khalil Ahmed. 1996. 'Elevated protein kinase CK2 activity in chromatin of head and neck tumors: association with malignant transformation', *Cancer Letters*, 101: 31-35.

Felton-Edkins, Z. A., J. A. Fairley, E. L. Graham, I. M. Johnston, R. J. White, and P. H. Scott. 2003. 'The mitogen-activated protein (MAP) kinase ERK induces tRNA synthesis by phosphorylating TFIIIB', *Embo j*, 22: 2422-32.

Fernández-Tornero, C., M. Moreno-Morcillo, U. J. Rashid, N. M. Taylor, F. M. Ruiz, T. Gruene, P. Legrand, U. Steuerwald, and C. W. Müller. 2013. 'Crystal structure of the 14-subunit RNA polymerase I', *Nature*, 502: 644-9.

Ferrari, R., and G. Dieci. 2008. 'The transcription reinitiation properties of RNA polymerase III in the absence of transcription factors', *Cell Mol Biol Lett*, 13: 112-8.

Ferrari, R., C. Rivetti, J. Acker, and G. Dieci. 2004. 'Distinct roles of transcription factors TFIIIB and TFIIIC in RNA polymerase III transcription reinitiation', *Proc Natl Acad Sci U S A*, 101: 13442-7.

Filer, D., M. A. Thompson, V. Takhaveev, A. J. Dobson, I. Kotronaki, J. W. M. Green, M. Heinemann, J. M. A. Tullet, and N. Alic. 2017. 'RNA polymerase III limits longevity downstream of TORC1', *Nature*, 552: 263-67.

Fishilevich, S., R. Nudel, N. Rappaport, R. Hadar, I. Plaschkes, T. Iny Stein, N. Rosen, A. Kohn, M. Twik, M. Safran, D. Lancet, and D. Cohen. 2017. 'GeneHancer: genome-wide integration of enhancers and target genes in GeneCards', *Database (Oxford)*, 2017.

Frank, Joachim, Haixiao Gao, Jayati Sengupta, Ning Gao, and Derek J. Taylor. 2007. 'The process of mRNA–tRNA translocation', *Proceedings of the National Academy of Sciences*, 104: 19671-78.

Frumkin, Idan, Marc J. Lajoie, Christopher J. Gregg, Gil Hornung, George M. Church, and Yitzhak Pilpel. 2018. 'Codon usage of highly expressed genes affects proteome-wide translation efficiency', *Proceedings of the National Academy of Sciences*, 115: E4940-E49.

Fuerstenau-Sharp, M., M. E. Zimmermann, K. Stark, N. Jentsch, M. Klingenstein, M. Drzymalski, S. Wagner, L. S. Maier, U. Hehr, A. Baessler, M. Fischer, and C. Hengstenberg. 2015. 'Generation of highly purified human cardiomyocytes from peripheral blood mononuclear cell-derived induced pluripotent stem cells', *PLOS ONE*, 10: e0126596.

Galli, Gabriella, Hans Hofstetter, and Max L. Birnstiel. 1981. 'Two conserved sequence blocks within eukaryotic tRNA genes are major promoter elements', *Nature*, 294: 626-31.

Gao, W., C. J. Gallardo-Dodd, and C. Kutter. 2022. 'Cell type-specific analysis by single-cell profiling identifies a stable mammalian tRNA-mRNA interface and increased translation efficiency in neurons', *Genome Res*, 32: 97-110.

Gardin, Justin, Rukhsana Yeasmin, Alisa Yurovsky, Ying Cai, Steve Skiena, and Bruce Futcher. 2014. 'Measurement of average decoding rates of the 61 sense codons in vivo', *eLife*, 3: e03735.

Geiduschek, E. P., and G. A. Kassavetis. 2001. 'The RNA polymerase III transcription apparatus', *J Mol Biol*, 310: 1-26.

Geiduschek, E. P., and G. P. Tocchini-Valentini. 1988. 'Transcription by RNA polymerase III', *Annu Rev Biochem*, 57: 873-914.

Gerber, A., K. Ito, C. S. Chu, and R. G. Roeder. 2020. 'Gene-Specific Control of tRNA Expression by RNA Polymerase II', *Mol Cell*, 78: 765-78.e7.

Gerber, A. P., and W. Keller. 1999. 'An adenosine deaminase that generates inosine at the wobble position of tRNAs', *Science*, 286: 1146-9.

Geslain, Renaud, Franck Martin, Alain Camasses, and Gilbert Eriani. 2003. 'A yeast knockout strain to discriminate between active and inactive tRNA molecules', *Nucleic Acids Research*, 31: 4729-37.

Ghavidel, A., and M. C. Schultz. 2001. 'TATA binding protein-associated CK2 transduces DNA damage signals to the RNA polymerase III transcriptional machinery', *Cell*, 106: 575-84.

Ghosh, S., A. J. Yates, M. C. Frühwald, J. C. Miecznikowski, C. Plass, and D. Smiraglia. 2010. 'Tissue specific DNA methylation of CpG islands in normal human adult somatic tissues distinguishes neural from non-neural tissues', *Epigenetics*, 5: 527-38.

Gillen, Sarah L., Joseph A. Waldron, and Martin Bushell. 2021. 'Codon optimality in cancer', *Oncogene*, 40: 6309-20.

Gingold, Hila, Disa Tehler, Nanna R Christoffersen, Morten M Nielsen, Fazila Asmar, Susanne M Kooistra, Nicolaj S Christophersen, Lise Lotte Christensen, Michael Borre, Karina D Sørensen, Lars D Andersen, Claus L Andersen, Esther Hulleman, Tom Wurdinger, Elisabeth Ralfkiær, Kristian Helin, Kirsten Grønbæk, Torben Ørntoft, Sebastian M Waszak, Orna Dahan, Jakob Skou Pedersen, Anders H Lund, and Yitzhak Pilpel. 2014. 'A Dual Program for Translation Regulation in Cellular Proliferation and Differentiation', *Cell*, 158: 1281-92.

Girbig, M., A. D. Misiaszek, M. K. Vorländer, A. Lafita, H. Grötsch, F. Baudin, A. Bateman, and C. W. Müller. 2021a. 'Cryo-EM structures of human RNA polymerase III in its unbound and transcribing states', *Nat Struct Mol Biol*, 28: 210-19.

Girbig, Mathias, Agata D. Misiaszek, Matthias K. Vorländer, Aleix Lafita, Helga Grötsch, Florence Baudin, Alex Bateman, and Christoph W. Müller. 2021b. 'Cryo-EM structures of human RNA polymerase III in its unbound and transcribing states', *Nature Structural & Molecular Biology*, 28: 210-19.

Girbig, Mathias, Juanjuan Xie, Helga Grötsch, Domenico Libri, Odil Porrua, and Christoph W. Müller. 2022. 'Architecture of the yeast Pol III pre-termination complex and pausing mechanism on poly(dT) termination signals', *Cell reports*, 40: 111316.

Giuliodori, Silvia, Riccardo Percudani, Priscilla Braglia, Roberto Ferrari, Elisa Guffanti, Simone Ottonello, and Giorgio Dieci. 2003. 'A Composite Upstream Sequence Motif Potentiates tRNA Gene Transcription in Yeast', *Journal of Molecular Biology*, 333: 1-20.

Gobet, C., B. D. Weger, J. Marquis, E. Martin, N. Neelagandan, F. Gachon, and F. Naef. 2020a. 'Robust landscapes of ribosome dwell times and aminoacyl-tRNAs in response to nutrient stress in liver', *Proc Natl Acad Sci U S A*, 117: 9630-41.

Gobet, Cédric, Benjamin Dieter Weger, Julien Marquis, Eva Martin, Nagammal Neelagandan, Frédéric Gachon, and Felix Naef. 2020b. 'Robust landscapes of ribosome dwell times and aminoacyl-tRNAs in response to nutrient stress in liver', *Proceedings of the National Academy of Sciences*, 117: 9630-41.

Gogakos, T., M. Brown, A. Garzia, C. Meyer, M. Hafner, and T. Tuschl. 2017. 'Characterizing Expression and Processing of Precursor and Mature Human tRNAs by Hydro-tRNAseq and PAR-CLIP', *Cell reports*, 20: 1463-75.

Gomez-Roman, N., C. Grandori, R. N. Eisenman, and R. J. White. 2003. 'Direct activation of RNA polymerase III transcription by c-Myc', *Nature*, 421: 290-4.

Goodarzi, H., H. C. B. Nguyen, S. Zhang, B. D. Dill, H. Molina, and S. F. Tavazoie. 2016. 'Modulated Expression of Specific tRNAs Drives Gene Expression and Cancer Progression', *Cell*, 165: 1416-27.

Goodenbour, J. M., and T. Pan. 2006. 'Diversity of tRNA genes in eukaryotes', *Nucleic Acids Res*, 34: 6137-46.

Graczyk, Damian, Małgorzata Cieśla, and Magdalena Boguta. 2018. 'Regulation of tRNA synthesis by the general transcription factors of RNA polymerase III - TFIIIB and TFIIIC, and by the MAF1 protein', *Biochimica et Biophysica Acta (BBA) - Gene Regulatory Mechanisms*, 1861: 320-29.

Graczyk, Damian, Janusz Dębski, Grażyna Muszyńska, Maria Bretner, Olivier Lefebvre, and Magdalena Boguta. 2011. 'Casein kinase II-mediated phosphorylation of general repressor Maf1 triggers RNA polymerase III activation', *Proceedings of the National Academy of Sciences*, 108: 4926.

Greulich, F., A. Mechtidou, T. Horn, and N. H. Uhlenhaut. 2021. 'Protocol for using heterologous spike-ins to normalize for technical variation in chromatin immunoprecipitation', *STAR Protoc*, 2: 100609.

Gu, Wanjun, Tong Zhou, and Claus O. Wilke. 2010. 'A Universal Trend of Reduced mRNA Stability near the Translation-Initiation Site in Prokaryotes and Eukaryotes', *PLOS Computational Biology*, 6: e1000664.

Guenther, M. G., S. S. Levine, L. A. Boyer, R. Jaenisch, and R. A. Young. 2007. 'A chromatin landmark and transcription initiation at most promoters in human cells', *Cell*, 130: 77-88.

Guimaraes, Joao C., Nitish Mittal, Alexandra Gnann, Dominik Jedlinski, Andrea Riba, Katarzyna Buczak, Alexander Schmidt, and Mihaela Zavolan. 2020. 'A rare codon-based translational program of cell proliferation', *Genome Biology*, 21: 44.

Guy, Michael P., David L. Young, Matthew J. Payea, Xiaoju Zhang, Yoshiko Kon, Kimberly M. Dean, Elizabeth J. Grayhack, David H. Mathews, Stanley Fields, and Eric M. Phizicky. 2014. 'Identification of the determinants of tRNA function and susceptibility to rapid tRNA decay by high-throughput in vivo analysis', *Genes & Development*, 28: 1721-32.

Hanahan, D., and R. A. Weinberg. 2011. 'Hallmarks of cancer: the next generation', *Cell*, 144: 646-74.

Harnett, D., M. C. Ambrozkiewicz, U. Zinnall, A. Rusanova, E. Borisova, A. N. Drescher, M. Couce-Iglesias, G. Villamil, R. Dannenberg, K. Imami, A. Münster-Wandowski, B. Fauler, T. Mielke, M. Selbach, M. Landthaler, C. M. T. Spahn, V. Tarabykin, U. Ohler, and M. L. Kraushar. 2022a. 'A critical period of translational control during brain development at codon resolution', *Nat Struct Mol Biol*, 29: 1277-90.

Harnett, Dermot, Mateusz C. Ambrozkiewicz, Ulrike Zinnall, Alexandra Rusanova, Ekaterina Borisova, Amelie N. Drescher, Marta Couce-Iglesias, Gabriel Villamil, Rike Dannenberg, Koshi Imami, Agnieszka Münster-Wandowski, Beatrix Fauler, Thorsten Mielke, Matthias Selbach, Markus Landthaler, Christian M. T. Spahn, Victor Tarabykin, Uwe Ohler, and Matthew L. Kraushar. 2022b. 'A critical period of translational control during brain development at codon resolution', *Nature Structural & Molecular Biology*, 29: 1277-90.

Haurie, Valérie, Stéphanie Durrieu-Gaillard, Hélène Dumay-Odelot, Daniel Da Silva, Christophe Rey, Martina Prochazkova, Robert G. Roeder, Daniel Besser, and Martin Teichmann. 2010. 'Two isoforms of human RNA polymerase III with specific functions in cell growth and transformation', *Proceedings of the National Academy of Sciences*, 107: 4176-81.

Hay, N., and N. Sonenberg. 2004. 'Upstream and downstream of mTOR', *Genes Dev*, 18: 1926-45.

Heinz, S., C. E. Romanoski, C. Benner, and C. K. Glass. 2015. 'The selection and function of cell type-specific enhancers', *Nat Rev Mol Cell Biol*, 16: 144-54.

Hellmuth, Klaus, Denise M. Lau, F. Ralf Bischoff, Markus Künzler, Ed Hurt, and George Simos. 1998. 'Yeast Los1p Has Properties of an Exportin-Like Nucleocytoplasmic Transport Factor for tRNA', *Molecular and cellular biology*, 18: 6374-86.

Henning, Robert H., and Bianca J. J. M. Brundel. 2017. 'Proteostasis in cardiac health and disease', *Nature Reviews Cardiology*, 14: 637-53.

Hernandez, Nouria. 2001. 'Small Nuclear RNA Genes: a Model System to Study Fundamental Mechanisms of Transcription*', *Journal of Biological Chemistry*, 276: 26733-36.

Hicks, David G., Bagi R. Janarthanan, Ramya Vardarajan, Swati A. Kulkarni, Thaer Khoury, Daniel Dim, G. Thomas Budd, Brian J. Yoder, Raymond Tubbs, Marshall T. Schreeder, Noel C. Estopinal, Rodney A. Beck, Yanling Wang, Brian Z. Ring, Robert S. Seitz, and Douglas T. Ross. 2010. 'The expression of TRMT2A, a novel cell cycle regulated protein, identifies a subset of breast cancer patients with HER2 over-expression that are at an increased risk of recurrence', *BMC Cancer*, 10: 108.

Hiller, D. A., V. Singh, M. Zhong, and S. A. Strobel. 2011. 'A two-step chemical mechanism for ribosome-catalysed peptide bond formation', *Nature*, 476: 236-9.

Hoffmann, Niklas A., Arjen J. Jakobi, María Moreno-Morcillo, Sebastian Glatt, Jan Kosinski, Wim J. H. Hagen, Carsten Sachse, and Christoph W. Müller. 2015. 'Molecular structures of unbound and transcribing RNA polymerase III', *Nature*, 528: 231-36.

Hofstetter, H., A. Kressman, and M. L. Birnstiel. 1981. 'A split promoter for a eucaryotic tRNA gene', *Cell*, 24: 573-85.

Homma, M. K., and Y. Homma. 2008. 'Cell cycle and activation of CK2', *Mol Cell Biochem*, 316: 49-55.

Hopper, Anita K., and Regina T. Nostramo. 2019. 'tRNA Processing and Subcellular Trafficking Proteins Multitask in Pathways for Other RNAs', *Frontiers in Genetics*, 10.

Hsieh, Y. J., Z. Wang, R. Kovelman, and R. G. Roeder. 1999. 'Cloning and characterization of two evolutionarily conserved subunits (TFIIIC102 and TFIIIC63) of human TFIIIC and their involvement in functional interactions with TFIIIB and RNA polymerase III', *Molecular and cellular biology*, 19: 4944-52.

Huber, Alexandre, Bernd Bodenmiller, Aino Uotila, Michael Stahl, Stefanie Wanka, Bertran Gerrits, Ruedi Aebersold, and Robbie Loewith. 2009. 'Characterization of the rapamycin-sensitive phosphoproteome reveals that Sch9 is a central coordinator of protein synthesis', *Genes & Development*, 23: 1929-43.

Hughes, Laetitia A., Danielle L. Rudler, Stefan J. Siira, Tim McCubbin, Samuel A. Raven, Jasmin M. Browne, Judith A. Ermer, Jeanette Rientjes, Jennifer Rodger, Esteban Marcellin, Oliver Rackham, and Aleksandra Filipovska. 2023. 'Copy number variation in tRNA isodecoder genes impairs mammalian development and balanced translation', *Nature Communications*, 14: 2210.

Hussmann, J. A., S. Patchett, A. Johnson, S. Sawyer, and W. H. Press. 2015. 'Understanding Biases in Ribosome Profiling Experiments Reveals Signatures of Translation Dynamics in Yeast', *PLoS Genet*, 11: e1005732.

Ingolia, Nicholas T., Sina Ghaemmaghami, John R. S. Newman, and Jonathan S. Weissman. 2009. 'Genome-Wide Analysis in Vivo of Translation with Nucleotide Resolution Using Ribosome Profiling', *Science*, 324: 218-23.

Ishimura, R., G. Nagy, I. Dotu, H. Zhou, X. L. Yang, P. Schimmel, S. Senju, Y. Nishimura, J. H. Chuang, and S. L. Ackerman. 2014. 'RNA function. Ribosome stalling induced by mutation of a CNS-specific tRNA causes neurodegeneration', *Science*, 345: 455-9.

Jahn, D., E. Wingender, and K. H. Seifart. 1987. 'Transcription complexes for various class III genes differ in parameters of formation and stability towards salt', *Journal of Molecular Biology*, 193: 303-13.

Jenner, L., A. L. Starosta, D. S. Terry, A. Mikolajka, L. Filonava, M. Yusupov, S. C. Blanchard, D. N. Wilson, and G. Yusupova. 2013. 'Structural basis for potent inhibitory activity of the antibiotic tigecycline during protein synthesis', *Proc Natl Acad Sci U S A*, 110: 3812-6.

Johnston, I. M., S. J. Allison, J. P. Morton, L. Schramm, P. H. Scott, and R. J. White. 2002. 'CK2 forms a stable complex with TFIIIB and activates RNA polymerase III transcription in human cells', *Molecular and cellular biology*, 22: 3757-68.

Joshi, Chintan J., Wenfan Ke, Anna Drangowska-Way, Eyleen J. O'Rourke, and Nathan E. Lewis. 2022. 'What are housekeeping genes?', *PLOS Computational Biology*, 18: e1010295.

Jühling, F., M. Mörl, R. K. Hartmann, M. Sprinzl, P. F. Stadler, and J. Pütz. 2009. 'tRNAdb 2009: compilation of tRNA sequences and tRNA genes', *Nucleic Acids Res*, 37: D159-62.

Kaiser, F., S. Krautwurst, S. Salentin, V. J. Haupt, C. Leberecht, S. Bittrich, D. Labudde, and M. Schroeder. 2020. 'The structural basis of the genetic code: amino acid recognition by aminoacyl-tRNA synthetases', *Sci Rep*, 10: 12647.

Kantidakis, T., B. A. Ramsbottom, J. L. Birch, S. N. Dowding, and R. J. White. 2010. 'mTOR associates with TFIIIC, is found at tRNA and 5S rRNA genes, and targets their repressor Maf1', *Proc Natl Acad Sci U S A*, 107: 11823-8.

Kantidakis, T., and R. J. White. 2010. 'Dr1 (NC2) is present at tRNA genes and represses their transcription in human cells', *Nucleic Acids Res*, 38: 1228-39.

Kapur, M., A. Ganguly, G. Nagy, S. I. Adamson, J. H. Chuang, W. N. Frankel, and S. L. Ackerman. 2020. 'Expression of the Neuronal tRNA n-Tr20 Regulates Synaptic Transmission and Seizure Susceptibility', *Neuron*, 108: 193-208.e9.

Karlsson, Max, Cheng Zhang, Loren Méar, Wen Zhong, Andreas Digre, Borbala Katona, Evelina Sjöstedt, Lynn Butler, Jacob Odeberg, Philip Dusart, Fredrik Edfors, Per Oksvold, Kalle von Feilitzen, Martin Zwahlen, Muhammad Arif, Ozlem Altay, Xiangyu Li, Mehmet Ozcan, Adil Mardinoglu, Linn Fagerberg, Jan Mulder, Yonglun Luo, Fredrik Ponten, Mathias Uhlén, and Cecilia Lindskog. 2021. 'A single–cell type transcriptomics map of human tissues', *Science Advances*, 7: eabh2169.

Kassavetis, G. A., J. A. Blanco, T. E. Johnson, and E. P. Geiduschek. 1992. 'Formation of open and elongating transcription complexes by RNA polymerase III', *J Mol Biol*, 226: 47-58.

Kassavetis, G. A., G. A. Letts, and E. P. Geiduschek. 2001. 'The RNA polymerase III transcription initiation factor TFIIIB participates in two steps of promoter opening', *Embo j*, 20: 2823-34.

Kassavetis, George A., Burkhard R. Braun, Lam H. Nguyen, and E. Peter Geiduschek. 1990. 'S. cerevisiae TFIIIB is the transcription initiation factor proper of RNA polymerase III, while TFIIIA and TFIIIC are assembly factors', *Cell*, 60: 235-45.

Katanski, C. D., H. Alshammary, C. P. Watkins, S. Huang, A. Gonzales-Reiche, E. M. Sordillo, H. van Bakel, K. Lolans, V. Simon, and T. Pan. 2022. 'tRNA abundance, modification and fragmentation in nasopharyngeal swabs as biomarkers for COVID-19 severity', *Front Cell Dev Biol*, 10: 999351.

Kenneth, N. S., L. Marshall, and R. J. White. 2008. 'Recruitment of RNA polymerase III in vivo', *Nucleic Acids Res*, 36: 3757-64.

Kessler, A. C., and R. J. Maraia. 2021. 'The nuclear and cytoplasmic activities of RNA polymerase III, and an evolving transcriptome for surveillance', *Nucleic Acids Res*, 49: 12017-34.

Khoo, S. K., C. C. Wu, Y. C. Lin, J. C. Lee, and H. T. Chen. 2014. 'Mapping the protein interaction network for TFIIB-related factor Brf1 in the RNA polymerase III preinitiation complex', *Molecular and cellular biology*, 34: 551-9.

Kilpinen, H., A. Goncalves, A. Leha, V. Afzal, K. Alasoo, S. Ashford, S. Bala, D. Bensaddek, F. P. Casale, O. J. Culley, P. Danecek, A. Faulconbridge, P. W. Harrison, A. Kathuria, D. McCarthy, S. A. McCarthy, R. Meleckyte, Y. Memari, N. Moens, F. Soares, A. Mann, I. Streeter, C. A. Agu, A. Alderton, R. Nelson, S. Harper, M. Patel, A. White, S. R. Patel, L. Clarke, R. Halai, C. M. Kirton, A. Kolb-Kokocinski, P. Beales, E. Birney, D. Danovi, A. I. Lamond, W. H. Ouwehand, L. Vallier, F. M. Watt, R. Durbin, O. Stegle, and D. J. Gaffney. 2017. 'Common genetic variation drives molecular heterogeneity in human iPSCs', *Nature*, 546: 370-75.

Kim, J., and H. Kim. 2012. 'Recruitment and biological consequences of histone modification of H3K27me3 and H3K9me3', *Ilar j*, 53: 232-9.

Klinge, S., F. Voigts-Hoffmann, M. Leibundgut, S. Arpagaus, and N. Ban. 2011. 'Crystal structure of the eukaryotic 60S ribosomal subunit in complex with initiation factor 6', *Science*, 334: 941-8.

Krahn, Natalie, Jonathan T. Fischer, and Dieter Söll. 2020. 'Naturally Occurring tRNAs With Non-canonical Structures', *Frontiers in Microbiology*, 11.

Kramer, E. B., and A. K. Hopper. 2013. 'Retrograde transfer RNA nuclear import provides a new level of tRNA quality control in Saccharomyces cerevisiae', *Proc Natl Acad Sci U S A*, 110: 21042-7.

Kudla, G., A. W. Murray, D. Tollervey, and J. B. Plotkin. 2009. 'Coding-sequence determinants of gene expression in Escherichia coli', *Science*, 324: 255-8.

Kulak, N. A., G. Pichler, I. Paron, N. Nagaraj, and M. Mann. 2014. 'Minimal, encapsulated proteomic-sample processing applied to copy-number estimation in eukaryotic cells', *Nat Methods*, 11: 319-24.

Kundu, T. K., Z. Wang, and R. G. Roeder. 1999. 'Human TFIIIC relieves chromatin-mediated repression of RNA polymerase III transcription and contains an intrinsic histone acetyltransferase activity', *Molecular and cellular biology*, 19: 1605-15.

Kutter, C., G. D. Brown, A. Gonçalves, M. D. Wilson, S. Watt, A. Brazma, R. J. White, and D. T. Odom. 2011a. 'Pol III binding in six mammals shows conservation among amino acid isotypes despite divergence among tRNA genes', *Nat Genet*, 43: 948-55.

Kutter, Claudia, Gordon D. Brown, Ângela Gonçalves, Michael D. Wilson, Stephen Watt, Alvis Brazma, Robert J. White, and Duncan T. Odom. 2011b. 'Pol III binding in six mammals shows conservation among amino acid isotypes despite divergence among tRNA genes', *Nature Genetics*, 43: 948-55.

Labbadia, J., and R. I. Morimoto. 2015. 'Repression of the Heat Shock Response Is a Programmed Event at the Onset of Reproduction', *Mol Cell*, 59: 639-50.

Lai, Lien B., Agustín Vioque, Leif A. Kirsebom, and Venkat Gopalan. 2010. 'Unexpected diversity of RNase P, an ancient tRNA processing enzyme: Challenges and prospects', *FEBS Letters*, 584: 287-96.

Lake, J. A. 1977. 'Aminoacyl-tRNA binding at the recognition site is the first step of the elongation cycle of protein synthesis', *Proc Natl Acad Sci U S A*, 74: 1903-7.

Landesman-Bollag, E., D. H. Song, R. Romieu-Mourez, D. J. Sussman, R. D. Cardiff, G. E. Sonenshein, and D. C. Seldin. 2001. 'Protein kinase CK2: signaling and tumorigenesis in the mammary gland', *Mol Cell Biochem*, 227: 153-65.

Landrieux, E., N. Alic, C. Ducrot, J. Acker, M. Riva, and C. Carles. 2006. 'A subcomplex of RNA polymerase III subunits involved in transcription termination and reinitiation', *Embo j*, 25: 118-28.

Landt, S. G., G. K. Marinov, A. Kundaje, P. Kheradpour, F. Pauli, S. Batzoglou, B. E. Bernstein, P. Bickel, J. B. Brown, P. Cayting, Y. Chen, G. DeSalvo, C. Epstein, K. I. Fisher-Aylor, G. Euskirchen, M. Gerstein, J. Gertz, A. J. Hartemink, M. M. Hoffman, V. R. Iyer, Y. L. Jung, S. Karmakar, M. Kellis, P. V. Kharchenko, Q. Li, T. Liu, X. S. Liu, L. Ma, A. Milosavljevic, R. M. Myers, P. J. Park, M. J. Pazin, M. D. Perry, D. Raha, T. E. Reddy, J. Rozowsky, N. Shoresh, A. Sidow, M. Slattery, J. A. Stamatoyannopoulos, M. Y. Tolstorukov, K. P. White, S. Xi, P. J. Farnham, J. D. Lieb, B. J. Wold, and M. Snyder. 2012. 'ChIP-seq guidelines and practices of the ENCODE and modENCODE consortia', *Genome Res*, 22: 1813-31.

Laplante, M., and D. M. Sabatini. 2012. 'mTOR signaling in growth control and disease', *Cell*, 149: 274-93.

Lareau, Liana F., Dustin H. Hite, Gregory J. Hogan, and Patrick O. Brown. 2014. 'Distinct stages of the translation elongation cycle revealed by sequencing ribosome-protected mRNA fragments', *eLife*, 3: e01257.

Lassar, Andrew B., Paul L. Martin, and Robert G. Roeder. 1983. 'Transcription of Class III Genes: Formation of Preinitiation Complexes', *Science*, 222: 740-48.

Ledoux, S., M. Olejniczak, and O. C. Uhlenbeck. 2009. 'A sequence element that tunes Escherichia coli tRNA(Ala)(GGC) to ensure accurate decoding', *Nat Struct Mol Biol*, 16: 359-64.

Lee, J., R. D. Moir, and I. M. Willis. 2009. 'Regulation of RNA polymerase III transcription involves SCH9-dependent and SCH9-independent branches of the target of rapamycin (TOR) pathway', *J Biol Chem*, 284: 12604-8.

Lefèvre, Stéphane, Hélène Dumay-Odelot, Leyla El-Ayoubi, Aidan Budd, Pierre Legrand, Noël Pinaud, Martin Teichmann, and Sébastien Fribourg. 2011. 'Structure-function analysis of hRPC62 provides insights into RNA polymerase III transcription initiation', *Nature structural & molecular biology*, 18: 352-58.

Lentini, J. M., H. S. Alsaif, E. Faqeih, F. S. Alkuraya, and D. Fu. 2020. 'DALRD3 encodes a protein mutated in epileptic encephalopathy that targets arginine tRNAs for 3-methylcytosine modification', *Nat Commun*, 11: 2510.

Levine, M., C. Cattoglio, and R. Tjian. 2014. 'Looping back to leap forward: transcription enters a new era', *Cell*, 157: 13-25.

Li, Y., C. K. Tsang, S. Wang, X. X. Li, Y. Yang, L. Fu, W. Huang, M. Li, H. Y. Wang, and X. F. Zheng. 2016. 'MAF1 suppresses AKT-mTOR signaling and liver cancer through activation of PTEN transcription', *Hepatology*, 63: 1928-42.

Liu, J., X. Wu, H. Zhang, G. P. Pfeifer, and Q. Lu. 2017. 'Dynamics of RNA Polymerase II Pausing and Bivalent Histone H3 Methylation during Neuronal Differentiation in Brain Development', *Cell reports*, 20: 1307-18.

Love, Michael I., Wolfgang Huber, and Simon Anders. 2014. 'Moderated estimation of fold change and dispersion for RNA-seq data with DESeq2', *Genome Biology*, 15: 550.

Loyfer, Netanel, Judith Magenheim, Ayelet Peretz, Gordon Cann, Joerg Bredno, Agnes Klochendler, Ilana Fox-Fisher, Sapir Shabi-Porat, Merav Hecht, Tsuria Pelet, Joshua Moss, Zeina Drawshy, Hamed Amini, Patriss Moradi, Sudharani Nagaraju, Dvora Bauman, David Shveiky, Shay Porat, Uri Dior, Gurion Rivkin, Omer Or, Nir Hirshoren, Einat Carmon, Alon Pikarsky, Abed Khalaileh, Gideon Zamir, Ronit Grinbaum, Machmud Abu Gazala, Ido Mizrahi, Noam Shussman, Amit Korach, Ori Wald, Uzi Izhar, Eldad Erez, Vladimir Yutkin, Yaacov Samet, Devorah Rotnemer Golinkin, Kirsty L. Spalding, Henrik Druid, Peter Arner, A. M. James Shapiro, Markus Grompe, Alex Aravanis, Oliver Venn, Arash Jamshidi, Ruth Shemer, Yuval Dor, Benjamin Glaser, and Tommy Kaplan. 2023. 'A DNA methylation atlas of normal human cell types', *Nature*, 613: 355-64.

Lund, R. J., N. Rahkonen, M. Malonzo, L. Kauko, M. R. Emani, V. Kivinen, E. Närvä, E. Kemppainen, A. Laiho, H. Skottman, O. Hovatta, O. Rasool, M. Nykter, H. Lähdesmäki, and R. Lahesmaa. 2017. 'RNA Polymerase III Subunit POLR3G Regulates Specific Subsets of PolyA(+) and SmallRNA Transcriptomes and Splicing in Human Pluripotent Stem Cells', *Stem Cell Reports*, 8: 1442-54.

Mandegar, M. A., N. Huebsch, E. B. Frolov, E. Shin, A. Truong, M. P. Olvera, A. H. Chan, Y. Miyaoka, K. Holmes, C. I. Spencer, L. M. Judge, D. E. Gordon, T. V. Eskildsen, J. E. Villalta, M. A. Horlbeck, L. A. Gilbert, N. J. Krogan, S. P. Sheikh, J. S. Weissman, L. S. Qi, P. L. So, and B. R. Conklin. 2016. 'CRISPR Interference Efficiently Induces Specific and Reversible Gene Silencing in Human iPSCs', *Cell Stem Cell*, 18: 541-53.

Marck, C, O Lefebvre, C Carles, M Riva, N Chaussivert, A Ruet, and A Sentenac. 1993. 'The TFIIIB-assembling subunit of yeast transcription factor TFIIIC has both tetratricopeptide repeats and basic helix-loop-helix motifs', *Proceedings of the National Academy of Sciences*, 90: 4027-31.

Marck, C., R. Kachouri-Lafond, I. Lafontaine, E. Westhof, B. Dujon, and H. Grosjean. 2006. 'The RNA polymerase III-dependent family of genes in hemiascomycetes: comparative RNomics, decoding strategies, transcription and evolutionary implications', *Nucleic Acids Res*, 34: 1816-35.

Marrone, L., H. C. A. Drexler, J. Wang, P. Tripathi, T. Distler, P. Heisterkamp, E. N. Anderson, S. Kour, A. Moraiti, S. Maharana, R. Bhatnagar, T. G. Belgard, V. Tripathy, N. Kalmbach, Z. Hosseinzadeh, V. Crippa, M. Abo-Rady, F. Wegner, A. Poletti, D. Troost, E. Aronica, V. Busskamp, J. Weis, U. B. Pandey, A. A. Hyman, S. Alberti, A. Goswami, and J. Sterneckert. 2019. 'FUS pathology in ALS is linked to alterations in multiple

ALS-associated proteins and rescued by drugs stimulating autophagy', *Acta Neuropathol*, 138: 67-84.

Marzouki, N., S. Camier, A. Ruet, A. Moenne, and A. Sentenac. 1986. 'Selective proteolysis defines two DNA binding domains in yeast transcription factor tau', *Nature*, 323: 176-8.

Mattison, J. A., R. J. Colman, T. M. Beasley, D. B. Allison, J. W. Kemnitz, G. S. Roth, D. K. Ingram, R. Weindruch, R. de Cabo, and R. M. Anderson. 2017. 'Caloric restriction improves health and survival of rhesus monkeys', *Nat Commun*, 8: 14063.

McFarlane, R. J., and S. K. Whitehall. 2009. 'tRNA genes in eukaryotic genome organization and reorganization', *Cell cycle (Georgetown, Tex.)*, 8: 3102-6.

Meggio, Flavio, and Lorenzo A. Pinna. 2003. 'One-thousand-and-one substrates of protein kinase CK2?', *The FASEB Journal*, 17: 349-68.

Michels, A. A., A. M. Robitaille, D. Buczynski-Ruchonnet, W. Hodroj, J. H. Reina, M. N. Hall, and N. Hernandez. 2010. 'mTORC1 directly phosphorylates and regulates human MAF1', *Molecular and cellular biology*, 30: 3749-57.

Mohr, S., E. Ghanem, W. Smith, D. Sheeter, Y. Qin, O. King, D. Polioudakis, V. R. Iyer, S. Hunicke-Smith, S. Swamy, S. Kuersten, and A. M. Lambowitz. 2013. 'Thermostable group II intron reverse transcriptase fusion proteins and their use in cDNA synthesis and next-generation RNA sequencing', *Rna*, 19: 958-70.

Moir, R. D., K. V. Puglia, and I. M. Willis. 2002. 'A gain-of-function mutation in the second tetratricopeptide repeat of TFIIIC131 relieves autoinhibition of Brf1 binding', *Molecular and cellular biology*, 22: 6131-41.

Moir, Robyn D., JaeHoon Lee, Rebecca A. Haeusler, Neelam Desai, David R. Engelke, and Ian M. Willis. 2006. 'Protein kinase A regulates RNA polymerase III transcription through the nuclear localization of Maf1', *Proceedings of the National Academy of Sciences*, 103: 15044-49.

Moore, Lisa D., Thuc Le, and Guoping Fan. 2013. 'DNA Methylation and Its Basic Function', *Neuropsychopharmacology*, 38: 23-38.

Moqtaderi, Z., J. Wang, D. Raha, R. J. White, M. Snyder, Z. Weng, and K. Struhl. 2010a. 'Genomic binding profiles of functionally distinct RNA polymerase III transcription complexes in human cells', *Nat Struct Mol Biol*, 17: 635-40.

Moqtaderi, Zarmik, Jie Wang, Debasish Raha, Robert J. White, Michael Snyder, Zhiping Weng, and Kevin Struhl. 2010b. 'Genomic binding profiles of functionally distinct RNA polymerase III transcription complexes in human cells', *Nature Structural & Molecular Biology*, 17: 635-40.

Mordret, E., O. Dahan, O. Asraf, R. Rak, A. Yehonadav, G. D. Barnabas, J. Cox, T. Geiger, A. B. Lindner, and Y. Pilpel. 2019. 'Systematic Detection of Amino Acid Substitutions in Proteomes Reveals Mechanistic Basis of Ribosome Errors and Selection for Translation Fidelity', *Mol Cell*, 75: 427-41.e5.

Murphy, Frank V., and V. Ramakrishnan. 2004. 'Structure of a purine-purine wobble base pair in the decoding center of the ribosome', *Nature Structural & Molecular Biology*, 11: 1251-52.

Nedialkova, D. D., and S. A. Leidel. 2015. 'Optimization of Codon Translation Rates via tRNA Modifications Maintains Proteome Integrity', *Cell*, 161: 1606-18.

Noack Watt, K. E., A. Achilleos, C. L. Neben, A. E. Merrill, and P. A. Trainor. 2016. 'The Roles of RNA Polymerase I and III Subunits Polr1c and Polr1d in Craniofacial Development and in Zebrafish Models of Treacher Collins Syndrome', *PLoS Genet*, 12: e1006187.

Oler, A. J., R. K. Alla, D. N. Roberts, A. Wong, P. C. Hollenhorst, K. J. Chandler, P. A. Cassiday, C. A. Nelson, C. H. Hagedorn, B. J. Graves, and B. R. Cairns. 2010a. 'Human RNA polymerase III transcriptomes and relationships to Pol II promoter chromatin and enhancer-binding factors', *Nat Struct Mol Biol*, 17: 620-8.

Oler, Andrew J., Ravi K. Alla, Douglas N. Roberts, Alexander Wong, Peter C. Hollenhorst, Katherine J. Chandler, Patrick A. Cassiday, Cassie A. Nelson, Curt H. Hagedorn, Barbara J. Graves, and Bradley R. Cairns. 2010b. 'Human RNA polymerase III

transcriptomes and relationships to Pol II promoter chromatin and enhancer-binding factors', *Nature Structural & Molecular Biology*, 17: 620-28.

Oliveira Andrade, M., M. L. Sforça, F. A. H. Batista, A. C. M. Figueira, and C. E. Benedetti. 2020. 'The MAF1 Phosphoregulatory Region Controls MAF1 Interaction with the RNA Polymerase III C34 Subunit and Transcriptional Repression in Plants', *Plant Cell*, 32: 3019-35.

Orellana, E. A., E. Siegal, and R. I. Gregory. 2022. 'tRNA dysregulation and disease', *Nat Rev Genet*, 23: 651-64.

Orioli, A. 2017. 'tRNA biology in the omics era: Stress signalling dynamics and cancer progression', *Bioessays*, 39.

Orioli, A., C. Pascali, A. Pagano, M. Teichmann, and G. Dieci. 2012. 'RNA polymerase III transcription control elements: themes and variations', *Gene*, 493: 185-94.

Orioli, A., V. Praz, P. Lhôte, and N. Hernandez. 2016. 'Human MAF1 targets and represses active RNA polymerase III genes by preventing recruitment rather than inducing long-term transcriptional arrest', *Genome Res*, 26: 624-35.

Orlando, David A, Mei Wei Chen, Victoria E Brown, Snehakumari Solanki, Yoon J Choi, Eric R Olson, Christian C Fritz, James E Bradner, and Matthew G Guenther. 2014. 'Quantitative ChIP-Seq Normalization Reveals Global Modulation of the Epigenome', *Cell reports*, 9: 1163-70.

Pai, D. A., and D. R. Engelke. 2010. 'Spatial organization of genes as a component of regulated expression', *Chromosoma*, 119: 13-25.

Panigrahi, Anil, and Bert W. O'Malley. 2021. 'Mechanisms of enhancer action: the known and the unknown', *Genome Biology*, 22: 108.

Parmley, Joanna L., Araxi O. Urrutia, Lukasz Potrzebowski, Henrik Kaessmann, and Laurence D. Hurst. 2007. 'Splicing and the Evolution of Proteins in Mammals', *PLOS Biology*, 5: e14.

Pekowska, A., T. Benoukraf, J. Zacarias-Cabeza, M. Belhocine, F. Koch, H. Holota, J. Imbert, J. C. Andrau, P. Ferrier, and S. Spicuglia. 2011. 'H3K4 tri-methylation provides an epigenetic signature of active enhancers', *Embo j*, 30: 4198-210.

Percudani, R., A. Pavesi, and S. Ottonello. 1997. 'Transfer RNA gene redundancy and translational selection in Saccharomyces cerevisiae', *J Mol Biol*, 268: 322-30.

Pluta, K., O. Lefebvre, N. C. Martin, W. J. Smagowicz, D. R. Stanford, S. R. Ellis, A. K. Hopper, A. Sentenac, and M. Boguta. 2001. 'Maf1p, a negative effector of RNA polymerase III in Saccharomyces cerevisiae', *Molecular and cellular biology*, 21: 5031-40.

Pombo, A., D. A. Jackson, M. Hollinshead, Z. Wang, R. G. Roeder, and P. R. Cook. 1999. 'Regional specialization in human nuclei: visualization of discrete sites of transcription by RNA polymerase III', *Embo j*, 18: 2241-53.

Pop, C., S. Rouskin, N. T. Ingolia, L. Han, E. M. Phizicky, J. S. Weissman, and D. Koller. 2014. 'Causal signals between codon bias, mRNA structure, and the efficiency of translation and elongation', *Mol Syst Biol*, 10: 770.

Porter, J. J., C. S. Heil, and J. D. Lueck. 2021. 'Therapeutic promise of engineered nonsense suppressor tRNAs', *Wiley Interdiscip Rev RNA*, 12: e1641.

Pratt-Hyatt, M. J., K. M. Kapadia, T. E. Wilson, and D. R. Engelke. 2006. 'Increased recombination between active tRNA genes', *DNA Cell Biol*, 25: 359-64.

Qin, Y., J. Yao, D. C. Wu, R. M. Nottingham, S. Mohr, S. Hunicke-Smith, and A. M. Lambowitz. 2016. 'High-throughput sequencing of human plasma RNA by using thermostable group II intron reverse transcriptases', *Rna*, 22: 111-28.

Quax, T. E., N. J. Claassens, D. Söll, and J. van der Oost. 2015. 'Codon Bias as a Means to Fine-Tune Gene Expression', *Mol Cell*, 59: 149-61.

Raab, Jesse R, Jonathan Chiu, Jingchun Zhu, Sol Katzman, Sreenivasulu Kurukuti, Paul A Wade, David Haussler, and Rohinton T Kamakaka. 2012. 'Human tRNA genes function as chromatin insulators', *The EMBO Journal*, 31: 330-50.

Rak, R., O. Dahan, and Y. Pilpel. 2018. 'Repertoires of tRNAs: The Couplers of Genomics and Proteomics', *Annu Rev Cell Dev Biol*, 34: 239-64.

Ramsay, Ewan Phillip, Guillermo Abascal-Palacios, Julia L. Daiß, Helen King, Jerome Gouge, Michael Pilsl, Fabienne Beuron, Edward Morris, Philip Gunkel, Christoph Engel, and Alessandro Vannini. 2020. 'Structure of human RNA polymerase III', *Nature Communications*, 11: 6409.

Rasmussen, E. B., and J. T. Lis. 1993. 'In vivo transcriptional pausing and cap formation on three Drosophila heat shock genes', *Proc Natl Acad Sci U S A*, 90: 7923-7.

Raymond, K. C., G. J. Raymond, and J. D. Johnson. 1985. 'In vivo modulation of yeast tRNA gene expression by 5'-flanking sequences', *Embo j*, 4: 2649-56.

Reinhardt, Peter, Michael Glatza, Kathrin Hemmer, Yaroslav Tsytsyura, Cora S. Thiel, Susanne Höing, Sören Moritz, Juan A. Parga, Lydia Wagner, Jan M. Bruder, Guangming Wu, Benjamin Schmid, Albrecht Röpke, Jürgen Klingauf, Jens C. Schwamborn, Thomas Gasser, Hans R. Schöler, and Jared Sterneckert. 2013. 'Derivation and Expansion Using Only Small Molecules of Human Neural Progenitors for Neurodegenerative Disease Modeling', *PLOS ONE*, 8: e59252.

Renaud, Marianne, Viviane Praz, Erwann Vieu, Laurence Florens, Michael P. Washburn, Philippe l'Hôte, and Nouria Hernandez. 2014. 'Gene duplication and neofunctionalization: POLR3G and POLR3GL', *Genome Research*, 24: 37-51.

Rideout, E. J., L. Marshall, and S. S. Grewal. 2012. 'Drosophila RNA polymerase III repressor Maf1 controls body size and developmental timing by modulating tRNAiMet synthesis and systemic insulin signaling', *Proc Natl Acad Sci U S A*, 109: 1139-44.

Rodnina, M. V., N. Fischer, C. Maracci, and H. Stark. 2017. 'Ribosome dynamics during decoding', *Philos Trans R Soc Lond B Biol Sci*, 372.

Rojas-Benítez, D., C. Eggers, and A. Glavic. 2017. 'Modulation of the Proteostasis Machinery to Overcome Stress Caused by Diminishe d Levels of t6A-Modified tRNAs in Drosophila', *Biomolecules*, 7.

Ross-Innes, C. S., R. Stark, A. E. Teschendorff, K. A. Holmes, H. R. Ali, M. J. Dunning, G. D. Brown, O. Gojis, I. O. Ellis, A. R. Green, S. Ali, S. F. Chin, C. Palmieri, C. Caldas, and J. S. Carroll. 2012. 'Differential oestrogen receptor binding is associated with clinical outcome in breast cancer', *Nature*, 481: 389-93.

Rosselló-Tortella, M., P. Llinàs-Arias, Y. Sakaguchi, K. Miyauchi, V. Davalos, F. Setien, M. E. Calleja-Cervantes, D. Piñeyro, J. Martínez-Gómez, S. Guil, R. Joshi, A. Villanueva, T. Suzuki, and M. Esteller. 2020. 'Epigenetic loss of the transfer RNA-modifying enzyme TYW2 induces ribosome frameshifts in colon cancer', *Proc Natl Acad Sci U S A*, 117: 20785-93.

Rubio, M. A., I. Pastar, K. W. Gaston, F. L. Ragone, C. J. Janzen, G. A. Cross, F. N. Papavasiliou, and J. D. Alfonzo. 2007. 'An adenosine-to-inosine tRNA-editing enzyme that can perform C-to-U deamination of DNA', *Proc Natl Acad Sci U S A*, 104: 7821-6.

Rudolph, Konrad L. M., Bianca M. Schmitt, Diego Villar, Robert J. White, John C. Marioni, Claudia Kutter, and Duncan T. Odom. 2016. 'Codon-Driven Translational Efficiency Is Stable across Diverse Mammalian Cell States', *PLOS Genetics*, 12: e1006024.

Sagi, Dror, Roni Rak, Hila Gingold, Idan Adir, Gadi Maayan, Orna Dahan, Limor Broday, Yitzhak Pilpel, and Oded Rechavi. 2016. 'Tissue- and Time-Specific Expression of Otherwise Identical tRNA Genes', *PLOS Genetics*, 12: e1006264.

Saitsu, H., H. Osaka, M. Sasaki, J. Takanashi, K. Hamada, A. Yamashita, H. Shibayama, M. Shiina, Y. Kondo, K. Nishiyama, Y. Tsurusaki, N. Miyake, H. Doi, K. Ogata, K. Inoue, and N. Matsumoto. 2011. 'Mutations in POLR3A and POLR3B encoding RNA Polymerase III subunits cause an autosomal-recessive hypomyelinating leukoencephalopathy', *Am J Hum Genet*, 89: 644-51.

Sakonju, Shigeru, Donald D. Brown, David Engelke, Sun-Yu Ng, B. S. Shastry, and Robert G. Roeder. 1981. 'The binding of a transcription factor to deletion mutants of a 5S ribosomal RNA gene', *Cell*, 23: 665-69.

Santos, Fenícia Brito, and Luiz-Eduardo Del-Bem. 2023. 'The Evolution of tRNA Copy Number and Repertoire in Cellular Life', *Genes*, 14: 27.

Sarin, L. P., and S. A. Leidel. 2014. 'Modify or die?--RNA modification defects in metazoans', *RNA Biol*, 11: 1555-67.

Saxton, R. A., and D. M. Sabatini. 2017. 'mTOR Signaling in Growth, Metabolism, and Disease', *Cell*, 168: 960-76.

Schmitt, B. M., K. L. Rudolph, P. Karagianni, N. A. Fonseca, R. J. White, I. Talianidis, D. T. Odom, J. C. Marioni, and C. Kutter. 2014. 'High-resolution mapping of transcriptional dynamics across tissue development reveals a stable mRNA-tRNA interface', *Genome Res*, 24: 1797-807.

Schneider-Poetsch, T., J. Ju, D. E. Eyler, Y. Dang, S. Bhat, W. C. Merrick, R. Green, B. Shen, and J. O. Liu. 2010. 'Inhibition of eukaryotic translation elongation by cycloheximide and lactimidomycin', *Nat Chem Biol*, 6: 209-17.

Schramm, L., and N. Hernandez. 2002. 'Recruitment of RNA polymerase III to its target promoters', *Genes Dev*, 16: 2593-620.

Schultz, P., N. Marzouki, C. Marck, A. Ruet, P. Oudet, and A. Sentenac. 1989. 'The two DNA-binding domains of yeast transcription factor tau as observed by scanning transmission electron microscopy', *Embo j*, 8: 3815-24.

Sepehri, S., and N. Hernandez. 1997. 'The largest subunit of human RNA polymerase III is closely related to the largest subunit of yeast and trypanosome RNA polymerase III', *Genome Res*, 7: 1006-19.

Shah, S. M., A. Kumar, E. P. Geiduschek, and G. A. Kassavetis. 1999. 'Alignment of the B" subunit of RNA polymerase III transcription factor IIIB in its promoter complex', *J Biol Chem*, 274: 28736-44.

Shor, Boris, Jiang Wu, Quazi Shakey, Lourdes Toral-Barza, Celine Shi, Max Follettie, and Ker Yu. 2010. 'Requirement of the mTOR Kinase for the Regulation of Maf1 Phosphorylation and Control of RNA Polymerase III-dependent Transcription in Cancer Cells', *Journal of Biological Chemistry*, 285: 15380-92.

Song, J., and J. L. Markley. 2007. 'Three-dimensional structure determined for a subunit of human tRNA splicing endonuclease (Sen15) reveals a novel dimeric fold', *J Mol Biol*, 366: 155-64.

Sørensen, Michael A., Johan Elf, Elli Bouakaz, Tanel Tenson, Suparna Sanyal, Glenn R. Björk, and Måns Ehrenberg. 2005. 'Over Expression of a tRNALeu Isoacceptor Changes Charging Pattern of Leucine tRNAs and Reveals New Codon Reading', *Journal of Molecular Biology*, 354: 16-24.

Spickler, C., and G. A. Mackie. 2000. 'Action of RNase II and polynucleotide phosphorylase against RNAs containing stem-loops of defined structure', *J Bacteriol*, 182: 2422-7.

Sriskanthadevan-Pirahas, Shrivani, Rujuta Deshpande, Byoungchun Lee, and Savraj S. Grewal. 2018. 'Ras/ERK-signalling promotes tRNA synthesis and growth via the RNA polymerase III repressor Maf1 in Drosophila', *PLOS Genetics*, 14: e1007202.

Stergachis, Andrew B., Eric Haugen, Anthony Shafer, Wenqing Fu, Benjamin Vernot, Alex Reynolds, Anthony Raubitschek, Steven Ziegler, Emily M. LeProust, Joshua M. Akey, and John A. Stamatoyannopoulos. 2013. 'Exonic Transcription Factor Binding Directs Codon Choice and Affects Protein Evolution', *Science*, 342: 1367-72.

Stillman, D. J., and E. P. Geiduschek. 1984. 'Differential binding of a S. cerevisiae RNA polymerase III transcription factor to two promoter segments of a tRNA gene', *Embo j*, 3: 847-53.

Sutcliffe, J. E., T. R. Brown, S. J. Allison, P. H. Scott, and R. J. White. 2000. 'Retinoblastoma protein disrupts interactions required for RNA polymerase III transcription', *Molecular and cellular biology*, 20: 9192-202.

Suzuki, Tsutomu. 2021. 'The expanding world of tRNA modifications and their disease relevance', *Nature Reviews Molecular Cell Biology*, 22: 375-92.

Takahashi, K., and S. Yamanaka. 2006. 'Induction of pluripotent stem cells from mouse embryonic and adult fibroblast cultures by defined factors', *Cell*, 126: 663-76.

Thiaville, P. C., D. Iwata-Reuyl, and V. de Crécy-Lagard. 2014. 'Diversity of the biosynthesis pathway for threonylcarbamoyladenosine (t(6)A), a universal modification of tRNA', *RNA Biol*, 11: 1529-39.

Thornlow, B. P., J. Armstrong, A. D. Holmes, J. M. Howard, R. B. Corbett-Detig, and T. M. Lowe. 2020. 'Predicting transfer RNA gene activity from sequence and genome context', *Genome Res*, 30: 85-94.

Thornlow, B. P., J. Hough, J. M. Roger, H. Gong, T. M. Lowe, and R. B. Corbett-Detig. 2018. 'Transfer RNA genes experience exceptionally elevated mutation rates', *Proc Natl Acad Sci U S A*, 115: 8996-9001.

Tohyama, S., F. Hattori, M. Sano, T. Hishiki, Y. Nagahata, T. Matsuura, H. Hashimoto, T. Suzuki, H. Yamashita, Y. Satoh, T. Egashira, T. Seki, N. Muraoka, H. Yamakawa, Y. Ohgino, T. Tanaka, M. Yoichi, S. Yuasa, M. Murata, M. Suematsu, and K. Fukuda. 2013. 'Distinct metabolic flow enables large-scale purification of mouse and human pluripotent stem cell-derived cardiomyocytes', *Cell Stem Cell*, 12: 127-37.

Torrent, M., G. Chalancon, N. S. de Groot, A. Wuster, and M. Madan Babu. 2018. 'Cells alter their tRNA abundance to selectively regulate protein synthesis during stress conditions', *Sci Signal*, 11.

Torres, A. G., D. Piñeyro, M. Rodríguez-Escribà, N. Camacho, O. Reina, A. Saint-Léger, L. Filonava, E. Batlle, and L. Ribas de Pouplana. 2015. 'Inosine modifications in human tRNAs are incorporated at the precursor tRNA level', *Nucleic Acids Res*, 43: 5145-57.

Torres, A. G., O. Reina, C. Stephan-Otto Attolini, and L. Ribas de Pouplana. 2019. 'Differential expression of human tRNA genes drives the abundance of tRNA-derived fragments', *Proc Natl Acad Sci U S A*, 116: 8451-56.

Torres, Adrian Gabriel. 2019. 'Enjoy the Silence: Nearly Half of Human tRNA Genes Are Silent', *Bioinformatics and Biology Insights*, 13: 1177932219868454.

Torres, Adrian Gabriel, David Piñeyro, Liudmila Filonava, Travis H. Stracker, Eduard Batlle, and Lluis Ribas de Pouplana. 2014. 'A-to-I editing on tRNAs: Biochemical, biological and evolutionary implications', *FEBS Letters*, 588: 4279-86.

Trotta, C. R., S. V. Paushkin, M. Patel, H. Li, and S. W. Peltz. 2006. 'Cleavage of pre-tRNAs by the splicing endonuclease requires a composite active site', *Nature*, 441: 375-7.

Tuller, Tamir, Asaf Carmi, Kalin Vestsigian, Sivan Navon, Yuval Dorfan, John Zaborske, Tao Pan, Orna Dahan, Itay Furman, and Yitzhak Pilpel. 2010. 'An Evolutionarily Conserved Mechanism for Controlling the Efficiency of Protein Translation', *Cell*, 141: 344-54.

Turowski, T. W., E. Leśniewska, C. Delan-Forino, C. Sayou, M. Boguta, and D. Tollervey. 2016. 'Global analysis of transcriptionally engaged yeast RNA polymerase III reveals extended tRNA transcripts', *Genome Res*, 26: 933-44.

Turowski, Tomasz W., and David Tollervey. 2016. 'Transcription by RNA polymerase III: insights into mechanism and regulation', *Biochemical Society Transactions*, 44: 1367-75.

Upadhya, R., J. Lee, and I. M. Willis. 2002. 'Maf1 is an essential mediator of diverse signals that repress RNA polymerase III transcription', *Mol Cell*, 10: 1489-94.

Valle, M., A. Zavialov, J. Sengupta, U. Rawat, M. Ehrenberg, and J. Frank. 2003. 'Locking and unlocking of ribosomal motions', *Cell*, 114: 123-34.

Van Bortle, K., D. P. Marciano, Q. Liu, T. Chou, A. M. Lipchik, S. Gollapudi, B. S. Geller, E. Monte, R. T. Kamakaka, and M. P. Snyder. 2022. 'A cancer-associated RNA polymerase III identity drives robust transcription and expression of snaR-A noncoding RNA', *Nat Commun*, 13: 3007.

Van Bortle, Kevin, Douglas H. Phanstiel, and Michael P. Snyder. 2017. 'Topological organization and dynamic regulation of human tRNA genes during macrophage differentiation', *Genome Biology*, 18: 180.

Vannini, A., and P. Cramer. 2012. 'Conservation between the RNA polymerase I, II, and III transcription initiation machineries', *Mol Cell*, 45: 439-46.

Vannini, Alessandro, Rieke Ringel, Anselm G. Kusser, Otto Berninghausen, George A. Kassavetis, and Patrick Cramer. 2010. 'Molecular Basis of RNA Polymerase III Transcription Repression by Maf1', *Cell*, 143: 59-70.

Vorländer, Matthias K., Florence Baudin, Robyn D. Moir, René Wetzel, Wim J. H. Hagen, Ian M. Willis, and Christoph W. Müller. 2020. 'Structural basis for RNA polymerase III transcription repression by Maf1', *Nature Structural & Molecular Biology*, 27: 229-32.

Waas, W. F., Z. Druzina, M. Hanan, and P. Schimmel. 2007. 'Role of a tRNA base modification and its precursors in frameshifting in eukaryotes', *J Biol Chem*, 282: 26026-34.

Wagner, E. J., and P. B. Carpenter. 2012. 'Understanding the language of Lys36 methylation at histone H3', *Nat Rev Mol Cell Biol*, 13: 115-26.

Wang, Jiaming, Yue Zhang, Craig A. Mendonca, Onur Yukselen, Khaja Muneeruddin, Lingzhi Ren, Jialing Liang, Chen Zhou, Jun Xie, Jia Li, Zhong Jiang, Alper Kucukural, Scott A. Shaffer, Guangping Gao, and Dan Wang. 2022. 'AAV-delivered suppressor tRNA overcomes a nonsense mutation in mice', *Nature*, 604: 343-48.

Wang, Qianmin, Shaobai Li, Futang Wan, Youwei Xu, Zhenfang Wu, Mi Cao, Pengfei Lan, Ming Lei, and Jian Wu. 2021. 'Structural insights into transcriptional regulation of human RNA polymerase III', *Nature Structural & Molecular Biology*, 28: 220-27.

Wang, Xiaoling, Alan Gerber, Wei-Yi Chen, and Robert G. Roeder. 2020. 'Functions of paralogous RNA polymerase III subunits POLR3G and POLR3GL in mouse development', *Proceedings of the National Academy of Sciences*, 117: 15702-11.

Wang, Z., and R. G. Roeder. 1997. 'Three human RNA polymerase III-specific subunits form a subcomplex with a selective function in specific transcription initiation', *Genes Dev*, 11: 1315-26.

Wei, Y. Y., and H. T. Chen. 2018. 'Functions of the TFIIE-Related Tandem Winged-Helix Domain of Rpc34 in RNA Polymerase III Initiation and Elongation', *Molecular and cellular biology*, 38.

Weinberg, D. E., P. Shah, S. W. Eichhorn, J. A. Hussmann, J. B. Plotkin, and D. P. Bartel. 2016. 'Improved Ribosome-Footprint and mRNA Measurements Provide Insights into Dynamics and Regulation of Yeast Translation', *Cell reports*, 14: 1787-99.

White, R J, S P Jackson, and P W Rigby. 1992. 'A role for the TATA-box-binding protein component of the transcription factor IID complex as a general RNA polymerase III transcription factor', *Proceedings of the National Academy of Sciences*, 89: 1949-53.

Whitfield, M. L., L. K. George, G. D. Grant, and C. M. Perou. 2006. 'Common markers of proliferation', *Nat Rev Cancer*, 6: 99-106.

Winter, A. G., G. Sourvinos, S. J. Allison, K. Tosh, P. H. Scott, D. A. Spandidos, and R. J. White. 2000. 'RNA polymerase III transcription factor TFIIIC2 is overexpressed in ovarian tumors', *Proc Natl Acad Sci U S A*, 97: 12619-24.

Wolin, Sandra L., and A. Gregory Matera. 1999. 'The trials and travels of tRNA', *Genes & Development*, 13: 1-10.

Wong, R. C., S. Pollan, H. Fong, A. Ibrahim, E. L. Smith, M. Ho, A. L. Laslett, and P. J. Donovan. 2011. 'A novel role for an RNA polymerase III subunit POLR3G in regulating pluripotency in human embryonic stem cells', *Stem Cells*, 29: 1517-27.

Wu, C. C., B. Zinshteyn, K. A. Wehner, and R. Green. 2019. 'High-Resolution Ribosome Profiling Defines Discrete Ribosome Elongation States and Translational Regulation during Cellular Stress', *Mol Cell*, 73: 959-70.e5.

Yenice, Sedef, Alan T. Davis, Said A. Goueli, Atif Akdas, Catherine Limas, and Khalil Ahmed. 1994. 'Nuclear casein kinase 2 (CK-2) activity in human normal, benign hyperplastic, and cancerous prostate', *The Prostate*, 24: 11-16.

Yong, Wai-Shin, Fei-Man Hsu, and Pao-Yang Chen. 2016. 'Profiling genome-wide DNA methylation', *Epigenetics & Chromatin*, 9: 26.

Yukawa, Y., G. Dieci, M. Alzapiedi, A. Hiraga, K. Hirai, Y. Y. Yamamoto, and M. Sugiura. 2011. 'A common sequence motif involved in selection of transcription start sites of Arabidopsis and budding yeast tRNA genes', *Genomics*, 97: 166-72.

Zakrzewski, Wojciech, Maciej Dobrzyński, Maria Szymonowicz, and Zbigniew Rybak. 2019. 'Stem cells: past, present, and future', *Stem Cell Research & Therapy*, 10: 68.

Zhang, Kuan, Erica Yao, Ethan Chuang, Biao Chen, Evelyn Y. Chuang, and Pao-Tien Chuang. 2022. 'mTORC1 signaling facilitates differential stem cell differentiation to shape the developing murine lung and is associated with mitochondrial capacity', *Nature Communications*, 13: 7252.

Zhang, Liying, Jing Guo, Pengyuan Zhang, Qiang Xiong, Steven C. Wu, Lily Xia, Samit Sunny Roy, Jakub Tolar, Timothy D. O'Connell, Michael Kyba, Kenneth Liao, and Jianyi

Zhang. 2015. 'Derivation and High Engraftment of Patient-Specific Cardiomyocyte Sheet Using Induced Pluripotent Stem Cells Generated From Adult Cardiac Fibroblast', *Circulation: Heart Failure*, 8: 156-66.

Zhang, M., J. S. Schulte, A. Heinick, I. Piccini, J. Rao, R. Quaranta, D. Zeuschner, D. Malan, K. P. Kim, A. Röpke, P. Sasse, M. Araúzo-Bravo, G. Seebohm, H. Schöler, L. Fabritz, P. Kirchhof, F. U. Müller, and B. Greber. 2015. 'Universal cardiac induction of human pluripotent stem cells in two and three-dimensional formats: implications for in vitro maturation', *Stem Cells*, 33: 1456-69.

Zhao, C., F. Liu, and A. M. Pyle. 2018. 'An ultraprocessive, accurate reverse transcriptase encoded by a metazoan group II intron', *Rna*, 24: 183-95.

Zheng, Guanqun, Yidan Qin, Wesley C. Clark, Qing Dai, Chengqi Yi, Chuan He, Alan M. Lambowitz, and Tao Pan. 2015. 'Efficient and quantitative high-throughput tRNA sequencing', *Nature Methods*, 12: 835-37.

Zhong, Zhaohui, Huiying Gu, Jirun Peng, Wenzheng Wang, Brian H. Johnstone, Keith L. March, Martin R. Farlow, and Yansheng Du. 2016. 'GDNF secreted from adipose-derived stem cells stimulates VEGF-independent angiogenesis', *Oncotarget*, 7.

Zhou, Jiaxi, Pei Su, Lu Wang, Joanna Chen, Maike Zimmermann, Olga Genbacev, Olubunmi Afonja, Mary C. Horne, Tetsuya Tanaka, Enkui Duan, Susan J. Fisher, Jiayu Liao, Jie Chen, and Fei Wang. 2009. 'mTOR supports long-term self-renewal and suppresses mesoderm and endoderm activities of human embryonic stem cells', *Proceedings of the National Academy of Sciences*, 106: 7840-45.

Zhou, Ying, Jeffrey M. Goodenbour, Lucy A. Godley, Amittha Wickrema, and Tao Pan. 2009. 'High levels of tRNA abundance and alteration of tRNA charging by bortezomib in multiple myeloma', *Biochemical and Biophysical Research Communications*, 385: 160-64.

Acknowledgements

Thanks for reading until here, and thanks for the ones that accompanied me in this remarkable journey:

My supervisor Danny. This PhD thesis would not be achievable in any possible way without the unparalleled guidance, expert advice, and constant encouragement from her. There are numerous things I observed and could learn from her: paying attention to details while staying mindful of the overarching concept, providing ample guidance with details and patience while maintaining efficiency, troubleshooting issues in a motivating and constructive manner, embracing and respecting the difference among individuals, cultivating young generations regardless of their current levels or abilities, showing concerns for the well-being of students, etc. I am lucky to work with Danny, especially early in my career, as she exemplifies what a true scientist should be, and I am sure that all the positive influence she had on me will be lasting and passed on.

My collaborator Drew, who is a great data scientist. This project would not be complete without all his computational expertise and excellent work. And many people in the lab, Sascha who is always optimistic and gave me encouragement whenever I question myself, Geri who is so professional and reliable that I never have doubts in any work that is given to her, Till who is so responsible and helped me solve troubles related to German speaking, Selay who is trustworthy, Felix, Sergio, etc.

My TAC members Annalisa Marsico and Till Bartke who provided great ideas in the progress of this project. Rinho and staff from the core facility, who always responded promptly to my requests with sequencing.

A lot of friends from and beyond Munich. Yong, who led me to research in the very beginning and gave me the opportunity of studying abroad. Kun, Huihui, Zeyuan, Ziqi, Wenxiu, Songwei, etc, for all the barbeques we had, the hotpot we enjoyed, the hiking we did, the roads and lakes we cycled, the short and long trips we traveled together.

My parents, who sometimes worried but still trusted and supported me, whom I care so much and desire the most recognition. My grandparents, who are my angels and gave me unconditional love that makes me feel rich and brave, for whom I wish I could have done more, who will be proud of their kid as always, no matter where they are. Kangren, with whom I would like to explore the uncertainty of life and future.

In a marathon that resembles the PhD study, after the initial excitement, more is the repetitive left-right moving forward, exhaustion and pain. I was fortunate enough to have you all who supported me in this battle of both body and mind. I wouldn't have made it this far without your companion in this extraordinary journey.